Metabolic Maturation of Induced Pluripotent Stem Cells derived Cardiomyocytes.



Colleen Lopez

St. Cross College

Department of Physiology, Anatomy, and Genetics

University of Oxford

A thesis submitted for the degree of

Doctor of Philosophy

Michaelmas Term 2018

Acknowledgements

It is difficult to believe that 3 years have gone by and this Thesis has come to an end. It has been a fascinating, enlightening and at times, turbulent journey which I could not have completed without the help and support of the following people and institutions.

First and foremost, I would like to thank my supervisor Professor Carolyn Carr for giving me the opportunity to work on this project and for her endless guidance and tireless support throughout the course of my DPhil. She has been extremely encouraging, and willing to answer questions or to discuss scientific ideas, alongside her help and patiences with me and my extra curriculum activities has allowed me to make the most of my experience here at Oxford. For all of this, I am extremely grateful. I also would like to thank my co-supervisor, Professor Damian Tyler, who consistently provided the extra support I needed and provided me valuable advice. In addition, I would like to thank the head of our research group Professor Kieran Clarke, for welcoming me into the group and for her constant motivation. None of this work would have been possible without the funding from the British Heart Foundation and Rosetrees Trust.

During these past three years, I received support from several members of the CMRG group. These individuals offered me encouragement, friendship, and help and made my time in lab a constant enjoyment. To start, Dr. Lisa Heather, you were an endless source of knowledge on any metabolism question. Thank you for helping me troubleshoot countless experiments from the radiation substrate assays, to OXbox, to westerns. Dr. Rhys Evans, you were another invaluable source of information to me. Not only did you assist in my radiation work but also mentored me on career choices. I'd also like to thank the lab managers. Dr. Vicky Ball, this lab would not run without you. For all the times I depended on your assistance, from techniques to housekeeping tasks, you were always there to help. You definitely showed us that your talents and insights extended far past the lab realm by teaching us about crepe day, cooking, and other life lessons. I truly enjoyed my time sitting across from you. Finally, I would also like to acknowledge both Nicola Dixon and Yvonne Green for running the day to day administration of the lab and assisting me in any way they could.

Next, I would like to thank the Stem Cell Group including Dr. Sophia Malandraki-Miller, Dr. Arne A. N. Bruyneel, Dr. Heba Al-Siddiqi, Rita

Alonaizan, Ujang Purnama and Fatemeh Kermani for their collaboration in the cell culture room and for their technical help and advice. Adding, to this list, I would like to thank all my students: Alyssas Borman, Samuel Sussmes, and Charlotte Ferguson for teaching me patience and assisting me on my experiments. I am also grateful to the other group members of the CRMG, both past and present for the friendship, advice, and entertaining working environment. These individuals include Dr. Michael Dodd, Dr. Jack Miller, Dr. Andrew Lewis, Dr. Latt Mansor, Dr. Brianna Stubbs, Dr. Lucia Giles, Dr. Cher-Rin Chong, Dr. Kerstin Timm, Dr. Angus Lau, Dr. Justin Lau, Maria de Luz Sousa Fialho, Dragana Savic, Matthew Kerr, Claudia Aparicio, Azrul Abdul Kadir, David Dearlove, Adrian Soto Mota, Giles McMullen-Klein, Tony Zhou and Javier Gilbert-Jaramillo. All of you provided a home away from home and I will always remember fondly our secret santas/xmas lunches, escape room adventures, lab outings, and endless supplies of cakes. From this lab I have learned the following very important life lessons...

- It's normal to take 5 tea breaks throughout the day.
- "You okay?" is a normal upbeat greeting.
- z's are actually pronounced as a zed's.
- If you are ever in doubt of spelling add a "u".
- Days come before months.
- Animals make different sounds depending on what country you ask.
- And finally, know how to cook a proper cake.

I definitely owe a special thank you to both Dr. Arne A. N. Brunyeel and Dr. Sophia Malandraki-Miller who initially trained me on all stem cell techniques, Maria de Luz Sousa Fialho for training me on the radiation experiments, Matthew Kerr for training me on the OXbox, Dr. Jack Miller for the constant Latex help, Megan Thomas for the graphic design of several of my images, and Dragana Savic for the constant motivation and day to day inspiration. All seven of you went out of your way to assist me on numerous occasions and always did so with a smile on your face!

I would also like to thank our collaborators at the University of Oxford Material Science Department including Professor Jan Czernuska, Dr. Qi Chen, Dr. Rabia Nazir, and Sonia Iftekhar for their support in the production of the collagen scaffolds as well as Dr. Michal Maj in the Pathology Department who assisted with the Flow Cytometry experiments. I would like to thank Professor Sian Harding and Dr. Thomas Owens at Imperial College, London for teaching me the EHT technology and Dr. Filippo Perbellini and Ifigeneia Bardi for the 3D printing of our OXbox ring and cryoslicing technique.

Additionally, I would like to thank all the members of the staff at DPAG,

BSB and other departments for their assistance and to the St. Cross College administration and Porters for all the help during my time there and during my Presidency role in the SRC. Lastly, I'd like to thank all my friends from Lab, College and from my several football team (Blues, Foxes, DPAG department, etc.) for providing me constant support, friendship, travel buddies, and an outlet from my work. Finally, I'd like to thank my family for their constant support and help even from a distance. They gave me the necessary encouragement and inspiration to finish.

Abstract

Cardiac metabolism and function are inherently linked, as substrate metabolism generates the energy needed for the heart to beat. With the development of protocols to differentiate human induced pluripotent stem cells (iPSCs) into beating cardiomyocytes (CMs), cardiac cells can now be studied in vitro. This promises valuable insights into the biology of human CMs, however it is hindered by the fact that induced pluripotent stem cell-derived cardiomyocytes (iPSC-CMs) have a very immature phenotype and do not recapitulate the properties of adult CMs. iPSC-CMs are immature in several ways including but not limited to morphologically, mitochondrial and sarcromeric structure, electrophysiological properties as well as their metabolism. iPSC-CMs reflect more of a foetal CM metabolism relying on glucose as their primary energy substrate, while an adult CM has more of an oxidative metabolism. This may, in part, be due to the fact that the iPSC-CMs are frequently grown as a monolayer in high glucose media and do not have the need to generate large amounts of energy for contraction and are metabolising non-physiologically relevant concentrations of nutrients. This does not change in the majority of cardiac differentiation protocols. Even though metabolic state affects marker expression, cellular function and activity, the substrate composition is currently being overlooked.

Several labs have tried different strategies to mature iPSC-CMs from long-term culture, applied mechanical and electrical stimulation, the use of maturation media containing chemicals or small compounds, to 3D culture. This thesis sought to investigate and address maturation of iPSC-CMs through stimulating fatty acid oxidation (FAO) using physiologically relevant methods of 3D culture in combination with PPARα activation via addition of the PPARα agonist WY-14643 and of the fatty acid, oleic acid (OA), into the culture media. By simultaneously targeting both maturation methods we have shown a degree of maturation through an increased movement towards reduced glycolysis and increased FAO in our iPSC-CMs.

Like others this thesis has shown that iPSC-CMs mature slowly over time with changes in structural genes occurring during the first month of differentiation and continuing to increase up to 3 months, whereas metabolic changes took longer to develop. 3D culture on collagen-derived scaffolds and engineered heart tissue (EHT) accelerated this maturation time and increased mitochondrial oxidative metabolism

while decreasing anaerobic glycolysis. This was also reflected genetically in the collagen-derived scaffolds with increased expression of a number of genes involved in regulating both FAO and reduced glycolytic gene expression. Treatment with OA + WY-14643 for 1 week enhanced FAO and oxygen consumption. Finally, EHTs treated for 1 week with both OA and WY-14643 were found to be generating 4 times the amount of ATP by oxidation than the 2D cultured iPSC-CMs and twice as much as the scaffolds.

Although, further work is still required to optimise culture conditions by reducing glucose levels in the media and investigating the effect of insulin stimulation, the work in this thesis confirms that the dual approach of 3D culture and enhancing the culture media with additional OA and PPARα agonists induces a degree of maturation in iPSC-CMs towards the metabolic flexibility of the adult heart.

Contents

1 Introduction **12**

1.1 Cardiovascular Disease . . . 12
1.1.1 Myocardial Infarction . . . 12
1.2 Stem Cell Therapies . . . 15
1.2.1 Types of Stem Cells for Therapy . . . 16
1.2.1.1 Bone Marrow-derived Stem Cells and Other Mesenchymal Stem Cells . . . 16
1.2.1.2 Adult Cardiac Stem Cells . . . 17
1.2.1.3 Embryonic Stem Cells . . . 18
1.2.1.4 Induced Pluripotent Stem Cells (iPSCs) . . . 19
1.3 Cardiac Metabolism . . . 23
1.3.1 Cardiac Metabolism During Development . . . 29
1.3.2 Cardiac Metabolism in MI and HF . . . 31
1.3.3 The Change in Cardiac Metabolism of Stem Cells to Adult CMs 33
1.4 Why Study Stem Cell Metabolism . . . 35
1.4.1 Assessing Cell Metabolism . . . 36
1.5 Cardiac Differentiation in Vitro . . . 38
1.5.1 EB-Based Protocols . . . 39
1.5.2 Monolayer Protocols . . . 42
1.5.3 The Role of Hypoxia and of Reactive Oxygen Species in Differentiation . . . 43
1.6 Future Strategies to Mature Cells . . . 45
1.6.1 Changing Media Composition to be More Physiologically Relevant . . . 45
1.6.2 Tissue Engineering Approaches for Disease Modelling . . . 47
1.6.2.1 Cell Sheeting . . . 48
1.6.2.2 Decellularized Hearts . . . 48
1.6.2.3 Constructing 3D scaffolds from (Semi-)Synthetic and Biological Materials . . . 49
1.6.2.4 Porous Scaffolds . . . 50
1.6.2.5 Fibrous Scaffolds . . . 50
1.6.2.6 Hydrogels . . . 51
1.7 Thesis Aims . . . 52
1.7.0.1 Specific Aims . . . 52

2 Methodology **54**
2.1 Methods . . . 54
2.1.1 iPSC Cell Culture . . . 54
2.1.1.1 Routine Culture, Media and Matrigel Coating . . . 54
2.1.1.2 Passaging Protocol . . . 54
2.1.1.3 Thawing Human iPSCs . . . 55
2.1.1.4 Freezing Down and Long Term Storage of iPSCs . . . 55
2.1.1.5 Cardiac Differentiation . . . 56
2.1.1.6 Dissociation and Re-plating of iPSC-CMs . . . 56
2.1.2 Collagen Scaffolds . . . 58
2.1.2.1 Scaffold Sterilisation . . . 59
2.1.2.2 Seeding Scaffolds with iPSC-CMs . . . 60
2.1.3 Engineered Heart Tissue . . . 61
2.1.3.1 Generation of EHT . . . 61
2.1.4 Flow Cytometry . . . 63
2.1.5 Quantitative PCR . . . 65
2.1.5.1 RNA Extraction . . . 65
2.1.5.2 cDNA Analysis . . . 65
2.1.5.3 Primer Design . . . 66
2.1.5.4 qPCR Reaction . . . 66
2.1.5.5 Analysis of qPCR Data: $\Delta\Delta C_T$ Method . . . 67
2.1.6 Total DNA Quantification . . . 68
2.1.7 Immunocytochemistry . . . 68
2.1.7.1 Mitotracker Staining . . . 69
2.1.7.2 Oil Red O Staining . . . 69
2.1.8 Assessing Cell Metabolism . . . 70
2.1.8.1 AlamarBlue Cell Viability . . . 70
2.1.8.2 ^{3}H Palmitate Oxidation . . . 70
2.1.8.3 ^{3}H Oleic Acid Oxidation . . . 74
2.1.8.4 Glycolytic Flux . . . 74
2.1.9 ^{14}C Glucose Oxidation . . . 79
2.1.9.1 Oxygen Consumption Rate Measurements Using the Clark Oxygen Electrode . . . 80
2.1.10 Statistics and Data Analysis . . . 83
2.1.10.1 T-Test . . . 84
2.1.10.2 Analysis of Variance (ANOVA) . . . 84
2.1.10.3 Tukey Test . . . 85
2.1.11 Extra Experiments . . . 86

3 3D culture on collagen-based scaffolds induces a more metabolically mature phenotype in induced pluripotent stem cell-derived cardiomyocytes. **87**
3.1 Introduction . . . 87
3.1.1 Activation and Inhibition of the Wnt Pathway in Cardiac Differentiation . . . 87

3.1.2 Accessing Maturation . . . 89
3.1.2.1 Cardiac Genes . . . 89
3.1.2.2 Metabolism Genes . . . 94
3.1.3 Tissue Engineering Approaches to Cell Maturation . . . 98
3.1.4 Chapter Aims . . . 99
3.2 Results . . . 99
3.2.1 Differentiating iPSCs into Beating Cardiomyocytes on Matrigel 99
3.2.2 Long Term Culture-induced Maturation of iPSC-CM . . . 102
3.2.2.1 Stability of the Reference Genes . . . 102
3.2.2.2 iPSC-CMs Long Term Culture Expression of CM Genes 105
3.2.2.3 iPSC-CMs Long Term Culture Expression of Metabolic Genes . . . 105
3.2.3 Metabolic Gene Expression Changes Between iPSCs and Beating Cardiomyocytes . . . 107
3.2.3.1 Glucose Consumption and Lactate Production in Culture Media . . . 107
3.2.4 Culture of iPSC-CMs on Different ECM Substrates . . . 109
3.2.5 ABA and Validating ABA . . . 110
3.2.6 Culture of iPSC-CMs on Collagen Scaffolds . . . 113
3.2.6.1 Determining iPSC-CMs Cell Count on Scaffolds . . . 116
3.2.7 ABA of Cultured iPSC-CMs on Collagen-Derived Scaffolds and ECM Substrate Coated Monolayer Plates. . . . 122
3.2.8 RF-Matrigel-Coated Scaffolds vs 100% Collagen Scaffolds . . . 123
3.2.9 Gene Expression Changes Between Cultured iPSC-CMs on Collagen-derived Scaffolds and ECM Substrate Coated Monolayer Plates . . . 126
3.2.10 Fatty Acid Oxidation of Cultured iPSC-CMs on Collagen-derived Scaffolds and ECM Substrate Coated Monolayer Plates 127
3.2.11 Glycolytic Flux of Cultured iPSC-CMs on Collagen-derived Scaffolds and ECM Substrate Coated Monolayer Plates . . . 130
3.3 Discussion . . . 130
3.3.1 iPSC-CMs Maturation Through Long-Term Culture . . . 133
3.3.2 iPSC-CMs Cultured on Different 2D ECM vs 3D Scaffolds . . . 135
3.3.3 Assessing 2D vs 3D Metabolic Flux . . . 137
3.4 Conclusion . . . 138

4 Treatment with Oleic Acid and a PPARα Agonist (WY-14643) with 3D Culture Induces Metabolic Maturation in Induced Pluripotent Stem Cell derived Cardiomyocytes. 139
4.1 Introduction . . . 139
4.1.1 Maturation of Stem Cell-Derived Cardiomyocytes . . . 139
4.1.1.1 Maturation Methods . . . 142
4.1.2 Peroxisome Proliferator-Activated Receptor . . . 143
4.1.2.1 PPAR Structure . . . 143
4.1.2.2 *PPARα* Activation . . . 143

4.1.2.3 PPARα Agonist - WY-14643 (Pirinixic Acid) 145
4.1.2.4 PPARα Target Genes 147
4.1.3 PPARα Expression in Developing and Adult Hearts. 147
4.1.3.1 PPARα Expression During Cardiac Differentiation. . 147
4.1.3.2 PPARα Expression Regulation of Cardiac Metabolism 149
4.1.4 Chapter Aims 150
4.2 Methods 151
4.2.1 Differentiation of iPSC-CMs and Treatment With OA ± WY-14643 151
4.2.2 OA Treatment 151
4.2.3 WY-14643 (Pirinixic Acid) Treatment 152
4.3 Results 152
4.3.1 iPSC-CM Treated With OA ± WY-14643 152
4.3.2 Monolayer qPCR Treated With OA ± WY-14643 for 24 Hours Versus 1 Week 153
4.3.2.1 Stability of the Reference Genes 153
4.3.2.2 Effects of OA ± WY-14643 on Relative Expression of Pyruvate Oxidation Genes. 153
4.3.2.3 Effects of OA ± WY-14643 on Relative Expression of Glycolysis Genes. 155
4.3.2.4 Effects of OA ± WY-14643 on Relative Expression of FAO Genes. 155
4.3.2.5 Effects of OA ± WY-14643 on Mitochondrial Relative Gene Expression. 157
4.3.3 FAO of Monolayer iPSC-CM Treated With OA ± WY-14643 for 24 Hours or 1 Week. 157
4.3.4 The Glycolytic Flux and Glucose Oxidation of Monolayer iPSC-CM Treated With OA ± WY-14643 157
4.3.5 Oxygen Consumption Rate of Treated iPSC-CMs With OA Alone or With WY-14643 Using the Clark-Type Oxygen Electrode 159
4.3.6 Westerns 162
4.3.7 Immunocytochemistry of iPSC-CMs Treated With OA ± WY-14643 166
4.3.8 FAO of iPSC-CMs Cultured on Scaffolds and Treated With OA ± WY-14643 for 24 Hours or 1 Week. 168
4.3.9 The Glycolytic Flux and Glucose Oxidation of Cultured iPSC-CMs on Scaffolds and Treated With OA ± WY-14643. . 169
4.3.10 Oxygen Consumption Rates in iPSC-CMs Cultured on 3D Scaffolds Treated with OA Alone or With WY-14643 Using the Clark-Type Oxygen Electrode 171
4.4 Discussion 176
4.4.1 Effects of OA ± WY-14643 Treatment on Gene Expression of Monolayer iPSC-CMs 176

4.4.2 Effects of OA ± WY-14643 Treatment on Monolayer iPSC-CMs Making a Metabolic Switch From a Glucose Metabolism Towards More FAO. . . . 178
4.4.3 Oxygen Consumption Rate on Monolayer iPSC-CMs Treated With OA Alone or With WY-14643 Using Clarke-Type Oxygen Electrode . . . 179
4.4.4 Effects of OA ± WY-14643 Treatment on iPSC-CMs Cultured in 3D . . . 180
4.5 Conclusion . . . 181

5 Developing Engineered Heart Tissue (EHT) for Metabolic Characterization and Maturation of Induced Pluripotent Stem Cell derived Cardiomyocytes. 182
5.1 Introduction . . . 182
5.1.1 Development of Engineered Heart Tissue . . . 182
5.1.1.1 EHTs Mimic Cardiac Tissue . . . 185
5.1.1.2 EHT Application in Stem Cell Therapies . . . 185
5.1.1.3 EHTs Application in Disease Modeling . . . 186
5.1.1.4 EHTs Application in Drug Toxicology . . . 187
5.1.2 iPSC-CM-Derived EHT Maturation . . . 188
5.1.3 Chapter Aims . . . 188
5.2 Methods . . . 189
5.2.1 Glucose-Free, Lactate-Enriched Treatment . . . 189
5.2.2 Glucose-Depleted Treatment . . . 189
5.2.3 Oleic Acid ± WY-14643 Treatment . . . 191
5.2.4 Protocol for the Generation of EHT . . . 191
5.3 Results . . . 191
5.3.1 Generating Engineered Heart Tissue . . . 192
5.3.2 Glucose-Depleted and Lactate-Enriched Culture Conditions to Purify CM Population. . . . 194
5.3.3 Transient Glucose-Depleted Treatments to Purify CM Population. 196
5.3.4 Gene Expression of EHTs Generated From iPSC-CMs Compared to Monolayer and Scaffolds . . . 196
5.3.5 Deciding Optimal Time Point in iPSC-CM's Differentiation Protocol to Generate EHTs. . . . 199
5.3.6 FAO of EHTs Generated From iPSC-CMs Treated with Oleic Acid ± WY-14643 for 1 Week. . . . 202
5.3.7 Glycolytic Flux of EHTs Generated From iPSC-CMs Treated with Oleic Acid ± WY-14643 for 1 Week. . . . 202
5.3.8 Gene Expression of EHTs Generated From iPSC-CMs Treated with Oleic Acid ± WY-14643 for 1 Week. . . . 205
5.4 Discussion . . . 206
5.4.1 Basic Characteristics of iPSC-CM-Derived EHTs . . . 206
5.4.1.1 Gene Expression of 3D EHT vs 2D Format . . . 206
5.4.2 Cell Population and Density Effects on EHT Culture . . . 209

5.4.3 Enhancing iPSC-CMs Differentiation Through the Use of Glucose-Depleted and Lactate-Enriched Treatments 210
5.4.4 Effects of OA ± WY-14643 Treatment on iPSC-CMs Cultured in 3D Scaffolds vs EHTs 211
5.4.4.1 Effects of OA ± WY-14643 Treatment on Gene Expression of iPSC-CMs Cultured in 3D Scaffolds vs EHTs 212
5.5 Conclusion 213

6 General Discussion **214**
6.1 The Quest to Mature iPSC-CMs 214
6.2 Thesis Findings 216
6.2.1 Thesis Obstacles 219
6.2.1.1 Purity Issues / Batch to Batch Variability 219
6.2.1.2 Bulk Analysis Methods vs Single Cell 220
6.2.1.3 Contamination 220
6.2.1.4 Standard Operating Procedures 221
6.2.1.5 Challenges of Working with 3D Constructs 222
6.3 The Future 223
6.3.1 Experiments to Complete This Story 223
6.3.2 Future Directions 223

A Additional Methods and Materials **225**
A.1 Extra Methodology 225
A.1.1 Tissue Fixation, Embedding and Sectioning 225
A.1.2 Immunohistochemistry 226
A.1.2.1 Measurement of Media Glucose and Lactate Concentration 226
A.1.3 Step By Step Protocol for Generation of Human Engineered Heart Tissue (EHT) 226
A.1.4 Trouble Shooting of Flow Cytometry 230
A.2 Additional Tables 230
A.3 PPARα Target Genes 238

B Research Outcomes **244**
B.1 Publications 244

Bibliography **287**

List of Figures

1.1 Myocardial Infarction Diagram 14
1.2 Adult vs Foetal Metabolic Pathways. 22
1.3 Glycolysis Diagram 24
1.4 β-Oxidation Diagram 26
1.5 TCA Cycle Diagram 27
1.6 Oxidative Phosphorylation Diagram 28
1.7 Cellular Respiration Diagram 28
1.8 Graphic of the Metabolic Switch During Cardiac Development, Differentiation, and During Heart Failure. 30

2.1 iPSC-CM Differentiation Protocol Timeline. 57
2.2 Collagenase Solution: Single-Cell Dissociation 59
2.3 Photo of Disc-Shape Scaffold 60
2.4 Loading iPSC-CMs Onto Scaffolds 61
2.5 EHT Teflon Spacers and Agarose Moulds 62
2.6 EHT Silicone Posts 62
2.7 Radiolabeled Metabolic Pathways 71
2.8 3H Palmitate Oxidation Chart 72
2.9 Glucose Oxidation Diagram 75
2.10 Glass Pipets Filled with Dowex 77
2.11 Side View of Dowex Racks 78
2.12 The Apparatus Constructed for Trapping $^{14}CO_2$ 81
2.13 $^{14}CO_2$ Contraption in a Metal Plate-sandwich 82
2.14 Measurement of the OCR at Baseline and Maximal Respiration . . . 83

3.1 Canonical Wnt/β-Catenin Biphasic Effects 89
3.2 Canonical Wnt/β-Catenin Pathway 90
3.3 Levels of Organization Within a Cardiac Muscle 91
3.4 Myosin Heavy Chain II 92
3.5 Regulation of Calcium Homeostasis Inside the Myoplasm. 94
3.6 Muscle Contraction Steps 95
3.7 Glucose and Pyruvate Oxidation Pathway 97
3.8 iPSC-CMs Morphology Changes During Differentiation. 100
3.9 Differentiation Efficiency of iPSCs into Beating-CMs. 101
3.10 Flow and Cardiac Expression of Sarcomeric Actinin and Troponin-T. 103
3.11 Aspecific Antibody: Staining for cTNT on a Whole Mount House Heart 104

3.12 Reference Gene Expression . . . 105
3.13 Contractile Gene Expression of iPSC-CMs Over 3 Months Culture-Induced Maturation . . . 106
3.14 iPSCs and iPSC-CMs Metabolic Gene Expression. . . . 108
3.15 Beating Efficiency of iPSC-CMs Cells on ECM Substrates . . . 109
3.16 CM Gene Expression of iPSC-CMs Cultured on Different of ECM Substrates. . . . 110
3.17 Metabolic Gene Expression of iPSC-CMs Cultured on Different of ECM Substrates. . . . 111
3.18 Reduction Reaction of Resazurin to Resorufin . . . 112
3.19 ABA Validation Experiments. . . . 114
3.20 Seeding Efficiency of iPSC-CMs on 3D Scaffolds . . . 115
3.21 Cell Proliferation Over Two Weeks. . . . 117
3.22 ABA: Long Term Culture of Non-Beating vs Beating iPSC-CMs . . . 117
3.23 Method 3: ABA Serial Dilutions with Regression Lines. . . . 121
3.24 ABA Reductions of Scaffolds Versus Monolayer . . . 123
3.25 Coll/C4S 1:1 Scaffold Had the Highest ABA Reduction. . . . 124
3.26 Seeding Efficiency of 100% Coll Cersus RF-Matrigel-Coated 100% Coll 125
3.27 ABA Reduction of 100% Coll Versus RF Coated 100% Coll. . . . 126
3.28 Gene Expression of iPSC-CMs on Collagen Scaffolds vs Monolayers (RF and Gel/FN) . . . 127
3.29 CM Gene Expression of iPSC-CMs on Collagen-Derived Scaffolds and Monolayers . . . 128
3.30 CM Gene Expression of iPSC-CMs on Collagen-Derived Scaffolds and Monolayers . . . 129
3.31 FAO of Monolayers vs Scaffolds. . . . 131
3.32 Glycolysis of Monolayers vs Scaffolds. . . . 132

4.1 PPARα Structure . . . 144
4.2 PPARα:RXRα Heterodimer . . . 146
4.3 WY-14643 Molecular Structure . . . 148
4.4 PPARα Target Genes . . . 149
4.5 Methods Protocol of iPSC-CM Treatment of OA $\pm$ WY-14643 . . . 151
4.6 Reference Genes . . . 153
4.7 Relative Gene Expression of iPSC-CM Treated with OA $\pm$ WY-14643 154
4.8 Relative Gene Expression of FAO Genes . . . 156
4.9 FAO of Monolayers iPSC-CMs Treated with OA $\pm$ WY-14642 for 24 Hours and 1-Week . . . 158
4.10 The Glycolytic Flux of Monolayers iPSC-CMs Treated with OA $\pm$ WY-14642 for 24 Hours and 1-Week . . . 159
4.11 Glucose Oxidation of Monolayers iPSC-CMs Treated with OA $\pm$ WY-14642 for 1-Week . . . 160
4.12 Dr. Al-Siddiqi's Oxygen Consumption Data. . . . 161
4.13 OCR Using the Clark-Type Oxygen Electrode in Gimish. . . . 163

4.14 OCR and RRC Using the Clark-type Oxygen Electrode in Culture Media with OA Respiring Substrates. 164
4.15 OCR and RRC Using the Clark-type Oxygen Electrode in Culture Media with Pyruvate and Malate Respiring Substrates. 165
4.16 Ponceau Staining Example from Westerns 166
4.17 Immunocytochemistry Microscopy. iPSC-CMs Treated with OA ± WY-14643 Staining for *GLUT4* and Sarcomeric Actinin. 167
4.18 iPSC-CMs Treated with OA ± WY-14643 Staining for Mitochondria Numbers 168
4.19 Staining for Oil Red O of iPSC-CMs Treated with OA ± WY-14643. 169
4.20 FAO of iPSC-CMs Cultured on Scaffolds Treated with OA ± WY-14642 for 1 Week 170
4.21 The Glycolytic Flux of iPSC-CMs Cultured on Scaffolds and Treated with OA ± WY-14642 for 1 Week 171
4.22 Glucose Oxidation of iPSC-CMs Cultured on Scaffolds and Treated with OA ± WY-14642 for 1-Week 172
4.23 Scaffold Oxbox 173
4.24 3D Printed Ring for Oxbox 173
4.25 3D Printed Ring Wedged into Oxbox 174
4.26 Oxygen Consumption Rate: Baseline for 5 Minutes 174
4.27 OCR Using the Clark-type Oxygen Electrode in Culture Media with OA Respiring Substrates for Scaffolds. 175

5.1 Generation of EHT Schematic. 183
5.2 Timeline of EHT Progression 184
5.3 Glucose-depleted, Lactate-enriched iPSC-CMs Treatment 190
5.4 Glucose-depleted iPSC-CMs Treatment 190
5.5 EHT Image With and Without Cells 192
5.6 ABA of EHT with iPSC-CMs 193
5.7 EHT Thinned After Three Days 194
5.8 Microscope of EHT with Cells 195
5.9 Image of a Beating EHT 195
5.10 Glucose-depleted and Lactate-enriched Treated Cells 197
5.11 Glucose-depleted Media Treatment. 198
5.12 Cardiac and Metabolic Gene Expression in 3D Culture vs 2D Monolayer. 200
5.13 FAO of EHTs Generated on DD7 vs DD15. 201
5.14 ^{3}H Palmitate Oxidation of RF Monolayer, 100% Collagen Scaffold and EHTs Treated with OA ± WY-14643. 203
5.15 ^{3}H Oleic Acid Oxidation of RF-Matrigel Monolayer, 100% Collagen Scaffold and EHTs Treated with OA ± WY-14643. 203
5.16 Glycolytic Flux of RF-Matrigel Monolayer, 3D Collagen-derived Scaffolds, and EHTs Treated with OA ± WY-14643. 204
5.17 Preliminary Relative Gene Expression of Metabolic Genes Comparing 100% Collagen Scaffolds and EHTs. 207

A.1 Trouble Shooting Flow: Gating for Singlets 233
A.2 Trouble Shooting Flow: Gating for Zombie Violet. 233
A.3 Example of Primer Melt Curve 234

List of Tables

1.1 Factors and Media Used by Different Labs to Differentiate Pluripotent Stem Cells to CMs. 40

2.1 List of the Cardiac Differentiation Compounds 56
2.2 ECM Substrate-coated Plates for iPSC-CMs Culture 57
2.3 Composition of EHT Medias 63
2.4 Flow Cytometry Antibodies 64
2.5 qPCR Reaction 67
2.6 Taqman qPCR Reaction 67
2.7 Mitochondrial Respiration Recorded by a Clark-type Oxygen Electrode 84

3.1 List of Gene Transcripts Accessed in the qPCRs 104
3.2 iPSCs and iPSC-CMs glucose and lactate concentration in the culture medium. 108
3.3 Different Collagen-Derived Scaffold Composition and ECM Substrate Used for Culturing iPSC-CMs for Maturation. 113
3.4 Method 1 - Cell Count on Scaffolds 118
3.5 Method 2 - Cell Count on Scaffolds 119
3.6 Method 3: Calculating ABA Dilution Linear Regression Equations. . 120
3.7 Method 3: Predicting Cell Count Using ABA Dilution Linear Regression Equations. 122

4.1 Summary of Differences Between Immature Stem Cell-derived CM and Mature Adult CMs, adapted from [1]. 140
4.2 Summary Table of Effects of OA ± WY-14643 on Monolayer Cells. . 177

5.1 RNA Values for 3D Constructs Treated with OA ± WY-14643 205

A.1 Primers for Quantitative PCR for the Analysis of Gene Expression in Human iPSCs and iPSC-CMs. 230
A.2 TaqMan Assays Used for Quantitative qPCR 232
A.3 Antibodies Used for Immunohistochemistry and Immunocytochemistry. 235
A.4 Secondary Antibodies Used for Immunocytochemistry and Immunohistochemistry 235
A.6 Reagent's Purchase List. 235
A.7 PPARα Target Genes With A Funtional PPRE 238
A.8 List of PPARα Dependent Gene Regulation with No Funtional PPRE 240

A.5 Western Blot Antibodies 243

Abbreviations

AA	Ascorbic acid
ABA	AlamarBlue Assay
ACSL1	Long-chain-fatty-acidCoA ligase 1
ACTC1	Actin, alpha, cardiac muscle 1
Acyl-CoA	Acetyl coenzyme A
ADP	Adenosine triphosphate
ADSCs	Adipose tissue-derived stem cells
AFP	Alpha fetoprotein
Akt/PKB	Phosphatidylinositol 3-kinase/Protein Kinase B
ALS	Amyotrophic Lateral Sclerosis
AMI	Acute myocardial infarction
ANOVA	Analysis of variance
APC	Adenomatous polyposis coli
aP2	Adipocyte protein 2
ARBs	Angiotensin II receptor blockers
ASCs	Adipose-derived stem cells
ATP	Adenosine-5-triphosphate
BADSCs	Bovine adipose tissue-derived stem cells
bFGF	Basic fibroblast growth factor
BMSCs	Bone marrow stem cells
BM-MNCs	Intra-artrial bone marrow mononuclear cells
BM-MSCs	Bone marrow-derived mesenchymal stem cells
BME	β-mercaptoethanol
BMP	Bone morphogenetic proteins
BMP4	Bone morphogenetic protein four
BNIP3	BCL2 interacting protein 3
BHF	British Heart Foundation

BMSCs	Bone marrow-derived mesenchymal cells
bp	base pairs
bpm	beats per minute
BSA	Bovine serum albumin
BTS	N-benzyl-p-toluene sulfonamide
B2M	Beta-2 microglobulin
Ca^{2+}	Calcium ion
CAD	Coronary artery disease
CASQ2	Calsequestrin-2
CB-MNCs	Human cord blood mononuclear cells
CD31	Cluster of differentiation 31
CD36	Cluster of differentiation 36
CDCs	Cardiosphere-derived stem cells
cDNA	Complementary deoxyribonucleic acid
C/EBPα	CCAAT/enhancer-binding protein alpha
CHD	Coronary heart disease
CICR	Calcium-induced calcium release
c-kit	Stem cell factor receptor (C-Kit +) cells or CD117
CLC	Cardiomyocyte-like cells
CM	Cardiomyocyte
CO_2	Carbon dioxide
$^{14}CO_2$	Radiolabelled Carbon 14 dioxide
COL1A1	Collagen, type I, alpha 1
COL3A1	Collagen, type III, alpha 1
COLL	Collagen I
COLL/CS	Collagen I/Chondritin-4-Sulfate Scaffolds 1:1
COLL/ELA	Collagen I/Elastin Scaffolds 1:1
CMs	Cardiomyocytes
CNT	Carbon nanotubes

CPC	Cardiac progenitor cells
CPT-1	Carnitine palmitoyltransferase I
CPT-II	Carnitine palmitoyltransferase II
cpm	counts per minute
CRISPER	Clustered Regularly Interspaced Short Palindromic Repeats
CS	Citrate synthase
CSCs	Cardiac stem cells
cTNT	Cardiac specific troponin T
cTNT+	Cardiac specific troponin T positive cells
CVD	Cardiovascular disease
CX43	Connexin 43
C4S	Chondritin-4-sulfate
DD-1	Differentiation Day -1
DD0	Differentiation Day 0
DD1	Differentiation Day 1
DD3	Differentiation Day 3
DD5	Differentiation Day 5
DD7	Differentiation Day 7
DD12-15	Differentiation Day 12-15
DD15	Differentiation Day 15
DD20+	Differentiation Day 20+
DAPI	4,6-diamidino-2-phenylindole
df	degrees of freedom
ddH_2O	deionized water
DLAT	Dihydrolipoyl transacetylase
DLD	Dihydrolipoyl dehydrogenase
DMEM	Dulbeccos modified eagle medium
DMSO	Dimethyl Sulfoxide
DNA	Deoxyribonucleic acid

dNTP	Deoxynucleotide triphosphate
DPBS	Dulbeccos phosphate buffered saline
Drp 1	Dynamin-related protein 1
ds	double stranded
DTEF-1	Cardiac muscle transcriptional enhancer factor-1
E10.5	Mouse embryonic Day 10.5
EB	Embryoid body
ECAR	Extracellular acidification rate
ECI	Enoyl CoA isomerase
ECs	Endothelial cells
ECM	Extracellular matrix
EDPVR	End-diastolic pressure volume relationship.
EDTA	Ethylenediaminetetraacetic acid
EHTs	Engineered heart tissues
EPCs	Epithelial cells
ERα	Estrogen-related receptor-alpha
ERγ	Estrogen-related receptor-gamma
Erk	Ras-Raf-MEK-ERK pathway
ESCs	Embryonic stem cells
ESC-CMs	Embryonic stem cell derived cardiomyocytes
ESRRA	Estrogen-related receptor a
ETC	Electron transport chain
FAs	Fatty acids
FAC	Fractional area change
FACs	Fluorescence-activated cell sorting
$FADH^2$	Flavin adenine dinucleotide
FAO	Fatty acid oxidation
FBS	Fetal bovine serum
FCCP	Carbonylcyanide-p-trifluoromethoxy-phenylhydrazone

FGF	Fibroblast growth factor
FGF2	Fibroblast growth factor 2
Flk-1	Foetal liver kinase-1
FN	Fibronectin
GAGs	Glycosaminoglycans
Gel/FN	Gelatin/fibronectin
GFs	Growth factors
GLUT1	Glucose transporter-1
GLUT4	Glucose transporter-4
GOI	Gene of interest
GSK3β	Glycogen synthase kinase 3 beta
GTP	Guanosine-5'-triphosphate, guanylyl imidodiphosphate
HA	Hyaluronic acid
HADHA	Hydroxyacyl-CoA dehydrogenase trifunctional multienzyme complex subunit alpha
HBSS	Hank's Balanced Salt Solution
HCl	Hydrogen chloride
HEPES	4-(2-hydroxyethyl)-1-piperazineethanesulfonic acid
HF	Heart failure
HIF	Hypoxia-inducible factor
HK	Hexokinase
HKG	Housekeeping gene
HPRT1	Hypoxanthine-guanine phosphoribosyltransferase
hr	hour
hrs	hours
HSCs	Hematopoietic stem/progenitor cells
H2AX	H2A histone family, member X
H_2O	Water
^3H	Tritium
^3H_2O	tritium water

I/R	Ischaemia/reperfusion
IGF-1	Insulin-like growth factor-1
IL-10	Interleukin-10
IL-6	Interleukin-6
iPS	Induced Pluripotent Stem
iPSCs	Induced Pluripotent Stem Cells
iPSC-CMs	Induced pluripotent stem cell derived cardiomyocytes
IRS1	Insulin receptor substrate-1
IRS2	Insulin receptor substrate-2
IWP4	Inhibitor of WNT Production-4
KCL	Potassium chloride
KDR	Kinase insert domain protein
kg	kilogram
KLF4	Kruppel-like factor 4
KO-	Knock out-
KOH	Potassium hydroxide
LCAD	Low expression of long-chain acyl-CoA dehydrogenase
LDH	Lactate dehydrogenase
LV	Left ventricle
LVFS	Left ventricular fractional shortening.
LVEF	Left ventricular ejection fraction.
LVEDP	Left ventricular end-diastolic pressure.
LVEDV	Left ventricular end-diastolic volume.
LVEDD	Left ventricular end-diastolic diameter.
LVESD	Left ventricular end-systolic diameter.
LVESV	Left ventricular end-systolic volume.
LVEDV	Left ventricular end-diastolic volume.
MAPK	Mitogen-activated protein kinase
MAP2	Microtubule associated protein 2

MBq	Megabecquerel
MCAD	Medium-chain acyl-CoA dehydrogenase
MEF2C	Myocyte Enhancer Factor 2C
mg	milligram
MHC	Myosin heavy chain
mLs	milliters
mm	milimeter
mM	milimolar
mN	meganewton
MSCs	Mesenchymal stem cells
MI	Myocardial infarction
mins	minutes
miRNA	micro ribonucleic acid
MSCs	Mesenchymal stem cells
mTDNA	Mitochondria DNA
MT-ND1	Mitochondrially Encoded NADH:Ubiquinone Oxidoreductase Core Subunit 1
MT-ND2	Mitochondrially Encoded NADH:Ubiquinone Oxidoreductase Core Subunit 2
MYH7	Myosin heavy chain 7
MYL3	Myosin light chain 3
MYL4	Myosin light chain 4
MYOD	Myogenic differentiation 1
NaCl	Sodium chloride
NAD+	Nicotinamide adenine dinucleotide
NADH	Reduced nicotinamide adenine dinucleotide
NANOG	Nanog homeobox
NaOH	Sodium hydroxide
NCX	Sodium calcium exchanger
NEAA	Non-essential amino acids
NFAT	Nuclear factor of activated T-cells

NFATC3	Nuclear factor of activated T-cells, cytoplasmic 3
NFATC4	Nuclear factor of activated T-cells, cytoplasmic 4
NKX2.5	NK2 homeobox 5
nm	nanometers
ng	nanograms
NOX-ROS	NADPH oxidase derived reactive oxygen species
NOX4	NADPH oxidase 4 protein
NRCM	Neonatal rat cardiomyocytes
NRF-1	Nuclear respiratory factor-1
NRF-2	Nuclear respiratory factor-2
NSTEMI	Non-ST-segment elevation myocardial infarction
OA	Oleic acid
OCR	Oxygen consumption rate
OCT4	Octamer-binding transcription factor 4
OXPHOS	Oxidative phosphorylation
PBMCs	Peripheral blood mononuclear cells
PBS	Phosphate buffered saline
PCL	Polycaprolactone
PCR	Polymerase chain reaction
PDC	Pyruvate dehydrogenase complex
PDH	Pyruvate dehydrogenase
PDHA1	Pyruvate dehydrogenase (lipoamide) alpha 1
PDK	Pyruvate dehydrogenase kinase
PDK4	Pyruvate dehydrogenase kinase, isozyme 4
PDP	Pyruvate dehydrogenase phosphatase
PEG	Poly ethylene-glycol
PFA	Paraformaldehyde
PFK	Phosphofructokinase
PGA	Polyglycolic acid

PGC1A	Peroxisome proliferator-activated receptor gamma coactivator
PGI_2	Prostaglandin I2
PGS	Poly(glycerol sebacate)
pH	Potential Hydrogen
PIPAAm	Poly(N-iso- propylacrylamide)
PKC	Protein kinase C, zeta
PLA	Polylactic acid
1. PLB	Phospholamban
PLGA	Poly(lactic-co-glycolic acid)
PLLA	Poly(L-lactic acid)
POLR2A	DNA-directed RNA polymerase II subunit RPB1
POU5F1	POU class 5 homeobox 1
PPARα	Peroxisome proliferator-activated receptor-alpha
PPARδ	Peroxisome proliferator-activated receptor-delta
PPARγ	Peroxisome proliferator-activated receptor-gamma
PPARGC1A	Peroxisome proliferator-activated receptor gamma coactivator
PPP	Pentose phosphate pathway
PSC-CMs	Pluripotent stem cells derived CMs
P/S	Penicillin/streptomycin
PTFE	Polytetrafluoroethylene
PTM	Placental tissue matrix
p38 MAPK	p38 mitogen-activated protein kinase
p70 S6K	p70S6 kinase
qPCR	Quantitative polymerase chain reaction
RAR	Retinoic acid receptor
RAREs	Retinoic acid response elements
RF	Reduced factor
RF-M	Reduced factor Matrigel
RI	Rock inhibitor

RNA	Ribonucleic acid
rpm	Rate per minute
RPMI	Roswell Park Memorial Institute
ROS	Reactive oxygen species
RT	Room temperature
RUNX1	Runt-related transcription factor 1
RV	Right ventricle
RXR	Retinoid X receptor
RYR2	Ryanodine receptor 2
Sca-1	Stem cell antigen (sca-1+) cells
SCIPIO	Stem Cell Infusion clinical trial for patients with Ischemic cardiomyopathy
SCT	Stem cell therapy
SERCα	Sarco/endoplasmic reticulum Ca^{2+}-ATPase
shRNA	Short hairpin RNA
SLC2A4	Solute carrier family 2 member 4
SMCs	Smooth muscle cells
SOX2	SRY (sex determining region Y)-box 2
SR	Sirius Red
ss	single stranded
StdDev	Standard deviation
SEM	Standard error of the mean
TBP	TATA-Box Binding Protein
TCA	tricarboxylic acid cycle
TDP43	TAR DNA-binding protein 43
TEM	Transmission electron micrograph
TGF	Transforming growth factor
TGFB	Transforming growth factor-beta
TIPS	Thermally induced phase seperation
TNNT2	Tropinin T 2

U	units
UBC	Ubiquitin C
UCP3	Mitochondrial uncoupling protein 3
UK	United Kingdom
μM	micromolar
USA	United States of America.
USF1	Upstream stimulatory factor 1
VAD	Ventricular assist device
VEGF	Vascular endothelial growth factor
v/v	Volume by volume
wt/v	Weight by volume
2D	Two-dimensional
3D	Three-dimensional

It's a dangerous business, Frodo, going out your door. You step onto the road, and if you don't keep your feet, there's no knowing where you might be swept off to ...

— J.R.R. Tolkien, The Lord of the Rings

1 Introduction

1.1 Cardiovascular Disease

Cardiovascular diseases (CVDs) are the leading cause of death worldwide, with myocardial infarction being the most prevalent. While infectious diseases are being successfully prevented, cardiac risk factors such as hypertension, obesity and diabetes continue to rise. The world health organization has reported that 17.7 million people die annually from CVDs, accounting for around 31% of deaths globally. In the USA, one in every nine deaths can be attributed to heart failure each year [2]. This breaks down to someone having a heart attack every 40 seconds [3]. In addition, heart disease costs the USA alone some $300 billion a year in the form of health care services, medication and lost productivity [4]. These costs are only expected to grow each year. As a result, it is paramount that the scientific and medical communities develop improved treatments and solutions to address the burden of all cardiovascular diseases.

1.1.1 Myocardial Infarction

Myocardial infarction (MI), commonly known as a heart attack, accounts for 80% of CVD deaths with no reliable therapy [2,5]. MI occurs when there is a blockage in a coronary

artery in the heart (usually due to atherosclerotic plaque build-up) which decreases or completely stops the blood flow to the ventricular muscle, triggering an ischemic cascade of events. Without constant perfusion, the cardiomyocytes (CMs) in the region of the blockage will die through necrosis and do not have the ability to regenerate the lost myocardium [6] (Fig. 1.1). As a protective measure, the heart produces a collagenous scar which forms over the infarcted region. This tissue, however, doesn't have the capability to properly reintegrate with the electrophysiological properties of the heart. Remaining cells lack the oxygen needed to produce ATP in mitochondria, which, in turn, is required to maintain electrolyte balance such as the NA^+/K^+-ATPase and to power contraction. As a result, the scar region will have impaired contractile ability [7]. The lack of sufficient cardiac muscle mass and contraction will ultimately lead to remodeling of myocardial structure and function such as an increase in left ventricular (LV) volume, increased wall stress and thinning, CM hypertrophy/polyploidisation, induction of extracellular matrix (ECM) protein synthesis [7,8], metabolic remodeling [9], which will ultimately lead to deterioration and increased cardiac dysfunction [10,11].

Current therapies attempt to prevent or minimize CM death, but to-date we have limited options and they are time-critical. The main strategies have concentrated on achieving reperfusion, thrombolysis and reducing the amount of workload on the heart. This is usually done through pharmacological approaches such as fibrinolytic agents which dissolve blood clots, β-adrenoceptor blockers that reduce blood pressure or nitro dilator drugs/ angiotensin-converting enzyme (ACE) inhibitors which promote vasodilation, anti-thrombotic, and anti-inflammatory responses. If further intervention is needed, surgical procedures such as coronary bypass, balloon angioplasty, stents, or ventricular assist device (VAD) can be implanted [13–15]. Recent advances have improved time to reperfusion, but progress to efficiently prevent, treat or reverse the lost myocardial tissue has yet to result in significant clinical benefit [16,17]. The only current long-term solution for end-stage heart failure is heart transplantation, but with limited donors, and the need for chronic immunosuppressants [18], the search for finding an alternative solution has becoming increasingly urgent. One pioneering approach that can potentially overcome the limitation

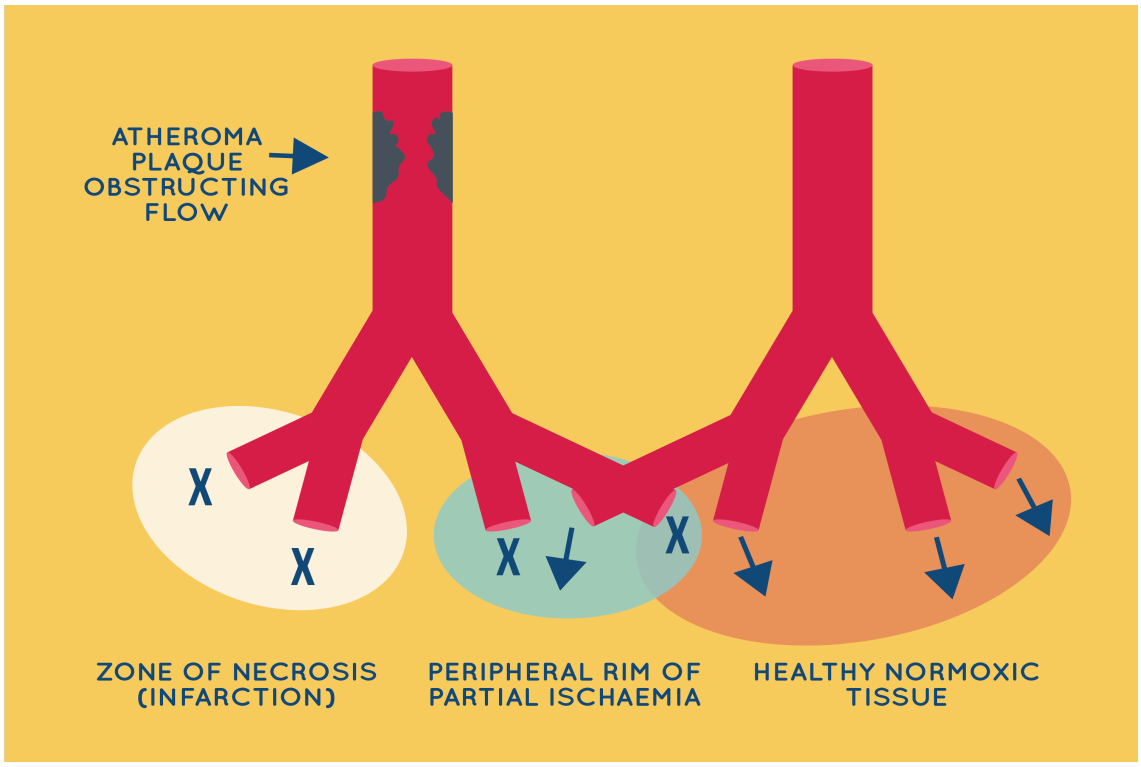

Figure 1.1: Myocardial infarction diagram, adapted from Levick *et al.* [12]. Image depicts the ends of a coronary arteries in which an atheroma plaque obstructing flow leads to a loss of blood flood and downstream necrosis.

of donor organ availability is stem cell-based replacement therapy. Here, the main goal is to improve function of the impaired tissue by integrating new CMs into the native organ architecture.

1.2 Stem Cell Therapies

MI can lead to a loss of around 1 billion CMs, which do not have the capability to be replaced due to the insufficient ability of the adult heart's proficiency to regenerate [19]. Although, contradicting what was once thought, the heart is no longer considered to be a post-mitotic organ (terminally differentiated), this dogma has been challenged in recent years by findings in both non-mammalian (newts [20–23] and zebrafish [24–27]) and mammalian systems [28–31]. Evidence has accumulated showing that adult CMs can be stimulated to re-enter the cell cycle and proliferate. It has been shown that an adult heart has the ability to turnover 1% of CMs annually [32], but this amount doesn't come close to counteracting the large numbers of CMs lost during a MI. Stem cell therapy (SCT) potentially holds the key to regenerating the impaired myocardium, restoring contractility, and avoiding any adverse remodeling post-MI [33,34].

There are different avenues which can be taken with stem cell therapies. The first is to induce existing CMs in the heart to re-enter into the cell cycle to replace lost myocardium [19,34,35]. Another approach is to use cells from other organs, such as skeletal myoblasts or bone marrow derived cells, which might substitute for lost CMs or induce positive effects on remodeling the myocardium. To date, there have a been a number of preclinical SCTs (in mice [36], rats [37–39], hamsters [40], dogs [41,42], pigs [43,44], sheep [45,46], and primates [47]) which showed promise. Clinical SCTs in patients with acute MIs or end-stage HF, gave mixed results [34,48–50] and meta-analyses have shown little or no significant improvement [51–53]. These approaches range from using a variety of therapeutic agents including a selection of different stem cells (skeletal myoblasts, bone marrow mononuclear cells, mesenchymal stem cells, CD34+ and CD133+ cells, adipose-derived cells, cardiac-derived cells, ESCs, and iPSCs) [54] with the addition of growth factors, hormones,

inflammatory mediators, to siRNA [54–58]. Specifically, strategies involving a combination of both cells and protein (such as GFs, 3D ECM components) therapy have been the most encouraging through enhancing endogenous angiogenic processes and thereby improving cardiac function and recovery [59–61]. It is important to note that the latest research strongly suggests that controlling the inflammatory response of the heart tissue after a MI may be the critical step to modulate in order to achieve full organ regeneration [62–64]. Nevertheless, although this strategy may be the most promising one, it is still a relatively new field of research, and further investigations are needed before obtaining conclusive results [65]. In recent years, identification of a number of cardiac resident progenitor cell population has given hope for alternative routes to regenerate damaged myocardium [34, 50, 66, 67].

1.2.1 Types of Stem Cells for Therapy

Several different types of stem cells have been used for testing in animal models and clinical studies to improve cardiac function [54, 68, 69]. Some of these include but are not limited to mesenchymal stem cells (such as bone-marrow derived cells) [38, 70, 71], cardiac progenitor cells [72–75], embryonic stem cell derived CMs (ESC-CM) [76–79] and human induced pluripotent stem cell derived CMs (iPSC-CMs) [80, 81].

1.2.1.1 Bone Marrow-derived Stem Cells and Other Mesenchymal Stem Cells

Bone marrow-derived stem cells (BMCs) can be selected from the bone marrow fraction using specific markers, such as the stem cell factor receptor C-kit, or can be expanded as mesenchymal stem cells by adherence to plastic. They have been shown to differentiate into non-hematopoietic cell types including brain [82–85], skeletal muscle [86, 87], liver and epithelium [88–90], endothelium [91–93] and heart [38, 94, 95]. BMCs were claimed to differentiate into beating CMs after two weeks in culture [70] through a variety of regulatory factors including 5-aza, miRNAs, cytokines, HDAC1, VR-1, Caveolin-1, and the microenvironment [96]. Although demonstrated by many elegant studies, this concept has also been met with enormous skepticism and resistance, with others suggesting that

BMCs do not possess differentiation plasticity of a true stem cell nor manage to produce beating derived CMs [97–101]. BMCs were first reported in 2002 to have the potential to regenerate significant amounts of lost myocardium in mice following MI [102,103]. These results created an overall eagerness in the field [104]. These cells were further explored and others have found that they may not only contribute to active myocardial repair as suggested by several groups [91,92,94,105–107], but also participate in the reconstitution of the cardiac progenitor cell pool [104,108]. In early studies it was reported that when bone marrow-derived C-kit positive/ linage negative (C-kit+/lin-) cells were used to treat infarcted tissue, they generated new cardiac cells and blood vessels and re-muscularised the damaged region [109,110]. Although BMCs have been shown to improve cardiac function following MI, it has been debated whether or not the repair was a result of the added cells or a delivery of a beneficial cocktail of cytokines which induced angiogenesis, limited scar fibrosis and activated endogenous cardiac progenitors [110–112]. In later studies, it was shown that bone marrow stem cells do not trans-differentiate into CMs but instead retained transplanted cells adopted a mature hematopoietic fate [98,99]. Other key types of mesenchymal stem cells such as **umbilical cord MSCs** [113,114], **adipose-derived MSCs** [115–117] and **amniotic fluid MSCs** [118], chosen for their ease of isolation and differentiation, have also been tested for therapeutic potential after MI.

1.2.1.2 Adult Cardiac Stem Cells

A series of cardiac progenitor cells (CPC) have been identified for potential use in SCT, that can be referred to by their surface markers. Beltrami *et al.* [119], first showed C-kit+ cardiac progenitor cells were self-renewing, clonogenic, multipotent, and able to differentiate into myocytes, smooth muscle, and endothelial cells. When these progenitor cells were injected into a rat MI model they were able to induce cardiac regeneration and improved heart function. A series of studies followed and supported this beneficial effect but debated the origin of the cells. Some suggested that the C-kit+ cells were of BM origin [109] while other considered them mast cells [120,121] or endothelial cells [121]. Ellison *et al.* [122] showed in 2013, that C-kit+ cells were required for significant cardiac recovery in rodent models,

but then, additional studies challenged these findings and showed opposing results [123–125]. In 2011, C-kit+ cells used in a phase-I Stem Cell Infusion clinical trial for patients with Ischemic cardiomyopathy (SCIPIO) showed promising results for post-MI treatment [126]. However, three years later, these results were questioned for their integrity [127].

Around the same time that C-kit+ cells were being identified, another cardiac progenitor cell was identified in the mouse heart by selection using stem cell antigen 1 (Sca-1+). Like C-kit+ cells they exhibited self-renewal characteristics, the ability to differentiate into myocytes both in vitro and in vivo [72] and showed beneficial effects on the injured myocardium [72, 128, 129]. A deletion of Sca-1 has been reported to cause cardiac defects in contractility, repair, and endogenous CPC proliferation [130].

Messina *et al.* [73] isolated a third population of progenitor cells from adult human and murine heart explants in 2004, referred to as **cardiosphere derived cells (CDCs)**. These cells were self-renewing and expressed known stem cell markers (*CD31*, *CD34*, C-kit, and Sca-1) [73]. In studies conducted by our group, CDCs were isolated from patients [131] or rodent models [132, 133] and were shown to improve cardiac function after being administered to a rat MI model [74]. This finding was also supported by others in studies in both rat [116] and pig [117] hearts. However, CDCs are a mixed population containing fibroblasts and hematopoietic cells as well. This raised concerns as to whether they would be the optimal cell type for regenerative applications [134]. There is also some controversy in the variability of reporting cell surface markers, suggesting that this culture method may be unreliable [131].

Adult cardiac progenitor stem cells have been heavily tested in animal models [74, 135, 136] and a clinical trial [53, 137]. The limited success is currently believed to be largely due to the paracrine effects of the injected cells.

1.2.1.3 Embryonic Stem Cells

In 1998, Thomson *et al.* [138], first derived human embryonic stem cells (ESCs) from the cleavage stage (the inner cell mass of blastocysts) of human embryos, produced by in vitro fertilization and donated for clinical research purposes. ESCs quickly became a potential cell type of interest for SCT because they had the capability to self-renew and differentiate into

any derivative cell type from the three germ layers: ectoderm, endoderm, and mesoderm. ESCs were the first pluripotent cell line to be expanded and differentiated into beating CMs and established as a potential pharmacological model [139]. Since then, others have shown transplantation of ESC-CMs after a MI in small animals results in the formation of stable CM grafts, attenuation of the remodeling process, and functional benefit [77,78,140–142]. Chong *et al.* [79] showed implantation of ESCs resulted in significant remuscularization after MI and reperfusion as well as complete electrical coupling in a pigtail macaque heart. However, the use of ESCs came with a lot of controversy on the ethics of using this cell type, as it came at the cost of destroying the embryos from which they were obtained. In addition to this morality concern, another obstacle involved in transplantation of ESC as a SCT is the risk of teratoma formation [143].

1.2.1.4 Induced Pluripotent Stem Cells (iPSCs)

Induced pluripotent stem cells (iPSCs) are derived from adult cells such as skin or blood cells that have been reprogrammed back into an embryonic like state [144]. They create an endless source of cells that can be differentiated into any cell in the body. This holds great potential for being a dynamic tool in the biomedical field for studying human diseases. iPSCs resemble ESCs in many aspects, such as transcription profiles, self-renewal while maintaining pluripotency, differentiability, metabolome profile, DNA methylation patterns, chimera formation, embryoid body formation, and teratoma formation [145–147]. In 2006, Shinya Yamanaka pioneered this technology, generating iPSCs by introducing four transcription factors: *OCT4*, *SOX2*, *CMYC*, and *KLF4* which had the capability to dedifferentiate adult cells back into a pluripotent stem cell state [148,149]. In 2012, he won the Nobel Prize with Sir John Gurdon.

Human iPSCs can be an appealing tool because they are patient-specific, overcoming the obstacle of immune rejection as well as the ethical concerns in using ESCs [143,150–154]. There are endless applications for iPSCs, from cell therapy, disease modelling, personalized medicine, to drug discovery and development, and toxicity analysis [155–164]. Furthermore, recent advances in gene editing technology (particularly CRISPER-Cas9 technology) opened

the door to genetically define human iPSC-based disease models [157]. iPSCs may also serve as an "off-the-shelf" cell type for regenerative therapy to treat heart disease as the establishment of banks of human leukocyte antigen haplotyped iPSCs may circumvent the time needed to generate and validate new cells for transplantation [157, 165] and save money. It costs around $800,000 to generate an iPSC-derived tissue product suitable for clinical use, the creation of banked iPSCs for allogeneic transplants can reduce that cost drastically since one production could be used for multiple patients [157].

iPSCs in Disease Modelling

Having the ability to generate large quantities of previously inaccessible cells such as neurons and CMs is the key to developing therapeutic strategies. These cells provide an invaluable tool for the identification of the underlying mechanism of diseases. iPSCs have been shown to model several diseases such as Alzheimer's [166–179], Schizophrenia [180–182], Parkinson's disease [183–201], amyotrophic lateral sclerosis (ALS) [202–205], spinal muscular atrophy [206] and more. iPSCs also provide a new way to successfully study sporadic diseases by created isogenic lines [166, 168, 176, 181, 191, 207, 207–211], which can help to identify the true pathology.

iPSCs in Drug Discovery and Screening

Patient derived iPSC models make it possible to recapitulate disease phenotypes and pathologies in a culture dish. The ability to mass produce genetically specific disease phenotypes allows for large scale drug screening. Burkhardt *et al.* [210] performed disease modelling and screening using iPSC derived from patients with sporadic ALS. The group identified an aggregation of TAR DNA-binding protein 43 (TDP43) in neurons which was then used for a high content drug screen (1,757 compounds screened) to identify compounds that reduced TDP43 aggregation. The same group also studied Alzheimer's disease and generated a therapeutic antibody against extracellular Tau [212] by screening 350 compounds. Overall, iPSC-based drug screening has been used to evaluate more than 1,000 compounds for several diseases [210, 213–215] and generated several clinical candidates [212, 216, 217].

iPSCs and iPSC-CMs in Cell Therapy

The first clinical study to evaluate iPSCs was done in 2014. iPSC-derived retinal pigment epithelial cells were used to treat macular degeneration [218] and were shown to improve patient's vision. To date, several diseases, such as sickle cell anaemia, [219] Parkinson's disease [220] and haemophilia A [221], have had successful treatment using iPSC-based therapy [222]. The cardiac field is not far behind and is currently investigating iPSCs derived from multiple species including: mice [223], rats [224], primates [225], and human [226]. All of these sources have been shown to differentiate in vitro into CMs and other cardiovascular cells such as smooth muscle cells and endothelial cells [227]. Nelson *et al.* [228] showed that intramyocardial delivery of iPSCs into a mouse MI model showed successful engraftment without disrupting the cytoarchitecture. The group also reported restored contractility, electrical stability, and an increase in ventricular wall thickness. In addition, it was also reported that the treatment regenerated cardiac, smooth muscle and endothelial tissue. Our lab has also previous demonstrated in Carpenter *et al.* [80] that efficient cardiac differentiation of iPSCs gave rise to progenitors that were retained within the infarcted rat heart, and reduced remodeling of the heart after ischemic damage. In another study, Mauritz *et al.* [223] showed that injection of iPSC-derived foetal liver kinase-1 (Flk-1) positive progenitor cells into a mouse MI model displayed improved cardiac function and showed that the Flk-1+ cells differentiated into cardiovascular lineages in vivo.

iPSC have also been used in combination with 3D technology to assist in the transition from benchtop to in vivo. In 2014, Ye *et al.* [229] administered insulin growth factors (IGF-1) microsphere-loaded fibrin patches with human iPSC-CMs to a porcine MI model. They showed retention of the transplanted cells, reduced ventricular wall stress and overall improved survival. Chow *et al.* [230] have also shown that human iPSC-CMs encapsulated in hydrogels improved heart function in a rat MI model.

Challenges with iPSC and iPSC-CMs

Although, the method of reprogramming iPSCs has been demonstrated for years, there are still challenges associated with this technology such as: low efficiency, genomic insertion,

tumorigenicity, limited donor cell retention and incomplete reprogramming [80,81,157,227]. Most importantly, in reference to this thesis, iPSC-CMs are immature and reflect more of a foetal phenotype than that of an adult CM [231,232]. Morphologically, they are small, circular or triangular and mono-nucleated, while adult CMs are large, rectangular, and multi-nucleated. iPSC-CMs do not have t-tubules [233], resulting in calcium primarily entering the cell through the sarcolemma, causing a slower excitation-contraction coupling then if the calcium was released from the sarcoplasmic reticulum. Metabolically, iPSC-CMs have fewer mitochondria [1,158,234–236] which affects energy output. In contrast to the adult heart, which generates most of its energy via fat oxidation, stem cells generate most of their energy by metabolising glucose and glutamine through aerobic glycolysis (regardless of oxygen availability) [1,234,237,238] (Fig. 1.2).

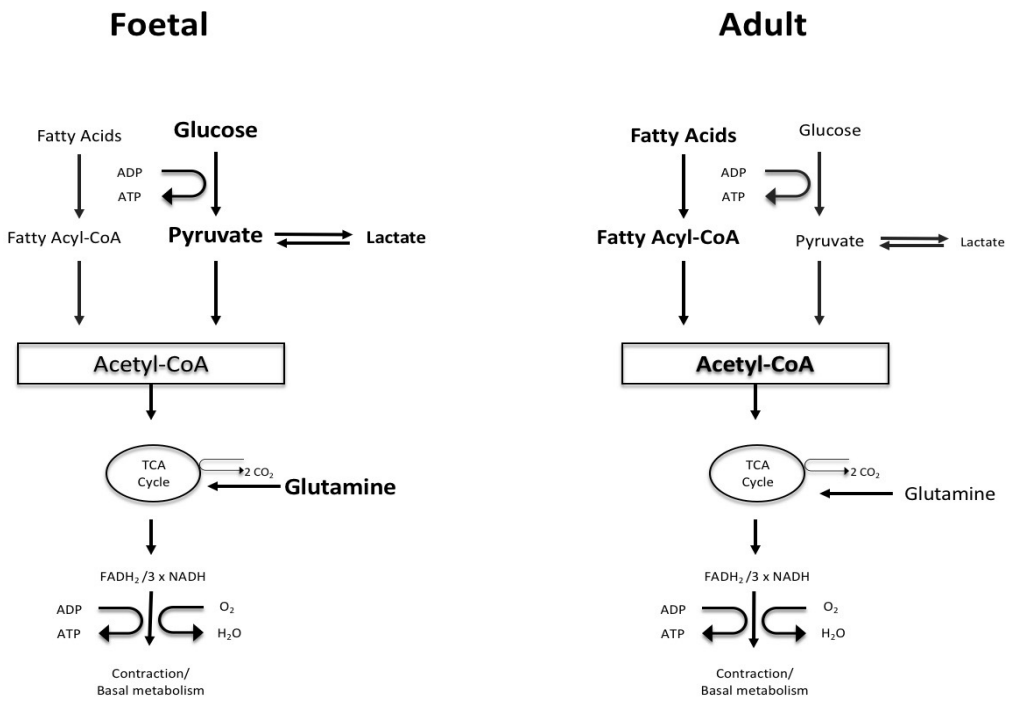

Figure 1.2: Adult vs foetal metabolic pathways, adapted from [239].

1.3 Cardiac Metabolism

An adult heart beats on average 80 times per minute, which calculates to 4,800 times per hour and 115,200 times per day. In order for the heart to sustain this heart rate it needs a constant and consistent supply of energy which is harvested from the hydrolysis of adenosine triphosphate (ATP). The heart requires around 6 kg of ATP per day, which is utilized at a rate of 30 mg/second to maintain contractions and sustain ion homeostasis [240, 241]. Since the heart has a low capacity to store energy [242], ATP is generated within CMs by utilizing a range of competing substrates (glucose, glycogen, fatty acids, pyruvate, lactate, triglycerides, ketone bodies, and certain amino acids) [242, 243]. These metabolic pathways are essential to life and strongly regulated on multiple levels based on demand.

Glycolysis is the first step in the metabolic pathway that breaks down glucose. It occurs in the cytoplasm and does not require the presence of oxygen. The pathway is outlined in Fig. 1.3 and involves a series of ten enzyme-catalyzed reactions. During these reactions, energy is released in the form of ATP and reduced Nicotinamide Adenine Dinucleotide Hydrogen (NADH). The breakdown per molecule of glucose ends with the formation of two molecules of pyruvate. Pyruvate has three potential fates. It can either be converted into acetyl-CoA (under aerobic conditions) by the pyruvate dehydrogenase complex (PDC) and enter the tricarboxylic acid (TCA) cycle [244] or be reduced to lactate by lactate dehydrogenase (LDH) (in anaerobic conditions), which regenerates nicotinamide adenine dinucleotide (NAD+). Although less relevant in cardiac tissue [245, 246], pyruvate can also be converted into oxaloacetate by pyruvate carboylase during gluconeogenesis. The heart doesn't do gluconeogenesis, so it has no major need for pyruvate carboxylase. The only use is in anaplerosis, which is not an energy generating pathway so is much lower in activity than the other pathways that utilise pyruvate (LDH and PDH).

A second pathway referred to as β-oxidation can also generate ATP via the breakdown of lipids (including triglycerides) into fatty acids (FAs). FAs enter the mitochondria in the form of Acyl-CoA via the assistance of carnitine. β-oxidation is then a stepwise dissociation of two carbon atoms from FAs, with coenzyme A creating the acetyl-CoA, which is oxidised

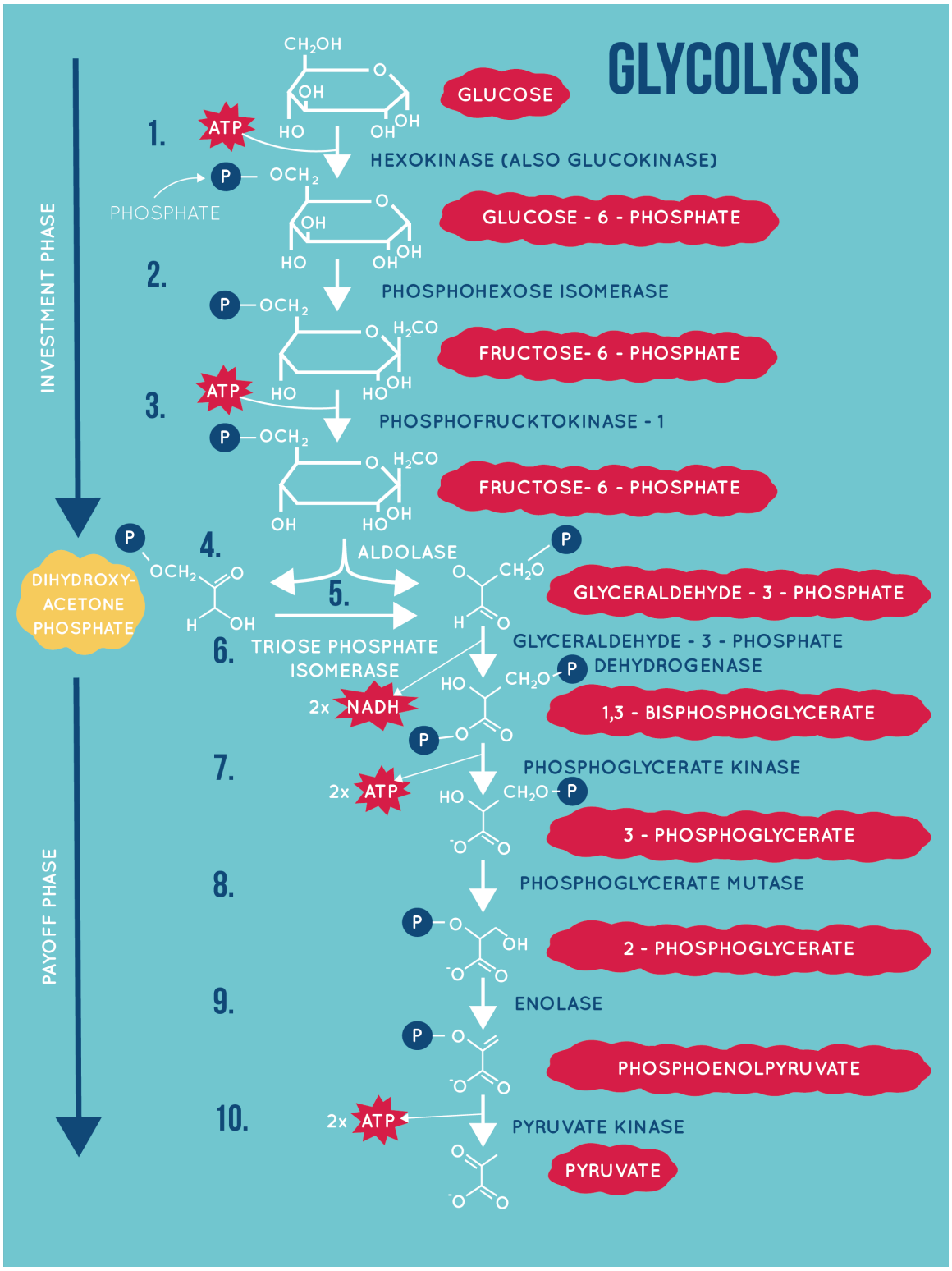

Figure 1.3: Diagram of glycolysis outlining the 10 enzyme-catalyzed reactions that break down glucose into two molecules of pyruvate, adapted from [247].

further in the TCA cycle [248] (Fig. 1.4). Energy is also released in these steps in the form of two hydrogen carriers: NADH and Flavin Adenine Dinucleotide Hydrogen ($FADH_2$). 50-80% of the energy in a healthy adult is generated through β-oxidation [249].

The TCA cycle, also known as the Krebs cycle or citric acid cycle, is a cyclic series of enzyme-catalyzed reactions to generate energy in the form of NADH, $FADH_2$ and guanosine triphosphate (GTP) in the presence of oxygen (Fig. 1.5). The cycle starts with the combination of acetyl-CoA (2-C) and oxaloacetate (4-C) to generate citrate (6-C). Citrate then continues to be broken down over a series of eight reactions to regenerate oxaloacetate with the release of two CO_2 molecules. The TCA cycle itself does not directly generate a lot of energy. For each turn of the cycle only one ATP is generated via a GTP intermediate. However, for each molecule of acetyl-CoA that enters the cycle, three NADH and one $FADH_2$ are produced. These coenzymes are then transported to the electron transport chain (ETC) on the inner mitochondrial membrane. In the ETC, a coupled-transfer of electrons and hydrogen ions (H^+) create an electrochemical proton gradient that generates ATP through a process called oxidative phosphorylation (OXPHOS) outlined in Fig. 1.6. Under aerobic conditions, OXPHOS generates more than 95% of ATP production [250].

Based on integer values for the stoichiometry of ATP synthase, the modern consideration is that oxidation phosphorylation yields 30-32 ATP per glucose molecule (depending on how the cytosolic NADH gets into the mitochondria) [251]. This is much more efficient than glycolysis which only yields 2 ATP per glucose molecule (Fig. 1.7). Lipids have a reduced state which makes them more oxygen-demanding than glucose, but they are also more energy dense which results in the production of more ATP per carbon. This greater yield of ATP is not due to ATP produced in the β-oxidative pathway, but rather due to the increased yield of acetyl-CoA produced from FAs. A single 6 carbon FA will produce 3 acetyl-CoA molecules while a 6 carbon glucose only yields 2 acetyl-CoA molecules [252], thus, depending on the chain length of the parent FA, oxidative phosphorylation can result in production of even more ATP [253, 254].

The healthy adult heart is a dynamic metabolic omnivore, which has the ability to switch to the most efficient substrate depending on availability or current physiological conditions

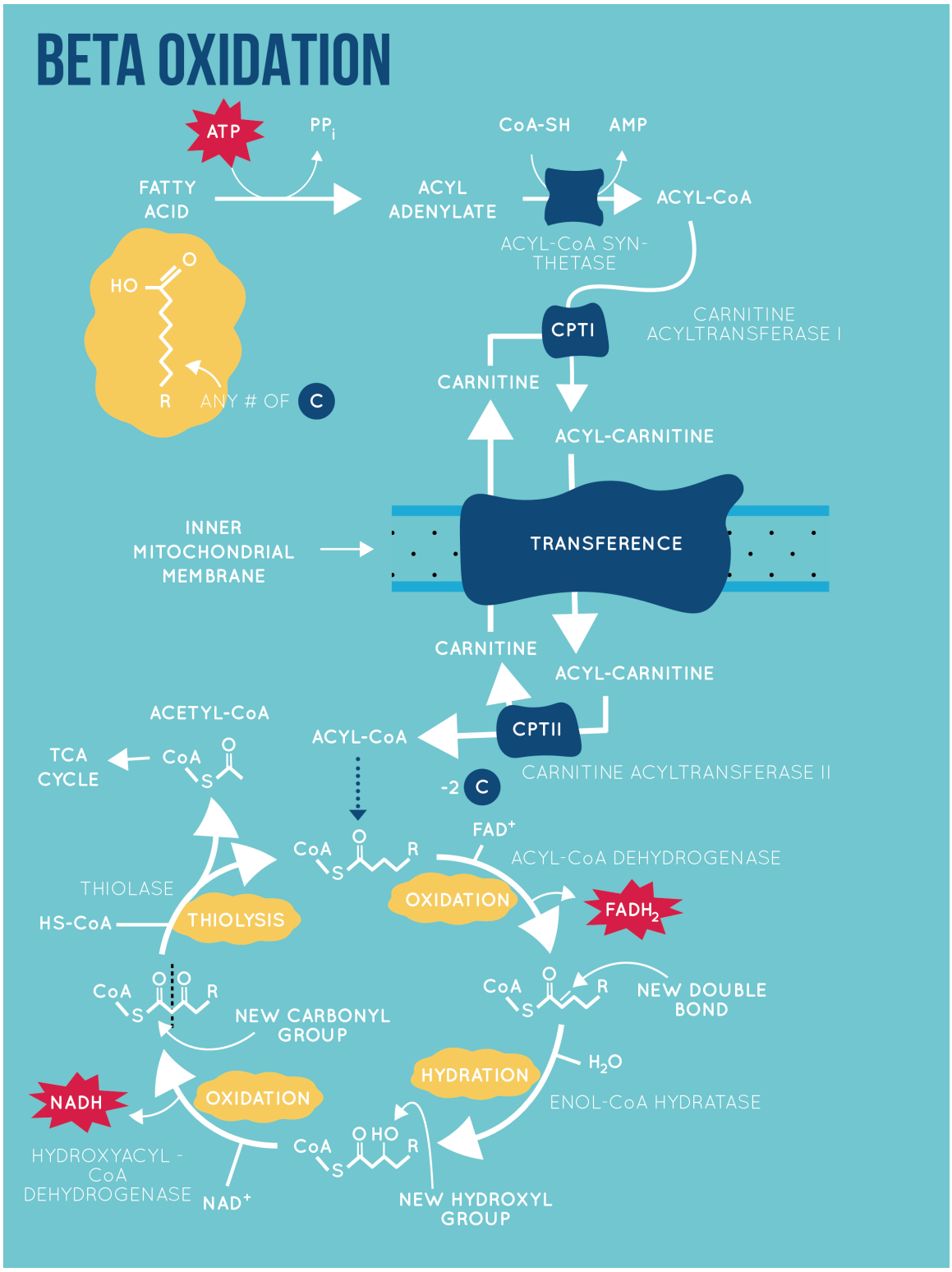

Figure 1.4: Diagram of β-oxidation outlining the stepwise dissociation of FAs into acetyl-CoA, adapted from [247].

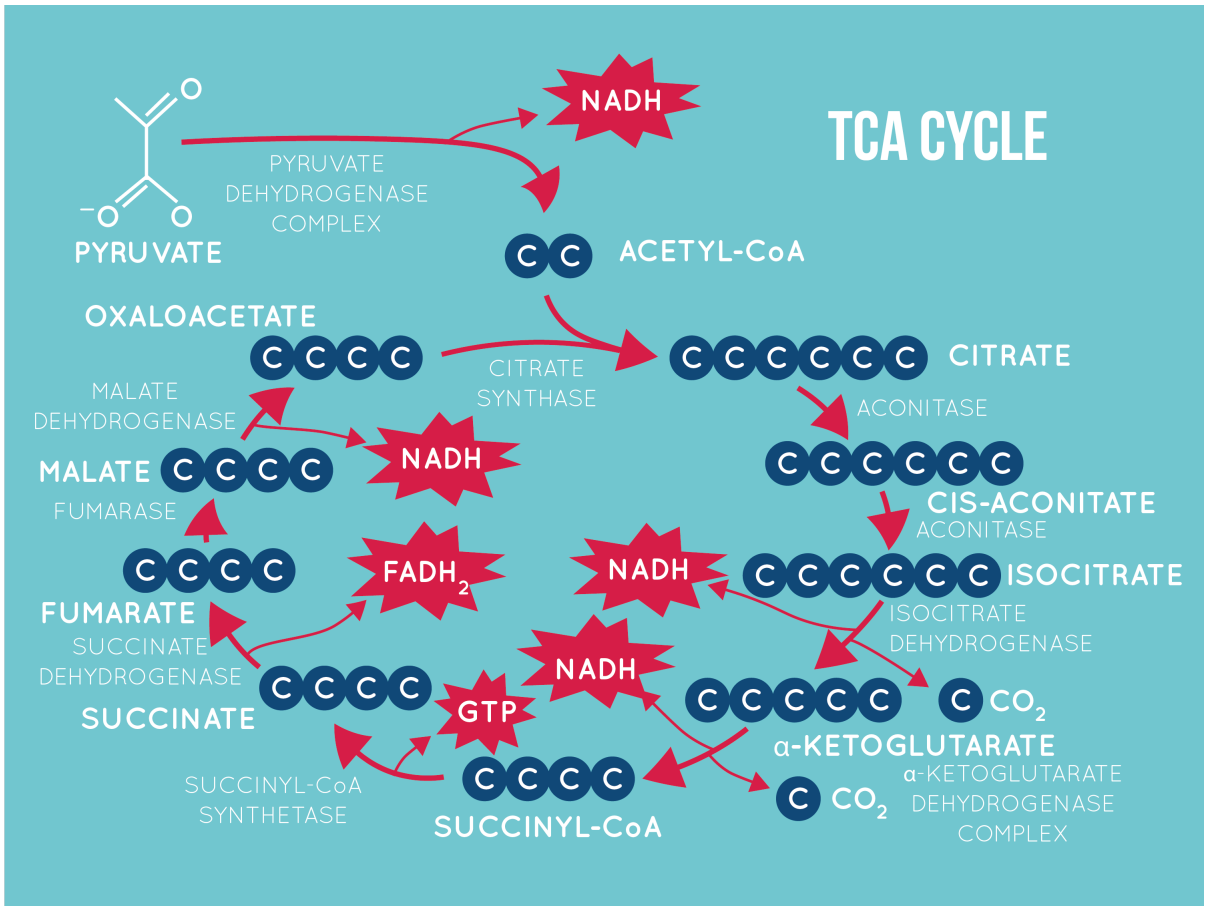

Figure 1.5: Diagram of the TCA cycle which is a cyclic series of enzyme-catalyzed reactions to generate energy in the form of NADH, $FADH_2$ and GTP in the presence of oxygen, adapted from [247].

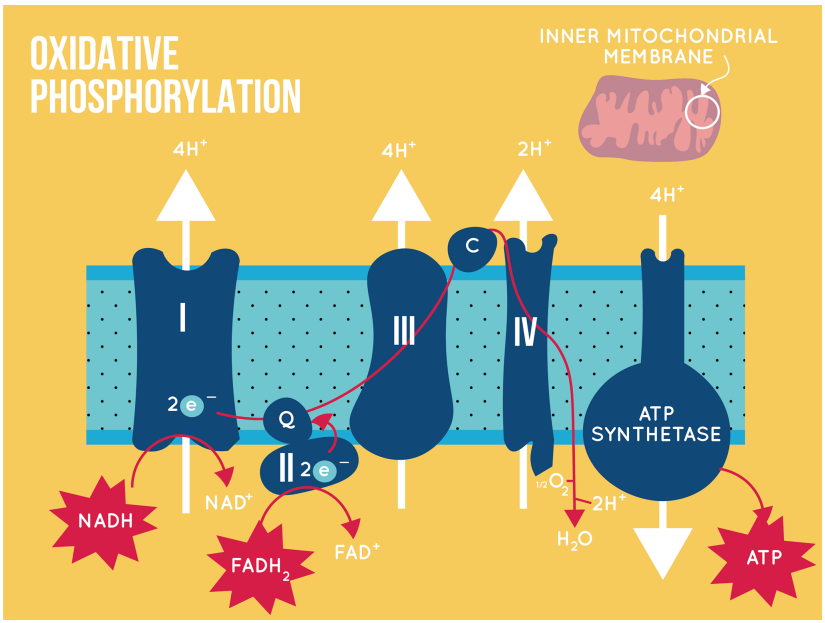

Figure 1.6: Diagram of oxidative phosphorylation which is a coupled-transfer of electrons and H^+ creating an electrochemical proton gradient that generates ATP, adapted from [247].

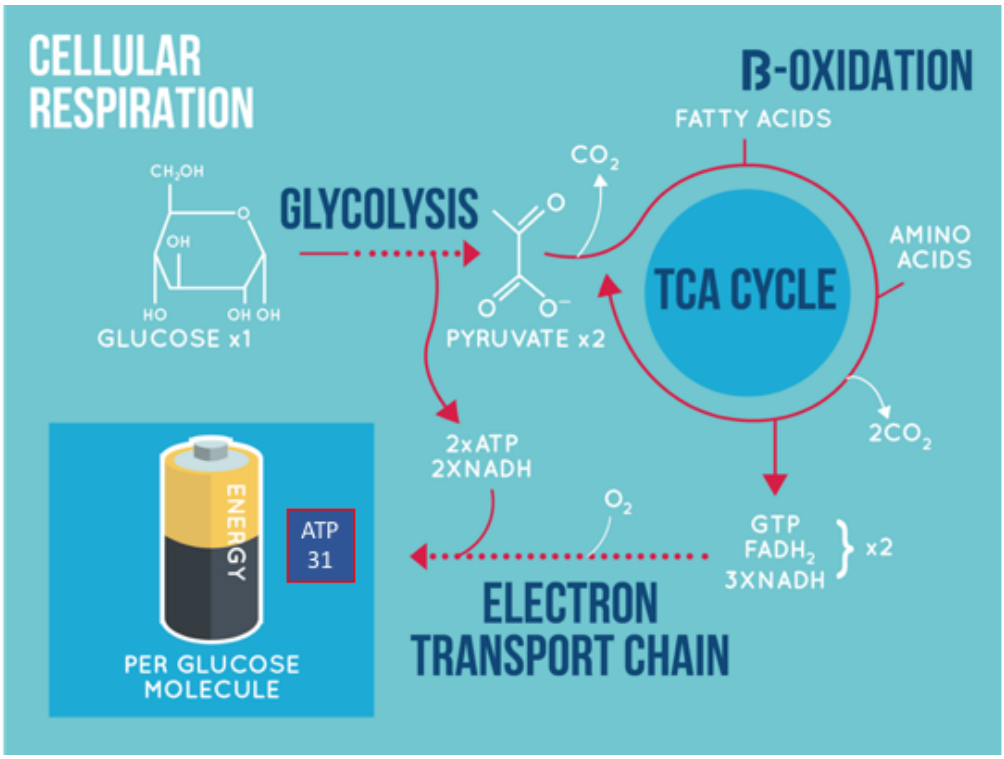

Figure 1.7: Overview of cellular respiration, adapted from [247].

to generate energy for contraction [255]. For example, FAs require more consumption of oxygen than glucose in order to generate the same amount of ATP [255,256]. Under hypoxic conditions there is an upregulation of the hypoxia-inducible factor (HIF) which leads to an increased glycolysis and reduced mitochondrial oxidative metabolism [257,258]. This shifts the metabolism towards the more oxygen-efficient fuel; glucose [257,258]. The heart has a network of interrelated signaling pathways that control the rapid flux of glucose and FA metabolism to enable the heart to switch substrates rapidly. This glucose/FA cycle was first described as the Randle cycle in 1963 [259] but is still being explored [260]. A healthy adult heart uses FAs for 70% of its ATP production, and glucose for only 30% of the total ATP production, even if FAs require more oxygen to generate a single ATP [256]. About 70% of this ATP produced is used just for contractile function [241,249].

1.3.1 Cardiac Metabolism During Development

The foetal heart relies on its mother for nourishment and oxygen. Since the fetus does not breath air, its blood does not circulate through the lungs to pick up oxygen, but instead has a connective vessel called the ductus arteriosus which connects the pulmonary artery and the aorta. As a result, prior to birth, the foetal heart lives in a low oxygen and FA environment. This leads to foetal CMs being highly dependent on glycolysis for ATP production [261] in addition to the lactate availability which allows for energy production through lactate oxidation to pyruvate, catalysed by lactate dehydrogenase. During the transition from development to after birth, the heart undergoes a major metabolic switch. From the transition to the post-natal stage there is an increased energy demand and work load that cannot be met in an hypoxic environment by glucose and lactate consumption alone [262,263]. Towards the end of gestation, the heart begins to store glucose as glycogen to prepare itself for immediately after birth [264,265], when the heart has to adapt to the loss of glucose, no longer provided directly by the mother, and the increased capability for oxidative phosphorylation. The increase in oxygen levels as well as of circulating levels of FAs (primarily due to the lipid content from the maternal milk) mediates a switch from glycolysis to relying on oxidative metabolism as mature CMs [261,266] (Fig. 1.8). Although some studies

still suggest that immediately after birth the main energy biogenesis mechanism is still glycolysis [267].

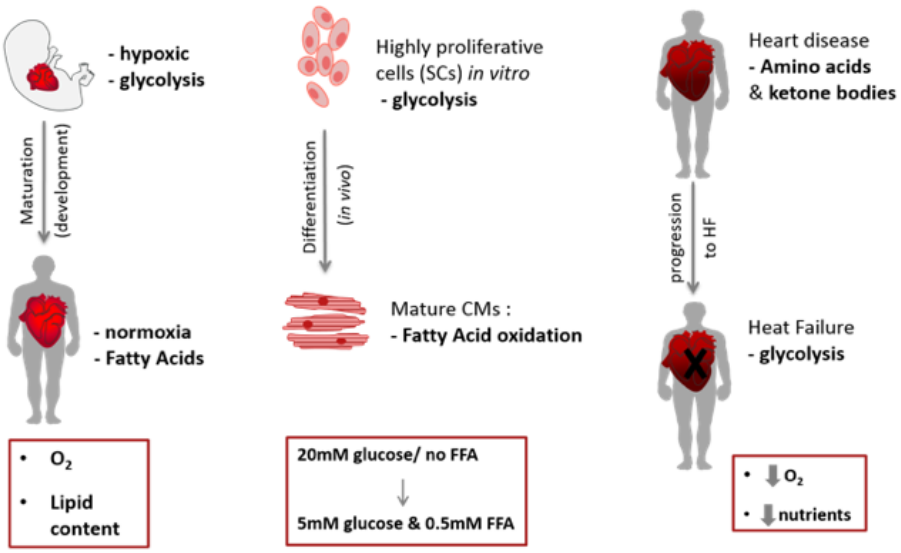

Figure 1.8: Graphic of the metabolic switch during cardiac development (left), differentiation (middle), and during heart failure (right). Taken from **Lopez** *et al.* 2018 [268]. See Appendix B for full PDF.

After birth, the "foetal switch" to oxidative metabolism of glucose and FAs has been linked to the loss of the regenerative phenotype [269]. Neonatal mouse hearts can regenerate in the first postnatal week, but this is lost after day 7 [270]. Puente *et al.* [269] investigated exposure of neonatal mice to hyperoxia (100% oxygen) or mild hypoxia (15% oxygen) and found that hyperoxia induced CM cell cycle to stop after birth whereas hypoxia prolonged the capability to regenerate. It was assumed that this effect resulted from the increased oxidative stress that accompanied the transition to oxidative metabolism and showed that treatment with an antioxidant resulted in increased proliferation in the first couple of weeks after birth.

Immediately after birth, cardiac energy demands and the number of mitochondria in CMs increases dramatically [271,272]. A recent study has shown that the localisation pattern of hypoxia-inducible factor (HIF-1) signaling controls the embryonic switch towards oxidative metabolism, the disruption of which affects cardiac maturation. Until midgestation myocardial metabolism is compartmentalized with a glycolytic signature

mainly in the compact myocardium and mitochondrial oxidative activity in the trabeculae. HIF-1 mirrors this compartmentalization patterns with expression predominating in the compact myocardium and scarece in the trabeculae where there was increased oxidative metabolism and higher mitochondrial content [273]. The transcription factors nuclear respiratory factor 1 and 2 (*NRF-1* and *NRF-2*) activate the expression of some key metabolic genes involved with respiration and mitochondrial ETC proteins [274,275]. Disruption of the ETC function during development leads to disorganized mitochondria and perturbed sarcomere formation and contraction [276] and eventually embryonic fatality [277]. In addition, signaling pathways involving the nuclear factor of activated T-cell (*NFAT*) family play a role in mitochondrial biogenesis and cardiac function. Mice with *NFATC3* and *NFATC4* deletion had abnormal mitochondrial structure and reduced oxidative capacity, eventually dying after E10.5 [278]. The estrogen-related receptor-α and -γ (ERRα/ERRγ) regulates genes involved in mitochondrial biogenesis [279], gluconeogenesis [280], oxidative phosphorylation [281] and FA metabolism [282] and deletion leads to premature fatality in mice [283]. Specifically, disruption of the ERRγ gene leads to impaired mitochondrial function, eventually blocking the switch from glycolysis to oxidative phosphorylation and leading to early prenatal death in mice [284].

1.3.2 Cardiac Metabolism in MI and HF

After an MI, the oxygen rich blood is blocked from reaching the desired tissue and the affected region experiences hypoxia, resulting in the activation of long-term HIF signaling in the myocardium [285]. The HIF signaling cascade regulates the effects of hypoxia and plays a key role in the mediation of human metabolism. During an infarction, the ischemic region relies mainly on glycogen as its anaerobic fuel for energy production [286]. HIF-1 activates the transcription of genes which encode for metabolic proteins such as lactate dehydrogenase (LDH), pyruvate dehydrogenase kinase (PDK) and BCL2 interacting protein 3 (BNIP3), a protein that triggers mitochondria-selective autophagy. All of these proteins play a pivotal role in reducing mitochondrial oxidative metabolism and thereby in reducing the generation of reactive oxygen species (ROS) [287]. Following reperfusion

post MI, oxidative metabolism is restored, but the resulting induction of ROS can lead to mitochondrial damage [288]. If the heart progresses to heart failure, there can be a decrease in pyruvate flux into the TCA cycle [289], reduced respiratory capacity [290,291], reduced oxidative phosphorylation [292–294], and mitochondria membrane and ETC defects [290,295]. All of these findings support the concept that during HF, the metabolic phenotype of the heart resembles that of a foetal heart. It switches back to predominately performing glycolysis over oxidative metabolism [248,296], with an increased glucose uptake [297] and a decrease or no change in glucose oxidation [297,298]. Progressive heart failure induces an increased conversion to lactate, which leads to a build-up of acid at the cellular level referred to as acidosis [299]. In addition, in heart failure patients there is a reduced availability of amino acids (aa), which play key roles in multiple cellular processes. This leads to the depletion of some important aa derivatives, that are vital for normal cardiac function, such as l-carnitine which helps facilitate FAs into the mitochondria for β-oxidation [300]. On the other hand, some studies have shown that there is an accumulation of aa during HF. Wende *et al.* [301] observed in a failing mouse heart, genes associated with aa catabolism were downregulated during compensated hypertrophy and overt failure. Others have shown that transcriptomic analyses showed downregulation of genes involved in amino acid degradation pathways (such as proline, alanine, tryptophan, and mainly branched-chain amino acids BCAAs) [302–304]. Using a genetic mouse model, Sun *et al.* [303] found that a deficiency in BCAA catabolism induced heart failure under mechanical overload, resulting from increased oxidative stress. Similarly, Li *et al.* [305] demonstrated in the healthy mouse heart, that while chronic accumulation of BCAAs did not affect cardiac energetics or function, glucose oxidation was decreased leading to an increased ischemic injury after MI.

Mitochondrial integrity plays a critical role in maintaining cardiac function. This is emphasized through several different conditions which are characterised by mitochondrial mutations or abnormalities including mitochondrial myopathy, cardiomyopathy, diabetes mellitus, neuromuscular dysfunction, and even sudden death [294,306]. In addition, the efficiency of the electron transport chain decreases with age and results in reduced ATP generation [306,307].

1.3.3 The Change in Cardiac Metabolism of Stem Cells to Adult CMs

An embryo developing from a single cell zygote, uses pyruvate oxidation for ATP production and low rates of glycolysis [308]. Before implantation, the embryo undergoes cell division into a blastocyst, which leads to a reduced mitochondrial DNA (mtDNA) number and density. With this reduction, the cell compensates with an increase in glycolysis and glucose uptake to support the exponential cell replication. After the blastocyst implants into the uterine wall, glycolysis reaches its maximum rates [308] as well as production of lactate which reflects specific metabolic requirements and mitochondrial regulation. During implantation, lactate production serves to facilitate several key functions including endometrial tissue breakdown, biosynthesis, the promotion of new blood vessel formation and induction of local immune-modulation of the uterine environment [309]. Similarly, ESCs derived from blastocysts [310] or cultured in vitro [311] show increased rates of glycolysis and lower oxidative phosphorylation. A comparison of iPSCs with ESCs showed many similarities between their energetics and metabolomics, confirming that somatic cells reprogrammed back to a pluripotent state switched back from an oxidative metabolism to a glycolytic one [312].

Reprogramming from a somatic cell to an iPSC has been shown to result in an upregulation in glycolytic enzymes such as the glucose transporter GLUT1, hexokinase (HK), phosphofructokinase (PFK) and LDH [313]. In addition, iPSCs have increased intracellular glucose-6-phosphate levels, used in the pentose phosphate pathway (PPP) to generate the reducing factor NADPH, which is used for biosynthesis of FAs and nucleotides necessary for rapid proliferation [313]. Mitochondrial morphological changes take place as well. They transition from being elongated and tubular-shaped with well-developed electron-dense cristae as in adult CMs, to being spherical with small-undeveloped cristae in iPSCs. They also go from an extensive cytoplasmic networks to a predominantly peri-nuclear location in iPSCs [314]. Prieto *et al.* [315] demostrated that this fragmentation was not associated with mitophagy, but was induced by activation of dynamin-related

protein 1 (Drp1), which fragments mitochondria in a GTPase-dependent manner. They also showed that early Erk activation induced Drp1 phosphorylation which was essential to the reprogramming pathway. These mitochondrial characteristics of being small numbered, rounded, immature with under-developed cristae have also been found in human and mouse ESCs [276,316] and in multipotent stem/progenitor cells (HSCs) [317].

There is still little known about the metabolism of cardiac stem cells in the adult heart. Most adult endogenous progenitor/stem cells reside in hypoxic niches [318], in what is thought to be a quiescent state, and therefore the metabolic rate is presumed to be low. In contrast, cells grown in culture are growing and proliferating in a culture media containing high levels of glucose with little to no FAs added. Basic cellular homeostasis consists of process like DNA repair, protein synthesis/degradation, and vesicle trafficking. As a result, these cells need energy for not only maintaining homeostasis requirements but also for anabolic processes like cell division and growth. Proliferative cells, such as cancer cells, have been thought to primarily rely on glycolysis for ATP production, regardless of oxygen presence. This metabolic paradox, first observed by Warburg in 1956 [319] has been termed aerobic glycolysis. Apart from Warburg's observations on cancer cells, human lymphocytes [320,321] along with chick embryo and skeletal muscle fibroblasts [322–324] have been reported to utilise aerobic glycolysis when stimulated to grow and proliferate. Several studies have supported the assumption that aerobic glycolysis's main function is to funnel glycolytic intermediates for anabolic reactions in the cell, implying that this metabolic pathway would be the ideal choice for cell proliferation [325]. Although cells in high glucose medium predominantly metabolise glucose, they can use other substrates if provided. Board, **Lopez** *et al.* [326] showed human bone marrow mesenchymal stem cells have an active oxidative metabolism with a range of substrates and can produce more ATP from substrate oxidation than glycolysis with certain substrates (full PDF in Appendix B). For example acetoacetate, the ketone body, can be oxidised 35 times faster than the rate of glucose. Many proliferating mammalian cells, such as human MSCs, also consume glutamine to be used as a source for biosynthesis [327]. Glutamine, is an amino acid, that can be used as a source of carbon that feeds into the TCA cycle with other intermediates to generate new

proteins.

When stem cells differentiate into CMs, they need to increase the number of their mitochondria and upregulate FA metabolism. A study comparing iPSC-CMs to iPSCs, showed a significant increase in mitochondrial relative abundance and membrane potential as a result of cardiac differentiation [328] and that further mitochondrial maturation in iPSC-CMs could be accomplished through long-term culture (3 months). Comparison of substrate metabolism in ESCs with that in ESC-derived CM has shown increased oxidative metabolism after differentiation [329] and that the respiratory capacity of CM was higher than in ESCs, resulting in an increased ATP:ADP ratio in the CM [276]. The mitochondria become elongated with abundant and organized cristae in CM and formed into networks which filled the cytoplasm [276].

1.4 Why Study Stem Cell Metabolism

The metabolism of any cell type in vitro depends on energy requirements and substrate availability. When expanded in vitro, cardiac progenitor cells reside in a high glucose environment and rely mainly on aerobic glycolysis for energy generation. Cells will experience a shift in substrate availability following in vivo transplantation. They go from being cultured in a media that contains anywhere from 5-25 mM of glucose (depending on the protocol) with no FAs, to an environment where substrates in plasma vary substantially. Glucose levels have been measured in different species and have been reported to be around 3.4-9.6 mM in mice (FAs around 0.18-0.6 mM [133]), and around 2.87.5 mM in rats [330,331]. While in humans, what is considered to be healthy plasma glucose levels are around 5 mM and 0.5 mM for FAs [332]. Higher circulating glucose levels are needed in the plasma because glucose usage is more rapidly adaptable than that of FAs. In addition there are some tissues in which glucose is the sole fuel source such as for the brain (except during prolonged starvation) [333–335]. The heart will selectively uptake and metabolize FA due to an increased energy output per mole from fat over sugar [333–335]. However, this difference in concentrations of substrates is exaggerated in culture media compared to these phyiological

levels since glucose concentration is doubled and the FA concentration is 100-fold lower or completely absent. So this alteration from in *vitro* to *vivo* is inevitably going to cause changes in the metabolic machinery of the cells, which most likely is one of the signals that induces differentiation of cells following transplantation, but may also result in increased release of ROS and cellular damage.

The various protocols used for ESCs and iPSCs differentiation mainly focus on small molecules to modulate signaling pathways, yet they do not take into consideration the substrate composition. This is unfortunate due to the considerations that knowing how metabolic changes, such as the transition from glycolysis to FA oxidation, could affect the function and maturation in CMs [237, 261, 313]. In various studies, iPSC-CMs have been reported to successfully integrate structurally and functionally in vivo with healthy cardiac tissue [79, 336, 337]. Despite the promising in vivo results, the initiation of beating in iPSC-CMs does not mean that these cells have the metabolic characteristics of mature CMs found in the heart. Multiple studies have shown that stem cell derived CMs have immature calcium handling [338, 339] and a drug response more analogous to CMs from a failing heart [340]. Regardless of the observed mitochondrial remodeling and upregulation of oxidative metabolism previously discussed, newly differentiated iPSC-CMs in culture have been shown to retain a predominantly glycolytic metabolism [341]. One of the major roles of iPSC-CMs is that of a drug-testing platform and this requires the differentiated cells to acquire a fully mature phenotype [342]. For example, a recent iPSC-CMs study showed that the electrophysiological responsiveness of iPSC-CMs was dependent on their maturation state [343].

1.4.1 Assessing Cell Metabolism

The main approaches for the investigation of substrate metabolism include the measurement of metabolic fluxes using radio-labelled substrates and of oxygen consumption.

Radio-Labelled Substrate Assays

Glucose oxidation rates are commonly measured using the method of Collins *et al.* [344] with

cell culture media containing D-U-^{14}C-glucose. Glucose oxidation results in the production of $^{14}CO_2$. The labelled CO_2 is trapped on filter papers, which are analysed using a scintillation counter, and the radiation counts per minute (cpm) are measured.

For ^{3}H-FA oxidation, the cells are incubated in media supplemented with the radioactive FA tracer of interest. FA oxidation rates are determined by the production of ^3H_2O from the mitochondria [345,346]. Media aliquots contain both ^3H_2O and ^{3}H-FA are collected, so the ^3H_2O is separated (via a Folch extraction), and radioactivity is counted again in cpm [345].

^{3}H glucose measurement of glycolytic flux is achieved after incubating the cells with media containing ^{3}H-glucose. Glycolytic rates are determined through the conversion of ^{3}H -glucose to ^3H_2O via enolase which converts 2-phosphoglycerate to phosphoenolpyruvate and releases H_2O as a by-product. As a result the samples contain both ^3H_2O and ^{3}H-glucose, and the ^3H_2O is collected using a Dowex mesh (Sigma, UK) anion exchange column, allowing for the ^{3}H-glucose to bind to the column and ^3H_2O to be eluted. Sample radioactivity is measured as before [346].

Oxygen Consumption

The rate of mitochondrial oxygen consumption (OCR) can be measured using the XF Extracellular Flux Analyzer (Seahorse Bioscience), the Oroboros O2K or the Clark-type oxygen electrode [347,348]. Seahorse XF Analyzers measure the concentration of dissolved oxygen and pH to quantify the oxygen consumption and extracellular acidification rates in the media of multi-well plates. There are four injection ports in each well to allow the addition of reagents. However, the Seahorse requires the cells to be adhered to the wells, which doesn't allow the addition of multiple substrates when the individual wells are not self-contained. Thus cells can be affected by gases from adjacent wells [347]. The Clark-type oxygen electrode is embedded in individual reaction chambers and cells are added in suspension in the respiration media [348]. Unlimited reagents and substrates can be added by manual addition. This system is more automated in the Oroboros O2K, which also includes optical sensors to allow for detection of fluorescent dyes, so that parameters

such as ATP production or mitochondrial membrane potential may be measured [347].

The OCR can be measured under baseline un-stimulated conditions in media containing the substrate of interest (such as pyruvate; palmitate; malate; or oleate). Addition of the ATP synthase inhibitor oligomycin provides a measure of contaminating ATP synthase activity from damaged mitochondria and of proton leak, whilst the metabolic uncoupler, carbonylcyanide-p-trifluoromethoxy-phenylhydrazone (FCCP) permits measurement of maximum respiration (fully uncoupled) [348]. Finally, mitochondrial inhibitors such as rotenone (complex I) and antimycin (complex III) will completely inhibit mitochondrial respiration. More delicate interrogation of the function of mitochondrial metabolism can be performed using substrates such as glutamate which assesses the second span of the Krebs cycle, succinate which enters the electron transport chain at complex II or β-hydroxybutyrate, a FA-derived substrate which bypasses β-oxidation and enters the Krebs cycle as acetyl CoA [288, 349].

Extracellular Measurement of Glucose Consumption and Lactate Production
Lactate production can be measured using the Seahorse Flux Analyzer from the extracellular acidification rate (ECAR) of the media. Glucose and lactate levels can also be determined using enzymatic assays or the ABX Pentra 400 Chemistry Analyser (Horiba Ltd. USA). In Glycolysis, one molecule of glucose yields two pyruvate molecules, which then can be converted into either acetyl CoA (through the TCA cycle) or lactate (through lactate dehydrogenase). Therefore, the ratio of glucose consumption to lactate production can be used as an indicator of how much pyruvate is being utilized in oxidative metabolism [350].

1.5 Cardiac Differentiation in Vitro

Cardiac directed differentiation protocols used for pluripotent stem cells can be divided into two main groups, the embryoid body (EB)-based method [234, 351, 352] and the monolayer-based method [80, 234, 353–356]. Although cardiac differentiation protocols vary, most of the monolayer-based methods involve specific activation and inhibition of signaling

pathways which have been shown to control heart development. They mimic three key early cardiac development stages, starting with the induction of an early mesoderm, cardiac mesoderm specification, and lastly the generation of CMs [357]. The two most common cardiac signaling pathways that protocols address are Activin/Nodal and bone morphogenetic proteins (BMP) signaling [351]. These both are members of the transforming growth factor beta (TGFB), the fibroblast growth factor (FGF) [80,351], and the Wnt signaling pathways [353–356]. Activin A, BMP4, and Wnt3 induce the initial mesoderm state, by upregulating the expression of Brachyury T. The Wnt signaling pathway is then inhibited at later stages of differentiation to induce a mesoderm cardiac specification [234]. From here, cells are then cultured in media with no growth factors, to allow CM maturation to give rise to spontaneous beating.

1.5.1 EB-Based Protocols

Originally, cardiac differentiation protocols were first established using ESCs and then were developed to iPSCs. Table 1.1 summarises and compares different published differentiation protocols showing the transition from the ESCs-derived EB-based model into the current most commonly used iPSC-CMs-derived monolayer-based model. Table 1.1 also takes note of the fact that all these protocols are differentiated in variable concentrations of glucose (4.5-25 mM) and insignificantly low amounts to no FAs (at most 2 μM). Broadly, EBs are cells in suspension cultured in a serum-based media in order to induce spontaneous cardiac differentiation [76,352,358]. The beating areas are then hand-picked from the rest of the EB or flow-sorted. In 2001, Kehat *et al.* [352] successfully created spontaneously beating ESCs derived EBs (8%), which reportedly expressed 30% cardiac specific troponin T positive cells (cTNT+). In 2002, Xu *et al.* [358] also was able to generate spontaneously beating EBs using the serum-induction method and enhanced the efficiency of differentiation by adding 5-Aza from days 6 to 8. The group also reported that DMSO or retinoic acid had no effect on the differentiation efficiency. In further studies the yield of beating areas was considerably increased by omitting serum from the EB culture medium [359,360] and subsequently by the addition of growth factors [351,357]. In 2011, Burridge *et al.* [361] systematically compared

45 variables added to EBs formed by forced aggregation which they tested on four ESC and seven iPSC lines. Their optimised method included addition of BMP4 and FGF2, with polyvinyl alcohol to aid EB formation, serum, and insulin and with staged exposure to physiological (5%) oxygen. The development of growth factor-directed differentiation enabled cells to be differentiated as monolayers, thereby introducing more straightforward, and hopefully more reproducible, methods of differentiation [234].

Table 1.1: Factors and media used by different labs to differentiate pluripotent stem cells to CMs. Abbreviations: B-ME = β-mercaptoethanol; mTG=monothioglycerol; P/S=penicillin/streptomycin; AA=ascorbic acid; NEAA=non-essential amino acids; P/S=penicillin/stretomyocin. It should also be mentioned that the existence of serum at percentages ranging from 2-20% does not allow for an absolutely clear image of the media composition. Table taken from **Lopez** *et al.* 2018 [268]. See Appendix B for full PDF.

Diff Method and Cell Type	**Growth factors or small molecules**	**Culture Media**	**Glucose Conc.**	**% of Cardiac Markers**
EB-Method (ESCs, iPSCs)	Cells in suspension - optionally differentiated with serum-based media, DMSO, all-trans retinoic acid or 5-Aza.	80% KO-DMEM, 1 mMol L-glutamine, 1.1-1.2 mMol B-ME, 1% NEAA, 20% FBS.	4.5mM	8.1% spontaneously beating EBs (29.4% cTNT+ cells) [352, 362]. By Day 8 of differentiation there are 25% beating EBs and 70% by Day 16; 5-Aza enhanced levels of cardiac *MHC*α [359, 363]. 10-15% positive for sarcomeric MHCs [142].

EB-Method (ESCs, iPSCs)	Guided differentiation: h-Activin A, h-BMP4 ± staged addition of hWnt3α and h-DKK1.	RPMI+B27	11.11mM (Note: 2 μM of oleic acid)	>30% CMs differentiated cells had Percoll gradient centrifugation for CM enrichment (69 ± 10% CMs) [76, 148]. Increase in sarcomeric MHC+ cells from 4 to 27% [356].
EB-Method (ESCs, iPSCs)	END-2 method (Insulin depletion, PGI_2, p38 inhibition).	80% KO-DMEM, 2 mMol L-glutamine, 10 ng/ml bFGF, 1.2 mMol B-ME, 7.5% FCS	4.5mM	50% beating CM [360, 364].
EB-Method (ESCs)	Guided differentiation: h-Activin A, h-BMP4, h-bFGF, h-VEGF, hDKK1.	StemPro-34 (Base) + [L-glutamine, AA, optional MTG, P/S]	>25 mM	KDR+ selected cells 35 ± 6% cTNT+, were enriched to 57 ± 4% by monolayer culture. DKK1 on Day 4 gave 2-fold enrichment of cTNT+ cells [357]. KDR+/ PDGFRA+ cells; in beating EBs, 50-70% cTNT+ cells. Monolayer culture on Day 5 KDR+/ PDGFRA+cells lead to 80% cTNT+ cells [351].
EB-Method (iPSCs)	Forced aggregation EBs with guided differentiation: BMP4, FGF_2, Staged O_2 levels.	RPMI (L-glutamine) 20% FBS on Day 3 Insulin on Days 0-2 and Day 4.	9-11 mM (Note: 2 μM FA)	Contracting EBs contained 64-89% of cTNT+ cells [361].
Monolayer (iPSCs)	Guided differentiation: h-Activin A, h-BMP4, h-bFGF	StemPro-34 + [L-glutamine, MTG, AA, P/S]	>25mM	Spontaneously beating sheets of CMs 40±15% CMs [80].

Monolayer (ESCs, iPSCs)	Guided differentiation method: h-Activin A, h-BMP4, h-bFGF, + Matrigel or CHIR99021, IWP4/IWP2.	RPMI+B27(-insulin) [Day 0-6 of differentiation]; RPMI+B27 [from Day 7 of differentiation].	11.11 mM (Note: 2 μM oleic acid)	With the addition of Matrigel on Day -1 and 0 of differentiation generated 80% cTNT+ cells [365]. Spontaneously beating sheets of CM, 87% cTNT+ CMs [353–355].
Monolayer (iPSCs)	Guided differentiation method: Ascorbic acid, h-BMP4, CHIR99021 (GSK-inhibitor), dorsomorphin (BMP-inhibitor), A83-01 (activin/nodal inhibitor), IWR1 (Wnt/β-catenin signaling inhibitor)	CVPC induction medium (CIM), CM differentiation medium 1 and 2 (CDM1 and CDM2) = RPMI+B27(-inslin)+ 1% glutamine + 1% P/S	11.11mM	Produced 80% CMs [366]
Monolayer (iPSCs)	Guided differentiation method: CHIR99021 (GSK-inhibitor), Wnt-C59 (Wnt inhibitor)	CDM3: RPMI 1640 + albumin + L-ascorbic acid 2-phosphate	11.11 mM with transient glucose depletion	Produced 85% to 95% CMs [361]

1.5.2 Monolayer Protocols

Laflamme *et al.* [142], played a pivotal role in optimising cardiac differentiation protocols by shifting the paradigm from the serum-induced EB-based method, which only generated around 10-15% beating EBs, to the serum-free monolayer method using Activin A and BMP4 generating >30% beating CMs [76]. In 2008, Yang *et al.* [357], also used this differentiation method with Activin A, BMP4, basic fibroblast growth factor (bFGF), and vascular endothelial growth factor (VEGF) to generate positive expression of the

kinase insert domain protein (KDR) marker representing the early stage in mesoderm cardiac specification. In addition, they showed that re-plating KDR+ cells in a monolayer generated 50% beating cTNT+ CMs [357]. Three years later, Kattman *et al.* [351] also generated spontaneously beating EBs using Activin A and BMP4. The derived cells were sorted for positive expression of both KDR and platelet-derived growth factor receptor alpha (PDGFR-α) and re-plated as a monolayer generating 80% cTNT+ cells. In 2011, Carpenter *et al.* [80] further optimised this protocol. These studies show the importance of the stage-specific manner of activating and inhibiting Activin/Nodal, and BMP4 signaling pathways in order to recapitulate and drive a cardiac linage of these cells as seen in heart development. To further enhance cardiac differentiation the Wnt signaling pathway was also exploited.

Differentiating cells using the Wnt signaling pathway is critically dependent on the time at which growth factors are added and removed. Canonical Wnt/B-catenin signaling is activated during mesoderm induction but inhibited during specification of cardiac mesoderm linage. Activating Wnt during this early stage and subsequently inhibiting it during cardiac mesoderm specification has been reported to enhance cardiac differentiation [355, 356]. Lian *et al.* [353] optimised this protocol by removing insulin during early stages of differentiation. They had found that when iPSCs were differentiated using Gsk3β inhibitor, Activin A, and BMP4, the presence of insulin in the early stages had a strong inhibitory effect but that this was not seen when cells were differentiated by manipulation of Wnt signaling. They identified an interplay between insulin signaling and Wnt signaling which coordinates to influence differentiation to CMs and therefore introduced staged removal and re-addition of insulin to their differentiation protocol [353].

1.5.3 The Role of Hypoxia and of Reactive Oxygen Species in Differentiation

Stem cells in vivo occupy an hypoxic niche and their energy yielding metabolism is likely to be hypoxic with a high reliance on glycolysis for ATP generation [367, 368]. There

are conflicting reports on the relationship between hypoxia and differentiation of stem cells. Hypoxia alone can revert ESC- or iPSC-derived differentiated cells back to a stem cell-like state, by re-activation of an OCT4-promoter reporter [369]. In contrast, exogenous expression of HIF has been shown to promote cardiac differentiation of ESCs [370]. During in vitro cardiac differentiation, transient hypoxia upregulated the Wnt signaling pathway which upregulated endogenous Wnt proteins (including: wnt3, wnt3a, wnt9a and wnt11) expression, which was reversed when cells were returned back into normoxia. This also resulted in the upregulation of cardiac markers Isl-1 and Troponin C, but decreased expression of MHC-β and a failure to develop the contractile phenotype [371]. To further complicate the picture, Gaber *et al.* [372] found a dose-dependent increase in expression of the DNA damage marker H2AX and of senescence in ESCs differentiated under increasing exposure to hypoxia. These differential reports may result from the different cell types (ESCs or iPSCs) and species studied. Fynes *et al.* [373] found that hypoxic culture of ESCs primed the cells for differentiation and resulted in increased differentiation along the mesoderm and endodermal lineages whereas iPSCs were pushed toward a more pluripotent state by hypoxia and were then primed for ectoderm differentiation.

As previously discussed, the loss of regenerative potential of the heart in the first weeks of life has been attributed to DNA damage resulting from the increase in ROS that accompanies upregulation of mitochondrial metabolism [269]. However, ROS have also been shown to signal differentiation to several cell types, including CMs. Transient expression of an NADPH oxidase-like enzyme with induction of ROS during embryoid body development of ESCs enhanced cardiomyogenesis, which was shown to occur via PI-3-kinase regulation and to be inhibited by the addition of radical scavengers [374]. Similarly, NADPH oxidase (NOX)-derived ROS induced cardiac differentiation via a p38 mitogen-activated protein kinase (MAPK)-dependent pathway [375]. In ESC-CMs, inhibition of mitochondrial biogenesis using shRNA targeting of *PGC1α* repressed mitochondrial respiration and beating frequency [376]. Levels of ROS increased during differentiation but were repressed by knockdown of *PGC1α*. However, decreasing ROS levels by differentiating cells under hypoxia decreased the rate of mitochondrial biogenesis, which was stimulated by induction

of ROS [376]. Interestingly, in addition to reducing the beating frequency, decreasing ROS levels increased the action potential and calcium transient amplitude, but made the cells vulnerable to metabolic stress. ESCs cultured in physiological levels of glucose (5 mMol) maintained their stemness and showed reduced levels of ROS, but failed to differentiate to fully-formed CMs [377]. This was associated with reduced levels of NOX4 and MAPK which were rescued by addition of the pro-oxidant ascorbic acid.

1.6 Future Strategies to Mature Cells

A range of strategies have been used to mature iPSC- and ESC-CMs, including time in culture [22,328,378,379], mechanical and electrical stimulation [380–382], genetic approaches [383,384], substrate stiffness [385], addition of small molecules [386], or 3D culture [387–390]. These are reviewed in other sections of this thesis (Section 3.1.3 and Section 4.1.1) as well in more detail elsewhere [342,391], but very few consider the medium in which the cells are cultured.

1.6.1 Changing Media Composition to be More Physiologically Relevant

During heart development, from the foetal to the adult phenotype, there is a switch in energy substrate availability and consumption. However, most published differentiation protocols do not address this change in metabolism. We have listed the substrate composition of differentiation media in Table 1.1. The majority of differentiation protocols into CMs had little to no lipids in the media composition. In culture media, the glucose concentration ranges from 4.5 mM - 25 mM. The variability of glucose concentration is striking, especially because glucose levels of 25 mM in vivo are considered to be hyperglycemic and can lead to mitochondrial network losses [392,393]. Therefore, a future strategy to try and mature cells is to investigate the concept of changing available substrates, for example adding FAs to the culture media could enhance fatty acid oxidation (FAO) in immature cells.

Maturation of ESC-CMs was induced by treatment with the thyroid hormone, tri-iodo-L- thyronine, which induced an enhancement in contractile kinetics, calcium release and reuptake rates and in sarcoendoplasmic reticulum ATPase expression. There was also a significant increase in the maximal mitochondrial respiratory capacity and respiratory reserve capability [386]. However, in that study the newly formed CMs were cultured in serum-free medium with no FAs. Similarly, where maturation of ESC-CMs was induced using members of the Let-7 family of microRNAs it resulted in an increased cell size, sarcomere length, force of contraction, and respiratory capacity [394]. There were no FAs added to the serum-free culture medium.

A few recent studies have begun to change media composition to induce a particular disease phenotype [329,341,395–398]. In 2013, Kim *et al.* [341] used a lipogenic medium made of insulin, -isobutyl-1-methylxanthine, and dexamethasone that reportedly increased FA metabolism in iPSC-CMs derived from patients with arrhythmogenic right ventricular dysplasia. They saw a mild increase in lipogenesis with minimal apoptosis after 45 weeks of treatment and increased expression of peroxisome proliferator-activated receptor-alpha (PPARα). Cell maturation revealed that metabolic derangement was implicated in the onset of arrhythmia. Wen *et al.* [399] also used a combination of insulin, dexamethasone and 3-isobutyl-1-methil-xanthine to increase FA synthesis and trigger the activation of PPARα, which led to enhanced mitochondrial oxidative phosphorylation. Drawnell *et al.* [395] induced a diabetic phenotype by treating differentiated iPSC-CMs with a maturation medium containing insulin and FAs, but no glucose for three days, followed by treatment with a diabetic milieu of glucose (10 mM), endothelin-1 (10 nM), and cortisol (1 μM). This treatment induced an increase in sarcomere length as well as velocity and duration of action potentials. In addition it increased the gene expression of myosin light chain genes such as *MYL2*, *MYL3* and *MYL4*, involved in regulation of sarcoplasmic reticulum calcium content and an associated repression of foetally enriched genes. More recently, Correia *et al.* [396] showed that by switching the iPSC-CM's culture media from a glucose-containing to galactose- and FA-containing one it induced an increased oxidative metabolism, contractility and more physiological action potential kinetics that reflected an adult CMs. Perhaps the

most comprehensive investigation into the effects of changing media is that of Rana *et al.* [398] who modified basal medium combinations of high or low glucose with galactose or FAs. They found that exclusion of glucose from the medium was needed to induce iPSC-CMs to switch from glycolysis to OXPHOS for their ATP production. Mills *et al.* [397] used a maturation media (containing 1 mM glucose and 10 or 100 μM palmitate with no insulin) in addition to culturing iPSC-CMs in organoids which obtained an increased contraction force, *MLC2v* expression and a reduction in proliferation pathway such as the β-catenin and Yes-Associated Protein 1 (YAP1) pathway.

1.6.2 Tissue Engineering Approaches for Disease Modelling

Traditionally, cells are grown in a monolayer environment, however in vivo cells are located within a 3D organ/tissue structure where there is cell to cell contact. It is hypothesized that culturing cells in 3D would better mimic conditions in vivo, such that differentiated cells would adopt a more mature phenotype. In addition, many studies mainly focus only on single cell functional assessment (such as patch clamp and action potentials) [400]. However, for many disease models, individual cell characterisation is insufficient and a 3D model should be explored and optimized.

There have been several success stories with 3D tissue engineering. Bian *et al.* [401] cultured neonatal rat CMs in a 3D environment and after 3 weeks saw aligned, electromechanically coupled CMs with capillary like structures, and improved calcium handling properties. The cells had action potentials which showed enhanced conduction velocities and directional dependence on the local CM orientation. Cardiac muscle strips which were fabricated from ESC-CMs and stromal cells in collagen-based biomaterials, showed higher passive and active twitch force, aligned sarcomeres, regularly dispersed connexin-43/N-cadherin and increased expression of maturation markers [387].

Overall there are four main types of tissue engineering strategies that have been developed to construct contractile heart muscle equivalents: stacking monolayer cell sheets to form multi-layered heart muscle [402], cells seeded onto decellularized native tissue, cells seeded onto synthetic or biologic scaffolds [403–408] and entrapment of cells in naturally

occurring biogels/hydrogels [409–411].

1.6.2.1 Cell Sheeting

Cell sheets are generated using temperature-responsive culture plates. These plates are coated with covalently attached temperature-responsive poly(N-iso-propylacrylamide) (PIPA-Am) polymers [402], which allows various types of cells to attach and proliferate at 37 °C. When the temperature is reduced below 32 °C, the polymer becomes hydrated, switching from being hydrophobic to hydrophilic and resulting in spontaneous detachment of the cells from the plate. These single continuous sheets of cells with intact cell junctions and deposited ECM can be harvested and stacked to generate a thicker construct [412, 413].

1.6.2.2 Decellularized Hearts

Potentially the "ultimate scaffold material" is that of decellularized heart tissue since it has the potential to provide the most appropriately structured scaffolds for an organ replacement [414]. The goal would be to design an organ that would be less likely to calcify, capable of harbouring cells and be able to remodel and grow [415]. Growing cells in native heart matrixes can also help induce cardiac differentiation of ESCs without supplemental growth factors [416].

There have only been a handful of labs investigating decellularized hearts but these have shown initial success in the method. Ott *et al.* [414] was the first to report the feasibility of this method by creating a decellularized rat heart by coronary perfusion of detergents, leaving an acellular scaffold with intact chambers and valves. The decellularized heart was then recellularized with neonatal cardiac cells via intramural injection. The cardiac cells were shown to contract and be drug responsive after 8 days in culture. Lu *et al.* [417] was also successful in creating a decellularized mouse heart seeded with iPSC-derived multipotent cardiovascular progenitor cells. After 20 days in culture the cells were reported to spontaneously contract and be drug responsive. In 2014, Robertson *et al.* [418] first re-endothelialized whole decellularized hearts with aortic endothelial cells throughout both arterial and venous cavities by a combination delivery strategy (through

arterial and venous) that reduced scaffold thrombogenicity and improved contractility of left ventricular-recellularized constructs. In 2016, Kitahara *et al.* [419] completed a heterotopic transplantation of a whole decellularized porcine heart seeded with MSCs and demonstrated short-term coronary artery perfusion in the transplanted scaffolds by angiography. Most recently, Duong *et al.* [420] showed that accessing and controlling the perfusion into the heart via 4-Flow cannulation allows for a more efficient decellularization and ensures efficient and proper distribution of perfusates.

1.6.2.3 Constructing 3D scaffolds from (Semi-)Synthetic and Biological Materials

Scaffolds can be formed from synthetic polymers from natural materials such as the cardiac **extracellular matrix (ECM)**. ECM is a complex mesh work of fibers decorated by matrix proteins in which fibroblasts, leukocytes and cardiac vascular cells reside. ECM is present in all tissues, deposited and maintained by the resident cells thereby creating a naturally occurring scaffold. Besides its structural role of giving support to surrounding cells, the ECM also has important non-structural properties that have important roles in cardiac development and remodeling. There are two main types of ECM that can be distinguished. The first is interstitial connective tissue matrix which surrounds cells and provides structural support to all tissues. And the second is the basement membrane which separates the lining of internal or external body surfaces (epithelium, mesothelium and endothelium) from the connective tissue.

The ECM contributes to cell signaling and is essential for life. It has been shown to help regulate cell survival, proliferation, migration and differentiation, for example by modulating the activity, bioavailability or presentation of growth factors to cell surface receptors [421, 422]. This can be demonstrated by mutations in ECM related genes that cause a large number of tissue defects and embryonic fatality [367]. The structure and composition of the ECM varies dramatically depending on the specific tissue type, developmental or disease stage, and age. There have been around 300 ECM proteins identified that encode for different substrates, including collagen [410, 423, 424], elastin [425], fibrin [426, 427] and glycosaminoglycans (GAGs)

like chondroitin-sulphate and hyaluronic acid [428, 429] that can be extracted from tissue and integrated in a 3D scaffolds [425, 429] or hydrogel [426].

Unlike natural materials, synthetic polymers are much more controllable and adjustable in when assessing mechanical properties. The most commonly used synthetic biomaterials used are polylactic acid (PLA), polyglycolic acid (PGA), and poly(lactic-co-glycolic acid) (PLGA) [403, 406, 430, 431]. They are often modified to incorporate adhesion peptides or release biological molecules [432].

1.6.2.4 Porous Scaffolds

Degradable porous scaffolds can be generated by several techniques that include freeze drying suspensions poured into moulds [425, 433, 434], leaching [435], 3D printing [436], electrospinning [437], and fiber extrusion [438]. Pores are essential to cardiac tissue scaffolds because they increase vascularization [439]. Using these types of manufacturing allows for complete control of the precise porous architecture (flexibility in size, shape and composition). However, the structure of these scaffolds limit cell seeding efficacy as the majority of seeded cells remain only attached to the scaffold top surface [425]. There has been varying success on seeding efficiency and the degree of cell penetration depending on the material used to make the scaffold, pore size and interconnectivity [440]. These parameters can be manipulated by adjusting the manufacturing conditions such as solvents used, freezing rates, and freeze-dry conditions [360, 441].

1.6.2.5 Fibrous Scaffolds

Fibrous scaffolds are manufactured from a large range of materials. Electrospinning is the most widely used method and gives control over the nano/micro-scale structure with interconnecting pores, resembling natural ECM in tissue. This technique has potential to facilitate formation of artificial functional tissue while managing mechanical properties of the scaffold [442]. Like the porous scaffold, this structure is also limited by cell seeding efficacy as the majority of seeded cells remain attached to the scaffold's surface [431]. Zhang *et al.* [389] compared 2D ESC-CMs to 3D ESC-CM-derived fibrin-based cardiac patches and

reported increased conduction velocities, longer sarcomeres, and an upregulation of cardiac contractile gene expression.

1.6.2.6 Hydrogels

Hydrogels are 3D polymeric networks that are capable of absorbing large amounts of biological fluids making them hydrophilic, but not dissolved in water [443]. They are soft, spongy, and have great diffusion properties [444] allowing them to closely resemble living tissue (more than any other class of synthetic biomaterials). Their high fluid content makes them appropriate for homogenous cell seeding and encapsulation during the synthesis of the gel. The manufacture can determine conductivity, cross-linking, degradation, shape, porosity, mechanical strength, density, chemical environment and interaction with therapeutic agents [445]. This ability to control the hydrogel at the microscopic level allows them to be designed to mimic ECM, which is the prime objective when developing analogues scaffolds to host tissue. There are three main types of hydrogels: natural-based (most promising results), synthetic-based, or hybrid hydrogels [65]. All three of these types of hydrogels have been explored as preclinical therapeutic options for cardiac tissue engineering.

Engineered Heart Tissue

One noteworthy 3D construct is the engineered heart tissue (EHT), which was pioneered two decades ago by Thomas Eschenhagen and Wolfram-Hubertus Zimmermann. It is potentially one of the most fully developed cardiac 3D model to date [410, 446]. EHTs are three-dimensional, hydrogel-based muscle constructs that are restrained between posts, thereby allowing the cells to contract against a force. EHTs can be generated from isolated heart cells from adult hearts, such as chicken [410] and rat [409] as well as from ESCs [447] and iPSCs [448]. iPSC-CMs in EHTs have shown an increased mitochondrial mass, DNA content, and protein abundance compared to their 2D counterparts. Moreover, EHTs were found to generate more energy via oxidation of glucose, lactate, and FAs with a decreased reliance on anaerobic glycolysis, generating 2 to 3 folds more ATP compared to

2D iPSC-CMs [390]. Complex, multi-cellular sheets are now being generated from a mixture of iPSC-CMs combined with fibroblasts and endothelial cells [449] or with mesenchymal cells [450] which display a more mature physiology or drug responses but these are still grown in non-physiologic culture media [449,450].

1.7 Thesis Aims

iPSC-CM have an immature phenotype including a glycolytic metabolism. The aim of this thesis was to mature the metabolic status of iPSC-CMs by targeting the PPARα pathway, which regulates the transcription of genes involved in FAO metabolism. Oleic acid (OA), a fatty acid, was added to current culture protocols on Day 15 of differentiation, when CMs generally begin beating, to enhance FAO in immature beating iPSC-CMs. Knowing FAs are natural ligands for PPARα, we added WY-14643 (a PPARα agonist) to further enhance the effects of PPARα activation and induce this metabolic shift towards FA metabolism. In parallel, we explored 2D vs 3D culture to maximize maturation in our iPSC-CMs using 3D constructs made from collagen in combination with different ECM materials and in engineered heart tissue. Lastly, the "maturation cocktail" was added to cells in 3D culture to maximize maturation in our iPSC-CMs.

1.7.0.1 Specific Aims

1. Characterize changes in gene expression and substrate metabolism during maturation of iPSC-CMs cultured over time as a monolayer on a variety of extracellular matrix substrates or in 3D collagen-derived porous scaolds. Initial studies of iPSC-CMs consisted of re-seeding cells at Day 7 (end of the dierentiation protocol) but then this was pushed back to Day 15 for the 3D culture, due to improve cell survival after seeding and the ability to verify differentiation due to observation of the beating phenotype.

2. Enhance metabolic maturation in immature iPSC-CMs by adding the FA, oleic acid, into the culture medium and activating PPARα by the addition of WY-14643 for a 24 hour and 1 week period starting on Day 15 of the cardiac differentiation protocol, characterised

by changes in gene expression and substrate metabolism.

3. Compare substrate metabolism in iPSC-CMs treated for one week with oleic acid and WY-14643 in a monolayer or on 3D collagen-derived scaffolds.

4. Establish the technology of engineered heart tissue in our lab and characterise the changes in gene expression and substrate metabolism of EHT, before and after treatment with oleic acid and WY-14643.

Why, sometimes I've believed as many as six impossible things before breakfast ...

— Lewis Carroll, Alice and Wonderland

2 Methodology

2.1 Methods

2.1.1 iPSC Cell Culture

2.1.1.1 Routine Culture, Media and Matrigel Coating

Induced pluripotent stem cells were cultured on Matrigel-coated plates or flasks. For coating, the Matrigel (Corning) was diluted according to the dilution factor provided per batch in DMEM/F12 (Gibco) and pipetted into either a six-well plate (1.5 mLs/well^{-1}), 4 mLs/T25 flask, or 10 mLs/T75 flask. The plates were then incubated for 60 mins at room temperature (RT) before using immediately, or being stored for up to two weeks in a normoxic incubator for later use. The iPSCs cultures were passaged (1:10; 1-2 million cells/T75) every 4-6 days when they became 90% confluent. The cells were cultured in mTeSR^{TM}1 media (10-12 mL/T75 flask; Stemcell Technologies) which was changed daily.

2.1.1.2 Passaging Protocol

When the cells were 90% confluent, the media was removed and the wells washed with Dulbeccos Phosphate Buffered Saline (DPBS, Sigma-Aldrich). 1 mL of TrypleExpress (Life

Technologies) was then added per well (six-well plate), 4 mLs/T25 flask, or 6 mLs/T75 flask and incubated for 6-8 minutes at 37 °C. The flask was then agitated by lightly knocking against a counter top to dislodge the cells from the bottom or through the use of a cell scraper. The cells were then washed with DPBS and collected in a 15 mL falcon tube to centrifuge for 4 mins at 1300 rpm. The supernatant was discarded and the pellet re-suspended in mTeSR^{TM}1 media containing rock inhibitor (10 μM Y-27632, Merck Chemicals Ltd) and then plated into freshly Matrigel-coated plates.

2.1.1.3 Thawing Human iPSCs

Cells were removed from the liquid nitrogen and the cryogenic storage vials were placed in a tip box for 30 seconds to thaw as protection in case of the plastic exploding. The vials were then held under running warm water from the sink until the pellet inside became loose when rotated up and down. The pellet was then immediately resuspended into 10 mLs of DPBS to dilute the DMSO and centrifuged (4 mins, 1300 rpm). The supernatant was discarded and the pellet re-suspended in mTeSR^{TM}1 media containing rock inhibitor (RI) and each vial was then plated into a freshly Matrigel-coated well of a 6-well plate.

2.1.1.4 Freezing Down and Long Term Storage of iPSCs

When iPSCs were 80-90% confluent the iPSCs were dissociated using the TripleExpress dissociation protocol above. The iPSCs were then collected again in DPBS and centrifuged (4 mins, 1300 rpm). The supernatant was discarded and the pellet resuspended in 10% Dimethyl Sulfoxide (DMSO, Sigma-Aldrich) and 90% mTeSR^{TM}1 media. The suspension was placed quickly into a prelabelled Cryogenic Storage Vial (Corning) and stored in a Mr. Frosty Freezing Container (Thermo Scientific) at −80 °C for 24 hours. The vials were then transferred to liquid nitrogen for long term storage. iPSC-CMs could also be frozen down with the same protocol and thawed for use on a later date. The iPSC-CMs can take 3-7 days to recover and regain a beating phenotype.

2.1.1.5 Cardiac Differentiation

iPSCs were cultured on Matrigel-coated T75 flasks until 90% confluent. The iPSCs were then dissociated and transferred to T25 flasks coated with reduced factor (RF) Matrigel for differentiation (DMEM/F12 (Gibco) at 1/100, 384k cells cm^{-2}). The following day (Day -1, Fig. 2.1), RF-Matrigel (1/200) was added into the mTeSR^{TM}1 media and the flask was transferred from the normoxic incubator (5% CO_2 and 21% O_2) into an hypoxia incubator (5% CO_2 and 5% O_2). The next day (Day 0), the media was changed to Roswell Park Memorial Institute (RPMI) 1640 (Gibco), supplemented with 1% B27 minus insulin (Gibco), 12 μM CHIR99201 (SelleckChem), 10 $ngmLs^{-1}$ Activin A (RD Systems Europe Ltd) and 1/200 RF-Matrigel (Table 2.1). The following day, the media was changed to RPMI 1640 with 1% B27 minus insulin with no additional factors. On Day 3, half of the media was changed to fresh RPMI containing 1% B27 minus insulin with the addition of 10 μM IWP4 (Tebu-bio, final concentration of IWP4 in medium is 5 μM). On Day 5, the medium was changed again to RPMI with 1% B27 minus insulin with no additional factors. On Day 7, the media was changed to RPMI 1640, containing 1% B27 Complete (Gibco), and the flasks were switched back to a normoxic incubator (room air with 5% CO_2). From this point on the culture media was changed every two-three days. This protocol was also completed without the use of an hypoxic incubator, on occasion, and also produced beating iPSC-CMs. A full list of all the reagents needed and company catalogue numbers can be found in Table A.6.

Table 2.1: List of the cardiac differentiation compounds.

Agent	Class	Function	Concentration
CHIRR-99021	GSK-3β inhibitor	Wnt activation	12 μM
Activin-A	Recombinant protein	TGF-β signaling	10 $ngmLs^{-1}$
IWP4	Compound	Wnt inhibitor	5 μM

2.1.1.6 Dissociation and Re-plating of iPSC-CMs

Human iPSCs were differentiated into CMs as described above in RF-Matrigel-coated T25 flasks (Corning). Depending on the experiment, the iPSC-CMs were harvested anywhere

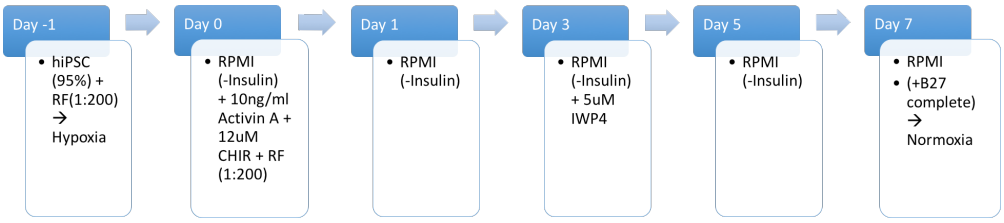

Figure 2.1: iPSC-CM differentiation protocol timeline.

between Days 7-45 of their differentiation protocol using two different collagenase-based methods and re-plated in the experimental design.

iPSC-CMs dissociated prior to Day 15 in their differentiation protocol used the following collagenase/trypsin method or the TrypleExpress method described above in Section 2.1.1.2. Briefly, the cells were incubated for 10 minutes in 2 mLs of 1 mgmLs^{-1} collagenase (Type I-A, C9722, Sigma-Aldrich, UK). An additional 2 mLs of a cell dissociation solution (40% RPMI, 40% enzyme-free cell dissociation buffer, and 20% 0.05% Trypsin-EDTA, all Gibco, Life Technologies^{TM}, UK) was added to the flask and then incubated for an additional 6 minutes at 37 °C. The flask was then agitated by lightly knocking against a counter top to dislodge the cells from the bottom or through the use of a cell scraper. In order to stop the reaction, the cells were collected in 4 mLs of foetal bovine serum (FBS) (Gibco, Life Technologies^{TM}, South America) and transferred to a 15 mL falcon tube and centrifuged. The supernatant was discarded and the pellets were washed with DPBS and subsequently re-suspended in RPMI media supplemented with B27 and RI (1:1000). These cells were then re-plated on a variety of different substrate-coated plate options (Table 2.2) or seeded on a collagen-derived scaffold. The media was changed the following day with fresh RPMI medium supplemented with B27 and subsequently every two days until cells were harvested.

Table 2.2: ECM substrate-coated plates for iPSC-CMs culture. A volume of 1 mL was used to coat a well in a 6-well plate and 500 μL per well in a 24-well plate.

ECM Component	**Manufacturer**	**Concentration**	**Coating**
Fibronectin	F1141, Sigma-Aldrich	20 μgmLs^{-1}, DPBS	>1 hr, 37 °C
Gelatin	G6144, Sigma-Aldrich, USA	1 mgmL^{-1}	>1 hr, 37 °C
Collagen I	C8919, Sigma-Aldrich, USA	100 μgmLs $^{-1}$, ddH_2O	>2 hrs, 37 °C
RF Matrigel	Corning, USA	1/100, DMEM/F12	>1 hr, RT

If the iPSC-CMs were re-plated between Day 15-45 (with a beating phenotype), a collagenase solution [collagenase II (200 U/ml, Worthington, LS004176 in HBSS minus Ca^{2+}/Mg^{2+}, Gibco, 14175-053), 1 mM HEPES (sterile filtered, pH 7.4), 10 μM Y-27632, 30 μM BTS Solution (30 mM in DMSO, PTFE-sterile filtered, TCI, 1576-37-0)] was used. Cells were washed twice with pre-warmed Ca^{2+}-free HBSS and incubated for 3.5 hours at 37 °C in the collagenase solution (added 1.5 mLs/2.5 mLs/7 mLs/14 mLs collagenase solution per 6-well/T25/T75/T175 flask respectively). Cells were titrated up to 10 times with a 10 mLs stripette at a gentle speed and placed in a universal/falcon tube. If cells were still not single-cell they were incubated for an additional 30 mins at 37 °C. The same volume of warm blocking buffer (24 μg DNase/mLs in RPMI, DNase was prepared at 12 mg/mLs 1:500) was added to each flask and washed up to 5 times and then placed in the same tube as the cell suspension. The cells were then centrifuged for 15 minutes at 100g (around 800 rpm/min^{-1}). The pellet was likely to be a bit loose, so was aspirated carefully and the final mLs taken with a pipette to avoid losing CMs. Cells were resuspended in warm RPMI (5 mLs for a small pellet, 10 mLs for a medium one, and 20 mLs for a large pellet) and titrated gently using a 10 mLs stripette again. Cells were then counted using a Countess Automated Cell Counter (Invitrogen, Fig. 2.2). A full list of all the reagents needed and company catalogue numbers can be found in Table A.6.

2.1.2 Collagen Scaffolds

Type I collagen (from bovine achilles tendon), chondroitin-4-sulfate (C4S) (from bovine trachea) and elastin (from bovine neck ligament), were selected as scaffold materials, and were all obtained from Sigma-Aldrich Ltd, UK. Scaffolds were fabricated by freeze-drying suspensions with various compositions, as required and previously described [425, 429]. The scaffolds were designed and manufactured in a collaboration with Prof. Jan Czernuszka's group in the Department of Material Science, Oxford. The scaffolds used in this thesis were made by either Dr. Qi Chen, Dr. Rabia Nazir, or Sonia Iftekhar.

For collagen and collagen-elastin scaffolds, a suspension was made with the desired weight ratio (100% collagen, 50% collagen-50% elastin, 20% collagen-80% elastin) in 0.05

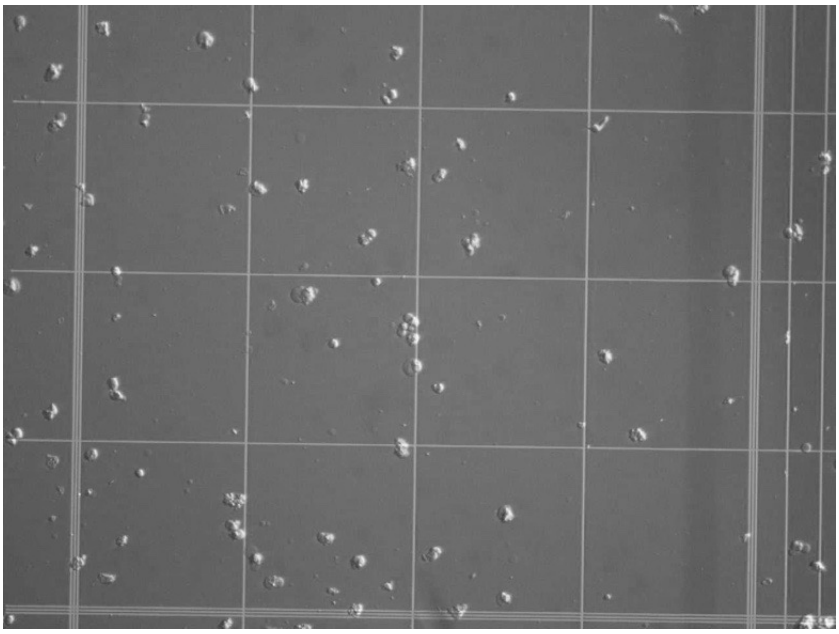

Figure 2.2: Image of single cell dissociation from the collagenase solution.

M acetic acid (pH 3.2). All the suspensions were of the same total concentration of 1% weight by volume (wt/v). For the 50% collagen-50% C4S scaffolds, collagen was first suspended in acetic acid, then the C4S was added into the suspension, and instantly the C4S co-precipitated with the collagen forming an agglomeration [425]. The suspension was reduced by a drop-wise addition of 2M sodium hydroxide until the pH value reached 7. This resulted in a homogeneous suspension of very fine collagen I-C4S co-precipitates [425, 429]. The total concentration of the suspension was 1% wt/v. The suspensions were degassed under a vacuum of 10 Pa before they were casted into polytetrafluoroethylene (PTFE) moulds to form disc-shaped scaffolds (diameter: 13 mm, height: 4 mm, Fig. 2.3). Next the moulds were frozen at −20 °C, and then freeze-dried (Christ I-5, Martin Christ) for 24 hours in a vacuum of 0.05 mbar. The ice crystals were removed by sublimation, leaving behind the porous solid scaffolds [425, 429].

2.1.2.1 Scaffold Sterilisation

The collagen-derived scaffolds were sterilised by submerging them in 100% ethanol (3 x 30 mins). For each wash they were just transferred to a new well/conical filled with fresh

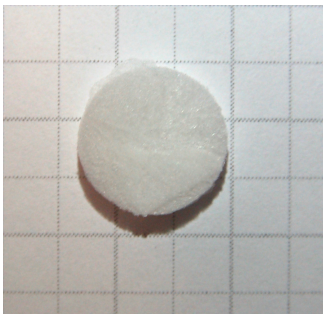

Figure 2.3: Photo taken by Dr. Arne Bruyneel of the top view of a disc-shaped 100% collagen scaffold on 5 mm graph paper.

100% ethanol. Next, in order to remove any and all traces of the ethanol, the scaffolds were washed again 3 x 30 mins with DPBS containing antibiotics (PSA made up of 100 U mLs^{-1} penicillin, 0.1 $mgmLs^{-1}$ streptomycin and 0.25 $\mu gmLs^{-1}$ amphotericin B, Sigma-Aldrich, UK) in the same manor. A final wash was conducted with RPMI with B27 supplement before being seeded with the cells.

2.1.2.2 Seeding Scaffolds with iPSC-CMs

iPSC-CMs were dissociated as described earlier, counted and then seeded onto different collagen-derived scaffolds. After sterilisation, each scaffold was placed in its own well of a 24-well plate. The top section of a 1 mL pipet tip was cut off and placed vertically on the scaffold to act as a mould (Fig. 2.4). When the scaffold was moist from the washes, the tip attached by suction to the scaffold and stood unassisted. Each scaffold was then loaded with 1,000,000 cells in 600 μL of media and 1/100 RI. The plate was then placed in the normoxic incubator for 5 hours, at which point the tips were removed and the well was loaded with an additional 500 μL of RPMI+B27 complete media with P/S. The media was changed the next day and every 2-3 days from then by manually picking up the scaffold with sterilized tweezers and transferring it to a new 24-well filled with 1.5 mLs of fresh media.

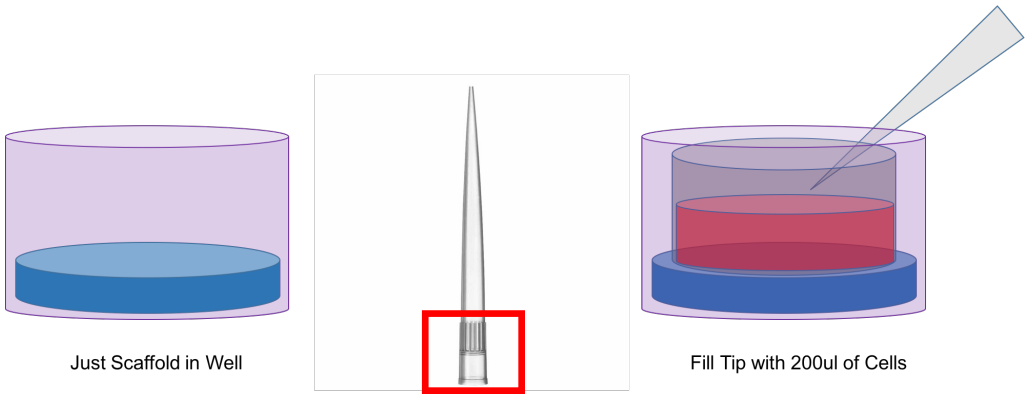

Figure 2.4: Picture diagram of loading collagen-derived scaffolds with iPSC-CMs.

2.1.3 Engineered Heart Tissue

2.1.3.1 Generation of EHT

Engineered heart tissue (EHT) was generated using the same protocol as previously described [426, 451]. 2% agarose (Invitrogen, 15510-027) was dissolved in DPBS by heating using a microwave oven for two minutes, swirled, and left to sit on the counter. While the mixture cooled, 1.6-1.8 mLs was pipetted into the wells of a 24-well plate. A teflon spacer (Fig. 2.5A) was used to create a casting mould by placement vertically along the 24-well plate while the agarose was in the process of cooling. The agarose was left for 15-30 minutes to set and then the teflon spacers were removed (Fig. 2.5B).

iPSC-CMs were dissociated using the same protocol as above and left in the pellet form after discarding the supernatant from the centrifuge spin. A master mix was prepared for EHTs in batches of 4-8. Looking at a single EHT, 10^6 iPSC-CMs were re-suspended in 92 μL of Non-CM media, 5.5 μL 2x DMEM, 0.425 μL aprotinin (Sigma). 3 μL bovine Thrombin was pipetted into individual PCR tubes. 2.5 μL of Fibrinogen was added last to the master mix and mixed by pipetting 10 times to thoroughly mix the solution. For a full list of media's composition see Table 2.3. 100 μL of the master mix was then pipetted into the PCR tubes containing the thrombin and pipetted up and down twice. Once the master mix was mixed with the thrombin the solution was transferred quickly into the agarose moulds with the silicone posts (Fig. 2.6) lined vertically along the plate. It's important to add that if there was a delay once the thrombin and fibrinogen were mixed then the

A 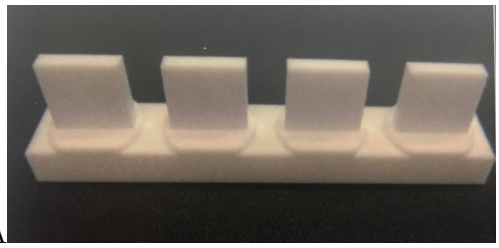 B 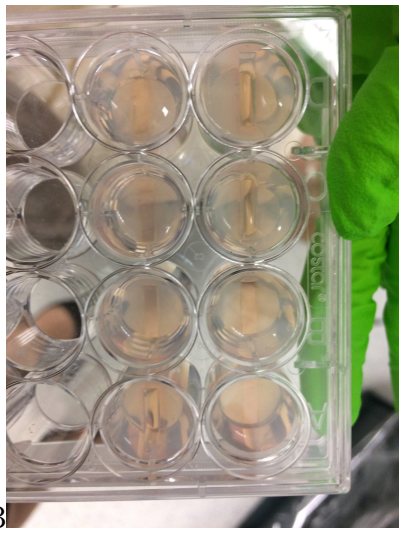

Figure 2.5: A) EHT teflon spacers and B) agarose moulds that have solidified post removal of the EHT teflon spacer.

hydrogel would solidify within the pipette tip.

A 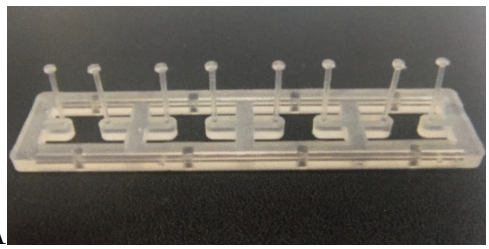 B 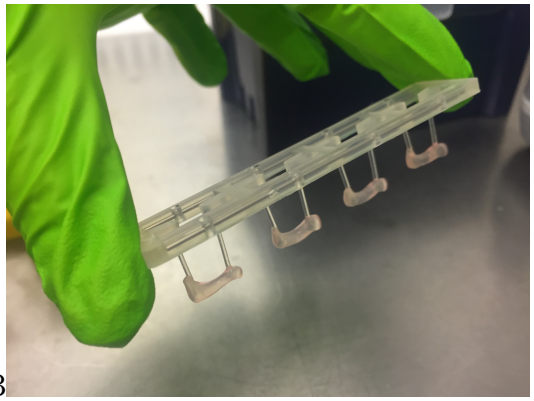

Figure 2.6: A) EHT silicone posts, B) silicone posts with EHTs attached.

EHTs were left to solidify for 90 minutes at 37 °C in a standard normoxic incubator. After the incubation, an additional 300 μL of EHT media was added to hydrate the gels and EHTs were left again for another 45-60 minutes. EHTs were then transferred out of the agarose moulds into 1.5 mLs of fresh EHT media in a new 24-well plate. EHTs were fed 1.5 mLs of new EHT media on Mondays, Wednesdays, and Fridays. Teflon spacers and silicone racks were washed in ethanol then DPBS and autoclaved for re-use. A step by step protocol can be found in Appendix A.1.3 and a full list of all the reagents needed with their company catalogue numbers can be found in Table A.6.

Table 2.3: Composition of EHT medias.

Media Name	Components
EHT media	45 mLs of DMEM (Biochrom F0415) incl. 1% P/S (Gibco 15140) + 5 mLs (10%) of Horse Serum (Gibco, 26050, Inactivated, store at −20 °C) + 50 μL (0.1%) of Insulin (Sigma, I9278) + 50 μL (0.1%) of Aprotinin (Sigma, A1153)
10x DMEM	Dissolve 670 mg DMEM powder (Gibco 52100-021, stored at 4 °C) in 5 mLs of water. Sterile Filter with 0.22 μm filter and store at (4 °C)
2x DMEM	2 mLs of 10x DMEM (Gibco 52100-021), store at 4 °C) + 2 mLs of Horse Serum (Gibco, 26050, Inactivated, store at −20 °C) + 0.2 mL of Penicillin/Streptomycin (Gibco 15140) + 5.4 mLs of water
Non-CM Media	44.5 mLs of DMEM (Bichrom F0415 incl. 1% P/S (Gibco 15140) + 5 mLs (10%) of fetal calf serum (FBS) heat inactivated + 500 μL (1%) of Glutamine (Life 25030-081, 200mM)
Fibrinogen	Sigma, F8630-5g: 200 mg/mL, Bovine. Pre-warm 0.9% NACL solution, 5g/25 mLs. Add 72.1 μL aprotinin (33 mg/mL stock) to 25 mLs of fibrinogen solution. Mix, aliquot and store at (−20 °C)
Thrombin	Biopur, BP11-10-1104, 100U/mL, Bovine Dissolve in 1.5 mLs DPBS and 1 mL water. Mix thoroughly, aliquot , and store at (−20 °C)
Aprotinin	Sigma, A1153-100mg: 33 mg/mL Dissolve 1g in 30.3 mLs of water. Mix aliquot, and store at (−20 °C)

2.1.4 Flow Cytometry

iPSC-CMs were dissociated to single-cell suspensions with the collagenase II solution (mentioned in the cell dissociation protocol) for 4 hours at 37 °C. Cells were incubated in 100 μL of Zombie Violet (ZV; 1:100, Biolegends, 405 nm wavelength) for 20 mins in the dark at RT. They were then spun down and supernatant discarded. The cells were then fixed with 4% PFA (20 min, 4 °C), washed in DPBS and stored long term in DPBS.

For the flow cytometer, 1 million cells per mL of DPBS were washed again with DPBS and incubated with blocking media (DPBS, 1% bovine serum albumin [BSA], 0.05% Triton) to limit aspecific staining (60 minutes, RT, in dark). Both conjugated and non-conjugated antibodies were used for flow cytometry as listed in Table 2.4.

For non-conjugated antibodies, the samples were incubated with the primary antibody, diluted (1:200) in blocking media (1 hour at RT, or overnight at 4 °C). The samples were then washed with DPBS containing 0.5% BSA, pelleted by centrifugation (2000 rpm, 4 minutes), and then incubated with a secondary antibody (1:200, one hour, RT), and washed

three more times with DPBS containing 0.5% BSA. For conjugated antibodies, the samples were incubated with the antibody, diluted (1:200) in blocking media (1 hour at RT, or overnight at 4 °C) and washed three times in DPBS containing 0.5% BSA.

After the last wash, each sample was resuspended in 600 μL - 1 mL of DPBS and transferred to an Eppendorf tube for flow cytometry. Each run also consisted of several controls: a negative (just fixed cells), ZV control (fixed ZV-treated cells), and secondary control (single stain antibody control). For conjugated antibodies, an isotype control was run as well. The samples were run at the Pathology Flow Cytometry facility, at the Dunn School, with the aid of Dr. Michal Maj (Dept. of Pathology, Oxford) on either the Cytek or BD FACS AriaIII machine. Each sample acquired 30,000 events and was analyzed with FlowJo Software 10.0. Analysis was presented in three plots: the 1st was a graph of side scatter (SSC-A) vs forward scatter (FSC-A) and gated down the diagonal for singlets. The next was graphed as ZV (405 nm) vs FSC and gated for live cells (the bottom population). For staining for cTNT with a FITC+ antibody, the third plot was graphed as ZV (405 nm) vs FITC (488 nm) to find the cTNT+ population (bottom right). This last graph was then presented as a histogram.

Table 2.4: Flow Cytometry Antibodies.

Antibody	**Manufacturer**	**Conc.**	**Wavelength**
Zombie Violet	Biolegend	1:200	405nm
Anti-Cardiac Troponin T	Abcam, ab10214	1:200	
Anti-Cardiac Troponin T, Conjugated	MACS:130-106-745	1:200	FITC
Donkey anti-Mouse IgG (H+L) Secondary	ThermoFisher: R37114	1:200	Alexa Fluor 488
Anti-α-Actinin (Sarcomeric), Mouse monoclonal	Sigma Aldrich, A7732	1:200	
Donkey anti-Mouse IgG (H+L) ReadyProbes Secondary	Thermo Fischer	1:200	Alexa Fluor 594

2.1.5 Quantitative PCR

2.1.5.1 RNA Extraction

Cells were collected using the dissociation methods described above and stored as pellets. Scaffolds and EHTs were isolated three at a time and could also be stored at −80 °C. It is important to note that the whole EHT was taken including the edges around the post to maximize the amount of RNA retrieved. Monolayer cells were thawed and lysed using RLT buffer supplemented with β-mercaptoethanol (B-ME) (Sigma-Aldrich, Germany) (as described in the Qiagen RNeasy protocol). Collagen scaffolds and EHTs were digested by incubation in TrypleExpress for 3 minutes at 37 °C. RTL buffer supplemented with the BME was added and then they were shredded using a QIAshredder^{TM} gun, prior to being processed further using the Qiagen RNeasy Kit (Qiagen, UK) for total ribonucleic acid (RNA) extraction according to the manufacturer's protocol.

Briefly, the same volume (600 μL) of 70% ethanol was added to the lysed samples, which were then loaded into RNeasy Mini spin columns and centrifuged (15 s, >8000 g). The flow through solution was discard and the column was then washed with 700 μL of RW1 (centrifuged for 15 s, >8000 g, discard flow through). Next, the column was washed twice with 500 μL RPE buffer (centrifuged for 15 s and 2 mins, >8000 g, discard flow through), and dried (centrifuged for 1 min, >8000 g, discard flow through). Finally, the RNA was eluted twice from the column using 20 μL of ddH_2O (1 min, >8000 g). RNA was then stored at −80 °C for further use.

2.1.5.2 cDNA Analysis

RNA concentration was determined using NanoDropUV spectrometry (NanoDrop ^{TM} Lite, Thermo Fisher Scientific), and 1 μg of RNA was converted into complementary deoxyribonucleic acid (cDNA) using a high capacity cDNA reverse transcriptase kit (Applied Biosystems^{TM}) according to the manufacturer's protocol. Briefly, 10 μg of RNA, 2 μL RT random primers, 2 μL RT buffer, 1 μL MultiScribe Reverse Transcriptase enzyme, 0.8 μL deoxynucleotide triphosphate (dNTP) mix and 4.2 μL of ddH_2O was used to make a total

volume of 20 μL per reaction. The samples were then incubated in a SensoQuest Basic Thermal Labcycler (SensoQuestGeneFlow): 10 min at 25 °C, 120 min at 37 °C, and 5 min at 85 °C. cDNA samples were stored at −20 °C for further use.

2.1.5.3 Primer Design

The primers used in this thesis for human iPSCs and iPSC-CMs, can be found in Table A.1. All primers were previously validated via melt curves (Fig. A.3) and percent efficiency recorded (Table A.1). When designing the thermocycler run, the denaturation was set to 95 °C for 5 minutes on the initial cycle and 30 seconds on the rest. The annealing temp was calculated 5 °C below the primer melting temperature (Tm) of the Primers (no lower than 40 °C) for 30 seconds. And the extension was set to 72 °C for 1 min/kb of expected products and 5-10 on the last cycle. There were 30 cycles.

Housekeeping genes were assessed for stability and consistency (Fig. 3.12). None of the housekeeping genes were significantly up or down regulated during differentiation or treatment in culture.

2.1.5.4 qPCR Reaction

qPCR was performed using either the SYBR detection method (Applied Biosystems^{TM}, REF 4309155, UK) or TaqMan Gene Expression Assay (Invitrogen) and TaqMan Fast Advanced PCR Master Mix (2x) (Invitrogen).

Briefly for the SYBR detection method, a 20 μL reaction volume was used per reaction, containing 12.5 ng cDNA, 10 μL SYBR reagent master mix, 3 μL of water, and 2 μL primers (10 μM stock). The samples were loaded in a 96-well format qPCR plate (MicroAmp Fast, Applied Biosystems ^{TM}, China), and a standard SYBR cycle (Table 2.6) was started using a StepOnePlus^{TM} Real-Time PCR System (Applied Biosystems^{TM}).

For the Taqman assay, amplification was carried out using TaqMan Fast Advanced PCR Master Mix (2x) (Invitrogen) according to the suppliers protocol. It involved a 10 μL reaction using 12.5 ng of cDNA, ddH_2O and the Taqman assays (Table A.2).

Table 2.5: qPCR reaction: two step SYBR green protocol (30 cycles).

Step	Time (s)	Temperature (°C)
Polymerase activation (Hold)	600	95
Denaturate	15	95
Anneal/extend	30	60

Table 2.6: qPCR reaction: Taqman Fast Advance Thermo cycler protocol (40 cycles).

Step	Time (s)	Temperature (°C)
UNG incubation (Hold)	120	50
Polymerase activation (Hold)	120	95
Denaturate	1	95
Anneal/extend	20	60

2.1.5.5 Analysis of qPCR Data: $\Delta\Delta C_T$ Method

The traditional method for relative quantification of qPCR data is the $\Delta\Delta C_T$ method (Livak Method [452]), plotting the fold change of $2^{-\Delta\Delta C_T}$.

Expression levels are measured by the cycle threshold (C_T) defined by the number of cycles it takes a sample's fluorescent signal to reach the threshold of background signal. The C_T of each target gene is normalized first to the average C_T value for housekeeping genes and then a second time to the experimental control sample. The $\Delta\Delta C_T$ analysis is calculated with the following steps:

- Calculate the average C_T per target gene (TG) and housekeeping gene (HKG)
- Calculate ΔC_T = C_T of TG - C_T of HKG
- Calculate $\Delta\Delta C_T$ = ΔC_T of test sample - ΔC_T of control sample
- Calculate and plot fold change: $2^{-\Delta\Delta C_T}$
- All statistical differences were assessed using the $2^{-\Delta\Delta C_T}$ values.

2.1.6 Total DNA Quantification

For determination of total cellular DNA, the CyQuant Cell Proliferation Assay kit (Invitrogen) standard methods were used. Cells were grown and treated in a 96-well plate (10k cells/well) and then frozen at $-80\,^{\circ}\mathrm{C}$ for 24 hours. The plate was then thawed at RT and re-suspended in a RNase treatment (1X cell-lysis buffer supplemented with 180 mM NaCl, 1 mM EDTA, and 1.35 Kunitz of RNase A) and incubated for 1 hour at RT. An equal volume of 2X solution of CyQuant GR dye diluted in cell-lysis buffer was added to each sample and incubated for 2-5 minutes at RT and the fluorescence signal was measured using a fluorescence microplate-reader with filters appropriate for around 480 nm excitation and around 520 nm emission maxima. Results were evaluated by plotting the samples' fluorescence signal against a generated standard curve prepared with serially diluted 200 μL samples of bacteriophage DNA using CyQuant GR/cell-lysis buffer (as prepared in preparing the reagent) with concentrations ranging from 50 pg/mLs to 1.0 μg/mL.

2.1.7 Immunocytochemistry

The cells were washed with DPBS, fixed in 4% PFA (20 mins, $4\,^{\circ}\mathrm{C}$), and washed again in DPBS. Following fixation, the cells were then permeabilized by incubated with 0.5% triton X for 10 mins at RT, then washed with DPBS. Then, the cells were incubated in blocking media (DPBS, 2% BSA) to limit aspecific staining for 60 mins at RT. Next, the samples were incubated with primary antibody (Table A.3), diluted in blocking media (1 hour at RT, or overnight at $4\,^{\circ}\mathrm{C}$). The samples were then washed with DPBS, incubated with secondary antibody (one hour, in the dark, RT, Table A.4), and washed twice again. DAPI stain (diluted in DPBS) was added for 5 minutes at RT, and then the slides were rinsed twice more in DPBS. The slides were mounted with 50:50 DPBS/glycerol and stored in the dark at $4\,^{\circ}\mathrm{C}$ until ready to be imaged. Images were taken using an Olympus Confocal Microscope at the Dunn School by either myself or Rita Al-Onaizan.

2.1.7.1 Mitotracker Staining

MitoTracker Red CMXRos dye (M7512; Invitrogen) diffuses passively across the mitochondrial membrane in live cells and accumulates in active mitochondria.

iPSC-CMs were incubated with RPMI+B27 media with 50 nM of MitoTracker Red CMXRos dye for 15 minutes at 37 °C. The cells were then washed twice with DPBS and fixed in 4% PFA for 20 minutes at 4 °C. After fixation, the cells were washed with DPBS and stored at 4 °C for further staining as described above or imaging.

Fixed cells were imaged using an Olympus Confocal Microscope and Image J was used to analyze the fluorescence intensity of MitoTracker Red CMXRos dye in the cells. The level of fluorescence of randomly selected cells was analyzed by measuring the grey value of stained areas and unstained areas (background). Fluorescence intensity was calculated by taking the average and StdDev of 10 mean grey values of selected cells minus the mean fluorescence of background [453].

2.1.7.2 Oil Red O Staining

The Lipid (Oil Red O) Staining Kit (MAK194; Sigma-Aldrich) was used to detect and stain neutral lipids in cultured iPSC-CMs. iPSC-CMs were washed twice with DPBS and fixed with 4% PFA at 4 °C for 20 minutes. After fixation, cells were washed with DPBS and stored at 4 °C for further staining as described above or for imaging. Fixed cells were then washed again with DPBS and 60% isopropanol was added to the cells and incubated for 5 minutes. The isopropanol was discarded and the cells were covered evenly with Oil Red O Working Solution. The plates were rotated and incubated for 10-20 minutes. The Oil Red O solution was discarded and cells were washed 25 times with water until no excess stain was seen. DAPI was added and incubated for 1 minute and discarded. The cells were again washed 3 times with water. Cells were left covered in water and were imaged using an Olympus Confocal Microscope. Lipid droplets appeared red and nuclei appeared blue.

2.1.8 Assessing Cell Metabolism

The main approaches for the investigation of substrate metabolism included the measurement of metabolic fluxes using radio-labelled substrates and of oxygen consumption (Fig. 2.7).

2.1.8.1 AlamarBlue Cell Viability

In a 24-well plate format the iPSC-CMs were treated using the standard manufacturers protocol. AlamarBlue reagent (ThermoFisher Scientific) was added (1/10) to the media to create an ABA solution and 1 mL was added directly into each well. The plates were then incubated at 37 °C for 4 hours to allow cells to convert resazurin to resorufin. A 1 mL negative control was collected of the ABA solution and stored in the fridge for the duration of the 4 hours, while a 1 mL positive control was incubated in a heat block at 90 °C for 4 hours to get a maximum colour change. After the 4 hours, 200 μL of each sample was collected and transferred to a 96-well plate where the absorbance was read at 570 nm (using 600 nm as a reference wavelength) in a plate-reader (Multiskan FC, Thermo Fisher Scientific). Results were evaluated by plotting the absorbance signal calculated by:

$$\text{Percent of ABA Reduction} = (\text{Sample-Negative})/(\text{Positive - Negative}) \tag{2.1}$$

2.1.8.2 ^{3}H Palmitate Oxidation

Palmitate oxidation rates were determined by the production of ^3H_2O from ^{3}H-palmitate in the electron transport chain as previously described [454, 455] (Fig. 2.8). A full list of all the reagents used and company catalogue numbers can be found in Table A.6.

On the day of the experiment, culture media was removed and the cells were rinsed with DPBS. The cells were then cultured with 1.5 mLs of the incubation media containing 2% BSA, 0.3 mM palmitate, and doped with 0.2 μCi/mL of Palmitic Acid, [9,10-^{3}H(N): 1mCi-37MBq] (PerkinElmer) per well of a 24-well plate (1.5 mLs per 1.9 cm^2 growth area). The palmitate had to be heated in advance to become liquid and added at the same time as the ^{3}H palmitate so both types have equally opportunity to bind to the BSA in the media.

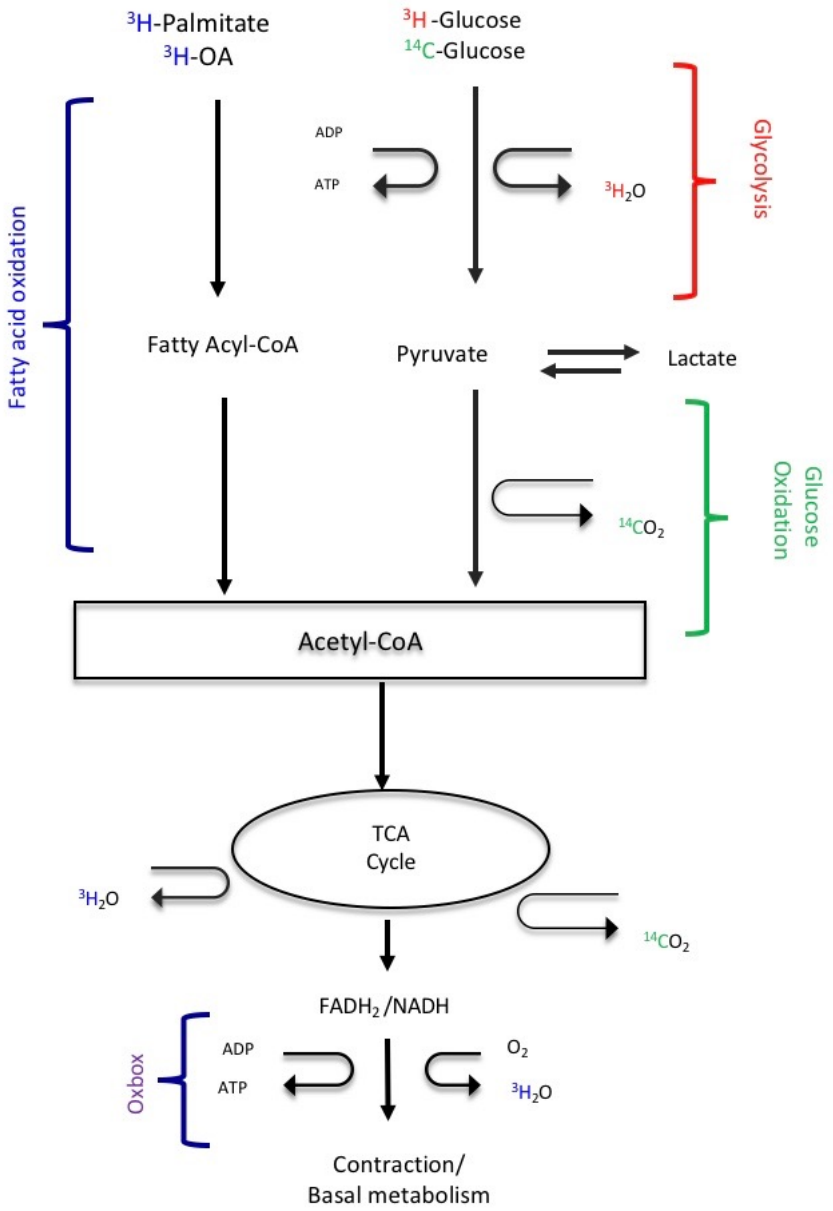

Figure 2.7: Overview of radiolabeled energy metabolic pathways in the heart, adapted from [239].

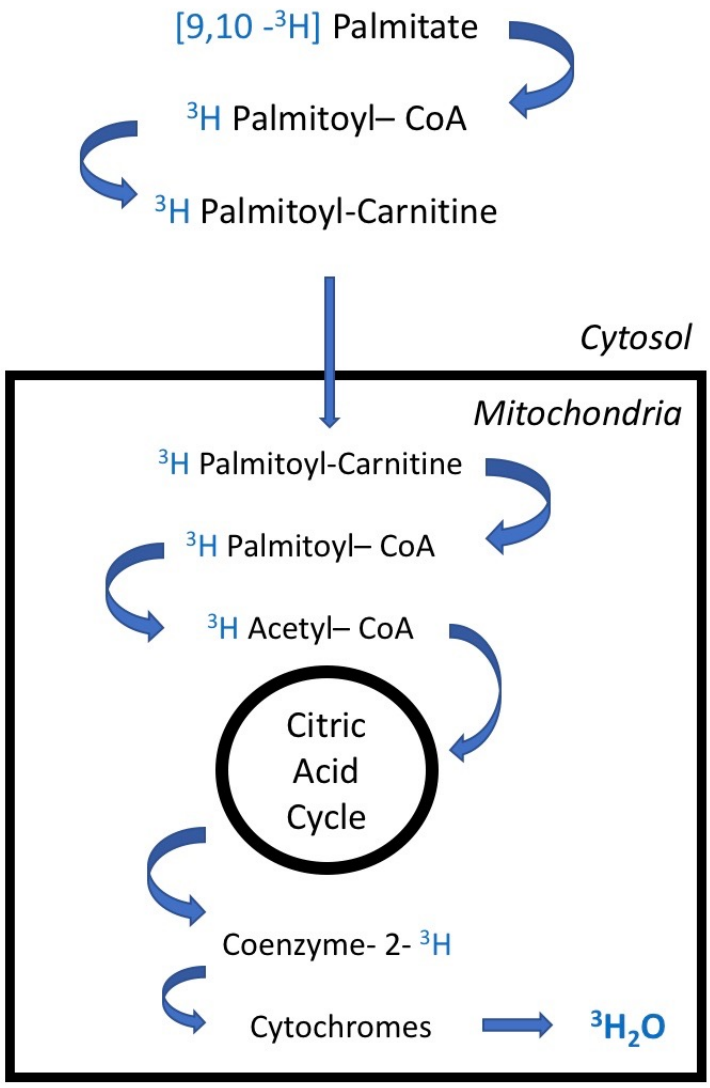

A

Figure 2.8: Tracking the radiolabeled substrates through palmitate oxidation, adapted from [454]. The square represents mitochondria.

Cells were cultured in a normoxic incubator (5% CO_2 and 21% O_2) at 37 °C for 8 hours. Each experiment also had a sample taken at timepoint zero where 4 mLs of media were collected that had not been exposed to any cells. During the incubation, ^3H_2O was released into the incubation media. After the incubation, the supernatant containing both ^3H_2O and remaining ^{3}H-palmitate was collected and frozen down at −20 °C so the ^3H_2O could be separated at a later date via Folch extraction.

A volume of 1.88 mLs of chloroform: methanol (1:2 v/v) solution, 625 μL chloroform and 625 μL KCl-HCl solution (2 M KCl, 0.4 M HCl) were added to 0.5 mLs of perfusate sample in a 15 mLs falcon tube. The mixture was rotated on a laboratory Stuart rotator SB3 at 40 rpm for 10 minutes and left in the hood for 1 hour to allow the different layers to separate. The top aqueous layer was then removed with a glass pipette and bulb into a new 15 mLs falcon tube while the organic (bottom) layer was discarded. To the extracted aqueous solution, 1 mL chloroform was added, with 1 mL methanol and 0.9 mLs KCl-HCl solution before it was mixed by rotation for another 10 minutes at 40 rpm and left to separate again for 1 hour in the hood. The top aqueous layer was once again removed via a glass pipette and retained, and 0.5 mLs (in duplicate) of this phase was added into a scintillation vial containing 10 mLs of Ecolite liquid scintillation cocktail (MP Biomedicals, USA). The radioactivity (cpm) of the sample was counted using a Tri-Carb 2800TR Liquid Scintillation Analyzer (PerkinElmer). In addition, a duplicate of 0.5 mLs of just the spiked media (not added to any cells) was extracted as a negative control to determine background noise. A second duplicate of 0.5 mLs of the spiked media (non-extracted) was added directly into scintillation vials as a positive control to determine the specific activity of the medium. For each sample, the machine will give two cpm readings (A and B). In calculating palmitate oxidation rates, the sample cpm used was an average of the cpmA and cpmB minus the negative control (background noise). Palmitate oxidation rates were calculated using the equations:

Total Palmitate oxidation per (nmol/10^6/hour):

$$\frac{17.1 * \ Sample\, cpm}{Counts\, per\, Mole\, Palmitate}/(\text{Cell Count})/(8 \text{ hours}) = \ nmol\, per\, 10^6\, cells\, per\, hour \quad (2.2)$$

The dilution factor of 17.1 was due to the dilution of the buffer aliquot during the extraction protocol [455]. As 0.5 mLs aliquots were diluted in scintillation fluid and counted for ^{3}H radioactivity, to normalise to count per mL values were multiplied by 2.

2.1.8.3 ^{3}H Oleic Acid Oxidation

Oleic acid oxidation rates were determined by the production of ^3H_2O from the electron transport chain as described by [454, 455]. Cells were cultured with incubation media that contained 2% BSA, 400 μM OA, and doped with 0.2 μCi/mL of Oleic Acid, [9,10-^{3}H(N): 1 mCi-37MBq] (PerkinElmer). The OA has to be left at RT in advance to become liquid and added at the same time as the ^{3}H OA so both types have equally opportunity to bind to the BSA in the media. On the day of the experiment the cells were washed with DPBS and 1.5 mLs of incubation media is added per well, incubated for 8 hours, and supernatant extracted as described in the palmitate oxidation protocol above.

2.1.8.4 Glycolytic Flux

Glycolytic rates were determined through the conversion of ^{3}H-glucose to ^3H_2O via enolase which converts 2-phosphoglycerate to phosphoenolpyruvate and releases H_2O as a byproduct (Fig. 2.9). A full list of all the reagents needed and company catalogue numbers can be found in Table A.6.

On the day of the experiment, culture media was removed and cells were rinsed with DPBS. The cells were then cultured with 1.5 mLs of the incubation media doped with 0.2 μCi/mL of Glucose, D-[5-^{3}H(N): 1 mCi-37MBq] (PerkinElmer) per well of a 24-well plate (1.5 mLs per 1.9 cm^2 growth area). Cells were cultured in a normoxic incubator (5% CO^2 and 21% O_2) at 37 °C for 8 hours. As in the palmitate oxidation experiments, 4 mLs of media at the zero hour time point was collected as well. During incubation, ^3H_2O

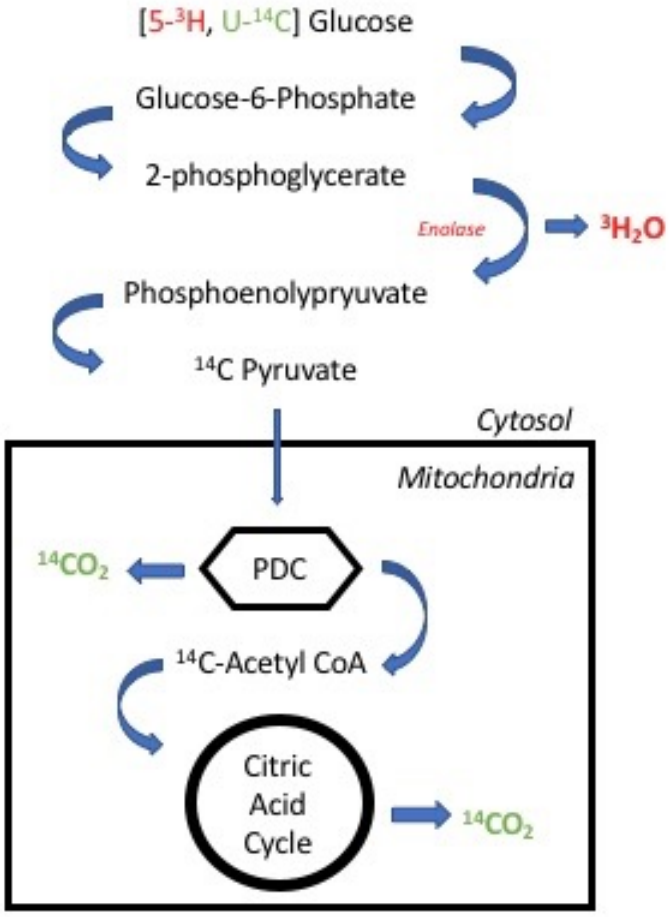

A

Figure 2.9: Tracking the radiolabeled substrates through glucose oxidation, adapted from [454]. PDC stands for pyruvate dehydrogenase and the square represents mitochondria.

was released into the incubation media. After the incubation, the supernatant containing both ^3H_2O and remaining [5-^{3}H]-glucose was collected and frozen down at $-20\,^{\circ}C$ so the ^3H_2O could be separated at a later date using the ion-exchange chromatography separation (Dowex) method [456–459].

The ^3H_2O was separated from the ^{3}H-glucose using a Dowex 1 x 4 chloride form, 100-200 mesh (Sigma, UK) anion exchange column. Preparation of the Dowex was made by adding 250 g of Dowex resin into a solution containing 1.25 M NaOH and 1.61 M boric acid. The mixture was then mixed gently and the beads were repeatedly washed with distilled H_2O until the mixture reached pH 7.5. The exchange columns were prepared in glass Pasteur pipettes (VWR 612-1701). The bases of the pipettes were filled with glass wool (Fig. 2.10) and placed in a rack (Fig. 2.11). The glass pasteur pipette was filled up to 2/3 with Dowex (Fig. 2.10). The columns were washed through twice with distilled H_2O and allowed to drain. Scintillation vials were filled with 10 mLs of scintillation fluid (Ecolite liquid scintillation cocktail, MP Biomedicals, USA), and placed underneath the columns to collect samples (Fig. 2.11). 200 μL of the collected incubation media from each sample was added to the Dowex column, and incubated for 15 minutes, allowing the ^{3}H-glucose to bind to the column and ^3H_2O to be eluted into the vials. Each dowex column was washed twice with 1 mL of distilled H_2O to wash down any residual samples. The scintillation vials were collected after the columns were fully drained and the radioactivity (cpm) was measured using a Tri-Carb 2800TR Liquid Scintillation Analyzer (PerkinElmer).

In addition, a duplicate of 200 μL sample at time zero was run through the dowex column and another added directly into scintillation vials in order to have its radioactivity counted to determine the specific activity of the buffer. For each sample, the machine will give two cpm readings (A and B). In calculating the glycolytic rates, the sample cpm used is an average of the cpmA and cpmB minus the 0 cpm. Glycolytic rates were calculated using the following equation:

Total glycolytic flux per (nmol/10^6/hour):

$$\frac{Sample\ cpm}{Counts\ per\ Mole\ Glucose}/(\text{Cell Count})/(8\text{ hours}) = nmol\ per\ 10^6\ cells\ per\ hour \quad (2.3)$$

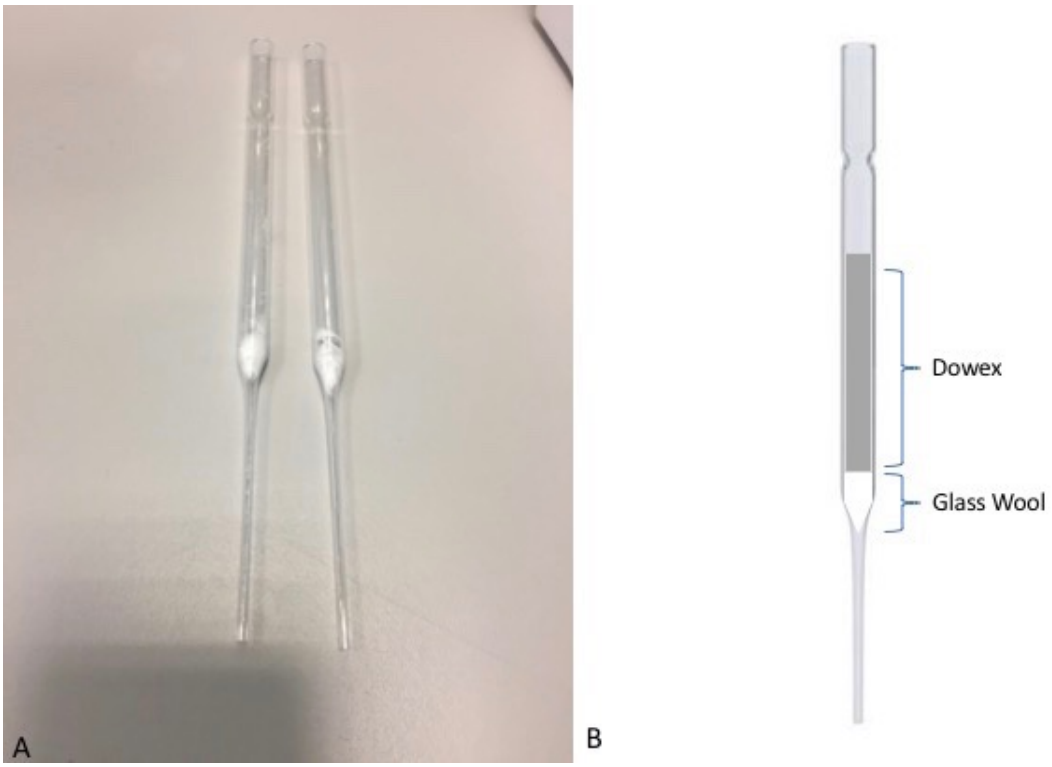

Figure 2.10: A) Glass pipets filled with the appropriate amount of glass wool. B) Diagram on proportions of Dowex and glass wool in the glass pipettes.

A

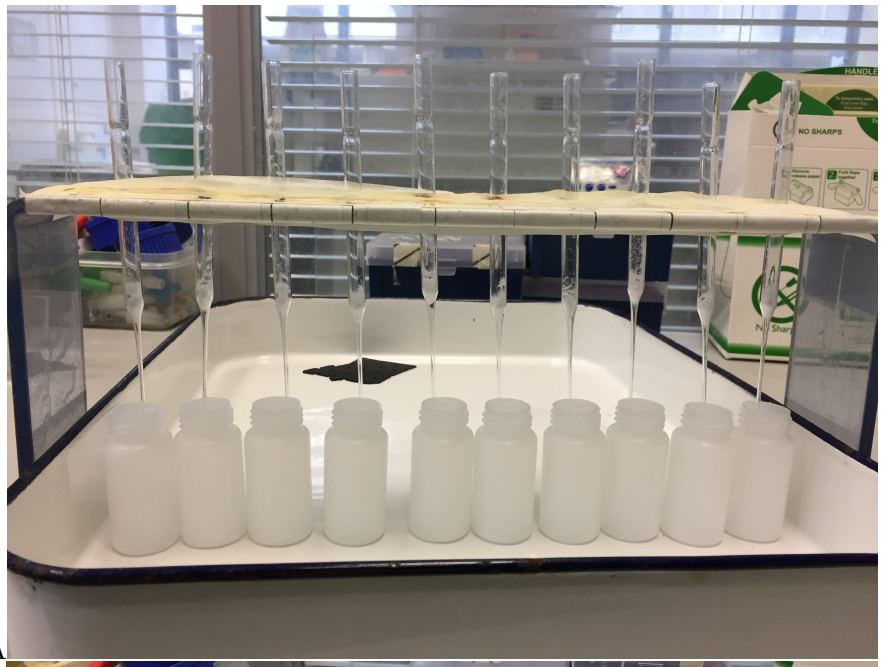

B

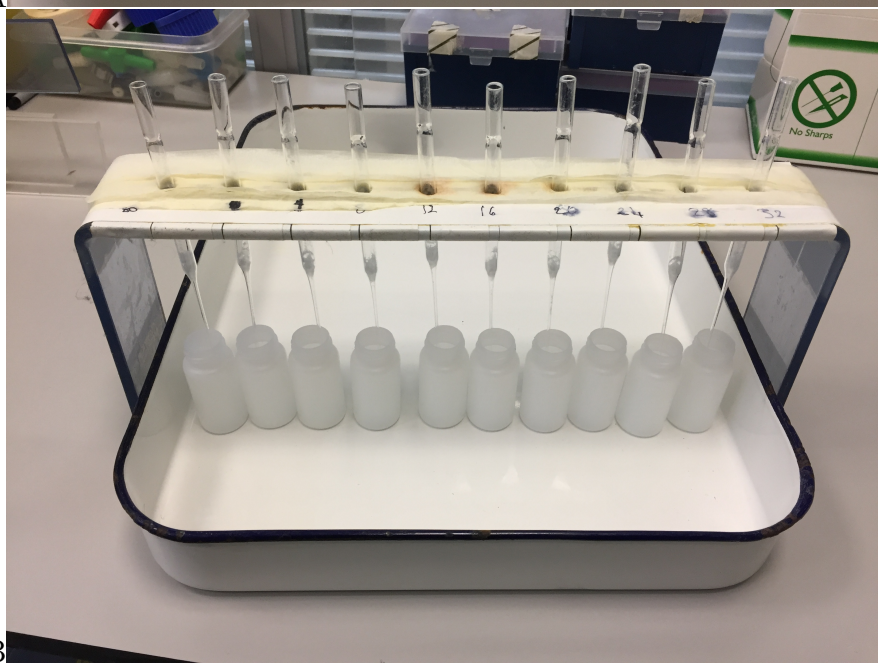

Figure 2.11: A) Side view and B) top view of rack holding 10 dowex columns. Each sample is held through a punctured hold covered in tape to keep them snug in place.

2.1.9 ^{14}C Glucose Oxidation

Glucose oxidation were determined through the use of a standard $^{14}CO_2$ capture technique [460,461] for evaluating the oxidation and decarboxylation reactions of substrates. Cells break down glucose and release carbon dioxide during the passage of acetyl-CoA through the citric acid cycle (Fig. 2.9). By labeling the glucose with a ^{14}C trace, the experimenter can quantitatively collect the $^{14}CO_2$ byproduct [454,455]. Collins *et al.* [344] had adapted these original methods to allow substrate oxidation rates of cells to be evaluated in a 24-well culture plate format. With further modifications we adapted their protocol again, published in Board, **Lopez**, *et al.* [326] (Appendix B) that allows the investigator to evaluate the $^{14}CO_2$ production of cells in culture with the ability to test multiple conditions simultaneously.

Cells were prepared in a 24-well or 6-well plate under experimental conditions. Cultured cells were washed with DPBS to remove remaining traces of the high-glucose culture media. 1 mL of RPMI-low glucose media (Sigma, D5546, 5.5 mmol/L) doped with 0.2 μCi/mL of Glucose, [D-[^{14}C(U): 1 mCi-37MBq] was added to each well of a 24-well plate. Depending on the experimental questions, the addition of fatty acids was added to the cocktail (2% BSA, 400 μM oleic acid or 0.3 mM palmitate). In addition, a well without cells, containing just the media with the radiolabeled glucose was used as a negative control.

The $^{14}CO_2$, produced from the glucose oxidation, was trapped on KOH-soaked filter papers covering the inside of an upside down 24-well plate that was used as a lid for the apparatus. During preparation, 1 mL of fresh 40% KOH dissolved in water, was pipetted onto rolled up Whatman grade 1 qualitative filter paper (Sigma-Aldrich, 1001-110) (Fig. 2.12) that were placed in each lid corresponding to an experimental well. A perforated rubber gasket, that had holes corresponding to each well of the 24-well plate, was placed between the two plates (Fig. 2.12). The plates were then sealed with parafilm (Sigma, P7793) to make sure there was no possibility for CO_2 leakage. The plate sandwich was then tightly screwed into a metal frame to hold down the plates and create a seal (Fig. 2.13). The whole apparatus was then placed inside a normoxic incubator (5% CO_2 and 21% O_2) and remained sealed for the length of the experiment (8 hours at 37 °C).

To trigger the release of the $^{14}CO_2$, 1 mL of 70-72% perchloric acid was injected through

the top holes in the top plate, through the gasket and into the well after the 8 hour incubation, to release the ^{14}C that was trapped as bicarbonate in the media. The new hole was instantly resealed with new parafilm. The samples were then kept for an additional 1-2 hours to allow for the complete release of the trapped $^{14}CO_2$ in the media as bicarbonate. Filter papers containing trapped $^{14}CO_2$ were manually placed into individual scintillation vials containing 10 mLs of Ecolite liquid scintillation cocktail (MP Biomedicals, USA) and analysed using a scintillation counter.

In calculating the glucose oxidation rates, only the sample cpmB minus the 0 cpm (negative control) was used. Glucose oxidation rates were calculated using the following equation:

Total glucose oxidation per (nmol/10^6/hour):

$$\frac{Sample\,cpmB\ -\ background}{umoles\,CO_2\,released}/(\text{Cell Count})/(5\text{ hours}) = nmol per 10^6 cells per hour \quad (2.4)$$

2.1.9.1 Oxygen Consumption Rate Measurements Using the Clark Oxygen Electrode

The rate of mitochondrial oxygen consumption (OCR) can be measured by using the Clark-type oxygen electrode [347, 348, 462–464]. Cells were rinsed with DPBS and dissociated into single cells using the dissociation protocol explained above. They were then counted into two million cells per 15 mLs falcon tube and centrifuged (1300 rpm, 4 minutes). Supernatant was discarded and the cell pellet was resuspended in 600 μL of respiration solution. There were two different respiration solutions used: Gimish (100 mM KCL, 50 mM MOPS, 1 mM EGTA, 5 mM KH_2PO_4, and 1 mg/mL BSA, prepared fresh on the day of the experiment) or the media in which the cells were routinely cultured in (RPMI+B27). Gimish is meant to mimic the intracellular cytoplasm in a cardiac cell, which is used normally for oxygen consumption measurements in isolated mitochondria, but the potassium levels might be too high to be a good extracellular medium for cells.

The Clark-type oxygen electrodes were embedded in the reaction chambers set to 37 °C. 600 μL of the cells in respiration solution were transferred into the respiratory chambers.

A

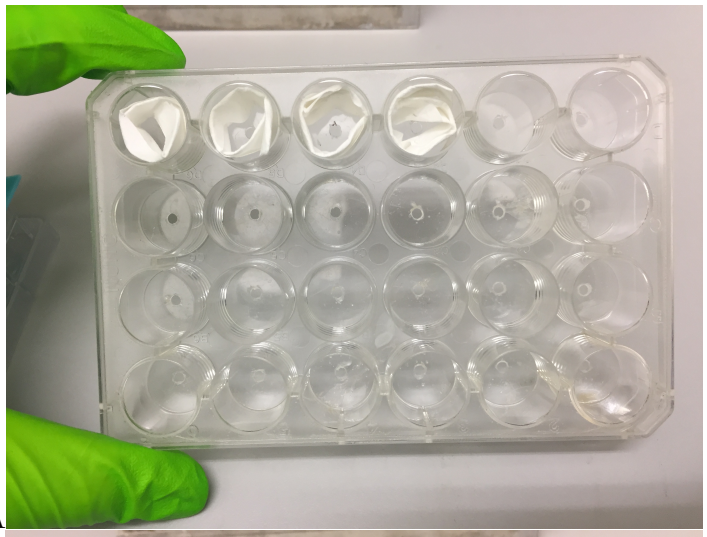

B



C



Figure 2.12: The apparatus constructed for trapping $^{14}CO_2$ A) with the KOH-soaked filter paper in the top right well B) with a blue rubber gasket C) the plate sandwich.

A



B

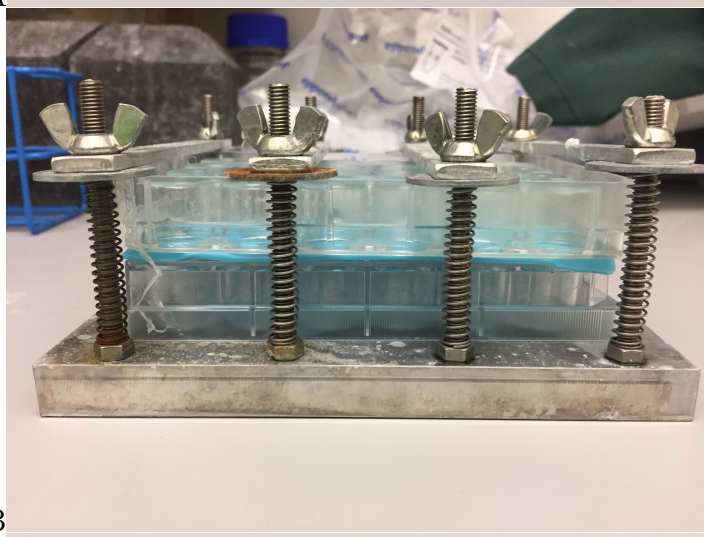

C

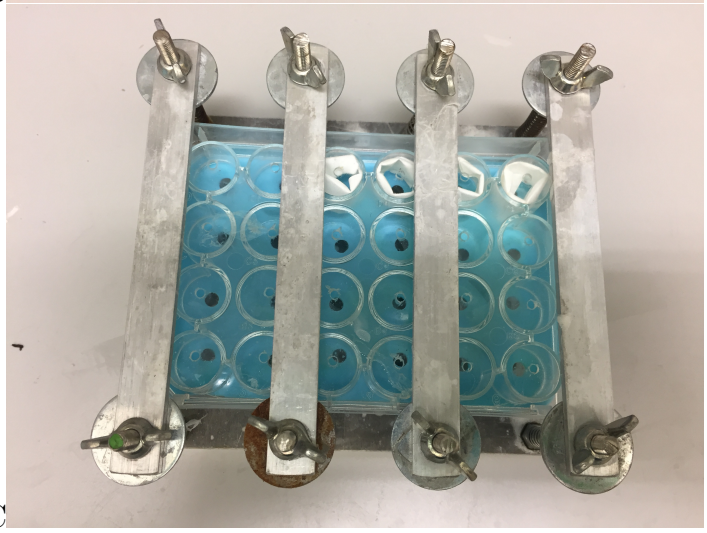

Figure 2.13: The apparatus constructed for trapping $^{14}CO_2$ A) The plate-sandwich is placed in the metallic contraption. B) side view. C) top view.

Respiration was then measured under baseline (un-stimulated conditions), and again after the addition of the energy substrate of interest (10 mM pyruvate + 5 mM malate, or 400 μM oleic acid), the ATP synthase inhibitor oligomycin (2 mM), and the metabolic uncoupler, carbonylcyanide-p-trifluoromethoxy-phenylhydrazone (10 mM FCCP) (Fig. 2.14 and Table 2.7). Due to slow penetration of the 3D constructs, two rounds of FCCP was used for in all conditions to confirm uniformity.

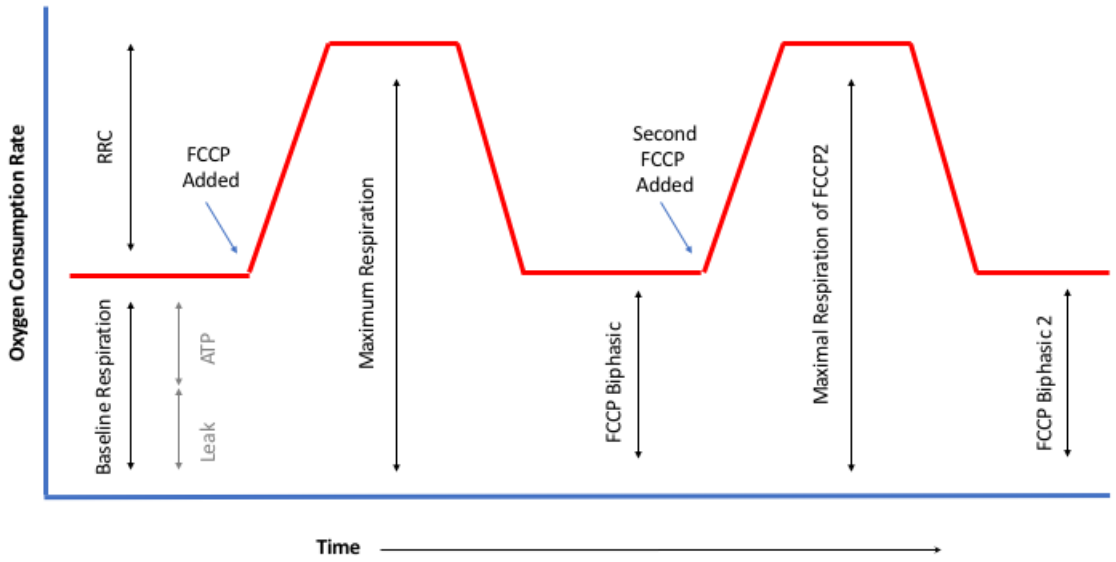

Figure 2.14: Measurement of the OCR at baseline and maximal respiration in iPSC-CMs. OCR of iPSC-CMs were measured at baseline and post FCCP (maximal respiration). Baseline respiration consists of ATP-synthesis linked OCR (ATP) and ATP synthesis independent OCR (leak). Adapted from [465].

2.1.10 Statistics and Data Analysis

All experimental samples were run in either duplicate or triplicate and in biological repeats. Gene expression data and ABA reductions are all presented as means ± standard errors. Differences between samples were considered significant if $p<0.05$ (i.e probability of the results occurring by chance <5%), as determined using either a Student's T-test or a one-way Analysis of Variance (ANOVA). Experiments with multiple variables and test groups were assessed using a two-way ANOVA with a Tukey post-hoc test in GraphPad Prism 7.

Table 2.7: The different stages of mitochondrial respiration recorded by a Clark-type oxygen electrode.

Stage	Treatment
Baseline Respiration	None
Respiring on Energy Substrate	Pyruvate (10 nM) and Malate (5 mM) or Oleic Acid (400 μM)
ATP Synthase Inhibitor	Oligomycin (2 mM)
Maximal Respiration Capacity FCCP Biphasic	FCCP (10 mM)
Maximal Respiration Capacity FCCP2 Biphasic	FCCP (10 mM)

2.1.10.1 T-Test

The T-test, also referred to the Students T-Test, expresses the difference between two means. The T-test also has the ability to convey how significant the differences are or if they could have happened by chance. The T-score is a ratio of the difference between two groups and the difference within the groups. The larger the T-score, the more difference there is between groups. A smaller T-score correlates to more similarity between groups. Each T-value is associated with a p-value, which tells if the results occurred by chance. P-values range from 0% to 100% and are written as a decimal. For example, a p-value of 1% is 0.01 or 5% is 0.05. Generally, p-values below 0.05 indicate an acceptable probability that the data did not occur by chance.

2.1.10.2 Analysis of Variance (ANOVA)

One-way ANOVA

One-way Analysis of Variance (ANOVA) is a statistics test that determines if the means of three or more samples are different. ANOVA looks at the spread of a group of means and compares them to how much you would expect the spread to be if all the samples were from the same population or had no difference between them.

The one-way ANOVA uses the F-test to determine whether the variability between group means is larger than the variability within the groups. A F-statistics is this ratio between two variances. A variance is basically a measurement of how far the data is scattered from

the mean. The F-statistic is measured by two independent chi-square variables divided by their degrees of freedom, expressed as the ratio shown below. If the null hypothesis is true (in other words, if no true difference exists between the groups), then the F ratio should be close to 1.

$$\text{F-Statistic} = \frac{\text{Variation Between the Sample Means}}{\text{Variation Within the Samples}} \tag{2.5}$$

If the p-value from the ANOVA is significant (less than 0.05), then you would reject the null hypothesis, concluding that at the groups are not all the same and at least one of the means is different. However, the ANOVA does not tell you where the difference lies. For this, you need another test, the Tukey test.

Two-Way ANOVA

A two-way ANOVA is an extension of a one-way ANOVA that examines the effect of two different categorical independent variable on a dependent variable. The goal of a two-way ANOVA is not only to assess and understand the main effect of each independent variable but also if there is any interaction between them.

2.1.10.3 Tukey Test

The Tukey test is also known as the Tukey's Honest Significant Difference (HSD) test, which is performed after an ANOVA. While the ANOVA can tell us whether our results are significant overall, it does not tell us which groups the differences lie in. The Tukey Test identifies which specific group's means (compared with each other) are different. This test compares all possible pairs of means. The HSD statistic is calculated, and compared to the Critical Value. The Critical Value is found in Table N in the Bluman text using the number of samples and degrees of freedom (for the within group variance). The null hypothesis is rejected if the absolute value of the test statistic is greater than the critical value. This would show the two means are significantly different.

2.1.11 Extra Experiments

Other experiments were completed over the span of my thesis but the data is not shown in the chapters either due to relevance or the need to optimise. Although, to not lose the description of the methods used, I have created an additional method section in Appendix A.1.

Some journeys take us far from home, Some adventures led us to our destiny.

– C.S. Lewis, The Chronicles of Narnia

3

3D culture on collagen-based scaffolds induces a more metabolically mature phenotype in induced pluripotent stem cell-derived cardiomyocytes.

3.1 Introduction

3.1.1 Activation and Inhibition of the Wnt Pathway in Cardiac Differentiation

There have been considerable improvements in the efficacy of generating CMs from ESCs and iPSCs over the last couple of decades (Table 1.1). Movement from the original EB-based method has given way to the more recent monolayer-based protocols that use transforming growth factor (TGFβ) and Wnt signaling to mimic a differentiation process more similar to that which occurs naturally in vivo.

Wnt genes encode for a series of glycoproteins that play key roles in embryonic development and adult tissue homeostasis [466, 467]. During early embryogenesis, Wnt signaling is necessary for primitive streak formation and mesoderm induction [468, 469]. Controversy exists over the extent of the effect Wnt signaling has on cardiac

development. In amphibians and avians, the Wnt/β-catenin pathway inhibits cardiac development [470–472] but in contrast, in many vertebrates such as Drosophila, it promotes heart formation [473, 474]. Wnt/β-catenin signaling also has been shown to induce CM differentiation in a P19CL6 mouse cell line [475, 476]. One possible reason to explain this discrepancy is that Wnt/β-catenin signaling has a two-phase effect on cardiac development depending on the stage of differentiation. For example, activation in the early stages of cardiac development promotes mesodermal cells into a cardiac lineage, while at a later stage, it inhibits proliferation and or maturation of committed CMs. Several studies have supported this notion. During P19CL6 cell differentiation into CMs, *Wnt2a* and *Wnt8a* gene expression were initially observed prior to early cardiac markers. When Wnt signaling was inhibited in this early stage, there was a reduction in cardiac marker gene expression, but there was no affect on mesodermal markers [475, 476]. Naito *et al.* [477] showed that activation of the Wnt/β-catenin pathway in the early development of EB formation enhanced CM gene expression while reducing that of hematopoietic and vascular cell markers (Fig. 3.1). However, activating the Wnt/β-catenin pathway in a later stage enhanced hematopoietic/vascular gene expression via the suppression of bone morphogenetic protein (BMP) signaling which led to inhibiting CM differentiation. Moreover, the initial enhancement followed by inhibition of Wnt/β-catenin signaling resulted in an increased efficiency in generating ESC-CMs. Lian *et al.* [354] translated this concept to iPSC differentiation and successfully produced 80-90% pure functional iPSC-CMs without cell sorting.

In this thesis a monolayer-based protocol utilizing Activin-A, CHIR99021 and IWP4 was used for the generation of beating iPSC-CMs, based on previous literature [353, 354], and optimized by a previous DPhil student in the lab, Dr. Heba Al-Siddiqi. Dr. Al-Siddiqi added the induction of hypoxia (5% O_2 and 5% CO_2) from Day 0 through Day 6 in the differentiation protocol to mimic in vivo changes in oxygen tension. Activin-A and CHIR99021, a Wnt signaling agonist, was used to induce mesoderm formation, while subsequent IWP4 inhibition of Wnt signaling drove the cells further towards cardiac mesoderm (Fig. 3.2). Insulin, present in the B27 supplement, largely inhibited

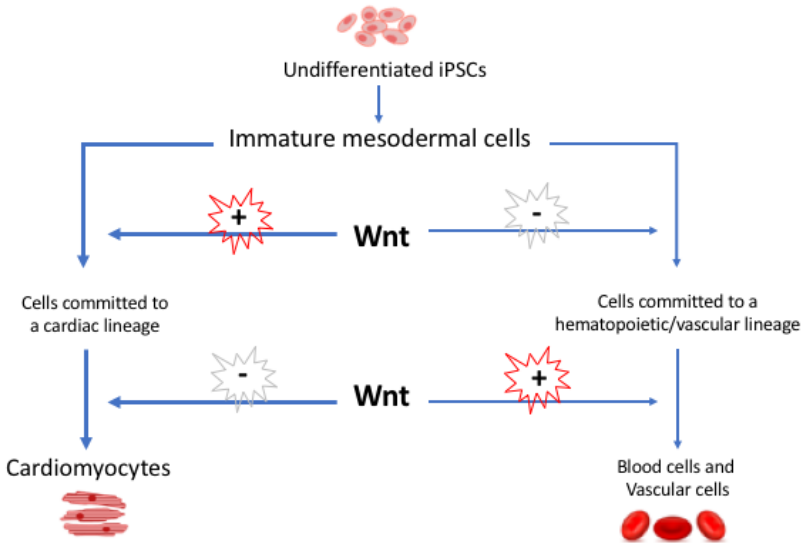

Figure 3.1: Canonical Wnt/β-Catenin signaling stage-specific effects on choosing a CM or hematopoietic fate, adapted from [477].

CM yield during the first 5 days of differentiation, which is consistent with previous reports [354, 478, 479]. Therefore, media with the addition of B27 lacking insulin was used from Days -1 to 6 to enhance cardiac differentiation.

3.1.2 Accessing Maturation

To assess maturation of our differentiated iPSC-CMs, this thesis focuses on the expression of a variety of different contractile and metabolic genes. The aim was to assess what machinery the cells expressed to support and confirm what metabolic pathways were activated and downregulated as a result of the different culture conditions.

3.1.2.1 Cardiac Genes

Cardiac Muscle

Cardiac muscles are intricate in their design but ultimately made up of repeating contractile units, referred to as sarcomeres, which give cardiac muscle its striation. Sarcomeres are lined up end to end to build myofibrils (Fig. 3.3). Myofibrils are surrounded by a covering known as the sarcoplasmic reticulum (SR), which is essentially a modified endoplasmic reticulum

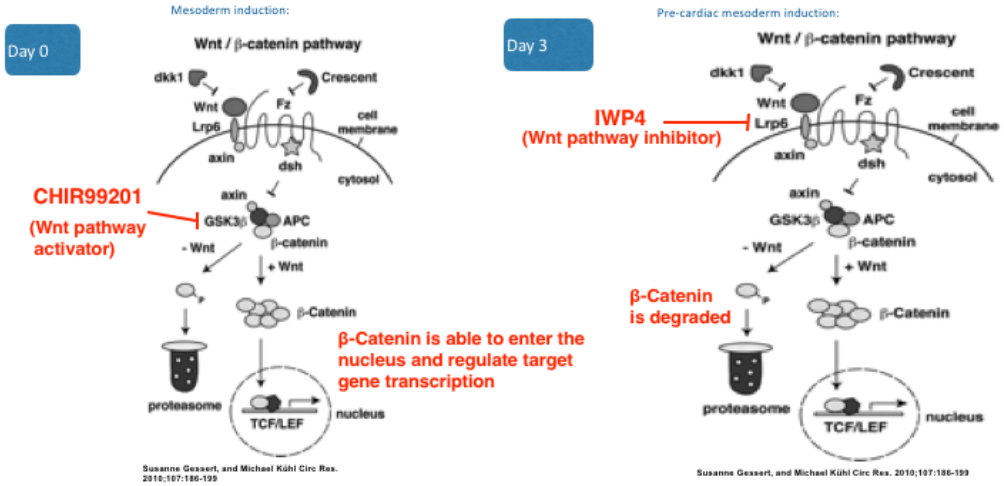

Figure 3.2: Canonical Wnt/β-Catenin pathway, adapted from [480]. In the presence of CHIR99021, the Wnt pathway is activated by blocking GSK3β. β-Catenin accumulates in the cytosol and activates the expression of target genes through interaction with the TCF/LEF transcription factors. On Day 3, IWP4 is added and inhibits Wnt. In the absence of Wnt, β-catenin binds to the destruction complex consisting of axin, adenomatous polyposis coli (APC), and GSK3β and is phosphorylated. This led to β-catenin being degraded by the proteasome.

that contains large amounts of Ca^{2+}. The SR is contained in the myoplasm (contractile region of muscle tissue and can be thought as a modified cytoplasm) and encapsulated within the sarcolemma (cell membrane). The sarcolemma is capable of propagating an action potential. T-tubules connected to the sarcolemma, oriented perpendicularly to the myofibrils, allow for the flow of ions. A single myocyte will contain many myofibrils.

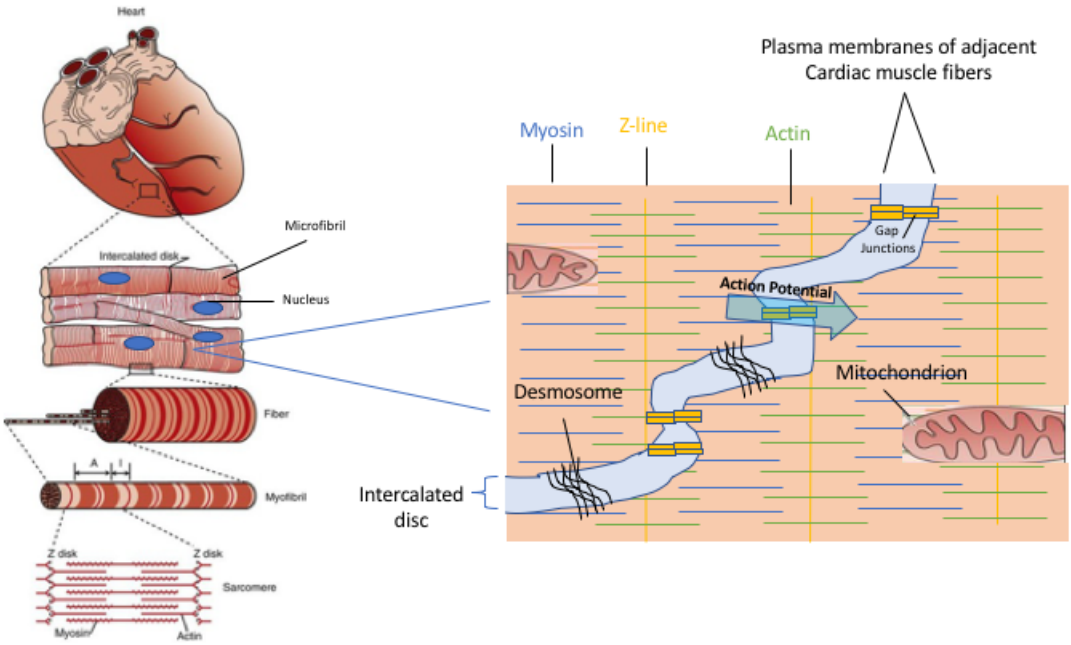

Figure 3.3: Levels of organization within a cardiac muscle, adapted from *VeterianKey.com*

Sarcomere

The sarcomere is the basic unit of muscle fibers, responsible for muscle contraction. It is made up of overlapping regions of thick (organized bundles of myosin) and thin filament (actin along with troponin and tropomyosin proteins) that crawl along each other in response to the binding of calcium ions that have been pumped in and out of the SR. The first genes of interest are the myosin heavy chain -6 and -7 (*MYH6* and *MYH7*), which encode for the contractile proteins alpha-myosin heavy chain (MHCα), and β-myosin heavy chain (MHCβ) in that order. These proteins are found in cardiac muscle and together form parts of a larger protein called type II myosin [481] which is one of the major components of the thick filament in the sarcomere that helps generate the mechanical force needed for cardiac muscle

contraction (Fig. 3.4). *MHCα* is considered to be the fast isoform and is expressed in both the atria and ventricle during embryonic development [482]. After birth, *MHCα* is mainly just expressed in the atria while *MHCβ*, the slow isoform, is predominately expressed in the ventricles. Assessing this switch between the isoforms can be used as a sign of maturation. Atrial Light Chain-2 (ALC-2), encoded by the *MYL7* gene is also expressed in atrial muscle, regulating cardiac development and contractility by the stabilization of thick filaments. Its expression is often correlated with that of MHCα. Another key protein located in the thin filament is cardiac muscle troponin-T (cTNT) which is encoded by the *TNNT2* gene and makes up the tropomyosin-binding subunit of the troponin complex. cTNT is pivotal in regulating muscle contractions in response to changes in intracellular calcium ions and it is often used in many labs as an indicator for CMs.

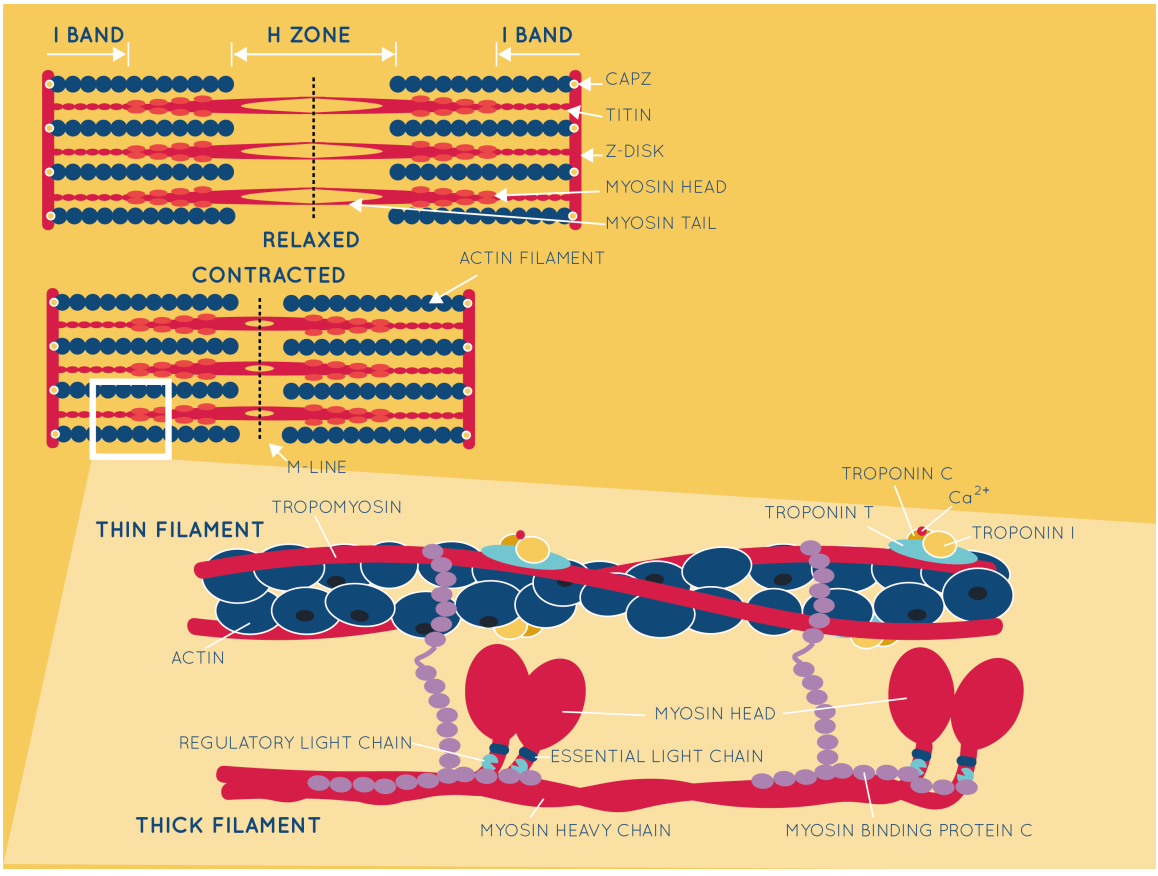

Figure 3.4: Myosin heavy chain II exists as a dimer, containing two regulatory and two essential light chains bound to each heavy chain. Image adapted from Sigma-Aldrich.

Muscle Contraction

Contraction of muscle requires a series of coordinated steps that are repeated to induce further shortening of the sarcomere (Fig. 3.4). Initially, the nervous system will send a signal to contract via a motor neuron. This signal reaches the nerve terminal (synaptic bouton) and releases neurotransmitters (e.g. acetylcholine) into the neuromuscular junction. If enough acetylcholine binds to the muscle cell, the muscle will be depolarized, and an action potential will be generated. The principal gap junction protein in the heart is referred to as alpha 1 connexin (Cx43). Cx43 regulates action potentials between cells to synchronize all cardiac contraction [483]. Cx43 are a cluster of closely packed channels, predominately located in the intercalated disks, that directly connect the cytoplasmic compartments and neighboring CMs, allowing the passage of small ions and secondary messengers to maintain homeostasis [484–486]. Due to its role in electrical coupling of cells, *CX43* has been correlated to the maturation of CMs. However, it is noteworthy to mention that CMs are not the only cells that express *CX43*. Boyer *et al.* [487] has shown they have also been paired to pluripotency.

There are channels made up with the ryanodine receptor 2 (RYR2) protein, encoded by the *RYR2* gene, that are embedded in the outer membrane of the SR, acting as a storage center for calcium ions. These RYR2 channels control the flow of calcium ions out of the SR and into the cytosol [488] (Fig. 3.5). The SR is structurally and functionally underdeveloped in a foetal heart, suggesting that expression of *RYR2* could be a target for maturation. After the calcium is released from the SR, it binds to troponin, causing tropomyosin to shift, exposing the myosin-binding site on actin (Fig. 3.6). The freed myosin heads then move towards and bind to the exposed actin site. A power-stroke occurs and the myosin pulls on the actin drawing the thin filaments towards the center of the H-zone, shortening the sarcomere [489]. ADP and P_i are released allowing for a new ATP molecule to bind to the myosin. This causes the dissociation of myosin from the thin filament and the sarcomere can reset to its original width in preparation for the next contraction. Calcium is necessary to reveal the myosin-binding site, so it is essential the SR has tight control and regulation over intracellular calcium so that the muscle only contracts when needed.

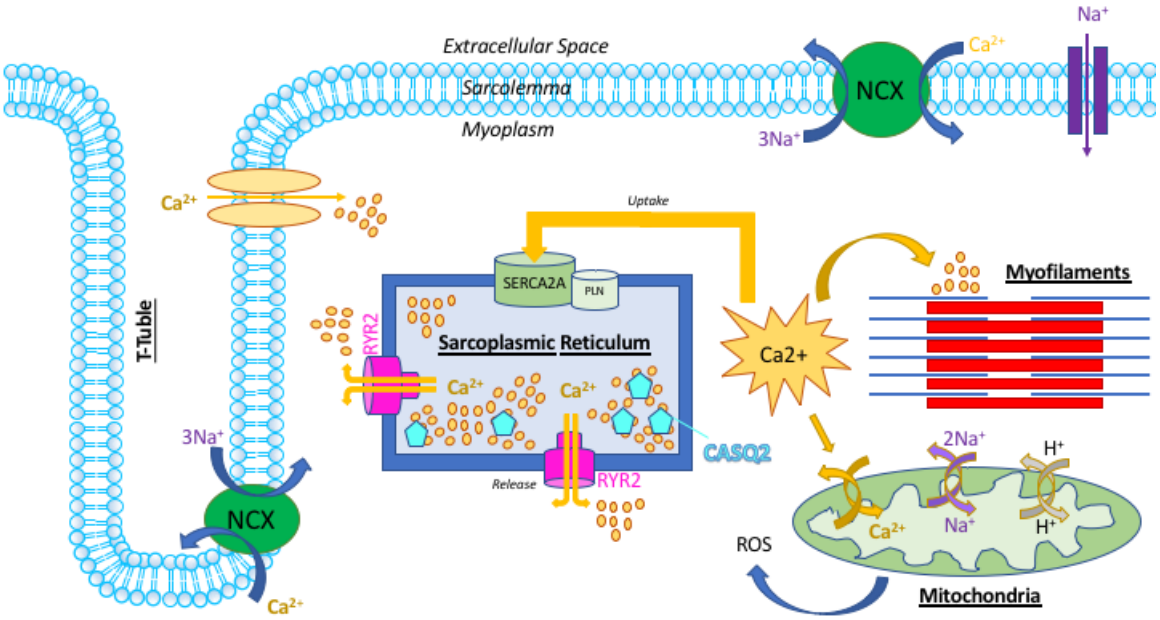

Figure 3.5: Regulation of calcium homeostasis inside the myoplasm.

Sarco/endoplasmic reticulum Ca^{2+}-ATPase (SERCA), a Ca^{2+} ATPase, transfers Ca^{2+} from the cytosol of the cell to the lumen of the SR at the cost of ATP hydrolysis during muscle relaxation (Fig. 3.5). The regulatory protein phospholamban (PLB/PLN), mediates the rate at which SERCA moves Ca^{2+} across the SR. When PLB is bound to SERCA, Ca^{2+} movement is reduced. Calsequestrin-2, encoded by the *CASQ2* gene, another calcium-binding buffer protein, helps reduce the concentration of free Ca^{2+} within the SR [490]. CASQ2 assists SERCA to hold calcium in the SR after a muscle contraction against its concentration gradient (SR has 10,000x higher concentration of Ca^{2+} than in the cytosol) [491]. The release of CASQ2-bound calcium triggers muscle contraction. CASQ2 also has an important role in lengthening the time to recharge the SR Ca^{2+} stores by mediating the calcium-induced calcium release (CICR) mechanism, which has been linked to maturation [383].

3.1.2.2 Metabolism Genes

An adult heart requires an efficient and sustainable source of ATP for muscle contraction in the presence of oxygen. As a result, FAs are the main fuel for adult CMs. In contrast, the

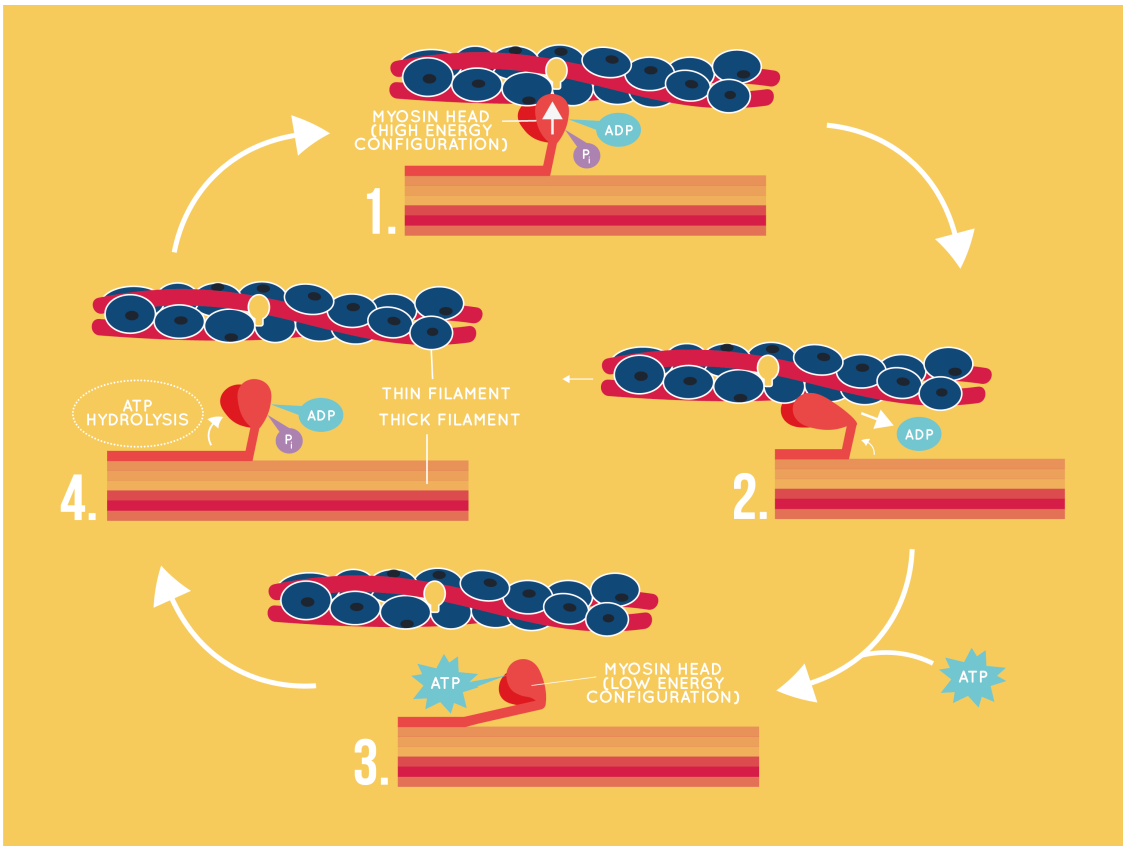

Figure 3.6: Muscle contraction steps. 1) The myosin head attaches to the actin myofilament to form a cross bridge. 2) Phosphate (P_i that was generated from the last contraction) is released initiating the power stroke. The myosin head pulls on the actin filament sliding it towards itself. The ADP is then released. 3) A new ATP attaches to the myosin head which weakens the link between myosin and actin allowing for the cross bridge to detach. 4) As ATP is hydrolysed and split into ADP and P_i, the myosin head is energized into a high-energy conformation ready to attach to actin again to repeat the cycle.

foetal heart requires a sufficient amount of ATP for development in an hypoxic environment, resulting in glucose and lactate as the major substrates consumed. Therefore, in this thesis, we will mainly be examining the metabolic pathways of glucose, pyruvate, and fatty acids.

Glucose Metabolism

To assess the ability of the cells to metabolise glucose, genes from both glycolysis and pyruvate oxidation were measured (Fig. 3.7). The first two genes look at the transportation of glucose into the cell. Glucose can be transported across the plasma membranes of mammalian cells through glucose transporter -1 and -4 (GLUT1 and GLUT4). GLUT1, encoded by the *SLC2A1* gene, is responsible for the low basal level of glucose uptake to sustain respiration in all cells [492]. GLUT4, encoded by the *SLC2A4* gene, is insulin-regulated and permits the diffusion of circulating glucose down its concentration gradient into the muscle cells [492]. Muscle contraction stimulates the translocation of more GLUT4 receptors to the surface based on demand. After birth, there is a switch in which GLUT isoform is most dominant in the heart [493–495]. *GLUT1*, originally predominant in the foetal heart is downregulated in adulthood, whereas *GLUT4* expression increases and becomes the dominant isoform in the adult heart [493–496]. Therefore, this switch from *GLUT1* to *GLUT4* isoforms were investigated to measure the degree of maturity in the iPSC-CMs. The second gene of interest is *PFKM* which encodes for one of the three subunits of the enzyme 6-phosphofructokinase. PFKm is involved in an irreversible reaction considered to be one of the major rate-limiting step of glycolysis, catalyzing the phosphorylation of fructose 6-phosphate to fructose 1,6-bisphosphate.

Pyruvate Oxidation

After glycolysis, pyruvate will be converted into either lactate or to acetyl-CoA to enter the TCA cycle. Pyruvate is converted into acetyl-CoA by the pyruvate dehydrogenase (PDH) complex by a process called pyruvate decarboxylation.

Pyruvate dehydrogenase "lipoamide" kinase isozyme 4 enzyme (PDK4) is encoded by *PDK4* gene, which is a member of PDK protein kinase family. They encode for a mitochondrial matrix protein that inhibits the pyruvate dehydrogenase complex, by

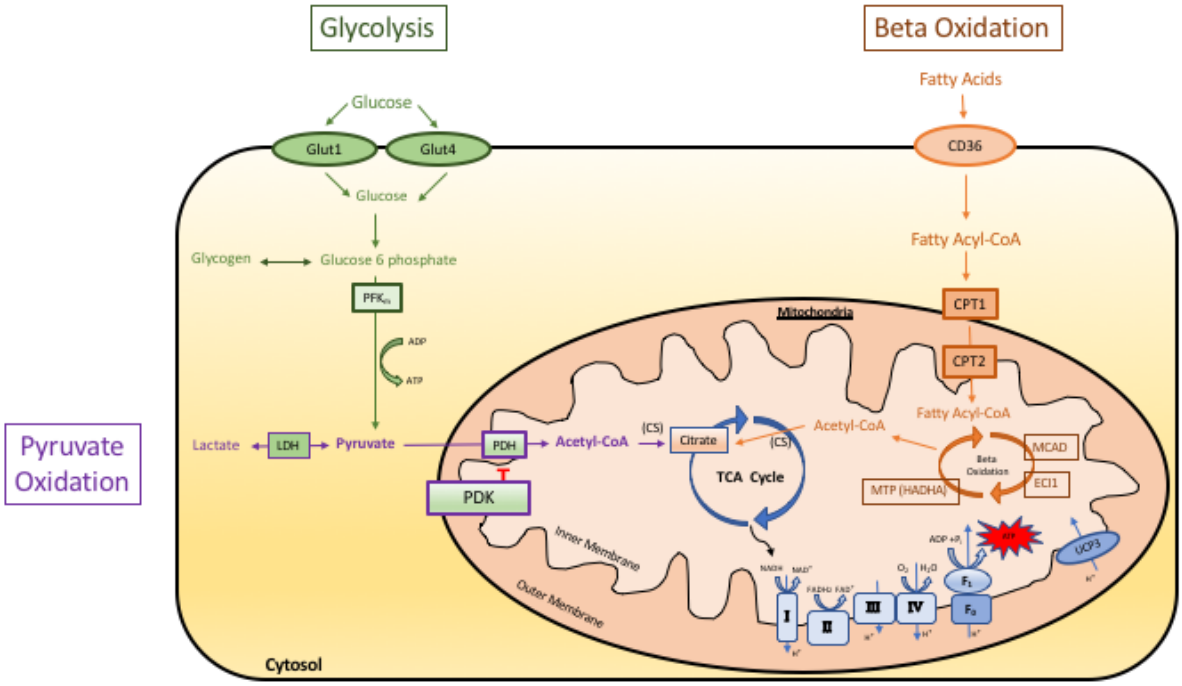

Figure 3.7: Glucose and pyruvate oxidation pathway and related genes.

phosphorylating one of its subunits. As PDK inhibits PDH, it decreases the overall conversion of pyruvate to acetyl-CoA and reduces glucose oxidation. Therefore, *PDK4* is considered to be a major regulator of glucose oxidation and its expression can be used to measure the degree of maturity by inducing the metabolic flexibility to switch between glucose and fatty acid metabolism in the iPSC-CMs.

Fatty Acid Oxidation

There are several genes involved in β-oxidation that were measured to indicate the ability of the cells to metabolise fatty acids. The first two transcription factors that are of interest in this thesis were the peroxisome proliferator-activated receptor alpha (*PPARα*) and peroxisome proliferator-activated receptor gamma coactivator 1-alpha (*PPARGC1A* or *PGC1A*). *PPARα* is a major regulator of lipid metabolism and, when activated, promotes uptake, utilization and catabolism of fatty acids, FA binding and activation, and peroxisomal and mitochondrial FA β-oxidation [497, 498]. *PGC1A* is a master regulator of mitochondrial biogenesis. PPARα and PGC1A will be discussed in more detail in Chapter

4.

Insulin signalling plays a major role in iPSC-CMs differentiation [478] and in the regulation of glucose metabolism. Insulin signalling inhibits gluconeogenesis and promotes fatty acid synthesis. Therefore, the expression of the insulin receptor substrate genes *IRS1* and *IRS2* were assessed to gauge maturation of iPSC-CMs. *IRS1* and *IRS2* are involved in both heart muscle growth and metabolism [499]. *IRS1* plays a key role in transmitting signals from the insulin and insulin-like factor 1 (IGF-1) receptors to intracellular pathways PI3K/AKt and Erk MAP kinase pathways [500]. *IRS2* is a cytoplasmic signalling molecule that mediates mitogenic and antiapoptotic signaling and participates in important biological processes such as cell proliferation, metabolism and survival [501, 502]. Qi *et al.* [503] showed that cardiac-specific *IRS1* and *IRS2* gene double-knockout mice showed impaired energy metabolism gene expression and heart failure.

Citrate synthase (CS) is an enzyme that exists in the mitochondrial matrix of all living cells. CS is involved in the first step of the TCA cycle and catalyzes a condensation reaction between acetyl-CoA (2 carbon) and oxaloacetate (four-carbon) into citrate (6-carbon). CS is also commonly used as a marker for intact mitochondria.

3.1.3 Tissue Engineering Approaches to Cell Maturation

As previously discussed, in vitro differentiation of pluripotent stem cells yields CMs with an immature phenotype which does not make them ideal models to mimic adult CMs. It is hypothesized that culturing cells in 3D would better mimic conditions in vivo, such that differentiated cells would adapt to a more mature phenotype.

Scaffolds can be formed from synthetic polymers or natural materials such as the cardiac ECM. Besides the structural role of giving support to surrounding cells, the ECM also has non-structural properties that have important roles in cardiac development and remodeling. There have been several ECM proteins that have been integrated into 3D scaffolds to try to enhance differentiation or used as a therapeutic tool. In this thesis, we will use porous scaffolds comprised of collagen, optionally integrated with elastin or C4S. The scaffolds in this thesis have been supplied by a collaborating lab that is researching artificial heart

valves comprised of these substrates.

A human heart valve consists of three layers: the fibrosa (predominantly collagen fibers), the ventricularis (elastin and collagen sheets), and the spongiosa GAGs and loosely arranged collagen) [504]. As a result, these scaffolds have been investigated with compositions resembling each layer of the native heart valve, i.e. collagen scaffolds, collagen-elastin scaffolds and collagen-GAGs scaffolds. The morphological, mechanical, and biological properties of the scaffolds have been previously characterized and assessed in vitro with CDCs [425]. The pore sizes of all the scaffolds fell in the range of 100-200 μm. These scaffolds will continue to be explored and assessed on their ability to mature iPSC-CMs compared to cells in 2D culture.

3.1.4 Chapter Aims

The aim of this chapter was to determine the maturation and metabolic phenotype of our iPSC-CMs cultured as a monolayer on a variety of extracellular matrix substrates and in 3D on porous scaffolds. Changes of gene expression were measured using qPCR, and glucose and fatty acid metabolism were measured using radiolabeled substrates and AlamarBlue assays.

3.2 Results

In the results, cells were used at different stages of the differentiation protocol and cultured for a number of days. For clarity, the number of days of differentiation on which the cells were used will be denoted as DD7, DD9 etc.

3.2.1 Differentiating iPSCs into Beating Cardiomyocytes on Matrigel

iPSCs were cultured on reduced factor (RF) Matrigel, a gelatinous protein mixture rich in laminin and collagen IV that is derived from Engelbreth-Holm-Swarm mouse sarcoma cells,

and then were successfully differentiated into beating CMs by a differentiation protocol that exploits the Wnt signalling pathway (Fig. 2.1, Table 2.1). In the first step, Activin-A, a RF-Matrigel sandwich, hypoxia (5% O_2 and 5% CO_2), and Wnt stimulation were used in the absence of insulin to generate mesoderm [351, 365, 480]. This step was particularly harsh and resulted in a loss of 30-70% of the cells (Fig. 3.8 C). Two days later, Wnt inhibition in the absence of insulin induced cardiac mesoderm [353, 354, 505]. Finally, insulin was introduced and the cells were switched to normoxia. Cardiac mesoderm formed spontaneous beating CMs around differentiation day (DD) 12-15 (around 50±3 bpm). The contractions at this stage were irregular and varied depending on location within the flask. Most beating clumps initiated along the parameter and edges of the flasks. Over the span of a week, the contractile areas grew larger and eventually started to beat in synchrony (Fig. 3.8 H-J). By DD20-30, there was a full synchronous sheet of cells beating at around 70±2 bpm (comparable to adult heart). Although, the efficiency of the differentiation protocol was no perfect and did not consistently generate beating colonies of CMs (Fig. 3.9).

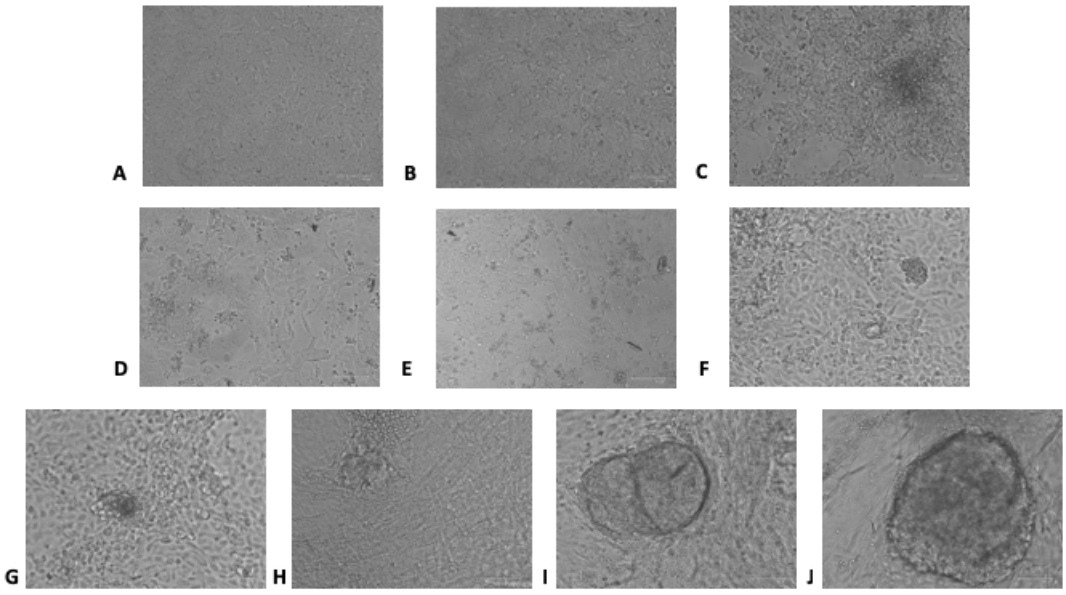

Figure 3.8: iPSCs morphology changes during differentiation into CMs. (A) DD-1, (B) DD0, (C) DD1, (D) DD3, (E) DD5, (F) DD7, (G) DD21, (H) one month (I) two months (J) three months post induction of CM differentiation.

Antibody staining for cardiac sarcomeric actinin (Fig. 3.10A) and cardiac troponin-T

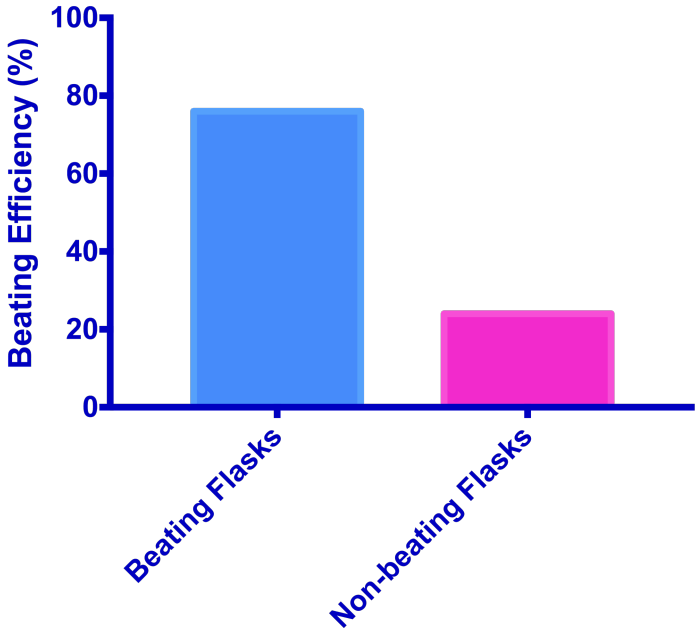

Figure 3.9: Differentiation efficiency of iPSCs into beating CMs. The graph represents the percentage of 50 independent T25 flasks of differentiated iPSC-CMs that either were successful or failed to generate full beating flasks. This measurement was taken visually on DD22.

(Fig. 3.10B) confirmed that the cells were positive for these cardiac markers on DD20+. Even though some of the iPSC-CMs showed the classic elongated morphology, unfortunately most did not. When looking at an n=3 of the cardiac sarcomeric actinin staining, around 80-85% of the cells stained positive for actinin. This was calculated by visually counting the nuclei surrounded by the actinin in ImageJ. Flow cytometry was attempted to get a quantitative measure of how many of our iPSC-CMs were positive for the cardiac-specific Troponin T (cTNT) marker. iPSCs were differentiated and cultured in a T25 flask for one month to generate a full-plate of synchronised beating cells. On DD31, the cells were harvested, stained, and fixed for flow cytometry. Several complications arose when attempting flow. The first was finding an optimal primary antibody. The initial attempts were with an Abcam cTNT (ab10214), which seemed to have non-specific binding to all the cells in each sample. This was later confirmed through confocal imaging taken by Rita Alonaizan of a whole mouse heart mount (Fig. 3.11). Not only was the cardiac region stained red, but also nonspecific binding outside the heart. A new cTNT conjugated antibody

(MACS:130-106-745) was purchased that was much more specific.

The second major problem with our flow was trying to dissociate the iPSC-CMs into single cells. The longer the cells were cultured the "stickier" they became and we were unable to separate them efficiently. This resulted in a smear like pattern when initially gating for live cells. There was an increased number of cells that were identified as dead because they were duplicates/clusters that didn't fit the correct size category. Only a few runs yielded useful data, but each of these reported a large number of "deceased" cells. However, flow cytometry performed on beating cells one-month post differentiation protocol yielded around 70% cTNT positive cells within the population of live cells (Fig. 3.10). More data on the flow troubleshooting can be found in Appendix A.1.4.

3.2.2 Long Term Culture-induced Maturation of iPSC-CM

Maturation of iPSC-CMs over long-term culture was assessed using qPCR on DD7, DD12-15, DD31, 2 months and 3 months of the differentiation protocol. A list of the target genes can be found in Table 3.1. DD7 cells were used as a control, representing the least mature cell type, which does not have a contractile phenotype and has only formed cardiac mesoderm. DD12-15 cells were chosen to represent the stage of the first spontaneous contractions while one month old cells represented a fully synchronized beating flask. The experiment was taken out to 3 months to capture slower gene expression changes. The experiments were run in three biological replicates for each time point from two independent batches of the same cell line. The qPCRs were analysed within each batch using $\Delta\Delta$CT qPCR analysis [452].

3.2.2.1 Stability of the Reference Genes

To determine the most stable reference genes for the Sybr Green qPCR studies, four different genes were assessed: *TBP*, *POLR2A*, *HPRT1*, and *B2M* (Fig. 3.12). Between the four different housekeeping genes, none of them were significantly up or down regulated. Thus a combination of at least two of these reference genes were used.

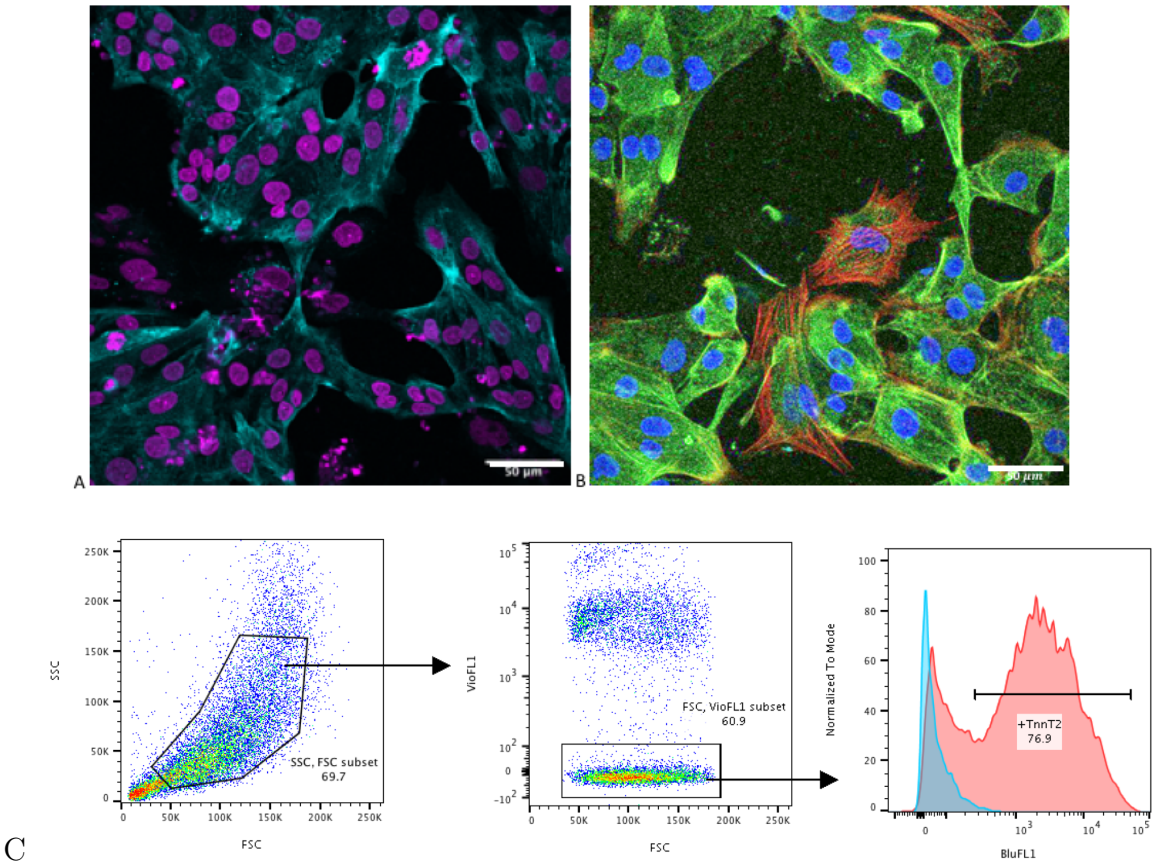

Figure 3.10: Cardiac expression of beating iPSC-CMs on DD20+. A) Cardiac sarcomeric actinin expression under 40X objective (actinin-cyan, DAPI-magenta) and was taken by Ujang Purnama. B) Cardiac troponin-T expression under 40X ojective (DAPI-blue, cTNT-green, and rhodamine phalloidin-red). Images were taken using an Olympus Confocal Microscope at the Dunns School. B) 70% of the iPSC-CMs were positive for cTNT after 1 month of differentiation. iPSC-CMs were harvest, stained for Zombie violet and fixed on DD31. Flow cytometry was performed on 1-2 million iPSC-CMs. They were first gated for normal shaped cells (single cells), then gated for Zombie Violet (live cells) and lastly for cTNT+ cells.

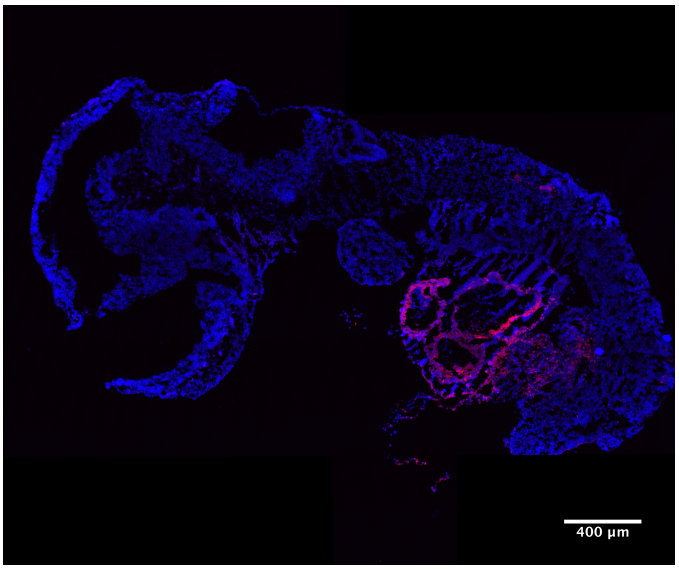

Figure 3.11: Aspecific antibody: whole mouse heart mount staining for cTNT.

Table 3.1: List of gene transcripts accessed in the qPCRs investigating long term culture-induced maturation of iPSC-CMs.

Gene Transcript	**Description**
B2M	housekeeping genes
HPRT1	housekeeping genes
POLR2α	housekeeping genes
TBP	housekeeping genes
MYH6	contractile protein
MYH7	contractile protein
MYL7	contractile protein
TNNT2	contractile protein
CASQ2	calcium handing
RYR2	calcium handing
SERCA2α	calcium handing
CX43	gap junction
PDK4	regulation of glucose metabolism
GLUT1	glucose transporter
GLUT4	glucose transporter
PGC1α	mitochondrial biogenesis
PPARα	metabolic transcription factor
CS	mitochondrial metabolism
IRS2	insulin signalling
IRS1	insulin signalling
COL3A1	ECM, collagen
COL1A1	ECM, collagen

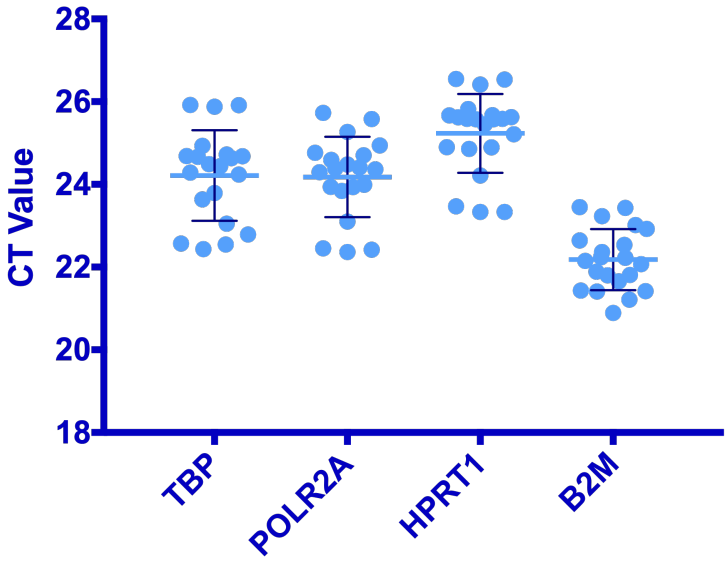

Figure 3.12: Reference gene expression. *TBP*, *POLR2A*, *HPRT1*, and *B2M* were assessed to determine the most stable reference gene for Syber qPCRs studies. The bar represents the mean, and the line represents the 95% confidence interval. n=20

3.2.2.2 iPSC-CMs Long Term Culture Expression of CM Genes

Quantitative PCR analysis was performed for expression of contractile and contraction associated genes (Fig. 3.13). *MYH6* was upregulated on DD31 compared to DD7. Additionally, at DD31 *MYH6* and *MYH7* were significantly higher than DD12. *MYL7* and *MYH6* were upregulated as early as DD12 when compared to DD7. Finally, *MYH7* continued to increase over the span of 3 months when compared to 1 and 2 months.

3.2.2.3 iPSC-CMs Long Term Culture Expression of Metabolic Genes

Quantitative PCR was performed for a series of metabolic genes such as the glucose transporters *GLUT1* and *GLUT4*, *PDK4* the mitochondrial regulator of glucose metabolism, *CS* which is involved in mitochondrial TCA cycle metabolism, *PGC1α*, a transcription cofactor of mitochondrial biogenesis, *IRS1* and *IRS2*, involved in insulin signalling and *PPARα*, a metabolic transcription regulator. The expression of *PDK4* and *GLUT4* were upregulated within the first month (Fig. 3.13 C), albeit at a relatively low level and with high variability, but continued to be upregulated at three months (Fig. 3.13

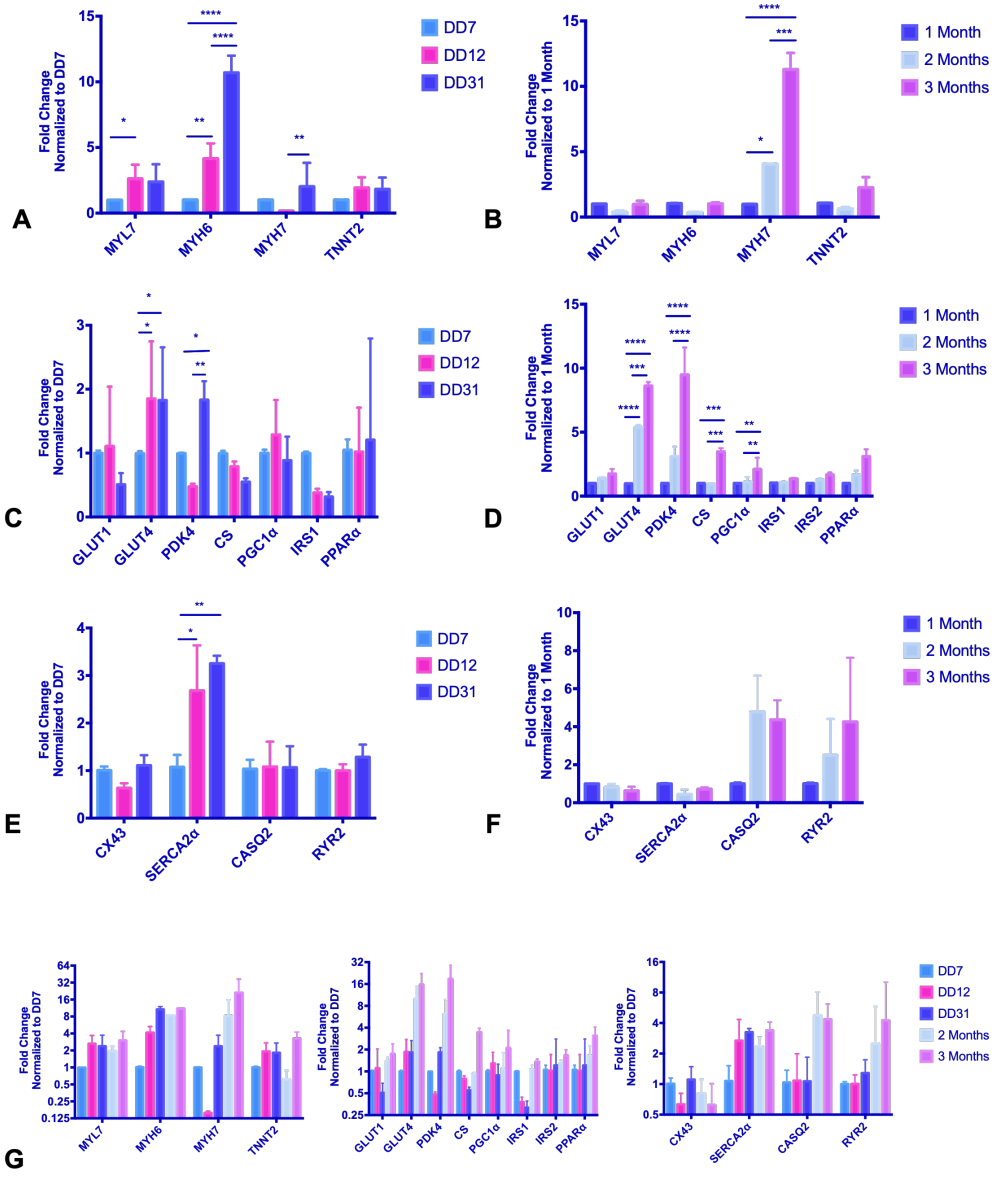

Figure 3.13: A,B) Contractile, C,D) metabolic and E,F) calcium handling gene expression between DD7 to DD31 (left panel) and 1 month to 3 months (right panel) cultured iPSC-CMs on RF-Matrigel-coated monolayer plates. The two panels of graphs represent dierent batches of iPSC-CM and therefore should not be be combined for statistical analysis. The experiment was run in 3-6 biological repeats in duplicates with 3 technical repeats. The bar represents the mean + SEM. The blue represents iPSC-CMs cultured for DD7, pink represents DD12, indigo represents 1 month, light blue represents 2 months, light pink represents 3 months. G) Shows the combined graphs with no stats to show more clearly the progression across the 3 months. "*" = $p<0.05$, "**" = $p<0.01$, "***" = $p<0.001$ and "****" = $p<0.0001$; analyzed using a two-way ANOVA and a Tukey's multiple comparison test.

D). *CS* and *PGC1A* were also upregulated by three months (Fig. 3.13 D).

Quantitative PCR was also performed on genes encoding for the calcium handling proteins *SERCA2α*, *CASQ2*, and *RYR2*, along with *CX43*, a gap junction protein. *SERCA2α* was significantly upregulated as early as DD12 compared to DD7 (Fig. 3.13 E). There were no significant changes amongst the other genes measured.

3.2.3 Metabolic Gene Expression Changes Between iPSCs and Beating Cardiomyocytes

Long term culture had no affect on some of the genes between DD7 and 3 months of differentiation. As a result, iPSC-CMs at 1 month were compared with undifferentiated cells to see if there had been any change overall. Gene expression of *IRS1*, *IRS2*, *GLUT1*, *GLUT4*, *CS*, *PPARα*, *PDK4*, and *PGC1α* were compared using qPCR (Fig. 3.14). The expression of *GLUT4*, *PPARα*, *PDK4* and *PGC1α* were significantly upregulated after differentiation, but the other transcripts were unaffected.

3.2.3.1 Glucose Consumption and Lactate Production in Culture Media

iPSCs and iPSC-CMs glucose consumption and lactate production were assessed by measuring substrate concentrations in the culture medium using the Horiba ABX Pentra 400 serum analyser. iPSCs were cultured in a six-well plate and the iPSC-CMs in a T25 flask until they were confluent (around 4M cells/well and 10M/T25 flask).

In 24 hours, the iPSCs consumed 21.8 μmoles of glucose and produced 35.6 μmoles of lactate (Table 3.2). In glycolysis, one mole of glucose can produce at most two moles of lactate, assuming there was no glucose used for oxidation. This translate to our cells using 1.6 moles of lactate per mole of glucose. However, since CMs can also consume lactate, the interpretation of the data is not straightforward.

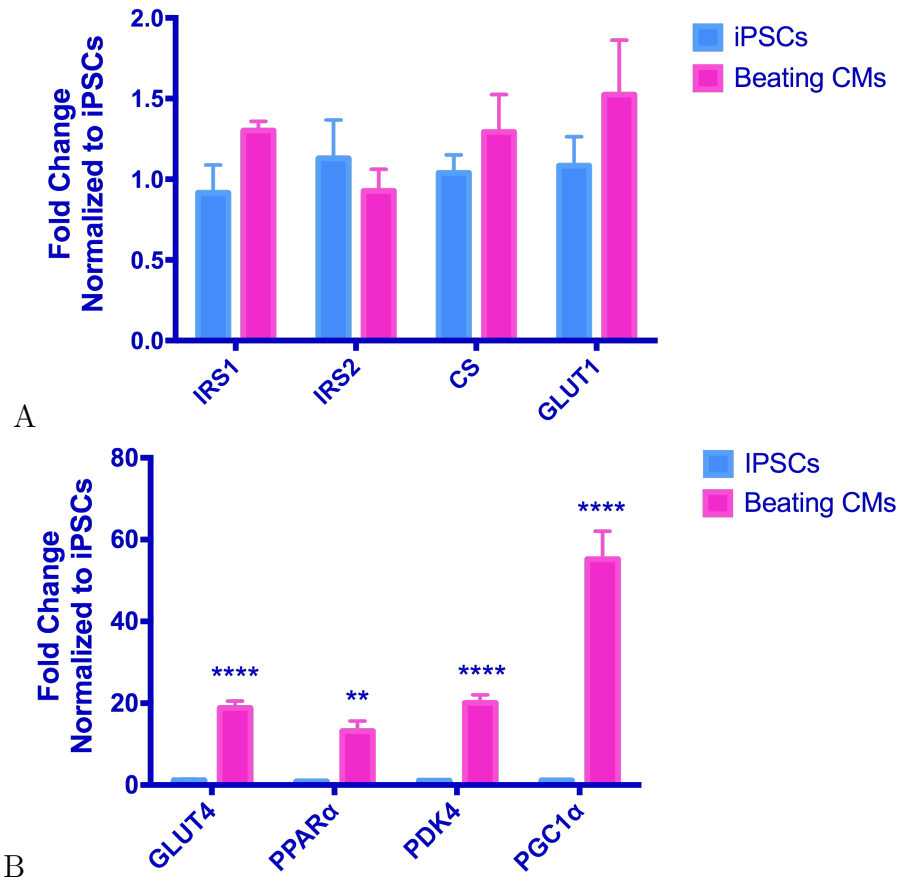

Figure 3.14: Metabolic gene expression of iPSCs and iPSC-CMs cultured for 1 month on RF-Matrigel-coated monolayer plates. The experiment was run in 8 biological repeats in duplicates with 3 technical repeats. The bar represents the mean + SEM. The blue represents iPSCs and the pink represents beating iPSC-CMs. The genes were normalized to iPSCs. The set of stars refers to the comparison between iPSCs and DD31 beating CMs. "*" = $p<0.05$, "**" = $p<0.01$, "***" = $p<0.001$, and "****" = $p<0.0001$; analyzed using a two-way ANOVA.

Table 3.2: Glucose and lactate were measured in the tissue culture media at the day of confluency using the Horiba ABX Pentra 400 serum analyser. Data is expressed as mean ± standard deviation. Control and one day culture were compared using the Welchs corrected t-test (* = $p<0.05$, ** = $p<0.01$, *** = $p<0.001$, and **** = $p<0.0001$).

Cell Type	**Treatment**	**Glucose**	**Lactate**
iPSCs	mTsER-1 media	15.6 ± 0.3	0.0 ± 0.0
iPSCs	1 Day confluent culture	4.7 ± 0.1**	17.8 ± 0.3****
iPSC-CMs	RPMI/B27 complete media	12.3 ± 0.1	0.0 ± 0.0
iPSC-CMs	2 days culture	0.25 ± 0.19****	19.3 ± 0.3****

3.2.4 Culture of iPSC-CMs on Different ECM Substrates

iPSCs are usually differentiated on RF-Matrigel instead of standard Matrigel because Matrigel contains a cocktail of different growth factors that limit and prevent differentiation. However, it has been shown that growing iPSC-CMs on different ECM substrates can promote differentiation [506]. To improve maturation and translate the iPSC-CMs to culture on collagen scaffolds, the feasibility of sub-culturing beating iPSC-CMs on a variety of other ECM substrates (such as collagen I, fibronectin, gelatin or other mixtures) were tested (Table 2.2). Five independent batches of iPSC-CMs were differentiated and re-plated on DD7 (the end of the differentiation protocol) onto different ECM coated surfaces and all conditions were able to generate beating colonies (Fig. 3.15).

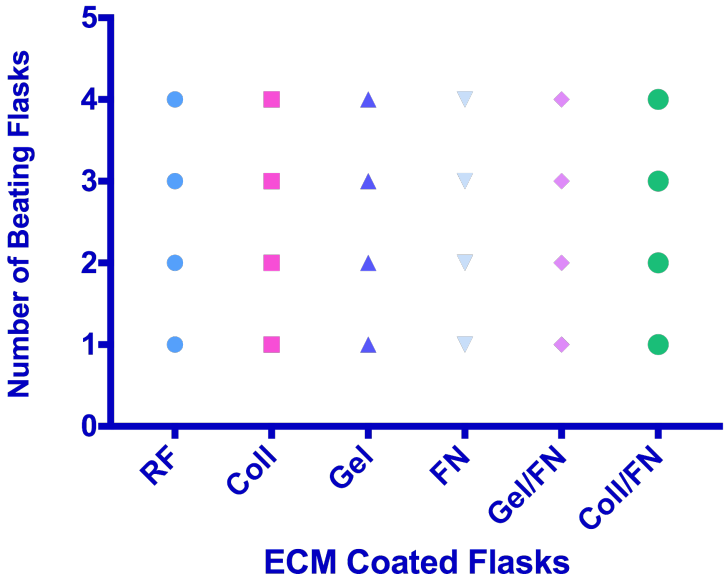

Figure 3.15: Beating efficiency of independent batches of iPSC-CMs on different ECM substrates. The beating count represents the number of flasks that led to beating cells post re-plating by DD22. n=5 independent flasks per ECM substrate.

The iPSC-CMs were harvested one week after re-plating on the different ECM substrates for RNA extraction. The expression of CM genes including *MYH6*, *MYH7* and *TNNT2* were assessed using qPCR (Fig. 3.16). There were no significant differences in expression between iPSC-CMs cultured for one week on the different ECM substrates. In addition, qPCR analysis was also performed to assess the expression of a number of metabolic genes

including *GLUT1*, *GLUT4*, *IRS1*, *IRS2*, *PDK4*, *PGC1α*, *CS* and *PPARα*. There was again no significant difference in the metabolic gene expression of iPSC-CMs cultured on the different ECM substrates (Fig. 3.17).

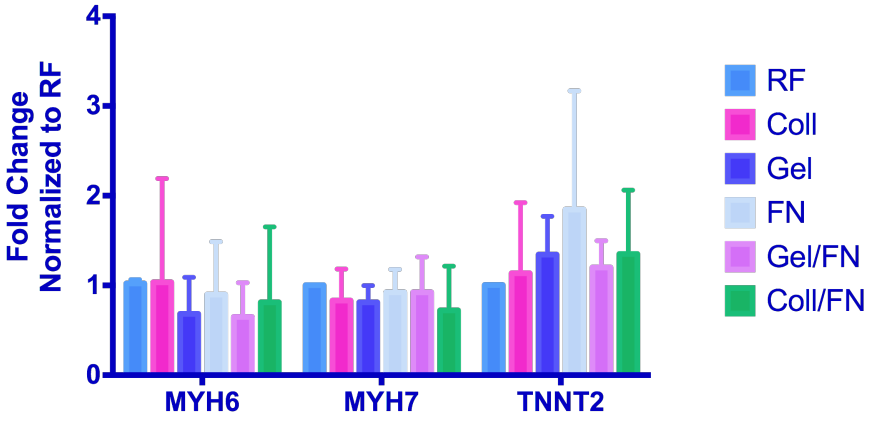

Figure 3.16: CM gene expression of iPSC-CMs re-plated on different ECM substrates on DD7 and cultured for 1 week. The experiment was run in 5 biological repeats in duplicates with 3 technical repeats. The bar represents the mean + SEM. The pink represents collagen, indigo: gelatin, light blue: fibronectin, light pink: gelatin/fibronectin, and green: collagen/fibronectin. All of the genes were normalized to the blue bar representing RF-Matrigel. The set of stars refers to significance in comparison to the cells cultured on RF-Matrigel. * denotes p-value$<$0.05; analyzed using a two-way ANOVA and a Tukey's multiple comparison test.

3.2.5 ABA and Validating ABA

AlamarBlue reagent was used to assess cell viability. Live cells maintain a reduced environment within the cytosol. Resazurin, a blue, non-fluorescent, non-toxic, permeable compound is the active ingredient of the AlamarBlue Assay (ABA). Upon entering cells, resazurin is reduced to resorufin, a red and highly fluorescent compound (Fig. 3.18). Viable and metabolically active cells continuously convert resazurin to resorufin, increasing the overall fluorescence and color of the media. Unlike other alternative kits, such as CellTiter-Glo, the ABA is one of the few non-destructive assays of cell viability and can be used to quantify cell activity in the same population over time. This means that viability measurements can be made on a well of iPSC-CMs without compromising the cells for their designated experiment. However, in a differentiating cell population, the

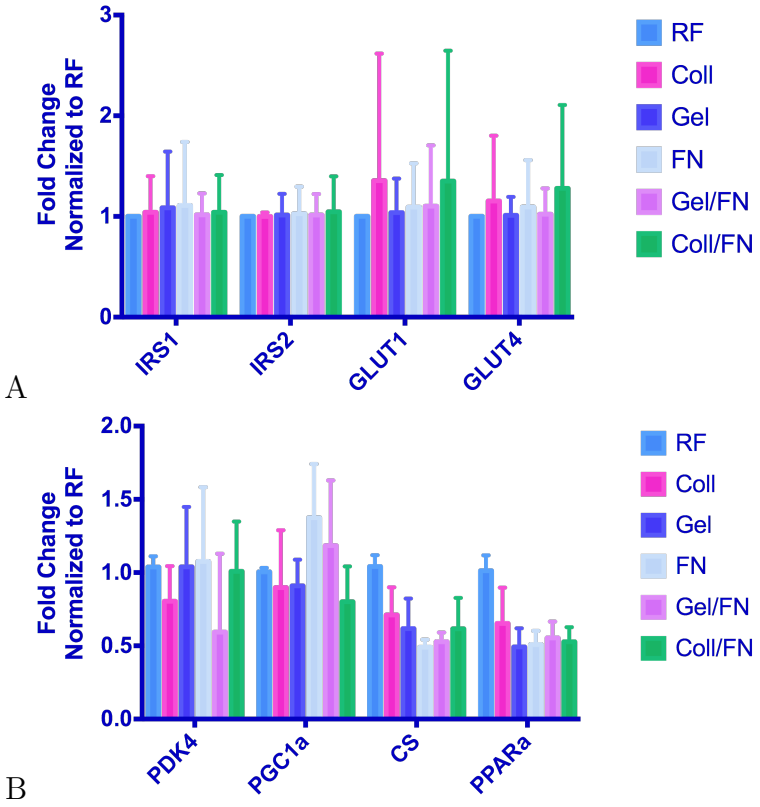

Figure 3.17: Metabolic gene expression of iPSC-CMs re-plated on different ECM substrates on DD7 and cultured for 1 week. The experiment was run in 5 biological repeats in duplicates with 3 technical repeats. The bar represents the mean + SEM. The pink represents RF, indigo: collagen, light blue: gel, light pink: FN, green: Gel/FN, blue: Coll/FN. All of these are normalized to the pink bar representing RF-Matrigel. The set of stars refers to significance in comparison to the cells cultured on RF-Matrigel. * denotes p-value$<$0.05; analyzed using a two-way ANOVA and a Tukey's multiple comparison test.

ABA percent reduction, measured by the absorbance change in the color of the media, can be due to cell proliferation or to up-regulated metabolism, so the results are not necessarily straightforward. As cells on scaffolds cannot be counted in the normal way, it was important to find a non-destructive method to determine cell number.

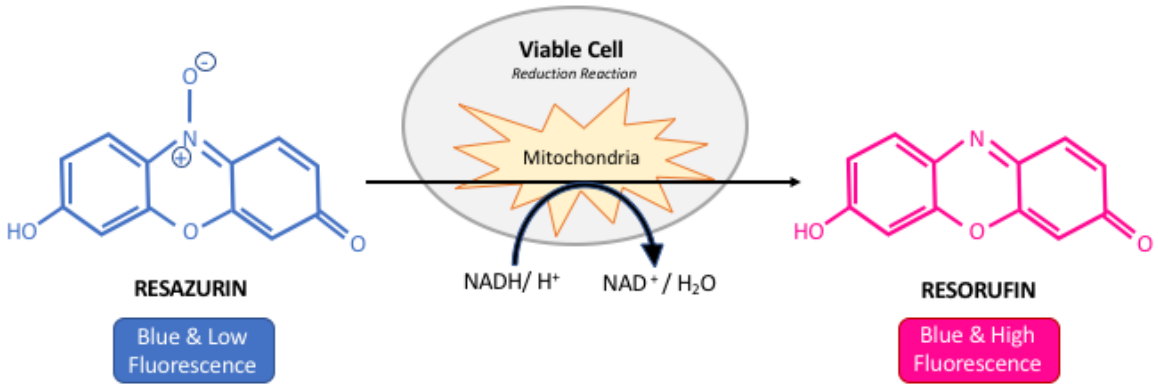

Figure 3.18: The AlamarBlue Assay's reduction reaction of Resazurin to Resorufin adapted from [507].

To establish whether ABA could be used to quantify proliferation or may be confounded by changes in metabolism, side experiments were performed to clarify the relationship between cell number and the colour change in differentiating cells. The first goal was to determine to what extent the cells grew over the span of a week.

Three independent batches of iPSC-CMs were re-plated on RF-Matrigel-coated 96-well plates and cultured for 1 week. On Days 1, 4, and 7 post re-plating, an ABA was performed per day group (n=4) and the corresponding cells were harvested to determine cell count using total DNA concentration over the span of the week (Fig. 3.19A). There was no significant change in cell count over the week. Reassuringly when comparing the cell count to the combined monolayer ABA results, the two displayed the same trend (Fig. 3.19B).

These results show strong support to the idea that the ABA reduction is mainly cell count in these cells. However, it is important to note that if more profound metabolic changes are induced, then the ABA may be confounded.

3.2.6 Culture of iPSC-CMs on Collagen Scaffolds

Since it proved possible to culture beating iPSC-CMs on different ECM substrates, the feasibility of culturing the iPSC-CMs on disc-shaped collagen-derived scaffolds was investigated. Collagen I was used as the primary ECM material because it is the most abundant ECM protein in the heart. To see whether composition affected the cell's retention rate, 100% collagen scaffolds were compared to collagen-derived scaffolds integrated with different ECM substrates. Mixed scaffolds of collagen with Elastin or Chondroitin-4-Sulfate (C4S) were used because these materials are found in the native heart.

Beating iPSC-CMs from three independent differentiation batches were harvested on DD7, DD9, DD12, DD20+ and 10^6 cells were seeded on each of the different collagen-derived scaffolds or ECM substrate coated well plates (Table 3.3), to compare 2D vs 3D environments.

Table 3.3: Different collagen-derived scaffold composition and ECM substrate used for culturing iPSC-CMs for maturation.

2D vs 3D	**Scaffold Composition**	**Abbreviation**
Scaffold	100% Collagen	100% Coll
Scaffold	100% Collagen coated in RF-Matrigel	RF/Coll
Scaffold	Collagen/Elastin 1:1	Coll/Ela 1:1
Scaffold	Collagen/Chondroitin-4-Sulfate 1:1	Coll/C4S 1:1
Monolayer	Collagen 1	Coll 1
Monolayer	Fibronectin	FN
Monolayer	Gelatin/Fibronectin	Gel/FN
Monolayer	RF-Matrigel	RF

Initial seeding methods consisted of pipetting 200 μL directly onto the scaffold, but this method had a seeding efficiency of only 50%. A new and improved way of seeding the scaffolds was developed (Section 2.1.2.2) which increased the seeding efficiency to around 80-92% (Fig. 3.20). Seeding efficiency was calculated the day after seeding when the scaffold

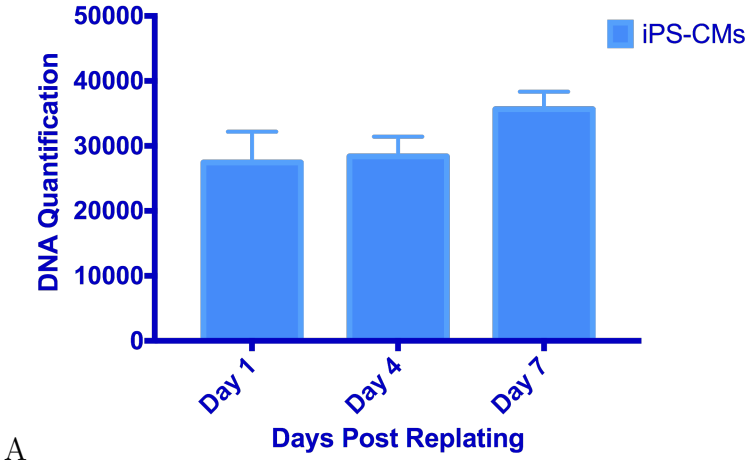

A

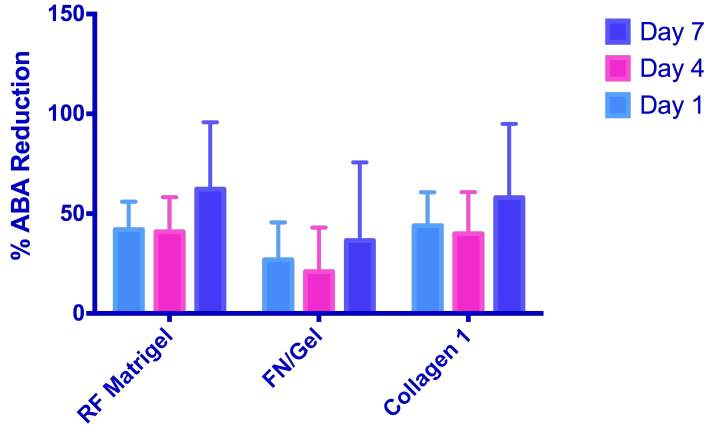

B

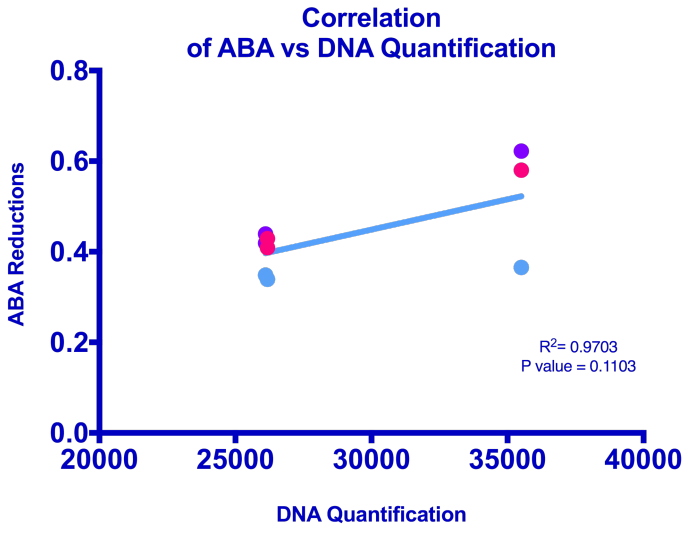

C

Figure 3.19: A) DNA quantification showing the total amount of DNA from iPSC-CMs harvested on Day 1, 4, and 7 post re-plating on DD7. Each time point was run in triplicates. B) Combined ABA reduction from 12 different batches of DD7 iPSC-CMs re-plated and cultured on three different ECM substrates (RF-Matrigel, Gel/FN, and Collagen I coated plates) for up to 1 week. C) Correlation between the two graphs. The bars represent the means + SEM. Each bar color represents the day the ABA was taken post re-plating. Analyzed using a two-way ANOVA.

was transferred to a new well. The number of cells attached was calculated by taking the total number of cells seeded minus the number of cells that didn't attach and were leftover in the well [Eq. (3.1)].

$$\text{Efficiency}(\%) = (\frac{\text{number of cells attached}}{\text{total number of cells}}) * 100 \tag{3.1}$$

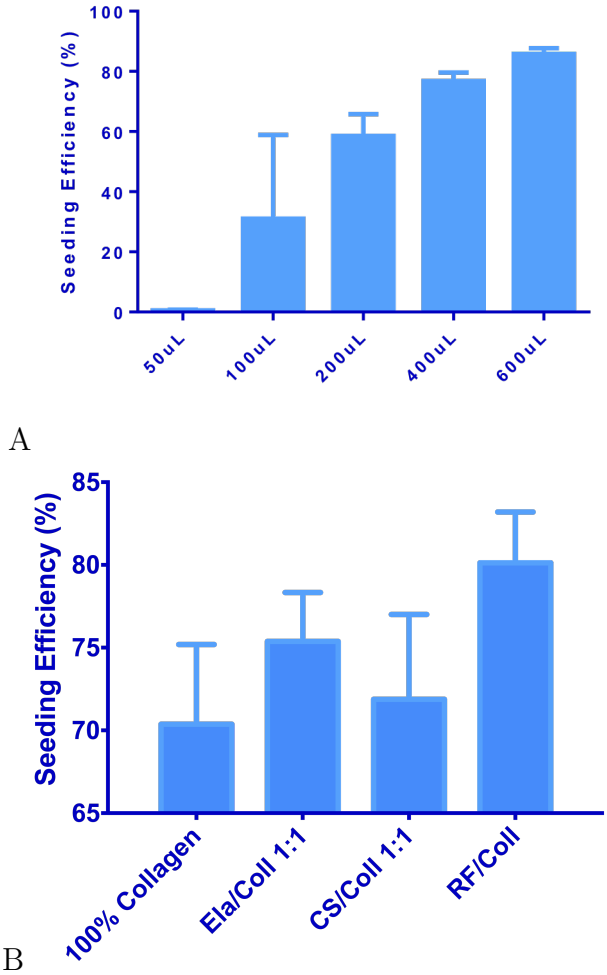

Figure 3.20: A) Seeding efficiency of 1 million DD15 iPSC-CMs (n=4) resuspended in different loading volumes of RPMI+B27 media and seeded onto 100% collagen scaffolds. B) Seeding efficiency of 1 million DD15 iPSC-CMs resuspended in a volume of 600 μL onto four different types of scaffolds. The experiment was run in 3 biological repeats in duplicates.

3.2.6.1 Determining iPSC-CMs Cell Count on Scaffolds

For measurements of substrate utilization, it is essential to know the cell count, so it is very crucial to find a consistent and reproducible way to determine how many cells are on scaffolds. We were able to gain an initial cell count during our single cell dissociation to have a fairly good estimate of how many cells were seeding on the scaffolds and monolayers. However, unlike the monolayers, there was no ability to take a cell count for the scaffolds at the moment of the experiment because there is no reproducible way to detach cells from a scaffold. As a result, several side experiments were run to help find a reliable cell count method for the scaffolds.

To start, we wanted to get an idea of how much cell proliferation occurs naturally over the span of 15 days. To do this the iPSC-CMs were dissociated into single cells on DD7 and counted. We then re-plated them in triplicates on a 24-well plate and counted them again at Days 0, 1, 3, 5, 7, and 15 post re-plating (Fig. 3.21). We saw an initial decrease in cell count which was probably from the cells being unhappy due to the dissociation into single cells when they prefer to maintain connection with each other. Within a week they had recovered and there was no significant change from the starting counts. If we extended past a week, the cells started to proliferate slowly. This is interesting since it was thought that the population was mainly CMs which are not thought to proliferate, suggesting that some degree of less differentiated cells remain that have the ability to proliferate.

A long term ABA was also performed from DD36 to DD66. There was no change in ABA reduction over time in the beating cells implying that the cells were not proliferating, but the non-beating cells had a slow, significant increase from the initial ABA readings taken, suggesting that there were less-differentiated cells in the non-beating population (Fig. 3.22).

Next, three different methods were explored to determine the optimal way to address cell count on scaffolds for the radiation experiments. The first method was to mirror the same number of cells seeded on a 3D scaffold with a 2D monolayer well where cells could be counted. 1 million iPSC-CMs were re-plated at different days of the differentiation protocol (DD7, DD9, DD12, and DD20+) and seeded onto 100% collagen scaffolds and in a parallel RF-Matrigel-coated monolayer. These cells were then cultured for 1 week, harvested, and

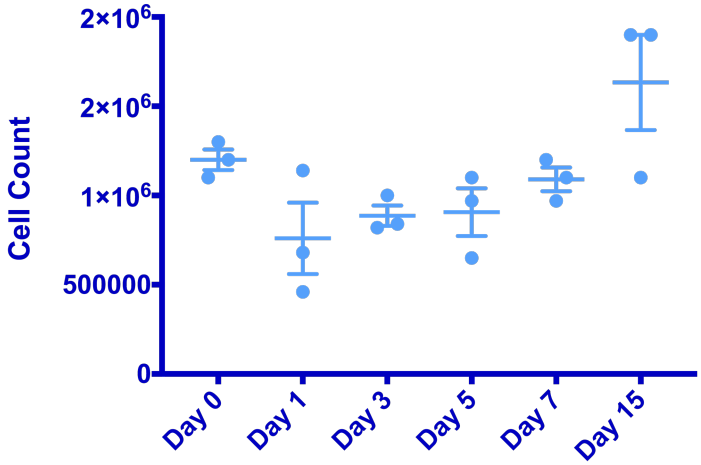

Figure 3.21: Cell proliferation data was obtained from three independent batches of iPSC-CMs by manually counting iPSC-CMs on an automated cell counter at different days up to two weeks post re-plating. Each time point was an average of triplicates, and the lines represents the mean + SEM.

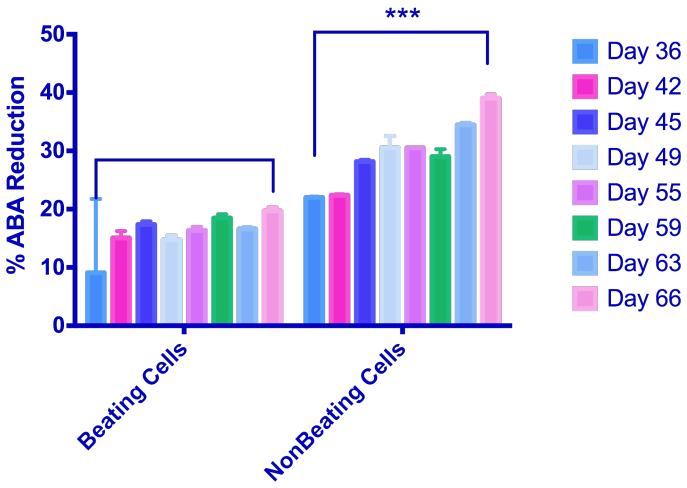

Figure 3.22: ABA percent reduction used to measure proliferation of 3 independent batches of non-beating versus beating iPSC-CMs during extended culture (up to around 3 months).

the monolayer cells were counted via an automated cell counter (Table 3.4) to obtain an estimated cell count. This cell count is then used as an estimated cell count number for the 3D scaffolds at that moment in time assuming the conditions were the same over the week.

Table 3.4: Method 1 to determine cell count on scaffolds, 1 million iPSC-CMs were re-plated at different differentiation days and seeded onto RF-Matrigel-coated 24-well plate monolayer. These cells were then cultured for 1 week and harvested to manually counted to obtain a estimated cell count.

RF-Monolayer	**Cell Count**
DD7 Seeded	$7.6x10^5$
DD9 Seeded	$7.8x10^5$
DD12 Seeded	$8.2x10^5$
DD20+ Seeded	$8.6x10^5$

The second method used the loading efficiency calculation [Eq. (3.1)] by taking the total number of cells seeded minus the cells that did not seed. Again new batches of iPSC-CMs were differentiated and 1 million cells were seeded on different days of the differentiation protocol (DD7, DD9, DD12, and DD20+) onto 100% collagen scaffolds. The following day post-seeding, the scaffolds were moved to a new well of fresh media. The original well was then harvested and counted to quantify how many cells did not seed onto the scaffold or died during the transition process. This number was then subtracted from the initial seeded cell count to get our second predicted cell count number (Table 3.5).

Since there is no ability to physically observe the cells on the scaffold and or detach them to count cells once they have been seeded, the only technique we can perform without being terminal for the cells is an ABA. From our previous experiments, it was assumed that the ABA reduction is proportional to cell number.

Method 3 tried to correlate ABA reductions with cell counts. For each differentiation day, a series of ABA serial dilutions were performed to see if we could determine a range of cell numbers corresponding to a specific range of colour change in the fluorescence. Scaffolds were seeded in triplicates with 250k, 500k, 1 million, 2M or 3M cells per scaffold. The ABA was performed the first day post-seeding and the fluorescence was plotted against cell number with linear regression lines calculated per DD (Table 3.6 and Fig. 3.23). These

Table 3.5: Method 2 to determine cell count on scaffolds. 1 million iPSC-CMs were re-plated at different days of the differentiation protocol and seeded onto 100% collagen scaffolds. After one day of culture, the scaffolds were moved to a fresh plate and the dead cells remaining in each well was manually counted. A total cell count was achieved by subtraction the assumed initial starting number of 1 million cells minus the cells that did not attach on the scaffold.

Day Seeded	Sample	Total	Left in well	Assumed Seeded	% Seeded
DD7	100% Coll 1	10^6	$2.8x10^5$	$7.2x10^5$	72%
DD7	100% Coll 2	10^6	$2.2x10^5$	$7.8x10^5$	78%
DD7	100% Coll 3	10^6	$2.6x10^5$	$7.4x10^5$	74%
DD9	100% Coll 1	10^6	$2.5x10^5$	$7.5x10^5$	75%
DD9	100% Coll 2	10^6	$2.4x10^5$	$7.6x10^5$	76%
DD9	100% Coll 3	10^6	$2.7x10^5$	$7.3x10^5$	73%
DD12	100% Coll 1	10^6	$2.0x10^5$	$8.0x10^5$	80%
DD12	100% Coll 2	10^6	$2.9x10^5$	$7.1x10^5$	71%
DD12	100% Coll 3	10^6	$2.1x10^5$	$7.9x10^5$	79%
DD20+	100% Coll 1	10^6	$2.9x10^5$	$7.1x10^5$	71%
DD20+	100% Coll 2	10^6	$1.4x10^5$	$8.6x10^5$	86%
DD20+	100% Coll 3	10^6	$1.3x10^5$	$8.7x10^5$	87%

equations were then used as method 3 to predict cell counts for new scaffolds based off their ABA reductions.

To test this method, a new set of 100% collagen scaffolds were seeded on different DD with 10^6 cells. After a week, an ABA was performed on each scaffold (incubated for 4 hours with 1:10 ABA). The scaffolds ABA reduction was then plugged into each DDs corresponding linear regression equation and the predicted cell count was calculated (Table 3.7). Overall this method could only predict within 20% of the initially seeded cell count and was discarded as a cell counting option. The fluorescence must not be comparable from day to day.

It was decided to proceed with a combination of method A and B for the official cell count number used in all the radiation experiment calculations. Each experiment would have a parallel monolayer that could be harvested the day of the experiment for an assumed cell count (method A). This number was then averaged with the predicted current seeded scaffold number calculated by the total seeded minus unattached cells harvested the following day post-seeded (method B). Knowing that the scaffolds have on average an 80%

Table 3.6: Method 3: Calculating ABA dilution linear regression equations. Different amounts of iPSC-CMs (2.5^5, 5.0^5, 1M, 2M and 3M) were re-plated at DD7, DD9, DD12, and DD20+ onto 100% collagen scaffolds. ABA was performed 1 week after re-plating.

Day Seeded	**Scaffold**	**Cell #**	**ABA% Reduction**
DD7	Coll 1	250000	0.029097
DD7	Coll 2	500000	0.056412
DD7	Coll 3	1000000	0.061383
DD7	Coll 4	2000000	0.093807
DD7	Coll 5	3000000	0.135706
DD9	Coll 1	250000	0.034667
DD9	Coll 2	500000	0.052615
DD9	Coll 3	1000000	0.073361
DD9	Coll 4	2000000	0.117749
DD9	Coll 5	3000000	0.15401
DD12	Coll 1	250000	0.064097
DD12	Coll 2	500000	0.084324
DD12	Coll 3	1000000	0.094324
DD12	Coll 4	2000000	0.12117
DD12	Coll 5	3000000	0.139583
DD20+	Coll 1	250000	0.043347
DD20+	Coll 2	500000	0.072058
DD20+	Coll 3	1000000	0.093576
DD20+	Coll 4	2000000	0.10308
DD20+	Coll 5	3000000	0.13277

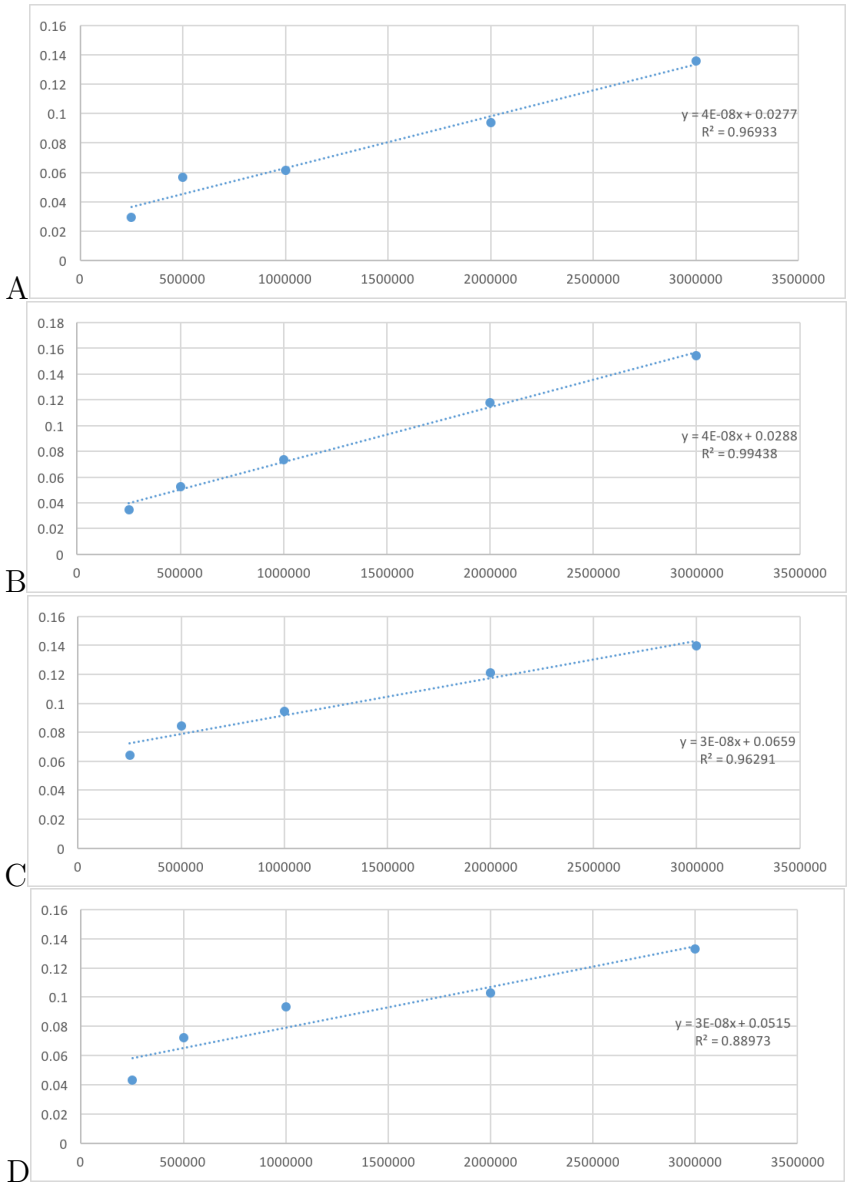

Figure 3.23: Method 3: The ABA reduction collected in Table 3.6 for A) DD7, B) DD9, C) DD12, D) DD20+ were plotted against their corresponding cell numbers and a linear regression equation was calculated to predict an assumed cell count number based off the level of ABA reduction. The experiment was run in 3 biological repeats in triplicates.

Table 3.7: Method 3 continues: 1 million iPSC-CMs were re-plated at DD7, DD9, DD12, and DD20+ onto 100% collagen scaffolds and an ABA was performed 1 week after re-plating. The ABA reduction measured was plugged into the previous linear regression equations calculated per time point in Fig. 3.23 to predict an assumed cell count number based off for each scaffold. From this number a percent seeding efficiency was calculated.

Day Seeded	Scaffold	ABA% Reduction	Predicted Seeded	% Seeded
DD7	Coll 1	0.049097	53493	5.3%
DD7	Coll 2	0.051383	59208	5.9%
DD7	Coll 3	0.044667	42418	4.2%
DD9	Coll 1	0.078191	123478	12%
DD9	Coll 2	0.056412	690300	6.9%
DD9	Coll 3	0.052615	59538	5.9%
DD12	Coll 1	0.0688365	97883	9.7%
DD12	Coll 2	0.135706	232687	23%
DD12	Coll 3	0.117749	172830	17%
DD20+	Coll 1	0.097125	152083	15%
DD20+	Coll 2	0.15401	341700	34%
DD20+	Coll 3	0.1361765	282255	28%

seeding efficiency, all scaffolds were seeded with 1.2 million cells accounting for a 20% loss giving an average of 1 million cells seeded per scaffold in each experiment moving forward.

3.2.7 ABA of Cultured iPSC-CMs on Collagen-Derived Scaffolds and ECM Substrate Coated Monolayer Plates.

For the next set of experiments, iPSC-CMs were seeded on four different collagen-derived scaffold compositions (100% Coll, Coll/Ela 1:1, Coll/C4S 1:1, and RF coated 100% Coll) and three monolayers (RF-Matrigel, collagen I and fibronectin) at 4 different time points (DD7, DD9, DD12, and DD20+). RF-Matrigel-coated wells were used as control and collagen I coated wells were chosen as the monolayer comparison for the 3D 100% collagen scaffold. Fibronectin was chosen because it has been shown that CDCs cultured on fibronectin differentiate further than those on collagen IV [508–510]. The ABA was performed on Days 1, 4, and 7 post seeding on the scaffolds and monolayers. Bearing in mind the variability

between cell batches, there are three main results that can be deduced. First, when data for all monolayers were combined and for all scaffolds, the monolayers had a higher ABA reduction than the scaffolds (Fig. 3.24). Second, the DD7 and DD9 cells were more fragile and tended to not survive as well over the next week on both the monolayers and the scaffolds, whereas the more mature cells survived longer, probably due to the fact they created the necessary connections to survive the re-plating and seeding process. Lastly, the Coll/C4S 1:1 scaffold had the highest initial ABA reduction at each DD seeded compared to all the other scaffold compositions, but this still tended to decrease with time (Fig. 3.25).

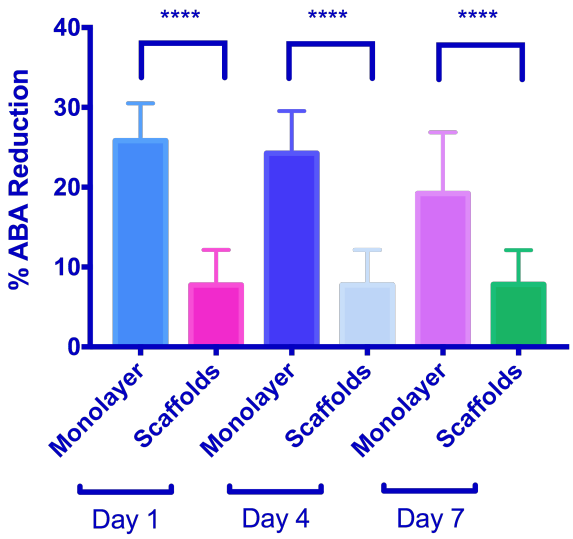

Figure 3.24: ABA reduction of combined iPSC-CMs cultured in a monolayer versus 3D scaffolds on Days 1, 4, and 7 post seeding and re-plating. The experiment was run in 3 biological repeats in triplicates. The bars represent the mean + SEM. Each bar color represents the day in which the ABA was done post re-plating/seeding and if that condition was a monolayer or scaffold. "*" denotes p-value of 0.05, "**" p-value of 0.01, and "***" p-value of 0.001. The set of stars refers to significance in comparing the monolayer versus scaffold at each day point. Analyzed using a two-way ANOVA.

3.2.8 RF-Matrigel-Coated Scaffolds vs 100% Collagen Scaffolds

Since the collagen scaffold coated with RF-Matrigel had a higher seeding efficiency, measured by counting cells remaining in the well, (probably due to its sticky nature), which

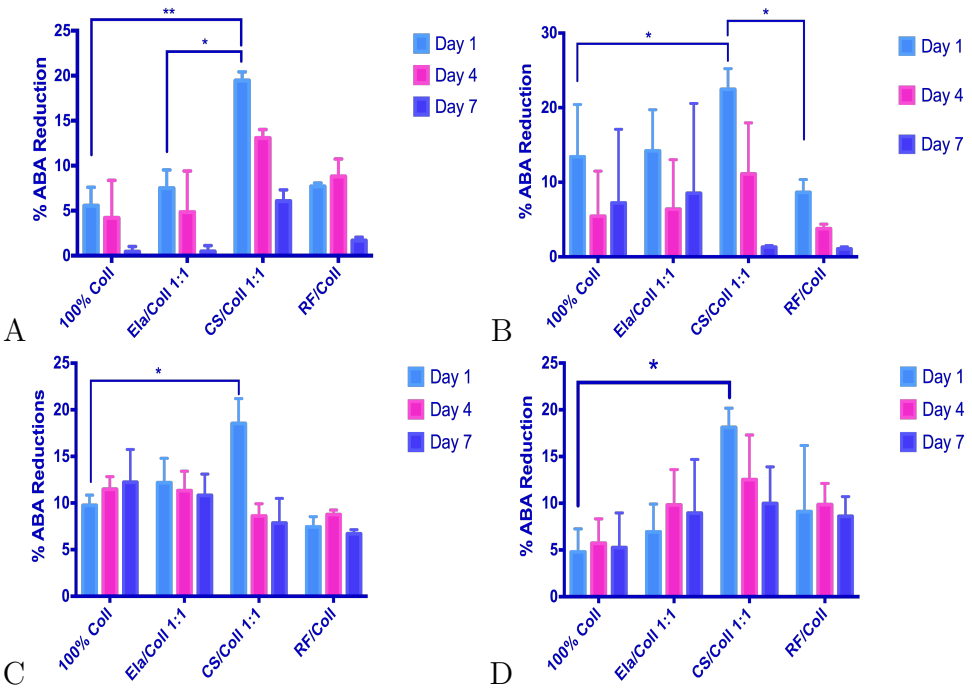

Figure 3.25: A) DD7 iPSC-CMs, B) DD9 iPSC-CMs, C) DD12 iPSC-CMs, and D) DD20+ iPSC-CMs seeded on scaffolds made from 100% Coll, Coll/Ela 1:1, Coll/C4S 1:1 and RF/Coll and cultured for 1 week. The experiment was run in 5 biological repeats in triplicates with 3 technical repeat. The bars represent the mean + SEM. Each bar color represents the day in which the ABA was done post re-plating/seeding. "*" denotes p-value of 0.05. The set of stars refers to significance in comparing Coll/C4S to the other scaffold compositions. Analyzed using a two-way ANOVA.

made it look like a desirable scaffold (Fig. 3.26), a closer look was taken at the ABA results from these scaffolds (Fig. 3.27). DD9 seeding had higher ABA reduction for the first day post re-plating for the 100% collagen scaffold compared to DD7 and DD9 RF-Matrigel-coated scaffolds cells seem to have significantly died off over the week. However, overall there was little to no significant difference in ABA reduction between collagen scaffolds and those scaffolds coated with RF-Matrigel. This is an interesting thought, since we calculated that the RF-Matrigel-coated scaffolds had a higher seeding efficiency (more cells seeded) but measured an equivalent ABA reduction, which reduces confidence in the conclusions that can be drawn from the ABA data.

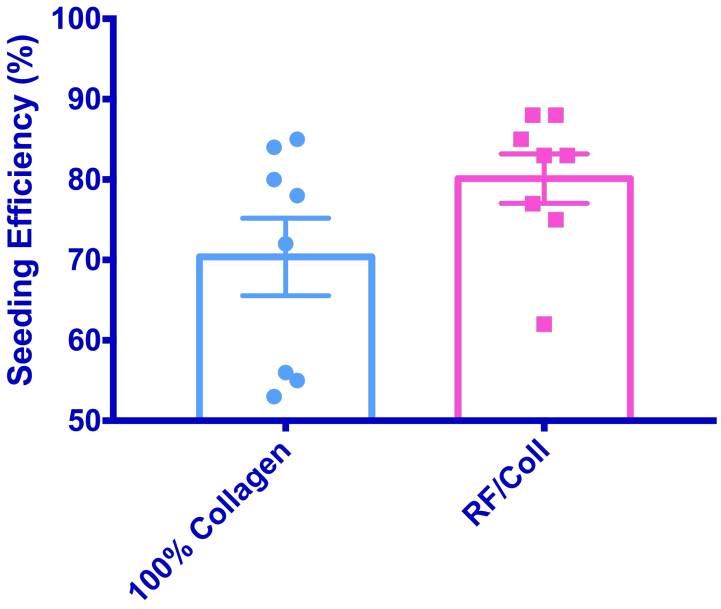

Figure 3.26: Seeding efficiency of 100% collagen scaffold versus RF-Matrigel-coated 100% collagen scaffolds. 1 million iPSC-CMs were re-plated on DD15 onto a 100% collagen scaffold. The following day the scaffolds were changed to a fresh new well of media and the remaining cells that did not seed onto the scaffold or died were manually counted via an automated cell counter. The seeding efficiency (%) was then calculated by 1 million cells minus remaining cells in the well x 100. The bars represent the mean + SEM; n=8.

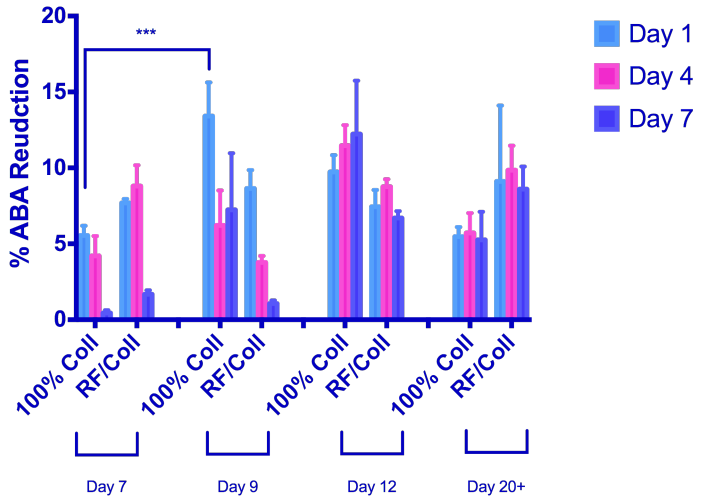

Figure 3.27: ABA reduction of 100% collagen scaffolds versus RF-Matrigel-coated 100% collagen scaffolds. 1 million iPSC-CMs were re-plated on different days of the differentiation protocol onto either a RF-Matrigel-coated or noncoated 100% collagen scaffold. ABA were performed on days 1, 4, and 7 after re-plating. The bars represent the mean + SEM; n=10.

3.2.9 Gene Expression Changes Between Cultured iPSC-CMs on Collagen-derived Scaffolds and ECM Substrate Coated Monolayer Plates

The scaffolds were seeded on DD7, DD9, DD12-15, and DD20+ and cultured for 1 week for the ABA experiments and were then harvested and RNA extracted for qPCR analysis. Unfortunately, due to the solid nature of the scaffolds, retrieving RNA proved to be difficult and not all scaffolds yielded sufficient RNA. As a result, only the qPCR analysis of DD12-15 seeded 100% collagen scaffolds versus iPSC-CMs cultured on RF-Matrigel and Gel/FN was performed. There was an increased expression in *MYH6*, *MYH7*, *PGC1α*, *PDK4* and *COL1* in cells cultured on scaffolds compared to those in the monolayers (Fig. 3.28), suggesting that maintaining iPSC-CMs on collagen scaffolds for a week may have induced a degree of maturation.

The experiment was repeated two more times to try and account for the low RNA yield and fill in the samples from each of the conditions for qPCR analysis. The scaffolds were again seeded on DD7, DD9, DD12-15, and DD20+ and cultured for 1 week. The gene

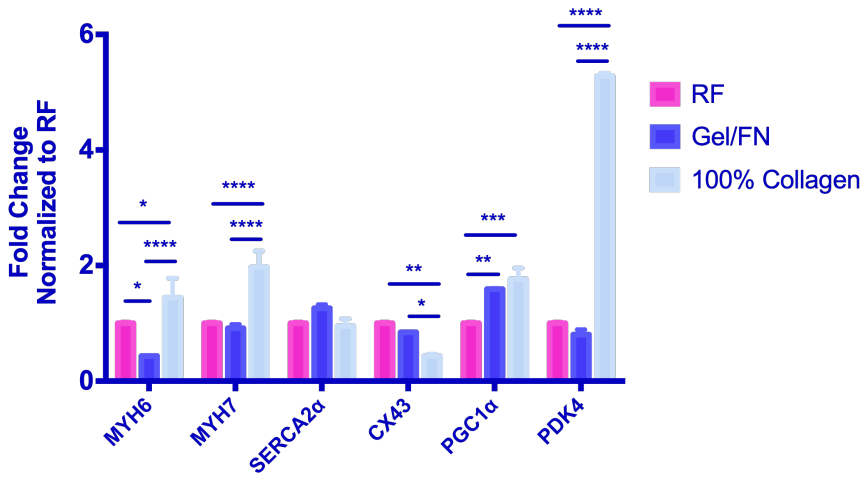

Figure 3.28: CM gene expression of DD15 re-plated iPSC-CMs cultured for 1 week. The experiment was run in 3 biological repeats in duplicates with 3 technical repeats. The bar represents the mean + SEM. The indigo represents the Gel/FN monolayer group, whereas blue represents the collagen scaffold group. Both normalized to the pink bar representing the monolayer DD12-15 iPSC-CMs seeded on RF-Matrigel. "*" = $p<0.05$, "**" = $p<0.01$, and "***" = $p<0.001$ or equivalent; analyzed using a two-way ANOVA and a Tukey's multiple comparison test.

expression of structural proteins had increased by DD20+ (Fig. 3.29). Cells cultured on FN, Coll 1, Coll/C4S and Coll/Ela had increased levels of *TNNT2* expression compared to the 2D RF-Matrigel at DD20+. In addition, cells cultured on FN, Coll I and Coll/C4S also had increased levels of *MYH6* expression compared to the 2D RF-Matrigel at DD20+. However, in contrast to the first experiment, the data from this set of samples were considerably more variable when looking at the metabolic gene expression. Due to the large variability in sample isolation, only two biological replicates were assessed and so no stats were performed (Fig. 3.30).

3.2.10 Fatty Acid Oxidation of Cultured iPSC-CMs on Collagen- derived Scaffolds and ECM Substrate Coated Monolayer Plates

Both palmitate and oleic acid oxidation rates were determined for DD15 iPSC-CMs seeded either as a monolayer (in wells coated with RF, Collagen, FN, or Gel/FN) or onto a scaffold

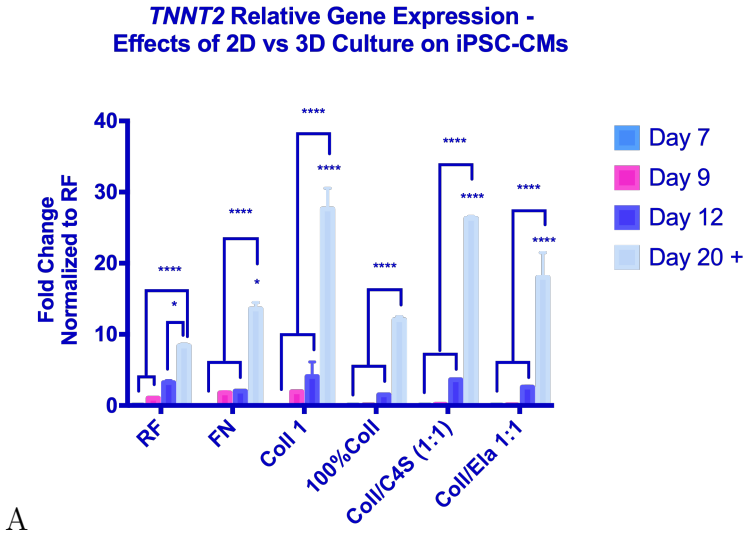

A

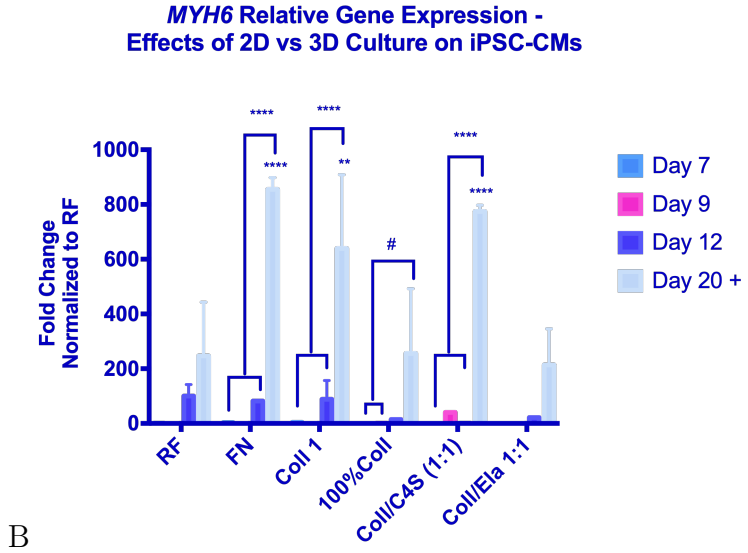

B

Figure 3.29: A) *TNNT2* and B) *MYH6* CM gene expression of iPSC-CMs re-plated on either DD7 (blue), DD9 (pink), DD12-15 (indigo), or DD20+ (light blue) and cultured for 1 week until harvested. The experiment was run in 3 biological repeats in duplicates with 3 technical repeats. The bar represents the mean + SEM. Each condition was normalized to the RF-Matrigel monolayers. For clarity, only the comparison to the DD20+ cultured on RF-Matrigel were shown. "*" = $p<0.05$, "**" = $p<0.01$, and "***" = $p<0.001$ or equivalent; analyzed using a two-way ANOVA and a Tukey's multiple comparison test.

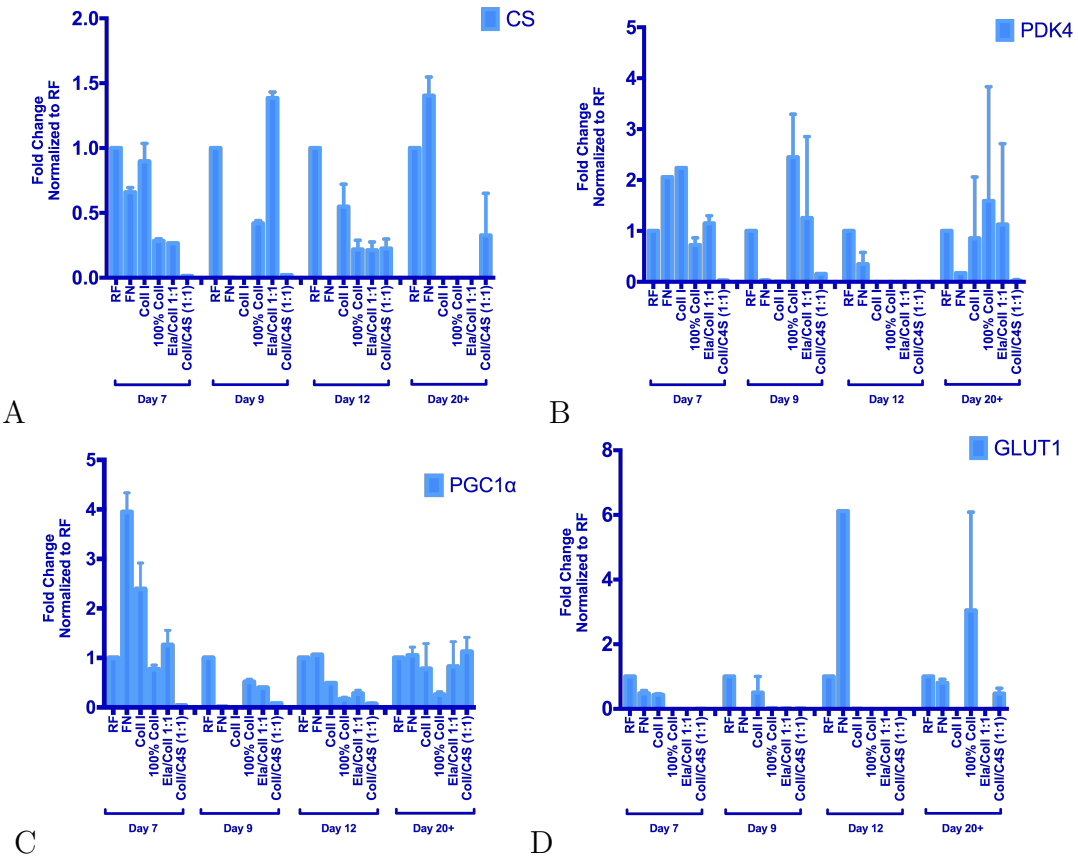

Figure 3.30: Gene expression of A) *CS* B)*PDK4* C) *PGCl*α D) *GLUT1* between 2 batches of biological repeats, each in duplicates. The bar represents the mean + SEM (n=2, no stats performed).

(100% Collagen, Coll/C4S 1:1, or Coll/Ela 1:1). The cells were cultured for a week in these conditions then incubated for 8 hours in RPMI+B27 media containing 2% BSA and either 0.3 mM palmitate doped with Palmitic Acid [9,10-^{3}H(N)] or 400 μL OA doped with Oleic Acid [9,10-^{3}H(N)]. Oxidation rates of both fatty acids increased in all the 3D constructs compared to the monolayers (Fig. 3.31).

3.2.11 Glycolytic Flux of Cultured iPSC-CMs on Collagen-derived Scaffolds and ECM Substrate Coated Monolayer Plates

Glycolytic rates were determined for DD15 iPSC-CMs seeded either as a monolayer (in wells coated with RF-Matrigel, Collagen, FN, or Gel/FN) or onto a scaffold (100% Collagen, Coll/C4S 1:1, or Coll/Ela 1:1). The cells were cultured for a week in these conditions then incubated for 8 hours in low-glucose RPMI media containing 2% BSA, 0.3 mM palmitate doped with D-[5-^{3}H(N)]-glucose. Glycolysis significantly decreased in all of the 3D constructs compared to the 2D monolayers (Fig. 3.32).

3.3 Discussion

iPSC-CMs have numerous applications and have been proposed to be an attractive candidate for modeling human diseases or the potential source for regeneration. In this Chapter, human iPSCs were differentiated into beating CMs and cultured in different environments to achieve a more mature phenotype. First, it was established that prolonged culture as a monolayer could induce a degree of maturation. Next, iPSC-CMs feasibility to grow on a variety of 2D ECM substrates was assessed and determined to not have a direct affect on metabolism over the time period chosen. Finally, iPSC-CMs were cultured on different 3D collagen-derived scaffolds and their genetic and metabolic phenotypes were characterized. Through radio-labelled substrate assays, it was shown that culturing in 3D decreased glycolysis and increased fatty acid oxidation.

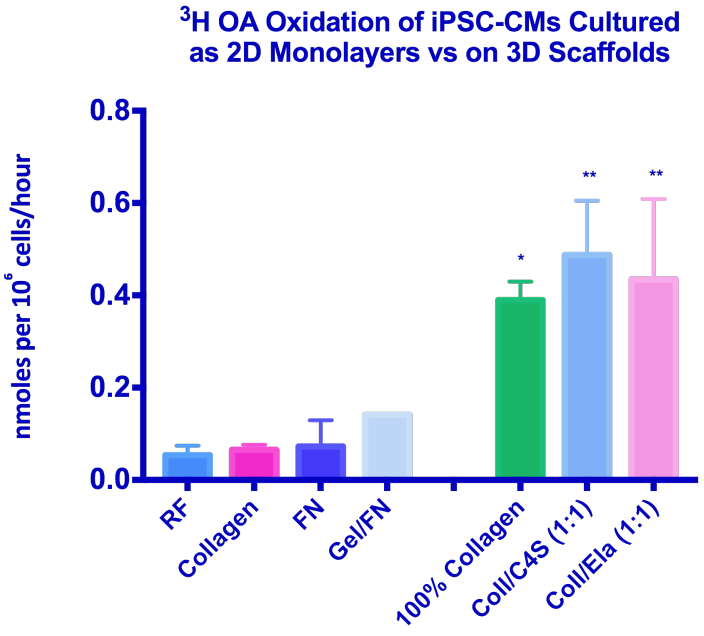

A

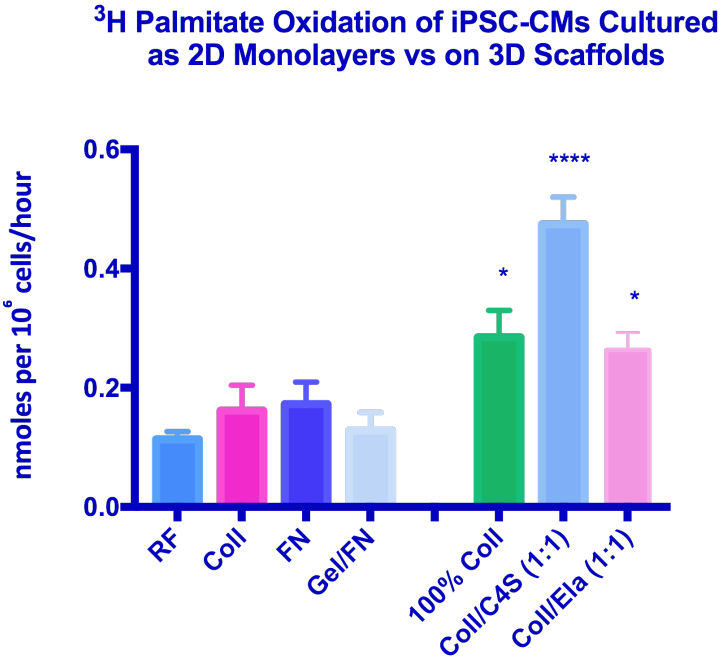

B

Figure 3.31: a) ^{3}H oleic acid oxidation B) ^{3}H palmitate oxidation of iPSC-CMs cultured on 2D ECM substrates or on 3D collagen-derived scaffolds. The experiment was run in 6-9 biological repeats in triplicates with 3 technical repeats. The bar represents the mean + SEM. The first four bars represent the monolayers (RF-Matrigel, collagen, FN, and Gel/FN consecutively). The next three bars represent the scaffolds (100% collagen, Coll/C4S, and Coll/Ela). Statistical analysis was performed against the blue bar representing the control RF-Matrigel monolayer. "*" = $p<0.05$, "**" = $p<0.01$, and "***" = $p<0.001$ or equivalent; analyzed using a two-way ANOVA and a Tukey's multiple comparison test.

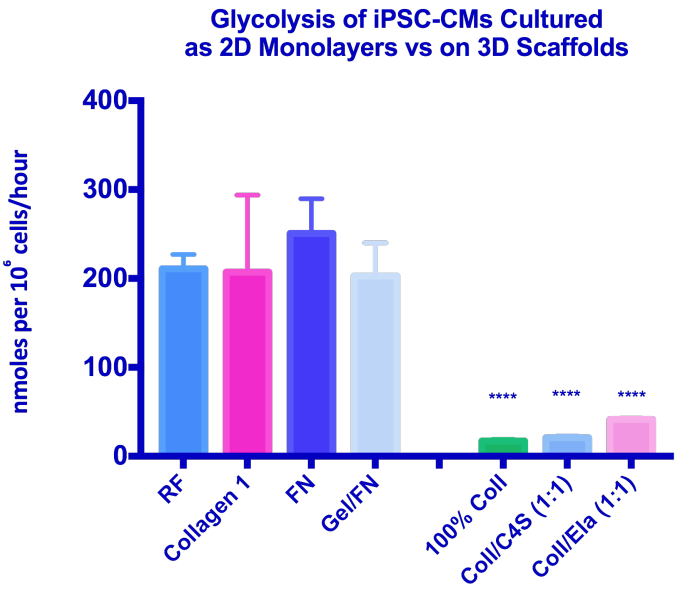

Figure 3.32: Glycolysis of iPSC-CMs cultured on 2D ECM substrates or on 3D collagen-derived scaffolds. The experiment was run in 6-9 biological repeats in triplicates with 3 technical repeats. The bar represents the mean + SEM. The first four bars represent the monolayers (RF-Matrigel, collagen, FN, and Gel/FN consecutively). The next three bars represent the scaffolds (100% collagen, Coll/C4S, and Coll/Ela). Statistical analysis was performed against the blue bar representing the control RF-Matrigel monolayer. "*" = $p<0.05$, "**" = $p<0.01$, and "***" = $p<0.001$ or equivalent; analyzed using a two-way ANOVA and a Tukey's multiple comparison test.

Most experiments started at with cells at one of two time points: DD7 and DD15. Initially DD7 was explored as the day the dierentiation protocol ended. The DD7 cells were used as a control, representing the least mature cell type as the cells would have only formed cardiac mesoderm without a contractile phenotype. After initial experiments, we used DD15 cells which represented the stage of first spontaneous contractions. Cells at DD15 survived the replating process better than DD7 cells and a visualization of beating allowed correct flask selection for experiments. Cells for each experiment were then cultured for 1 week in each condition to give enough time induce genetic eects. Although, beating CMs were successfully generated in most cases, not every batch would beat to the same extent leading to a considerable amount of batch to batch variation. This was not unexpected, as it is a well-known obstacle that iPSCs dierentiation ecacy varies greatly even within the same cell line [511]. This inconsistency added a level of complication to the analysis and interpretation of the data as it could result from things like cell cycle differences or differing ratios of CMs to non-CMs (such as fibroblasts) produced in individual batches. For this reason, qPCR analysis was performed on iPSC-CMs in triplicates derived from three independent batches to assess maturation.

3.3.1 iPSC-CMs Maturation Through Long-Term Culture

The gene expression results supported what others have shown, that a degree of maturation can be achieved through prolonged culture [328, 378, 512]. After three months our iPSC-CMs gained a more mature contractile and metabolic gene expression phenotype. Piccini *et al.* [513] performed transcriptome analysis on iPSC-CMs and observed only marginal differences between one and two month old iPSC-CMs. Lundy *et al.* [378] also assessed long term culture to induce maturation by comparing ESCs and iPSC-CMs after 20-40 and 80-120 days of differentiation. The older cells were larger, less spherical, and more multi-nucleated. Similar to our data, Lundy saw with prolonged culture the same switch in relative expression of the faster alpha isoform (*MYH6*) towards the slower beta isoform (*MYH7*) which was accompanied by increased expression of *SERCA2α* in late stage hESC-CMs. Jung *et al.* [514] generated iPSC-CMs using an EB differentiation system and

allowed for further maturation through prolonged culture of an addition 2-4 months. After two months, the expression of most genes involved in calcium handling reached similar levels to that of a foetal human heart. However, there were nearly undetectable levels of *CASQ2* observed and it took 4 months of culture for these to reach foetal heart levels. Similarly, in this study, *CASQ2* was unchanged during the 3 months of culture.

Overall it took around 3 months to get a significant upregulation in expression of oxidative metabolism genes. The isoform switch between *GLUT1* and *GLUT4* was observed as early as DD12. While *GLUT1* expression was unaffected over the 3 months, *GLUT4* was continually increasing with the maturation of the cells. The gene expression of PGC1α and *CS* were upregulated by 3 months. Dai *et al.* [328] also observed in iPSC-CMs an upregulation in *CS*, along with increased mitochondrial number and membrane potential after 12-15 weeks of culture. The expression of *PDK4* was upregulated with maturation in 2D within the first month but *PPAR*α was unchanged. However, there were no FAs in the culture media used in this study, so it is possible that FAs supplementation could have activated *PPAR*α signalling, altering the cell's metabolic phenotype. There was also no alteration in the levels of *IRS1* and *IRS2* expression observed. The lack of changes in expression with maturation of CMs suggests that the iPSC-CMs were insensitive to insulin-dependent regulation.

This study reflected what others have shown that iPSC-CMs can be matured with long term culture, but it is expensive and time consuming. Due to the costly nature of culturing cells for 3 months only gene expression was used as a measure of maturation. While investigating some of the distinctive isoform switches such as *MYH6/7* and *GLUT1/4* to show parameters of maturation this study could have also addressed others such *ssTn1/cTNT*, *N2BA/N2B*, or *MYL2/7*. These markers could have complimented the other maturation indicators and also helped define the population phenotype as being more atrial or ventricular. Overall, waiting 2 to 3 months for metabolic maturation is impractical for scientific applications, so other culture methods were investigated to try and improve that time to a more applicable range.

3.3.2 iPSC-CMs Cultured on Different 2D ECM vs 3D Scaffolds

2D iPSC-CMs are usually cultured and differentiated on RF-Matrigel, a poorly-defined, biological substrate. To try and induce maturation quicker the iPSC-CMs were cultured on a range of different ECM substrates to try and mimic in vivo. Others have shown the importance of ECM in cardiac development. Fibronectin, is highly expressed at the foetal stage and promotes cell migration [515]. Collagen, laminin, glycoproteins and proteoglycans increase sarcomere organization and density during neonatal development and then take on more structural support roles during CM adulthood [516,517]. To mirror the long term culture experiments, iPSC-CM were replated on DD7 after completion of their differentiation protocol. However, when culturing our iPSC-CMs for one week we observed no particular maturation benefit amongst the gene expression of the cells cultured on the different ECM substrates. Due to high cost of keeping the cells in culture, after a week of no results the experiments were left and assumed that iPSC-CMs had no preference on what substrates they were cultured on for at least the time parameters used.

Knowing that iPSC-CMs can be dissociated and then successfully re-plated on a variety of different ECM substrates in 2D, 3D culture was developed for different collagen-derived scaffolds. There were two options to translate these cells onto 3D constructs, the first is to seed the undifferentiatied cells and differentiate directly within the scaffold or to re-plate the iPSC-CMs post differentiation. While some studies differentiate the stem cells within the scaffold, given the batch to batch variability and limited visual aspect to monitor the cells, a pre-differentiation and reseeding method was used in this thesis.

Porous scaffolds were chosen as they enable perfusion of media into the structure. A former student previously showed that histological analysis revealed that the CMs adopt a similar morphology to that seen in 2D and formed small contractile clumps on the collagen-derived scaolds as seen in monolayer culture [429]. They also previously showed, via SEM micrographs, that the CDCs penetrated the collagen-derived scaffold and settled into pores (average size ranging from 115.6 μm to 187.6 μm) after 1-week in culture [429].

In this thesis, it was observed that the majority of cells mainly resided on the top surface which was also seen with endogenous rat cardiac progenitors [429]. The exact depth of cell penetration in our scaffolds could be confirmed via SEM micrographs, cyrosectioning and immunohistochemistry analysis at a later date. If given enough time, the cells would eventually secrete enzymes that would remodel the scaffold and generate new ECM proteins. This suggests that over time a scaffold would be degraded and replaced with self-secreted matrix, allowing for colonization of deeper layers.

Different timepoints were tested for the optimal seeding range of the collagen scaffolds. Initial results showed that DD7 was too early and iPSC-CM survival rate was not as prominent as DD15+. This was most likely due to the fact DD15+ cells were beating and naturally maturing, allowing them to handle the replating process. As a result DD15 was chosen for a starting timepoint for the rest of the thesis due to higher retention rate and the ability to visualize intial contraction in order to select beating flasks for experiments.

Culture of iPSC-CMs on porous collagen scaffolds induced a 2-fold increase in mRNA expression of *MYH6* and *MYH7* and a 5-fold increase in mRNA expression of *PDK4*, indicating a degree of both structural and metabolic maturation over 1 week of culture. 3D culture conditions have been explored for CMs maturation previously. Bian *et al.* [401] cultured neonatal rat CMs in a 3D environment and after 3 weeks saw aligned, electromechanically- coupled CMs with capillary-like structures, improved calcium handling properties, and the action potentials of the cells showed directional dependence on local CM orientation and enhanced conduction velocities. Zhang *et al.* [387] showed, a 3D environment used to culture ESC-CMs with cardiac niche cells, which generated higher passive and active twitch forces, aligned sarcomeres, regularly dispersed CX43 and N-Cadherin, and overall an upregulation of genes indicating maturation. Another group reported seeded of ESC-CMs on a tissue patch induced longer sarcomeres, higher conduction velocities, and enhanced expression of contractile genes [389]. Fong *et al.* [518] cultured iPSC-CMs on a 3D scaffold made from native cardiac ECM and produced CMs with improved expression of calcium handling genes and calcium handling properties. 3D culturing has been shown to increase multiple morphological and functional properties of immature CMs including

increased binucleation, rod-like cell shape, sarcomere alignment, electrophysiology, and calcium handling properties [391].

3.3.3 Assessing 2D vs 3D Metabolic Flux

Metabolism has an important role in differentiation potential and can be a used as a target for maturation. While adult CMs mainly use FAs for ATP production, it is known that iPSC-CMs have a very foetal metabolism where the main substrate is glucose. Chung *et al.* [276] showed that the switch from an anaerobic glycolysis into a more FAO metabolism is critical for cardiac specification and excitation-contraction coupling. Accomplishing this switch in the iPSC-CM's metabolism towards increased FAO could show a sign of maturation.

ABA is not a straightforward technique to analyze due to the duality of its interpretation. It correlated well with cell number in 2D but the results with the 3D scaffolds were not consistent. To properly assess the maturation and functional metabolism in iPSC-CMs, metabolic flux analysis using radio-labelled substrates, was used to give a more accurate measurement of the contribution of glycolysis versus FAO being used for ATP generation. There was no difference in substrate utilisation when comparing the monolayer iPSC-CMs grown on different ECMs but, when iPSC-CMs were grown on 3D scaffolds the oleic acid and palmitate oxidation increased significantly across all 3D constructs compared to cells grown in 2D. To complement this increase in lipid metabolism, there was a significant decrease in glycolysis for these conditions. Thus a single week of culturing cells in 3D caused a 2-3 fold increase in FAO. After one week of 3D culture on a collagen-derived scaffold, the rate of glycolysis was averaging around 40 nmoles/10^6 cells/hour while the monolayers averaged around 200 nmoles/10^6 cells/hour. As glycolysis produces 2 ATP/mole of substrate the rate of ATP production was 80 or 400 nmoles ATP/mole of substrate for 3D vs 2D culture respectively. In parallel, the rate of FAO averaged 0.5 nmoles/10^6 cells/hour for the scaffolds and 0.1 nm nmoles/10^6 cells/hour for the monolayers. As β-oxidation of OA produces 120 moles ATP/mole of substrate, the rate of ATP production was 60 or 12 nmoles ATP/mole of substrate, for 3D vs 2D culture respectively. This shows that

even though scaffolds are increasing utilization of FAs, glycolysis is still the main source of ATP. Ulmer *et al.* [390] recently reported a similar increase in relative ATP production from glycolysis/oxidation (2D iPSC-CMs = 51%/49% versus 3D iPSC-CMs derived hydrogels = 14%/86%). These increases in oxidative metabolism are indicators of energy metabolism maturation due to 3D culture.

The 3D Coll/C4S (1:1) scaffold had the highest levels of FAO reaching as much as 2-3 fold more than the 2D RF-Matrigel monolayer. This was an interesting outcome. Others have shown chondroitin sulfate (CS) in compositions of scaffolds but mainly in applications with progenitor and stem cells functioning for tissue repair in cartilage, bone, cornea, skin and brain [519]. Very recently, Saporito *et al.* [520] showed the presence of CS in nanofibrous scaffolds was crucial for the adhesion and proliferation of cardiac cells for myocardial repair. With this logic, our Coll/C4S scaffolds may have permitted better adhesion over the pure collagen or integrated collagen/elastin scaffolds giving its added benefit.

3.4 Conclusion

The aim of this work was to increase metabolic flexibility in iPSC-CMs. As has been shown by others, we found that the cells matured slowly over time with changes in structural genes occurring during the first month of differentiation and continuing to increase up to 3 months whereas metabolic gene changes took longer to develop. Culturing the cells on different ECM substrates in 2D for the first week did not improve their maturation time. However, culturing the cells on 3D collagen scaffolds for only 1-week significantly affected the metabolic profile of the cells, by increasing fatty acid oxidation and lowering glycolysis compared with the 2D equivalents. Specifically, the Coll/C4S 1:1 scaffold was of interest having the highest increase in FAO and ABA reduction. Overall, however, despite the increase in FAO in the iPSC-CMs cultured on 3D scaffolds, anaerobic glycolysis remained the main source of energy generation.

I solemnly swear that I am up to no good.
— J.K. Rowling, Harry Potter and the Prisoner of Azkaban

4

Treatment with Oleic Acid and a PPARα Agonist (WY-14643) with 3D Culture Induces Metabolic Maturation in Induced Pluripotent Stem Cell derived Cardiomyocytes.

4.1 Introduction

4.1.1 Maturation of Stem Cell-Derived Cardiomyocytes

Energy substrate availability goes through changes during heart development from the foetal to adult heart, which results in a metabolic switch from a primarily glucose-based to FA. However, this switch in metabolism is not reproduced in the majority of published iPSC differentiation protocols. A number of labs are working on optimising cardiac differentiation, but consistently, the derived CMs remain immature [1, 158, 234–236]. Table 4.1 compares the differences in maturation between stem cell derived CMs and adult CMs. Morphologically, they are small, circular, and mono-nucleated, while adult CMs are large, rod-shaped, and multi-nucleated. Stem cell derived CMs lack t-tubules [233], causing calcium to slowly diffuse through the sarcolemma resulting in unsynchronised Ca^{2+} transients. The sarcomere

is a fundamental unit for CM contraction and in stem cell derived CMs its structure is disorganised with an average length of 1.6 μM [378] in comparison to the adult CM's organised sarcomere averaging around 2.2 μM long [521]. Overall, this affects the action potential rates causing slower-excitation and contraction coupling. Differentiating CMs undergo several myofibrillar protein isoform switches modulating the contractile function of the cell such as in Titin (N2BA switches to N2B), Troponin I (ssTnI switches to cTNT) and Myosin Heavy Chain (MHC) [1]. Differentiated stem cell derived CMs express *MHC*α more than *MHC*β and myosin light chain 2 atrial over ventricular, which is the opposite of that seen in adult CMs [1, 234, 235]. Metabolically, iPSC-CMs are known to have fewer, long and slender mitochondria which occupy only a fraction of the cell's volume, usually clustered by the nucleus or in the cell periphery [1]. These mitochondria form irregular networks in the cytoplasm, whereas in the adult CM mitochondria networks occupy up to 20-40% of the cell's volume [1, 158, 234–236]. In agreement with their immature nature, glucose is the primary energy substrate used by iPSC-CMs, whereas adult CMs rely more on FAO [1, 234].

Table 4.1: Summary of Differences Between Immature Stem Cell-derived CM and Mature Adult CMs, adapted from [1].

Parameters	**Stem Cell-derived CMs**	**Adult CMs**
Morphology	Cell shape: small, circular, and triangular; Membrane capacitance is 17.5 $\pm$ 7.6 pF [522].	Cell shape: large, rectangular, rod-shaped; Membrane capacitance is 150 pF [523].
Sarcomere	Structure: disarrayed; Length: 1.6 μm [378]	Structure: highly organised; Length: 2.2 μm [521]
Myofibrillar Isoform Switching	Titin: N2BA; Troponin I: ssTnI; and MHCα >MHCβ	Titin: N2B; Troponin I: cTnT; and MHCβ >MHCα
T-tubules	No [233]	Yes
Mitochondria	Irregular reticular network in cytoplasm; occupies only a small fraction of the cell's volume	Distributed evenly; Occupies 20-40% of cell's volume [1]
Metabolic Substrates	Glucose	Fatty Acids

Multinucleation	Mononucleated	25% Multinucleated
Electrophysiological Properties	Upstroke velocity: 50 V/sec [378]; Resting membrane potential: -60mV [378]	Upstroke velocity: 250 V/sec [523]; Resting membrane potential: -90mV [523].
E-C Coupling	Partially developed	Mature
Contractile force	Range: nN/cell	Range: μN/cell
Gap Junction Distribution	Circumferential	Polarized to intercalated disks
Conduction Velocity	0.1 m/sec [524]	0.3-1.0 m/sec
Responses to β-Adrenergic Stimulation	Chronotropic response: no inotropic reaction [525]	Chronotropic response: inotropic reaction

Another factor that potentially contributes to the immature metabolic nature of iPSC-CMs is the fact that they are routinely cultured in high-glucose media. Table 1.1 shows the substrate composition for a variety of media used in differentiation protocols from a range of labs. In culture media, the glucose concentration ranges from 4.5 mM - 25 mM. The variability in glucose concentration is of concern, especially when, in vivo, a glucose level of 25 mM is considered hyper-glycemic, which could lead to a loss of mitochondrial networks and eventually induce apoptosis [392, 393, 526]. In addition, the majority of these differentiation medias contain little to no lipids. For example, our differentiation media cocktail includes 1% of the additive B27, both during differentiation and for the length of their culture. Unfortunately, the exact composition of B27 is not disclosed, but it has been reported to contain around 0.2 mM OA [361], this would suggest a final concentration of only 2 μM FAs in the final culture media. This concentration of FAs is much lower than the 0.1-2mM of physiologically relevant levels [332], in contrast to the 11-25 mM of glucose which is much higher than the corresponding 6 mM of physiologically relevant level. This might contribute to the slow maturation of iPSC-CMs as the cells would not have the substrates required to switch from a predominately glucose metabolism to a FA-based metabolism. If there were potentially more FAs available to them in their culture media, would they be able to make that metabolic switch towards a more mature FAO?

4.1.1.1 Maturation Methods

Labs have attempted to mature cells in countless ways. The most consistent one to date is through long-term culture which was previously discussed in detail in Chapter 1. Others have shown that by using biochemical cues such as adrenergic receptor agonists, triiodothyronine, insulin-like growth factors or microRNA, they have been able to induce a degree of maturation [1]. Deng *et al.* [527] treated ESC-CMs with an α-AR/GR agonist phenylephrine resulting in a significant increase in cell volume, number of organised sarcomeric structures and total cellular protein to DNA content. Yang *et al.* [386] matured iPSC-CMs through the addition of the growth hormone tri-iodothyronine (T3). This treatment increased contractile force and calcium release rates in addition to inducing changes in morphology. They also measured mitochondrial metabolism using a Seahorse Analyser and found increased oxygen consumption in T3 treated iPSC-CMs, although they only measured glucose oxidation. Others have also reported that long-term culture increased activity in the ETC complex I and II in iPSC-CMs [328]. Ito *et al.* [528] showed treatment with insulin growth factor 1 (IGF-1) in neonatal rat ventricular myocytes (NRVM) led to increased expression of Troponin-1 and MLC-2, cell size, and protein synthesis. This treatment has also reported to induce maturation by increasing FAO enzymes such as medium chain acyl-CoA dehydrogenase and carnitine palmitoyltransferase I and enhance effects of PPARα [529]. Fu *et al.* [530] identified miR-1 as a potential modulator for CM maturation. They showed overexpression of MiR-1 decreased action potential duration and hyperpolarized both the resting membrane potential as well as the maximum diastolic potential in ESC-CMs. Others believe that, due to its role in thyroid hormone responsiveness, the myosin isoform switch microRNA, miR208, could also be a potential modulator in promoting maturation [531, 532].

4.1.2 Peroxisome Proliferator-Activated Receptor

4.1.2.1 PPAR Structure

The peroxisome proliferator-activated receptor (PPAR) is a transcription factor belonging to the ligand-activated nuclear hormone receptor superfamily and is a major regulator of lipid metabolism in the liver. There are three main isoforms of PPAR (PPARα, PPARβ/δ, and PPARγ) that have been identified in many species including mouse, rat, guinea pig, human, chicken, fish and amphibians [533]. For the most part, they share a highly conserved structure and molecular mode of action, but vary in tissue distribution and activation. Expression of PPARα has been the most characterised and is expressed most highly in tissue that oxidizes FAs [534–538]. In rodents, the highest gene expression of *PPAR*α is found primarily in the liver and brown adipose tissue, followed by the heart and kidneys [534]. Human *PPAR*α seems to be expressed more equally across a range of tissues, but with highest expression in the liver [498, 533, 534, 539–545], heart [498, 533, 534, 539–545], kidney [498, 533, 534, 539–541, 543, 544], and intestine [498, 533, 534, 544]. It is also expressed to a lesser degree in skeletal muscle [498, 533, 534, 539, 541–545] and brown adipose tissue [498, 533, 540, 541, 545]. PPARβ/δ can be found in brain [542, 543], adipose tissue [542, 545], skin [542], intestine [543, 545], and kidney [543, 545], while PPARγ is found in adipose tissue [534, 539–542, 544, 545], intestine [539, 541, 543, 545], and the immune system [539, 541]. Structurally, PPARs are composed of four domains: the ligand-independent activation domain (A/B), the DNA binding domain (C), the cofactors domain (D), and the ligand dependent domain (E/F) [539–543, 545] (Fig. 4.1). PPARs regulate the rate of gene transcription and in return control development, homeostasis, and metabolism in a range of organs in the body [539–543, 545].

4.1.2.2 *PPAR*α Activation

PPARα can be activated by either natural or synthetic ligands. The most important class of synthetic PPARα ligands is the fibrates including gemfibrozil, fenofibrate, clofibrate, bezafibrate, and WY-14643 [547–551]. Natural ligands include saturated FAs [541, 543, 545, 552, 553], unsaturated FAs [498, 533, 539–541, 543, 545, 552–556] and

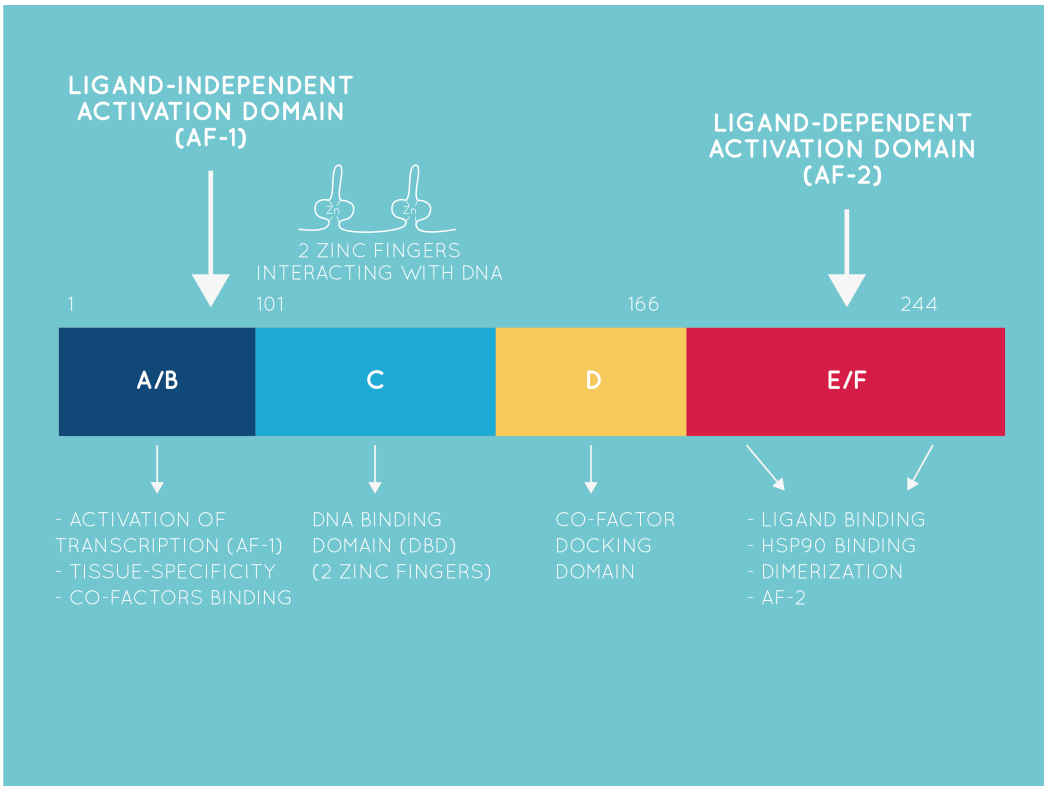

Figure 4.1: PPARα structure adapted from [546]. PPARα has four domains: the ligand-independent activation domain (A/B) including an activation function-1 (AF-1), the DNA binding domain (C), the cofactors docking domain (D) also known as the hinge region, and the C-terminal E/F domain including a ligand binding domain and activation function-2 (AF-2).

eicosanoids [543,555]. FAs have different binding affinity to PPARα and therefore may not necessarily result in its activation.

Activation of PPARα, through ligand binding, promotes uptake, utilization, and catabolism of FAs by upregulating genes involved in FA transport, binding and activation, and peroxisomal/ mitochondrial FAO [557]. FA binding proteins (FABPs) transfer long chain FAs intercellularly to enzymes involved in FA metabolism [558]. FAs are chaperoned into the nucleus where they can interact with transcription factors, such as members of the PPAR family [559]. L-FABP (FABP1) interacts with PPARα as a co-activator in PPAR-mediated gene regulation [560]. Similarly, E-FABP (FABP5) interacts with PPARδ and A-FABP with PPARγ [561].

Binding of a FA to PPARα facilitates the formation of an obligate heterodimer with another nuclear receptor: retinoid X receptor (RXR) (Fig. 4.2) [562]. The PPARα/RXR heterodimers bind to a specific nucleotide sequence referred to as a peroxisome proliferator response element (PPRE), which is located in the promoter region of the target genes [563,564]. The PPRE consists of a common core repeating sequence, AGGTCA, spaced by any single nucleotide, allowing the proper binding of PPARα and its partner RXRα [565]. The PPARα/RXR heterodimer complex recruits different co-activators or co-repressors that modulate transcription activity of PPAR genes [565].

4.1.2.3 PPARα Agonist - WY-14643 (Pirinixic Acid)

WY-14643 (pirinixic acid) is an agonist for PPARα, which binds with high affinity and activates *PPARα* (Fig. 4.3). PPARα then binds to RXR forming its heterodimer complex and activates target genes transcription (Fig. 4.2). [567–569]. WY-14643 was discovered in 1974 to act as a potent antihypercholesterolemic agent and reduce serum cholesterol [570]. Since then WY-14643 has been explored for prevention of cardiac dysfunction, cardiomyopathy and heart failure as a result of lipid accumulation within CMs. Wolkart *et al.* [571] have shown in pre-clinical trials that adipose triglyceride lipase (ATGL) deficient mice treated with WY-14643 have reduced cardiac hypertrophy and improved heart function. They saw the activation of *PPARα* genes involved in lipid metabolism that

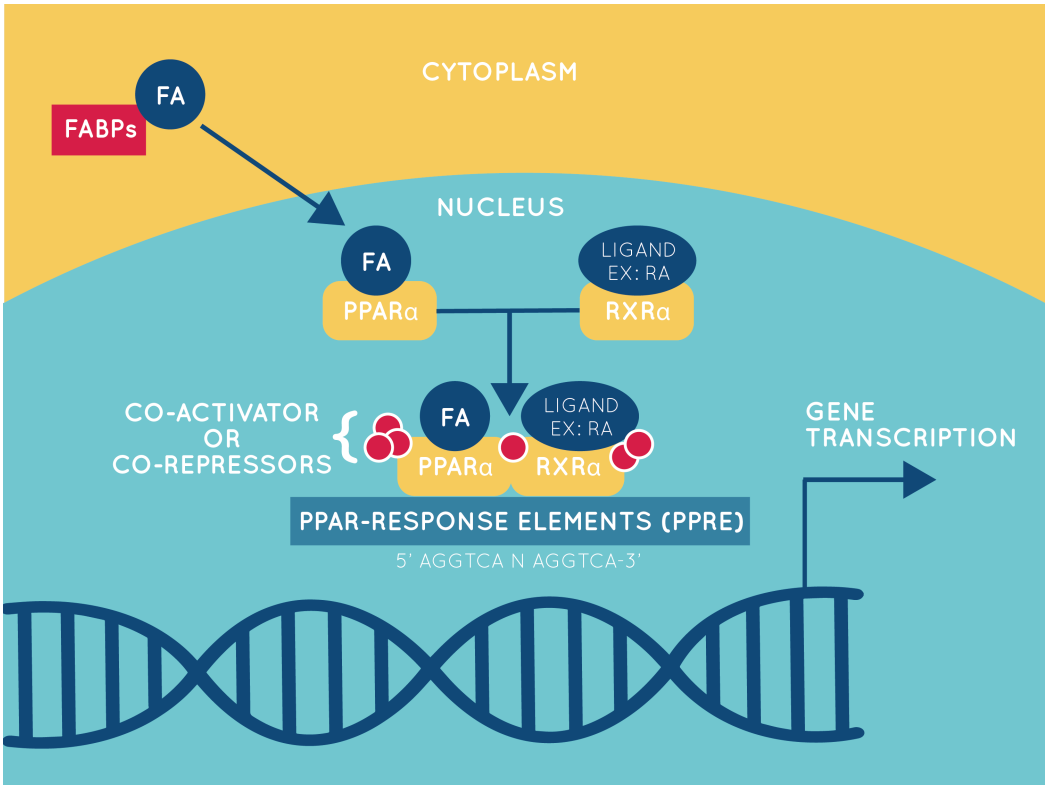

Figure 4.2: FAs are chaperoned into the nucleus by FABPs and bind to PPAR to form the heterodimer complex with the retinoid X receptor (RXR). This complex then binds to the specific PPRE and recruits coactivators and corepressors to activate target gene transcription. RA, 9-cis retinoic acid, is a metabolite required for growth and development. RA binds to the retinoic acid receptor (RAR), which attaches as a heterodimer with the RXR in a region called retinoic acid response elements (RAREs). This image has been adapted from [566].

led to an increased mitochondrial FAO and improved cardiac myocyte energy supply.

4.1.2.4 PPARα Target Genes

Gene expression profiling studies have indicated that *PPARα* has hundreds of target genes [557]. One of the criteria to classify PPARα target genes is by identifying the ones with a functional PPRE within a promoter region [533] (Table A.7). However, there is also a large number of genes involved in mitochondrial β-oxidation that have been shown to be PPARα-dependently regulated that have been characterised through functional assays but a functional PPRE has yet to be identified at this time although it most likely exists [533] (Table A.8).

The target genes relevant to this thesis are *CPT-I* [572,573], *CPT-II* [574], *MCAD* [575], *PDK4* [576,577], *CD36* [578], *UPC3* [576,579], and *ACSL1* [580–584]. For which the signaling pathways are depicted in Fig. 4.4. By altering the expression of these genes, PPARα can mediate lipid metabolism by impacting FA uptake/intracellular binding, mitochondrial β-oxidation, peroxisomal FAO, ketogenesis, triglyceride turnover, and gluconeogenesis.

4.1.3 PPARα Expression in Developing and Adult Hearts.

4.1.3.1 PPARα Expression During Cardiac Differentiation.

PPARα is highly expressed in the adult heart [249,250,534,539–541,543–545,585] and can be first detected as early as E13.5 - E15.5 during rodent embryogenesis [544]. There have been previous studies that show all isoforms of PPAR are expressed at different time points in CM differentiation, specifically there are two spikes at DD12 and DD20, which also might correlate to peaks in the expression of *MHCα* [586]. Sharifpanah *et al.* [586] activated *PPARα* during ESC-CM differentiation with the addition of WY-14643, GW7647, and ciprofibrate and increased cardiomyogenesis and expression of the transcription factors (*GATA4*, *NKXX2.5*, *DTEF-1*, and *MEF2C*), cardiac genes (*MHCβ*, *MHC2α*, and *MLC2v*) and increased beating area of embryonic bodies. Inhibiting *PPARα* resulted in the reduction of beating cells and expression of the cardiac genes *MHCα*, *MLC2v*, actinin-α and troponin

A

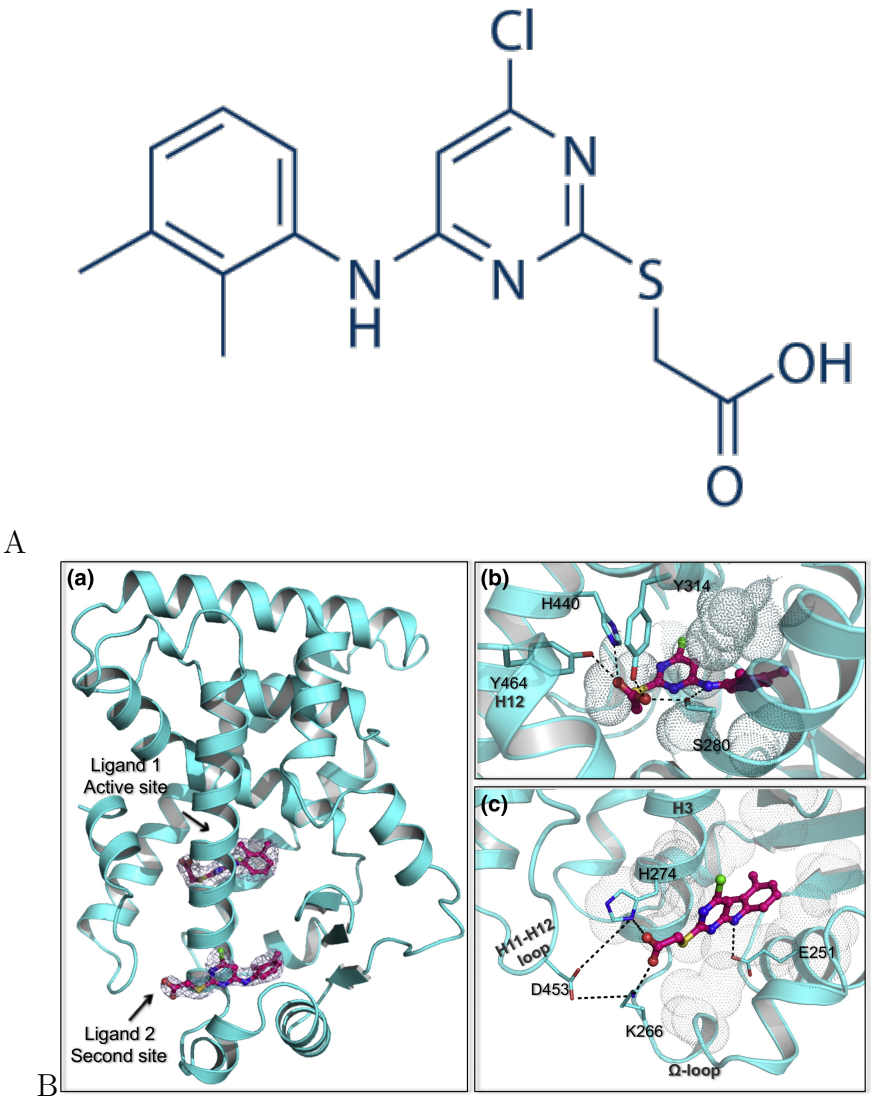

B

Figure 4.3: A) WY-14643 molecular structure. B) Image taken from [569]. PPARα crystal structure showing binding of two WY-14643 molecules (a). There are two ligand domain binding sites: in the first (b), the WY-14643 molecule occupies the standard PPARα agonist position and interacts with helix 12, via polar and hydrophobic contacts with the protein; in the second (c), the WY-14643 molecules binds to a secondary ligand binding domain stabilized by nonpolar interactions and salt bridge networks. The dashed lines represent hydrogen bonds and dotted spheres represent residues involved in hydrophobic interactions.

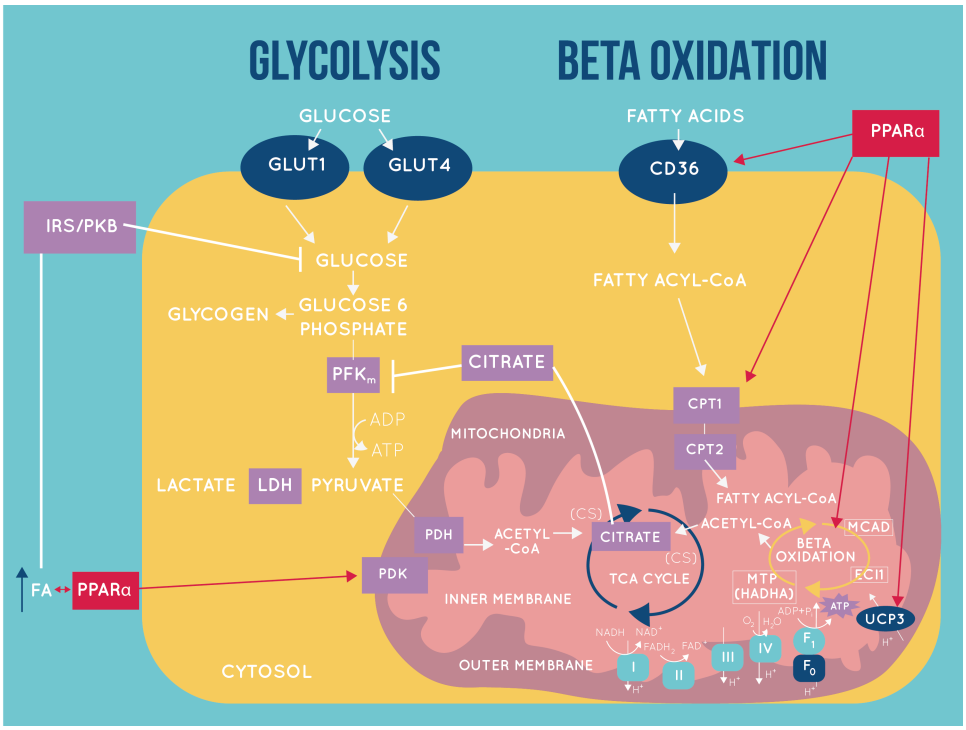

Figure 4.4: PPARα target genes and their downstream affects on Glycolysis and β-oxidation.

T [562,587]. It has been debated as to the mechanism by which *PPARα* activation occurs during CM differentiation, but it is thought that the mechanism could involve the p38 MAPK signalling pathway [562] while others think it may involve ROS and NADPH oxidase activity [586].

4.1.3.2 PPARα Expression Regulation of Cardiac Metabolism

From previous studies, it has been shown PPARα has a major role in regulating cardiac metabolism [256,572–575,578,588–594]. PPARα activates genes that regulate various steps of FAO from cellular transport [578,588,589,591,594], mitochondrial uptake [573,588,592,593], to mitochondrial oxidation [256,575,588,593]. In PPARα knockout mouse models, cardiac FAO decreased [256] and there was a 30-60% reduction in the cardiac gene expression of *MCAD*, *LCAD*, and *VLCAD172* [591]. Whereas when mice were treated with WY-14643, PPARα was activated, FAO increased [572–575,578,588–595] and the expression of LCAD was upregulated [591].

In parallel, PPARα has been reported to have effects on glucose metabolism in the heart [256,589,591,595]. In PPARα knockout mice, PPARα activation via natural [572,591] or synthetic ligands [595] resulted in the reduction of *GLUT4* expression and increased cardiac glycolysis [256]. In other PPARα knockout mice experiments, *PDK4* expression was downregulated [256], but WY-14643 treatment to activate PPARα showed increased *PDK4* expression [595,596] and reduced *PFK* [595] in the heart.

Another PPARα target gene in the heart is *UCP3* [256,533,597,598]. A study of WY-14643 treated wild-type animal models showed elevated levels of *UCP3* [533,597], whereas, in a *PPARα* knock out mouse model, *UCP3* was downregulated [256,597]. In addition, due to increased FA levels in circulation, there was an upregulation of *PGC1α* gene expression [543].

4.1.4 Chapter Aims

iPSC-CMs have an immature phenotype including a glycolytic metabolism. In this chapter, the aim was to mature the metabolic status of iPSC-CMs by targeting the PPARα pathway, which regulates the transcription of genes involved in FA metabolism. Oleic acid (OA) is an 18-carbon unsaturated FA that is classified as a monounsaturated omega-9 FA. It is considered to be one of the most widely distributed and abundant FAs in nature [599] and is one of the two FAs predominately oxidized by the heart, the other being palmitic acid. OA was added to current culture protocols on DD15 to enhance FAO in immature beating iPSC-CMs. Although FAs are natural ligands for PPARα, we also added WY-14643 (a PPARα agonist) to further increase the effects of PPARα activation and induce the metabolic shift towards FA utilisation. Lastly, this "maturation cocktail" was added to cells in 3D culture to maximize maturation in our iPSC-CMs. OA and WY-14643 were chosen both for their relevance in cardiac metabolism and because they have previously been used in the lab and we already have optimized protocols with historical data that can be used as a comparison. Here we aimed to build upon that previous work and complete a larger story by assessing the metabolic phenotype of our iPSC-CMs using qPCR, radiolabeled substrate assays to measure palmitate and glucose uptake, oxygen consumption measurements using a Clarke-type oxygen electrode and immunocytochemistry.

4.2 Methods

4.2.1 Differentiation of iPSC-CMs and Treatment With OA ± WY-14643

iPS cells were differentiated into CMs by the Wnt-modulation based protocol explained in Section 2.1.1.5 which usually resulted in cells that started spontaneously beating around DD12-15. The cells were either re-plated on DD15 onto a 2D RF-Matrigel coated 24-well plate or seeded onto collagen-derived scaffolds as per the experimental design. Beating iPSC-CMs were then treated with either 400 μM of OA alone or in combination with 120 μM WY-14643 for 24 hours or 1 week (Fig. 4.5). Untreated iPSC-CMs were used as controls for all the experiments.

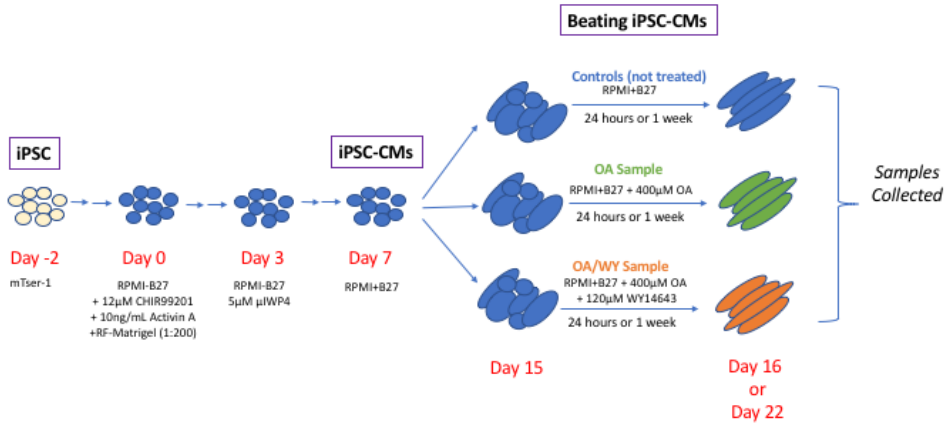

Figure 4.5: Methods for iPSC-CM differentiation and treatment with OA ± WY-14643. Cells were differentiated and re-plated on DD15, in either a 2D RF-Matrigel coated 24-well plate or onto a 3D collagen-derived scaffold. iPSC-CMs were then treated for 24 hours or one week with OA ± WY-14643.

4.2.2 OA Treatment

As palmitate and oleate are extremely water insoluble, they have to be pre-bound to albumin to increase solubility in aqueous solutions.

OA was bought pre-conjugated to albumin (OA-BSA; 1:2) from Sigma (Cat: 03008-5mL). iPSC-CMs were treated with 400 μM OA-BSA on DD15 for either 24 hours or 1 week. For the 1 week treatment, OA was always added fresh into the RPMI+B27 culturing media, and the media was changed every two days.

4.2.3 WY-14643 (Pirinixic Acid) Treatment

WY-14643 was bought from Selleckchem (Cat: S8029) and used to treat the iPSC-CMs at a concentration of 120 μM. WY-14643 was added in combination with 400 μM OA directly into the RPMI+B27 culturing media on DD15. The iPSC-CMs were either treated for 24 hours or 1 week. For the 1 week treatment, the WY-14643 in combination with the 400 μM OA was always added fresh into the RPMI+B27 culturing media, and the media was changed every two days.

4.3 Results

4.3.1 iPSC-CM Treated With OA ± WY-14643

iPSC-CM were successfully differentiated into CMs and started spontaneously beating around DD12-15. They were then treated with OA ± WY-14643 on DD15 for 24 hours or 1 week. The one week treated iPSC-CM progressed to full plate beating around DD20-22. The control (untreated cells) averaged 70±2 bpm, while the OA alone treated averaged 68±1 bpm and the OA + WY-14643 averaged 67±1 bpm. Although this isn't a significant decrease in average frequency, visually the treated cells contracted more strongly and deeply which could be a sign of maturation.

4.3.2 Monolayer qPCR Treated With OA ± WY-14643 for 24 Hours Versus 1 Week

4.3.2.1 Stability of the Reference Genes

Two new reference genes were assessed for Taqman assays for stability across each treatment and time variable (Fig. 4.6). Neither of the reference genes were significantly up or down regulated, and both were used in combination and averaged per qPCR experiment.

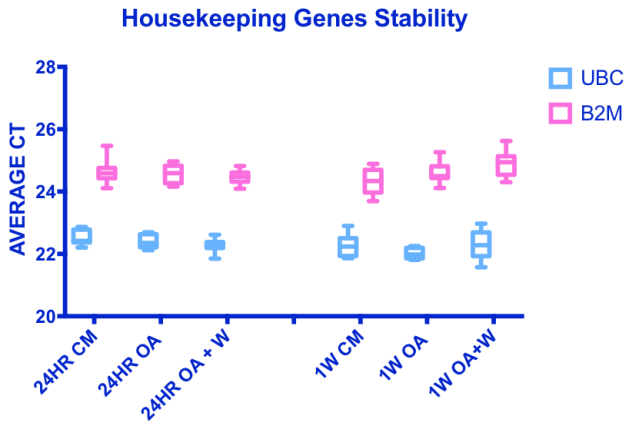

Figure 4.6: Reference gene expression after 24 hours and 1 week of treatment with OA ± WY-14643. *UBC* and *B2M* were assessed to determine the most stable reference gene for Taqman qPCRs studies. The bar represents the mean, and the line represents the 95% confidence interval; n=8.

4.3.2.2 Effects of OA ± WY-14643 on Relative Expression of Pyruvate Oxidation Genes.

Under aerobic conditions, pyruvate can be converted into acetyl-CoA by the enzyme pyruvate dehydrogenase (PDH), which is then further regulated by PDH kinase (PDK) and PDH phosphatase (PDP). *PDK4* expression increased at both time points after the treatment of OA ± WY-14643 compared to the untreated iPSC-CMs, although to a greater extent after 1 week of treatment (Fig. 4.7B). There was no significant difference in *PDHA1* expression between the treatment groups and the untreated controls, although there was a significant reduction comparing the 24 hours to 1 week OA-treated cells and the 24 hours vs 1 week OA + WY-14643 treated cells (Fig. 4.7A).

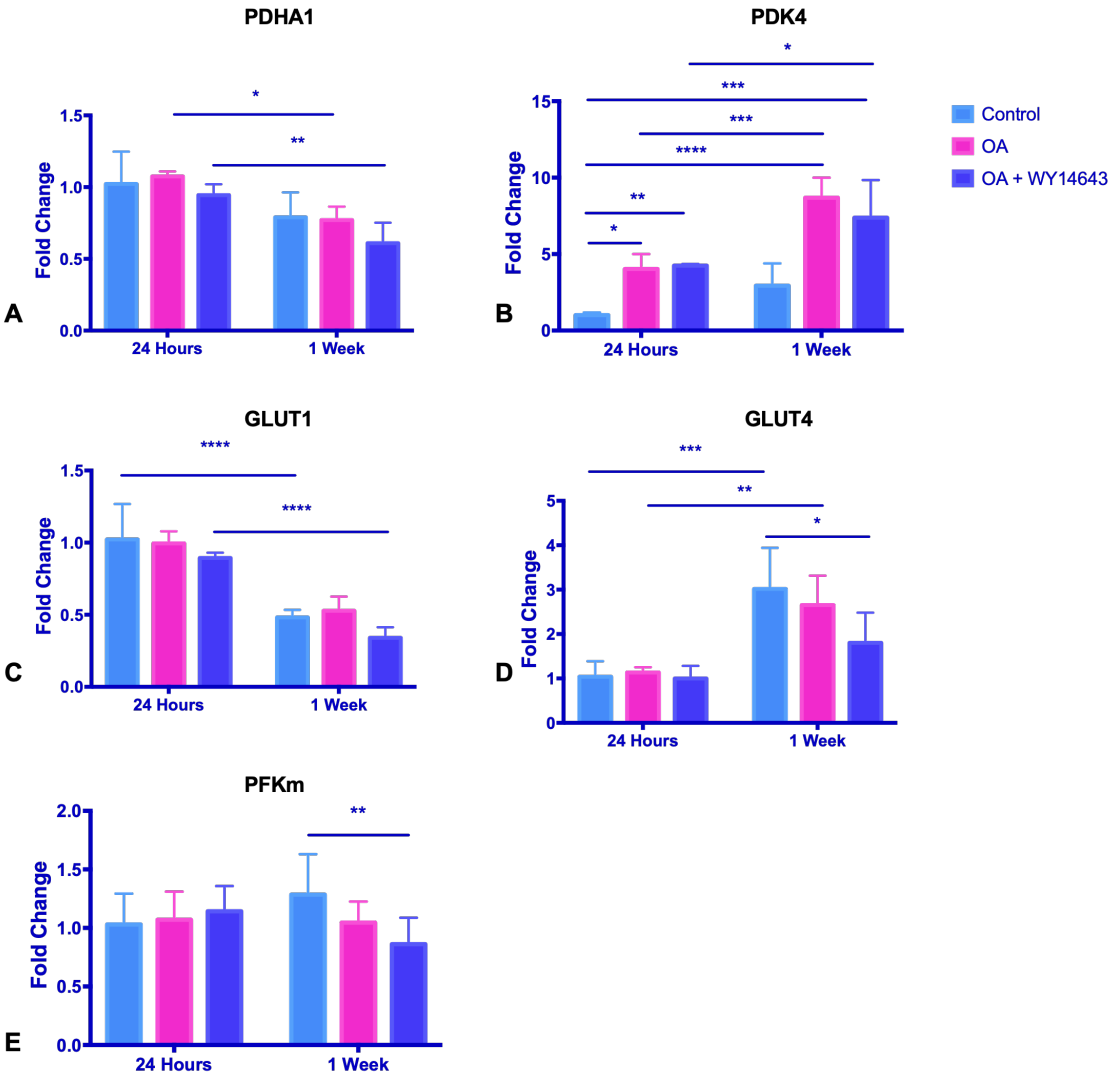

Figure 4.7: A) *PDHA1*, B) *PDK4*, C) *GLUT1*, D) *GLUT4*, E) *PFKm*, relative gene expression on treated iPSC-CMs. iPSC-CMs were differentiated and treated with OA ± WY-14642 on DD15 for either 24 hours (blue bar) or 1 week (pink bar). The experiment was run in 4 biological repeats in triplicates with 3 technical repeat. The bar represents the mean + SEM. The genes are normalised to the untreated controls at 24 hours. "*" = $p<0.05$, "**" = $p<0.01$, and "***" = $p<0.001$ or equivalent; analyzed using a two-way ANOVA and a Tukey's multiple comparison test.

4.3.2.3 Effects of OA ± WY-14643 on Relative Expression of Glycolysis Genes.

The relative gene expression of *GLUT1*, *GLUT4*, and *PFKM* was measured following a 24 hours and 1 week treatment of OA ± WY-14642. Relative gene expression of *GLUT1* decreased in all conditions after the 1 week of culture compared to the iPSC-CMs treated for only 24 hours. However, there was no difference in expression between the 1 week treatment groups (Fig. 4.7C). Relative gene expression of *GLUT4* increased in the 1 week controls and OA treated cells compared to the 24 hour groups. *GLUT4* expression in the iPSC-CMs treated with both OA and the WY-14643 compound was significantly less than in the corresponding 1 week control cells (Fig. 4.7D).

The enzyme phosphofructokinase catalyses the rate-limiting and irreversible step in glycolysis. *PFKM* expression decreased after 1 week of treatment with OA + WY-14643 compound compared to the untreated control. There were no significant changes after any of the 24 hour treatments (Fig. 4.7E).

4.3.2.4 Effects of OA ± WY-14643 on Relative Expression of FAO Genes.

Relative gene expression levels were measured for a number of enzymes involved in FAO such as *ACSL1*, *CPT1B*, *CD36*, *HADHA*, *MCAD*, and *ECI1*, which are known to be PPARα target genes. *ACSL1* relative gene expression increased when cells were treated with OA alone for 1 week compared to the OA 24 hours' treatment (Fig. 4.8A). There were no other significant differences between the treatments. *CPT1B* gene expression increased with the treatment of OA + WY-14643 after 1 week compared to the untreated control (Fig. 4.8B). There were no significant differences in the relative expression of *CD36* (Fig. 4.8C), *HADHA* (Fig. 4.8D), or *MCAD* (Fig. 4.8E) after 24 hours or 1 week for either treatment.

Since OA is an unsaturated FA, the relative expression of enoyl CoA isomerase was measured. The data showed that *ECI1* was downregulated only after the 1 week OA + WY-14643 treatment compared to the control (Fig. 4.8F).

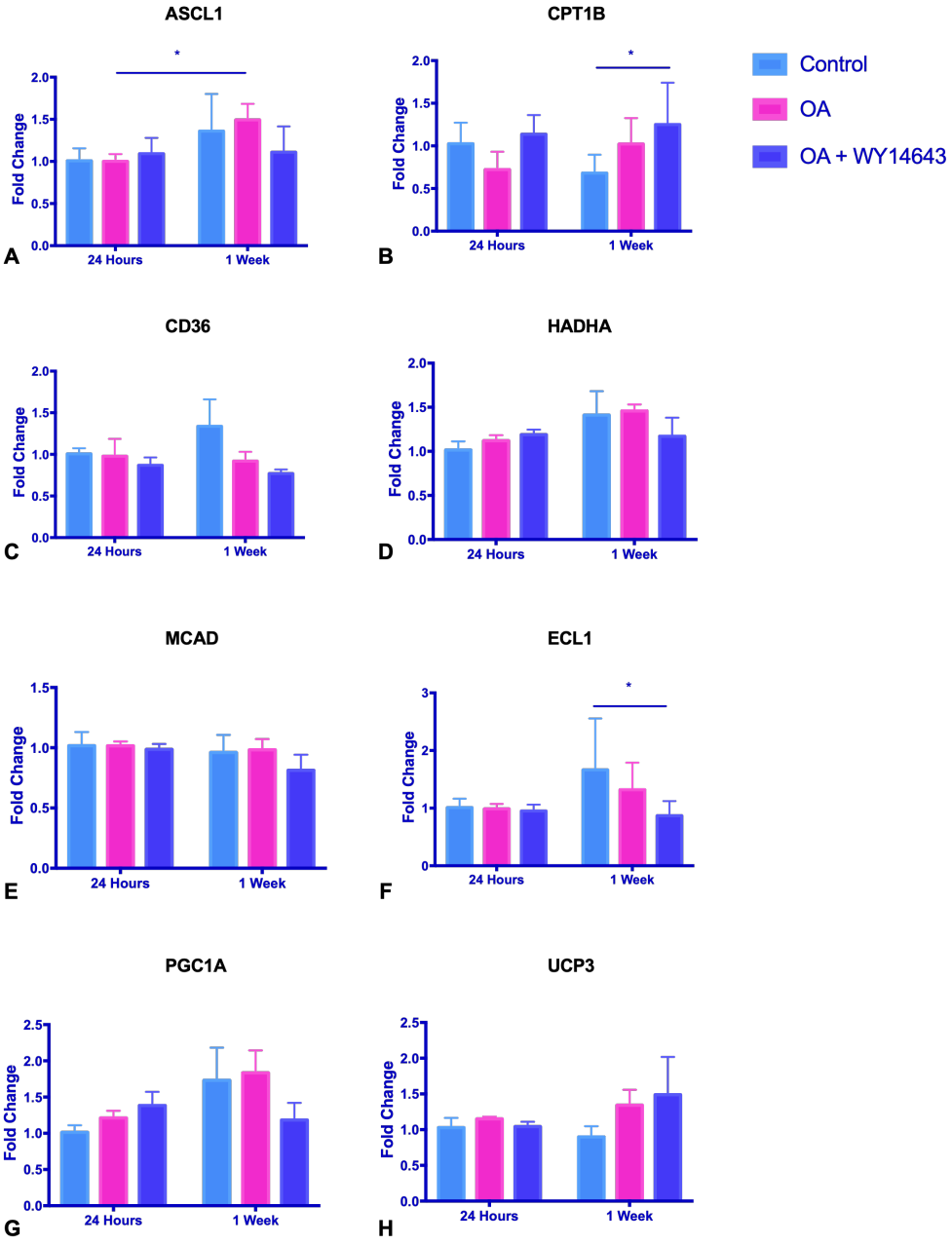

Figure 4.8: A) *ASCL1*, B) *CPT1B*, C) *CD36*, D) *HADHA*, E) *MCAD*, F) *ECL1*, G) *PGC1A*, and H) *UCP3* relative gene expression on treated iPSC-CMs. iPSC-CMs were differentiated and treated with OA ± WY-14642 on DD15 for either 24 hours (blue bar) or 1 week (pink bar). The experiment was run in 4 biological repeats in triplicates with 3 technical repeat. The bar represents the mean + SEM. The genes are normalised to the untreated controls at 24 hours. "*" = $p<0.05$, "**" = $p<0.01$, and "***" = $p<0.001$ or equivalent; analyzed using a two-way ANOVA and a Tukey's multiple comparison test.

4.3.2.5 Effects of OA ± WY-14643 on Mitochondrial Relative Gene Expression.

The relative gene expression of *PGC1A* and *UCP3* were measured following a 24 hour and 1 week treatment. There were no significant differences in gene expression in either treatments or time points for *PGC1A* (Fig. 4.8G) and *UCP3* (Fig. 4.8H). However, there was a non-significant increase in expression of *UCP3* after addition of OA + WY-14643 which may have become significant with increased numbers or an extended treatment.

4.3.3 FAO of Monolayer iPSC-CM Treated With OA ± WY-14643 for 24 Hours or 1 Week.

Both palmitate and OA oxidation rates were determined by comparing iPSC-CMs treated with 400 μM OA alone or with the addition of 120 μM WY-14643. Overall, FAO increased with the addition of OA ± WY-14642. OA oxidation significantly increased in iPSC-CMs, regardless of treatment, after 1 week of culture compared to just 24 hours. In addition, the 1 week OA + WY-14643 treatment resulted in higher OA oxidation than the untreated control (Fig. 4.9A). Interestingly, palmitate oxidation increased after 24 hours of the OA treatment and with a greater increase after the addition of the WY compound. There was an additional increase in each treatment group when comparing the 1 week cultured cells to those treated for 24 hours (Fig. 4.9B).

4.3.4 The Glycolytic Flux and Glucose Oxidation of Monolayer iPSC-CM Treated With OA ± WY-14643

Both glycolytic flux and glucose oxidation rates were determined by comparing iPSC-CMs treated with 400 μM OA alone or with the addition of 120 μM WY-14643. Treating iPSC-CMs with OA alone for 1 week significantly reduced glycolytic rates compared to the untreated or OA + WY-14643 treated iPSC-CMs (Fig. 4.10). There was no significant difference in glucose oxidation after 1 week treating the cells with either OA alone or with

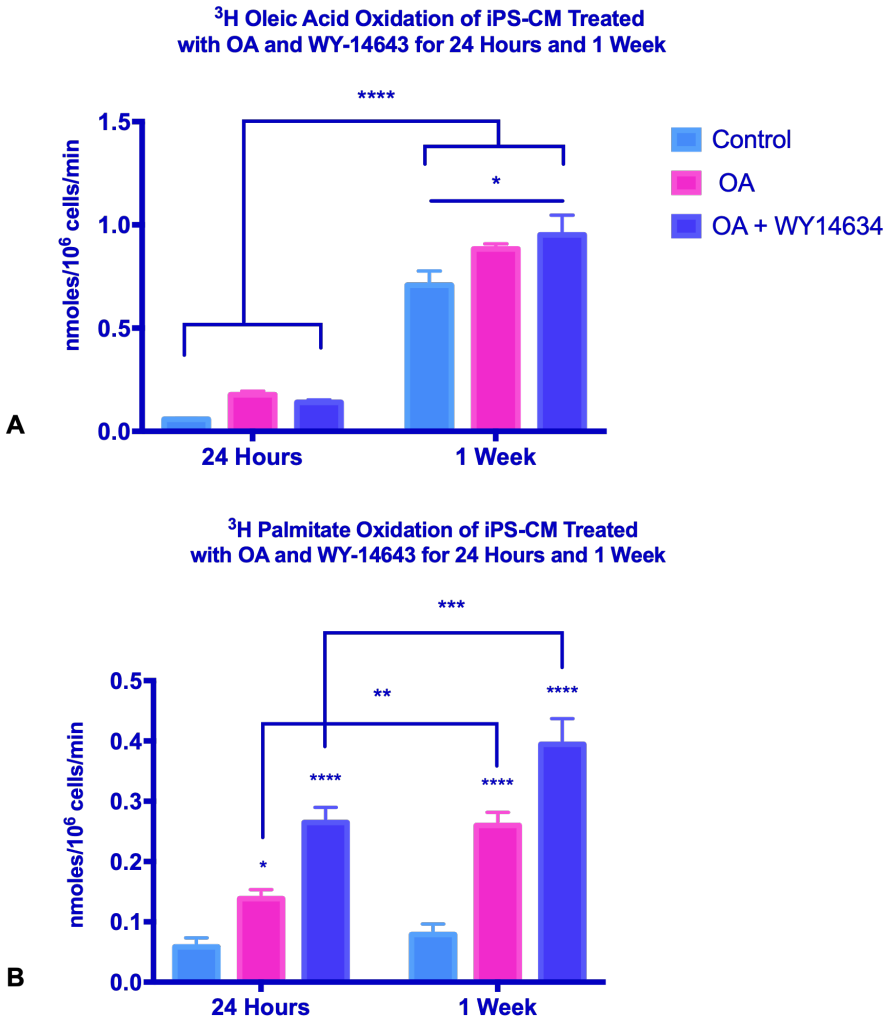

Figure 4.9: A) ^{3}H OA oxidation and B) ^{3}H palmitate oxidation of monolayer iPSC-CMs treated with OA ± WY-14642 for 24 hours and 1 week. iPSC-CMs were re-plated on DD15 to RF-Matrigel coated 24-well plate (10^6 cells/well). The cells were incubated for 8 hours in RPMI+B27 media containing 2% BSA and either 0.3mM palmitate doped with of palmitic acid [9,10-^{3}H(N)] + their assigned OA/WY treatment or 400 μL OA doped with OA [9,10-^{3}H(N)] + their assigned OA/WY treatment. The bar represents the mean + SEM (n=8-14). The blue represents iPSC-CMs treated for 24 hours, and the pink represents the iPSC-CMs treated for 1 week. "*" = $p<0.05$, "**" = $p<0.01$, and "***" = $p<0.001$ or equivalent; analyzed using a two-way ANOVA and a Tukey's multiple comparison test.

the WY compound.

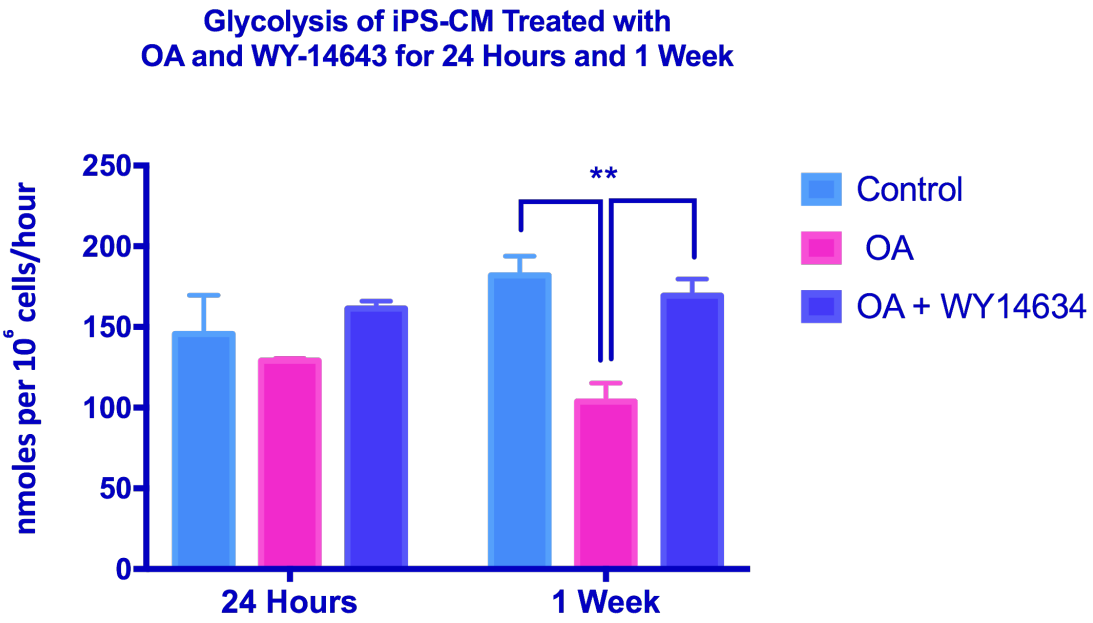

Figure 4.10: The glycolytic flux of monolayers iPSC-CMs treated with OA ± WY-14642 for 24 hours and 1 week. iPSC-CMs were re-plated on DD15 to RF-Matrigel coated 24-well plate (10^6 cells/well). The iPSC-CMs were incubated for 8 hours in low-glucose RPMI media containing 2% BSA, 0.3 mM palmitate doped with D-[5-^{3}H(N)]-glucose + their assigned OA/WY treatments. For glucose oxidation cells were incubated in low-glucose RPMI media containing 2% BSA, 0.3 mM palmitate and doped with D-[^{14}C(U)] glucose + their assigned OA/WY treatments. The bar represents the mean + SEM (n=3). The blue represents iPSC-CMs treated for 24 hours, and the pink represents the iPSC-CMs treated for 1 week. "*" = $p<0.05$, "**" = $p<0.01$, and "***" = $p<0.001$ or equivalent; analyzed using a two-way ANOVA and a Tukey's multiple comparison test.

4.3.5 Oxygen Consumption Rate of Treated iPSC-CMs With OA Alone or With WY-14643 Using the Clark-Type Oxygen Electrode

A previous DPhil student in our lab, Dr. Heba Al-Siddiqi, measured oxygen consumption rate (OCR) using the Clarke-Type Oxygen Electrode which we refer to as the OXbox (short for OXPHOS box). She treated the iPSC-CMs with 400 μM OA alone or with the addition

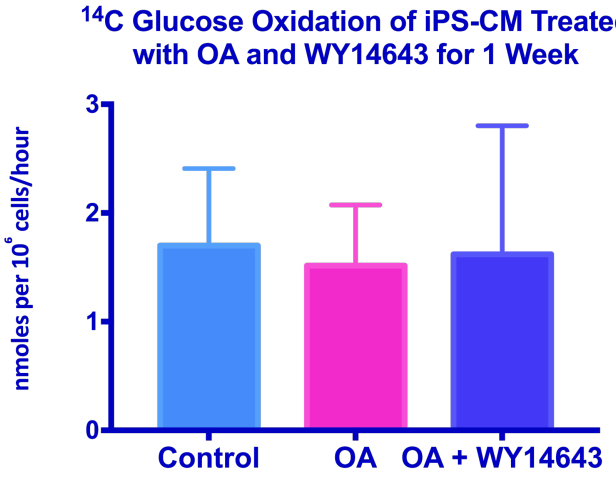

Figure 4.11: Glucose oxidation of monolayers iPSC-CMs treated with OA ± WY-14642 for 1 week. iPSC-CMs were re-plated on DD15 to RF-Matrigel coated 24-well plate (10^6 cells/well). The cells were incubated for 8 hours in RPMI-low glucose media media containing 2% BSA, 0.3 mM palmitate doped with D-[14C(U)] Glucose. The bar represents the mean + SEM (n=8). The blue is the untreated iPSC-CMs (controls), the pink represents the iPSC-CMs treated with OA alone, and the indigo represents the iPSC-CMs treated with OA + WY-14643. The set of stars represents the comparison of the treatments to their controls. "*" = $p<0.05$, "**" = $p<0.01$, and "***" = $p<0.001$ or equivalent; analyzed using a two-way ANOVA.

of 120 μM WY-14643 for 24 hours. OCR was measured using two million iPSC-CMs resuspended in Gimish and respiring on either OA or the combination of pyruvate and malate during the experiment. Measurements were collected at baseline after oligomycin was added, and again at maximal respiration (after FCCP treatment). Dr. Al-Siddiqi reported that, when the cells were respiring on OA, there was no difference between the treated and untreated iPSC-CMs in the rate of oxygen consumption either at baseline or with the addition of oligomycin (Fig. 4.12). OCR at maximal respiration (FCCP) was significantly higher in the iPSC-CM treated with both OA and WY-14643 combined compared with untreated iPSC-CMs and those treated with OA alone.

I expanded on her experiment and mimicked her parameters, but treated the iPSC-CMs for 1 week instead of 24 hours. In the initial runs using Gimish, there was no difference observed in the OCR across the treatment groups (Fig. 4.13). It was also noted that the cells were not surviving long in the chamber and did minimal respiration. Overall, we were not able to observe cellular oxygen consumption comparable to that seen in Dr. Al-Siddiqi's

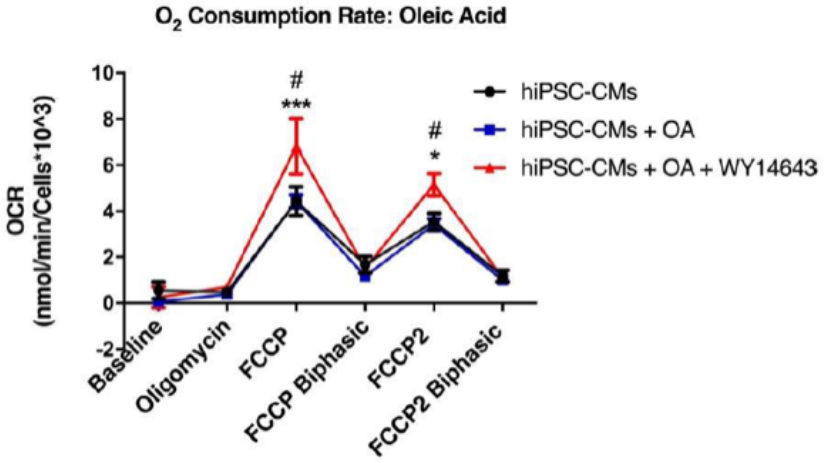

A

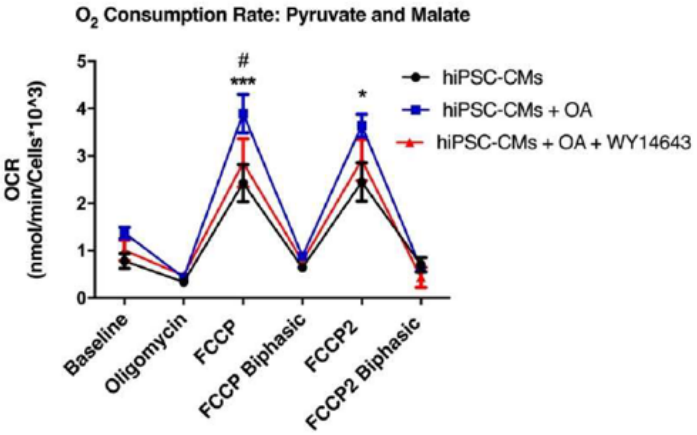

B

Figure 4.12: Dr. Al-Siddiqi's cellular oxygen consumption data taken from her thesis. iPSC-CMs were treated with OA alone (blue) or with WY-14643 (red) for 1 week. Untreated iPSC-CMs (black) were used as a control. On the day of the experiment, 2 million iPSC-CMs were resuspended in Gimish and supplemented with respiration substrates of either A) 400 μM OA or B) 10 mM pyruvate and 5 mM malate. Measurements were collected at baseline, after the oligomycin treatment, and at maximal respiration. The cells were then allowed to reset from the FCCP treatment and a second FCCP treatment was applied for a second measure of maximal respiration. The data is presented as mean $\pm$ SEM (n=6), and analysed using a one-way ANOVA with Tukey post hoc test. "*" compared with untreated controls, while "#" compared OA treated iPSC-CMs. P value<0.05 "*", P value<0.01 "**", P value<0.001 "***", and P value<0.001 "****" or equivalents.

results (n=6). As a result, we switched to running our cells in their standard culture media (RPMI+B27) to see if the cells would survive longer inside the OXbox chamber.

Under these conditions, when cells were respiring on media containing OA, the OCR at the maximal respiration was significantly higher in the treated OA + WY-14643 iPSC-CMs than it was in the OA alone or untreated iPSC-CMs (Fig. 4.14A). When respiring on media containing pyruvate and malate, the baseline oxygen consumption of the treated OA + WY-14643 iPSC-CMs was significantly higher than the other two conditions as was the FCCP1 Biphasic oxygen consumption (Fig. 4.15A). Because of this increased baseline, there was a significant decrease in the reserved respiratory capacity (RRC) for the OA + WY-14643 treated iPSC-CMs compared to the OA treated and untreated iPSC-CMs while respiring on pyruvate and malate (Fig. 4.15B). There was no difference when cells were respiring on OA (Fig. 4.14B).

4.3.6 Westerns

Seeing an elevated baseline in the WY-14643 treated cells in the oxygen consumption data led to the hypothesis that since the WY compound activated PPARα target genes, an explanation could be an upregulation in the mitochondria uncoupling protein 3 (*UCP3*). If this gene was upregulated, then this could explain the elevated baseline respiration, and the lack of difference after addition of FCCP, because proton leak through *UCP3* could already have uncoupled the electron transport chain from oxidative phosphorylation. However, when examining the gene expression data previously in Fig. 4.8, we did not see a significant upregulation of *UCP3* in cells treated with the WY compound for a week. Nevertheless, the mRNA expression could have been upregulated earlier in the treatment and already reset, so we decided to look at protein levels of *UCP3*. My Part II student (Charlotte Ferguson) attempted to run westerns on the cells used in the OXBox (untreated control, 1 week treated with OA alone and 1 week treated with OA + WY-14643). Sadly, she was unsuccessful with optimizing the protocol in time for this thesis. Staining with Ponceau S (Fig. 4.16) confirmed that adequate protein was extracted, separated and transferred (from both the monolayers and scaffolds). Unfortunately, only data from the loading control, cyclophilin

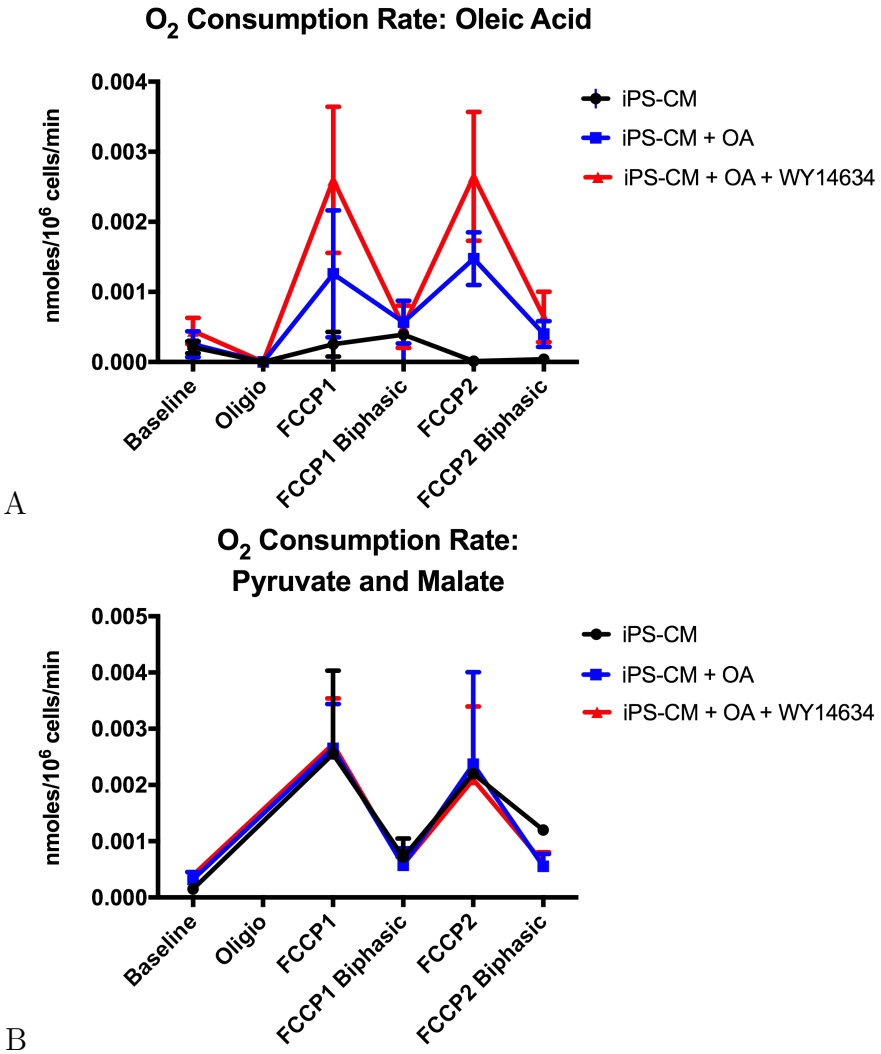

Figure 4.13: OCR using the Clark-Type Oxygen Electrode in Gimish. iPSC-CMs were treated with OA alone (blue) or with WY-14643 (red) for 1 week. Untreated iPSC-CMs (black) were used as a control. On the day of the experiment, 2 million iPSC-CMs were resuspended in Gimish and supplemented with respiration substrates of either A) 400 μM OA or B) 10 mM pyruvate and 5 mM malate. Measurements were collected at baseline, after the oligomycin treatment, and at maximal respiration. The cells were then allowed to reset from the FCCP treatment and a second FCCP treatment was applied for a second measure of maximal respiration. The data is presented as mean ± SEM (n=6), and analysed using a one-way ANOVA with Tukey post hoc test. P value<0.05 "*" compared with untreated controls. P value <0.05 "#" compared with OA + WY-14643 treated iPSC-CMs.

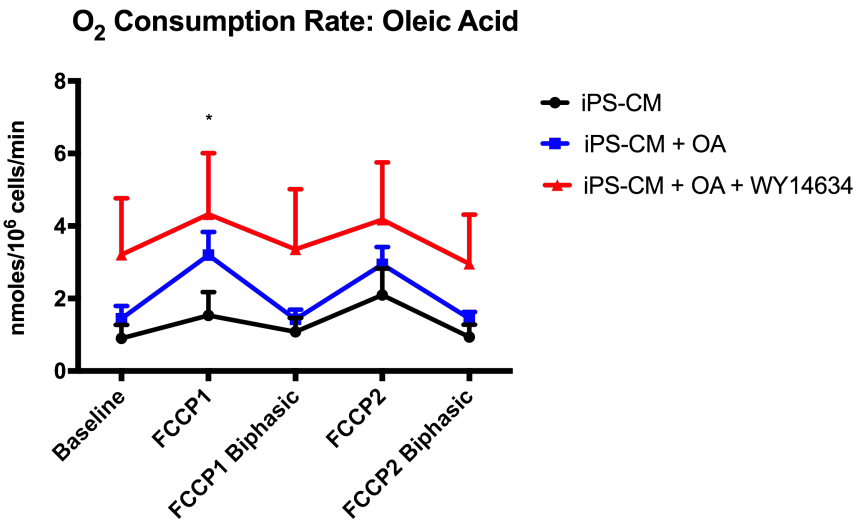

Figure 4.14: A) OCR using the Clark-type oxygen electrode in culture media containing OA. iPSC-CMs were treated with OA alone (blue) or in combination with WY-14643 (red) for 1 week. Untreated iPSC-CMs (black) were used as a control. On the day of the experiment, 2 million iPSC-CMs were resuspended in media and supplemented with 400 μM OA as the respiring substrate. Measurements were collected at baseline, after the oligomycin treatment, and at maximal respiration. The cells were then allowed to reset from the FCCP treatment and a second FCCP treatment was applied again for a second measure of maximal respiration. The data is presented as mean ± SEM (n=6) and analysed using a one-way ANOVA with Tukey post hoc test. P value<0.05 "*" compared with untreated controls. P value <0.05 "#" compared with OA + WY-14643 treated iPSC-CMs. B) RRC during OA respiration on untreated vs treated iPSC-CMs. RRC was calculated as the difference between maximal respiration and baseline. Untreated iPSC-CMs were used as a control. Data are presented as mean ± SEM (n=4) and analysed using a one-way ANOVA with Tukey post doc) test.

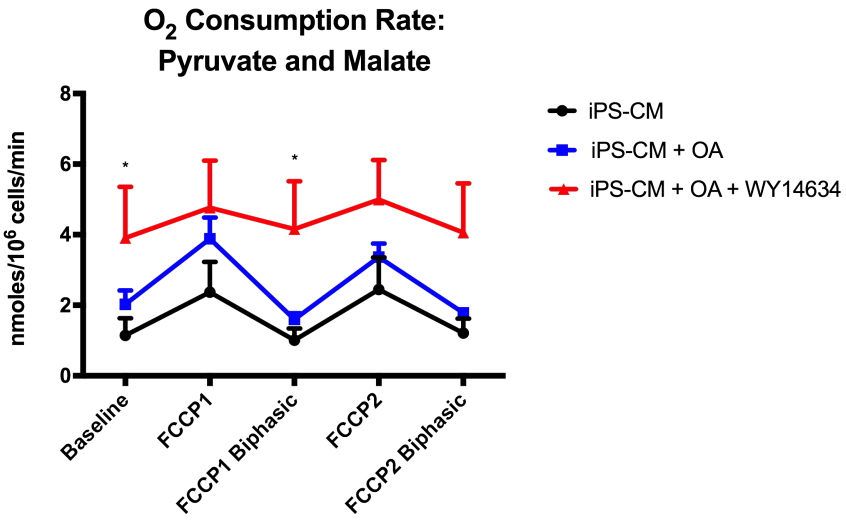

Figure 4.15: A) OCR using the Clark-type oxygen electrode in culture media with pyruvate and malate respiring substrates. iPSC-CMs were treated with OA alone (blue) or in combination with WY-14643 (red) for 1 week. Untreated iPSC-CMs (black) were used as a control. On the day of the experiment, 2 million iPSC-CMs were resuspended in media and supplemented with 10 mM pyruvate and 5 mM malate as the respiring substrate. Measurements were collected at baseline, after the oligomycin treatment, and at maximal respiration. The cells were then allowed to reset from the FCCP treatment and a second FCCP treatment was applied again for a second measure of maximal respiration. The data is presented as mean ± SEM (n=6) and analysed using a one-way ANOVA with Tukey post hoc test. P value<0.05 "*" compared with untreated controls. P value <0.05 (#) compared with OA + WY-14643 treated iPSC-CMs. B) RRC during pyruvate and malate respiration on untreated vs treated iPSC-CMs. RRC was calculated as the difference between maximal respiration and baseline. Untreated iPSC-CMs were used as a control. Data are presented as mean ± SEM (n=4) and analysed using a one-way ANOVA with Tukey post doc) test.

B, was successfully obtained. This was probably due to a lack of antibody optimisation used on the blots (anti-UCP3, anti-PDK4 and anti-MCAD, Table A.5). It was assumed the antibody concentrations were either too low or unsuited for this cell type. This experiment will have to be optimised and explored in more detail by the next incoming DPhil student.

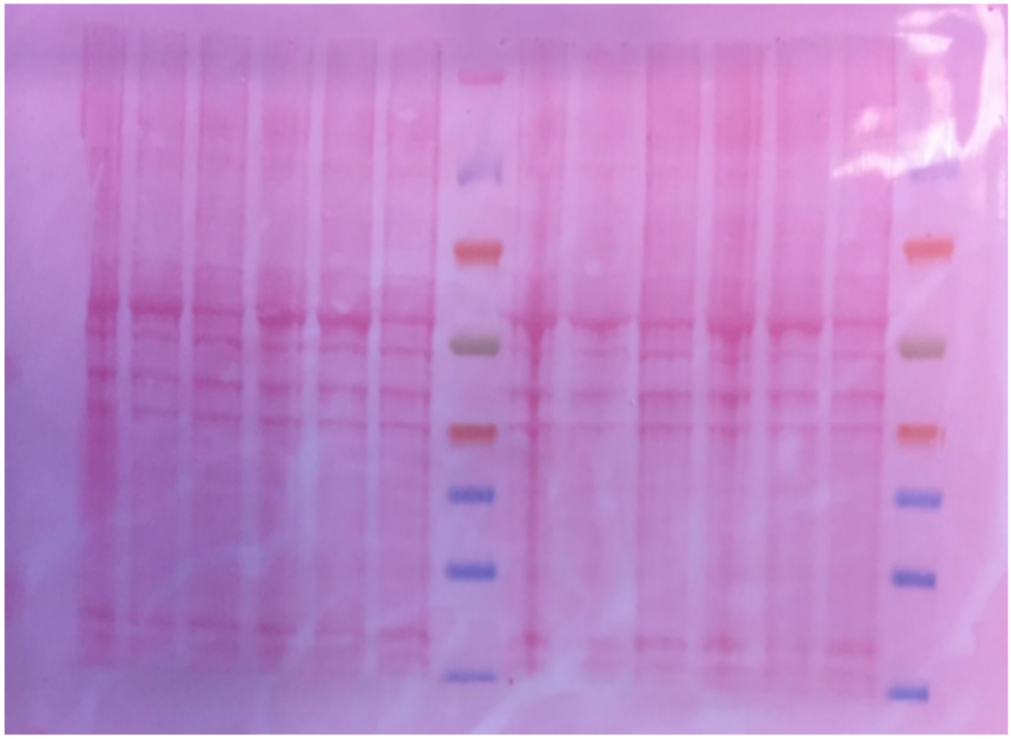

Figure 4.16: Ponceau Staining Example from Westerns

4.3.7 Immunocytochemistry of iPSC-CMs Treated With OA ± WY-14643

Immunocytochemistry was performed on iPSC-CMs treated with OA ± WY-14643. The cells were differentiated and re-plated onto RF-Matrigel coated coverslips in a 24-well plate on DD15. Each sample was treated for 1 week with OA ± WY-14643 and then fixed for staining. The iPSC-CMs were stained for GLUT4, Sarcomeric Actinin, Mitotracker and Oil Red O (Table A.3). The GLUT4 expression increased when treated with the OA and WY-14643 when compared to the untreated controls even when cell numbers were decreasing (Fig. 4.17A-C). Sarcomeric actinin seemed to decrease with treatment, but this

was associated with a decrease in cell number so proportional expression may have remained constant (Fig. 4.17D-F). Unfortunately these samples had died, either due to the treatment or just to being re-plated on a glass cover slip which the cells did not particularly like.

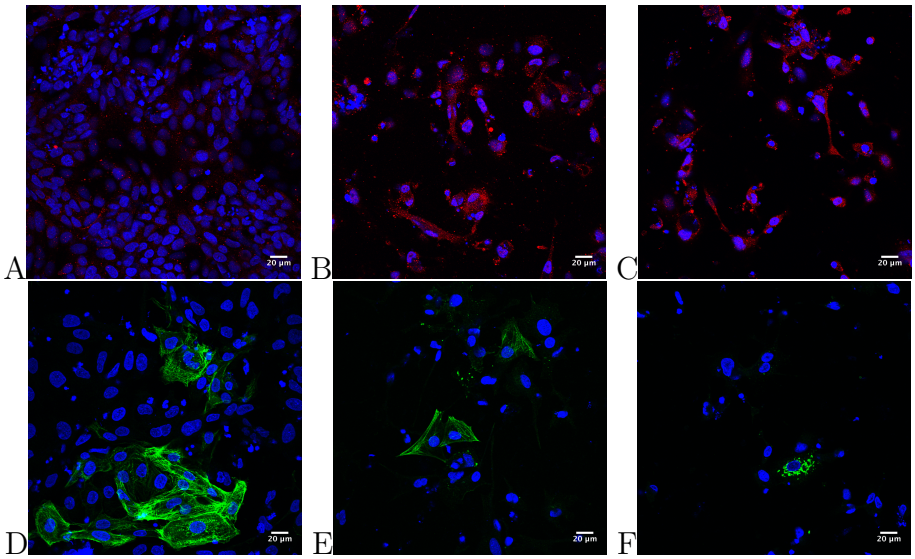

Figure 4.17: Staining of iPSC-CMs treated with OA ± WY-14643. Dapi (blue) stains for the nucleus. A) iPSC-CMs (control) stained for GLUT4. B) iPSC-CMs treated with OA stained for GLUT4. C) iPSC-CMs treated with OA + WY-14643 stained for GLUT4 (red). D) iPSC-CMs (control) stained for sarcomeric actinin (green). E) iPSC-CMs treated with OA stained for sarcomeric actinin (green). F) iPSC-CMs treated with OA + WY-14643 stained for sarcomeric actinin (green). Images were taken using an Olympus Confocal Microscope at the Dunn School by Rita Al-Onaizan.

Next, the mitochondrial number was looked at by incubating the iPSC-CMs with 50 nM MitoTracker Red CMXRos dye for 15 minutes, at 37 °C, prior to fixation. Here we saw again the same decrease in cell number with treatment as we did before, but interestingly even with the decreased number, when just looking at individual cells treated with OA + WY-14643, they had the same fluorescence intensity as the controls (Fig. 4.18A-D). Treatment with OA alone did result in a reduction in fluorescence intensity. Overall the cells did not like being re-plated onto glass and other experiments could be considered in the future to quantify mitochondrial mass such as flow or qPCR for mitochondrial DNA. Lastly, Oil Red O (ORO) staining was attempted but there was no visualization of lipid droplets in any of the conditions (Fig. 4.19A-C). This protocol needs to be optimised further and run with controls (e.g. fat cells, MSCs, etc) to verify accuracy of the staining versus a

false negative result.

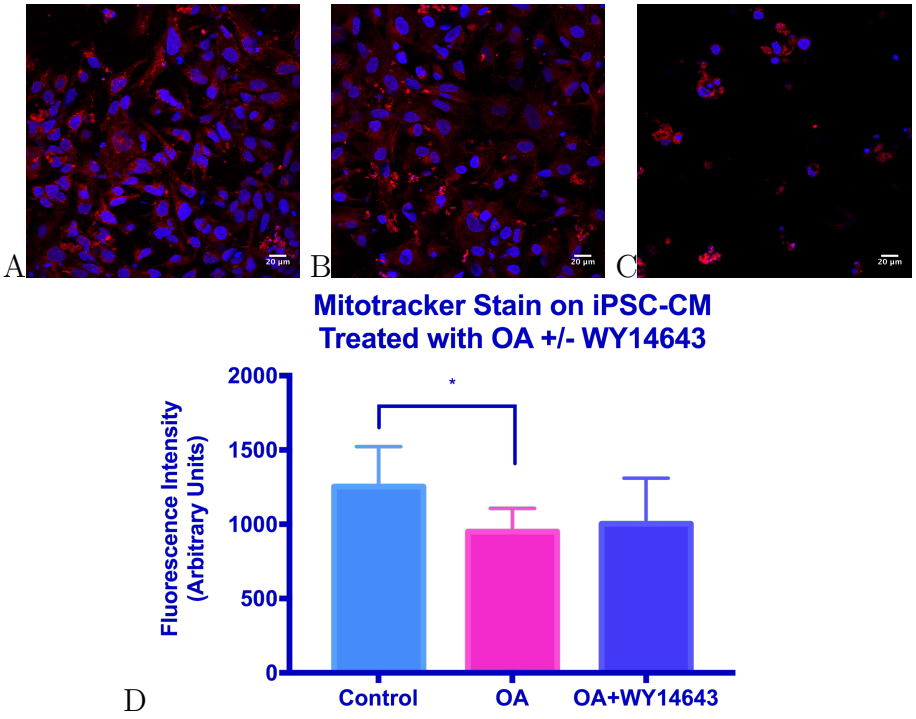

Figure 4.18: Staining of iPSC-CMs treated with OA ± WY-14643. Dapi (blue) stains for the nucleus A) iPSC-CMs (control) B) iPSC-CMs treated with OA C) iPSC-CMs treated with OA + WY-14643 stained with Mitotracker (red). D) fluorescence intensity. The bar represents the mean of grey value collected from 10 independent stained cells + StdDev. The pink represents the iPSC-CMs treated with OA alone and indigo represents the iPSC-CMs treated with both OA + WY-14643 for 1 week. All of these are normalised to the blue bar representing the control (iPSC-CMs untreated at Day 22). "*" denotes p-value<0.05 and refers to significance in comparison to the control iPSC-CMs. Images were taken using Olympus Confocal Microscope at the Dunns School by Rita Al-Onaizan.

4.3.8 FAO of iPSC-CMs Cultured on Scaffolds and Treated With OA ± WY-14643 for 24 Hours or 1 Week.

Both palmitate and OA oxidation rates were determined by comparing iPSC-CMs treated with 400 μM OA alone or in combination with 120 μM WY-14643 cultured either as a monolayer or on a 3D scaffold. iPSC-CMs were differentiated and re-plated on DD15 (10^6 cells) to either a 24-well plate coated with RF-Matrigel (control) or onto one of three

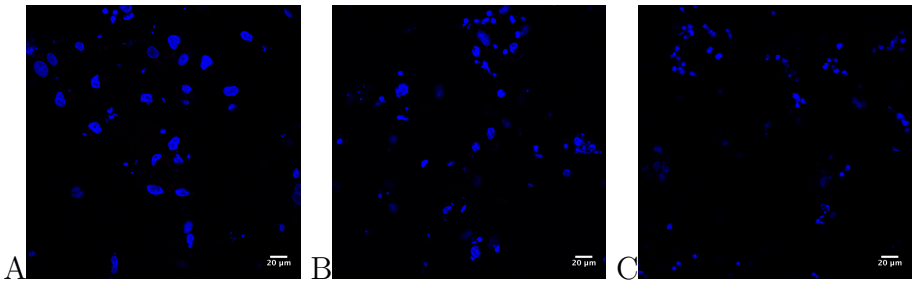

Figure 4.19: Staining of iPSC-CMs treated with OA ± WY-14643. Dapi (blue) stains for the nucleus. A) iPSC-CMs (control) B) iPSC-CMs treated with OA alone C) iPSC-CMs treated with OA + WY-14643 stained for ORO (red). Images were taken using Olympus Confocal Microscope at the Dunns School by Rita Al-Onaizan. The protocol was unsuccessful.

different collagen-derived scaffolds (100% Coll, Coll/C4S 1:1, or Coll/Ela 1:1). Each scaffold was cultured for 1 week with the assigned OA/WY treatment.

Both palmitate and OA oxidation increased when cells were grown on Coll/C4S 1:1 or Coll/Ela 1:1 scaffolds when compared to the RF-Matrigel monolayer (Fig. 4.20). The OA/WY treatment did not provide any further increase in oxidation of OA (Fig. 4.20A). However, palmitate oxidation increased with the addition of OA and with OA + WY-14643 in the iPSC-CMs grown on Coll/Ela 1:1 scaffolds, albeit with high variability (Fig. 4.20B).

4.3.9 The Glycolytic Flux and Glucose Oxidation of Cultured iPSC-CMs on Scaffolds and Treated With OA ± WY-14643.

Both glycolytic flux and glucose oxidation rates were determined by comparing iPSC-CMs cultured on scaffolds treated with 400 μM OA alone or with the addition of 120 μM WY-14643. As shown before in Chapter 3, the cells grown on 3D scaffolds had significantly decreased glycolysis compared to the RF-Matrigel monolayer controls (Fig. 4.21A). However, treating the iPSC-CMs with OA + WY-14643 for 1 week did not further reduce glycolytic rates.

There was a non-significant increase in glucose oxidation after 1 week of treating the cells with either OA ± WY-14643 in the 100% Coll or Coll/C4S scaffolds (Fig. 4.22). However,

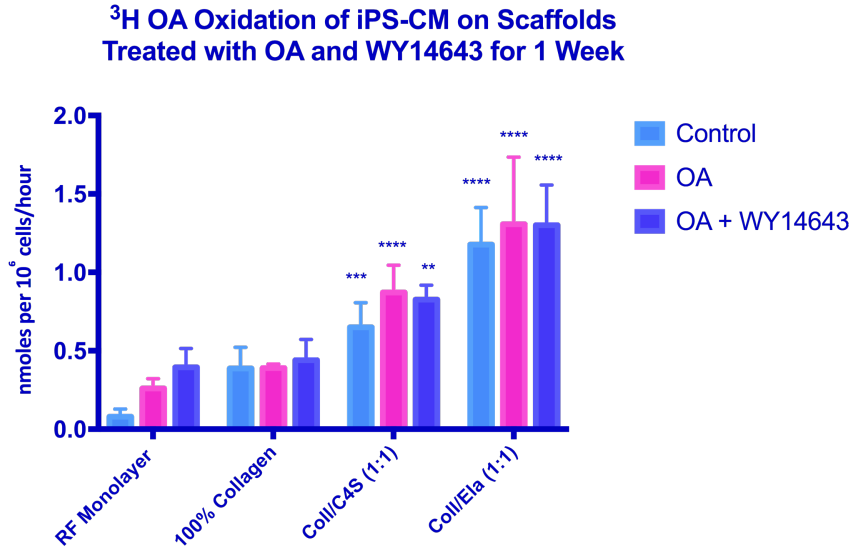

A

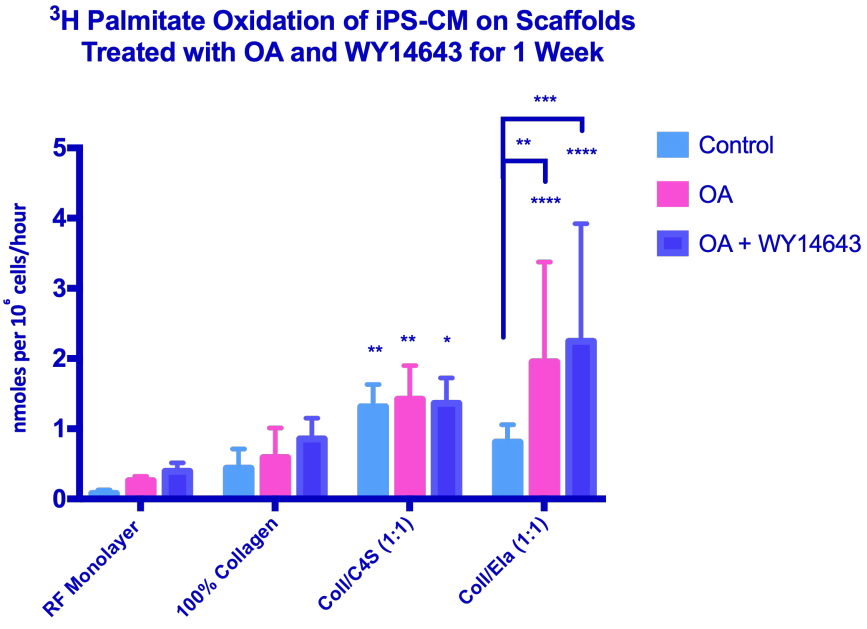

B

Figure 4.20: A) ^{3}H OA oxidation B) ^{3}H palmitate oxidation of 10^6 iPSC-CMs re-plated on DD15 and cultured on scaffolds treated with OA ± WY-14642 for 1 week. On the day of the experiment the iPSC-CMs were incubated for 8 hours in RPMI+B27 media containing 2% BSA and either 0.3 mM palmitate dpped with palmitic acid [9,10-^{3}H(N)] + their assigned OA/WY treatment or 400 μL OA doped with OA [9,10-^{3}H(N)] + their assigned OA/WY treatment. The bar represents the mean + SEM (n=6-10). The blue represents the control (untreated iPSC-CMs), the pink represents treated with OA alone, and indigo represents treated with OA + WY-14643. The set of stars represents the comparison of the treatments to the RF-Matrigel monolayer control, while the "*" = $p<0.05$, "**" = $p<0.01$, and "***" = $p<0.001$ or equivalent. The data was analyzed using a two-way ANOVA and a Tukey's multiple comparison test.

cells on the Coll/Ela scaffold showed significantly increased glucose oxidation after the treatment with OA and with OA + WY-14643 (Fig. 4.22). The glucose oxidation of treated OA + WY-14643 cells on the Coll/Ela scaffold was also significantly higher than that of the treated OA + WY-14643 on the 100% Coll scaffold.

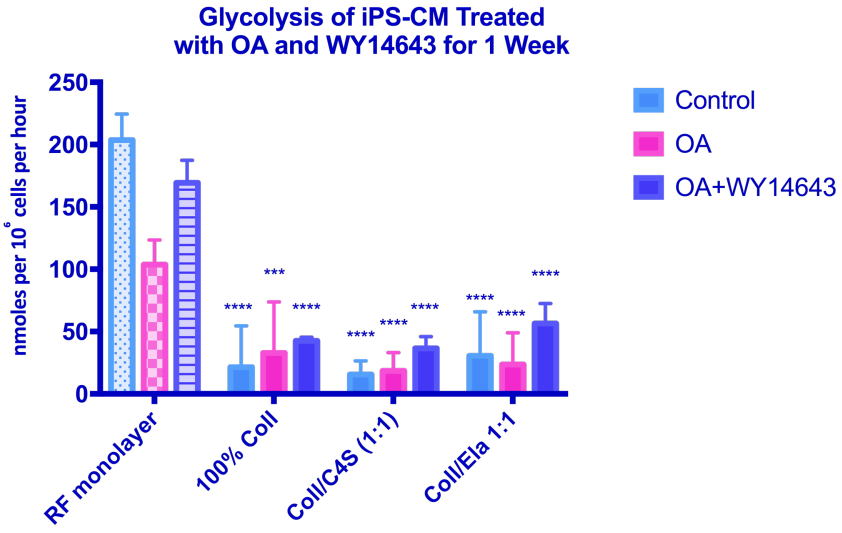

Figure 4.21: The glycolytic flux of 10^6 iPSC-CMs re-plated on DD15 cultured on scaffolds and treated with OA ± WY-14642 for 1 week. The scaffolds were incubated for 8 hours in low-glucose RPMI media containing 2% BSA, 0.3 mM palmitate doped with D-[5-^{3}H(N)]-glucose + their assigned OA/WY treatments. The bar represents the mean + SEM (n=8-12). The blue represents iPSC-CMs untreated for 1 week (control), the pink represents treated with OA, and indigo represents treated with OA + WY-14643. The set of stars compares each treatment group to the RF-Matrigel monolayers. "*" = $p<0.05$, "**" = $p<0.01$, and "***" = $p<0.001$ or equivalent. The data was analyzed using a two-way ANOVA and a Tukey's multiple comparison test.

4.3.10 Oxygen Consumption Rates in iPSC-CMs Cultured on 3D Scaffolds Treated with OA Alone or With WY-14643 Using the Clark-Type Oxygen Electrode

The Clarke-type oxygen electrode chamber in our lab was designed for use with mitochondria or isolated cells. When used with a large semi-solid item, such as a scaffold, the flea (spinner) at the bottom of the chamber knocked against the scaffold, causing interference in the oxygen electrode used to measure the OCR (Fig. 4.23). A collaborating student, Ifigeneia

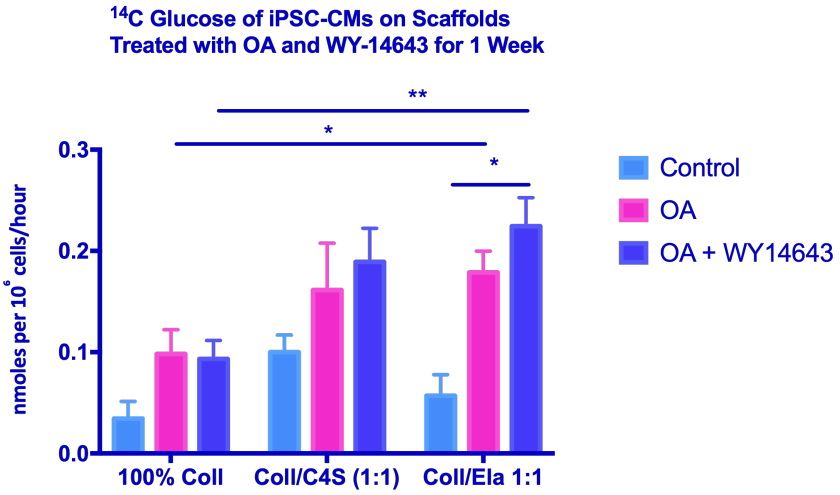

Figure 4.22: Glucose oxidation of iPSC-CMs cultured on scaffolds and treated with OA ± WY-14642 for 1 week. Scaffolds were then incubated in low-glucose RPMI media containing 2% BSA, 0.3 mM palmitate and 0.185 MBq D-[^{14}C(U)] Glucose + their assigned OA/WY treatments. The bar represents the mean + SEM (n=6). The blue represents iPSC-CMs untreated for 1 week (control), the pink represents treated with OA, and indigo represents treated with OA + WY-14643. "*" = $p<0.05$, "**" = $p<0.01$, and "***" = $p<0.001$ or equivalent.

Bardi from Imperial College, 3D printed a 7 mm silicon ring (Fig. 4.24) that wedged into the chamber and supported the scaffold right above the flea, eliminating the interference with the pressure sensors (Fig. 4.25). The gratings in the ring allowed for the liquid to pass through but did impede mixing. As a result when adding substrates, it would take an extra 10-15 seconds to obtain a fully homogeneous solution.

A baseline measurement test was performed to see how long the cells survived on each of the scaffolds in the chamber, but after five minutes there was no respiration occurring for any of the scaffolds (Fig. 4.26), suggesting that the cells were not happy in the chamber. A series of runs were completed with the addition of Oligo and FCCP. Although changes in respiration were detected for all scaffolds, respiring on oleate or on pyruvate and malate, there was no significant difference between the three different types of scaffolds (Fig. 4.27). A second FCCP experiment was not performed since the cells did not survive long enough to get a useful response. In addition, the rapidly declining rate of oxygen consumption resulted in a lower rate after addition of FCCP rate than the initial baseline rate in some cases, suggesting that the data were confounded. It is probable that the impaired mixing

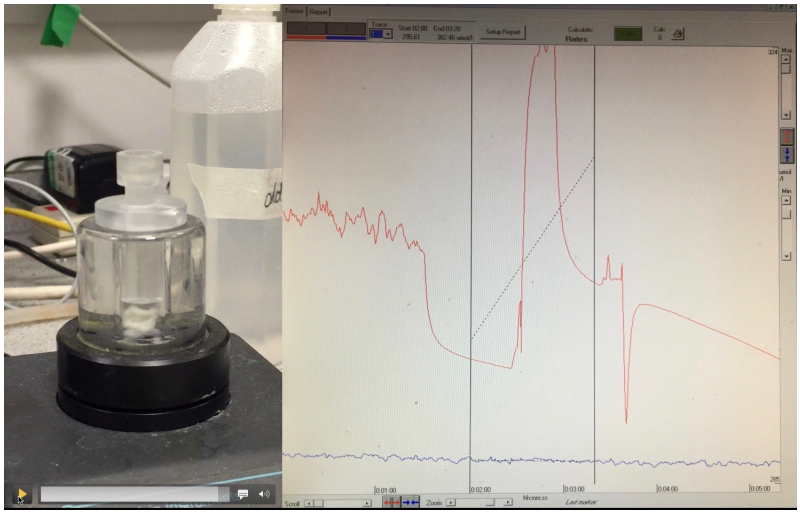

Figure 4.23: Image of a 100% Coll scaffold free floating in the chamber and interfering with the spinner at the bottom. To the right is an image of the OCR sensor's trace that is being affected by the pressure changes and showing as spikes in the rate.

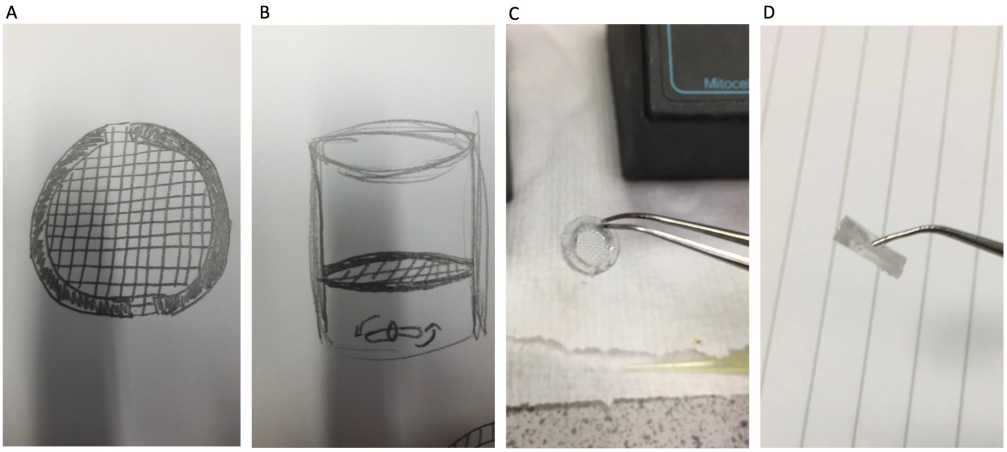

Figure 4.24: A) Top view of design, B) side view of design and C) top image D) side image of the 3D printed silicon ring that held the scaffolds above the flea to eliminate interference with the oxygen electrode.

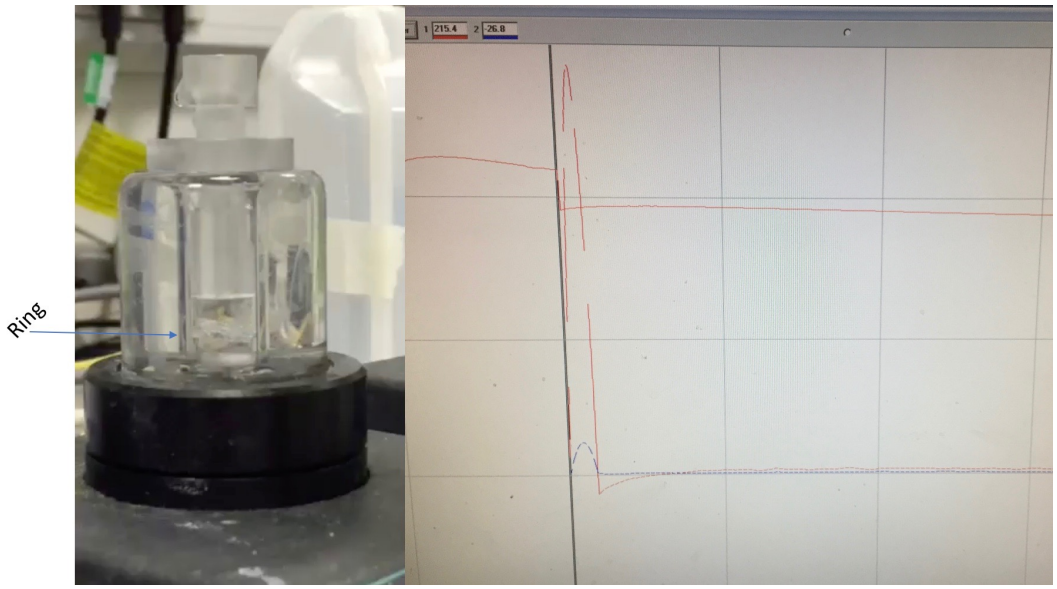

Figure 4.25: Image of 3D printed ring wedged into the chamber. To the right is an image of the sensor's rate that is now unaffected.

in the chamber meant that oxygen and/or substrate levels rapidly depleted in the region of the well containing the scaffold and caused the cells to stop respiration. As a result, this technique needs to be further optimised for use with the 3D constructs.

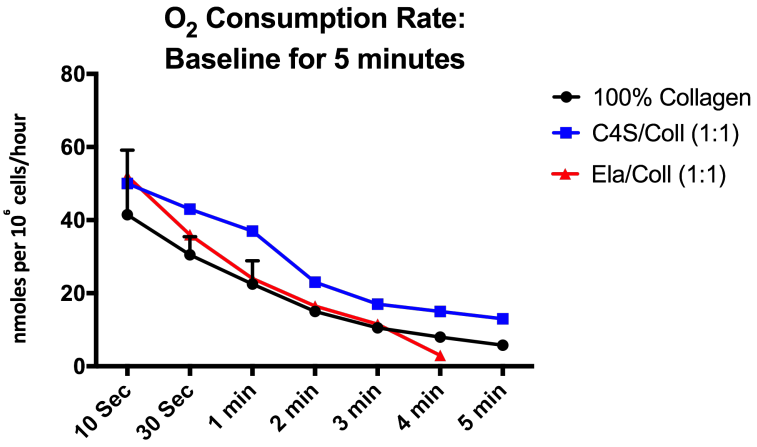

Figure 4.26: OCR for iPSC-CMs cultured on different collagen-derived scaffolds for 5 minutes with no added respiring substrates to gain a baseline to determine how long the cells survive in the chamber (n=3).

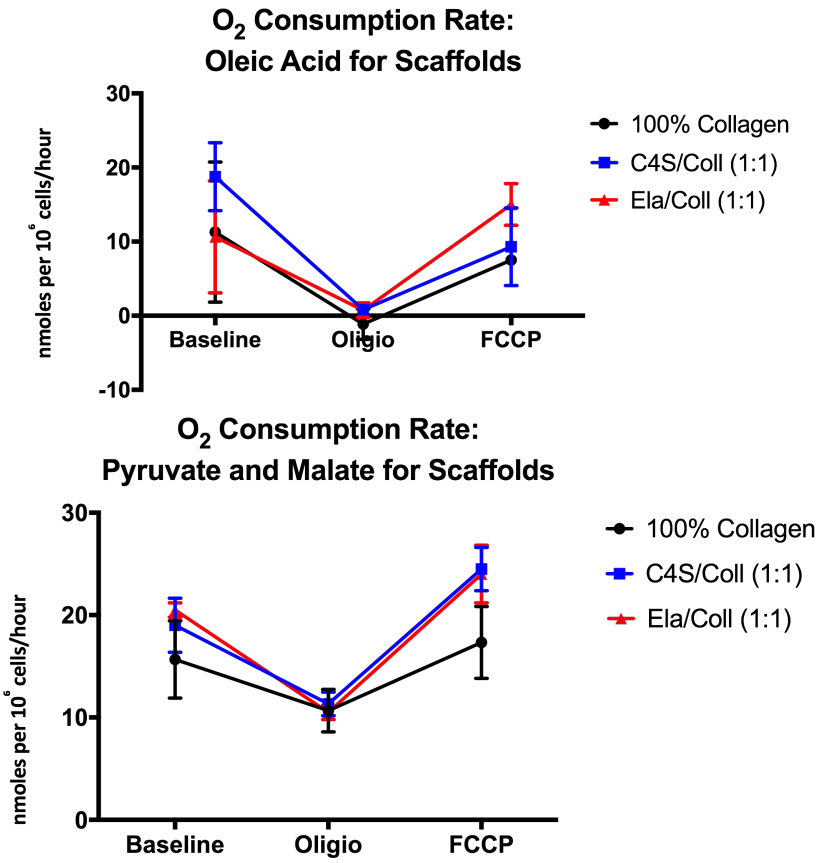

Figure 4.27: A) OCR using the Clark-type oxygen electrode in culture media containing A) OA and B) pyruvate and malate as respiring substrates for scaffolds. 2 million iPSC-CMs were cultured for 1 week on 100% coll (black), C4S/Coll (Blue) or Ela/Coll (red) scaffolds. Measurements were collected at baseline, after the oligomycin treatment, and at maximal respiration. The data is presented as mean ± SEM (n=6), and analysed using a one-way ANOVA with Tukey post hoc test. P value<0.05 "*" compared with untreated controls. P value <0.05 "#" compared with OA + WY-14643 treated iPSC-CMs.

4.4 Discussion

Immediately after birth, there are several changes to the heart's environment that affect its metabolism such as substrate levels, hormone concentrations, and increased oxygen availability [264, 265, 494, 600]. The foetal heart is equipped to survive in an environment of low oxygen and FA content (0.025 mmol/L). Due to these conditions, foetal CMs are primarily dependent on glycolysis for energy production [261] although, large lactate availability also allows for energy production via lactate oxidation. After birth, the heart undergoes a major metabolic switch, with an increased workload and demand for growth, the energy necessary cannot be met by glucose and lactate consumption alone [262, 263]. There is a rapid increase in circulating levels of FAs (ranging from 0.2 to 0.8 mM due to dietary changes and the lipid content in maternal milk) as well as increased oxygen levels which mediate a switch from relying on glycolysis towards oxidative metabolism in mature CMs [261, 266].

Despite changes in the energy substrate levels, in many cases the same culture media is used for differentiating iPSCs into CMs as for their long-term culture. Most culture media for iPSC-CMs are high in glucose and have little to no FA content. Therefore it was hypothesized that the addition of the fatty acid, oleic acid, along with the PPARα agonist, WY-14643 into their daily culture media would enhance metabolic maturation through *PPARα* activation. This would mature the mitochondria through the upregulation of these genes involved in FAO which would facilitate the consumption of the FAs and increase oxidative metabolism.

4.4.1 Effects of OA ± WY-14643 Treatment on Gene Expression of Monolayer iPSC-CMs

As confirmed in chapter 3 as well as by others, we found that the cells matured slowly over time with changes in structural genes occurring as early as the first month of differentiation whereas metabolic changes took longer to develop. The addition of OA and WY-14643 accelerated changes in some genes involved in oxidative metabolism (Table 4.2). Expression of *PDK4*, which controls the flux of pyruvate into the TCA cycle, was increased, with an

associated decrease in *PFKm* expression. There were also small increases in the PPARα target genes *ACSL1* and *CPT1*. In vivo, treatment with WY-14643 caused upregulated *PDK4* expression in control and cardiac myosin heavy chain (MHC)-PPARα mice [595]. Gilde *et al.* [591] showed increased *ACSL1* expression after treatment of neonatal rat CM with a combination of FAs (palmitic and OA) and even more when WY-14643 was added, compared to the glucose-treated CMs controls. Treatment of neonatal rat CMs cultured in glucose only media with WY-14643 also resulted in 2-3 times increased *ACSL1* expression compared to that in the DMSO treated CMs [590]. WY-14643 treatment has also been shown to upregulate *CPT1* expression in rat neonatal CMs [590, 591], MHC-PPARα transgenic mice [595], and in hESC-derived ventricular CMs [601].

Table 4.2: Summary Table of Effects of OA ± WY-14643 on Monolayer Cells.

Gene	**24Hrs+OA**	**1W+OA**	**24Hrs+OA+WY**	**1W+OA+WY**
PDK4	* ↑	**** ↑	**↑	**** ↑
GLUT4				* ↓
PFKM				** ↓
CPT1B				* ↑
EC1				* ↓
OA oxidation				* ↑
Palm. oxidation	* ↑	**** ↑	**** ↑	**** ↑
Glycolysis		** ↓		

Our data also showed that the isoform switch from *GLUT1* to *GLUT4* expression occurred over 1 week of culture, indicative of an increase in more mature, insulin-responsive metabolism. Treatment with OA ± WY-14643 resulted in a small decrease in GLUT4 expression compared with control. Others have also shown downregulation in *GLUT4* expression when culturing rat neonatal CMs with FAs (palmitic and OA) [591]. The reduced mRNA expression with OA + WY-14643 treatment suggests that there is a reduced requirement for *GLUT4* due to more FAO being performed. These results are complemented by the *PFKM* gene expression being significantly downregulated after 1 week of treatment with OA + WY-14643.

4.4.2 Effects of OA ± WY-14643 Treatment on Monolayer iPSC-CMs Making a Metabolic Switch From a Glucose Metabolism Towards More FAO.

Activation of PPARα downregulates glucose uptake and glucose utilization [585, 595] which may be because of direct activation of PPARα or in response to the increased FAO. PPARα knockout mice showed increased glucose uptake and oxidation while overexpression of PPARα reduced glucose uptake and transporter expression [554, 602]. Thus, we expected to see similar results with a reduction of glucose uptake and utilization from the OA ± WY-14643 treatment.

While a lot of studies have measured downstream PPARα effects and inferred increased FAO there are a limited number of studies that have shown direct measures of FAO. Here we saw, as expected, that addition of OA decreased the rate of glycolysis and increased that of fatty acid oxidation. There was an additional increase in palmitate oxidation between cells treated with OA and those treated with OA + WY-14643. The addition of this agonist also induced a greater difference from untreated cells. It should be noted, however, that glucose metabolism remained the predominant source of energy, although to a much lower extent than in untreated cells. After a week of treatment with OA + WY-14643, the rate of glycolysis was around 160 nmoles/10^6 cells/hour, that of glucose oxidation was around 1.6 nmoles/10^6 cells/hour whilst that of OA was around 1 nmole/10^6 cells/hour. As glycolysis, glucose oxidation and β-oxidation of OA produce 2, 32 and 120 moles ATP/10^6 cells/hour, respectively, the rate of ATP production was 320/51/120 nmoles ATP/10^6 cells/hour, respectively.

Interestingly, when iPSC-CMs were treated with both OA + WY-14643, *PDK4* gene expression increased yet there was no change in glucose oxidation. This could be due to a couple reasons. First, the increase in *PDK4* gene expression may have been transient but not resulted in a significant increase in PDK4. Furthermore, increased levels of *PDK4* mRNA or protein do not necessarily translate into increased phosphorylation and inactivation of PDH. In order to verify these ideas, westerns could be performed to determine these protein

levels and PDH activity could be quantified.

The RPMI media used in everyday culture contains around 11.11 mM glucose, and as a result the treated iPSC-CMs always had the choice of using either glucose or OA for energy production. Our data infers that even if treated OA + WY-14643 iPSC-CMs have developed more mature mitochondria, when they have a choice between glucose and FAs the cells will continue to use glucose as their primary energy substrate. So moving forward, to further enhance the usage of FAs in OA + WY-14643 treated iPSC-CMs, the iPSC-CMs should be cultured in a media with low or no glucose.

4.4.3 Oxygen Consumption Rate on Monolayer iPSC-CMs Treated With OA Alone or With WY-14643 Using Clarke-Type Oxygen Electrode

OCR was measured in untreated and OA ± WY-14643 treated iPSC-CMs. Interestingly, treatment for 24 hours with OA + WY-14643, as previously shown in Dr. Al-Siddiqi's thesis, induced an increased oxygen consumption rate in cells respiring on OA whereas cells treated with OA alone had increased oxygen consumption on pyruvate and malate, suggesting that the PPARα agonist was having some effect, even if small. This thesis continued this work measuring iPSC-CM treated for a week. Due to the design of the OXBOX, cells are inserted as a suspension and so it is hard to maintain their viability for a prolonged period of time. Originally cells suspended in glucose-free respiration medium was attempted but was unsuccessful. The cells quickly died most likely to a combination of being in suspension and a lack of nutrients. The protocol was then adapted so the cells were tested in their culture medium which prolong their survival in order to take consistent measurements. Treatment with OA + WY-14643 resulted in a 2-fold increase in baseline respiration (although this was not significant in cells respiring on OA) and a reduced response to the uncoupler FCCP. This may indicate that oxidative metabolism in the mitochondria was increased by the treatment or that the cells had increased proton leak at baseline caused, perhaps, by an increase in damage from reactive oxygen species.

Pfleger *et al.* [603] measured OCR using the Seahorse XF24-3 Analyzer of iPSC-CMs and neonatal rat CMs while respiring on palmitate, glucose, and a combination of both. These cells were treated for 24 hours with the same substrates they received during OCR measurements. They showed that the CMs respired more on 100μM palmitate alone or in combination with 17.5mM glucose [603]. We had observed previously that treating the cells with OA alone for 24 hours was not enough to increase OCR when respiring on OA but required the addition of WY-14643 suggesting that the untreated iPSC-CMs did not have the metabolic flexibility of neonatal rat CMs. Other labs have also shown that WY-14643 treatment increased mitochondrial membrane potential, another indication of maturation [601].

4.4.4 Effects of OA ± WY-14643 Treatment on iPSC-CMs Cultured in 3D

It has been previously shown in chapter 3 that iPSC-CMs prefer to be cultured in 3D over a 2D environment to more mimic in vivo conditions. There we showed that culture of iPSC-CM on porous collagen scaffolds induced a 2-fold increase in mRNA from *MYH6* and *MYH7* and a 5-fold increase in mRNA from *PDK4*, indicating both structural and metabolic maturation over 1 week of culture. This was associated with a decreased rate of glycolysis and a moderate increase in FAO. Addition of OA ± WY-14643 did not induce any further changes except where cells were cultured on scaffolds comprised of 1:1 collagen/elastin where increased glucose and palmitate oxidation were observed. It may be that the increased elasticity of the collagen/elastin scaffold permitted greater contraction of the cells, thereby increasing the energy demand and the benefit from upregulating fatty acid oxidation. Even though the iPSC-CMs have been shown to have an increased ability to oxidise OA, there was no change to the overall glucose metabolism. This may be because the cells are still cultured in large amounts of glucose from their basal media and are not having to do any substantial amount of work, so the need for ATP is not high especially as they do not really proliferate much on the scaffolds. As a result, the more mature cells still retained a

glycolytic phenotype, but were able to oxidise the fatty acid when supplied.

To the best of my knowledge, there is not another lab that is currently treating iPSC-CMs with both FAs and 3D constructs to use as a comparison. Overall it can be concluded that both the addition of OA and a PPARα agonist to the culture media and culturing on 3D constructs are having a small effect on the substrate metabolism of the iPSC-CM but for some reason these effects are not cumulative.

4.5 Conclusion

In conclusion, treating beating iPSC-CMs with 400 μM OA with the addition of 120 μM WY-14643 for 1 week enhanced metabolic maturation by upregulating FAO and regulators of pyruvate oxidation genes, increased palmitate utilization, and mitochondrial oxidative respiration. Overall, glucose oxidation was not affected by the treatment of OA alone or with the addition of WY-14643. Further increases in glucose and palmitate oxidation were observed when the treated iPSC-CMs were cultured on the collagen/elastin (1:1) scaffolds. This suggests that changing the culture media or growing the cells on 3D scaffolds is a start in the right direction but is not sufficient to induce enough maturation to switch these immature iPSC-CMs from a glycolytic metabolism to an oxidative one.

The greatest secrets are always hidden in the most unlikely places ...

— Roald Dahl, Charlie and the Chocolate Factory

5

Developing Engineered Heart Tissue (EHT) for Metabolic Characterization and Maturation of Induced Pluripotent Stem Cell derived Cardiomyocytes.

5.1 Introduction

5.1.1 Development of Engineered Heart Tissue

The engineered heart tissue (EHT) technique was pioneered by Thomas Eschenhagen and Wolfram-Hubertus Zimmermann in 1997. The initial EHTs were generated using isolated embryonic chick CMs mixed with collagen to form a 3D contracting construct [410]. Eschenhagen *et al.* [410] showed that these newly formed EHTs resembled heart tissue in vivo. They observed increased extracellular Ca^{2+} with an increased beating frequency, and exhibited a positive Frank-Starling mechanism. Zimmerman *et al.* [411] improved the initial design by moulding the EHT in the shape of a 3D ring by casting them around silicon tubing glued to the surface of a culture dish. These circular EHTs were created from the combination of neonatal rat CMs and collagen I with the addition of Matrigel.

This new model reportedly improved contractile function, myofiber organisation, and cell differentiation.

The ability to reproduce large quantities of EHTs make them an excellent tool for tissue regeneration, disease modeling, and drug screening/toxicity analysis. In 2010, Hansen *et al.* [426] developed a medium through-put method of generating fibrin-based EHTs. The fibrin EHTs took advantage of the rapid solidification reaction between fibrinogen and thrombin allowing them to be quickly casted into a gel suspended between two silicone posts, providing an auxotonic load /tension to the tissue while contracting. When the CMs start spontaneous beating, this is detected by the bending and movement of the silicone posts. The force generated by an individual EHTs can be measured automatically using a custom system made of a cell culture incubator, overhead camera, and analysis program (Fig. 5.1). More complex designs have now been tested in vivo and a timeline of the progression of EHT technology can be found in Fig. 5.2A.

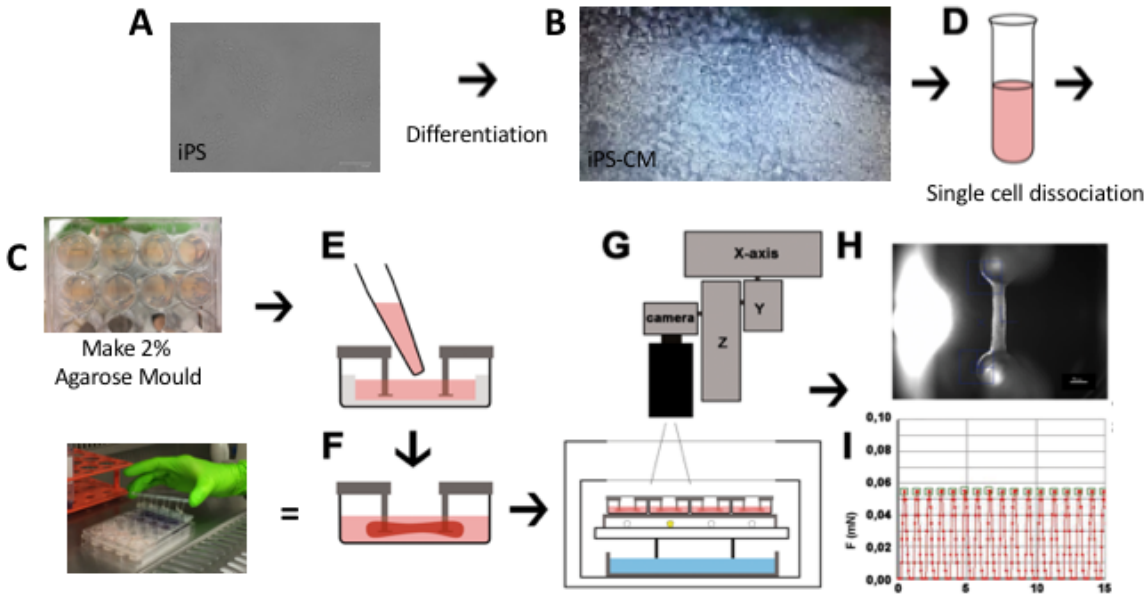

Figure 5.1: Generation of EHT schematic, adapted from [447]. A) iPS cells differentiated to B) iPSC-CMs. D) The cells are then dissociated into a single-cell solution and pipetted into E) 2% agarose moulds. F) EHTs solidificy around two silicon post and G) their contractility measurements can be measured.

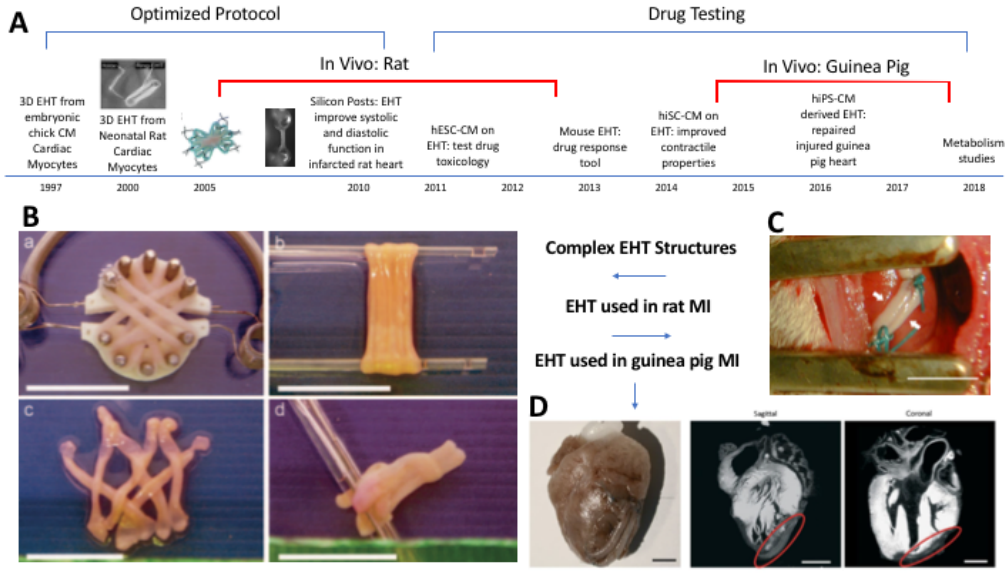

Figure 5.2: A) Timeline of EHT progression both in vitro and in vivo. B) Generation of different complex EHT geometries. Top left: Star-shaped EHTs generated by stacking 5 EHTs, fused in the center. Top right: 6 EHTs grown horizontally on two glass pipettes, adjacent EHTs fused to form a tubular construct. Bottom left: 3 EHTs cut open and layered to form a contracting network. Bottom right: EHTs rotated together to form a long rope structure. Scale bar=10mm. Image from [604]. C) Implantation of a circular EHT onto a Fischer 344 rat heart post-MI. Image from [426]. D) Implantation of a circular EHT on injured guinea pig heart post-MI. Scale bar=3mm. Image from [448]

5.1.1.1 EHTs Mimic Cardiac Tissue

To be practical and worthwhile, tissue engineering technology should meet specific criteria and, where possible, the construct should mimic host tissue. EHTs can recapitulate cardiac tissue in many ways. In the early stages of the technique, it was observed that the cells inside an EHT become aligned and the contraction force generated was calculated to be around 0.3 mN [410]. Initially, this measure was far below the desired force seen in human cardiac tissue. Others have improved the method by the addition of insulin and an auxotonic load resulting in increased force production and contraction rate of EHTs derived from rat neonatal ventricular CMs [424]. In 2013, Kensha *et al.* [605] continued to optimise the collagen/Matrigel-based EHT technique by using a custom made bioreactor, adding vitamin C, fibroblasts, and increased static stress. They also used a novel approach for using murine and human embryonic/iPSC-derived CMs from an EB-based differentiation protocol, where they generated cardiac bodies (CBs) and did not disassociate the cells prior to seeding them in the EHTs. A combination of all these new strategies yielded an improved force generation of 4.4 mN/mm^2. Unfortunately, this measurement is still lower than adult human cardiac muscle measuring around 20 mN/mm^2.

The approach in which these contraction forces are being calculated is not ideal, as they are measured using the cross-sectional area of an individual EHT [606, 607]. While the active levels of force do not change substantially amongst different batches, the width of the EHTs becomes thinner over time, causing the force per unit area to increase. This thinning is thought to be due to fibroblasts pulling CMs closer together. The concept has been investigated and reported to show that around 10% of fibroblasts are essential for optimum EHT performance and thinning [605].

5.1.1.2 EHT Application in Stem Cell Therapies

EHT holds the potential to be a great vehicle to facilitate replacement and regeneration of CMs in cardiac tissue. These 3D beating constructs can be engrafted onto injured myocardium and provide in vivo aid in the contraction of heart tissue and replacement of lost CMs [426, 448, 608]. For engraftment purposes, a range of large complex EHTs have been

designed to cover more area and be easily attached over an infarcted region [604] (Fig. 5.2 B-D).

Zimmerman *et al.* [426,609] fused together several EHTs creating a single large contracting construct (15 mm in diameter and 1-4 mm in length) that was surgically grafted to a MI rat model and was reported to improve cardiac function. The engrafted large EHT showed structural integration and electrical coupling up to 28 days after implantation. In addition, it induced thickening of the systolic wall and improved fractional area shortening. More recently, EHTs have been tested on a larger animal model in the process of up-scaling towards more human-like conditions. The EHTs were engrafted over cryo-injury induced MIs in guinea pig hearts and resulted in CM proliferation and improved left ventricular function, including increased fractional shortening [448]. These studies have been a proof of concept in both small and larger animal models that EHTs could be used for a regenerative medicine approach. However, if translated to humans, a larger hydrogel would have to be produced to compensate for the substantial loss of CM numbers during ischemia and there may be problems in maintaining viable cells in a thicker construct.

5.1.1.3 EHTs Application in Disease Modeling

Disease modelling is used to investigate mechanisms behind diseases which would otherwise be extremely difficult or unethical to perform in humans. EHTs have been shown to be a promising method to model certain cardiac diseases, such as hypertrophic cardiomyopathy and heart failure, thereby helping to identify cardiac phenotypes crucial to pathogenesis [610–613]. This range of diseases were previously difficult to model in a 2D system as the contraction of a cell sheet does not accurately recapitulate the contraction parameters of cells in an electrically coupled tissue. Hirt *et al.* [614] developed a method of placing metal braces, onto the silicone posts to increase the load on neonatal rat-derived EHT by around 12 fold, inducing hypertrophic cardiomyopathy. This resulted in an activation of foetal genes that caused increased glucose consumption and extracellular collagen-1 deposit. After the release of the metal braces, the EHTs experienced a reduced contractile force and impaired diastolic relaxation that could be preventable by endothelin-A

blockade [614]. This approach showed proof of concept that EHTs can be used as an experimental model for hypertrophy and potentially other complex cardiac diseases while using fewer animals. The model can be useful to investigate novel therapeutic approaches in a fast and straightforward manner.

Tiburcy *et al.* [613] have demonstrated that a version of EHTs referred to as engineered heart myocardium (EHM) have important structural and functional characteristics that resemble the postnatal myocardium such as morphology, systolic twitch forces, positive force-frequency responses, inotropic responses to β-adrenergic stimulation, and advanced molecular maturation by transcriptome profiling. These properties allow the iPSC-derived EHM to model and respond to chronic catecholamine toxicity with contractile dysfunction, CM hypertrophy, and CM death which are all hallmarks to heart failure. Recently, Lemoine *et al.* [615] showed that iPSC-derived EHTs promote a higher I_{Na} density and showed similar upstroke velocities in EHT (219±15 V/s, n=13) compared to human left ventricle tissue (LV, 253±7 V/s, n=25). They also demonstrated that iPSC-derived EHTs displayed a resemblance in CM morphology and subcellular $Na_V1.5$ distribution to left ventricular tissue which indicates its usefulness as a model for excitability of human cardiac tissue.

5.1.1.4 EHTs Application in Drug Toxicology

EHTs are easily reproducible with minimal variation and can mimic several characteristics of endogenous cardiac tissue making it an encouraging model for drug screening studies. Eschenhagen's group has set up a system in which multiple drugs can be tested simultaneously for abnormalities in contractions or cardiotoxic action in both rat and human-derived EHTs [616,617]. The system allows analysis of contractile force with high precision of up to 24 x EHTs (10^6 cells/EHT) for a 14 day incubation after casting. Mannahardt *et al.* [617] used this system for quantifying changes in beating frequency after addition of isoprenaline, SEA-0400, ryanodine, ivabradine, and Tetrodotoxin suggesting both calcium- and membrane-clock mechanisms are involved in spontaneous pacemaking of iPSC-CM-derived EHTs. These findings reflected a similarity to newborn sinoatrial node pacemaking. They also observed among others, canonical responses to adenylyl cyclase

(cAMP) -dependent and -independent positive and negative inotropic drugs.

Eder *et al.* [616] also used this medium-throughput system to conduct the largest head to head comparison of proarrhythmic drugs performed to date. In this study, using rat EHTs, they observed drug effects on contractile activity, electrical pacing, action potentials and Ca^{2+} transients. For example, they reported that the I_{to}-blocker 4-aminopyridine increased action potential duration, time of relaxation and caused after contractions which were reversed by inhibitors of RYR2 or sodium calcium exchanger (NCX). These findings support the proposal that iPSC-CM-derived EHTs can be a promising model for preclinical drug screening and allow the opportunity for large drug companies to improve rejection rates of drugs prior to phase one clinical trials.

5.1.2 iPSC-CM-Derived EHT Maturation

iPSC-derived EHTs were first established in 2016 by adapting former EHT technology from the neonatal rat/mouse and ESC-CMs models [426, 618, 619]. These iPSC derived EHTs were able to demonstrate maturation in morphology such as sarcomeric organization and cellular alignment. They also showed responses to physiological and pharmacological stimuli similar to healthy human heart tissue [620, 621]. In 2018, Ulmer *et al.* [390] expanded on this work and reported iPSC-CM derived EHTs led to a maturation of energy metabolism when compared to 2D culture. They showed the EHTs had an increase in mitochondrial mass, glucose, lactate, and FAO metabolism while having a reduction in anaerobic glycolysis. These results strongly support the notion that contractile work contributed to metabolic maturation of iPSC-CMs.

5.1.3 Chapter Aims

The aims of this chapter were first to set up the EHT technology in our lab and then adapt our existing protocols for metabolic characterization for use with the contracting heart tissue. Next, we aimed to compare iPSC-CMs gene expression and metabolic characterization when iPSC-CMs were cultured in 2D versus 3D either on one of our three

collagen derived scaffolds or in our newly developed EHTs.

In addition, we aimed to try and maximize metabolic maturation by the addition of the fatty acid, oleic acid, and the PPARα agonist, WY-14643. Characterization of changes in gene expression and substrate metabolism were performed to compare the different 3D culture conditions.

5.2 Methods

5.2.1 Glucose-Free, Lactate-Enriched Treatment

To purify iPSC-CMs, a glucose-depleted, lactate-enriched treatment was attempted. The iPSCs were differentiated into CMs by the Wnt-modulation based protocol explained in Section 2.1.1.5 until DD10. On DD10, the media was replaced with a glucose-depleted DMEM (ThermoFisher) supplemented with 5mM lactate (Sigma). This medium was made fresh and replaced every two days for a total of 10 treatment days (until DD20, Fig. 5.3). The iPSC-CMs were then switched back to their usual RPMI + B27 media replaced every two days for the rest of their span in culture.

5.2.2 Glucose-Depleted Treatment

A second method to purify iPSC-CMs was attempted using transient glucose-depleted treatment. The iPSCs were differentiated into CMs by the Wnt-modulation based protocol explained in Section 2.1.1.5 until DD7. On DD7, instead of switching to the RPMI + B27 media, the medium was replaced with a glucose-depleted DMEM (ThermoFisher). This medium was left for two days until DD9 and then switched back to the normal RPMI + B27 for two days. On DD11, the medium was again replaced with the DMEM minus glucose for an additional two days. From DD11 forward, the media switched back to RPMI + B27 was used and was changed every two days for the rest of the time in culture Fig. 5.4.

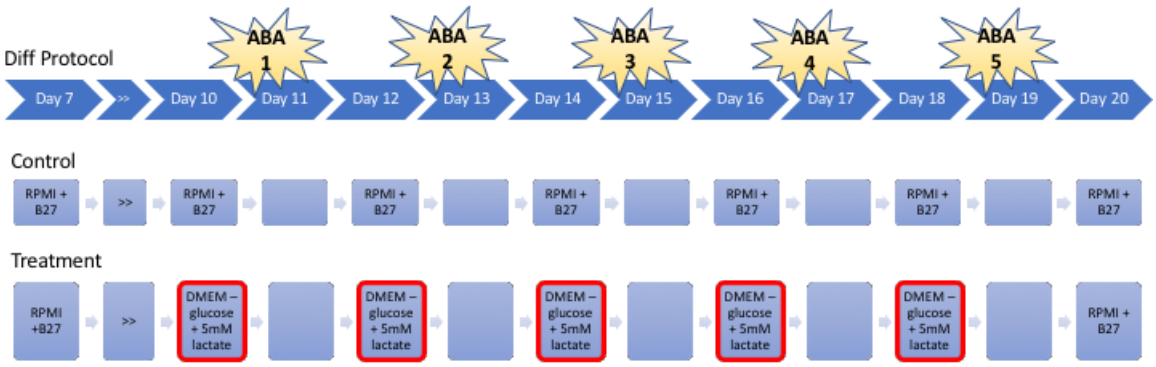

Figure 5.3: Glucose-depleted, lactate-enriched iPSC-CMs treatment timeline. iPSC-CMs were treated with the lactate media on DD10, DD12, DD14, DD16, and DD18 for a total exposure of 10 consecutive days. AlamarBlue assays were performed on DD11, DD13, DD15, DD17, and DD19.

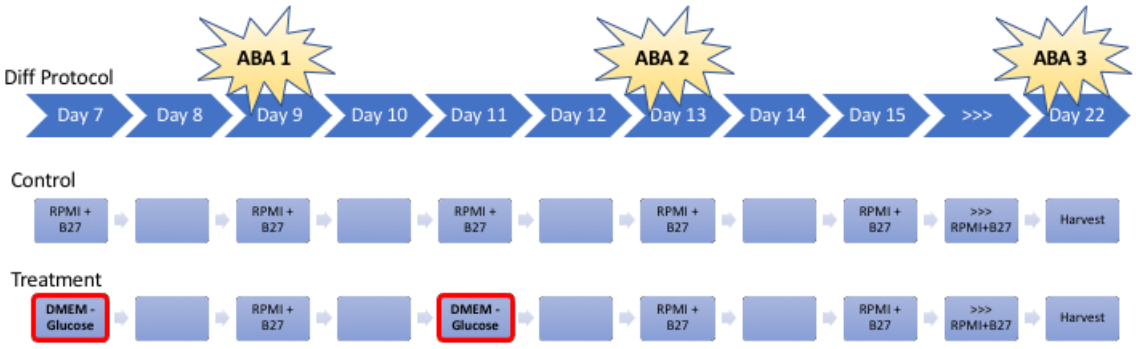

Figure 5.4: Glucose-depleted iPSC-CMs treatment timeline. iPSC-CMs were treated with the glucose-depleted media on DD7 and DD11 for a total time of 2 sets of 2 days. AlamarBlue assays were performed on DD9, DD13, and DD22.

5.2.3 Oleic Acid ± WY-14643 Treatment

As in Chapter 4, the iPSC-CMs were treated with oleic acid ± WY-14643 to further enhance maturation (see Section 4.2.1 for protocol). Briefly, the iPSCs were differentiated into CMs by the Wnt-modulation based protocol explained in Section 2.1.1.5 and usually start spontaneously beating around DD12-15. 10^6 iPSC-CMs were then re-plated on DD15 onto either a 2D RF-Matrigel-coated 24-well plate, seeded onto a 3D collagen-derived scaffold, or encapsulated in an EHT. Each condition was then treated with either 400 μM OA ± 120 μM WY-14643 for 1 week. The untreated iPSC-CMs were used as controls for all the experiments.

5.2.4 Protocol for the Generation of EHT

Engineered heart tissue was generated using the protocol as previously described [426,451]. Briefly, iPSC-CMs were differentiated and dissociated on DD15 into single cells. For a single EHT, 10^6 iPSC-CMs were re-suspended in 92 μL of Non-CM media, 5.5 μL 2xDMEM, 0.425 μL aprotinin (Sigma), 3 μL bovine Thrombin, and 2.5 μL of Fibrinogen. Each mixture was then pipetted into a pre-casted 2% agarose mould and solidified around two silicone posts over a 3 hour span. A step-by-step protocol for EHT generation can be found in Appendix A.1.3 and a full list of the necessary reagents and media compositions can be found in Table 2.3 and Table A.6. Oleic acid and WY-14643 treatment were always added the day the EHTs were generated (DD15) and made fresh every two days for 1 week.

5.3 Results

I wanted to note in this chapter during our EHT project, we suffered from problems of infection in the cell culture lab at a crucial time. This meant that on certain experiments there was less time available for trouble shooting and we had to decide which experiments to prioritise. As a result in certain sections we were only able to obtain preliminary data.

5.3.1 Generating Engineered Heart Tissue

The EHTs in this thesis were generated by casting 10^6 iPSC-CMs in a fibrinogen and thrombin gel mixture in a pre-designed mould, generating a 3D hydrogel construct that contracted between two flexible silicone posts. I learned this technique from Dr. Thomas Owen in Professor Sian Harding's lab at Imperial College.

After a preliminary experiment to make EHTs without cells, the protocol was repeated with the addition of iPSC-CMs (Fig. 5.5). To determine if the iPSC-CMs were surviving the seeding process, an ABA was performed the day after casting. After a 4 hours incubation of ABA, there was a notable color change which corresponded to a 40% ABA reduction (double the reduction from the scaffolds presented in Chapter 3 over the same time period). This confirmed the iPSC-CMs were viable and metabolically active inside the EHTs (Fig. 5.6).

A 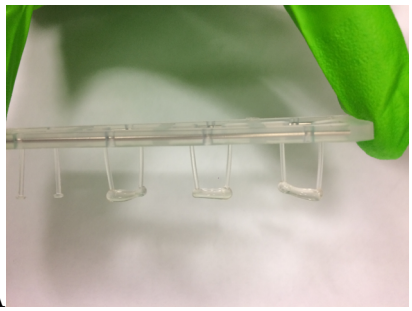 B 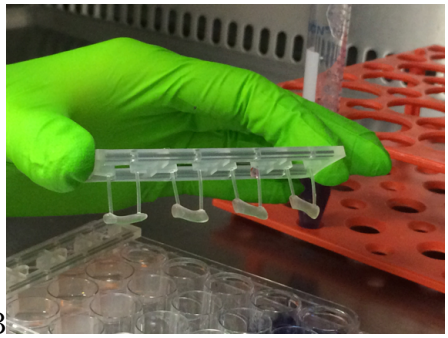

Figure 5.5: Image of EHTs generated A) without cells and B) with iPSC-CMs attached to silicone posts.

Within just three days after generating iPSC-CMs-EHTs, the EHTs started to drastically thin, resulting in 80% of them breaking completely (Fig. 5.7). After troubleshooting, it was confirmed there was not enough Aproptin in the master mix. All future batches used a concentration of 33 mg/mL and did not have this problem.

The next batch of EHTs looked thick and were viable. Over the span of the week the EHTs had a limited amount of thinning, but this was in the normal range that others observed. After a week of culture, there was no visible sign of contraction. When examining the EHTs further under a microscope, there seemed to be largely independent clusters of spontaneous beating cells near the silicone posts but they were not synchronised. After

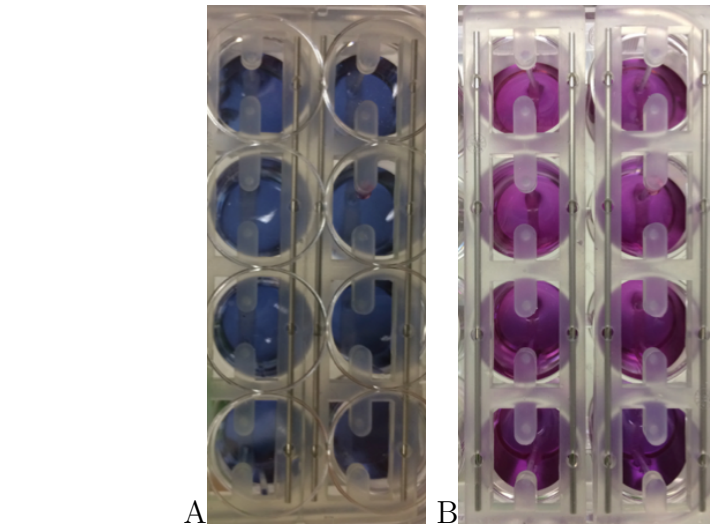

A B

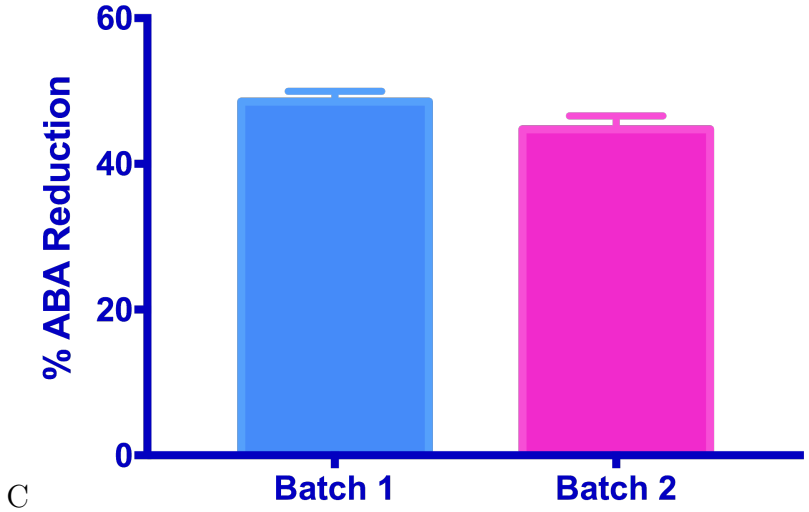

C

Figure 5.6: A) Image of ABA reduction colour of EHTs at the start of an ABA (timepoint 0) and B) after 4 hours of ABA incubation. C) ABA reduction calculation of EHTs. Each batch had 4 EHTs and the bar represents mean + SEM (n=8). There was no significant difference between the two batches.

A 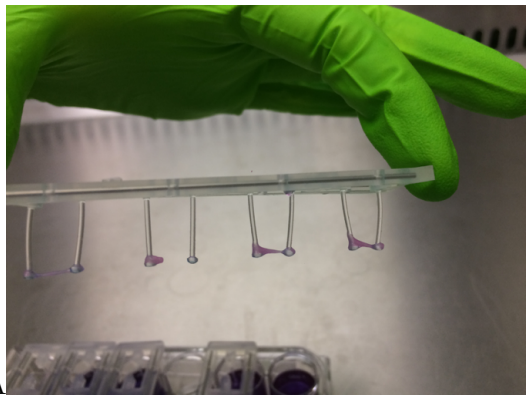 B 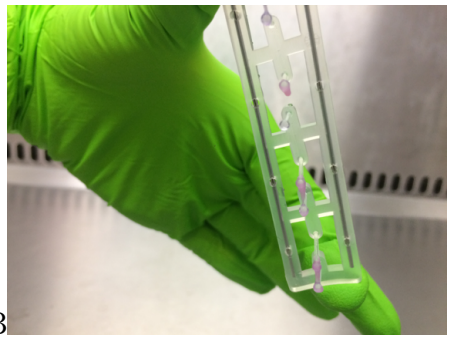

Figure 5.7: Image of EHT that thinned within 3 days of casting due to insufficient amounts of aproptin added. A) Side view. B) Bottom view.

discussing with Dr. Thomas Owen, we optimised our single cell dissociation protocol and were able to produce a more homogeneous seeding of the EHTs (Fig. 5.8). The following batch of EHTs started physically beating after culture for 2-3 weeks. There was minimal post deflection, but a rate of around 80 bpm (Fig. 5.9). This culture time was two to three times longer than what was seen with EHTs constructed at Imperial using iCell Cardiomyocytes from Cellular Dynamics (CMC-100-010-001) which are reported to be 99% pure, so the increased time to beating could be due to a more robust CM population then our differentiation protocol.

5.3.2 Glucose-Depleted and Lactate-Enriched Culture Conditions to Purify CM Population.

To try and enrich our iPSC derived CM population, the culture media was changed for glucose-depleted DMEM with the addition of 5 mM lactate on DD10 for 10 days. An AlamarBlue Assay was performed every other day during the treatment to check the viability of the cells. Within the first 5 days, the majority of the lactate treated cells had died and the number continued to decline (Fig. 5.10). The corresponding readings from the ABA also fell in parallel to the decline in cell number. The small (around 14%) of remaining cells were presumably CMs but there was no way to verify how many CMs could have also died in the treatment. Flow cytometry for the marker cardiac troponin T

A 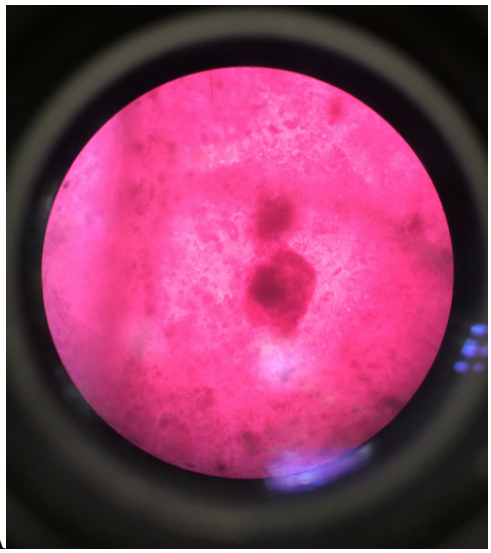 B 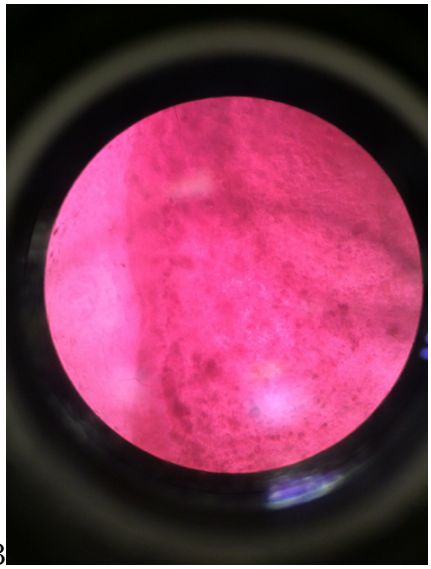

Figure 5.8: Microscope image at 40x of the side of EHTs attached to the south post. A) Image of original cell dissociation and generation of EHTs with iPSC-CMs clumped into large clusters of beating cells. B) Improved dissociation protocol eliminated clumps into a more homogeneous seeding.

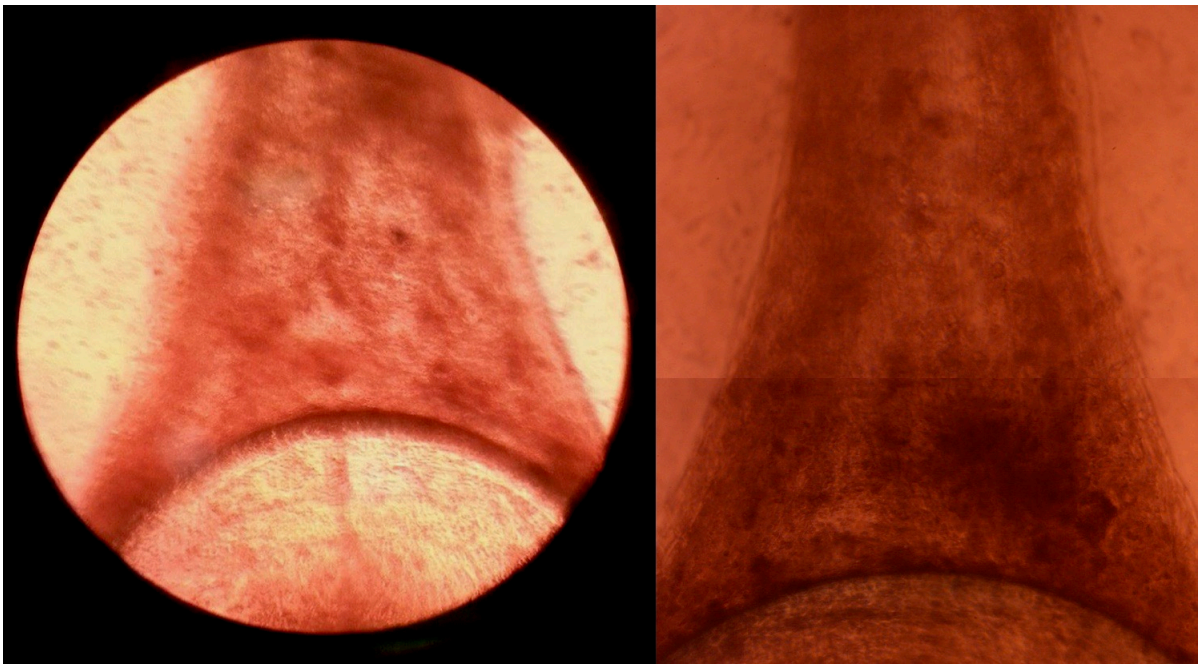

Figure 5.9: A) Image of a beating EHT attached to a silicone post on the south end (40x). B) Two images stacked to give a longer view of the bridge component of an EHT attached to a silicone post.

was attempted, but failed due to unoptimised dissociation procedures.

Multiple lactate treated flasks were collected and re-plated into a single flask to gain an enriched purity of CM population. However, due to the small yield it would take around 18-20 flasks to reach our initial 10 million cells. This made the method impractical and too costly to continue.

5.3.3 Transient Glucose-Depleted Treatments to Purify CM Population.

A second less harsh method was applied to try and enrich our iPSC-CMs population by incorporating a transient treatment of glucose-depleted media for two days intermixed with 2 days of the normal RPMI + B27 media. An AlamarBlue assay was performed on DD9, DD13, and DD22. There was no significant difference in ABA reduction between the control iPSC-CMs and the treated glucose-depleted group (Fig. 5.11A) which suggested that there was no difference in cell number or metabolic activity after the glucose-depletion treatment and making this a viable option with respect to cell viability. Flow cytometry was attempted to investigate cardiac troponin T expression, but again failed due to unoptimised dissociation procedures. It was later successfully accomplished by Ujang Purnama using a sarcomeric actinin antibody and showed that the glucose-depleted media treatment improved iPS-CM purity to 89% (Fig. 5.11B).

5.3.4 Gene Expression of EHTs Generated From iPSC-CMs Compared to Monolayer and Scaffolds

Gene expression of selected cardiac and metabolism genes were investigated to compare EHTs (both non-beating and beating) to iPSC-CMs on collagen-derived scaffolds and in RF-Matrigel-coated monolayers. iPSC-CMs were differentiated and re-plated on DD15 into one of the listed conditions. They were cultured for an additional two weeks until the EHTs were visually beating and harvested for RNA extraction on DD31. Retrieving RNA from both scaffolds and EHT was not an easy task and yielded very low levels of RNA.

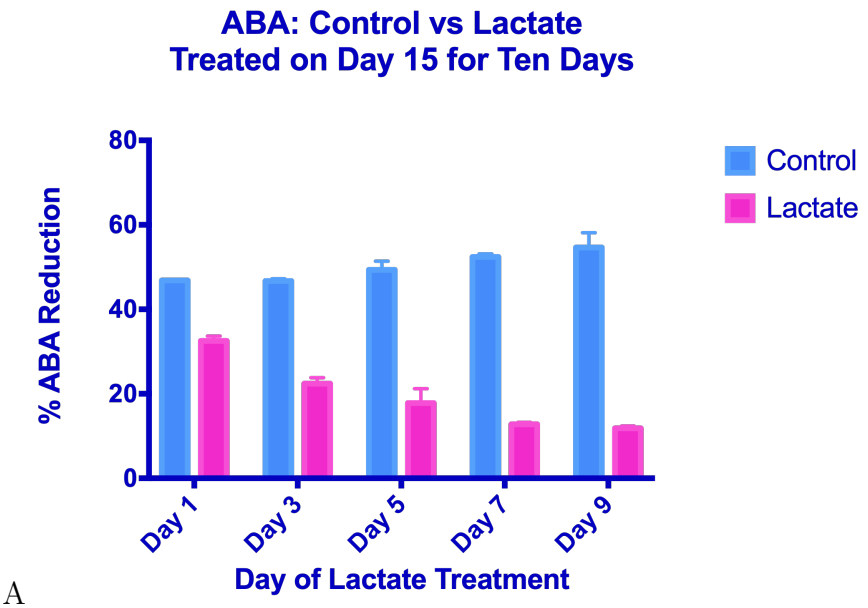

A

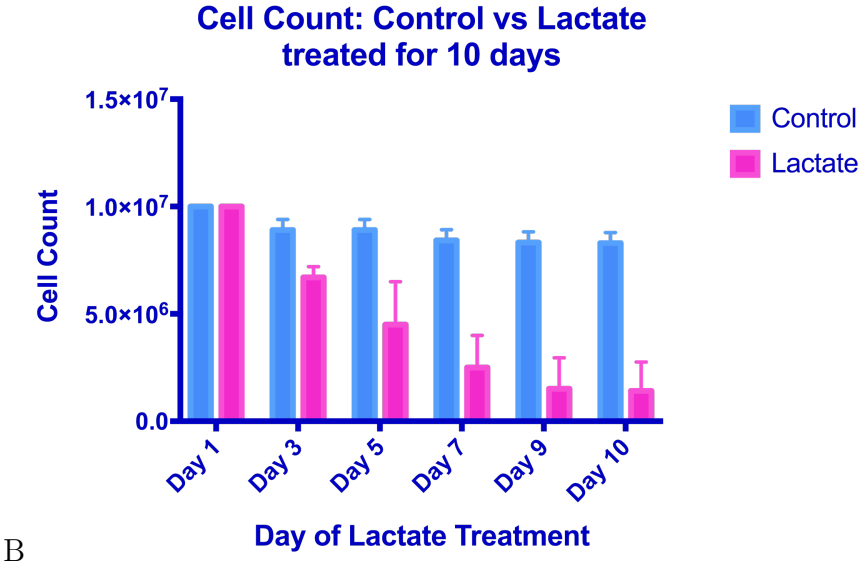

B

Figure 5.10: Glucose-depleted and lactate-enriched treated iPSC-CMs. A) AlamarBlue assay was performed every other day for the 10 days treatment period. Each ABA had a 4 hour incubation. B) Cell count of the total number of detached iPSC-CMs each day, counted using an automatic cell counter collected each media change. The experiment was run in 2 biological repeats in triplicates. The bar represents mean + SEM.

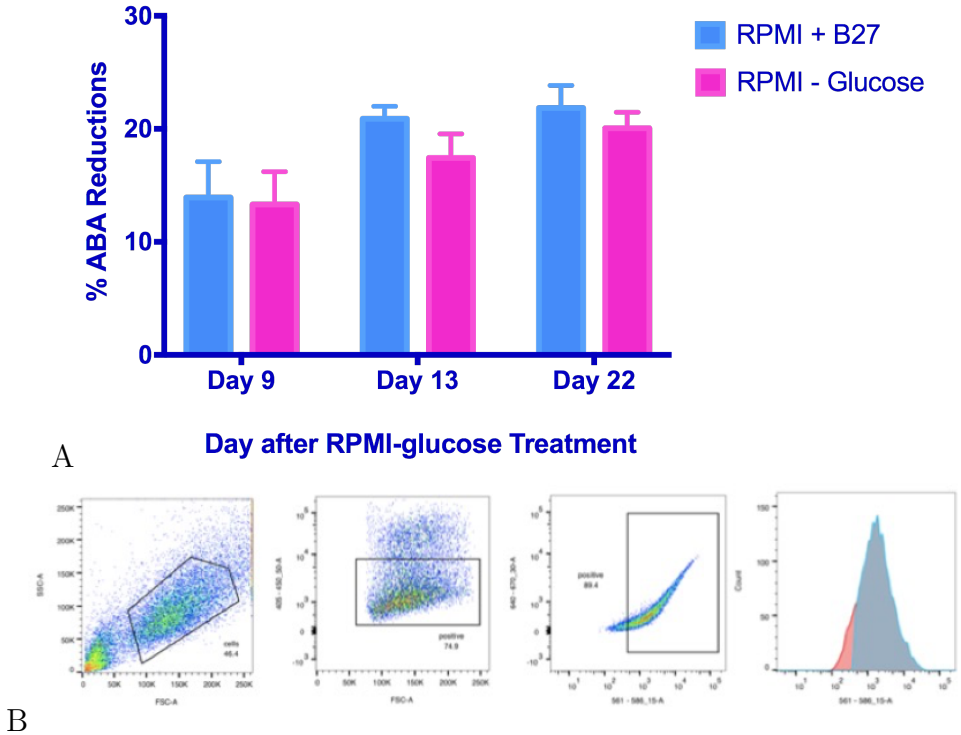

Figure 5.11: A) AlamarBlue assay performed after every glucose-depleted media treatment on iPSC-CMs during DD9 and DD22. Each ABA had a 4 hour incubation and the bar represents mean + SEM. The experiment was run in 3 biological repeats in triplicates. B) Flow cytometry performed by Ujang Purnama using a sarcomeric actinin antibody showed that the glucose-depleted media treatment yielded around 89% actinin + iPS-CM (n=2).

As a result, each RNA sample was a combination of at least 3 separate scaffolds or EHTs. Unfortunately, due to time constraints of this thesis and unsuccessful RNA extractions on some of the samples leaving only a sample size of 1, statistics were not performed. The apparent increases will be discussed but are not claimed to be significant. The number of biological repeats are shown in the key to the right of each graph.

After the successful generation of EHTs, qPCR analysis were performed for expression of contractile and metabolic associated genes (Fig. 5.12). *TNNT2* and *MYH6* were upregulated in the non-beating and beating EHTs when compared to the RF-Matrigel monolayer and C4S/Coll scaffolds. *GLUT1* expression decreased in all conditions compared to the untreated monolayer while, *GLUT4* expression increased in the non-beating EHTs and was highest in the beating EHTs. There was a large visible increase in *IRS1* and *PGC1A* in beating EHTs compared to the other culture conditions. Based off the limited biological repeats there appeared to be no difference in *PDK4*, *CS*, or *PPARα* expression amongst the different conditions.

5.3.5 Deciding Optimal Time Point in iPSC-CM's Differentiation Protocol to Generate EHTs.

Both palmitate and oleic acid oxidation rates were determined to compare iPSC-CMs encapsulated into EHTs on two different time points (DD7 and DD15) to gauge the optimal seeding frame. EHTs were cultured for a week post casting and then incubated for 8 hours in EHT media containing 2% BSA and either 0.3 mM palmitate doped with palmitic acid [9,10-^{3}H(N)] or 400 μL OA doped with oleic acid [9,10-^{3}H(N)]. Both palmitate and oleic acid oxidation were higher in the DD15 seeded EHTs than in those seeded on DD7 (Fig. 5.13). Moving forward EHTs were generated at day 15 of the iPSC-CMs differentiation protocol.

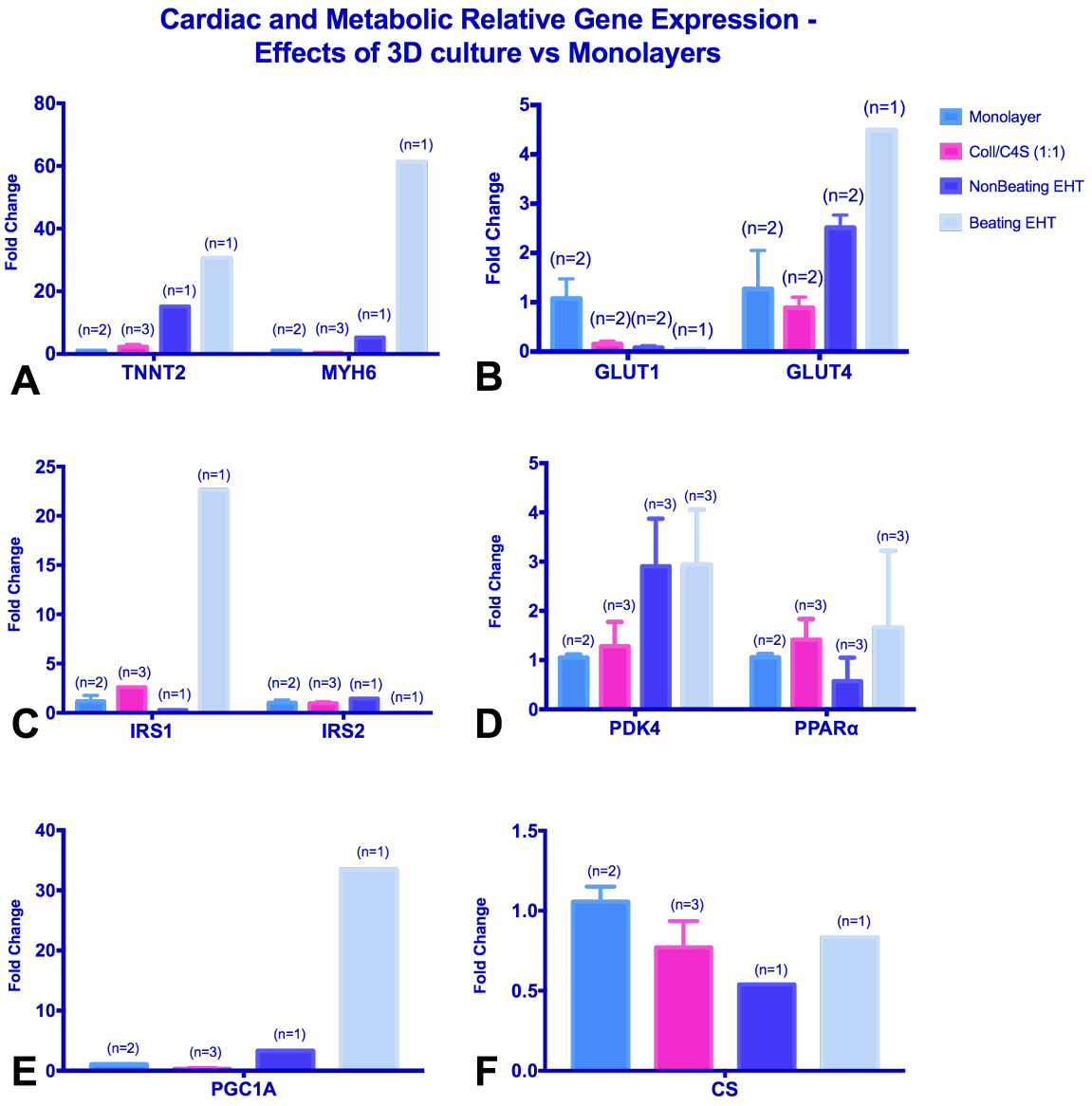

Figure 5.12: Relative gene expression of A) *TNNT2* and *MYH6* B) *GLUT1* and *GLUT4* C) *IRS1* and *IRS2* D) *PDK4* and *PPARα* E) *PGC1A* F) *CS* in 3D culture vs 2D monolayer. iPSC-CMs were differentiated and re-plated on DD15 onto either a 2D RF-Matrigel monolayer, 3D collagen-derived scaffolds or encapsulated into an EHT. The iPSC-CMs were then cultured for an additional 2 weeks before being harvested for RNA extraction. The bar represents the mean + SEM. The blue represents the monolayer, pink represents the C4S/Coll 1:1 scaffold, indigo represents the non-beating EHTs, and the light blue represents the beating EHTs. There were no stats performed in non-beating and beating EHTs as a single sample size.

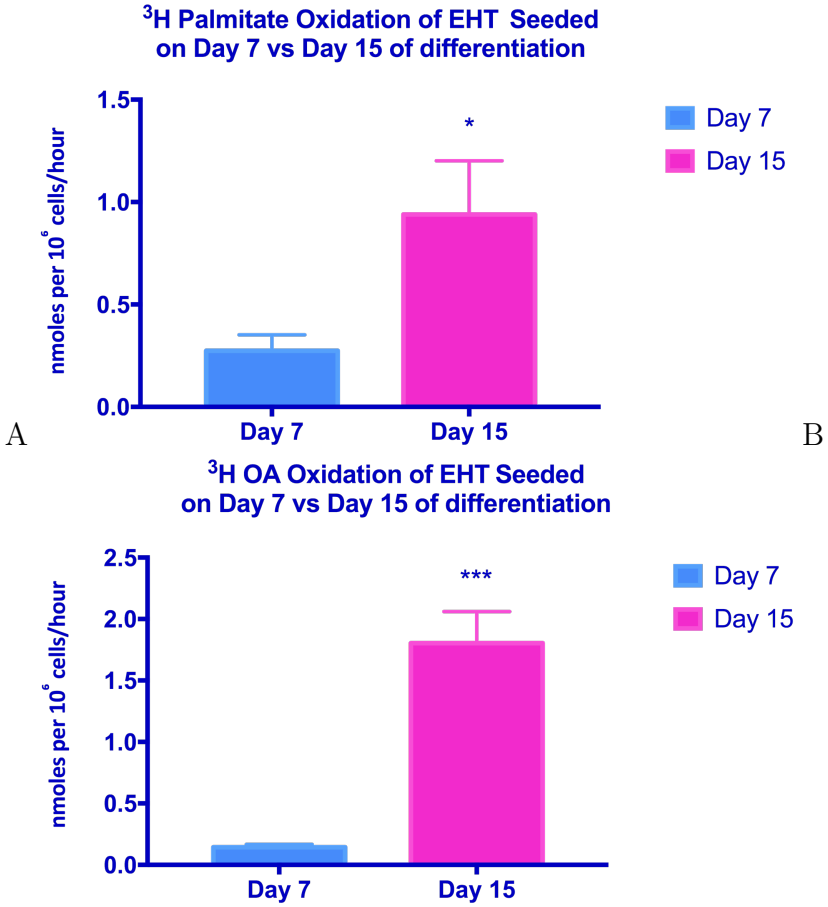

Figure 5.13: A) ^{3}H palmitate oxidation B) ^{3}H oleic acid oxidation of EHTs generated on DD7 vs DD15. The experiment was run in 3 biological repeats in triplicates. The bar represents the mean + SEM. The pink bar represents the EHTs made on DD15 of differentiation protocol which is normalised to the blue bar represents EHTs made on DD7. * = $p<0.05$, ** = $p<0.01$, and *** = $p<0.001$.

5.3.6 FAO of EHTs Generated From iPSC-CMs Treated with Oleic Acid ± WY-14643 for 1 Week.

Both palmitate and oleic acid oxidation rates were determined to compare iPSC-CMs treated with 400 μM ± 120 μM WY-14643 cultured either as a monolayer or on a 3D scaffold. iPSC-CMs were differentiated and re-plated on DD15 (10^6 cells) to either a 24-well plate coated with RF-Matrigel (control), onto 100% collagen scaffold, or encapsulated into an EHT. Each condition was cultured for 1 week with the assigned OA/WY treatment. On the day of the experiment, the iPSC-CMs were incubated for 8 hours in RPMI+B27 media containing 2% BSA and either 0.3 mM palmitate doped with palmitic acid [9,10-^{3}H(N)] + the assigned OA/WY treatment or 400 μL OA doped with oleic acid [9,10-^{3}H(N)] + the assigned OA/WY treatment.

Overall, both palmitate (Fig. 5.14) and oleic acid oxidation (Fig. 5.15) increased in the EHTs when compared to the untreated monolayer and scaffolds. Moreover, when treating the EHTs with OA alone there was an additional increase in palmitate oxidation and when treated in combination with WY-14643 there was an even further increase. Treatment did not have an effect on oleic acid oxidation.

5.3.7 Glycolytic Flux of EHTs Generated From iPSC-CMs Treated with Oleic Acid ± WY-14643 for 1 Week.

Glycolytic flux was determined to compare iPSC-CMs treated with 400 μM OA alone or with the addition of 120 μM WY-14643. iPSC-CMs were differentiated and seeded on DD15 (10^6 cells) per scaffold and EHT. They were then cultured for 1 week with either treatment. Untreated iPSC-CMs were used as controls. The day of the experiment, the iPSC-CMs were incubated for 8 hours in low-glucose RPMI media containing 2% BSA, 0.3 mM palmitate and 0.00148 MBq of D-[5-^{3}H(N)]-glucose + the assigned OA/WY treatments.

When comparing the glycolytic rates with the RF-Matrigel-coated monolayers from Chapter 4, there was a substantial decrease in the rate of glycolysis for all the iPSC-CMs cultured in a 3D construct over the 2D monolayers (Fig. 5.16). There was also an additional

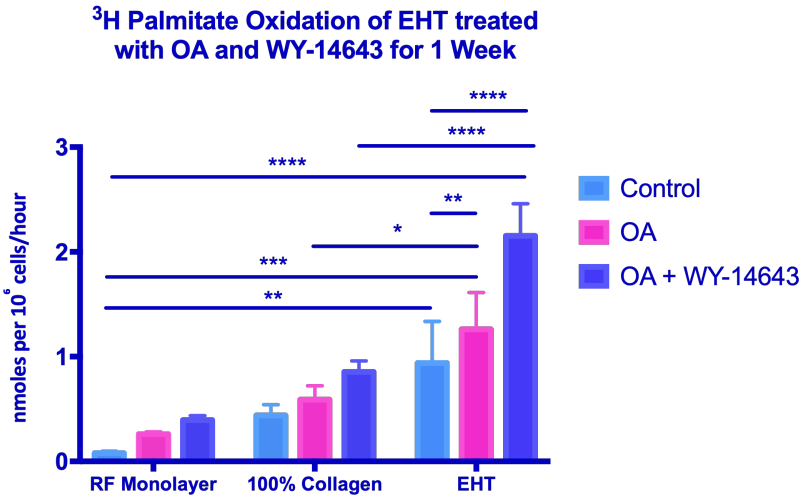

Figure 5.14: ^{3}H palmitate oxidation of RF-Matrigel monolayer, 100% collagen scaffold and EHTs treated with OA ± WY-14643. The experiment was run in 3 biological repeats in triplicates with 3 technical repeat. The bar represents the mean + SEM. The data is normalised to the untreated RF-Matrigel monolayer (control). * = $p<0.05$, ** = $p<0.01$, and *** = $p<0.001$, or their equivalent; analyzed using a two-way ANOVA and a Tukey's multiple comparison test.

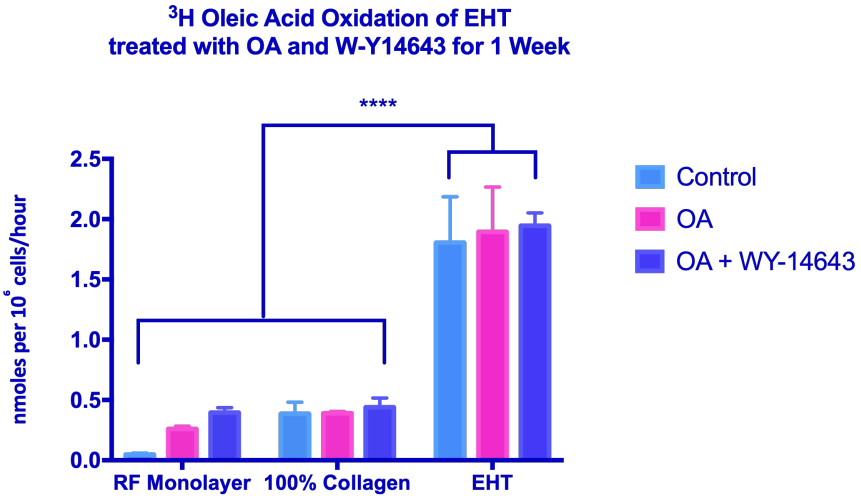

Figure 5.15: ^{3}H oleic acid of RF-Matrigel monolayer, 100% collagen scaffold and EHTs treated with OA ± WY-14643. The experiment was run in 3 biological repeats in triplicates with 3 technical repeat. The bar represents the mean + SEM. The data is normalised to the untreated RF-Matrigel monolayer (control). * = $p<0.05$, ** = $p<0.01$, and *** = $p<0.001$, or their equivalent; analyzed using a two-way ANOVA and a Tukey's multiple comparison test.

reduction of the EHTs compared to the 100% coll and Ela/Coll scaffold. There was no additional difference in treated vs untreated cells amongst the different 3D constructs.

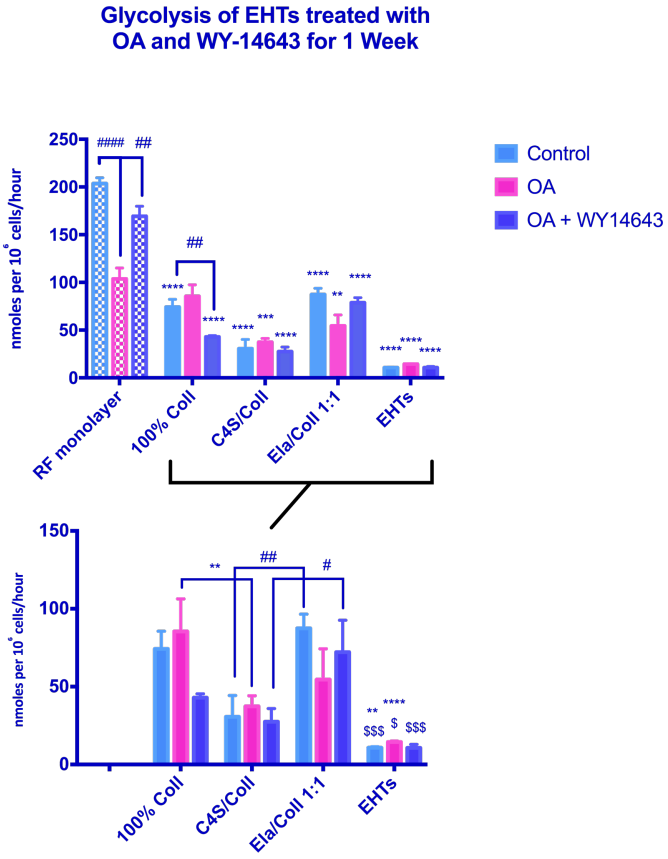

Figure 5.16: Glycolytic flux of RF-Matrigel monolayer, 3D collagen derived scaffolds, and EHTs treated with OA ± WY-14643. A) The "*" represents the comparison against the untreated RF-Matrigel monolayer in each condition. The "#" represents the comparison of the treated groups within each culture category. B) Zoomed in on just the scaffolds and EHTs. "*" represents the comparison against the 100% collagen scaffolds, "#" - C4S/Coll and "$" - Ela/Coll 1:1. The experiment was run in 3 biological repeats in triplicates with 3 technical repeat. The bars represent the mean + SEM. The data is normalised to the untreated RF-Matrigel monolayer (control). * = $p<0.05$, ** = $p<0.01$, and *** = $p<0.001$, or their equivalent; analyzed using a two-way ANOVA and a Tukey's multiple comparison test.

5.3.8 Gene Expression of EHTs Generated From iPSC-CMs Treated with Oleic Acid ± WY-14643 for 1 Week.

To complement the metabolic assay, preliminary relative gene expression was performed on a handful of metabolic genes. As mentioned before, retrieving RNA was difficult for scaffolds and EHTs, so they were collected in batches of three. Even with combining the EHTs and scaffolds the yield of RNA values were still low (Table 5.1). Due to time constraints of this thesis and limited RNA levels there was only a n=1 for each graph and no statistics were performed.

Table 5.1: RNA Values for 3D Constructs Treated with OA ± WY-14643

Sample	ng/uL
EHT Control	9.7
EHT OA	49.7
EHT OA+WY	36.5
100% Coll Control	9.4
100% Coll OA	14.8
100% Coll OA+WY	5.1
C4S/Coll Control	7.5
C4S/Coll OA	16.4
C4S/Coll OA+WY	10.6
Ela/Coll Control	6.7
Ela/Coll OA	4.6
Ela/Coll OA+WY	9.7

Relative Gene Expression

The relative gene expression of *GLUT1*, *GLUT4*, *PDK4*, *UCP3*, *CD36*, and *ASCL1* were measured (Fig. 5.17). Overall, relative mRNA expression of *GLUT1* decreased more in the EHTs then compared to the C4S/Coll scaffolds. There was potentially a further reduction with the treatment of OA ± WY-14643 in the scaffolds, but more repeats would be needed to confirm. *GLUT4* expression increased in the OA + WY-14643 treated EHT. There was higher expression in both *PPARα* and *PDK4* in the EHTs compared to the scaffolds. There did not seem to be any indication that the treatment had an effect, except potentially in the *PDK4* expression of EHT treated with both OA and WY-14643. Both *CD36* and *ASCL1*

expression seems to be higher in scaffolds but had no apparent difference between treatment groups and controls.

5.4 Discussion

5.4.1 Basic Characteristics of iPSC-CM-Derived EHTs

Generating EHTs involved mixing a mastermix containing 10^6 iPSC-CMs master mix with fibrinogen and combining this with thrombin. The addition of the thrombin enzyme causes the polymerisation of fibrinogen to fibrin. The mixture was then pipetted into a mould and left to set around two silicone posts. The critical aspect of the casting process was the concentration of thrombin and fibrinogen. Bovine fibrinogen was used in generating the EHTs because it was produced at a higher and more accurate concentration, which made it easier to handle and led to more standardised conditions.

Depending on the quality of the batch of cells, small individual clusters could be seen to beat as early as 5-6 days and progressed to spontaneous whole construct contractile activity 2-3 weeks post casting. Over time the EHTs thinned and reduced in size along the x-axis. As the length of EHTs reduced this caused a preload on the construct, bending the silicone post inward.

5.4.1.1 Gene Expression of 3D EHT vs 2D Format

Unfortunatly, we experienced 6 months of delay due to infection and incubator breakdown in the cell culture lab at a crucial time in the work for this EHT chapter. This involved repurchasing almost every media, reagent, and factor in the lab and repeated thorough cleaning of incubators and shared lab space. This limited the available time for trouble shooting and completing sucient number of biological repeats to gain statistical significance. As a result the qPCR sections contain only preliminary data and no real conclusion can be drawn. The apparent increases will be discussed but are not claimed to be significant.

The whole construct of the EHT was used for RNA extraction to maximize the amount

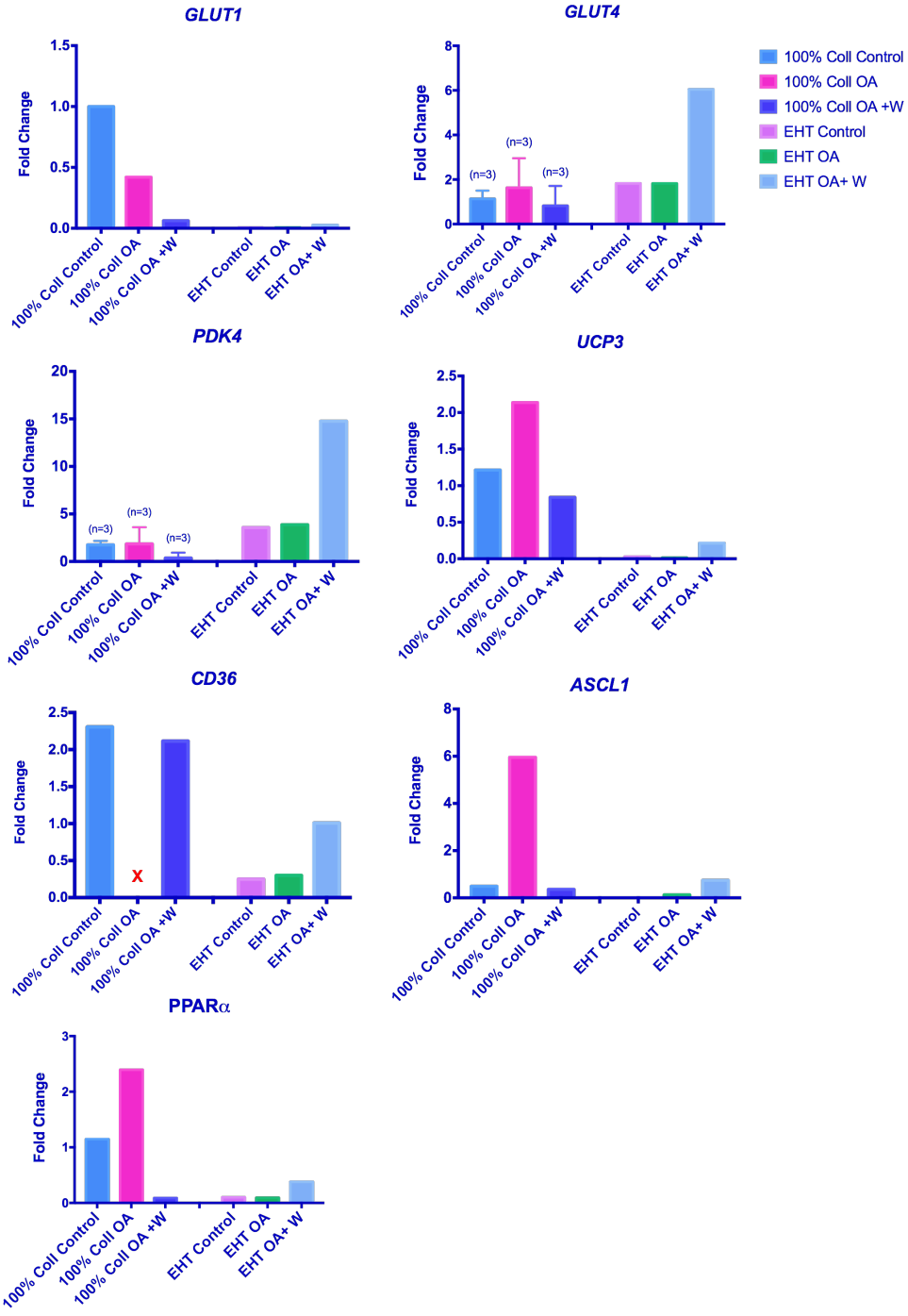

Figure 5.17: Preliminary relative gene expression of A) *GLUT1*, B) *GLUT4*, C) *PDK4*, D) *UCP3*, E) *CD36*, F) *ASCL1* and G) PPARα between 100% collagen scaffolds and EHTs. Bars represent means + SEM. The red X represents samples that were unsuccessful at retreiving RNA from. No stats were performed due to an n=1.

of RNA retrieval. It is important to note a limitation of using the whole EHT for the qPCR data, because the gene expression might vary slightly from the cells around the post to the ones in the center. Ideally, we would have liked just to take the center length of an EHT, but due to the complications of obtaining enough RNA we had to take everything.

Cardiac Gene Expression

The beating iPSC-CM derived EHTs showed an apparent increase in cardiac gene expression of *TNNT2* and *MYH6* when grown in 3D over 2D. Ulmer *et al.* [390] also looked at cardiac gene expression in EHTs compared to their 2D format and found no significant difference in the expression of cardiac (*MYL3*, *MYL4*, *cTNT1*), or fibroblast (Vimentin, Periostin), and endothelial (*CD31*) markers. However, Duan *et al.* [416] reported that in a different hybrid hydrogel construct (composed of ESCs/native heart matrix/collagen) they saw significant upregulation in cardiac troponin T expression within 8 days post casting. Similarly cardiosphere-derived cells in hydrogel had high expression of cardiac markers (*cTNT* and *MYH6*) a week after casting [622].

Metabolic Gene Expression

There was an apparent reduction in *GLUT1* and increase in *GLUT4* in our EHTs compared to the 2D format. Even though no other lab has investigated the glucose transporter genes in EHTs to date, Wittmann *et al.* [623] saw the same trend in human adipose-derived stem cells (ASCs) encapsulated in a stable fibrin hydrogel. They reported upregulation of adipogenic marker (*GLUT4*, *PPAR*γ, *C/EBP*α, and *aP2*). The upregulation and translocation of the Glut4 was also shown in skeletal muscle cells on a hydrogel sheet [624].

There was also an apparent increase in *PGC1A* in our 3D beating EHTs which is supported by others who also showed significant higher expression of *PGC1A* and estrogen-related receptor A in 3D EHTs over 2D iPSC-CMs counterparts [390]. To date, no other labs have looked at gene expression of *IRSs*, *CS*, *PDK4*, or *PPAR*α in EHTs or hydrogels.

5.4.2 Cell Population and Density Effects on EHT Culture

Rat EHTs composed of 0.8-3x10^6 cells, started coherently beating between days 2-5 [409]. ESC-CM derived EHTs, composed of 6x10^5 cells/EHT, beat between days 5-10 with a rate of 40-70 bpm, and 40% differentiated efficiency [447]. iPSC-CM derived EHTs composed of 10^6 cells/EHT started spontaneously beating 10-14 days after casting with a 61 bpm rate and 88% differentiation efficiency [617]. Sian Harding's lab at Imperial College, London uses a 90-99% pure CM populations and sees post deflecting beating within 3-5 days of casting. In comparison our iPSC-CM derived EHTs (10^6 cells/EHT) started contracting (but with minimal post deflection to the naked eye) between days 14-20 post casting at a rate of 80 bpm. One explanation for the difference could be due to the differentiation efficiency (70% CMs) and cell density. This concentation dierence could have affected both the beating rates and also on the gene expression data and metabolic measurements.

The ability to contract earlier is most likely due to the early establishment of cell to cell contact allowing for the proper coordination and communication to occur for synchronised beating. In addition, the higher contraction force is most likely correlated to increased cell survival in the hydrogel during EHT generation. By optimising our differentiation protocol to yield more CM cells, we could address both of these limitations and increase the force of our EHT contractions, thereby increasing maturation even further. As cells mature their beating slows, but gets stronger.

However, an adult human heart is a mixture of different types of cells consisting of CMs and non-myocytes, which make up 70% of total cell content [625,626]. Natio *et al.* [604] showed that generating EHTs from a mixture of native heart cell populations (63±2% CMs, 33±3% fibroblasts, 3-4% smooth muscle cells and 2-3% endothelial cells) improved contractile function (0.7±0.06mN vs 0.3±0.03mN) and formation of primitive capillaries compared to cardiac myocyte enriched EHTs. To complement this idea, Kensha *et al.* [605] reported that having around 10% fibroblasts in addition to CMs was essential for EHT performance and thinning. Others have suggested either a 1:1 composition of CMs: fibroblast [604] or a 70%/30% CMs: fibroblast ratio to achieve maximal peak contraction force [613]. In these cases, having a heterogenous population may be more ideal for EHT generation. Our

differentiation protocol should be further examined into what cell population exists and investigate different seeding ratios to optimize our EHT generation.

One overall limitation to keep in mind, is that an EHT's density made from 1 million cells is still far below the density of an adult myocardium. An average EHT made from 10^6 cells has a volume of 0.14 cm^3 while the cardiac tissue is estimated at a density of 0.5-1x10^8 cells/cm^3. This is 400-700 times larger than an EHT, which needs to be taken into consideration when using an EHT to mimic an adult myocardium [627].

5.4.3 Enhancing iPSC-CMs Differentiation Through the Use of Glucose-Depleted and Lactate-Enriched Treatments

Several labs have explored the use of transient glucose-depleted, lactate-enriched media to increase cardiac differentiation efficiency. In 2013, Tohyama *et al.* [628], cultured both ESCs and iPSCs derivative with glucose-depleted culture media containing 4 mM lactate on DD20-30, reporting that only CMs survived. Using this approach, the percentage of positive α-actinin-positive cells went from 8.1% to 98.3%. As with our attempt utilizing the lactate method, they also found that using this approach killed every other type of cell (88-92% of total cell number) within 96 hours in the glucose-depleted conditions. Only the CMs were able to survive (8-12% of cell population). Overall, the lactate method increased cardiac gene expression of *MYH6*, *ACTC1* and *NKX2.5* and eliminated noncardiac genes expression of *NANOG*, *MYOD*, *AFP*, *MAP2*, and *POU5F1*. In 2014, Burridge *et al.* [361], also enriched their cardiac differentiation protocol by replacing their RPMI+B27 media with a RPMI minus glucose supplemented with 5 mM sodium D L-lactate on DD10-20. They found that 6-10 days of glucose deprivation enriched CMs from 85% TNNT2+ to >95% TNNT2+ cells. This approach could not be used in the media containing B27 because it contains a source of glucose (D(+)-galactose). More recently, Huebsch *et al.* [388] added a lactate purification step in the same Wnt based iPSC-CMs differentiation protocol that is used in this thesis. They re-plated cells on DD15 and exchanged out the RPMI+B27 with a glucose-depleted DMEM supplemented with 4 mM lactate on DD20-24. This purification

step increased TNNT2 + cells from 53.7% to 94.6%. Our results appear to fall into the same pattern as these previous publications and should continue to be investigated further. With the glucose-depleted purity step, our differentiation improved 13% and yielded around 89% iPS-CM. Achieving a high purity CM population could potentially add to the improvement and maturation of our generation of iPSC-CM derived EHTs.

5.4.4 Effects of OA ± WY-14643 Treatment on iPSC-CMs Cultured in 3D Scaffolds vs EHTs

Previous studies have shown that iPSC-CMs prefer to be cultured in 3D constructs rather than in a 2D environment, which was confirmed in Chapter 3 and 4, showing cultured iPSC-CMs on scaffolds had increased FAO and decreased glycolysis. In comparison to these previous conditions, after a week of treatment with OA, EHTs had a significant increase in FAO (both in palmitate and oleic acid oxidation) and a substantial decrease in glycolysis compared to the RF-Matrigel-coated monolayer and 100% collagen scaffold. With the additional treatment of WY-14643, there was a further increase in palmitate oxidation. The rate of glycolysis for the OA + WY-14643 treatment in 2D/100% collagen scaffold/EHTs were around 160/50/10 nmoles /10^6 cells/hour while that of palmitate was around 0.5/1/2.2 nmole/10^6 cells/hour, respectively. As glycolysis and β-oxidation of palmitate produces 2 and 120 moles ATP/mole of substrate, respectively, the rate of ATP production from glycolysis/palmitate oxidation was 320/60 nmoles ATP/10^6 cells/hour for the RF-monolayers, 100/120 nmoles ATP/10^6 cells/hour for the 100% collagen scaffolds, and 20/264 nmoles ATP/10^6 cells/hour for the EHTs, respectively. EHTs were generating 4 times the amount of ATP by oxidation than the 2D RF-Matrigel-coated iPSC-CMs and twice as much as the scaffolds.

As to date, there is only one other group looking at the energetics and substrate metabolism of EHTs. Ulmer *et al.* [390], also showed that culture of iPSC-CM derived EHTs perform more glucose, lactate, and FAO and less anaerobic glycolysis than cells in the 2D format. EHTs generated 2-3-fold more ATP by oxidation than the 2D iPSC-CMs and had

increased mitochondria, mass, DNA (Mt-ND1, Mt-ND2), and protein abundance [390]. This thesis observed similar results, but also expanded on this work with the pre-treatment of FAs, such as OA, and activating PPARα target genes through WY-14643 to try and further increase maturation in EHTs.

5.4.4.1 Effects of OA ± WY-14643 Treatment on Gene Expression of iPSC-CMs Cultured in 3D Scaffolds vs EHTs

Glycolytic Gene Expression

Our preliminary gene expression partly supports the switch in energetics from anaerobic glycolysis to FAO. We saw a switch from *GLUT1* to *GLUT4* expression in EHTs over scaffolds. As mentioned before, there is no current lab that investigated the GLUT genes in hydrogels or EHTs to reference, but this switch reflects the in vivo state, when *GLUT1*, the predominant isoform in the foetal heart becomes downregulated, and *GLUT4* becomes upregulated to the dominant isoform in adulthood [493–496]. We also saw an increase in the expression of *PDK4* in EHTs when treated for a week with OA and WY-14643.

Fatty Acid Oxidation

The rest of the genes investigated showed opposite trends to those expected. There was decreased gene expression of *PPARα*, *CD36*, and *ASCL1* in EHTs compared to scaffolds. Others have shown in different cell types that culturing in a hydrogel has previously increased gene expression of *CD36* and *ASCL1* [629–631]. Kim *et al*, showed that genes associated with adipogenic differentiation (including but not limited to (*CD36*, *ACSL1*, and *PPARG*) were consistently increased in bone-marrow-derived porcine stem cells cultured in alginate hydrogels [630]. The expression of *PPARα* has not been thoroughly investigated in hydrogels. Although, other labs have shown increased gene expression of its other isoform, *PPARγ*, when MSCs/ASCs/HSCs were cultured in different hydrogels [632–634].

5.5 Conclusion

In conclusion, we were able to establish an iPSC-CM derived EHTs protocol in our lab that generated spontaneous beating EHTs 2 weeks after casting. However, due to technical difficulties and problems of cell culture infection, we were only able to obtain preliminary data which suggested that the rate of FAO was significantly greater in EHTs than in collagen scaffolds. In addition, treatment with OA ± WY-14643 for 1 week enhanced palmitate oxidation even further. EHTs were generating 4 times the amount of ATP by oxidation than the 2D RF-Matrigel-coated iPSC-CMs and twice as much as the 100% collagen scaffold. This confirms that 3D culture in EHTs and enhancing the culture media with additional FAs and PPARα agonists does induce a degree of maturation in iPSC-CMs.

The more that you read, the more things you will know. The more that you learn, the more places you'll go.
— Dr. Seuss, I Can Read With My Eyes Shut!

6 General Discussion

6.1 The Quest to Mature iPSC-CMs

Human induced pluripotent stem cells can be an appealing tool for biomedical research because they are patient-specific and have endless applications from cell therapy, disease modelling and personalized medicine, to drug discovery and development and toxicity analysis [155–164]. Furthermore, recent advances in gene editing technology (particularly CRISPR-Cas9 technology) have enabled the capability to genetically define iPSCs-based disease model [157]. However, if iPSC-CMs are going to be used for disease modelling or drug testing, it is essential that they mimic an adult CM expressing the same range of proteins, receptors, enzymes and ion channels.

As already discussed, iPSC-CM are immature in almost every way and reflect more of a foetal phenotype than an adult CM [1, 158, 231, 232, 234–236] despite a range of different strategies for maturation. The most consistent method remains maturation through long-term culture, but this is both time and money consuming [22, 328, 378, 379, 635]. Maturation through changing metabolism has only rarely been investigated.

Drawnell *et al.* [395] showed that you can modify the medium to induce a diabetic model, by treating differentiated iPSC-CMs with a maturation medium containing insulin and FAs,

with no glucose for three days, followed by treatment with a diabetic milieu of glucose (10 mM), endothelin-1 (10 nM), and cortisol (1 μM) they induced an increase in sarcomere length, velocity, and duration of an action potential. In addition there were increases in gene expression associated with myosin light chain (*MYL2*, *MYL3* and *MYL4*), regulation of sarcoplasmic reticulum calcium content, and the repression of foetal enriched genes. Although, this was an extensive study the group did not investigate the bioenergetics of the cells. Rana *et al.* [398] undertook perhaps the most comprehensive investigation into the effects of changing media, by modifying a basal medium with a combination of high or low glucose with galactose or FAs. They found that they could eliminate a cell's choice in substrate metabolism by excluding glucose from the medium forcing the iPSC-CMs to utilise the galactose and switch from glycolysis to OXPHOS for their ATP production. Both of these groups laid the foundation showing that you could modify medium to direct a specific phenotype and drive iPSC-CMs into using a particular metabolic pathway.

Tissue engineering has also become an attractive avenue used to induce a more mature phenotype in iPSC-CMs by creating a more physiological relevant culture condition that better mimics the environment of the cell in vivo. However, the metabolic changes in the cells are rarely considered, possibly because metabolism in 3D constructs cannot be quantified using the Seahorse, which is the strategy used most frequently to give an indication of metabolic changes. Recent work by Ulmer *et al.* [390] showed, using radiolabeled substrate measurements, that culture of iPSC-CM in EHTs led to maturation of energy metabolism when compared to 2D culture. They showed the EHTs had an increase in mitochondrial mass, glucose, lactate, and FA oxidative metabolism while having a reduction in anaerobic glycolysis. These results strongly support the notion that contractile work contributed to the metabolic maturation of iPSC-CMs. However, this lab only looked into the use of 3D culture and mechanical load/stimulation to induce maturation and did not target any modification of the medium.

It has been previously shown that PPARα is a critical component in driving metabolic maturation in the heart post-birth [585, 636]. The aims of this thesis were to investigate and address maturation of iPSC-CMs through stimulating FA oxidation using physiologically

relevant methods of 3D culture in combination with PPARα activation via the PPARα agonist, WY-14643, and/or the addition of the fatty acid, oleic acid, into the culture media. Unlike others, simultaneously targeting two maturation methods we have shown a degree of maturation through an increased movement towards reduced glycolysis and increased FA oxidation in our iPSC-CMs.

6.2 Thesis Findings

This work aimed to increase metabolic flexibility in iPSC-CMs. Human iPSCs were successfully differentiated into beating CMs by a differentiation protocol adapted from Liam *et al.* [355] that exploits the Wnt signalling pathway. As has been shown by others [512], we found that the cells matured slowly over time with changes in structural genes occurring during the first month of differentiation and continuing to increase up to 3 months while metabolic changes took longer to develop. This was not accelerated when iPSC-CMs were cultured on different ECM substrates. The cardiac genes *MYL7*, *MYH6*, and *MYH7*, were upregulated during the first weeks of differentiation and expression of *MYH7* continued to increase up to 3 months of culture. In the adult human heart *MYH6* is primarily expressed in the atria with very low levels found in the ventricles while *MYH7* is expressed mainly in the ventricle [637]. Expression of SERCA2α increased in the first weeks of differentiation but did not change significantly after DD31. When cells were re-plated at DD12-15 and cultured for one week, a clear switch in expression from *GLUT1* to *GLUT4* was evident, indicative of an increase in more mature, insulin-responsive metabolism. Interestingly, this was associated with an increase in the ability of the cells to oxidise OA, but there was no change to glucose metabolism. This may be because the more mature cells retained a glycolytic phenotype, but were able to oxidise the fatty acid when supplied.

We hypothesized that the iPSC-CMs are unlikely to upregulate FA oxidation associated pathways while being cultured in high glucose media containing little to no FAs. Therefore we aimed to stimulate FA metabolism in DD15 iPSC-CMs by adding OA to the medium alongside the addition of a PPARα agonist which regulates the expression of genes involved

in β-oxidation [588]. Addition of OA to the culture medium for 1 week increased *PDK4* expression, which controls the flux of pyruvate into the TCA cycle, but did not change any of the other metabolic genes that were assessed. Further addition of the PPARα agonist had minimal effect on mRNA expression, with a small increase in the FA transporter *CPT1* and a decrease in expression of *GLUT4*. Expression of the pyruvate dehydrogenase gene *PDHA1* decreased after 1 week of treatment with OA whereas that of the long chain fatty acyl-CoA ligase, *ACSL1*, increased. Addition of OA decreased the rate of glycolysis and increased that of FA oxidation. There was an additional increase in palmitate oxidation between cells treated with OA and those treated with OA + WY-14643. The addition of this agonist also induced a greater difference from untreated cells. It should be noted, however, that glucose metabolism remained the predominant pathway, although to a much lower extent than in untreated cells. After a week of treatment with OA + WY-14643, the rate of glycolysis was around 160 nmoles/10^6 cells/hour, that of glucose oxidation was around 1.6 nmoles/10^6 cells/hour while that of OA was around 1 nmole/10^6 cells/hour. As glycolysis, glucose oxidation and β-oxidation of OA produces 2, 32 and 120 moles ATP/mole of substrate, respectively, the rate of ATP production was 320/51/120 nmoles ATP/10^6 cells/hour, respectively. Interestingly, from Dr. Al-Siddiqi's thesis we learned that treatment for 24 hours with OA + WY-14643 induced an increased oxygen consumption rate in cells respiring on OA whereas cells treated with OA alone had increased oxygen consumption on pyruvate and malate, suggesting that the PPARα agonist was having some effect, even if small. After longer treatment with OA + WY-14643, shown in this thesis, iPSC-CM had increased baseline respiration (although this was not significant in cells respiring on OA) and a reduced response to the uncoupler FCCP. This may indicate that the treatment increased oxidative metabolism in the mitochondria or that the cells had increased proton leak at baseline caused, perhaps, by an increase in damage from reactive oxygen species. Overall, this first part of the project suggests that iPSC-CM are responsive to the addition of FAs into the culture medium and that the additional stimulation of the PPARα pathway, beyond that from OA itself, has only a small effect.

Prof Jan Czernuszka in the Department of Materials generates porous collagen scaffolds

comprising a mixture of collagen with elastin or C4S for the manufacture of heart valves [429]. We questioned whether culturing iPSC-CMs in 3D within these scaffolds would increase cell maturation. iPSC-CM cultured on porous collagen scaffolds induced a 2-fold increase in mRNA from *MYH6* and *MYH7* and a 5-fold increase in mRNA from *PDK4*, indicating both structural and metabolic maturation over 1 week of culture. This was associated with a decreased rate of glycolysis and a moderate increase in FA oxidation. Addition of OA ± WY-14643 did not induce any further changes except where cells were cultured on scaffolds comprised of 1:1 collagen/elastin where increased glucose and palmitate oxidation were observed. It may be that the increased elasticity of the collagen/elastin scaffold permitted greater contraction of the cells, thereby increasing the energy demand which required the benefit provided by upregulating FA oxidation. One explanation that could explain why the combined treatment did not further upregulate FA oxidation in the other scaffolds could be that the medium still contains large amounts of glucose.

The final aspect of this project was to explore these effects further in engineered heart tissue (EHT), a three-dimensional, hydrogel fibrin-based muscle construct that is restrained between two flexible posts, thereby allowing the cells to perform increased contractile work [409, 410, 447, 448]. Ulmer *et al.* [390] have shown that iPSC-CM grown in EHTs have increased ability for glucose and FA oxidation even though the EHTs were cultured in FA-free media. However, due to technical difficulties and problems of cell culture infection, we were only able to obtain preliminary data which agreed with the findings from Ulmer *et al.* [390] that the rate of FA oxidation was significantly greater in EHTs than in collagen scaffolds. Building on this, treatment with OA ± WY-14643 for 1 week enhanced palmitate oxidation even further. Using the prior calculation of rate of ATP production, after a week of treatment with OA+ WY-14643, the rate of glycolysis/palmitate oxidation was 320/60 nmoles ATP/10^6 cells/hour for the RF-monolayers, 100/120 nmoles ATP/10^6 cells/hour for the the 100% collagen scaffolds, and 20/264 nmoles ATP/10^6 cells/hour for the EHTs, respectively. EHTs were generating 4 times the amount of ATP by oxdiation than the 2D RF-coated iPSC-CMs and twice as much as the scaffolds. This confirms that 3D culture in EHTs and enhancing the culture media with additional FAs and PPARα agonists does induce a degree of maturation

in iPSC-CMs. Further work is required to optimise culture conditions by reducing glucose levels in the media and investigating the effect of insulin stimulation.

6.2.1 Thesis Obstacles

6.2.1.1 Purity Issues / Batch to Batch Variability

There are various cardiac differentiation protocols [80, 142, 351–357, 363, 365] that have been extensively studied by numerous groups. The efficiency of the different protocols seems to vary between cell lines, and in a single protocol there may be large batch to batch variability in the yield, purity and reproducibility of the iPSC-CMs [234, 638–640]. This is a big problem that we also faced in the work presented here. We used the Wnt-modulation protocol with a few modifications that improved efficiency of cardiac differentiation, as assessed by upregulation of cardiac genes like *MYH6* and *TNNT2*. However, throughout this thesis, even though we used the same conditions and cell lines, we had a wide range in the success of our differentiation and yield of CMs. We achieved successful batches that were fully beating as one synchronised sheet, others that were partially successful with unsynchronised scattered beating areas and some with non-beating iPSC-CMs. One explanation for this inconsistency could be due to using different batches of Matrigel and growth factors as there may be batch dependent variation in bioactivity and protein concentration. These discrepancies may also have occurred during the enzymatic dissociation of iPSCs for cardiac differentiation. Although the same reagent is used each time, detachment time of the cells varies from flask to flask. Some would have to be manually disassociated using a cell scraper which would add extra stress to the cells. Also, despite efforts to maintain consistent technique, there will always be some variability in differentiation efficiency due to human technical variation that naturally occurs when working (i.e. treating cells at different times of the day, mixing too vigorously, etc.). Most likely, these small variations can lead to a range in concentration of CMs versus fibroblast-like population of non-cardiomyocytes. The presence of this non-CM population, in varying amounts, is likely to be a contributing factor to problems such as the non-beating flasks. All of these factors can contribute to

variation between experiments, impacting the assessment of our iPS-CMs.

6.2.1.2 Bulk Analysis Methods vs Single Cell

The issue of the methods used for assessing differentiation and purity of the iPSC-CM population is relevant throughout this thesis and needs to be taken into consideration. Our initial differentiation protocol yielded around 70% CMs but also contained other mixed populations. We have made assumptions in all our experiments that it is the CMs driving the metabolic changes, but we cannot be 100% sure that the results are not also due to the presence of subpopulations. The majority of the experiments in this thesis were run as bulk analysis (e.g. qPCR, metabolic assays, ABA, westerns, etc) with limited single cell analysis (e.g. flow, histology, patch clamp, etc) to compliment them. As a result, when taking an average of change from an entire population we cannot be sure if the whole group equally shares the same metabolic activity or if small populations within the group are more metabolically active while other groups lie dormant. Both situations could generate the same results. In order to strengthen the conclusions in this thesis, more single cell analysis should be made to get a better understand of the average population and to validate the bulk measurements of maturation.

6.2.1.3 Contamination

As faced by any tissue culture lab, we suffered from problems of infections in the cell culture lab which came at a crucial time during our EHT project. There were a few potential causes to these two separate back to back contaminations. We had recently taken on two FHS students in the lab that were believed to be the source of the cause. The incubators are shared amongst different projects and without knowing right away their flasks were contaminated, the infection spread to the different subgroups. As one group would be clearing it they would be getting reinfected by the other in the shared space. It took a complete spring cleaning and many thorough washes of the lab before we were able to clear it. This was further complicated by one incubator failing to maintain the level of CO_2 at 5%. This was not detected immediately as the resulting cell death was

attributed to the infection rather than the mechanical fault. We went through a measure of precautions, including adding antibiotics to our media, using sterilized filters, ordering new stocks of every reagent, and conducting weekly incubator cleans. These contaminations were extremely costly and timely. This delayed several experiments and created time constraints for troubleshooting others so that we had to decide which experiments to prioritise. As a result, in certain sections of this thesis, we were only able to obtain preliminary data.

6.2.1.4 Standard Operating Procedures

As any new scientist in a tissue culture lab, I became aware of the importance of accuracy of standard operating procedures to overcome issues caused by human error. There is always a learning curve when starting any new technique and as a result the first couple of runs of each experiment were not necessarily used in statistical significance calculations but more as practice. After a practice round or two, experiments were then collected for data. Each experiment was run in a minimum of three biological repeats with three technical repeats. If there was a data point that was an extreme outlier, the experiment would have to repeated a fourth time or even more.

Working with stem cells can be very tedious and requires a large amount of consistency and precision. When experiencing a lot of batch to batch variability in our beating flasks we were able to troubleshoot problems down to something as small as not feeding the cells at the same time of day. If that window stretched more than a couple hours for the daily feed the cells were noticeable unhappy and this often would result in unbeating flasks. Sometimes over the three years, a single daily time point became difficult to maintain, particularly at the weekend or when there were several experiments going on simultaneously and all needed to be treated at once. Most of the differentiation protocols were also time sensitive and it was important that the factors were added at exact time points. This had to be planned a couple weeks in advance but could always be affected by unexpected delays and could have been one of the contributors to the batch to batch variation.

6.2.1.5 Challenges of Working with 3D Constructs

Working with the 3D constructs was a challenge. Throughout the thesis, we ran into several obstacles from determining optimal seeding techniques for our collagen-derived scaffolds, poor cell survival in the oxbox, to not being able to unload our EHTs for the more complicated metabolic assays. One of the most challenging components that affected the overall limitations of this thesis was dealing with cell count on our scaffolds. All the metabolic assays are driven by obtaining a reliable cell count, which proved difficult with some of our 3D constructs. A substantial part of Chapter 3 discussed all the potential methods used to determine cell count when seeding our collagen-derived scaffolds but overall we relied on our best reproducible estimation. Unfortunately, errors in this estimation could generate or remove a significant difference in data. We tried to take as many precautions as possible, by double and triple checking cell count along the way and ran several repeats in our radiation data (some as high of n=20). We consistently saw a difference in metabolic activity between our 2D and 3D cultures and can be confident with those findings, but when it came down to smaller differences, such as those between the different scaffold types, this concern should be mentioned. This thesis also has a limitation on how many of the metabolic assays were suited for 3D constructs. For example we don't have any oxygen consumption data or glucose oxidation measurements for our EHTs due to the nature of the assays. Removing the EHTs from their silicone post would be counterintuitive since the load is what makes this model so successful. We couldn't fit the EHTs loaded on their silicone posts into the OXBOX or a seal a container for the $^{14}CO_2$ release in the glucose oxidation measurements so, in order to get the full metabolic phenotype for these EHTs, workarounds would need to be developed.

6.3 The Future

6.3.1 Experiments to Complete This Story

If more time permitted, there are several experiments that I would have liked to have finished to close this story completely. We have laid a great foundation towards demonstrating that the combination of growing immature iPSC-CMs in 3D EHTs with a maturation media of OA plus the WY-14643 enhanced maturation towards a more oxidative metabolism. However, we need to repeat the EHT versus scaffold gene expression experiments to validate the results. In addition to this, I would have liked to have spent time optimising the flow protocol to obtain quantitative numbers of cTNT+ cells in each condition and treatment. It would also be interesting through FACS to see how many of our cells express atrial or ventricular markers.

To complement the work in this thesis, it would be nice to have corresponding protein levels alongside our gene expression data and to optimize the immunocytochemistry specifically to investigate the oil red O lipid staining for the different treatments. Although we spent a fair amount of time brainstorming, we were unable to design a device that would be suitable for sealing the EHTs into a closed environment to measure glucose oxidation. This box would have to be custom built, or 3D printed but is an interesting avenue to explore. Lastly, it would be interesting to have oxygen consumption data on the EHTs, but again we could not use the current system without having to remove the EHTs from their mechanical load silicone posts, which I believed would have confounded the data since the EHTs would no longer be contracting against a force.

6.3.2 Future Directions

The field of cardiac stem cell biology has come a long way over the last 20 years. Beating sheets of CMs can now be generated routinely from ESCs and iPSCs in large numbers. However, the maturity of the CMs remains a cause for concern if they are to be used to validate new drug compounds, detect cardiotoxicity or recapitulate the cardiac physiology of

patients with genetic disorders. We have shown that long-term culture, maturation media, and culture on 3D constructs can all aid towards a degree of maturation. However, further work is still required to determine appropriate cell culture conditions to enable pluripotent stem cell-derived CM to achieve the metabolic flexibility of the adult heart. EHTs look like a promising 3D model because they can recapitulate many of CM characteristics as well as having been shown to induce increased ability for glucose and FA oxidation [390]. However, we have just scratched the surface in maturating iPSC-CMs and even though we have induced a movement towards FA oxidation, anaerobic glycolysis is still the predominant source of energy in these cells, and there is still room for further optimization.

In this thesis, we focused solely on changing metabolism through the use of a maturation media and 3D culture but found that was not enough to fully mature these cells to an adult phenotype. Changing metabolism is only one aspect of cardiac maturation when in vivo this results from a combination of numerous factors. Future steps could involve combinations of other strategies such as 3D culture, electrical stimulation, force and metabolic maturation. Ulmer *et al.* [390], have started the groundwork for this topic, but our dual angle of both the addition of FA and PPARα activation is a novel approach and has shown to be beneficial to a degree in overall maturation. We have shown that changes can be induced in iPSC-CMs in 2D and translated across to 3D so it would be interesting to test out a range of different maturation media in multi-well plates in 2D and then take the most promising across to the EHTs. Maturation media have been building traction [329, 341, 386, 395–398] and may prove to be a solid cornerstone to enhancing maturation by better mimicking in vivo conditions. Exploring different media compositions such as alternative FAs, low glucose or the addition of ketones could be interesting to investigate. Further studies should include electrophysiological measurements of EHT contractility resulting from the implemented maturation media. Targeting maturation from multiple sides will hopefully be the edge needed to generate an ideal phenotype to model human adult cardiomyocytes and push the cardiac regenerative field forward.

The moment you doubt whether you can fly, you cease forever to be able to do it ...

– Peter Pan, J.M. Barrie

A

Additional Methods and Materials

A.1 Extra Methodology

A.1.1 Tissue Fixation, Embedding and Sectioning

Tissue was removed and instantly placed in Krebs buffer to allow the heart to continue pumping out the blood. The tissue was then cleaned up by removing the lungs and excess fat. The heart was then washed twice with PBS and fixed in 4% paraformaldehyde (PFA) (4 °C or RT, overnight). The sample was then washed twice again in DPBS and embedded in optimal cutting temperature (OCT). Before OCT embedding, the samples were equilibrated in 30% sucrose in phosphate buffered saline (DPBS) overnight (or until the heart sank).

Then with increasing ratios the heart was soaked in 1:5 OCT and then 1:1 OCT. The heart was then positioned in a mould and 100% OCT was added with no bubbles until fully submerged. In order to prevent the OCT or tissue from cracking, the samples were immediately placed in a zip lock bag and immersed slowly in cold isopentane until frozen. The samples are stored at −80 °C until ready to section. Samples were then sectioned using a cryostat and mounted on cover slips for staining.

A.1.2 Immunohistochemistry

Frozen sections were defrosted and allowed to dry, washed with DPBS, permeabilised (0.5% triton X-100 (TX-100) in DPBS) and incubated with blocking solution (DPBS, 10% donkey serum, 1% bovine serum albumin (BSA), and 0.1% TX-100) at RT for 90 minutes. Then, the samples were incubated with primary antibody (Table A.3) diluted in blocking solution (4 °C, overnight). The next day, the samples were washed three times (5 minutes, DPBS 0.1% TX-100) and incubated with the appropriate secondary antibodies (one hour, RT, Table A.4). Then, the slides were washed three times (10 minutes, DPBS 0.1% TX-100). 4,6-diamidino-2-phenylindole (DAPI) staining was added to the final wash, and then the slides were rinsed twice in DPBS. The slides were mounted with 50:50 DPBS/glycerol and stored in the dark at 4 °C.

A.1.2.1 Measurement of Media Glucose and Lactate Concentration

Glucose and lactate concentrations were determined after 24 hours by collecting the culture media and using a Horiba ABX Pentra 400 blood plasma analyser according to manufacturer's protocols.

A.1.3 Step By Step Protocol for Generation of Human Engineered Heart Tissue (EHT)

Aliquot the Following Reagents:

1. Aprotinin- 33 mg/mL

    - Dissolve 1 g aprotinin in 30.3 mLs cell culture grade water for injections (filter-sterilise)
    - 250 μL aliquots, store at $-20\,^{\circ}$C

2. Fibrinogen Bovine - 200 mg/mL (sterile)

    - In pre-warmed 0.9% NaCl solution (5 g/25 mLs) made up in sterilised cell culture water.
    - Optional: Add 72.1 μL aprotinin (33 mg/mL) to 25 mLs fibrinogen solution, mix, aliquot.
    - store at $-20\,^{\circ}$C and don't repeat thaw (lasts 2-3 weeks).

3. Thrombin Bovine - 100 U/mL

    - Dissolve in 1.5 mLs DPBS and 1.0 mL injectable water (mix thoroughly).
    - Aliquot into 500 μL (stock) and 3 μL for daily use.
    - store at $-20\,^{\circ}$C.

Prepare the following Reagents:

1. EHT - medium

    - 45 mLs of DMEM (Biochrom F0415) incl. 1% P/S
    - 10% Horse Serum inactive - (5 mLs)
    - 0.1% Insulin - (50 μL)
    - 0.1% Aprotinin - (50 μL)
    - store at $4\,^{\circ}$C

2. 10x DMEM solution

- 670 mg DMEM (powder)
- 5 mLs diH_2O (must be filtered with 0.22 μm filter and store at 4 °C)

3. 2x DMEM solution (make fresh each time)
    - 20% 10x DMEM solution - 2 mLs
    - 20% Horse serum (inactive) - 2 mLs
    - Penicillin/streptomycin - 0.2 mLs
    - Sterile water - 5.4 mLs
    - Store at 4 °C
4. NKM medium
    - DMEM (Biochrom F0415) incl. 1% P/S - 45 mLs
    - 10% Fetal calf serum inactive - 5 mLs
    - 1% Glutamine - 500 μL
    - store at 4 °C

Protocol:

1. Make agarose mould
    - Make 2% agarose (1 g agarose + 50 mLs of DPBS) and microwave for 2-3 minutes until powder dissolves.
    - When it cools slightly add 1.6 mLs of 2% agarose solution per well of 24-well plate. Place Teflon spacer on top of agarose solution. Let sit for 15-30 minutes until it solidifies and turns opaque colour.
    - Note: Agarose solidifies very fast so pipette max 8 wells before placing spacer and do NOT leave agarose solution at RT for longer than 5 minutes.

2. Prepare Master Mix (per EHT) in universal tube, on ice - recommended for 4 EHTs (+ 10% extra).

    - 1 million iPSC-CMs - concentration/EHT
    - NKM - 92 μL/EHT
    - 2x DMEM - 5.5 μL/EHT
    - Aprotinin - 0.425 μL/EHT (Note** if you already added this to the Fibrinogen stock sample then just add this amount to the fibrinogen amount.)
    - Fibrinogen - 2.5 μL/EHT (5 mg/mLs)
    - Thrombin - 3 μL/EHT (3 U) (Note** do NOT add to Master Mix but instead in a 3 μL aliquots in individual PCR tubes.)
    - NOTE** Fibrinogen has to be luke-warm for pipetting. Slowly fill the tip of the pipet and do not touch the surface of the ice cold Master Mix with the fibrinogen containing pipet - the viscosity of the fibrinogen would increase immediately.

3. When the agarose is solid, remove the spacer and place the silicone racks inside the open slits. Try and make sure that the post are in the center of the agarose slots and don't touch the edges.

4. Triturate (stripette) the Master Mix 10-15 times until the fibrinogen clot is dissolved (check the Master Mix in the pipette for homogeneity).

5. For each EHT pipette 100 μL Master Mix in one thrombin aliquot (3 μL), mix and pipet the mixture into the agarose slots quickly. Stripette mix the Master Mix after 8 EHTs.

6. Place in the 37 °C incubator for 2 hours.

7. Cover each well with a small amount of NKM (200-500 μL). Shake the plate gently and incubate again at 37 °C for 60 minutes.

8. Prepare a new 24-well plate with 1.5 mLs EHT medium per well.

9. Remove the silicone racks carefully from the agarose casting moulds and transfer them to the new medium filled plate.

10. Place EHTs in the incubator, and feed every 2-3 days.

A.1.4 Trouble Shooting of Flow Cytometry

There were a lot of complications with attempting flow cytometry with these cells. A series of attempts were made but very few were only partially successful. As mentioned in the chapter the first problem was that we had large amounts of cells dying off in the collection process. In Fig. A.1, you can see that in the first runs there was around 85% of the cells rendering as "dead". This could be due to the harvest process or the fact we weren't able to get them to truly single cells. We went back and optimised our dissociation protocol and saw significant improvements with our survival rate. The next run (Fig. A.1B) the alive count jumped to 31% and then another attempt to 52% (Fig. A.1C). This ratio is now comparable to ThermoFisher's expected rates for measurements using zombie violet (viability marker) (Fig. A.2.

Another problem we ran into was aspecific binding of the antibody which was confirmed through confocal of a whole mouse heart slide that can be seen in Chapter 5, (Fig. 3.11). We then attempted a series of runs with the new conjugated antibody. The first set of runs were on Days 7, 9, 15, 20 and 25 of the iPSC-CMs differentiation protocol. The second set were on iPSC-CM treated with OA ± WY-14643 for 1 week on Day 15 of the differentiation protocol. Although, we are getting closer, we still need to optimize further with the goal of getting distinct populations.

A.2 Additional Tables

Table A.1: Primers for Quantitative PCR for the Analysis of Gene Expression in Human iPSCs and iPSC-CMs.

Category	**Gene**	**sequence direction**	**E%**

Housekeeping	POLR2A	AGTCCGGATGAACTGAAGCG (FW)	[641]
		CACGTGAAACACAGGCTTGG (RV)	
Housekeeping	TBP	TGACCCAGCATCACTGTTTCTT (FW)	[642]
		CAAGCCCTGAGCGTAAGGTG (RV)	
Housekeeping	HPRT1	CCTGGCGTCGTGATTAGTGA (FW)	[643]
		GGGCTACAATGTGATGGCCT (RV)	
Housekeeping	B2M	AGCAGCATCATGGAGGTTTGA (FW)	[497]
		AGCCCTCCTAGAGCTACCTG (RV)	
Heart	RYR2	CTAATGTCTGGGTGGGCTGG (FW)	[643]
		TGCTGCGTTTGATGCTTTCA (RV)	
Heart	CX43	TACCAAACAGCAGCGGAGTT (FW)	[642]
		TGGGCACCACTCTTTTGCTT (RV)	
Heart	SERCA2A	CGAACCCTTGCCACTCATCT (FW)	[644]
		CCAGTATTGCAGGTTCCAGGT (RV)	
Heart	CASQ2	ACTTTCCTCTGCTCGTTGCC (FW)	[478]
		GCTCCTCAGCAGTTGGAAGA (RV)	
Heart	MYL7	GGAGTTCAAAGAAGCCTTCAGC (FW)	[641]
		GTCCCATTGAGCTTCTCCCC (RV)	
Heart	MYH6	TCCTGCGGCCCAGATTCTTC (FW)	[480]
		TCTTCCTTGTCATCGGGCAC (RV)	
Heart	MYH7	AAGGTCAAGGCCTACAAGCG (FW)	[364]
		CCAGGGCTGAGCAGATCAA (RV)	
Heart	TNNT2	GACAGAGCGGAAAAGTGGGA (FW)	[645]
		CTCCTTGGCCTTCTCCCTC (RV)	
Mesoderm	RUNX1	AACCTCGAAGACATCGGCAG (FW)	[646]
		GGCTGAGGGTTAAAGGCAGT (RV)	
Metabolism	GLUT1	TGGCATCAACGCTGTCTTCT (FW)	[644]
		CTAGCGCGATGGTCATGAGT (RV)	
Metabolism	GLUT4	GTTCTTTCATCTTCGCCGCC (FW)	[478]
		CAATCACCTTCTGAGGGGCA (RV)	
Metabolism	CS	CCAGTGCTTCCTCCACGAAT (FW)	[647]
		GGAAACGGATGCCCTCATCA (RV)	

Metabolism	IRS1	ACTGGACATCACAGCAGAATGA (FW)	[478]
		ACTGAAATGGATGCATCGTACC (RV)	
Metabolism	IRS2	GCCACCATCGTGAAAGAGTG (FW)	[648]
		CCATCCGGGAACAAGGGAAA (RV)	
Metabolism	PDK4	TGGTCCAAGATGCCTTTGAGT (FW)	[648]
		GTTGCCCGCATTGCATTCTT (RV)	
Metabolism	PPARα	GGACAAGGCCTCAGGCTATC (FW)	[641]
		AACGAATCGCGTTGTGTGAC (RV)	
Metabolism	PGC1a	TCTCAGTAAGGGGCTGGTTG (FW)	[360]
		ACCAGAGCAGCACACTCGAT (RV)	
ECM	COL1A1	GGACACAGAGGTTTCAGTGGT (FW)	[497]
		GCACCATCATTTCCACGAGC (RV)	
ECM	COL3A1	GCTGGCATCAAAGGACATCG (FW)	[643]
		GGGAGCCCTCAGATCCTCTT (RV)	

Table A.2: TaqMan Assays Used for Quantitative qPCR

Gene	**Full Name**	**Gene Expression Assay ID**
UBC	House Keeping Gene	Hs00824723L
B2M	House Keeping Gene	Hs99999907
PPARα	Cardiac Metabolism	Hs00947536
PGC1α	Mitochondrial Biogenesis	Hs01016719
UCP3	Mitochondrial uncoupling protein and PPARα target gene	Hs01106052
GLUT1	Glucose Transport	Hs00892681
GLUT4	Glucose Transport	Hs00168966
PFKM	Glycolysis	Hs00175997
PDK4	Pyruvate Oxidation	Hs01037712
PDHA1	Pyruvate Oxidation	Hs01049345
CD36	Fatty Acid Uptake	Hs01567185
ACSL1	Fatty Acid Activation	Hs00960561
CPT1B	Mitochondrial Fatty Acid Uptake (muscle type)	Hs03046298
HADHA	Fatty Acid Oxidation	Hs00426191
ACADM	Fatty Acid Oxidation	Hs00936584
ECI1	Unsaturated Fatty Acid Oxidation	Hs00157239
CS	TCA Enzyme	Hs02574374

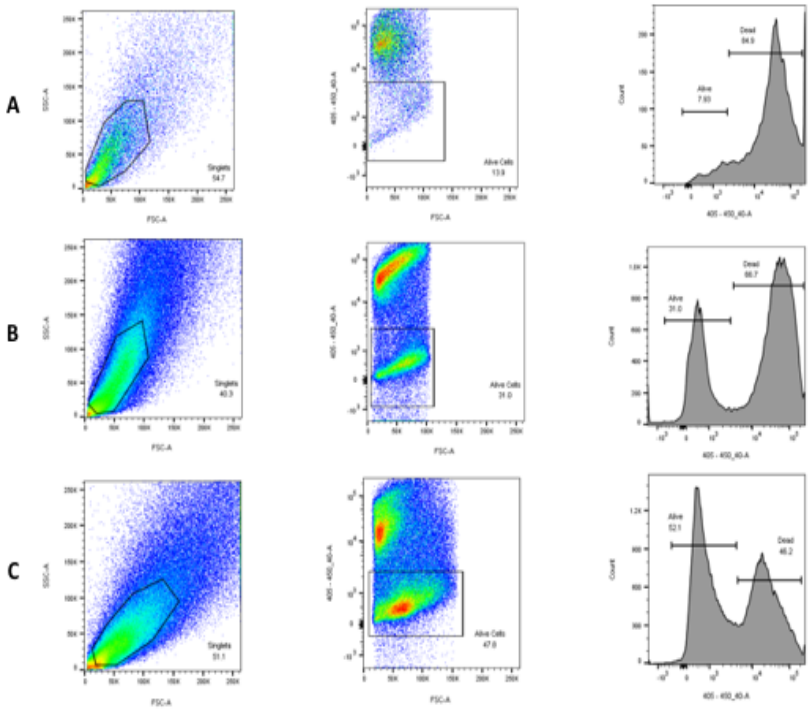

Figure A.1: Trouble Shooting Flow: Gating for Singlets and Alive cells A) Original poor dissociation method. B-C) Improved dissociation method more cells surviving. Although, it's supposed to be two distinct populations and you can see a smear which implies there is a range of size and not all singlets.

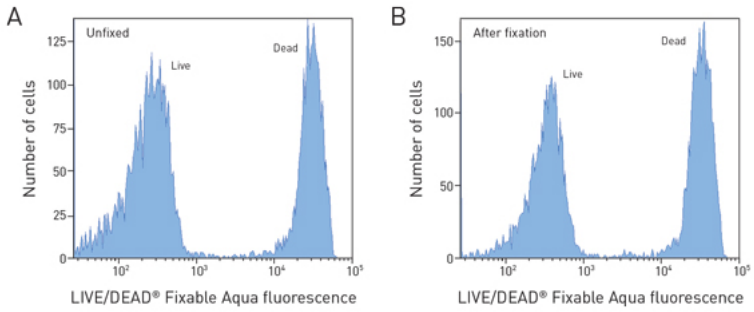

Figure A.2: ThermoFisher's Zombie Violet retention of LIVE/DEAD Fixable Dead Cell Stains after fixation. The LIVE/ DEAD Fixable Aqua Dead Cell Stain Kit was used to differentially stain a mixture of live (left peak) and heat-treated Jurkat cells (right peak). Cells in (A) were not fixed; cells in (B) were fixed in 3.7% formaldehyde following staining. Samples were analyzed by flow cytometry using 405 nm excitation and 525 nm emission. Image taken from ThermoFisher website.

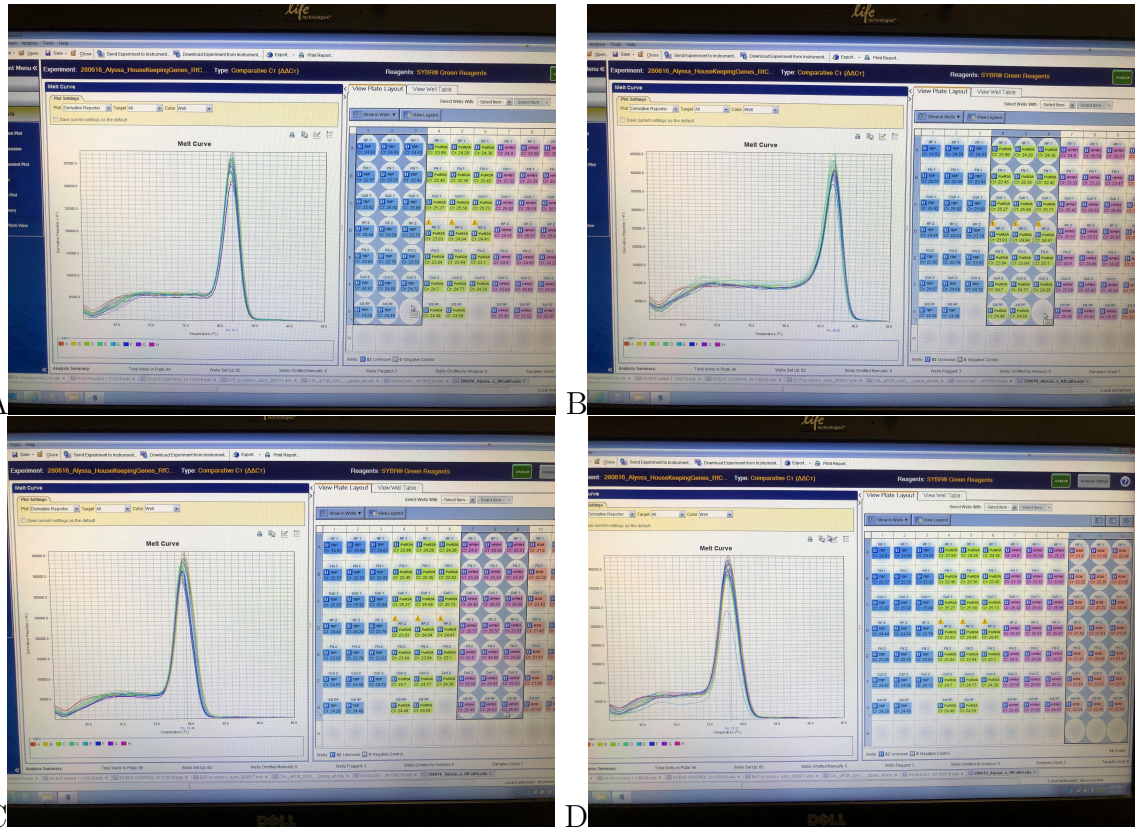

Figure A.3: All primers were previously validated via melt curves and percent efficiency recorded. Here is an example of the melt curve for a housekeeping primer. A) *TBP* B) *POLR2A* C) *HPRT1* D) *B2M* melt curves. Photos of the thermocycler taken via iPhone.

A)TBP B) POLR2A C) HPRT1 D) B2M

Table A.3: Antibodies Used for Immunohistochemistry and Immunocytochemistry.

Target	Manufacturer	Dilution
Anti-Cardiac Troponin T	Abcam, ab10214	1:200
Anti-Cardiac Troponin T antibodies	MACS, 130-106-745	1:200
Myosin Heavy Chain	Abcam, ab50967	1:200
Monoclonal Anti--Actinin (Sarcomeric)	Sigma A7811	1:500
Glut 4	Abcam, ab654	1:1000
Lipid (Oil Red O)	Sigma-Aldrich, MAK:194	3:2
DAPI (nucleus)	Life Technologies	1:1000

Table A.4: Secondary Antibodies Used for Immunocytochemistry and Immunohistochemistry

Label	Manufacturer	Species reactivity	Dilution
Alexa-488	Life Technologies Ltd	donkey anti-goat	1/200
Alexa-488	Life Technologies Ltd	donkey anti-rabbit	1/200
Alexa-488	Life Technologies Ltd	goat anti-rat	1/200
Alexa-568	Life Technologies Ltd	donkey anti-rabbit	1/200
Alexa-568	Life Technologies Ltd	goat anti-rabbit	1/200
Alexa-647	Life Technologies Ltd	donkey anti-mouse	1/200

Table A.6: Reagent's Purchase List.

Experiment	Reagent	Company	Catalog Number
iPSC maintenance	MTSER	StemCell	85850
iPSC maintenance	Matrigel	Corning	354277
iPSC maintenance	TripleExpress	Gibco	12604-013
iPSC-CM Differentiation	RPMI 1640 1X Medium + L-glutamine	ThermoFisher	11875093
iPSC-CM Differentiation	B-27 Supplement minus insulin	ThermoFisher	A1895601
iPSC-CM Differentiation	B-27 supplement (50x), serum free	ThermoFisher	17504044
iPSC-CM Differentiation	Rock Inhibitor (Y-27632)	Millipore	688000-1MG
iPSC-CM Differentiation	IWP4	StemCell	72552
iPSC-CM Differentiation	Activin A (Recombinant Human/Mouse/Rat)	R& D Systems	338-AC-010

iPSC-CM Differentiation	CHIR-99021 (CT99021)	Selleckchem	S1263
iPSC-CM Differentiation	growth factor reduced (RF)-Matrigel	Corning	354230
EHT	Aprotinin	Sigma-Aldrich	A1153-100mg
EHT	Fibrinogen	Sigma-Aldrich	F8630-5g
EHT	Thrombin	Biopur	BP11-10-1104
EHT	Agarose	Invitrogen	15510-027
EHT	10xDMEM	Gibco	52100-021
EHT	Penicillin/streptomycin (P/S)	Gibco	15140
EHT	DMEM	Biochrom	F0415
EHT	Horse Serum inactivated	Gibco	1209534
EHT	Insulin	Sigma-Aldrich	I9278
EHT	Glutamine	Life Technologies	25030-081
EHT	Silicone racks	EHT Technologies	C0001
EHT	Teflon Spacers	EHT Technologies	C0002
Single Cell Dissociation	Collagenase II	Worthington Biochemical Corporation	LS004176
Single Cell Dissociation	HEPES	ThermoFisher	15630106
Single Cell Dissociation	N-Benzyl-p-toluenesulfonamide (BTS)	TCI America	B3082
Single Cell Dissociation	Dimethyl Sulfoxide (DMSO)	Sigma-Aldrich	D2650
Single Cell Dissociation	DNase I, RNase-free	ThermoFisher	EN0521
Single Cell Dissociation	Fetal Bovine Serum	ThermoFisher	16000044
Single Cell Dissociation	Calcium free HBSS	ThermoFisher	14175095
^{3}H Glycolysis	Glucose, D-[5-3H(N)]-, 1mCi (37MBq)	PerkinElmer	NET531001MC
^{3}H Glycolysis	Dowex	Sigma-Aldrich	428590-500g
^{3}H Glycolysis	Glass Pasteur Pipettes	ThermoFisher	FB50251
^{3}H Glycolysis	Glass Wool	Sigma-Aldrich	18421-500g
^{3}H Glycolysis	Sodium Hydroxide (NAOH) 1kg	ThermoFisher	S/4920/60
^{3}H Glycolysis	Boric Acid - 1KG	ThermoFisher	B/3800/60
^{3}H Glycolysis	Ecolite(+) Liquid Scintillation Cocktail	MP	0188247501 - 1 gal

^{3}H Glycolysis	Super Polyethylene Vial 20mL Quick Closure Case of 1000	PerkinElmer	6008117
^{3}H Glycolysis	DMEM (Low glucose) (x1)	Sigma-Aldrich	D5546-500mLs
^{14}C Glucose	Glucose, D-[^{14}C(U)]-, 1mCi (37MBq)	PerkinElmer	NEC042A001MC
^{14}C Glucose	Potassium Hydroxide (KOH) - 500g	ThermoFisher	P/5640/53
^{14}C Glucose	70%-72% Perchloric Acid (1 Liter)	Merck Millipore	1005191001
^{14}C Glucose	Whatman 1001-110 Grade 1 Qualitative Filter Paper Standard Grade, circle, 110 mm, 100 per pack	Sigma-Aldrich	1001-110
^{14}C Glucose	1 mL syringes	DPAG stores	BS01T
^{14}C Glucose	21 gauge needles	DPAG stores	NN2138R
^{14}C Glucose	Parafilm M (4in x 125ft)	Sigma-Aldrich	P7793-1EA
^{14}C Glucose	Ecolite(+) Liquid Scintillation Cocktail	MP	0188247501 - 1 gal
^{14}C Glucose	Super Polyethylene Vial 20mL Quick Closure Case of 1000	PerkinElmer	6008117
^{14}C Glucose	DMEM (Low glucose) (x1)	Sigma-Aldrich	D5546-500mLs
^{3}H Palmitate	Palmitic Acid, [9,10-3H(N)]-, 1mCi (37MBq)	PerkinElmer	NET043001MC
^{3}H Palmitate	Centrifuge Tube 15ml (Falcon 2097) Rack of 50	DPAG stores	352097-SP
^{3}H Palmitate	Chloroform - 1 liter	ThermoFisher	C/4966/15
^{3}H Palmitate	Methanol (2.5L)	Honeywell	32213-2.5L
^{3}H Palmitate	Potassium Chloride (KCL) - 500g	Sigma-Aldrich	P9541-500g
^{3}H Palmitate	Hydrochloric Acid Solution 1M (HCL) - 1Liter	ThermoFisher	J/4320/15
^{3}H Palmitate	Glass Pasteur Pipettes	ThermoFisher	FB50251
^{3}H Palmitate	Ecolite(+) Liquid Scintillation Cocktail	MP	0188247501 - 1 gal
^{3}H Palmitate	Super Polyethylene Vial 20mL Quick Closure Case of 1000	PerkinElmer	6008117

^{14}C Palmitate	Palmitic Acid, [14C(U)]-, 50Ci (1.85MBq)	PerkinElmer	NEC534050UC
^{3}H Oleic Acid	Oleic Acid, [9,10-3H(N)]-, 1mCi (37MBq)	PerkinElmer	NET289001MC
OA/WY Treatment	Oleic acid-BSA (5mLs)	Sigma-Aldrich	03008-5mL
OA/WY Treatment	WY Pirinixic Acid	selleckchem.com	S8029
Lactate Treatment	DMEM (No glucose) (x1)	ThermoFisher	11966025
Lactate Treatment	sodium DL lactate solution	Sigma-Aldrich	71723
MISC	AlamarBlue Assay (x1)	BioRad	BUF012B

A.3 PPARα Target Genes

Table A.7: PPARα Target Genes with a PPRE Within the Promoter Sequence, Adapted from [533].

Gene	**Function of the gene**	**Ref**
Heart		
Acl-CoA oxidase (ACO-A)	peroxisomal β-oxidation	[649]
Carnitine palmitoyl-transferase I	FAO	[572, 573]
Carnitine palmitoyl-transferase II	FAO	[574]
Long-chain acyl-CoA synthetase	FA activation	[580]
Medium-chain acyl-CoA dehydrogenase	FA oxidation	[575]
Liver		
Acyl-CoA binding protein	fatty acyl-CoA ester transport	[650]
Acyl-CoA oxidase (ACO)	peroxisomal β-oxidation	[649]
Apolipoprotein-AI	plasma HDL metabolism	[651]
Apolipoprotein-AII	plasma HDL metabolism	[652]
Apolipoprotein-AV	plasma HDL metabolism	[653, 654]

Apolipoprotein-CIII	plasma HDL metabolism	[655]
Bifunctional enzyme (BIEN or BE)	FA β-oxidation	[656–658]
Carnitine palmitoyl-transferase I	FAO	[572, 573]
Carnitine palmitoyl-transferase II	FAO	[574]
Cytochrome P450 4A6-Z	FA w-hydroxylation	[659, 660]
Cytochrome P450 4A1	FA w-hydroxylation	[661]
Cytochrome P450 7A1 (CYP12A1)	bile acid metabolism	[662]
Cytochrome P450 12A1 (CYP12A1)	cholesterol metabolism	[663]
delta-6-Desaturase	desaturation of fatty-acyl CoA	[664]
Cytosolic FA binding protein	FA binding/transport	[665]
FA transport protein-1	FA transport	[581, 666]
Lipoprotein lipase (LPL)	triglyceride clearance	[667]
Liver X receptor α (LXRα)	cholesterol metabolism	[668]
Long-chain acyl-CoA synthetase (LCAS)	FA activation	[580]
Malic enzyme (ME)	FA synthesis	[575]
Mitochondrial HMG-CoA synthase	ketogenesis	[669]
Medium-chain acyl-CoA dehydrogenase	FAO	[575]
Phospholipid transfer protein (PLTP)	plasma HDL metabolism	[670]
Rev-Erbα	repressor of gene transcription	[651]
Stearoyl-CoA desaturase I	desaturation of fatty acyl CoA	[671]
Sterol carrier protein-X	FAO	[672]
Superoxide dismutase	oxygen free radical metabolism	[673]
Transferrin	iron transport	[674]
Thiolase B	FA oxidation	[675]
UDP-glucuronosyltransferase 1A9	biotransformation	[676]
Muscle		
Carnitine palmitoyl-transferase-1	FA transport	[572]
Brown adipose tissue		
Uncoupling protein-1	thermogenesis	[677]
White adipose tissue		
Lipoprotein lipase (LPL)	triglyceride clearance	[667]
Acyl-CoA oxidase (ACO)	peroxisomal β-oxidation	[649]
Small intestine		

Apolipoprotein C-III (apo-III)	plasma HDL metabolism	[655]
Cytosolic FA binding protein	FA binding/transport	[665]

Table A.8: List of PPARα Dependent Gene Regulation with No Functional PPRE Reported Yet, Adapted from [533].

Gene	**Function of the gene**	**Ref**
Heart		
Cytoplasmic acyl-CoA thioesterase	Hydrolysis of Acyl-CoA	[678]
Malonyl-CoA decarboxylase	FAO	[679, 680]
Mitochondrial acyl-CoA thioesterase	Hydrolysis of Acyl-CoA	[678]
Uncoupling protein-2 (UCP-2)	ROS production	[579]
Uncoupling protein-3 (UCP-3)	body energy metabolism	[576, 579]
Pyruvate dehydrogenase kinase isoform-4	glucose oxidation	[576, 577]
Liver		
ABCA-1 (via LXRα)	Cholesterol transport	[681]
ABCG-5 (via LXRα)	Cholesterol transport	[681]
ABCG-8 (via LXRα)	Cholesterol transport	[681]
Alanine aminotransferase	amino acid metabolism	[682]
Alanine-glyoxylate transaminase	amino acid metabolism	[683]
alpha-1 Acid glycoprotein (AGP)	acute phase response	[684]
Arginase	amino acid metabolism	[683]
Arginosuccinate lyase	amino acid metabolism	[683]
Arginosuccinate synthase	amino acid metabolism	[683]
Carbamoyl-phosphate synthase-1	amino acid metabolism	[683]
c-myc (protooncogene)	cell cycle	[685]
Cyclin D1	cell cycle	[685]
Cytochrome P450 2AS	Biotransformation	[686]
Cytochrome P450 2C11	steroid hydroxylase	[684]
Cytochrome P450 2C12	steroid hydroxylase	[684]
Cytochrome P450 2C29	Biotransformation	[686]
Cytochrome P450 3A11	steroid hydroxylase	[686]
Cytochrome P450 4A3	FA hydroxylation	[687–691]

Cytochrome P450 4A14	FA hydroxylation	[685, 686]
Cytochrome P450 4A10	FA w-hydroxylation	[686]
Cytochrome P450 27A1	cholesterol metabolism	[681, 692]
Cytosolic acyl-CoA thioesterase-I	Hydrolysis of Acyl-CoA	[678]
Cytosolic acyl-CoA thioesterase-II	Hydrolysis of Acyl-CoA	[582]
Cytosolic epoxide hydrolase	biotransformation	[693]
delta-5-Desaturase	Desaturation of FAs	[671, 694]
Dodec Enoyl-CoA delta-isomerase	FAO	[695]
Farnesoid X receptor (FXR)/Bile acid receptor (BAR)	hepatic sterol metabolism	[681]
Fasting-induced adipose factor	lipid metabolism	[696]
FA translocase (FAT/CD36)	FA transport	[578]
Fibrinogen	acute phase response	[684, 697]
Glucose-regulated protein-94	cellular proliferation	[698]
Glutaminase	amino acid metabolism	[683]
Glutathione-S-transferase alpha	Biotransformation	[699]
Glyoxylate/hydroxypyruvate reductase	amino acid metabolism	[683]
Interleukin-6	vascular inflammation	[685]
Interleukin-1 receptor type 1	vascular inflammation	[685]
Interleukin-6 receptor	vascular inflammation	[685]
Lactoferrin	Iron-binding protein	[700]
Long-chain acyl-CoA dehydrogenase	FAO	[582, 690]
Mitochondrial acyl-CoA thioesterase-I	hydrolysis of acyl-CoA	[678]
Mitochondrial aspartate aminotransferase	AA metabolism	[682, 683]
Multidrug resistance 2	Hepatobiliary lipid transport	[681, 701]
Ornithine transcarbamylase	amino acid metabolism	[683, 698]
Peroxisomal acyl-CoA thioesterase 1A	Hydrolysis of acyl-CoA	[683, 698]
Peroxisomal acyl-CoA thioesterase 1B	Hydrolysis of acyl-CoA	[678, 695]
Peroxisomal acyl-CoA thioesterase 2	Hydrolysis of acyl-CoA	[702]
Pyruvate dehydrogenase kinase isoform 4	glucose oxidation	[703]
scavenger receptor B-type 1	plasma HDL metabolism	[704]
Short chain specific 3 ketoacyl-CoA thiolase (T1)	FAO	[582]

short chain acyl-CoA dehydrogenase	FAO	[582, 705]
Uncoupling protein 2 (UCP2)	ROS production	[705–707]
Very long chain acyl-CoA dehydrogenase	FAO	[582]
Aortas		
interleukin-6	vascular inflammation	[708]
White adipose tissue		
Fasting-induced adipose factor	lipid metabolism	[696]
Resistin	Insulin resistance	[709]
FA translocase (FAT/CD36)	FA transport	[710]
Uncoupling protein 2 (UCP2)	ROS production	[710]
Brown adipose tissue		
Uncoupling protein 2 (UCP2)	ROS production	[705]
Kidney		
17-β-hydroxysteroid dehydrogenase	steroid metabolism	[711]
pyruvate dehydrogenase kinase isoform-4	glucose oxidation	[577]
Monocytes/macrophages		
Scavenger receptor type B class I	HDL metabolism	[712]
Muscle		
pyruvate dehydrogenase kinase isoform-4	glucose oxidation	[713]
Uncoupling protein 2 (UCP2)	ROS production	[579]
Uncoupling protein 3 (UCP3)	body energy metabolism	[579]

Table A.5: Western Blot Antibodies

Antibody	**Species**	**Company**	**Cat number**
Anti-PDK4	Human, Mouse	Abgent	AP7041b
Anti-UCP3	Human, Dog, Mouse, Rat	Abcam	ab3477
Anti-MCAD	Human, Mouse, Rat	Santa Cruz	sc-49047
Anti-cyclophilin B	Human, Dog, Mouse, Rat, Horse, Chicken	Abcam	ab16045

You are BRAVER then you believe, and STRONGER than you seem, and SMARTER than you think . . .

— A.A. Milne, Winnie the Pooh

B Research Outcomes

B.1 Publications

During my time at Oxford University, these are the following publications that have been accepted or are currently in review.

Publications:

- Sophia Malandraki-Miller, **Colleen A. Lopez**, Rita Alonaizan, Ujang Purnama, Filippo Perbellini, Kathy Pakzad, Carolyn A. Carr. (2019) Metabolic flux analyses to assess the differentiation of adult cardiac progenitors after fatty acid supplementation. Stem Cell Research. https://doi.org/10.1016/j.scr.2019.101458
- **Colleen A Lopez**, Sophia Malandraki-Miller, Heba Al-Siddiqi, Carolyn A Carr. "Changing Metabolism in differentiating cardiac progenitor cells - can stem cells become metabolically flexible cardiomyocytes?" *Frontiers in Cardiovascular Medicine*, vol 5, no. 119, 2018 [268].
- Mary Board, **Colleen A Lopez**, Christian Bos Van Den, Richard Callaghan, Kieran Clarke, & Carolyn A Carr. "Acetoacetate is a more efficient energy-yielding substrate for human mesenchymal stem cells than glucose and generates fewer reactive oxygen species." *Int J of Biochem Cell Biol*, vol. 88. pp 75-83, 2017. http://dx.doi.org/10.1016/ j.biocel.2017.05.007 [326].
- Ashton Faulkner, Rob Purcell, **Colleen Lopez**, Mary Board, Carolyn Carr, Nicole Wagner. "Context-dependent regulation of endothelial cell metabolism: Diggerential effects of PPARβ/γ agonist GW0742 and VEGF-A." *Scientific Reports (Nature)* (in review: 01/18/19).

Abstracts and Scientific Presentations:

- **Colleen A Lopez[1]**, Pooja Basnett[2], Sonia Iftekhar[2], Rita Alonaizan[1], Esra Sengul[1], Junyan Wang[1], Arne Bruyneel[1], Jan Czernuszka[2], Ipsita Roy[2] and Carolyn Carr[1].

[1]Department of Physiology, Anatomy & Genetics, [2]Department of Material Science, University of Oxford. [3]Department of Life Sciences, University of Westminster. Acellular scaffolds to deliver paracrine factors for myocardial repair. Oxford British Heart Foundation Centre of research excellence (Oxford BHF CRE) annual research symposium. Oxford, England November 22, 2018; Poster Presentation.

- **Colleen A Lopez*[1]**, Charlotte Ferguson[1], Arne Bruyneel[1], Sonia Iftekhar[2], Jan Czernuszka[2] and Carolyn Carr[1]. [1]Department of Physiology, Anatomy & Genetics, [2]Department of Material Science, University of Oxford. 3D culture on collagen-based scaffolds induce a more metabolically mature phenotype in iPS derived Cardiomyocytes. MitOX, Oxford, England December 1, 2017; Poster Presentation. **Portland Press Poster Prize**.

- Heba Al-Siddiqi, **Colleen A Lopez**, Lisa C Heather, Carolyn Carr. Department of Physiology, Anatomy and Genetics, University of Oxford. Treatment with Oleic acid and a PPARα agonist increases fatty acid oxidation in beating human inducible pluripotent stem cell derived cardiomyocytes. BSCR Autumn Meeting. September 11-12th, 2017, University of Oxford. Poster Presentation; **Published Abstract**.

- Sophia Malandraki-Miller, **Colleen A Lopez**, Carolyn A. Carr. Activating Mitochondrial Metabolism in Adult Cardiac Progenitors. Department of Physiology, Anatomy, and Genetics, University of Oxford, Oxford, UK. MitOX. Academic Centre, John Radcliffe Hospital, Oxford, England. December 6, 2016; Poster Presentation; **Poster Prize**.

- **Colleen A Lopez[1]***, Arne Bruyneel[1], Rabia Nazir[2], Jan Czernuszka[2] and Carolyn Carr[1]. [1]Department of Physiology, Anatomy & Genetics, [2]Department of Material Science, University of Oxford, UK. Does Prolonged Culture and/or Culture in 3D Collagen-based Scaffolds Induce Maturation of iPS-derived Cardiomyocytes? DPAG Second Year Dphil Studies Semeniar. October 27, 2016 University of Oxford, Oxford, UK. Poster Presentation.

- Arne Bruyneel[1], Rabia Nazir[2], Qi Chen[2], **Colleen A Lopez[1]***, Jan Czernuska[2], Carolyn Carr[1].[1]Department of Physiology, Anatomy & Genetics, [2]Department of Material Science, University of Oxford, UK. Cardiosphere- derived cell-seeded porous collagen scaffolds for cardiac repair. BSCR/BAS annual Conference. Manchester, England. June 6-7, 2016. Presenting Author - Poster Presentation; **Published Abstract**

Stem Cell Research 38 (2019) 101458

Contents lists available at ScienceDirect

Stem Cell Research

journal homepage: www.elsevier.com/locate/scr

Metabolic flux analyses to assess the differentiation of adult cardiac progenitors after fatty acid supplementation

Sophia Malandraki-Miller[a,*], Colleen A. Lopez[a], Rita Alonaizan[a], Ujang Purnama[a], Filippo Perbellini[b], Kathy Pakzad[a], Carolyn A. Carr[a]

[a] Department of Physiology, Anatomy, and Genetics,Sherrington Building, University of Oxford, Oxford, UK
[b] National Heart and Lung Institute, Imperial College London, London, W12 0NN, UK

ARTICLE INFO

Keywords:
Cardiac stem cells
Differentiation
Metabolism
Oleic acid OA
Fatty acid oxidation
PPARα

ABSTRACT

Myocardial infarction is the most prevalent of cardiovascular diseases and pharmacological interventions do not lead to restoration of the lost cardiomyocytes. Despite extensive stem cell therapy studies, clinical trials using cardiac progenitor cells have shown moderate results. Furthermore, differentiation of endogenous progenitors to mature cardiomyocytes is rarely reported.

A metabolic switch from glucose to fatty acid oxidation occurs during cardiac development and cardiomyocyte maturation, however *in vitro* differentiation protocols do not consider the lack of fatty acids in cell culture media. The aim of this study was to assess the effect of this metabolic switch on control and differentiated adult cardiac progenitors, by fatty acid supplementation.

Addition of oleic acid stimulated the peroxisome proliferator-activated receptor alpha pathway and led to maturation of the cardiac progenitors, both before and after transforming growth factor-beta 1 differentiation. Addition of oleic acid following differentiation increased expression of myosin heavy chain 7 and connexin 43. Also, total glycolytic metabolism increased, as did mitochondrial membrane potential and glucose and fatty acid transporter expression.

This work provides new insights into the importance of fatty acids, and of peroxisome proliferator-activated receptor alpha, in cardiac progenitor differentiation. Harnessing the oxidative metabolic switch induced maturation of differentiated endogenous stem cells.

(200 words)

1. Introduction

The heart uses a variety of substrates for energy production, while an array of metabolic networks guides adenosine triphosphate (ATP) production rates (Evans and Heather, 2016)·(Taegtmeyer et al., 2016). ATP can be produced *via* glycolysis (non-oxidative breakdown of glucose) (DeBerardinis et al., 2007), alternatively, pyruvate can enter the mitochondria and be metabolised *via* oxidative phosphorylation (Madeira, 2012) (Fig. S1).

A well-studied metabolic switch characterises the transition from

Abbreviations: A.A, Ascorbic Acid; BSA, Bovine Serum Albumin; CKIT, proto-oncogene Ckit / tyrosine-protein kinase Kit (CD117); CDM, Cardiac Differentiation Medium; CPC, Cardiac Progenitor Cell; CX43, Connexin 43; DIFF, Differentiation samples; DIFF + OA, Differentiation samples + Oleic Acid; DMSO, DiMethylSulfOxide; EB, Embryoid Body; FA, Fatty Acid; FBS, Fetal Bovine Serum; FLK1, Fetal Liver Kinase 1 / (KDR) (Type III Receptor Tyrosine Kinase); HF, Heart Failure; HRPT, Hypoxanthine-guanine phosphoribosyltransferase; GATA4, GATA binding protein 4; GLUT1, Glucose transporter type 1; GLUT4, Glucose transporter type 4; ISL-1, ISL1 transcription factor/ (Insulin gene enhancer protein – Islet1); mESC, mouse Embryonic Stem Cells; MEF2C, Myocyte Enhancer Factor 2C; MI, Myocardial Infarction; MYH7, myosin, heavy chain 7, cardiac muscle, beta; NKX2.5, NK2 homeobox 5; OA, Oleic Acid (unsaturated fatty acid); OCT-3/4, Octamer-binding Transcription factor 4 / (POU5F1); Px, Passage x (x = number); PDK4, Pyruvate Dehydrogenase Kinase-4; PGC-1A, Peroxisome Proliferator-Activated Receptor Gamma Coactivator 1; PFA, Paraformaldehyde; PPARA, Peroxisome Proliferator Activated Receptor Alpha; RXR, Retinoid X Receptor; SCA1, Stem cells antigen-1; SDHA, Succinate Dehydrogenase complex, subunit A; TERT, telomerase reverse transcriptase; TGF-β1, Transforming Growth Factor Beta 1; TNNT2, (Cardiac) Troponin T2

* Corresponding author at: Department of physiology, Anatomy & Genetics, Sherrington Building, Parks Road, Oxford OX1 3PT, UK.
E-mail addresses: sophia.malandraki-miller@dpag.ox.ac.uk (S. Malandraki-Miller), colleen.lopez@dpag.ox.ac.uk (C.A. Lopez), rita.alonaizan@dpag.ox.ac.uk (R. Alonaizan), ujang.purnama@dpag.ox.ac.uk (U. Purnama), f.perbellini@imperial.ac.uk (F. Perbellini), khadij.pakzad@icloud.com (K. Pakzad), carolyn.carr@dpag.ox.ac.uk (C.A. Carr).

https://doi.org/10.1016/j.scr.2019.101458
Received 21 September 2018; Received in revised form 11 April 2019; Accepted 6 May 2019
Available online 08 May 2019
1873-5061/ © 2019 Published by Elsevier B.V. This is an open access article under the CC BY-NC-ND license (http://creativecommons.org/licenses/BY-NC-ND/4.0/).

cardiac stem cells to cardiomyocytes (CMs), highlighted by a shift from anaerobic to oxidative metabolism (Kolwicz et al., 2013), which allows for the increased yield of ATP to sustain contraction (Schönfeld et al., 1996). Another metabolic shift is also experienced by cardiac progenitor cells (CPCs) during transplantation *in vivo*, since CPCs are transferred from the culture medium, which can contain between 5.5 mM – 25 mM glucose and no fatty acids (FAs), to substrates in plasma that vary substantially. In mice, glucose levels have been measured between ~3.4–9.6 mM (Wolfensohn and Lloyd, 2003), while FAs in the range of ~0.18–0.6 mM (Perbellini et al., 2014).

In addition, both oleic acid (OA) and Transforming Growth Factor-Beta 1 (TGF-β1) are naturally found in the body, so in the context of cell therapy it is necessary to understand their effect on the transplanted cells. FAs (including oleic, palmitic, linoleic, and arachidonic acid) are natural ligands for Peroxisome Proliferator-Activated Receptor α (PPARα) (Göttlicher et al., 1992). The PPARα signalling pathway comprise a group of nuclear receptor proteins (Nuclear Receptors Nomenclature, C, 1999), and their target genes are involved in fatty acid (Gulick et al., 1994) and glucose metabolism (Finck et al., 2002). Ding et al. showed that PPARα levels were upregulated during differentiation of Embryonic Stem Cells (ESCs) to beating CMs, and that PPARα inhibition prevented differentiation (Ding et al., 2007a). Furthermore, PPAR co-activator 1α (PGC-1α) (Sanderson et al., 2009), is involved in metabolic processes (Handschin and Spiegelman, 2006) including regulation of genes involved in FA oxidation (Vega et al., 2000). Interestingly, a study conducted in 2014 on the HepG2 hepatic cell line, showed that not all FAs have the same binding affinity to PPAR-alpha and therefore, do not necessarily result in its activation. While OA and palmitoleic acid increased PPRAα transactivation, palmitate and stearic acid inhibited it (Popeijus et al., 2014).

Various strategies have been applied to develop the optimal protocol for *in vitro* cardiac differentiation of stem cells (Malandraki-Miller et al., 2018). Goumans et al. used TGF-β1 for differentiation of human adult atrial stem cell antigen-1-positive ($Sca1^+$) CPCs (Goumans et al., 2008; Smits et al., 2009).

Recently, there have been studies exploring metabolic manipulation and the subsequent effect on cell differentiation and maturation, in hPSC-CMs. In 2017, Correia et al. investigated how different substrates affect the functional maturation of hPSC-CMs (Correia et al., 2017). By testing different media compositions, they demonstrate that culture medium supplemented with fatty acids and galactose, lacking glucose, forced the cells to shift to oxidative phosphorylation. That resulted in a phenotype more similar to human adult CMs than previously reported. In addition, Hu et al. investigated the mechanism that links metabolism and the maturation of hPSC-CMs, showing that reliance on glucose and the HIF1α-LDHA axis are involved in the immature phenotype of hPSC-CMs (Hu et al., 2018). They afterwards proved that metabolic shift towards oxidative metabolism led to maturation of the hPSC-CMs. Hitherto, to the best of our knowledge, no cardiac differentiation protocol has investigated the effect of FA supplementation on adult CPCs' metabolism and differentiation.

On the basis of the link between metabolic state and cell phenotype, we suggest that manipulating substrate availability *in vitro* could trigger differentiation of CPCs. In addition, the different layers of regulation that PPARα and PGC-1α exert on differentiation and metabolism lead us to hypothesise that stimulating this axis could enhance cell differentiation. Here we reveal the effect of fatty acid (OA) availability, in culture, on the metabolic maturation of adult CPCs. We also elucidate the effect that OA has on control and differentiated CPCs.

2. Materials & methods

2.1. Animals

Male C57BL/6 mice (Harlan, Oxon, UK) were housed in a 12-h light–dark cycle, controlled temperature and humidity, with water and food *ad libitum*. All animal procedures were reviewed and approved by the University of Oxford Animal Welfare and Ethical Review Board and conforms to the Animals (Scientific Procedures) Act 1986 incorporating Directive 2010/63/EU of the European Parliament.

2.2. Isolation and expansion of mouse cardiac progenitor cells (CPCS)

Mouse atria were excised, washed with Dulbecco's phosphate buffered saline (DPBS) (Invitrogen, Fisher Scientific – UK Ltd) containing Penicillin / Streptomycin (P/S) and minced mechanically. The tissue-pieces were transferred in 0.5 ml of the digestion solution (comprising of 0.1% trypsin and 0.1% Collagenase II (Calbiochem, 286 U/ mg), incubated in a shaking water bath at 37 °C for 1 h. Every 10′ the digestion-mix was mechanically triturated, the supernatant was collected, neutralized with CPC medium and plated on fibronectin-coated 6-well plates. CPC medium comprised of Iscove's modified Dulbecco's medium (IMDM) (Invitrogen, Fisher Scientific – UK Ltd) with 20% foetal bovine serum (FBS) (Invitrogen, Fisher Scientific – UK Ltd), 1 U/ ml penicillin, 1 μg/ ml streptomycin and 0.2 mM L-glutamine (P/S/G), (Gibco, Life Technologies, Fisher Scientific – UK Ltd). Fresh digestion solution was added to the remaining tissue pieces as before, until 1 h was reached. This digestion produced surviving fibroblast-like cells, named “CPCs”, attaching after 2 days. The CPCs were passaged when they reached 90% confluency, for further experiments and analysis.

2.3. RNA extraction, reverse transcription &qPCR reaction

Total RNA was extracted from frozen cell pellets, using the RNeasy Mini Kit (QIAGEN Ltd. – Manchester UK), following the manufacturer's protocol. Complementary DNA was synthesized, using the High Capacity cDNA Reverse Transcription kit (Life Technologies, Fisher Scientific – UK Ltd), following the manufacturer's protocol. cDNA aliquots were kept at −20 °C for further use. qPCR was performed using the StepOnePlus Real-Time PCR System (Applied Biosystems, Life Technologies, Fisher Scientific – UK Ltd). Relative mRNA levels were normalised to Sdha and Hrpt housekeeping genes. As detection system for the reaction SYBR green fluorescent intercalating dye was used (SYBR Green PCR mastermix, Life Technologies, Fisher Scientific – UK Ltd). For primer information see Supplementary material. Data was analysed using the published ΔΔCt method Livak method (Livak and Schmittgen, 2001), plotting the data as $2^{-\Delta\Delta Ct \pm SE}$.

2.4. Immunocytochemistry

CPCs P4 were seeded in 24-well plates, on fibronectin-coated cover slips (2 × 104 cells / well) and were fixed with 4% paraformaldehyde for 30′ at 4 °C. For intracellular proteins, cells were permeabilised with 0.2% Triton X for 10′. Then cells were blocked with a 2% FBS and 2% bovine serum albumin (BSA, Sigma-Aldrich Ltd. – Dorset, UK) solution for 30′. Primary antibody staining followed overnight at 4 °C. After washing with PBS, when required, cells were labelled with secondary antibody (30′, room temperature). Afterwards samples were co-stained with 0,1% 4′,6-diamidino-2-phenylindole (DAPI, Sigma-Aldrich Ltd. – Dorset, UK), and mounted on glass slides using a 50% PBS and 50% Glycerol (Fisher Scientific – UK Ltd) solution. Slides were kept at 4 °C protected from light, until imaging. Immunostaining was assessed using light confocal microscopy (Inverted Olympus Fluoview FV1000 Confocal system). For image analysis FIJI software (“Fiji Is Just ImageJ”) was used. Positive staining was assessed compared to a negative control; either cells stained only with 4′,6-diamidino-2-phenylindole (DAPI) or with just the secondary antibody and DAPI. For antibody information see Supplemental material.

2.5. Mitochondrial staining

For mitochondrial imaging, the MitoTracker® Red CMXRos (Fisher

Scientific – UK Ltd) intracellular dye was used, following manufacturer's protocol. CPCs at P4 were incubated for 40'with 10 nM MitoTracker in non-FBS medium. After washing with DPBS, they were fixed with 4% paraformaldehyde and imaged using light confocal microscopy. The average fluorescence intensity was analysed using the FIIJI image analysis software.

2.6. Mouse-esc differentiation – Embryoid bodies

The differentiated mouse ESCs, which were used as a positive control for comparison with differentiated CPCs in RT-PCR experiments, were donated by Dr. Richard Tyser (Prof. Paul Riley group, DPAG, Oxford). The samples were collected either at day 4, day 7,or day 14 of differentiation. Differentiation was induced using the hanging drop culture – embryoid body formation method (Boheler et al., 2002) (EBs d4, EBs d7, EBs d14).

2.7. TGF-β1 differentiation

Cardiac differentiation was induced using TGF-β1 (Smits et al., 2009). CPCs were seeded in CPC medium on gelatine-coated flasks 0,1% (Sigma-Aldrich Ltd. – Dorset, UK); at a density of 25×10^4 cells per 25 cm^2 flask or at 2×10^4 cells per well in a 24-well plate. The next day, the medium was replaced with Cardiac Differentiation Medium (CDM) (47% IMDM, 47% Ham's F12 – GlutaMAX-I, 2% Horse serum, 1% MEM non-essential amino acids, 1% Insulin-Transferrin-Selenium, 2% Pen/Strep, containing 5 μM 5-Azacytidine. 5-Azacytidine was also added at the next 2 days, and then the medium was refreshed. From day 6 forward, 1 mM Ascorbic Acid (AA) was added every 2 days and 1 ng/ml TGF-β1 twice weekly, while medium was refreshed every 2 days. The cells were collected after 25 days of differentiation for analysis. Undifferentiated, but over-confluent, cells were used as a control.

2.8. Oleic acid supplementation

CPCs P4 were seeded in 6-well plated for either 48 h, 1 week or 1 month, with the CDM basal medium (without any drug addition) supplemented with 75 μM, 150 μM and 300 μM OA conjugated to BSA. As a control, BSA supplemented CDM was used. The media was replenished every 2 days in all conditions.

Following the 25-day TGF-β1 differentiation, as described above, the differentiating cells were cultured in OA 300 μM-supplemented CDM, for either 1 week or 1 month.

2.9. ^{14}C-glucose oxidation measurement

Glucose oxidation was measured using the method of the Collins et al. (Wolfensohn and Lloyd, 2003) with some modifications. CPCs were seeded on gelatine-coated 24-well plates (20×10^4 cells/ well) and were grown in basal CDM medium as untreated "control" condition (CNTRL), differentiated or treated with OA for 48 h or 1 week. Subsequently, they were incubated for 4 h in no-glucose DMEM (A14430, Gibco, Life Technologies, Fisher Scientific – UK Ltd) supplemented with 12 mM glucose containing 0.185 MBq D-U-^{14}C-glucose (0.5 ml/ well). DMEM-alone was used as a negative CNTRL and wells without cells containing DMEM with ^{14}C-glucose were used to measure background radioactivity. A 24-well plate formed the lid of the apparatus with a perforated rubber gasket, with holes corresponding to each well, separating the two plates. The $^{14}CO_2$ produced by the glucose oxidation was trapped on KOH-soaked filter papers in the upper wells. To trigger the release of the $^{14}CO_2$, perchloric acid was added to the well, at each desired time-point, to kill the cells. Subsequently, the samples were kept for 1 h to allow for the release of dissolved $^{14}CO_2$. Filter papers containing trapped $^{14}CO_2$ were analysed using a scintillation counter, and the radiation counts per minute (CPM) were measured.

2.10. ^{3}H palmitate oxidation

CPCs were seeded in gelatine-coated 24-well plates (20×10^4 cells/ well) and were grown in basal CDM medium, as untreated CNTRL, differentiated or treated with OA for 48 h and 1 week. Subsequently the cells were incubated in no-glucose DMEM medium that was supplemented with 12 mM glucose, 300 μM palmitate, conjugated to 20 μM albumin and 0.022 MBq ^{3}H-palmitate for 6 h. Palmitate oxidation rates were determined by the production of ^3H_2O from the mitochondria (Barr and Lopaschuk, 1997; Belke et al., 1999). Perfusate aliquots contained both ^3H_2O and ^{3}H-palmitate, so the ^3H_2O was separated *via* Folch extraction. 1.88 ml of chloroform:methanol (1:2 *v*/v) solution, 625 μl chloroform and 625 μl KCl-HCl solution (2 M KCl, 0.4 M HCl) were added to 0.5 ml of the perfusate sample. The solution was rotated on a laboratory Stuart rotator SB3 at 40 rpm for 1 h before removing the top aqueous layer, while the organic layer was discarded. A solution of 1 ml choloform, 1 ml methanol and 0.9 ml KCl-HCl was added to the extracted aqueous solution, before further rotation for 1 h at 40 rpm. The top aqueous layer was once again removed and retained, and radioactivity was counted in counts per minute (CPM) using a scintillation counter. 0.5 ml medium at time 0 was used as a control to determine the specific activity of the buffer. For each aliquot sample, palmitate oxidation rates were calculated (Barr and Lopaschuk, 1997).

2.11. ^{3}H glucose measurement of glycolytic flux

CPCs were seeded in gelatine-coated 24-well plates (20×10^4 cells/ well) and were grown in in basal CDM medium, as an untreated CNTRL, differentiated or treated with OA for 48 h and 1 week. Subsequently, they were incubated for 6 h in no-glucose basal DMEM supplemented with 12 mM glucose containing 0.118 MBq ^{3}H-glucose. Glycolytic rates were determined through the conversion of ^{3}H -glucose to ^3H_2O *via* enolase which converts 2-phosphoglycerate to phosphoenolpyruvate and releases H_2O as a by-product. The samples contained both ^3H_2O and ^{3}H-glucose. Therefore, the ^3H_2O was separated from the ^{3}H-glucose using a Dowex 1 × 4 chloride form 100–200 mesh (Sigma, UK) anion exchange column. 250 g of Dowex resin was added to a 1.25 M NaOH and 1.61 M boric acid solution, and washed with distilled H_2O until pH < 7.5. Dowex resin was added to glass Pasteur pipettes plugged with glass wool and the columns were washed with distilled H_2O and allowed to drain. Then 200 μl of sample was added to each column allowing for the ^{3}H -glucose to bind to the column for 15′, and ^3H_2O to be eluted into scintillation vials. Distilled H_2O (2 ml) was added into the column to wash down any residual samples. Sample radioactivity was counted in counts per minute (CPM) using a scintillation counter.

2.12. Cell viability

To assess cell viability after Oleic Acid supplementation in the cell medium, treated CPCs were washed with PBS, trypsinised, and then counted using trypan blue stain, using both the standard haemocytometer approach and a Countess Automated Cell Counter (Invitrogen, Fisher Scientific – UK Ltd).

2.13. Statistical analysis

For all experiments (except for the case of mESCs) the 'n' number refers to biological replicates, that represent cells originating from different mice, and each tested once. The 'n' number for the EB mESCs represents technical replicates, of the donated cell line samples. Results are presented as means ± SE for qPCR and metabolic flux analyses, and means ± SD for other analyses. Differences were considered significant at $p < .05$, determined using analysis of variance with a Student's *t*-test. Experiments with > 2 test groups were assessed by a one-way analysis of variance (ANOVA) with a Tukey post-hoc test (GraphPad Prism 7).

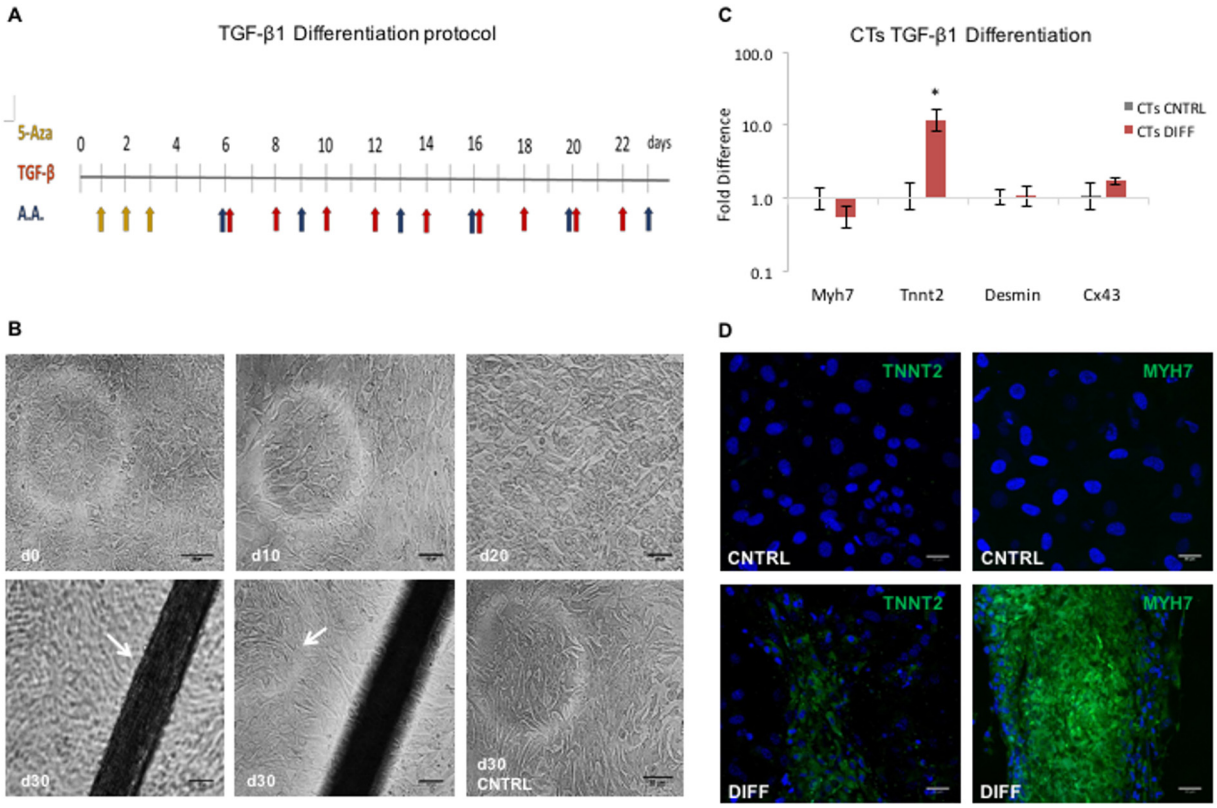

Fig. 1. Differentiation of CPCs: (A) Schematic representation of the timeline of the TGF-β1 differentiation protocol; yellow arrows mark the days when 5-Aza was added, blue is for Ascorbic Acid and red for TGF-β1. (B) Cell morphology of differentiating CPCs, at day 0, 10, 20 and 30, under light microscope. Arrow at d30 left image: indicating the tubular structure, at d30 right image: indicating the cell layer underneath the tubular structure (scale bars: 100 μm). (C) qPCR of differentiating CPCs normalised to the respective undifferentiated control samples ($n = 4$, $^*p < .002$, error bars: standard error). (D) Differentiated CPCs, expression of MYH7 and TNNT2 shown in green; a,b: control samples, c,d: differentiated samples. (blue: DAPI, scale bars: 30 μm). (For interpretation of the references to colour in this figure legend, the reader is referred to the web version of this article.)

3. Results

3.1. TGF-β1 differentiation increases expression of TNNT2 in mouse adult CPCs

To assess the differentiation potential of the CPCs (for CPC characterisation profile see Supplementary Material and Fig. S2), the TGF-β1/5-Azacytidine/Ascorbic Acid (A.A.) protocol was used (Fig. 1A). The differentiating CPCs ("DIFF") were monitored throughout, and at day 30 formed tubular structures (Fig. 1B). Gene expression analysis *via* qPCR showed a significant increase in cardiac troponin-T 2 (TnnT2) levels (Fig. 1C). The presence of TNNT2 and myosin heavy chain β (MYH7) was confirmed by immunocytochemistry, with the latter being confined to the organoids (Fig. 1D).

3.2. Stages of mESC differentiation VIA embryoid body formation

To characterise the metabolic changes we should expect to see during *in vitro* differentiation, a differentiating mESC line was used as a positive control. Agreeing with the anticipated genetic changes, the stemness genes (Oct4, Sox2, Sca1, Ckit) showed reduced expression as mESCs progressed from day 4 (EBs d4) to day 7 (EBs d7) of differentiation, while the early-onset cardiac markers (Gata4, Mef2c, Nkx2.5, Isl1) increased, as did the endothelial marker Flk1 (Fig. 2A). The gene expression of late-onset cardiac markers (Tnnt2 and Myh7) increased from day 4, through day 7 to day 14 (EBs d14) of differentiation. Expression of the insulin-sensitive glucose transporter Glut4 and the fatty acid transporter CD36 increased, while that of the glucose transporter Glut1, predominant at the fetal stage, was reduced (Fig. 2B). PPARα expression was unchanged from day 4 to day 7 of embryoid body differentiation and then showed an 8-fold increase. Pgc-1α was upregulated on day 7 and then downregulated when the cells were terminally differentiated (Fig. 2C).

3.3. Oleic acid supplementation stimulates the PPARα pathway in mouse adult CPCs

To investigate the effect of FAs as a cell culture substrate, the CPC culture medium was supplemented with OA. The effect of 75 μM, 150 μM or 300 μM of OA on cell viability was checked and was not found to be toxic (Fig. 3B). 300 μM was selected as the highest dose because high levels of FA have been shown to be cytotoxic (De Sousa Andrade et al., 2005; Haeiwa et al., 2014). PGC-1α expression was significantly upregulated as the concentration of OA increased, but PPARα expression did not change (Fig. 3C). Since the OA supplement was pre-conjugated with BSA, the gene expression of PPARα and PGC-1α was also compared to the untreated controls which had been supplemented with BSA, at the respective concentrations. Both PPARα and PGC-1α expression increased > 5-fold with 300 μM of OA, compared to the BSA controls (Supplementary Fig. S3).

3.4. Oleic acid supplementation metabolically matures mouse adult CPCs

To test the long-term effect of OA treatment on the metabolism of CPCs, gene expression levels were investigated after treatment of CPCs with OA 300 μM for 48 h, 1 week and 1 month. The CPC morphology was observed for whole period, during which cells kept proliferating and no cell death was observed (Fig. 4A).

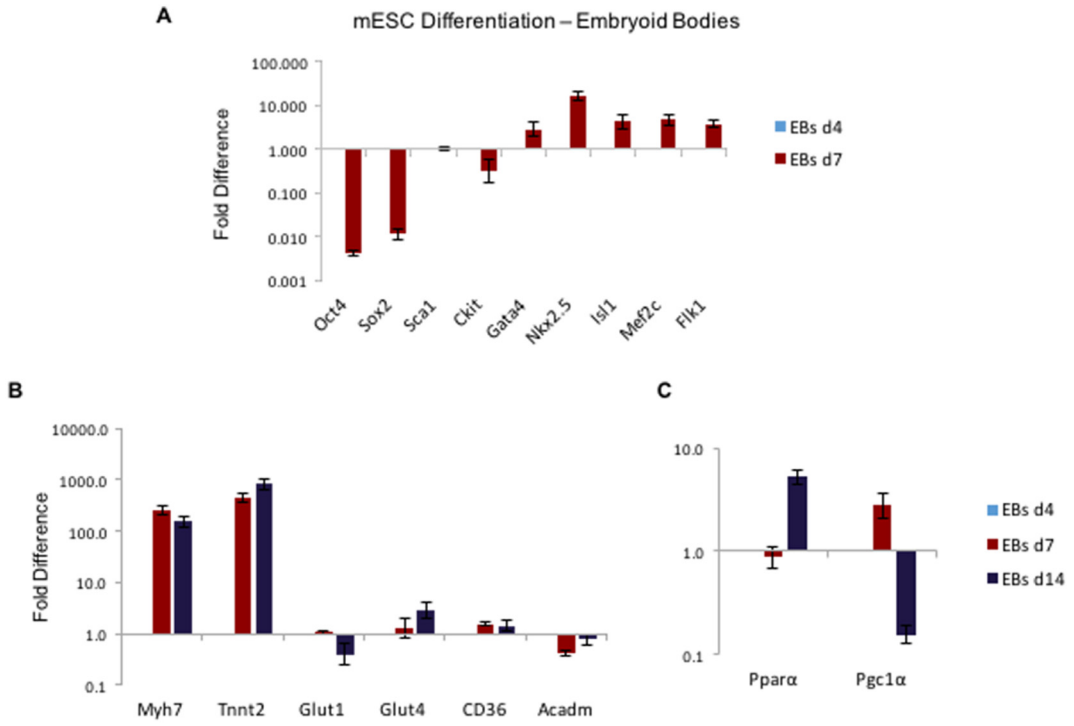

Fig. 2. Gene expression in differentiating ESCs: (A) Gene expression levels of stemness markers (Oct4, Sox2, Sca1, Ckit), early-onset cardiac (Gata4, Mef2c, Nkx2.5, Isl1) and endothelial (Flk1) markers in mESCs at d4 and d7 of differentiation of ESCs to CMs, normalised to EBs d4. (B) Gene expression levels of late-onset cardiac markers (TnnT2 and Myh7) and Glut1, Glut4 in mESCs at d4, d7 and d14 of differentiation to CMs, normalised to EBs d4. (C) Gene expression levels of PPARα and Pgc1α in mESCs at d4, d7 and d14 of differentiation to CMs, normalised to EBs d4 ($n = 3$).

PGC-1α gene expression was significantly upregulated after 48 h and then decreased (Fig. 4B). PPARα and Glut4 were also significantly upregulated with OA supplementation (Fig. 4B). Pdk4 significantly increased with OA addition at all time-points, as did the fatty acid translocase receptor CD36, which functions as an OA receptor (Fig. 4B). No change in gene expression of citrate synthase (Cs) was observed (Fig. 4B).

To investigate mitochondrial activity, CPCs were incubated with

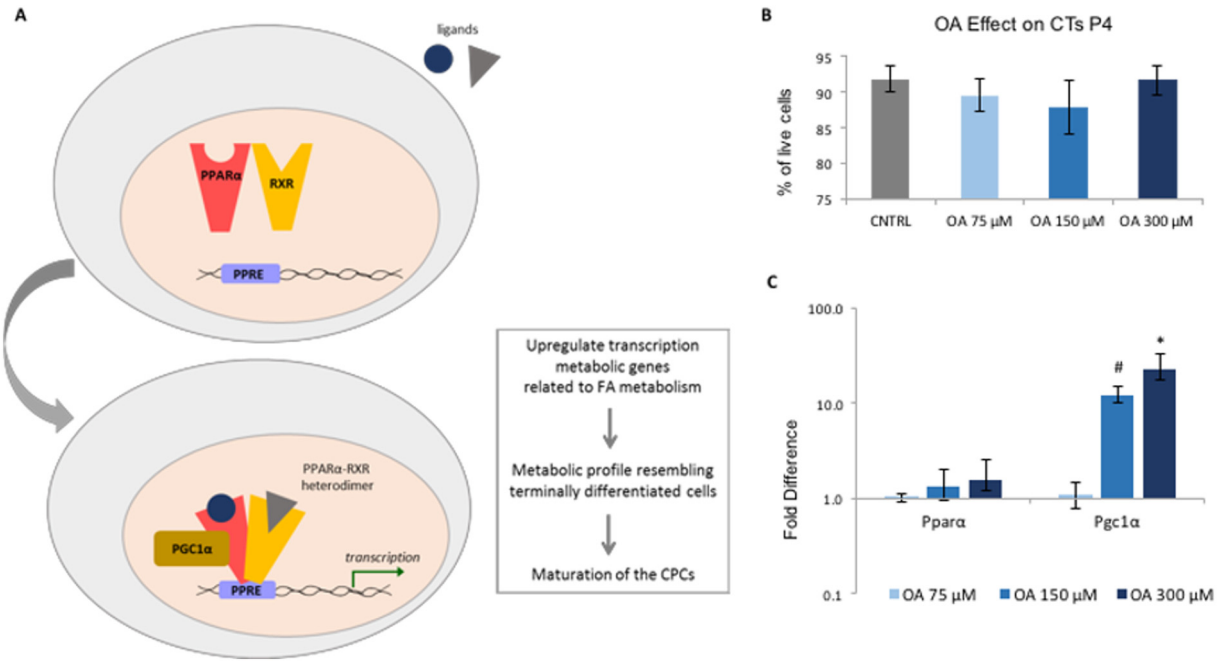

Fig. 3. OA stimulation of the PPARα pathway: (A) Schematic representation of the PPARα/PGC-1α axis: PPARα binds to RXR, the heterodimer is activated by ligands and PGC-1α acts as a co-activator for PPARα. The heterotrimer binds to the PPARα response element (PPRE), in the promoter of target genes. (B) The effect of 75 µM, 150 µM or 300 µM of OA on cell viability after 1 week of incubation. (C) Effect of 48 h supplementation with OA at increased concentrations. Effect of OA 75 µM, 150 µM, 300 µM on the expression of PPARα, PGC-1α in P4 CPCs, normalised to OA 75 µM. (n = 4, $*p < .02$, $\#p < .01$, indicating difference to OA 75 µM; error bars: standard error).

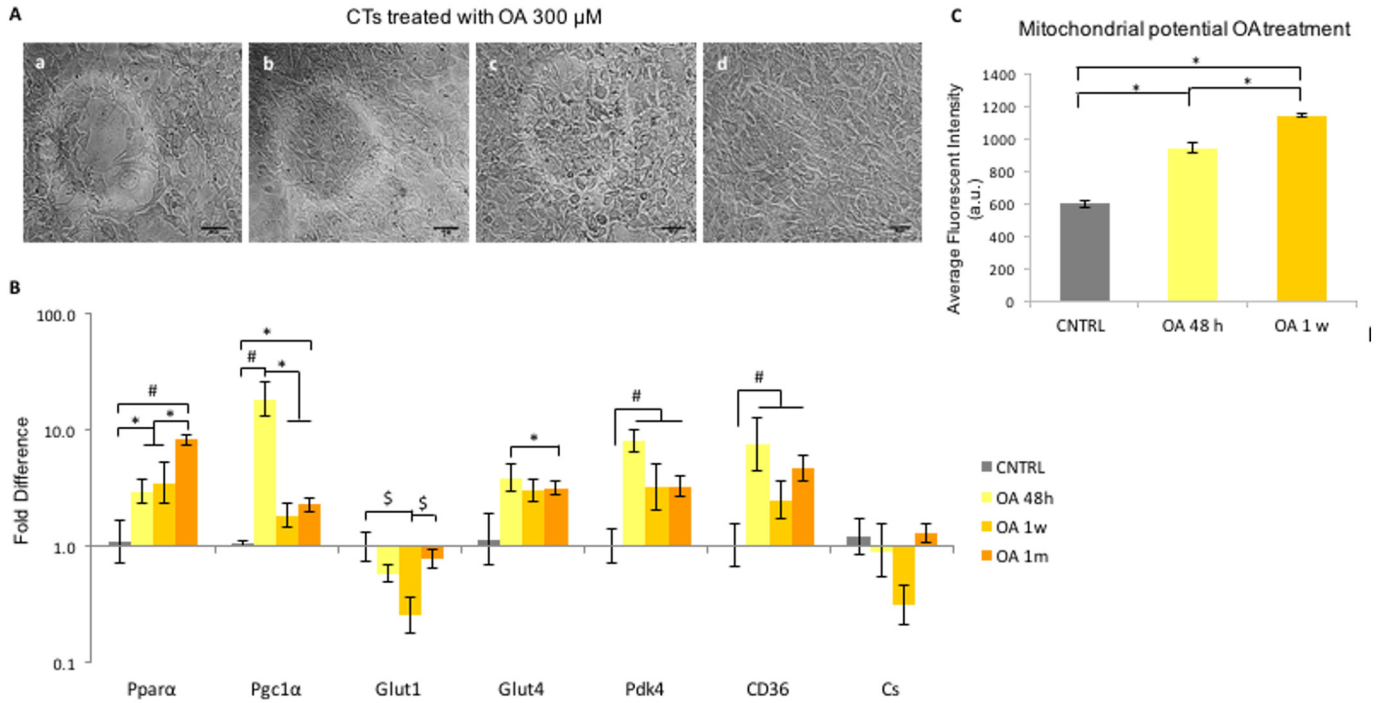

Fig. 4. Long-term stimulation with OA: (A) P4 CPCs treated with OA for 48 h (4a), 1 week (4b) and 1 month (4c), as well as untreated CPCs grown for 1 month (scale bars: 100 μm). (B) Effect of 48 h, 1 week, 1 month supplementation of P4 CPCs with OA on the expression of metabolic genes, normalised to control untreated CPCs. (n = 3; error bars: standard error, $*p < .05$, #p < .02). (C) Effect of OA treatment for 48 h and 1 week, estimated as average fluorescent intensity, after staining with MitoTracker Red CMXRos red. $*p <$ 0,00001 normalised to untreated CNTRL, and OA 48-h treatment, respectively. (For interpretation of the references to colour in this figure legend, the reader is referred to the web version of this article.)

MitoTracker® Red CMXRos. CNTRL untreated CPCs were compared to 48 h of OA treatment, and 1 week of OA supplementation (Fig. 4C). A significant increase in fluorescence was observed following prolongation of the OA treatment (Fig. 4C, Supplemental Fig. S4), suggesting that the mitochondria were more active, since the CMXRos dye accumulates in live cells based on the mitochondrial membrane potential (Cottet-Rousselle et al., 2011).

The level of substrate utilisation was assessed using radioactive tracer analysis. After supplementing the CPCs with OA for 48 h and 1 week, glucose oxidation was increased significantly (Fig. 5A), glycolytic flux was significantly reduced after 1 week of OA incubation (Fig. 5B), while FA oxidation remained unchanged (Fig. 5C). Despite these changes, qPCRanalysis showed no significant change in the gene expression of Tnnt2 or Cx43 after treatment with OA at any time point (Fig. 5D). Myh6 and Myh7 were not expressed under any of the conditions.

3.5. Oleic acid addition further matures differentiated CPCS functionally and metabolically

Based on the data indicating upregulation of the PPARα pathway after OA treatment of CPCs, OA was used after TGF-β1 differentiation ("DIFF + OA") to assess whether differentiated cells could be matured metabolically. The differentiating CPCs formed cell clusters as before (Fig. 6A), but with the OA treatment the cells surrounding them were smaller than in the non-treated samples. qPCR analysis of mature cardiac genes (Myh7, Tnnt2, Cx43) showed that both Myh7 and Cx43, which were unchanged after differentiation (Fig. 1C), were significantly upregulated after OA treatment. Tnnt2 gene expression did not increase further (Fig. 6B). Immunocytochemistry confirmed the expression of MYH7 and TNNT2 in the differentiated CPCs treated with OA (Fig. 6C). Filamentous actin (fActin) staining, to assess the shape and structural components of the cells, did not indicate any CM-like striations (Fig. 6C).

The TGF-β1 protocol increased gene expression of both PPARα and PGC-1α. Addition of OA for 1 week maintained the PPARα gene expression at the same level, but PGC-1α expression decreased (Fig. 7A). Glut1 gene expression was significantly downregulated after OA treatment, accompanied by a significant increase in Glut4 expression after TGF-β1 differentiation, which increased further following OA treatment. Pdk4 and Cs expression remained unchanged in both treatments (Fig. 7A). Assessment of the mitochondrial membrane potential, showed an increase in the fluorescence between the CNTRL undifferentiated CPCs, compared to the DIFF group and the DIFF + OA differentiated CPCs (Supplemental Fig. S5), (Fig. 7B).The glucose oxidation rates were increased after differentiation with TGF-β1, and afterwards further in differentiated cells treated with OA compared with rates in CNTRL undifferentiated cells (Fig. 7C). FA oxidation (Fig. 7E) increased in differentiated cells treated with OA, whereas rates of glycolytic flux which had been significantly increased by differentiation alone, were further elevated with OA treatment (Fig. 7D).

4. Discussion

To our knowledge, this is the first report that investigates the effect of fatty acid supplementation on adult cardiac progenitors, using metabolic flux analyses, focusing on optimising differentiation efficiency. Our results shed light on the metabolic profile of differentiating CPCs and highlight the importance of substrate availability, and the PPARα pathway, in this process.

Different groups have used the TGF-β1 family (Smits et al., 2009; Goumans et al., 2008; Ye et al., 2012) and 5-Aza (Oh et al., 2003; Qian et al., 2012; Goumans et al., 2008) on various cardiac cell types to induce cardiac differentiation *in vitro*. The methods of assessment of the level of CPC differentiation vary, but entail changes in cell morphology, as well as expression of markers such as Tnnt2, Myh7 and Cx43 (Goumans et al., 2008; Qian et al., 2012; Linke et al., 2005). Smits et al. (Smits et al., 2009) observed that cells formed multiple layers with

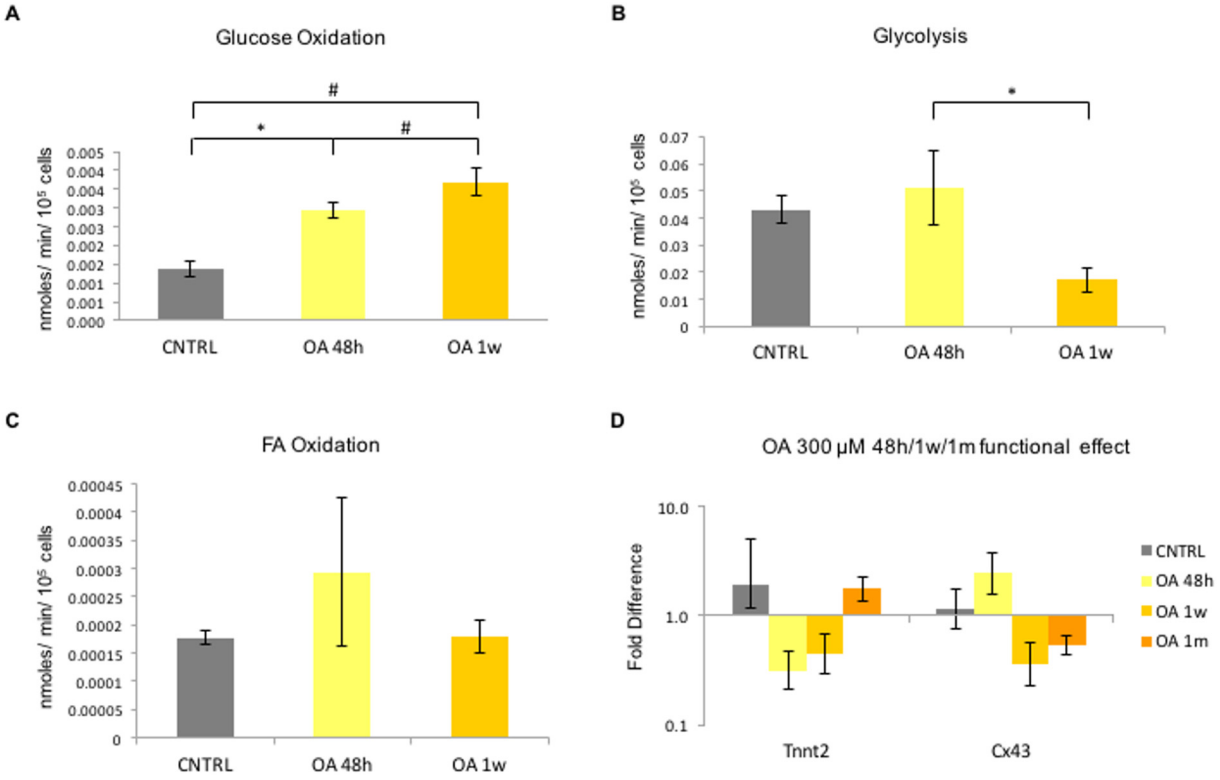

Fig. 5. OA supplementation affects substrate metabolism: Effect of supplementation with OA on (A) glucose oxidation levels, (B) Glycolysis and (C) FA Oxidation levels, measured as nMoles/min/10^5 cells, compared to control untreated CPCs. (n = 4; *$p < .04$, #$p < .01$ indicating differences amongst the groups, error bars: standard error); and D) on the expression of differentiation genes in P4 CPCs normalised to control untreated CPCs. (n = 3; error bars: standard error).

different alignments and confluency, after TGF-β1 differentiation of selected Sca1$^+$ CPCs, as well as upregulation in Tnnt2, Cx43 and Myh7, which agrees with our observation of cell culture morphology and marker expression (Fig. 1B and C). The pattern of MYH7 expression was concentrated within the tubular structures (Fig. 1D), suggesting that there was still a fraction of undifferentiated cells growing around the differentiating ones, which may indicate that cells need to be highly confluent for efficient differentiation. The main cell culture issue that we faced, had to do with the fact that the cells were difficult to dissociate as they formed clumps after the differentiation of month. Subsequently, the cells were trypsinised, before pelleting for RNA extraction, which did not work well with the cell clusters in the differentiated samples, which may have biased the analysis of gene expression to the easily-dissociated monolayer cells (Fig. 1C).

The upregulation of cardiac transcription factors, shown in studies of hESC differentiation (Kehat et al., 2004; Xu, 2002) and mESC (Sachinidis et al., 2003; Fijnvandraat et al., 2003) into CMs, as well as MHC and Troponin (Fijnvandraat et al., 2003; Van Laake et al., 2005), matched those seen in the differentiating mESCs at d4, d7 and d14. (Fig. 2A). The downregulation of Glut1 and upregulation of Glut4 observed has been reported as an indication of the metabolic maturation of cells (Wang and Hu, 1991; Studelska et al., 1992; Postic et al., 1994) (Fig. 2B). The early increase in PGC-1α could indicate upregulation of the mitochondrial metabolism early in the differentiating SCs (Chung et al., 2010; Porter et al., 2011; Lehman et al., 2000), followed by an increase in PPARα, as seen previously in murine cardiac differentiation *in vitro* (Ding et al., 2007b; Vega et al., 2000) (Fig. 2C). These observations suggested that the mESCs differentiating to beating CMs *in vitro* recapitulate the metabolic shift towards oxidative metabolism and express mature cardiac cell markers, rendering them a good control for this study.

After identifying the metabolic changes characterising successful differentiation of mESCs to beating CMs, we proceeded to study the metabolism of differentiating mouse adult CPCs. The upregulation of PPARα and PGC-1α after OA supplementation (Fig. 2C &3C) agrees with OA, and FAs in general, being activators of the PPARα pathway (Popeijus et al., 2014; Göttlicher et al., 1992). Pdk4, which has been shown to be upregulated by PGC-1α (Wende et al., 2005) was upregulated at 48 h, while CD36, which mediates the uptake of fatty acids in a variety of cell types (Pepino et al., 2014); Coburn et al., 2001), was upregulated at all time-points (Fig. 3B). The shift from Glut1 to Glut4 was similar to that seen with mESC differentiation, consistent with cell maturation (Wang and Hu, 1991; Studelska et al., 1992; Postic et al., 1994) (Figs. 3B & 2B). Also, OA treatment increased mitochondrial membrane potential (Figs. 4C & Supplementary Figs. S4 & S5) after 48 h and 1 week of treatment. The effect was on mitochondrial activity, rather than the mitochondrial numbers, since CS was found unchanged – both of which are necessary for cell maturation (Porter et al., 2011).

Glucose oxidation was upregulated significantly, while glycolytic flux decreased, after 1 week of OA treatment, suggesting a shift towards a more mature metabolic phenotype, but FA oxidation rates were unchanged (Fig. 5A, B and C). This is the first study assessing the metabolism of differentiating adult CPCs *in vitro,* so there is no prior evidence of the expected metabolic profile. It may be that the OA-treated cells required a longer supplementation period in order to significantly upregulate FA oxidation, or that the undifferentiated cells obtained sufficient energy from glucose oxidation.

To investigate whether the metabolic effect that followed the OA treatment could assist the differentiation of adult CPCs, the cell culture medium was supplemented for 1 week following the TGF-β1 differentiation protocol. The gene expression changes of the OA-treated differentiated CPCs revealed a more structurally mature phenotype, with both Myh7 and Cx43 being significantly upregulated (Fig. 6B). In addition, TGF-β1 differentiation alone was sufficient to stimulate the PPARα – PGC-1α pathway, as well as a shift from Glut1 to Glut4 gene expression (Fig. 7A), as seen during the mESC differentiation

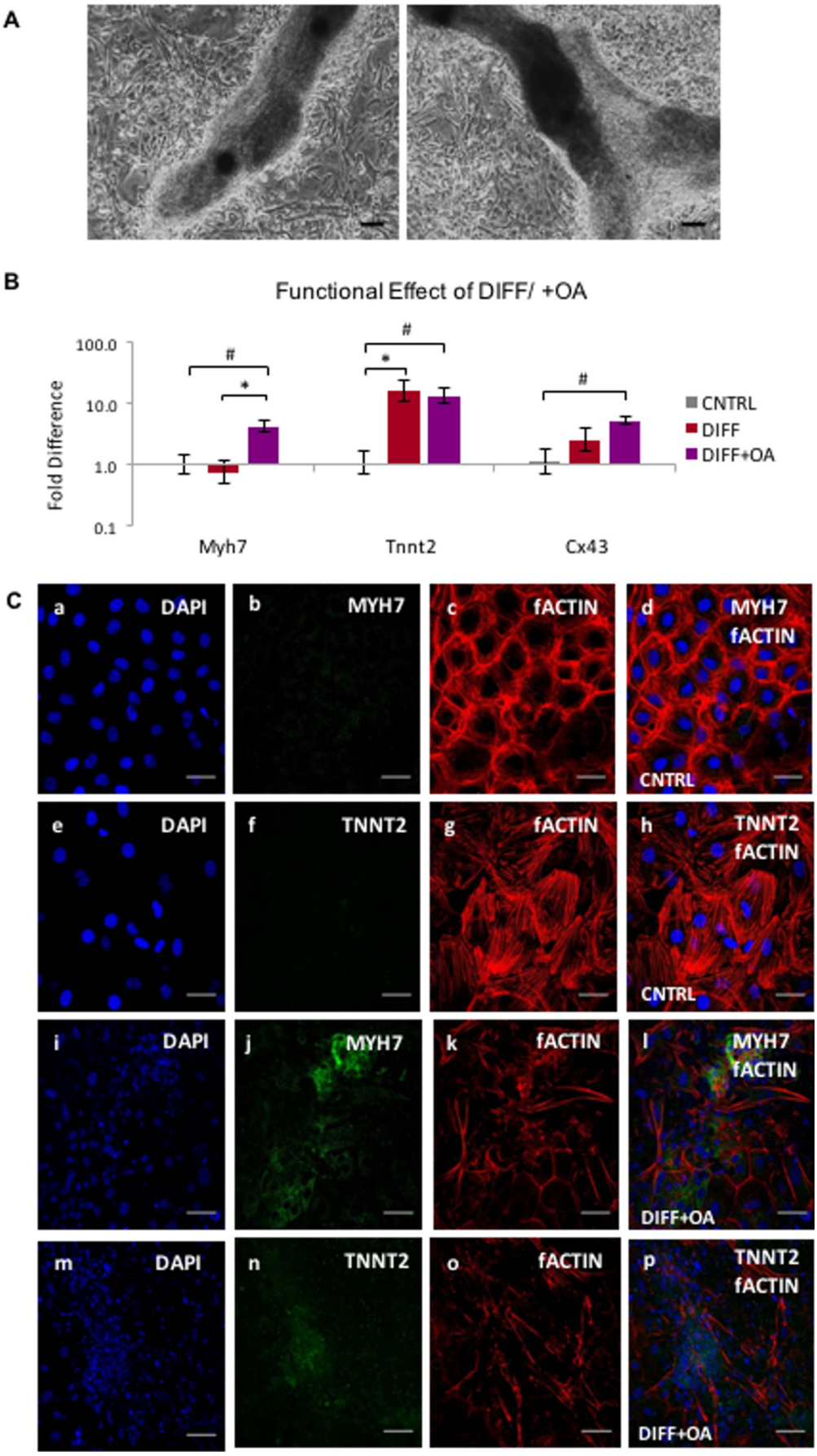

Fig. 6. OA supplementation of differentiating CPCs: (A) Cell morphology of CPCs differentiated using the TGF-β1 protocol, followed by 1 week of OA 300 μM supplementation, under light microscope (scale bars: 100 μM). (B) Effect of OA treatment post-differentiation on CPCs, compared to non-treated differentiated CPCs and CNTRL undifferentiated P4 CPCs. (n = 4, *p < .02, $p < .01 compared to CNTRL, error bars: standard error). (C) Immunocytochemistry on control undifferentiated samples (top two rows) and differentiated samples with OA addition (DIFF + OA; bottom two rows). (MYH7 and TNNT2 shown in green, co-stained with DAPI in blue, scale bars: 50 μm). (For interpretation of the references to colour in this figure legend, the reader is referred to the web version of this article.)

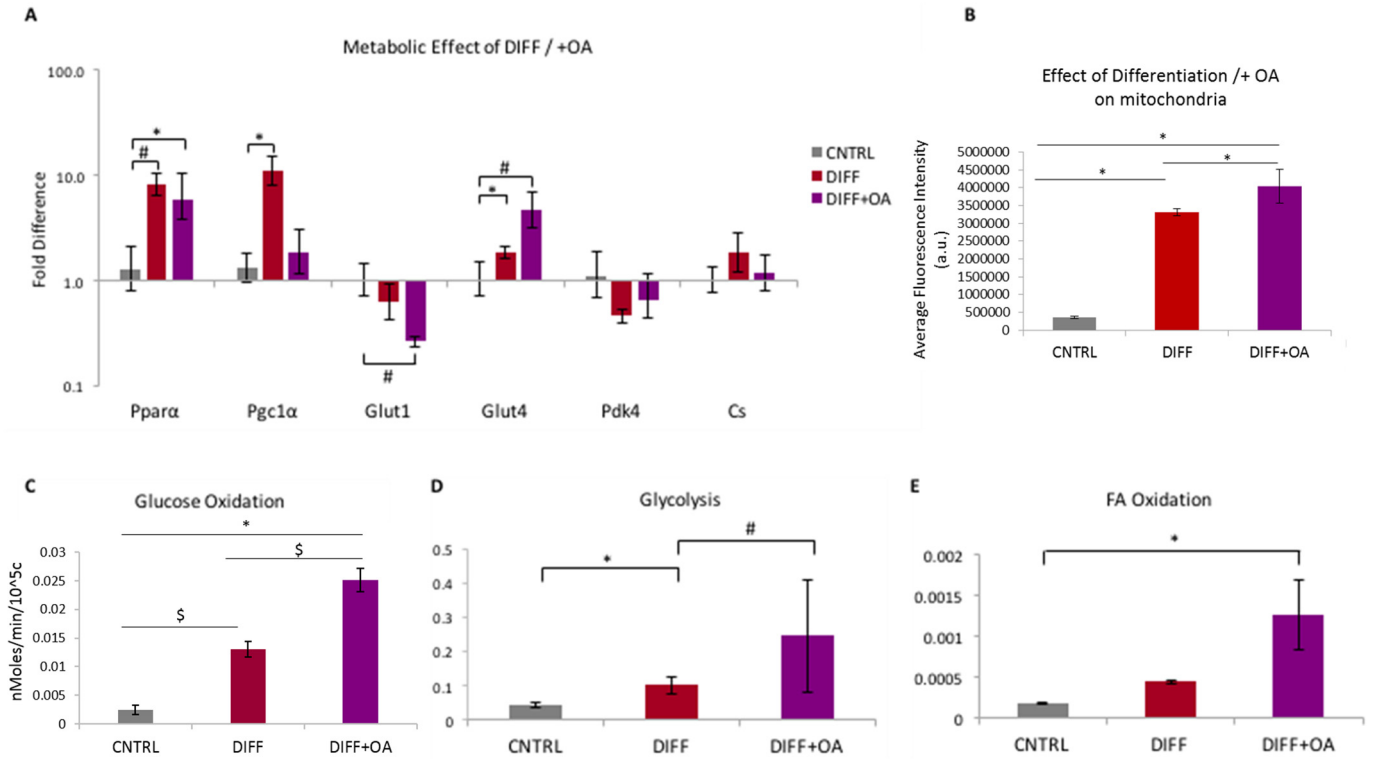

Fig. 7. OA supplementation affects substrate metabolism in differentiated CPCs: (A) Metabolic effect of 1 week supplementation with OA post-differentiation on gene expression in CPCs, compared to non-treated differentiated CPCs and CNTRL undifferentiated CPCs. (n = 4, *p < 0,05, $p < 0,01 indicating difference to CNTRL, error bars: standard error). (B) Effect of differentiation, and differentiation followed by 1 week of OA 300 μM, on cell mitochondria, estimated as average fluorescent intensity, after staining with MitoTracker Red CMXRos red. (n = 12 cells, 3 replicates, *p < .001). (C) Effect of TGF-β1 differentiation, and differentiation followed by 1 week supplementation with OA, on the glucose oxidation levels, (D) Glycolysis, and E) FA Oxidation, measured as nMoles/ min/ 10^5 cells, normalised to control untreated CPCs. (n = 3; *p < .03, #p < .01, $p < .001 indicating differences amongst the groups, error bars: standard error). (For interpretation of the references to colour in this figure legend, the reader is referred to the web version of this article.)

previously. PPARα and PGC-1α are upregulated during differentiation (Ding et al., 2007b), and the expression of GLUT4 is higher in adult tissues (Wang and Hu, 1991; Studelska et al., 1992; Postic et al., 1994), suggesting that TGF-β1 differentiation induces a degree of metabolic maturation.

Addition of OA after differentiation retained the levels of PPARα, Glut1 and Glut4, but led to a reduction in PGC-1α (Fig. 7A), a decrease that was also seen at d14 of mESCs progressing to terminal differentiation (Fig. 2C), and after long-term exposure of CNTRL cells with OA (Fig. 4B). This could suggest that PGC-1α does not need to be constitutively upregulated after changes have been induced, although Birket et al. reported consistent activation of PGC-1α in ESCs during cardiomyocyte differentiation (Birket et al., 2013).

Glucose and FA oxidation, as well as glycolytic flux, were significantly upregulated in the TGF-β1 differentiated CPCs treated with OA (Fig. 7C, D and E), indicating a holistic metabolic maturation of the differentiated cells after OA supplementation. The TGF-β1 differentiated CPCs seem to acquire a more mature metabolic phenotype (because of the pharmacological agent), and respond differently to undifferentiated CPCs when OA is added, by upregulating FA oxidation. The fact that OA supplementation had a positive effect in the maturation of the differentiated CPCs came as no surprise, given the recent study from Correia et al. (Correia et al., 2017) that demonstrated the importance of the metabolic shift in the maturation of hPSC-CMs. The hPSCs that were supplemented with FAs had enhanced differentiated profile with increased oxidative metabolism and functional maturation, compared to those grown in the standard glucose media, a finding that agrees with our observations. In this study the FA treatment entailed combination of both oleic and palmitic acids, as well as galactose, whereas we only used oleic acid, but it would be interesting to explore a better combination of substrates that can enhance cardiac differentiation to mature CMs from adult cardiac progenitors.

5. Conclusions

This is the first study that uses radiolabelled substrate consumption for metabolic flux analyses of adult cardiac progenitors, after FA supplementation, with the aim to enhance their cardiac differentiation. In addition, we explore the role of the PPARα/PGC-1α axis during metabolic manipulation.

We have shown that OA supplementation matured both control and differentiated cells metabolically, while also increased the expression of cardiac markers in the latter. In addition we highlight that the PPARα pathway was stimulated by cardiac differentiation in both CPCs and mESCs. Our results allow for a better understanding of the effect of fatty acids, on cardiac differentiation of adult cardiac progenitors, complementing the metabolic manipulation studies of hPSC-CMs, and development of a protocol that would allow for more efficient differentiation to mature CMs.

Supplementary data to this article can be found online at https://doi.org/10.1016/j.scr.2019.101458.

Acknowledgements

We thank Dr. Richard Tyser and Professor Paul Riley for donation of the differentiating mESCs.

We would also like to thank Dr. Vicky Ball for her technical support and training she provided for the radioactive experiments.

Author contributions

Sophia Malandraki-Miller: Conception and design, Collection and assembly of data, Data analysis and interpretation, Manuscript writing, Manuscript revisions and final approval.

Colleen Lopez: Collection and assembly of data, Data analysis and interpretation.

Ujang Purnama: Collection and assembly of data for the revision corrections.

Rita Alonaizan: Collection and assembly of data for the revision corrections.

Filippo Perbellini: Provided support and consulting for experimental techniques.

Kathy Pakzad: Initial set up of the ^{14}C-Glucose Oxidation Measurement technique.

Carolyn Carr: Conception and design, Financial support, Administrative support, Data analysis and interpretation, Manuscript writing, Final approval of manuscript.

Funding

This work was supported by the British Heart Foundation (PG/13/34/30216) and the Rosetrees Trust (M315).

Declarations of interest

None.

References

Barr, R.L., Lopaschuk, G.D., 1997. Direct measurement of energy metabolism in the isolated working rat heart. J. Pharmacol. Toxicol. Methods 38, 11–17. https://doi.org/10.1016/S1056-8719(97)86574-4.

Belke, D.D., Larsen, T.S., Lopaschuk, G.D., Severson, D.L., 1999. Glucose and fatty acid metabolism in the isolated working mouse heart. Am. J. Phys. 277, R1210–R1217.

Birket, M.J., Casini, S., Kosmidis, G., Elliott, D.A., Gerencser, A.A., Baartscheer, A., Schumacher, C., Mastroberardino, P.G., Elefanty, A.G., Stanley, E.G., Mummery, C.L., 2013. PGC-1?? and reactive oxygen species regulate human embryonic stem cell-derived cardiomyocyte function. Stem Cell Rep. 1, 560–574. https://doi.org/10.1016/j.stemcr.2013.11.008.

Boheler, K.R., Czyz, J., Tweedie, D., Yang, H.T., Anisimov, S.V., Wobus, A.M., 2002. Differentiation of pluripotent embryonic stem cells into cardiomyocytes. Circ. Res. https://doi.org/10.1161/01.RES.0000027865.61704.32.

Chung, S., Arrell, D.K., Faustino, R.S., Terzic, A., Dzeja, P.P., 2010. Glycolytic network restructuring integral to the energetics of embryonic stem cell cardiac differentiation. J. Mol. Cell. Cardiol. 48, 725–734. https://doi.org/10.1016/j.yjmcc.2009.12.014.

Correia, C., Koshkin, A., Duarte, P., Hu, D., Teixeira, A., Domian, I., Serra, M., Alves, P.M., 2017. Distinct carbon sources affect structural and functional maturation of cardiomyocytes derived from human pluripotent stem cells. Sci. Rep. https://doi.org/10.1038/s41598-017-08713-4.

Cottet-Rousselle, C., Ronot, X., Leverve, X., Mayol, J.F., 2011. Cytometric assessment of mitochondria using fluorescent probes. Cytom. Part A. https://doi.org/10.1002/cyto.a.21061.

De Sousa Andrade, L.N., De Lima, T.M., Curi, R., De Lauro Castrucci, A.M., 2005. Toxicity of fatty acids on murine and human melanoma cell lines. Toxicol. in Vitro 19, 553–560. https://doi.org/10.1016/j.tiv.2005.02.002.

DeBerardinis, R.J., Mancuso, A., Daikhin, E., Nissim, I., Yudkoff, M., Wehrli, S., Thompson, C.B., 2007. Beyond aerobic glycolysis: transformed cells can engage in glutamine metabolism that exceeds the requirement for protein and nucleotide synthesis. Proc. Natl. Acad. Sci. U. S. A. 104, 19345–19350. https://doi.org/10.1073/pnas.0709747104.

Ding, L., Liang, X.-G., Lou, Y.-J., 2007a. Time-dependence of cardiomyocyte differentiation disturbed by peroxisome proliferator-activated receptor alpha inhibitor GW6471 in murine embryonic stem cells in vitro. Acta Pharmacol. Sin. 28, 634–642. https://doi.org/10.1111/j.1745-7254.2007.00558.x.

Ding, L., Liang, X., Zhu, D., Lou, Y., 2007b. Peroxisome proliferator-activated receptor alpha is involved in cardiomyocyte differentiation of murine embryonic stem cells in vitro. Cell Biol. Int. 31, 1002–1009. https://doi.org/10.1016/j.cellbi.2007.03.013.

Fijnvandraat, A.C., Van Ginneken, A.C.G., Schumacher, C.A., Boheler, K.R., Lekanne Deprez, R.H., Christoffels, V.M., Moorman, A.F.M., 2003. Cardiomyocytes purified from differentiated embryonic stem cells exhibit characteristics of early chamber myocardium. J. Mol. Cell. Cardiol. 35, 1461–1472. https://doi.org/10.1016/j.yjmcc.2003.09.011.

Finck, B.N., Lehman, J.J., Leone, T.C., Welch, M.J., Bennett, M.J., Kovacs, A., Han, X., Gross, R.W., Kozak, R., Lopaschuk, G.D., Kelly, D.P., 2002. The cardiac phenotype induced by PPARa overexpression mimics that caused by diabetes mellitus. J. Clin. Invest. 109, 121–130. https://doi.org/10.1172/JCI200214080.

Göttlicher, M., Widmark, E., Li, Q., Gustafsson, J.A., 1992. Fatty acids activate a chimera of the clofibric acid-activated receptor and the glucocorticoid receptor. Proc. Natl. Acad. Sci. U. S. A. 89, 4653–4657. https://doi.org/10.1073/pnas.89.10.4653.

Goumans, M.-J., de Boer, T.P., Smits, A.M., van Laake, L.W., van Vliet, P., Metz, C.H.G., Korfage, T.H., Kats, K.P., Hochstenbach, R., Pasterkamp, G., Verhaar, M.C., van der Heyden, M.A.G., de Kleijn, D., Mummery, C.L., van Veen, T.A.B., Sluijter, J.P.G., Doevendans, P.A., 2008. TGF-β1 induces efficient differentiation of human cardiomyocyte progenitor cells into functional cardiomyocytes in vitro. Stem Cell Res. 1, 138–149. https://doi.org/10.1016/j.scr.2008.02.003.

Gulick, T., Cresci, S., Caira, T., Moore, D.D., Kelly, D.P., 1994. The peroxisome proliferator-activated receptor regulates mitochondrial fatty acid oxidative enzyme gene expression. Proc. Natl. Acad. Sci. U. S. A. 91, 11012–11016.

Haeiwa, H., Fujita, T., Saitoh, Y., Miwa, N., 2014. Oleic acid promotes adaptability against oxidative stress in 3T3-L1 cells through lipohormesis. Mol. Cell. Biochem. 386, 73–83. https://doi.org/10.1007/s11010-013-1846-9.

Handschin, C., Spiegelman, B.M., 2006. Peroxisome proliferator-activated receptor a coactivator 1 coactivators, energy homeostasis, and metabolism. Endocr. Rev. 27, 728–735. https://doi.org/10.1210/er.2006-0037.

Hu, D., Linders, A., Yamak, A., Correia, C., Kijlstra, J.D., Garakani, A., Xiao, L., Milan, D.J., van der Meer, P., Serra, M., Alves, P.M., Domian, I.J., 2018. Metabolic maturation of human pluripotent stem cell-derived cardiomyocytes by inhibition of HIF1α and LDHA. Circ. Res. https://doi.org/10.1161/CIRCRESAHA.118.313249.

Kehat, I., Khimovich, L., Caspi, O., Gepstein, A., Shofti, R., Arbel, G., Huber, I., Satin, J., Itskovitz-Eldor, J., Gepstein, L., 2004. Electromechanical integration of cardiomyocytes derived from human embryonic stem cells. Nat. Biotechnol. 22, 1282–1289. https://doi.org/10.1038/nbt1014.

Kolwicz, S.C., Purohit, S., Tian, R., 2013. Cardiac metabolism and its interactions with contraction, growth, and survival of cardiomyocytes. Circ. Res. https://doi.org/10.1161/CIRCRESAHA.113.302095.

Lehman, J.J., Barger, P.M., Kovacs, A., Saffitz, J.E., Medeiros, D.M., Kelly, D.P., 2000. Peroxisome proliferator-activated receptor gamma coactivator-1 promotes cardiac mitochondrial biogenesis. J. Clin. Invest. 106, 847–856. https://doi.org/10.1172/JCI10268.

Linke, A., Müller, P., Nurzynska, D., Casarsa, C., Torella, D., Nascimbene, A., Castaldo, C., Cascapera, S., Böhm, M., Quaini, F., Urbanek, K., Leri, A., Hintze, T.H., Kajstura, J., Anversa, P., 2005. Stem cells in the dog heart are self-renewing, clonogenic, and multipotent and regenerate infarcted myocardium, improving cardiac function. Proc. Natl. Acad. Sci. U. S. A. 102, 8966–8971. https://doi.org/10.1073/pnas.0502678102.

Livak, K.J., Schmittgen, T.D., 2001. Analysis of relative gene expression data using real-time quantitative PCR and the 2ˆ- ΔΔCT Method. Methods 25, 402–408. https://doi.org/10.1006/meth.2001.1262.

Madeira, V.M.C., 2012. Overview of mitochondrial bioenergetics. Methods Mol. Biol. 810, 1–6. https://doi.org/10.1007/978-1-61779-382-0_1.

Malandraki-Miller, S., Lopez, C.A., Al-Siddiqi, H., Carr, C.A., 2018. Changing metabolism in differentiating cardiac progenitor cells-can stem cells become metabolically flexible cardiomyocytes? Front Cardiovasc Med. 5, 119. https://doi.org/10.3389/fcvm.2018.00119.

Nuclear Receptors Nomenclature, C, 1999. A unified nomenclature system for the nuclear receptor superfamily. Cell 97, 161–163. https://doi.org/10.1016/S0092-8674(00)80726-6.

Oh, H., Bradfute, S.B., Gallardo, T.D., Nakamura, T., Gaussin, V., Mishina, Y., Pocius, J., Michael, L.H., Behringer, R.R., Garry, D.J., Entman, M.L., Schneider, M.D., 2003. Cardiac progenitor cells from adult myocardium: homing, differentiation, and fusion after infarction. Proc. Natl. Acad. Sci. U. S. A. 100, 12313–12318. https://doi.org/10.1073/pnas.2132126100.

Pepino, M.Y., Kuda, O., Samovski, D., Abumrad, N. a, 2014. Structure-function of CD36 and importance of fatty acid signal transduction in fat metabolism. Annu. Rev. Nutr. 34, 281–303. https://doi.org/10.1146/annurev-nutr-071812-161220.

Perbellini, F., Gomes, R.S.M., Vieira, S., Buchanan, D., Malandraki-Miller, S., Bruyneel, A., et al., 2015. Chronic high-fat feeding affects the mesenchymal cell population expanded from adipose tissue but not cardiac atria. Stem Cells Transl. Med. 4, 1403–1414. https://doi.org/10.5966/sctm.2015-0024.

Popeijus, H.E., van Otterdijk, S.D., van der Krieken, S.E., Konings, M., Serbonij, K., Plat, J., Mensink, R.P., 2014. Fatty acid chain length and saturation influences PPARα transcriptional activation and repression in HepG2 cells. Mol. Nutr. Food Res. https://doi.org/10.1002/mnfr.201400314.

Porter, G.A., Hom, J.R., Hoffman, D.L., Quintanilla, R.A., Bentley, K.L. de M., Sheu, S.S., 2011. Bioenergetics, mitochondria, and cardiac myocyte differentiation. Prog. Pediatr. Cardiol. 31, 75–81. https://doi.org/10.1016/j.ppedcard.2011.02.002.

Postic, C., Leturque, A., Printz, R.L., Maulard, P., Loizeau, M., Granner, D.K., Girard, J., 1994. Development and regulation of glucose transporter and hexokinase expression in rat. Am. J. Phys. 266, E548–E559.

Qian, Q., Qian, H., Zhang, X., Zhu, W., Yan, Y., Ye, S., Peng, X., Li, W., Xu, Z., Sun, L., Xu, W., 2012. 5-Azacytidine induces cardiac differentiation of human umbilical cord-derived mesenchymal stem cells by activating extracellular regulated kinase. Stem Cells Dev. 21, 67–75. https://doi.org/10.1089/scd.2010.0519.

Sanderson, L.M., Degenhardt, T., Koppen, A., Kalkhoven, E., Desvergne, B., Müller, M., Kersten, S., 2009. Peroxisome proliferator-activated receptor beta/delta (PPARbeta/delta) but not PPARalpha serves as a plasma free fatty acid sensor in liver. Mol. Cell. Biol. 29, 6257–6267. https://doi.org/10.1128/MCB.00370-09.

Smits, A.M., van Vliet, P., Metz, C.H., Korfage, T., Sluijter, J.P., Doevendans, P. a, Goumans, M.-J., 2009. Human cardiomyocyte progenitor cells differentiate into functional mature cardiomyocytes: an in vitro model for studying human cardiac physiology and pathophysiology. Nat. Protoc. 4, 232–243. https://doi.org/10.1038/

nprot.2008.229.
Studelska, D.R., Campbell, C., Pang, S., Rodnick, K.J., James, D.E., 1992. Developmental expression of insulin-regulatable glucose transporter GLUT-4. Am. J. Physiol. Endocrinol. Metab. 263, E102–E106.
Taegtmeyer, H., Young, M.E., Lopaschuk, G.D., Abel, E.D., Brunengraber, H., Darley-Usmar, V., Des Rosiers, C., Gerszten, R., Glatz, J.F., Griffin, J.L., Gropler, R.J., Holzhuetter, H.-G., Kizer, J.R., Lewandowski, E.D., Malloy, C.R., Neubauer, S., Peterson, L.R., Portman, M.A., Recchia, F.A., Van Eyk, J.E., Wang, T.J., 2016. Assessing cardiac metabolism a scientific statement from the American Heart Association. Circ. Res. https://doi.org/10.1161/RES.0000000000000097.
Van Laake, L.W., Van Hoof, D., Mummery, C.L., 2005. Cardiomyocytes derived from stem cells. Ann. Med. 37, 499–512. https://doi.org/N782Q30313536680 [pii]\r. https://doi.org/10.1080/07853890500327843.
Coburn, C.T., Hajri, T., Ibrahimi, A., Abumrad, N.A., 2001. Role of CD36 in membrane transport and utilization of long-chain fatty acids by different tissues. J. Mol. Neurosci. 16, 117–121. discussion 151–7. https://doi.org/10.1385/JMN:16:2-3:117.
Evans, R.D., Heather, L.C., 2016. Metabolic pathways and abnormalities. Surg. 1–7. https://doi.org/10.1016/j.mpsur.2016.03.010.
Sachinidis, A., Fleischmann, B.K., Kolossov, E., Wartenberg, M., Sauer, H., Hescheler, J., 2003. Cardiac specific differentiation of mouse embryonic stem cells. Cardiovasc. Res. https://doi.org/10.1016/S0008-6363(03)00248-7.
Schönfeld, P., Schild, L., Bohnensack, R., 1996. Expression of the ADP/ATP carrier and expansion of the mitochondrial (ATP + ADP) pool contribute to postnatal maturation of the rat heart. Eur. J. Biochem. 241, 895–900.
Vega, R.B., Huss, J.M., Kelly, D.P., 2000. The coactivator PGC-1 cooperates with peroxisome proliferator-activated receptor alpha in transcriptional control of nuclear genes encoding mitochondrial fatty acid oxidation enzymes. Mol. Cell. Biol. 20, 1868–1876. https://doi.org/10.1128/MCB.20.5.1868-1876.2000.
Wang, C., Hu, S.M., 1991. Developmental regulation in the expression of rat heart glucose transporters. Biochem. Biophys. Res. Commun. 177, 1095–1100.
Wende, A.R., Huss, J.M., Schaeffer, P.J., Giguère, V., Kelly, D.P., 2005. PGC-1α coactivates PDK4 gene expression via the orphan nuclear receptor ERRα: a mechanism for transcriptional control of muscle glucose metabolism. Mol. Cell. Biol. 25, 10684–10694. https://doi.org/10.1128/MCB.25.24.10684-10694.2005.
Wolfensohn, S., Lloyd, M., 2003. Handbook of Laboratory Animal Management and Welfare, 3rd ed. Blackwell Publishing Ltd.
Xu, C., 2002. Characterization and enrichment of cardiomyocytes derived from human embryonic stem cells. Circ. Res. 91, 501–508. https://doi.org/10.1161/01.RES.0000035254.80718.91.
Ye, J., Boyle, A., Shih, H., Sievers, R.E., Zhang, Y., Prasad, M., Su, H., Zhou, Y., Grossman, W., Bernstein, H.S., Yeghiazarians, Y., 2012. Sca-1 + cardiosphere-derived cells are enriched for isl1-expressing cardiac precursors and improve cardiac function after myocardial injury. PLoS One 7. https://doi.org/10.1371/journal.pone.0030329.

frontiers in Cardiovascular Medicine

REVIEW
published: 19 September 2018
doi: 10.3389/fcvm.2018.00119

Changing Metabolism in Differentiating Cardiac Progenitor Cells—Can Stem Cells Become Metabolically Flexible Cardiomyocytes?

*Sophia Malandraki-Miller†, Colleen A. Lopez†, Heba Al-Siddiqi and Carolyn A. Carr**

Department of Physiology, Anatomy and Genetics, University of Oxford, Oxford, United Kingdom

The heart is a metabolic omnivore and the adult heart selects the substrate best suited for each circumstance, with fatty acid oxidation preferred in order to fulfill the high energy demand of the contracting myocardium. The fetal heart exists in an hypoxic environment and obtains the bulk of its energy via glycolysis. After birth, the "fetal switch" to oxidative metabolism of glucose and fatty acids has been linked to the loss of the regenerative phenotype. Various stem cell types have been used in differentiation studies, but most are cultured in high glucose media. This does not change in the majority of cardiac differentiation protocols. Despite the fact that metabolic state affects marker expression and cellular function and activity, the substrate composition is currently being overlooked. In this review we discuss changes in cardiac metabolism during development, the various protocols used to differentiate progenitor cells to cardiomyocytes, what is known about stem cell metabolism and how consideration of metabolism can contribute toward maturation of stem cell-derived cardiomyocytes.

Keywords: heart, progenitor cells, substrate metabolism, mitochondria, differentiation, cardiomyocytes

OPEN ACCESS

Edited by:
Gabor Foldes,
Imperial College London,
United Kingdom

Reviewed by:
Silvia Martin-Puig,
Centro Nacional De Investigaciones Cardiovasculares (CNIC), Spain
Praphulla C. Shukla,
Indian Institute of Technology Kharagpur, India

****Correspondence:***
Carolyn A. Carr
carolyn.carr@dpag.ox.ac.uk

†These authors have contributed equally to this work

Specialty section:
This article was submitted to Cardiovascular Biologics and Regenerative Medicine, a section of the journal Frontiers in Cardiovascular Medicine

Received: *30 April 2018*
Accepted: *10 August 2018*
Published: *19 September 2018*

Citation:
Malandraki-Miller S, Lopez CA, Al-Siddiqi H and Carr CA (2018) Changing Metabolism in Differentiating Cardiac Progenitor Cells—Can Stem Cells Become Metabolically Flexible Cardiomyocytes? Front. Cardiovasc. Med. 5:119. doi: 10.3389/fcvm.2018.00119

STEM CELL THERAPY FOR THE HEART

Myocardial infarction (MI) is the primary cause of disease-related death in the world with no reliable therapy (1). Acute coronary syndromes, like MI, account for half of all cardiovascular deaths in the industrialized world, with around 20% of patients developing heart failure (HF) and having a 1-year mortality rate (2, 3). Current therapeutic strategies focus on reperfusion, thrombolysis and reducing the workload of the heart using pharmacological agents or surgical procedures (4–6). Recent advances in treatment have improved time to reperfusion, but progress in identifying efficient therapies to offer more than symptom alleviation and support the surviving myocardium is yet to result in substantial clinical benefit (7, 8). The only current long-term solution is heart transplantation but with the limited numbers of donors, and the need for chronic immunosuppressants (9), the search to find an alternative solution to the problem of end stage HF is becoming increasingly urgent. MI can lead to a loss of up to 1 billion cardiomyocytes, which cannot be replaced due to the insufficient degree of regeneration in the adult heart (10). Although the heart is no longer considered a post-mitotic organ, the turnover of cardiomyocytes in the adult heart is around 1% per year (11) which is insufficient to counter the loss caused by MI. Stem cell therapy (SCT) has the potential to regenerate the damaged tissue and restore its

contractility, harnessing the self-renewal and differentiation potential of stem cells (SCs) (12). *In vivo*, the transplanted cells can act *via* a combination of the following mechanisms; (a) replicate themselves and/or differentiate to mature cardiomyocytes; (b) stimulate the endogenous cardiac cells to regenerate; (c) exert a beneficial effect via paracrine mechanisms of action (13) (**Figure 1**).

TYPES OF STEM CELLS FOR THERAPY

A wide range of cells have been tested both in animal models or early-stage human clinical trials in order to find the appropriate source for SCT (14, 15). These include bone-marrow derived cells (16–18), cardiac stem or progenitor cells (19–25), human embryonic stem cell-derived cardiomyocytes (26–29) and human inducible-pluripotent stem cell-derived cardiomyocytes (30, 31).

Bone marrow-derived stem cells were claimed to differentiate into cardiomyocytes that spontaneously beat after 2 weeks in culture (17) or into myotubules that, when injected into infarcted hearts, stimulated angiogenesis and generated cardiac-like cells (16). In addition, it was reported that when bone marrow-derived stem cell growth factor receptor-positive/linage negative (c-kit+/lin-) cells were injected into infarcted tissue, they generated new cardiac cells and blood vessels and re-muscularised the damaged region (18). However, later studies showed that bone marrow-derived cells do not trans-differentiate into cardiomyocytes and that retained transplanted cells adopted a mature haematopoetic fate (32, 33). Bone-marrow derived mesenchymal cells have also been shown to improve cardiac function following MI, although repair is now thought to result from the delivery of a cocktail of beneficial cytokines which induce angiogenesis, limit scar fibrosis and may activate endogenous cardiac progenitors (34–36). Other key types of mesenchymal stem cells (MSCs) such as umbilical cord MSCs (37, 38), adipose-derived MSCs (39–41) and amniotic fluid MSCs (42), chosen for their ease of isolation and differentiation, have also been tested for therapeutic potential after infarction. As with bone marrow cells, any beneficial effect was deemed to be paracrine.

In 2003, a population of cardiac progenitor cells called stem cell growth factor receptor-positive (c-kit+) cells were identified (19). *In vitro*, these proliferative cells can self-renew and differentiate into myocytes. When injected into infarcted hearts, c-kit+ cells were shown to differentiate into cardiomyocytes resulting in myocardium regeneration and improved heart function (19). Subsequent studies supported the beneficial effect after cardiac injury, but suggested that the c-kit+ cells were of bone marrow origin (43) or were mast cells (44), endothelial cells (45) or maybe a mixed population of both (46). Studies looking at the issue from a developmental perspective suggested that c-kit+ cells contribute to new cardiomyocytes after injury in the neonate, but they were unable to do so in the adult heart (47), in line with previous observations regarding the role of c-kit+ cells in the neonatal heart (48). In 2011, the Anversa group used c-kit+ cardiac progenitor cells (CPCs) in a phase-I Stem Cell Infusion in Patients with Ischemic cardiomyopathy (SCIPIO) clinical trial showing encouraging results for post-MI treatment (49). However, in 2014 the results were questioned for their integrity (50). In 2013, Ellison et al. showed that c-kit+ CPCs were necessary and sufficient for cardiac recovery in rodent models of diffuse myocardial damage causing acute heart failure (51). This was subsequently challenged by studies using c-kit+ lineage tracing mouse models, and reporter lines, where it was shown that cardiac c-kit+ cells contribute to cardiomyocytes only minimally, but mainly and substantially generate cardiac endothelial cells (52–54). The debate continues, with recent publications showing that selected c-kit+ cardiac cells contain a low level (about 1%) of clonal cells that can be expanded and differentiated into spontaneously beating cardiomyocytes (55) and that c-kit expression can be identified on both CPCs and a subpopulation of cardiomyocytes and is upregulated in response to pathological stress (56).

Also in 2003, another population of cardiac progenitor cells was identified, the stem cell antigen 1 (sca-1+) cells, in the mouse heart, having stem-like self-renewal characteristics and the ability to home to the injured myocardium (20). Later it was shown that this cell population led to increased ejection fraction and neoangiogenesis, after injection into the acutely infarcted mouse heart (57). It was also shown that sca-1+ CPCs contribute to the generation of cardiomyocytes during normal aging and after injury sca-1+ cells were induced to differentiate to three cardiac cell types (44). In line with these observations, a genetic deletion of sca-1 caused primary cardiac defects in heart contractility, an impaired damage response and reduced CPC proliferation (58). Although the human sca-1 isoform does not exist, a sca-1-like cell population has been isolated from the human heart using the murine antibody and has been extensively studied by the Goumans group (59). In a similar manner to the isolation of a clonal c-kit+ population, clonal cells have been identified within selected sca-1+, PDGRFα+ mouse cells and have been shown to improve cardiac function after MI, but again by a largely paracrine mechanism (60).

In addition, a population of progenitor cells were derived, via the formation of cardiospheres, from cells migrating from adult human and murine heart explants, called cardiosphere-derived cells (CDCs) (21). It was reported that human CDCs have the ability to self-renew in culture and express the endothelial kinase insert domain receptor (KDR) and other known stem cell markers (CD-31, CD-34, c-kit, and sca-1) (21). This heterogeneous cell population has also been shown to have beneficial effects, both in animal models (22, 61) and in a clinical trial (62), but again via the release of paracrine factors.

CPCs have been also identified by markers of embryonic origin, like Insulin gene enhancer protein 1 (Isl1) and NK2 homeobox 5 (Nkx2.5). Isl1 is a cardiac transcription factor expressed in second heart field progenitors and cardiac neural crest cells, involved in cardiovascular development, and leading to severely deformed hearts in rodents after genetic deletion (24, 63). Nkx2.5, a homeobox-containing transcription factor, has been identified via its involvement in cardiac looping (64, 65). Isl1+ and Nkx2.5+ CPCs have been shown to differentiate into

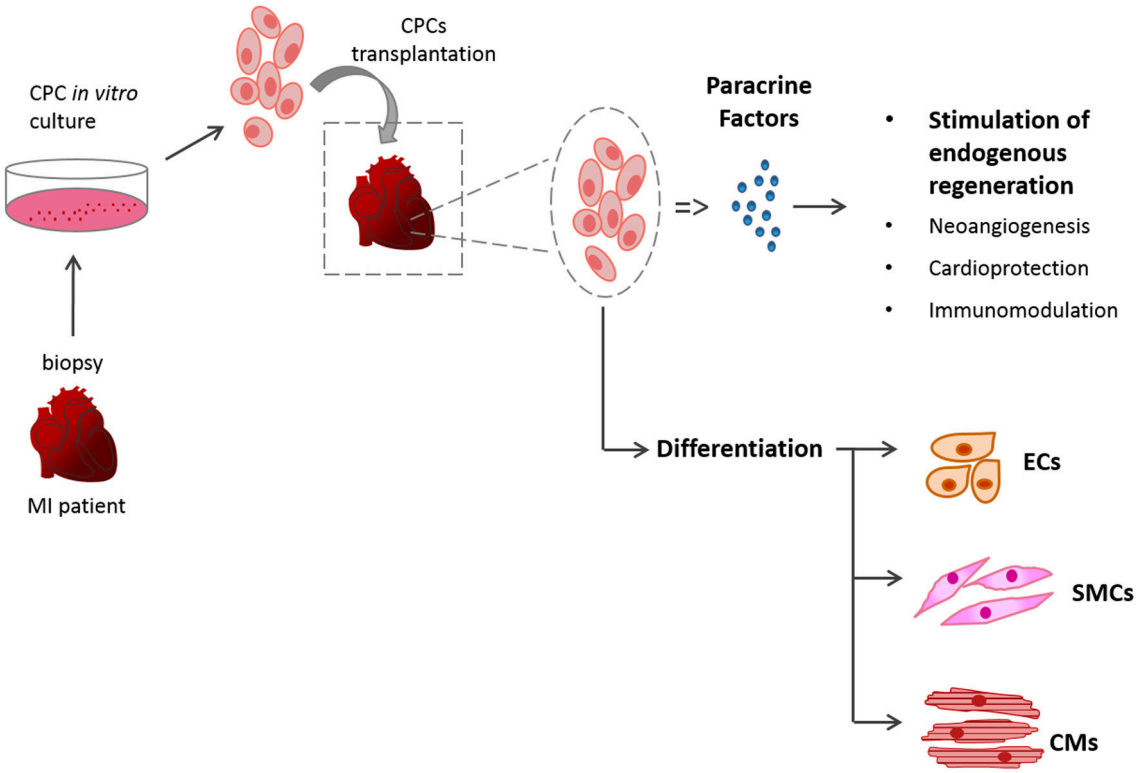

FIGURE 1 | Schematic of SCT. The mechanisms of action of the transplanted cardiac stem cells (CSCs) can be by differentiation of the donor cells or via paracrine mechanisms.

major cardiac lineages, mainly contributing to proepicardium during development (25).

Human embryonic stem cells (hESCs) are derived from the inner cell mass (ICM) of blastocysts from donated fertilized eggs (66). Human ESCs have the ability to continuously proliferate in an undifferentiated state and, when given the appropriate signals, will differentiate into any cell type. An interesting tool for cell therapy that originated from this field, are the *in vitro*–generated, stem cell–derived cardiomyocytes (SC-CMs). These have been shown to integrate structurally and functionally with healthy host cardiac tissue *in vivo* in various studies (26, 67, 68). These cells show great promise, but there are ethical concerns using hESCs in the clinic and the risk of teratoma formation (69). In 2007, Yamanaka's group were the first to report the reprogramming of human somatic cells into induced pluripotent stem cells (iPSCs), by overexpression of the transcription factors: Oct4, Sox2, KLF4, and c-myc (70). The reprogrammed hiPSCs resembled hESCs and had the ability to self-renew while maintaining pluripotency (70). Human iPSCs can be produced from patient-specific somatic cells, therefore overcoming the problem of immune rejection and the ethical concerns of using hESCs (69). hiPSCs have been shown to improve cardiac function, albeit with limited donor cell retention (30, 31) and used extensively as *in vitro* human-cell-based models to study basic biology and development (71), to model diseases (72) and to screen for drugs (73, 74). This is particularly important for the heart, since adult cardiomyocytes do not survive *in vitro*, as morphological and functional changes occur in long-term culture and so there has been no easy way to determine whether the effect of genetic mutations or of drug compounds that were observed in animal models would also be seen in a human cardiomyocyte. However, despite the promising *in vivo* results, the initiation of beating in SC-derived cardiomyocytes does not mean that these cells have the maturity or metabolic characteristics of mature cardiomyocytes found in the healthy heart (75). Studies have shown that SC-derived cardiomyocytes have immature calcium handling (76) and a response to drugs more akin to cardiomyocytes from the failing heart (77).

The effect of the transplantation environment on enhancing the maturation of human pluripotent SC-derived cardiomyocytes has been studied in rats. Despite their capacity to survive and form grafts, they failed to improve adverse remodeling or overall cardiac function after chronic MI (28). Approaches to enhance their efficacy, via preconditioning the cells and host environment, are currently being investigated [reviewed here (78)].

CARDIAC METABOLISM

The heart is a fascinating organ that beats 100,000 times a day and pumps 7,200 L of blood through the body, in the same period using 35 L of O_2 for energy production. It requires

about 6 kg of adenosine triphosphate (ATP), which it utilizes at a rate of 30 mg per second to sustain myocardial contraction and maintain ion homeostasis (79, 80). Since the heart has a low capacity for energy storage (81), an array of metabolic networks guides ATP production rates, based on demand. The heart has been characterized as a metabolic omnivore, being able to use a variety of substrates for energy production [see reviews (82, 83)]. Glucose, pyruvate, triglycerides, glycogen, lactate, ketone bodies, fatty acids (FAs) of different chain-lengths and certain amino acids are among the energy-providing substrates of the heart. It is responsible for almost 10% of the whole body fuel consumption; with FAs accounting for 70% of ATP production and carbohydrates for the remaining 30%.

Energy, in the form of ATP, can be produced in the cytosol via glycolysis (**Figure 2**); catabolism of glucose derived from carbohydrates. The end-product of glycolysis is pyruvate, which can be further reduced to produce lactate. In case of carbohydrate shortage, gluconeogenesis of pyruvate, re-oxygenation of lactate or glycerol metabolism, can be used as sources of glucose synthesis (82, 84). Alternatively, pyruvate can enter the mitochondria in the form of acetyl-coenzyme A (Acetyl-CoA) and be oxidized in the TCA cycle (also known as the Krebs cycle), in a process called oxidative phosphorylation (85). The reducing equivalents of this chained reaction act as hydrogen carriers (Nicotinamide Adenine Dinucleotide Hydrogen; NADH and Flavin Adenine Dinucleotide Hydrogen; $FADH_2$) and enter the electron transport chain (ETC). There the coupled-transfer of electrons and H^+ creates an electrochemical proton gradient that leads to the production of ATP.

ATP can also be generated by the degradation of lipids (including triglycerides) into FAs, which are metabolized in the mitochondria via beta-oxidation (**Figure 2**), which converts Fatty Acyl-CoA to Acetyl-CoA for flux into the TCA cycle and ATP synthesis as above (86). Under aerobic conditions, more than 95% of ATP production comes from oxidative phosphorylation (86) and in the healthy heart 50–80% of the energy is generated via beta-oxidation (87). Oxidative phosphorylation yields 36 ATP/glucose molecule, being more efficient than glycolysis (2 ATP/glucose). Lipids, due to their reduced state are more oxygen-demanding than glucose (producing 2.8 ATP/O_2, vs. 3.7 ATP/O_2), but they are more energy-dense with a much higher yield of ATP/carbon (depending on the chain length of the parent FA) (79, 88).

The heart has a remarkable ability to adapt to changes in its physiological state by selecting the most efficient substrate, depending on the conditions of its environment (82). For example, as FAs require more oxygen than glucose, to generate the same amount of ATP (82, 89), upregulation of the hypoxia-inducible factor (HIF) under hypoxia has been shown to increase

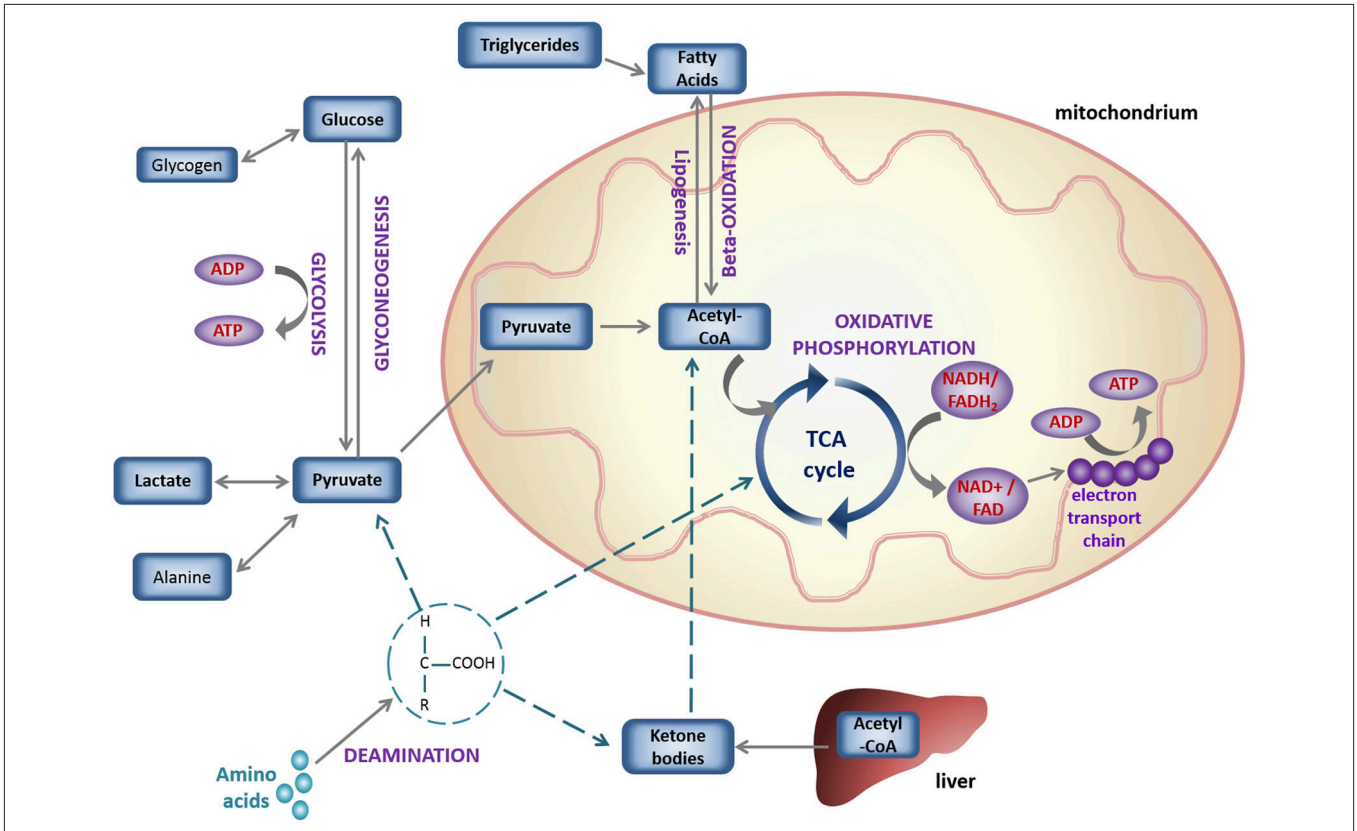

FIGURE 2 | Schematic overview of basic cell metabolic pathways for energy production.

glycolysis and suppress mitochondrial oxidative metabolism (83, 90), shifting toward the more oxygen-efficient fuel: glucose. A network of interrelated signaling pathways control the flux of glucose and fatty acid metabolism to enable the heart to switch substrates rapidly. This was first described as the glucose-fatty acid cycle by Randle in 1963 (91), but the complexity of this network is yet to be fully explored (92). Under conditions of starvation, acetyl-CoA in the liver can form ketone bodies, that are water-soluble forms of this metabolite, and can be efficiently used by the brain and other oxidative organs (82) (**Figure 2**).

Cardiac Metabolism During Development—Metabolic Switch (1)

The fetal heart is adapted to an environment of low oxygen and low fatty acid content, so fetal cardiomyocytes are highly dependent on glycolysis for ATP production (93). In addition, lactate availability allows for energy production via lactate oxidation. During development, the heart undergoes a major metabolic alteration; the main physiological changes during the transition to the post-natal stage are the increased workload, and the demand for growth, that cannot be met by glucose and lactate consumption alone (94, 95). Interestingly, immediately after birth some studies suggest that the main energy biogenesis mechanism is still glycolysis (96). The post-natal increase in both circulating levels of free FAs (due to dietary alteration and lipid content in maternal milk) and in O_2 levels mediates a switch from glycolysis-dependence, to predominantly relying on oxidative metabolism as mature cardiomyocytes (93, 97) (**Figure 3**). After birth, the "fetal switch" to oxidative metabolism of glucose and fatty acids has been linked to the loss of the regenerative phenotype (98). Neonatal mouse hearts can regenerate in the first postnatal week but this is lost after day 7 (99). Puente et al. investigated exposure of neonatal mice to hyperoxia (100% oxygen) or mild hypoxia (15% oxygen) and found that hyperoxia induced cardiomyocyte cell cycle arrest after birth whereas hypoxia prolonged the regenerative window (98). They hypothesized that this effect resulted from increased oxidative stress that accompanied the induction of oxidative metabolism and showed that treatment with an antioxidant resulted in a significant increase in cardiomyocyte mitosis in the first weeks after birth. During the early postnatal period, as cardiac energy demands increase, the number of mitochondria in cardiomyocytes increases dramatically (100, 101). A recent study has shown that the HIF1 signaling localisation pattern controls the embryonic switch toward oxidative metabolism, disruption of which affects cardiac maturation. The cardiac compartment where HIF was absent, the trabeculae, has increased oxidative metabolism, as well as higher mitochondrial content (102). Several studies demonstrated an increase in PPAR coactivator 1α (PGC-1), as well as Peroxisome Proliferator-Activated Receptor α (PPARα), mRNA levels in mice or rats during development (103, 104). The regulatory mechanism involves genes encoding several key mitochondrial ETC proteins, specifically the transcription factors nuclear respiratory factors-1 and−2 (NRF-1 and−2) (103, 105). Disruption of the ETC function, during cardiac development, leads to disrupted mitochondrial organization in the cardiomyocytes, resulting in perturbed sarcomere formation and contraction (106). Various

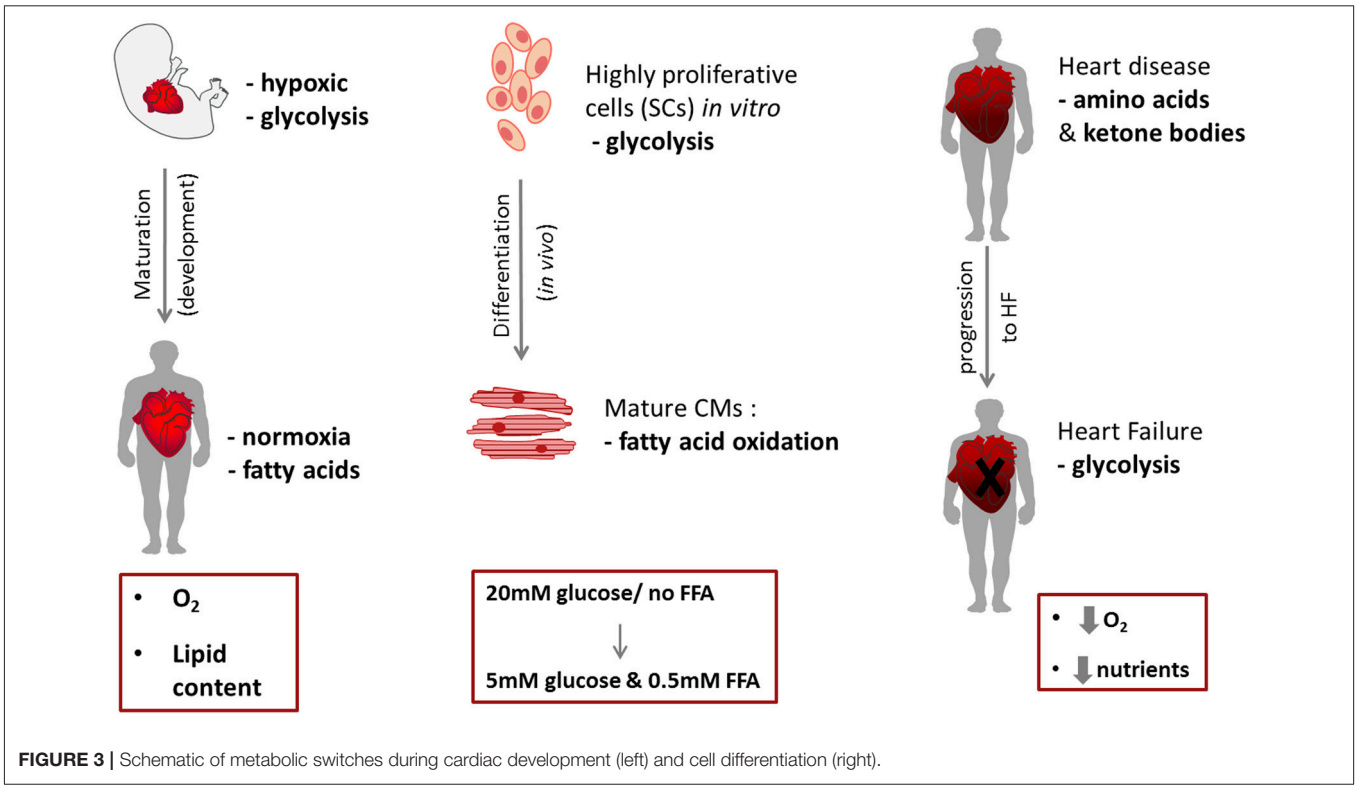

FIGURE 3 | Schematic of metabolic switches during cardiac development (left) and cell differentiation (right).

mouse models have revealed that disruption in mtDNA processes leads to embryonic lethality (107). In addition, signaling pathways involving the Nuclear factor of activated T-cell (NFAT) family of transcription factors play a role in mitochondrial biogenesis and cardiac function. Mice with nfatc3 and nfatc4 deletion had abnormal mitochondrial structure and reduced oxidative capacity, eventually dying after E10.5 (108). The ERRα/ERRγ axis plays a crucial role in mitochondrial energy production, as well, and their deletion leads to premature lethality in mice (109). Disruption of the ERRγ gene leads to impaired mitochondrial function, eventually blocking the switch from glycolysis to oxidative phosphorylation and leading to early prenatal death in mice (110).

Cardiac Metabolism in MI and HF—Metabolic Switch (2)

Following MI, tissue ischaemia leads to hypoxia, which in turn activates long-term HIF signaling in the myocardium (111). During MI, the ischemic region relies solely on glycogen, as an anaerobic fuel for energy production (112). The absence of oxygen for OXPHOS means that NADH and FADH2 are accumulated, affecting fatty acid enzyme reactions and leading to a build-up of fatty acid intermediates and resulting in disruption of mitochondrial cristae and function (87). Reduction in fatty acid oxidation upregulates anaerobic glycolysis and lactate production leading to intracellular acidosis (87). HIF1α activation upregulates the transcription of Bcl-2 adenovirus E1B 19 kDa-interacting protein 3 (BNIP3), which triggers selective mitochondrial autophagy (113, 114). Under normal conditions, BNIP3 expression is suppressed by the nuclear factor kappa beta (NF-κB) pathway (114). In addition, HIF1α upregulates the transcription of pyruvate dehydrogenase kinase 1 (PDK1), which inactivates pyruvate dehydrogenase, thereby blocking the entry of pyruvate into the mitochondria for oxidative phosphorylation (113). These HIF-1 mediated changes play key roles in reducing mitochondrial oxidative metabolism and thereby in reducing the generation of reactive oxygen species (ROS) (115). Following reperfusion, oxidative metabolism is restored but the resulting induction of ROS can lead to mitochondrial damage (116). As the heart progresses to failure, flux from pyruvate into the TCA cycle decreases (117). Mitochondria can be found with membrane and ETC defects (118, 119), as well as reduced respiratory capacity (119, 120) and reduced oxidative phosphorylation (121–123). These findings are consistent with the concept that, during HF, the metabolic state of the heart resembles that of the fetal stage, switching to glycolysis rather than mitochondrial oxidative metabolism (124); with increased glucose uptake (125) and glycolysis (86) and either no change or a decrease in glucose oxidation (125, 126).

The aforementioned perturbations in cardiac metabolism lead to a dangerous environment, due to the excess of lactate and oxidative metabolic intermediates. Progressive heart failure induces, at a cellular level, increased conversion to lactate, increasing cell acidosis (127). However, amino acids such as aspartate play a role in reducing damage that occurs as a result of lactate accumulation via upregulating the conversion of pyruvate to alanine. Glutamate and aspartate improve the production of ATP as they produce intermediates that feed the TCA cycle for further oxidation (128). Studies have reported the reduced availability of amino acids in heart failure patients, leading to the depletion of some valuable amino acid derivatives that are important for normal cardiac function (l-carnitine and creatine) (129). However, there is also evidence of their accumulation during HF, as seen in a study on failing mouse hearts where genes associated with amino acid catabolism were downregulated during compensated hypertrophy and overt failure (130). Transcriptomic analyses reflected downregulation of genes involved in amino acid degradation pathways [proline, alanine, tryptophan, and mainly branched-chain amino acids (BCAAs)] (131–133). Using a genetic mouse model, Sun et al. demonstrated that a deficiency in BCAA catabolism induced heart failure under mechanical overload, resulting from increased oxidative stress (132). Similarly, Li et al. found that whilst chronic accumulation of BCAAs did not affect cardiac energetics and function in the healthy mouse heart, glucose oxidation was decreased which increased ischaemic injury after myocardial infarction (134).

The importance of mitochondrial integrity for maintenance of cardiac function has been also highlighted through several conditions which are characterized by mitochondrial mutations or abnormalities, causing among others: cardiomyopathy, neuromuscular dysfunction, diabetes mellitus and even sudden death (122, 135). In addition, the efficiency of the ETC is found to decline with age, which in turn decreases ATP generation (135, 136).

Cardiac Metabolism From Stem Cells to Adult Cells and Vice Versa—Metabolic Switch (3)

Metabolic changes during embryonic development have been reviewed in detail by Johnson et al. (137). Mammalian oocytes contain low levels of glycogen and fat but have substantial stores of amino acids and protein which have been estimated to be sufficient for the energetic needs of the first few days of development (137). The preimplantation embryo relies on the mitochondria inherited from the oocyte and on pyruvate oxidation for ATP production (138, 139). There is a gradual switch in metabolism during the preimplantation stage (morula, blastocyte) from aerobic oxidation to anaerobic glycolysis in preparation of the low-oxygen environment in the uterine wall (137). As the preimplantation embryo undergoes cell division there is a reduction in mitochondrial DNA copy number (mtDNA) and mitochondrial density (138) and an upregulation of glucose transporter 3 and hexokinase gene expression until anaerobic glycolysis increases to maximal rates as the blastocyst implants into the uterus (137). ESCs originate from the inner cell mass of preimplantation blastocyst, therefore, these cells show high rates of glycolysis and low oxidative phosphorylation to support the rapid cell proliferation (138, 140). Similarly, ESCs derived from *in vitro* cultured ICMs (141) or ESCs cultured *in vitro* (142) show high rates of glycolysis and low oxidative phosphorylation. A comparison of the metabolomics and energetics of iPSCs with those of ESCs showed many

similarities and confirmed that, during reprogramming, somatic cells convert from an oxidative state to a glycolytic state in pluripotency (143).

The reprogramming factors, c-Myc and Lin28, have been shown to enhance glycolysis and nuclear reprogramming (140) and reprogrammed pluripotent stem cells show upregulation of glycolytic enzymes such as the glucose transporter GLUT1, hexokinase (HK), phosphofructokinase (PFK) and LDH (144). In addition, hiPSCs have increased levels of intracellular glucose-6-phosphate, which feeds into the pentose phosphate pathway (PPP) to generate the reducing factor NADPH, which is used for biosynthesis of FAs and nucleotides necessary for rapid proliferation (144). Stimulation of glycolysis with D-fructose-6-phosphate or by PDK1 activation has been shown to enhance the efficiency of iPSC reprogramming (145). Mitochondrial morphology changes from being elongated and tubular-shaped with well-developed electron-dense cristae in somatic cells, to being spherical with small-undeveloped cristae in hiPSCs, with a transition from an extensive cytoplasmic networks in somatic cells, to a predominantly peri-nuclear location in hiPSCs (146). Prieto et al. found that this fragmentation was not associated with mitophagy but was induced by activation of dynamin-related protein 1 (Drp1), which fragments mitochondria in a GTPase-dependent manner (147). They showed that Erk activation in early reprogramming induced Drp1 phosphorylation which was critical to the reprogramming pathway. Studies in human and mouse ESCs have also found a small number of rounded and immature mitochondria with under-developed cristae (106, 148). Moreover, multipotent stem/progenitor cells show the same characteristics; for example, mitochondria in HSCs are relatively inactive and ATP content increases in lineage-committed progenitors compared with HSCs (149).

Due to the ongoing controversy as to whether the heart contains resident progenitor cells (150), little is known about the metabolism of cardiac stem cells in the adult heart. However most adult endogenous progenitor/stem cells reside in hypoxic niches (151), in a quiescent state, and therefore the metabolic rate is presumed to be low. CPCs isolated from the heart, by marker selection, tissue digestion or from explants, and expanded *in vitro*, are proliferative and grown in culture medium containing high levels of glucose and little or no FAs. Basal cellular homeostasis involves processes like protein turnover, DNA repair, and vesicle trafficking and therefore proliferating cells, in addition to homeostasis maintenance, need energy for anabolic processes such as cell division and growth. Proliferative cells, such as cancer cells, have been suggested to predominantly rely on glycolysis for ATP production, irrespective of oxygen presence; this metabolic paradox, first observed by Warburg in 1956 (152) has been termed "aerobic glycolysis." Apart from Warburg's observations on cancer cells, mouse fibroblasts (153) and human (154) and mouse (155) lymphocytes have been shown to utilize "aerobic glycolysis," when stimulated to proliferate. Various studies have supported the conclusion that the major function of aerobic glycolysis is to supply glycolytic intermediates for anabolic reactions in cells, thus being the metabolic pathway of choice during cell proliferation [for Review see (156)]. Although cells in high glucose medium predominantly metabolise glucose, they can use other substrates if provided. Human bone marrow MSCs have an active oxidative metabolism with a range of substrates and can produce more ATP from substrate oxidation than glycolysis with certain substrates (157). For example, the ketone body, acetoacetate, can be oxidized at up to 35 times the rate of glucose. Many proliferating mammalian cells, such as human MSCs, also consume glutamine to provide material for biosynthesis (158). Glutamine, as a carbon source, can supply the TCA cycle with intermediates that can be used for the production of new macromolecules in cells. A recent study by Hosios et al., in 2016, argued that glutamine contributes most to protein synthesis, suggesting that anaplerosis of glutamine in the TCA cycle is serving mainly amino acid biosynthesis (159).

When stem/progenitor cells differentiate to cardiomyocytes they need to increase the number of their mitochondria and upregulate FA metabolism (**Figure 3**). A study comparing hiPSC-derived cardiomyocytes (hiPSC-CM) to hiPSCs, showed an increase in mitochondrial relative abundance and activity (mitochondria membrane potential) as a result of cardiac differentiation (160) and that additional mitochondrial maturation in hiPSC-CMs could be achieved by long-term culture (3 months). Comparison of substrate metabolism in ESCs with that in ESC-derived cardiomyocytes has shown increased oxidative metabolism after differentiation (161) and that the respiratory capacity of cardiomyocytes was higher than in ESCs, resulting in an increased ADP:ATP ratio in the cardiomyocytes (106). The mitochondria become elongated with abundant and organized cristae in cardiomyocytes and formed into networks which filled the cytoplasm (106).

WHY STUDY STEM CELL METABOLISM

The metabolism of any cell type *in vitro* depends on energy requirements and substrate availability. Cardiac progenitor cells, when expanded *in vitro*, reside in a high glucose environment and rely on aerobic glycolysis for energy generation. CPCs will experience a shift in substrate availability following transplantation *in vivo* (**Figure 3**), being transferred from the culture medium, which contains about 5–25 mM glucose (depending on the culture protocol) and no FFA, to substrates in plasma that vary substantially. Glucose levels in mice have been measured at between ∼3.4 and 9.6 mM (2.8–7.5 mM in rats) (162, 163) and ∼0.18–0.6 mM FFA (164). In humans, healthy plasma glucose levels are around 5 mM and FFA 0.5 mM (165). This alteration is bound to cause changes in the metabolic machinery of the cells which might be one of the stimuli that induce differentiation following transplantation, but may also result in increased release of ROS and cellular damage.

The various protocols used for CPC differentiation focus on pharmacological reagents and cytokines, and do not refer to or take into account the substrate composition. This is a striking fact especially knowing how metabolic changes affect the function of the cells (166) and how transition from glycolysis to FA oxidation affects cell maturation (93), and *vice-versa* (144). iPSC-CM have been shown to integrate structurally and functionally with healthy host cardiac tissue *in vivo* in

various studies (26, 67, 68). Despite the promising *in vivo* results, the initiation of beating in iPSC-CM does not mean that these cells have the metabolic characteristics of mature cardiomyocytes found in the heart. Studies have shown that SC-CMs have immature calcium handling (76, 167) and a response to drugs more akin to cardiomyocytes from the failing heart (77). Despite the observed mitochondrial remodeling and upregulation of oxidative metabolism previously discussed, newly differentiated iPSC-CM in culture have been shown to retain a predominantly glycolytic metabolism (168). One of the major roles of iPSC-CM is that of a drug-testing platform and this requires the differentiated cells to acquire a fully mature phenotype (74). For example, a recent iPSC-CM study showed that the electrophysiological responsiveness of iPSC-CM was dependent on their maturation state (169).

ASSESSING CELL METABOLISM

The main approaches for the investigation of substrate metabolism include the measurement of metabolic fluxes using radio-labeled substrates and of oxygen consumption.

Radio-Labeled Substrates Assays

Glucose oxidation rates are commonly measured using the method of the Collins et al. (163) with cell culture media containing D-U-^{14}C-glucose. Glucose oxidation results in the production of $^{14}CO_2$ which is trapped for analysis using a scintillation counter. For ^{3}H-FA oxidation the cells are incubated in media supplemented with the radioactive FA tracer of interest. FA oxidation rates are determined by the production of ^3H_2O from the mitochondria (170, 171). Media aliquots contain both ^3H_2O and ^{3}H-FA, so the ^3H_2O is separated via a Folch extraction (170). Glycolytic rates are determined through the conversion of ^{3}H-glucose to ^3H_2O via enolase which converts 2-phosphoglycerate to phosphoenolpyruvate and releases ^3H_2O as a by-product that is collected using a Dowex mesh (Sigma, UK) anion exchange column, allowing for the ^{3}H-glucose to bind to the column and ^3H_2O to be eluted (171).

Oxygen Consumption

The rate of mitochondrial oxygen consumption (OCR) can be measured using the XF Extracellular Flux Analyzer (Seahorse Bioscience), the Oroboros O2K or the Clark-type oxygen electrode (172, 173). Seahorse XF Analyzers measure the concentration of dissolved oxygen and pH to quantify the oxygen consumption and extracellular acidification rate in the media in multi-well plates. Four injection ports in each well allow for addition of reagents. However, the Seahorse requires cells to be adhered to the wells, multiple additions of substrates are not possible and the individual wells are not self-contained and thus cells can be affected by gases from adjacent wells (172). The Clark-type oxygen electrode is embedded in individual reaction chambers and cells are added in suspension in the respiration media (173). Unlimited reagents and substrates can be added by manual addition. This system is more automated in the Oroboros O2K which also includes optical sensors to allow for detection of fluorescent dyes so that parameters such as ATP production or mitochondrial membrane potential may be measured (172).

The OCR can be measured under baseline un-stimulated conditions in media containing the substrate of interest (such as pyruvate; palmitate; malate; or oleic acid). Addition of the ATP synthase inhibitor oligomycin provides a measure of contaminating ATP synthase activity from damaged mitochondria and of proton leak, whilst the metabolic uncoupler, carbonylcyanide-p-trifluoromethoxy-phenylhydrazone (FCCP) permits measurement of fully uncoupled or maximal respiration (173). Finally, mitochondrial inhibitors such as rotenone (complex I) and antimycin (complex III) will completely inhibit mitochondrial respiration. More exquisite interrogation of the function of mitochondrial metabolism can be performed using substrates such as glutamate which assesses the second span of the Krebs cycle, succinate which enters the electron transport chain at complex II, or β-hydroxybutyrate, a fatty acid-derived substrate which bypasses β-oxidation and enters the Krebs cycle as acetyl CoA (116, 174).

Extracellular Measurement of Glucose Consumption and Lactate Production

Lactate production can be measured using the Seahorse Flux Analyzer from the extracellular acidification rate (ECAR) of the media. Glucose and lactate levels can also be determined using enzymatic assays or the ABX Pentra 400 Chemistry Analyser (Horiba Ltd. USA). Glycolysis yields two molecules of pyruvate, which can be converted to either lactate or acetyl CoA. Therefore, the ratio of glucose consumption to lactate production can be used as an indicator of the level of utilization of pyruvate in oxidative metabolism (175).

CARDIAC DIFFERENTIATION *IN VITRO*

Various methods and strategies have been applied to develop the optimal protocol for directing *in vitro* cardiac differentiation of stem cells. *In vitro* differentiation of adult endogenous CPCs is very challenging, due to their limited plasticity. Despite a variety of differentiation studies, the ability of adult progenitors for differentiation, is still under debate (176, 177). Different approaches, utilizing various differentiation factors have been used on both pluripotent SCs and CPCs, with the main ones being; DMSO, 5-Azacytidine, Ascorbic Acid, members of the TGF-β superfamily, oxytocin, dexamethasone and retinoic acid (see **Table 1**).

More specifically, 5-azacytidine (5-Aza) is a demethylating agent that allows for the exposure of genes that are normally silenced, due to hypermethylation, by inhibiting DNA methyltransferase (191, 192). Several *in vitro* studies suggested that 5-Aza can induce cardiac differentiation, on different MSC types, such as human umbilical cord-derived MSCs (186) and adult human bone marrow-derived MSCs (17, 187). Other studies have demonstrated the inefficiency of 5-Aza as a cardiac differentiation agent, showing transdifferentiation to skeletal muscle cells, rather than cardiac cells (193) as well as unsuccessful differentiation of adipose-derived stem cells (ASCs) (194) and adult mouse Sca-1+ CPCs (182). Ascorbic Acid (A.A.), is an antioxidant compound which has been shown to increase the expression of cardiac genes and their proteins

TABLE 1 | Factors and media used to differentiate adult stem cells to cardiomyocytes.

Differentiation approaches	References	Differentiated cell type	Cell culture medium and differentiation factors	Glucose concentration
TGF-β1 family	(178)	Human atria Sca-1$^+$; clonally isolated & magnetic-sorting	5 μM 5-Aza, TGF-β1 1 ng/ml, 10^{-4} M AA, IMDM/Ham's F12 GlutaMAX, 2% serum, 1% MEM amino acids, 1% insulin–transferrin–selenium	
	(179)	Human fetal and adult atrial biopsies, Sca-1$^+$ magnetic-sorting		12.5 mM
	(180)	Whole mouse heart Sca-1$^+$/ CD45$^-$ magnetic-sorting CDCs (Isl1$^+$)		
Oxytocin	(181)	Mouse or rat whole hearts, c-kit$^+$/CD45$^-$/Tryp$^-$ magnetic-sorting	DMEM 100 nM oxytocin acetate, 50 μg/ml AA, 2% serum, 1 μM dexamethasone, beta-glycerol phosphate 10 mM, TGF-β1, 5 ng/ml, BMP2 10 ng/ml, BMP4 10 ng/ml, Dkk1 150 ng/ml	5.5. mM
	(182)	Mouse whole heart Sca-1+ magnetic-sorting	IMDM, 10% serum, 100 nm oxytocin	22.5 mM
	(183)	Rat, mouse ventricles side population cells		
5-Azacytidine	(184)	Mouse bone marrow stroma MSCs	IMDM, 20% serum, 3 μmol/L 5-Aza	20 mM
	(185)	Human adipose MSCs	RPMI + 15% FCS, 1–9 μmol/L 5-Aza	9.4 mM
	(20)	Mouse whole heart Sca-1$^+$ magnetic-sorting	Medium 199, 2% FBS, 3 μM 5-Aza	5.5. mM
	(186)	Human umbilical cord MSCs	LG-DMEM, 10% FBS, 10 μM 5-Aza	5.0. mM
	(187)	Human bone marrow MSCs	LG-DMEM, 20% serum, 3 μM 5-Aza	4.4 mM
	(188)	Rat bone marrowMSCs	DMEM, 10% FBS, 10 μM 5-Aza	5.0. mM
Dexamethasone	(189)	Human atrial or ventricular c-kit$^+$ -sorted	F12 medium 10% serum, 10 nM dexamethasone	9 mM
	(19)	Rats c-kit$^+$/ Lin$^-$ magnetic-sorting	F12 medium 10% serum, 10 nM dexamethasone	9 mM
	(190)	Dog left ventricle c-kit$^+$/ Lin$^-$ and Sca-1$^+$/ Lin$^-$ magnetic-sorting	F12 medium 10% serum, 10 nM dexamethasone	9 mM
	(53)	mouse whole heart c-kit$^+$	DMEM, 10% serum, 10 nM dexamethasone	9 mM

5-Aza, 5-azacytidine; AA, Ascorbic acid; BMP, Bone morphogenic protein; Dkk1, Dickkopf-related protein 1; DMEM, Dubecco Modified Eagle Medium; MDMD, Iscove's Modified Dulbecco's Medium; LG-DMEM: low glucose DMEM; MEM, Minimum Essential Medium; RPMI, Roswell Park Memorial Institute medium; TGFβ, transforming growth factor β.

and to lead to beating cardiomyocytes in mouse ES cells (195). Cao et al. in 2012 demonstrated that A.A. was able to induce cardiac differentiation and maturation in several human and mouse iPSC lines (196). In contrast, treatment of BM-derived MSCs with A.A. triggered their proliferation and differentiation into osteoblasts and adipocytes (197). Another key player in cardiac differentiation is transforming growth factor-beta 1 (TGF-β1) which is thought to drive cardiac differentiation by inducing the cardiac transcription factor Nkx2.5 (198). Goumans et al. used TGF-β1 to induce differentiation of adult atrial Sca-1$^+$ CPCs, in combination with 5-Aza and A.A (178, 179). The mechanism of action involves phosphorylation of Smad2, that leads to the expression of cardiac-specific proteins (179). Dexamethasone is a glucocorticoid compound with immunomodulatory properties. Initial studies showed that it stimulates differentiation and maturation of osteogenic progenitor cells (199). The osteogenic effect of dexamethasone has since been demonstrated on MSCs (200–202). Interestingly, various groups have used it as the main agent of differentiation of adult selected c-kit+ CPCs to cardiomyocytes (19, 181, 189, 190). One of the most successful *in vitro* differentiation protocols for adult cardiac progenitors uses staged treatment with oxytocin, BMP2/4, TGF-β, and DKK1 which has been shown to induce cloned c-kit+ progenitor cells to form beating cardiomyocytes (181)

Cardiac directed differentiation protocols used for pluripotent SCs can be divided into two main groups, the Embryoid Body (EB)-based method (203, 204) and the monolayer-based method (30, 205–208). These protocols are discussed briefly here but a more comprehensive review has been given by Mummery et al. (209). Although cardiac differentiation protocols vary, most monolayer-based methods involve stage-specific activation and inhibition of signaling pathways that control heart development, replicating the early cardiac developmental stages in the early embryo (mesoderm induction, mesoderm cardiac specification, and generation of cardiomyocytes). The signaling pathways that

are involved in most directed cardiac differentiation protocols are Activin/Nodal and bone morphogenetic protein (BMP) signaling (203), which are members of the (TGFβ) signaling pathway and the fibroblast growth factor (FGF) (30, 203), and the Wnt signaling pathways (205–208). Activin A, BMP4, and Wnt3 induce the mesoderm, and upregulate the expression of Brachyury T, whereas inhibition of Wnt signaling at later stages of differentiation has been shown to induce mesoderm cardiac specification (209). Following these steps, cells are generally cultured with media in the absence of growth factors, to allow cardiomyocyte maturation to give spontaneous beating. The distinct effects of Wnt signaling during various stages of cardiac development has been thoroughly investigated, both *in vitro* and *in vivo* (210). More specifically, it was shown with *in vivo* gene function studies in the mouse that Wnt initially enhances mesoderm commitment, while it later hinders the induction of cardiogenesis, and that it stimulates the proliferation of Isl1+ cardiac progenitors (211, 212). In addition, a study in zebrafish embryos demonstrated the switch from the inductive to the inhibitory role, of Wnt on cardiac formation, during a short 1-hour window prior to gastrulation (213). In chick embryos, treatment with Wnt antagonists *in vivo* enhanced expression of cardiac muscle differentiation markers and increased expression of Isl1 and Nkx2.5 in splanchnic mesoderm (214). *In vitro,* Murry's lab in 2010 showed that supplementation with exogenous Wnt at the point of initiation of cardiogenic differentiation of hESC enhanced the cardiac marker expression, while the same effect was induced by antagonism of endogenous Wnts at a later stage (208).

Differentiation protocols were first developed using hESCs and then were translated to iPSCs. **Table 2** summarizes and compares some of the published differentiation protocols and shows a shift from the EB-based model using hESCs to the monolayer-based model using hiPSCs, which is the commonly model used currently. **Table 2** also takes note of the fact that all these protocols are differentiated in variable concentrations of glucose (4.5–25mM) and insignificantly low amounts to no fatty acids (at most 2 μM). In general, spontaneously beating EBs are generated from cells in suspension using a serum-based media to induce spontaneous cardiac differentiation (27, 204, 216). The beating areas are then hand-picked from the rest of the EB or flow-sorted. Laflamme et al., played a key role in the enhancement of cardiac differentiation protocols by shifting from the serum-induced EB-based differentiation protocol that generated 10–15% spontaneously beating EBs (218) to the serum-free monolayer-based differentiation generating >30% cardiomyocytes using Activin A and BMP4 (27). In 2011, Burridge et al. systematically compared 45 variables added to EBs formed by forced aggregation which they tested on four hESC and seven hiPSC lines (222). Their optimized method included addition of BMP4 and FGF2, with polyvinyl alcohol to aid EB formation, serum and insulin to induce oxidative metabolism and with staged exposure to physiological (5%) oxygen. The growth factor-directed differentiation enabled cells to be differentiated as monolayers, thereby introducing more straightforward, and hopefully more reproducible, methods of differentiation (209). Lian et al. also optimized the Wnt-based protocol by removing insulin during early stages of differentiation (205). They had found that when iPS cells were differentiated using a Gsk3β inhibitor, Activin A, and BMP4, the presence of insulin in the early stages had a strong inhibitory effect but that this was not seen when cells were differentiated by manipulation of Wnt signaling. They identified an interplay between insulin signaling and Wnt signaling which coordinates to influence differentiation to cardiomyocytes and therefore introduced staged removal and re-addition of insulin to their differentiation protocol (205).

MEDIA COMPOSITION DURING/AFTER DIFFERENTIATION

As shown in **Tables 1**, **2**, the majority of differentiation protocols for CPCs to cardiomyocytes had a no lipids in the media composition whilst the glucose concentration in culture media ranged from 4.5 mM to 25 mM (Here it should be mentioned that the addition of serum at percentages ranging from 2 to 20% does not allow for an absolutely clear image of the media composition). The variability of glucose concentration is striking, especially bearing in mind that a glucose level of 25 mM *in vivo* is considered hyperglycemic and leads to loss of mitochondrial networks (224, 225).

The Role of Hypoxia and of Reactive Oxygen Species in Differentiation

Stem cells *in vivo* occupy an hypoxic niche and their energy yielding metabolism is likely to be hypoxic with a high reliance on glycolysis for ATP generation (226, 227). There are conflicting reports on the relationship between hypoxia and differentiation of stem cells. Hypoxia alone can revert hESC- or iPSC-derived differentiated cells back to a stem cell-like state, by re-activation of an Oct4-promoter reporter (228). In contrast, exogenous expression of HIF has been shown to promote cardiac differentiation of ESC (229). Transient hypoxia during *in vitro* cardiac differentiation upregulated the Wnt signaling pathway with increased expression of the endogenous Wnt proteins (wnt3, wnt3a, wnt9a, and wnt11), which was lost when the cells were transferred back to normoxia. This resulted in increased expression of cardiac markers such as Isl-1 and Troponin C but decreased expression of βMHC and a failure to develop the contractile phenotype (230). To further complicate the picture, Gaber et al. found a dose-dependent increase in expression of the DNA damage marker γH2AX and of senescence in ESCs differentiated under increasing exposure to hypoxia (231). These differential reports may result from the different cell types (ESC or iPSC) and species studied. Fynes et al. found that hypoxic culture of mESCs primed the cells for differentiation and resulted in increased differentiation along the mesoderm and endodermal lineages whereas hiPSCs were pushed toward a more naïve pluripotent state by hypoxia and were then primed for ectoderm differentiation (232).

As previously discussed, the loss of regenerative potential of the heart in the first weeks of life has been attributed

TABLE 2 | Factors and media used to differentiate pluripotent stem cells to cardiomyocytes.

Different-iation method cell type	Growth factor or small molecules	Culture media	Glucose concent-ration	% of Cardiac markers	References
EB-Method hESCs iPSc	Cells in suspension -optionally differentiated with serum-based media, DMSO, all-trans retinoic acid or 5-Aza	80% KO-DMEM, 1 mMol L-glutamine, 1.1-1.2mMol B-ME,1% NEAA, 20% FBS	4.5mM	8.1% spontaneously beating EBs. In beating EBs, 29.4% cTnI+ cells. 25% spontaneously beating EBs by day 8 and 70% by day 16 of differentiation 5-Aza enhanced levels of cardiac α-MHC 10 to 15% positive for sarcomeric MHC	(204) (215) (216) (217) (218)
Monolayer hESCs hiPSC	Guided differentiation: h-Activin A, h-BMP4 +/- staged addition of h-Wnt3a & h-DKK1	RPMI+B27	11.1mM Note: 2uM of oleic acid	> 30% CMs Differentiated cells underwent Percoll gradient centrifuge for CM enrichment (69 ± 10% CMs) Increase in sarcomeric MHC+ cells from 4 to 27%	(27) (70) (208)
EB-Method hESCs hiPSC	END-2 method (Insulin depletion, PGI2, p38 inhibition)	80% KO-DMEM, 2 mMol L-glutamine,10ng/ml bFGF, 1.2 mMol B-ME, 7.5% FCS	4.5mM	50% beating CM	(219) (220)
EB-Method hESCs	Guided differentiation: h-Activin A, h-BMP4, h-bFGF, h-VEGF, h-DKK1	StemPro-34 (Base) + [L-glutamine, AA, optional MTG, P/S]	>25mM	KDR+ selected cells 35 ± 6% cTNT+, enriched to 57±4% by monolayer culture. DKK1 on day 4 gave 2-fold enrichment of CTNT+ cells KDR+/PDGFRA+ cells, 50–70% cTNT+ cells in beating EBs. 80% cTNT+ cells by monolayer culture	(221) (203)
EB-method iPSCs	Forced aggregation EBs with guided differentiation:BMP4, FGF2, Staged O_2 levels	RPMI (L-glutamine) 20% FBS on day 3 Insulin on days 0-2 and day 4	9–11mM Note: 2uM FA	Contracting EBs contained 64–89% of cardiac troponin I^+cells	(222)
Monolayer hiPSCs	Guided differentiation: h-Activin A, h-BMP4, h-bFGF	StemPro-34 + [L-glutamine,MTG, AA, P/S]	>25mM	Spontaneously beating sheets of CMs 40 ± 15% CMs	(30)
Monolayer hESCs hiPSCs	Guided differentiation method: h-Activin A, h-BMP4, h-bFGF, + Matrigel or CHIR99021, IWP4/IWP2	RPMI+B27(-insulin) [d0-6 of differentiation]; RPMI+B27 [from d7 of differentiation]	11.1mM Note: 2uM oleic acid	Matrigel addition on day−2 and day 0 generated 80% cTnT+ CMs Spontaneously beating sheets of CMs, 87% cTNT+ CMs	(223) (207) (206) (205)

B-ME, beta-mercaptoethanol; CM, cardiomyocytes; MTG, monothioglycerol; P/S, penicillin/streptomycin; AA, ascorbic acid; NEAA, non-essential amino acids.

to DNA damage resulting from the increase in ROS that accompanies upregulation of mitochondrial metabolism (98). However, ROS have also been shown to signal differentiation to several cell types, including cardiomyocytes. Transient expression of an NADPH oxidase-like enzyme with induction of ROS during embryoid body development of ESCs enhanced cardiomyogenesis, which was shown to occur *via* PI-3-kinase regulation and to be inhibited by the addition of radical scavengers (233). Similarly, NADPH oxidase (NOX)-derived ROS induced cardiac differentiation via a p38 mitogen-activated protein kinase (MAPK)-dependent pathway (234). Inhibition of mitochondrial biogenesis using shRNA targeting of PGC-1α, in hESC differentiation to cardiomyoytes, repressed mitochondrial respiration, and beating frequency (161). Levels of ROS increased during differentiation but were repressed by knockdown of PGC-1α. However, decreasing ROS levels by differentiating cells under hypoxia decreased the rate of mitochondrial biogenesis, which was stimulated by induction of ROS (161). Interestingly, in addition to reducing the beating frequency, decreasing ROS levels increased the action potential and calcium transient amplitude, but made the cells vulnerable to metabolic stress. ES cells cultured in physiological levels of glucose (5 mmol) maintained their stemness and showed reduced levels of ROS, but failed to differentiate to fully-formed cardiomyocytes (235). This was associated with reduced levels of NOX4 and MAPK which were rescued by addition of the pro-oxidant ascorbic acid.

STRATEGIES TO MATURE CELLS

A range of strategies have been used to mature iPS- and ESC-CMs, including time in culture (236), mechanical and electrical stimulation (237, 238), addition of small molecules (239), substrate stiffness (240), genetic approaches (241–243) and growth in 3D tissues (244–246). These are reviewed in detail elsewhere (74, 247) but very few consider the medium in which the cells are cultured.

CHANGING MEDIA COMPOSITION TO BE MORE PHYSIOLOGICALLY RELEVANT

There is a change in energy substrate availability and metabolism during heart development from the embryo into the adult stage. However, this change in metabolism is not mimicked in most published differentiation protocols. Maturation of ESC-CMs was induced by treatment with the thyroid hormone, tri-iodo-L-thyronine, which induced an enhancement in contractile kinetics, in rates of calcium release and reuptake and in sarcoendoplasmic reticulum ATPase expression, and a significant increase in maximal mitochondrial respiratory capacity and respiratory reserve capability (239). However, in that study the newly formed cardiomyocytes were cultured in serum-free medium with no fatty acids. Similarly, where maturation of ESC-CMs was induced using members of the Let-7 family of microRNAs, increasing cell size, sarcomere length, force of contraction, and respiratory capacity, no fatty acids were added to the serum-free culture medium (243).

A few recent studies have begun to change media composition to induce a particular disease phenotype. Kim et al. used a lipogenic medium comprising insulin, dexamethasone and 3-isobutyl-1-methylxanthine to induce fatty acid metabolism in iPSC-CM derived from patients with arrhythmogenic right ventricular dysplasia. They saw a mild increase in lipogenesis with minimal apoptosis after 4–5 weeks of treatment and increased expression of PPARα. Cell maturation revealed that metabolic derangement was implicated in the onset of arrhythmia (168). Drawnell et al. induced a diabetic phenotype by treating differentiated iPSC-CM with a maturation medium containing insulin and fatty acids, but no glucose for three days, followed by treatment with a diabetic milieu of glucose (10 mM), endothelin-1 (10 nM), and cortisol (1 μM) (248). This induced an increase in sarcomere length, and in velocity and duration of action potential, in addition to increases in the myosin light chain genes, MYL2, MYL3 and MYL4; of genes involved in regulation of sarcoplasmic reticulum calcium content and an associated repression of fetally enriched genes. Correia et al. reported that shifting hPSC-CMs from glucose-containing to galactose- and fatty acid-containing medium induced fast maturation into adult-like cardiomyocytes with higher oxidative metabolism, enhanced contractility and more physiological action potential kinetics (249). Perhaps the most comprehensive investigation into the effects of changing media is that of Rana et al., who modified a basal medium with combinations of high or low glucose with galactose or fatty acids (250). They found that exclusion of glucose from the medium was needed to induce iPSC-CM to switch from glycolysis to OXPHOS for their ATP production.

TISSUE ENGINEERING APPROACHES

It is hypothesized that culturing cells in 3D would better mimic conditions *in vivo*, such that differentiated cells would adopt a more mature phenotype. There are four main types of tissue engineering strategies that have been developed to construct contractile heart muscle equivalents: stacking monolayer cell sheets to form multi-layered heart muscle (251), cells seeded onto decellularized native tissue, cells seeded onto synthetic or biologic scaffolds (252–257) and entrapment of cells in naturally occurring biogels or hydrogels (258–260). Bian et al. cultured neonatal rat cardiomyocytes in a 3D environment and after 3 weeks saw aligned, electromechanically coupled cardiomyocytes with capillary-like structures, improved calcium handling properties. The cells had action potentials which showed enhanced conduction velocities and directional dependence on the local cardiomyocytes orientation (261). Cardiac muscle strips which were fabricated from hESC-CMs and stromal cells in collagen-based biomaterials, showed higher passive and active twitch force, aligned sarcomeres, regularly dispersed connexin-43 and N-cadherin and increased expression of maturation markers (262).

Scaffolds can be formed from synthetic polymers or from natural materials such as the cardiac extracellular matrix (ECM). Besides its structural role of giving support to surrounding cells, the ECM also has important signaling roles in cardiac development and remodeling. In recent years, it has been shown to help regulate cell survival, proliferation, migration and differentiation, for example by modulating the activity, bioavailabilty or presentation of growth factors to cell surface receptors (263, 264). ECM macromolecular proteins such as collagen (259, 265, 266), elastin (267), fibrin (268, 269) and glycoaminoglycans (270, 271) can be extracted from tissue and integrated in 3D scaffolds (267, 271) or hydrogels (268) to explore further the retention and maturation of SCs seeded. Material properties are more controllable in synthetic polymers which can be modified to incorporate adhesion peptides or release biological molecules (272).

In the hydrogel approach, cells are encapsulated in the scaffold during synthesis of the gel which allows homogenous seeding. Hydrogels have also been shown to induce cell maturation and differentiation which makes them an attractive system for basic studies of cardiac development and potential for the delivery of therapeutics to the heart (273, 274). Suspension of CDCs in a hydrogel formed from serum and the glycosoaminoglycan hyaluronic acid, increased the oxygen consumption rate from that of cells in suspension and increased cell retention after transplantation *in vivo* (275). Porous scaffolds can be generated by freeze-drying suspensions poured in molds (267, 276). This type of manufacturing gives flexibility in shape and composition, but limits cell seeding efficacy as most seeded cells remain attached to the scaffold surface (267). Fibrous

scaffolds can be manufactured from a large variety of materials by electrospinning which gives control over the nano-scale structure and mechanical properties of the scaffold, but again limits the seeding efficiency (277). Zhang et al. found that, compared to 2D hESC monolayers, hESC-CM in a 3D fibrin-based cardiac patch exhibited significantly higher conduction velocities, longer sarcomeres and enhanced expression of genes involved in cardiac contractile function (244). Potentially the "ultimate scaffold material" is that of decellularized heart tissue since it has the potential to give rise to appropriately structured scaffolds for organ replacement (278).

One noteworthy 3D construct is the engineered heart tissue (EHT) which is a three-dimensional, hydrogel-based muscle construct that is restrained between posts, thereby allowing the cells to contract against a force. EHTs can be generated from isolated heart cells from adult hearts, such as chicken (259) and rat (258) as well as from hESC (279) and hiPSC (280). iPSC-CM EHTs have showed to increase mitochondrial mass, DNA content, and protein abundance (proteome) compared to their 2D counterparts. Moreover they were found to generate more energy via oxidation of glucose, lactate, and fatty acid with a decreased reliance on anaerobic glycolysis, generating 2.3-fold more ATP by oxidation than 2D hiPSC-CMs (245). Mills et al. have developed a technique for growing 3D cardiac organoids in 96 well plates (281). The cells form dense muscle bundles in serum-free conditions developed to promote metabolic and proliferative maturation. They found that addition of palmitate increased the force of contraction and expression of ventricular myosin light chain 2. Interestingly, addition of insulin promoted cell cycling and so was not included in the maturation medium comprising 1 mM glucose and 0.1 mM palmitate. By comparing contractile properties of organoids grown in maturation medium with those in control medium, they found that maturation medium reduced activation time and relaxation time, thereby recapitulating changes seen during human cardiomyocytes development.

Thus, three-dimensional culture conditions have induced binucleation, rod-like cell shape, increased sarcomere alignment, more mature electrophysiology, and calcium handling properties (247). Complex, multi-cellular cell sheets are now being developed from mixtures of iPSC-CMs with fibroblasts and endothelial cells (282) or with mesenchymal cells (283) which exhibit more mature physiology or drug responses but these are still grown in non-physiologic culture media (282, 283). What is needed now, is routine modulation of the culture medium, as discussed above, to cells in 3D constructs to fully induce metabolic maturation.

CONCLUSIONS

The field of CPC biology has come a long way over the last 20 years. Beating sheets of cardiomyocytes can now be generated routinely from ESCs and iPSCs in large numbers. However, the maturity of the cardiomyocytes remains a cause for concern if they are to be used to validate new drug compounds, detect cardiotoxicity or recapitulate the cardiac physiology of patients with genetic disorders. Long term culture can aid maturation, as can culture in 3D constructs, but a fully mature cardiomyocytes should express the appropriate level of substrate transporters and mitochondrial proteins. Further work is required to determine appropriate cell culture conditions to enable pluripotent stem cell-derived cardiomyocytes to achieve the metabolic flexibility of the adult heart.

AUTHOR CONTRIBUTIONS

All authors contributed conception and design for the manuscript. SM-M and CL wrote the first draft of the manuscript. All authors wrote sections of the manuscript and contributed to manuscript revision, read and approved the submitted version. SM-M and CL are joint first authors.

FUNDING

This work was supported by the Rosetrees Trust (Grant # M624), the British Heart Foundation (Grant # PG/13/14/30216) and the BHF Centre of Research Excellence, Oxford (Grant # RE/13/1/3018).

ACKNOWLEDGMENTS

We thank the Oxford Clarendon Fund for a studentship for SMM and the Qatar Foundation for funding for HAS.

REFERENCES

1. Velagaleti RS, Pencina MJ, Murabito JM, Wang TJ, Parikh NI, D'Agostino RB, et al. Long-term trends in the incidence of heart failure after myocardial infarction. *Circulation* (2008) 118:2057–62. doi: 10.1161/CIRCULATIONAHA.108.784215
2. Go AS, Mozaffarian D, Roger VL, Benjamin EJ, Berry JD, Blaha MJ, et al. Heart disease and stroke statistics—2014 update: a report from the american heart association. *Circulation* (2014) 129:e28–292. doi: 10.1161/01.cir.0000441139.02102.80
3. Fuster V. Global burden of cardiovascular disease: time to implement feasible strategies and to monitor results. *J Am Coll Cardiol*. (2014) 64:520–2. doi: 10.1016/j.jacc.2014.06.1151
4. Goldfinger JZ, Adler ED. End-of-life options for patients with advanced heart failure. *Curr Heart Fail Rep*. (2010) 7:140–7. doi: 10.1007/s11897-010-0017-5
5. Kumar A, Cannon CP. Acute coronary syndromes: diagnosis and management, part I. *Mayo Clin Proc*. (2009) 84:917–38. doi: 10.4065/84.10.917
6. Kumar A, Cannon CP. Acute coronary syndromes: diagnosis and management, part II. *Mayo Clin Proc*. (2009) 84:1021–36. doi: 10.1016/S0025-6196(11)60674-5
7. Kirklin JK, Naftel DC, Pagani FD, Kormos RL, Stevenson LW, Blume ED, et al. Sixth INTERMACS annual report: a 10,000-patient database. *J Hear Lung Transplant*. (2014) 33:555–64. doi: 10.1016/j.healun.2014.04.010
8. Perricone AJ, Vander Heide RS. Novel therapeutic strategies for ischemic heart disease. *Pharmacol Res*. (2014) 89:36–45. doi: 10.1016/j.phrs.2014.08.004

9. Toyoda Y, Guy TS, Kashem A. Present status and future perspectives of heart transplantation. *Circ J*. (2013) 77:1097–110. doi: 10.1253/circj.CJ-13-0296
10. Laflamme MA, Murry CE. Heart regeneration. *Nature* (2011) 473:326–35. doi: 10.1038/nature10147
11. Bergmann O, Bhardwaj RD, Bernard S, Zdunek S, Barnabé-Heider F, Walsh S, et al. Evidence for cardiomyocyte renewal in humans. *Science* (2009) 324:98–102. doi: 10.1126/science.1164680
12. Gersh BJ, Simari RD, Behfar A, Terzic CM, Terzic A. Cardiac cell repair therapy: a clinical perspective. *Mayo Clin Proc*. (2009) 84:876–92. doi: 10.4065/84.10.876
13. Vincent SD, Buckingham ME. How to make a heart. The origin and regulation of cardiac progenitor cells. *Curr Top Dev Biol*. (2010) 90:1–41. doi: 10.1016/S0070-2153(10)90001-X
14. Lalit PA, Hei DJ, Raval AN, Kamp TJ. Induced pluripotent stem cells for post-myocardial infarction repair: remarkable opportunities and challenges. *Circ Res*. (2014) 114:1328–45. doi: 10.1161/CIRCRESAHA.114.300556
15. Bruyneel AAN, Sehgal A, Malandraki-Miller S, Carr C. Stem cell therapy for the heart: blind alley or magic bullet? *J Cardiovasc Transl Res*. (2016) 9:405–18. doi: 10.1007/s12265-016-9708-y
16. Tomita S, Li RK, Weisel RD, Mickle DA, Kim EJ, Sakai T, et al. Autologous transplantation of bone marrow cells improves damaged heart function. *Circulation* (1999) 100(19 Suppl.):II247–56. doi: 10.1161/01.CIR.100.suppl_2.II-247
17. Makino S, Fukuda K, Miyoshi S, Konishi F, Kodama H, Pan J, et al. Cardiomyocytes can be generated from marrow stromal cells *in vitro*. *J Clin Invest*. (1999) 103:697–705. doi: 10.1172/JCI5298
18. Orlic D, Kajstura J, Chimenti S, Jakoniuk I, Anderson SM, Li B, et al. Bone marrow cells regenerate infarcted myocardium. *Nature* (2001) 410:701–5. doi: 10.1038/35070587
19. Beltrami AP, Barlucchi L, Torella D, Baker M, Limana F, Chimenti S, et al. Adult cardiac stem cells are multipotent and support myocardial regeneration. *Cell* (2003) 114:763–76. doi: 10.1016/S0092-8674(03)00687-1
20. Oh H, Bradfute SB, Gallardo TD, Nakamura T, Gaussin V, Mishina Y, et al. Cardiac progenitor cells from adult myocardium: homing, differentiation, and fusion after infarction. *Proc Natl Acad Sci USA*. (2003) 100:12313–8. doi: 10.1073/pnas.2132126100
21. Messina E, De Angelis L, Frati G, Morrone S, Chimenti S, Fiordaliso F, et al. Isolation and expansion of adult cardiac stem cells from human and murine heart. *Circ Res*. (2004) 95:911–21. doi: 10.1161/01.RES.0000147315.71699.51
22. Carr C, Stuckey DJ, Tan JJ, Tan SC, Gomes RSM, Camelliti P, et al. Cardiosphere-derived cells improve function in the infarcted rat heart for at least 16 weeks - an mri study. *PLoS ONE* (2011) 6:e25669. doi: 10.1371/journal.pone.0025669
23. Smart N, Bollini S, Dube KN, Vieira JM, Zhou B, Davidson S, et al. *De novo* cardiomyocytes from within the activated adult heart after injury. *Nature* (2011) 474:640–4. doi: 10.1038/nature10188
24. Cai CL, Liang X, Shi Y, Chu PH, Pfaff SL, Chen J, et al. Isl1 identifies a cardiac progenitor population that proliferates prior to differentiation and contributes a majority of cells to the heart. *Dev Cell*. (2003) 5:877–89. doi: 10.1016/S1534-5807(03)00363-0
25. Zhou B, Gise AV, Ma Q, Rivera-Feliciano J, Pu WT. Nkx2-5- and Isl1-expressing cardiac progenitors contribute to proepicardium. *Biochem Biophys Res Commun*. (2008) 375:450–3. doi: 10.1016/j.bbrc.2008.08.044
26. Chong JJH, Yang X, Don CW, Minami E, Liu YW, Weyers JJ, et al. Human embryonic-stem-cell-derived cardiomyocytes regenerate non-human primate hearts. *Nature* (2014) 510:273–7. doi: 10.1038/nature13233
27. Laflamme MA, Chen KY, Naumova AV, Muskheli V, Fugate JA, Dupras SK, et al. Cardiomyocytes derived from human embryonic stem cells in pro-survival factors enhance function of infarcted rat hearts. *Nat Biotechnol*. (2007) 25:1015–24. doi: 10.1038/nbt1327
28. Fernandes S, Naumova AV, Zhu WZ, Laflamme MA, Gold J, Murry CE. Human embryonic stem cell-derived cardiomyocytes engraft but do not alter cardiac remodeling after chronic infarction in rats. *J Mol Cell Cardiol*. (2010) 49:941–9. doi: 10.1016/j.yjmcc.2010.09.008
29. Shiba Y, Fernandes S, Zhu WZ, Filice D, Muskheli V, Kim J, et al. Human ES-cell-derived cardiomyocytes electrically couple and suppress arrhythmias in injured hearts. *Nature* (2012) 489:322–5. doi: 10.1038/nature11317
30. Carpenter L, Carr C, Yang CTCT, Stuckey DJDJ, Clarke K, Watt SMSM. Efficient differentiation of human induced pluripotent stem cells generates cardiac cells that provide protection following myocardial infarction in the rat. *Stem Cells Dev*. (2012) 21:977–86. doi: 10.1089/scd.2011.0075
31. Kadota S, Pabon L, Reinecke H, Murry CE. *In vivo* maturation of human induced pluripotent stem cell-derived cardiomyocytes in neonatal and adult rat hearts. *Stem Cell Rep*. (2017) 8:278–89. doi: 10.1016/j.stemcr.2016.10.009
32. Murry CE, Soonpaa MH, Reinecke H, Nakajima H, Nakajima HO, Rubart M, et al. Haematopoietic stem cells do not transdifferentiate into cardiac myocytes in myocardial infarcts. *Nature* (2004) 428:664–8. doi: 10.1038/nature02446
33. Balsam LB, Wagers AJ, Christensen JL, Kofidis T, Weissman IL, Robbins RC. Haematopoietic stem cells adopt mature haematopoietic fates in ischaemic myocardium. *Nature* (2004) 428:668–73. doi: 10.1038/nature02460
34. Hatzistergos KE, Quevedo H, Oskouei BN, Hu Q, Feigenbaum GS, Margitich IS, et al. Bone marrow mesenchymal stem cells stimulate cardiac stem cell proliferation and differentiation. *Circ Res*. (2010) 107:913–22. doi: 10.1161/CIRCRESAHA.110.222703
35. Loffredo FS, Steinhauser ML, Gannon J, Lee RT. Bone marrow-derived cell therapy stimulates endogenous cardiomyocyte progenitors and promotes cardiac repair. *Cell Stem Cell* (2011) 8:389–98. doi: 10.1016/j.stem.2011.02.002
36. Abdel-Latif A, Bolli R, Tleyjeh IM, Montori VM, Perin EC, Hornung CA, et al. Adult bone marrow-derived cells for cardiac repair: a systematic review and meta-analysis. *Arch Intern Med*. (2007) 167:989–97. doi: 10.1001/archinte.167.10.989
37. Breymann C, Schmidt D, Hoerstrup SP. Umbilical cord cells as a source of cardiovascular tissue engineering. *Stem Cell Rev*. (2006) 2:87–92. doi: 10.1007/s12015-006-0014-y
38. Fang CH, Jin J, Joe JH, Song YS, So BI, Lim SM, et al. *In vivo* differentiation of human amniotic epithelial cells into cardiomyocyte-like cells and cell transplantation effect on myocardial infarction in rats: comparison with cord blood and adipose tissue-derived mesenchymal stem cells. *Cell Transplant*. (2012) 21:1687–96. doi: 10.3727/096368912X653039
39. Gimble JM, Katz AJ, Bunnell BA. Adipose-derived stem cells for regenerative medicine. *Circ Res*. (2007) 100:1249–60. doi: 10.1161/01.RES.0000265074.83288.09
40. Li B, Zeng Q, Wang H, Shao S, Mao X, Zhang F, et al. Adipose tissue stromal cells transplantation in rats of acute myocardial infarction. *Coron Artery Dis*. (2007) 18:221–7. doi: 10.1097/MCA.0b013e32801235da
41. Valina C, Pinkernell K, Song YH, Bai X, Sadat S, Campeau RJ, et al. Intracoronary administration of autologous adipose tissue-derived stem cells improves left ventricular function, perfusion, and remodelling after acute myocardial infarction. *Eur Heart J*. (2007) 28:2667–77. doi: 10.1093/eurheartj/ehm426
42. De Coppi P, Bartsch G Jr, Siddiqui MM, Xu T, Santos CC, Perin L, et al. Isolation of amniotic stem cell lines with potential for therapy. *Nat Biotech*. (2007) 25:100–6. doi: 10.1038/nbt1274
43. Fazel S, Cimini M, Chen L, Li S, Angoulvant D, Fedak P, et al. Cardioprotective c-kit+ cells are from the bone marrow and regulate the myocardial balance of angiogenic cytokines. *J Clin Invest*. (2006) 116:1865–77. doi: 10.1172/JCI27019
44. Uchida S, De Gaspari P, Kostin S, Jenniches K, Kilic A, Izumiya Y, et al. Sca1-derived cells are a source of myocardial renewal in the murine adult heart. *Stem Cell Rep*. (2013) 1:397–410. doi: 10.1016/j.stemcr.2013.09.004
45. Sandstedt J, Jonsson M, Lindahl A, Jeppsson A, Asp J. C-kit+ CD45- Cells found in the adult human heart represent a population of endothelial progenitor cells. *Basic Res Cardiol*. (2010) 105:545–56. doi: 10.1007/s00395-010-0088-1
46. Sandstedt J, Jonsson M, Dellgren G, Lindahl A, Jeppsson A, Asp J. Human C-kit+CD45- cardiac stem cells are heterogeneous and display both cardiac and endothelial commitment by single-cell qPCR analysis. *Biochem Biophys Res Commun*. (2014) 443:234–8. doi: 10.1016/j.bbrc.2013.11.086
47. Jesty SA, Steffey MA, Lee FK, Breitbach M, Hesse M, Reining S, et al. c-kit+ precursors support postinfarction myogenesis in the neonatal, but not adult, heart. *Proc Natl Acad Sci USA*. (2012) 109:13380–5. doi: 10.1073/pnas.1208114109

48. Tallini YN, Greene KS, Craven M, Spealman A, Breitbach M, Smith J, et al. C-Kit expression identifies cardiovascular precursors in the neonatal heart. *Proc Natl Acad Sci USA*. (2009) 106:1808–13. doi: 10.1073/pnas.0808920106
49. Bolli R, Chugh AR, D'Amario D, Loughran JH, Stoddard MF, Ikram S, et al. Cardiac stem cells in patients with ischaemic cardiomyopathy (SCIPIO): initial results of a randomised phase 1 trial. *Lancet* (2011) 378:1847–57. doi: 10.1016/S0140-6736(11)61590-0
50. The Lancet Editors. Expression of concern: the SCIPIO trial. *Lancet*. (2014) 383:1279. doi: 10.1016/S0140-6736(14)60608-5
51. Ellison GM, Vicinanza C, Smith AJ, Aquila I, Leone A, Waring CD, et al. Adult c-kitpos cardiac stem cells are necessary and sufficient for functional cardiac regeneration and repair. *Cell* (2013) 154:827–42. doi: 10.1016/j.cell.2013.07.039
52. Molkentin JD, Houser SR. Are resident c-Kit+ cardiac stem cells really all that are needed to mend a broken heart? *Circ Res*. (2013) 113:1037–9. doi: 10.1161/CIRCRESAHA.113.302564
53. van Berlo JH, Kanisicak O, Maillet M, Vagnozzi RJ, Karch J, Lin SCJ, et al. c-kit+ cells minimally contribute cardiomyocytes to the heart. *Nature* (2014) 509:337–41. doi: 10.1038/nature13309
54. Sultana N, Zhang L, Yan J, Chen J, Cai W, Razzaque S, et al. Resident c-kit(+) cells in the heart are not cardiac stem cells. *Nat Commun*. (2015) 6:8701. doi: 10.1038/ncomms9701
55. Vicinanza C, Aquila I, Scalise M, Cristiano F, Marino F, Cianflone E, et al. Adult cardiac stem cells are multipotent and robustly myogenic: C-kit expression is necessary but not sufficient for their identification. *Cell Death Differ*. (2017) 24:2101–16. doi: 10.1038/cdd.2017.130
56. Gude NA, Firouzi F, Broughton KM, Ilves K, Nguyen KP, Payne CR, et al. Cardiac c-Kit biology revealed by inducible transgenesis. *Circ Res*. (2018) 123:57–72. doi: 10.1161/CIRCRESAHA.117.311828
57. Wang X, Hu Q, Nakamura Y, Lee J, Zhang G, From AHL, et al. The role of the sca-1+/CD31- cardiac progenitor cell population in postinfarction left ventricular remodeling. *Stem Cells* (2006) 24:1779–88. doi: 10.1634/stemcells.2005-0386
58. Bailey B, Fransioli J, Gude NA, Alvarez R, Zhan X, Gustafsson AB, et al. Sca-1 knockout impairs myocardial and cardiac progenitor cell function. *Circ Res*. (2012) 111:750–60. doi: 10.1161/CIRCRESAHA.112.274662
59. van Vliet P, Roccio M, Smits AM, van Oorschot AAM, Metz CHG, van Veen TAB, et al. Progenitor cells isolated from the human heart: a potential cell source for regenerative therapy. *Neth Heart J*. (2008) 16:163–9. doi: 10.1007/BF03086138
60. Noseda M, Harada M, McSweeney S, Leja T, Belian E, Macaulay I, et al. PDGFRα demarcates the cardiogenic and clonogenic Sca-1^{+} stem cell. *Cardiovasc Res*. (2014) 103:S107. doi: 10.1038/ncomms7930
61. Smith RR, Barile L, Cho HC, Leppo MK, Hare JM, Messina E, et al. Regenerative potential of cardiosphere-derived cells expanded from percutaneous endomyocardial biopsy specimens. *Circulation* (2007) 115:896–908. doi: 10.1161/CIRCULATIONAHA.106.655209
62. Malliaras K, Makkar RR, Smith RR, Cheng K, Wu E, Bonow RO, et al. Intracoronary cardiosphere-derived cells after myocardial infarction: evidence of therapeutic regeneration in the final 1-year results of the CADUCEUS trial (CArdiosphere-derived aUtologous stem CElls to reverse ventricular dysfunction). *J Am Coll Cardiol*. (2014) 63:110–22. doi: 10.1016/j.jacc.2013.08.724
63. Lin L, Bu L, Cai CL, Zhang X, Evans S. Isl1 is upstream of sonic hedgehog in a pathway required for cardiac morphogenesis. *Dev Biol*. (2006) 295:756–63. doi: 10.1016/j.ydbio.2006.03.053
64. Wu SM, Fujiwara Y, Cibulsky SM, Clapham DE, Lien CL, Schultheiss TM, et al. Developmental origin of a bipotential myocardial and smooth muscle cell precursor in the mammalian heart. *Cell* (2006) 127:1137–50. doi: 10.1016/j.cell.2006.10.028
65. Tanaka M, Chen Z, Bartunkova S, Yamasaki N, Izumo S. The cardiac homeobox gene Csx/Nkx2.5 lies genetically upstream of multiple genes essential for heart development. *Development* (1999) 126:1269–80.
66. Thomson JA, Itskovitz-Eldor J, Shapiro SS, Waknitz MA, Swiergiel JJ, Marshall VS, et al. Embryonic stem cell lines derived from human blastocysts. *Science* (1998) 282:1145–7. doi: 10.1126/science.282.5391.1145
67. Kehat I, Khimovich L, Caspi O, Gepstein A, Shofti R, Arbel G, et al. Electromechanical integration of cardiomyocytes derived from human embryonic stem cells. *Nat Biotechnol*. (2004) 22:1282–9. doi: 10.1038/nbt1014
68. Xue T, Cho HC, Akar FG, Tsang SY, Jones SP, Marban E, et al. Functional integration of electrically active cardiac derivatives from genetically engineered human embryonic stem cells with quiescent recipient ventricular cardiomyocytes: insights into the development of cell-based pacemakers. *Circulation* (2005) 111:11–20. doi: 10.1161/01.CIR.0000151313.18547.A2
69. Zimmermann WH. Embryonic and embryonic-like stem cells in heart muscle engineering. *J Mol Cell Cardiol*. (2011) 50:320–6. doi: 10.1016/j.yjmcc.2010.10.027
70. Takahashi K, Tanabe K, Ohnuki M, Narita M, Ichisaka T, Tomoda K, et al. Induction of pluripotent stem cells from adult human fibroblasts by defined factors. *Cell* (2007) 131:861–72. doi: 10.1016/j.cell.2007.11.019
71. Karakikes I, Ameen M, Termglinchan V, Wu JC. Human induced pluripotent stem cell-derived cardiomyocytes: insights into molecular, cellular, and functional phenotypes. *Circ Res*. (2015) 117:80–8. doi: 10.1161/CIRCRESAHA.117.305365
72. Lan F, Lee AS, Liang P, Sanchez-Freire V, Nguyen PK, Wang L, et al. Abnormal calcium handling properties underlie familial hypertrophic cardiomyopathy pathology in patient-specific induced pluripotent stem cells. *Cell Stem Cell* (2013) 12:101–13. doi: 10.1016/j.stem.2012.10.010
73. Liang P, Lan F, Lee AS, Gong T, Sanchez-Freire V, Wang Y, et al. Drug screening using a library of human induced pluripotent stem cell-derived cardiomyocytes reveals disease-specific patterns of cardiotoxicity. *Circulation* (2013) 127:1677–91. doi: 10.1161/CIRCULATIONAHA.113.001883
74. Denning C, Borgdorff V, Crutchley J, Firth KSA, George V, Kalra S, et al. Cardiomyocytes from human pluripotent stem cells: from laboratory curiosity to industrial biomedical platform. *Biochim Biophys Acta Mol Cell Res*. (2016) 1863:1728–48. doi: 10.1016/j.bbamcr.2015.10.014
75. Veerman CC, Kosmidis G, Mummery CL, Casini S, Verkerk AO, Bellin M. Immaturity of human stem-cell-derived cardiomyocytes in culture: fatal flaw or soluble problem? *Stem Cells Dev*. (2015) 24:1035–52. doi: 10.1089/scd.2014.0533
76. Satin J, Itzhaki I, Rapoport S, Schroder EA, Izu L, Arbel G, et al. Calcium handling in human embryonic stem cell-derived cardiomyocytes. *Stem Cells* (2008) 26:1961–72. doi: 10.1634/stemcells.2007-0591
77. Brito-Martins M, Harding SE, Ali NN. Beta(1)- and Beta(2)-adrenoceptor responses in cardiomyocytes derived from human embryonic stem cells: comparison with failing and non-failing adult human heart. *Br J Pharmacol*. (2008) 153:751–9. doi: 10.1038/sj.bjp.0707619
78. Don CW, Murry CE. Improving survival and efficacy of pluripotent stem cell-derived cardiac grafts. *J Cell Mol Med*. (2013) 17:1355–62. doi: 10.1111/jcmm.12147
79. Bing RJ, Siegel A, Ungar I, Gilbert M. Metabolism of the human heart: II. studies on fat, ketone and amino acid metabolism. *Am J Med*. (1954) 16:504–15. doi: 10.1016/0002-9343(54)90365-4
80. Neubauer S. The failing heart–an engine out of fuel. *N Engl J Med*. (2007) 356:1140–51. doi: 10.1056/NEJMra063052
81. Neely JR, Morgan HE. Relationship between carbohydrate and lipid metabolism and the energy balance of heart muscle. *Annu Rev Physiol*. (1974) 36:413–59. doi: 10.1146/annurev.ph.36.030174.002213
82. Evans RD, Heather LC. Metabolic pathways and abnormalities. *Surgery* (2016) 34:266—72. doi: 10.1016/j.mpsur.2016.03.010
83. Taegtmeyer H, Young ME, Lopaschuk GD, Abel ED, Brunengraber H, Darley-Usmar V, et al. Assessing cardiac metabolism. *Circ Res*. (2016) 118:1659–701. doi: 10.1161/RES.0000000000000097
84. Bar-Even A, Flamholz A, Noor E, Milo R. Rethinking glycolysis: on the biochemical logic of metabolic pathways. *Nat Chem Biol*. (2012) 8:509–17. doi: 10.1038/nchembio.971
85. Madeira VMC. Overview of mitochondrial bioenergetics. *Methods Mol Biol*. (2012) 810:1–6. doi: 10.1007/978-1-61779-382-0_1
86. Lopaschuk G. The role of fatty acid oxidation in cardiac ischemia and reperfusion. *Adv Stud Med*. (2004) 4:S803–7.

87. Lopaschuk GD, Ussher JR, Folmes CDL, Jaswal JS, Stanley WC. Myocardial fatty acid metabolism in health and disease. *Physiol Rev*. (2010) 90:207–58. doi: 10.1152/physrev.00015.2009
88. van der Vusse G, Glatz J, Stam H, Reneman R. Fatty acid homeostasis in the normoxic and ischemic heart. *Physiol Rev*. (1992) 72:881–940. doi: 10.1152/physrev.1992.72.4.881
89. Cole MA, Jamil AHA, Heather LC, Murray AJ, Sutton ER, Slingo M, et al. On the pivotal role of PPARa in adaptation of the heart to hypoxia and why fat in the diet increases hypoxic injury. *FASEB J*. (2016) 30:2684–97. doi: 10.1096/fj.201500094R
90. Kim JW, Tchernyshyov I, Semenza GL, Dang CV. HIF-1-mediated expression of pyruvate dehydrogenase kinase: a metabolic switch required for cellular adaptation to hypoxia. *Cell Metab*. (2006) 3:177–85. doi: 10.1016/j.cmet.2006.02.002
91. Randle, PJ, Garland PB, Hales CN, Newsholme EA. The glucose fatty-acid cycle its role in insulin sensitivity and the metabolic disturbances of diabetes mellitus. *Lancet* (1963) 281:785–9. doi: 10.1016/S0140-6736(63)91500-9
92. Hue L, Taegtmeyer H. The Randle cycle revisited: a new head for an old hat. *Am J Physiol Endocrinol Metab*. (2009) 297:E578–91. doi: 10.1152/ajpendo.00093.2009
93. Lopaschuk GD, Jaswal JS. Energy metabolic phenotype of the cardiomyocyte during development, differentiation, and postnatal maturation. *J Cardiovasc Pharmacol*. (2010) 56:130–40. doi: 10.1097/FJC.0b013e3181e74a14
94. Lai L, Leone TC, Zechner C, Schaeffer PJ, Kelly SM, Flanagan DP, et al. Transcriptional coactivators PGC-lα and PGC-lβ control overlapping programs required for perinatal maturation of the heart. *Genes Dev*. (2008) 22:1948–61. doi: 10.1101/gad.1661708
95. Kolwicz SC, Purohit S, Tian R. Cardiac metabolism and its interactions with contraction, growth, and survival of cardiomyocytes. *Circ Res*. (2013) 113:603–16. doi: 10.1161/CIRCRESAHA.113.302095
96. Lopaschuk GD, Spafford MA, Marsh DR. Glycolysis is predominant source of myocardial ATP production immediately after birth. *Am J Physiol*. (1991) 261(6 Pt 2):H1698–705.
97. Breckenridge RA, Piotrowska I, Ng KE, Ragan TJ, West JA, Kotecha S, et al. Hypoxic regulation of hand1 controls the fetal-neonatal switch in cardiac metabolism. *PLoS Biol*. (2013) 11:e1001666. doi: 10.1371/journal.pbio.1001666
98. Puente BN, Kimura W, Muralidhar SA, Moon J, Amatruda JF, Phelps KL, et al. The oxygen-rich postnatal environment induces cardiomyocyte cell-cycle arrest through DNA damage response. *Cell* (2014) 157:565–79. doi: 10.1016/j.cell.2014.03.032
99. Mahmoud AI, Kocabas F, Muralidhar SA, Kimura W, Koura AS, Thet S, et al. Meis1 regulates postnatal cardiomyocyte cell cycle arrest. *Nature* (2013) 497:249–53. doi: 10.1038/nature12054
100. Attardi G, Schatz G. Biogenesis of mitochondria. *Annu Rev Cell Biol*. (1988) 4:289–333. doi: 10.1146/annurev.cb.04.110188.001445
101. Mayor F, Cuezva JM. Hormonal and metabolic changes in the perinatal period. *Biol Neonate*. (1985) 48:185–96.
102. Menendez-Montes I, Escobar B, Palacios B, Gómez MJ, Izquierdo-Garcia JL, Flores L, et al. Myocardial VHL-HIF signaling controls an embryonic metabolic switch essential for cardiac maturation. *Dev Cell* (2016) 39:724–39. doi: 10.1016/j.devcel.2016.11.012
103. Lehman JJ, Barger PM, Kovacs A, Saffitz JE, Medeiros DM, Kelly DP. Peroxisome proliferator-activated receptor gamma coactivator-1 promotes cardiac mitochondrial biogenesis. *J Clin Invest*. (2000) 106:847–56. doi: 10.1172/JCI10268
104. Steinmetz M, Quentin T, Poppe A, Paul T, Jux C. Changes in expression levels of genes involved in fatty acid metabolism: upregulation of all three members of the PPAR family (a,c,d) and the newly described adiponectin receptor 2, but not adiponectin receptor 1 during neonatal cardiac development of the. *Basic Res Cardiol*. (2005) 100:263–69. doi: 10.1007/s00395-005-0520-0
105. Virbasius CMA, Virbasius JV, Scarpulla RC. NRF-1, an activator involved in nuclear-mitochondrial interactions, utilizes a new DNA-binding domain conserved in a family of developmental regulators. *Genes Dev*. (1993) 7:2431–45.
106. Chung S, Dzeja PP, Faustino RS, Perez-Terzic C, Behfar A, Terzic A. Mitochondrial oxidative metabolism is required for the cardiac differentiation of stem cells. *Nat Clin Pr Cardiovasc Med*. (2007) 4 (Suppl. 1):S60–7. doi: 10.1038/ncpcardio0766
107. Larsson NG, Wang J, Wilhelmsson H, Oldfors A, Rustin P, Lewandoski M, et al. Mitochondrial transcription factor A is necessary for mtDNA maintenance and embryogenesis in mice. *Nat Genet*. (1998) 18:231–6. doi: 10.1038/ng0398-231
108. Bushdid PB, Osinska H, Wacław RR, Mołkentin JD, Yutzey KE. NFATc3 and NFATc4 are required for cardiac development and mitochondrial function. *Circ Res*. (2003) 92:1305–13. doi: 10.1161/01.RES.0000077045.84609.9F
109. Wang T, McDonald C, Petrenko NB, Leblanc M, Wang T, Giguere V, et al. Estrogen-Related Receptor α (ERRα) and ERRγ are essential coordinators of cardiac metabolism and function. *Mol Cell Biol*. (2015) 35:1281–98. doi: 10.1128/MCB.01156-14
110. Alaynick WA, Kondo RP, Xie W, He W, Dufour CR, Downes M, et al. ERRγ directs and maintains the transition to oxidative metabolism in the postnatal heart. *Cell Metab*. (2007) 6:13–24. doi: 10.1016/j.cmet.2007.06.007
111. Lee SH, Wolf PL, Escudero R, Deutsch R, Jamieson SW, Thistlethwaite PA. Early expression of angiogenesis factors in acute myocardial ischemia and infarction. *N Engl J Med*. (2000) 342:626–33. doi: 10.1056/NEJM200003023420904
112. Cross HR, Opie LH, Radda GK, Clarke K. Is a high glycogen content beneficial or detrimental to the ischemic rat heart? A controversy resolved. *Circ Res*. (1996) 78:482–91. doi: 10.1161/01.RES.78.3.482
113. Majmundar AJ, Wong WJ, Simon MC. Hypoxia-inducible factors and the response to hypoxic stress. *Mol Cell*. (2010) 40:294–309. doi: 10.1016/j.molcel.2010.09.022
114. Gustafsson ÅB. Bnip3 as a dual regulator of mitochondrial turnover and cell death in the myocardium. *Pediatr Cardiol*. (2011) 32:267–74. doi: 10.1007/s00246-010-9876-5
115. Semenza GL. Hypoxia-inducible factor 1 and cardiovascular disease. *Annu Rev Physiol*. (2014) 76:39–56. doi: 10.1146/annurev-physiol-021113-170322
116. Heather LC, Carr CA, Stuckey DJ, Pope S, Morten KJ, Carter EE, et al. Critical role of complex III in the early metabolic changes following myocardial infarction. *Cardiovasc Res*. (2010) 85:127–36. doi: 10.1093/cvr/cvp276
117. Dodd MS, Atherton HJ, Carr CA, Stuckey DJ, West JA, Griffin J, et al. Impaired *in vivo* mitochondrial krebs cycle activity after myocardial infarction assessed using hyperpolarized magnetic resonance spectroscopy. *Circ Cardiovasc Imaging* (2014) 7:895–904. doi: 10.1161/CIRCIMAGING.114.001857
118. Sharov VG, Goussev A, Lesch M, Goldstein S, Sabbah HN. Abnormal mitochondrial function in myocardium of dogs with chronic heart failure. *J Mol Cell Cardiol*. (1998) 30:1757–62. doi: 10.1006/jmcc.1998.0739
119. Sharov VG, Todor AV, Silverman N, Goldstein S, Sabbah HN. Abnormal mitochondrial respiration in failed human myocardium. *J Mol Cell Cardiol*. (2000) 32:2361–7. doi: 10.1006/jmcc.2000.1266
120. Gong G, Liu J, Liang P, Guo T, Hu Q, Ochiai K, et al. Oxidative capacity in failing hearts. *Am J Physiol Heart Circ Physiol*. (2003) 285:H541–8. doi: 10.1152/ajpheart.01142.2002
121. Casademont J, Miró O. Electron transport chain defects in heart failure. *Heart Fail Rev*. (2002) 7:131–9. doi: 10.1023/A:1015372407647
122. Marin-Garcia J, Goldenthal MJ, Moe GW. Mitochondrial pathology in cardiac failure. *Cardiovasc Res*. (2001) 49:17—26. doi: 10.1016/S0008-6363(00)00241-8
123. Quigley AF, Kapsa RM, Esmore D, Hale G, Byrne E. Mitochondrial respiratory chain activity in idiopathic dilated cardiomyopathy. *J Card Fail*. (2000) 6:47–55. doi: 10.1016/S1071-9164(00)00011-7
124. Taegtmeyer H, Sen S, Vela D. Return to the fetal gene program: a suggested metabolic link to gene expression in the heart. *Ann NY Acad Sci*. (2010) 1188:191–8. doi: 10.1111/j.1749-6632.2009.05100.x
125. Leong HS, Grist M, Parsons H, Wambolt RB, Lopaschuk GD, Brownsey R, et al. Accelerated rates of glycolysis in the hypertrophied heart: are they a methodological artifact? *Am J Physiol Endocrinol Metab*. (2002) 282:E1039–45. doi: 10.1152/ajpendo.00507.2001
126. Ellen Kreipke R, Wang Y, Miklas JW, Mathieu J, Ruohola-Baker H. Metabolic remodeling in early development and cardiomyocyte maturation. *Semin Cell Dev Biol*. (2016) 52:84–92. doi: 10.1016/j.semcdb.2016.02.004
127. Fragasso G. Deranged cardiac metabolism and the pathogenesis of heart failure. *Card Fail Rev*. (2016) 2:8–13. doi: 10.15420/cfr.2016:5:2

128. Marazzi G, Rosanio S, Caminiti G, Dioguardi FS, Mercuro G. The role of amino acids in the modulation of cardiac metabolism during ischemia and heart failure. *Curr Pharm Des*. (2008) 14:2592–604. doi: 10.2174/138161208786071227
129. Carubelli V, Castrini AI, Lazzarini V, Gheorghiade M, Metra M, Lombardi C. Amino acids and derivatives, a new treatment of chronic heart failure? *Heart Fail Rev*. (2014) 20:39–51. doi: 10.1007/s10741-014-9436-9
130. Wende AR, Brahma MK, McGinnis GR, Young ME. Metabolic origins of heart failure. *JACC Basic Translational Sci*. (2017) 2:297–310. doi: 10.1016/j.jacbts.2016.11.009
131. Lai L, Leone TC, Keller MP, Martin OJ, Broman AT, Nigro J, et al. Energy metabolic reprogramming in the hypertrophied and early stage failing heart a multisystems approach. *Circ Heart Fail*. (2014) 7:1022–31. doi: 10.1161/CIRCHEARTFAILURE.114.001469
132. Sun H, Olson KC, Gao C, Prosdocimo DA, Zhou M, Wang Z, et al. Catabolic defect of branched-chain amino acids promotes heart failure. *Circulation* (2016) 133:2038–49. doi: 10.1161/CIRCULATIONAHA.115.020226
133. Wang W, Zhang F, Xia Y, Zhao S, Yan W, Wang H, et al. Defective branched chain amino acids catabolism contributes to cardiac dysfunction and remodeling following myocardial infarction. *Am J Physiol Hear Circ Physiol*. (2016) 311:H1160–9. doi: 10.1152/ajpheart.00114.2016
134. Li T, Zhang Z, Kolwicz SC, Abell L, Roe ND, Kim M, et al. Defective branched-chain amino acid catabolism disrupts glucose metabolism and sensitizes the heart to ischemia-reperfusion injury. *Cell Metab*. (2017) 25:374–85. doi: 10.1016/j.cmet.2016.11.005
135. Biala AK, Dhingra R, Kirshenbaum LA. Mitochondrial dynamics: orchestrating the journey to advanced age. *J Mol Cell Cardiol*. (2015) 83:37–43. doi: 10.1016/j.yjmcc.2015.04.015
136. Lesnefsky EJ, Gudz TI, Moghaddas S, Migita CT, Ikeda-Saito M, Turkaly PJ, et al. Aging decreases electron transport complex III activity in heart interfibrillar mitochondria by alteration of the cytochrome c binding site. *J Mol Cell Cardiol*. (2001) 33:37–47. doi: 10.1006/jmcc.2000.1273
137. Johnson MT, Mahmood S, Patel MS. Intermediary metabolism and energetics during murine early embryogenesis. *J Biol Chem*. (2003) 278:31457–60. doi: 10.1074/jbc.R300002200
138. Folmes CDL, Dzeja PP, Nelson TJ, Terzic A. Metabolic plasticity in stem cell homeostasis and differentiation. *Cell Stem Cell*. (2012) 11:596–606. doi: 10.1016/j.stem.2012.10.002
139. Fisher SA, Zhang H, Doree C, Mathur A, Martin-Rendon E. Stem cell treatment for acute myocardial infarction. *Cochrane database Syst Rev*. (2015) 9:CD006536. doi: 10.1002/14651858.CD006536.pub4
140. Zhang J, Nuebel E, Daley GQ, Koehler CM, Teitell MA. Metabolic regulation in pluripotent stem cells during reprogramming and self-renewal. *Cell Stem Cell*. (2012) 11:589–95. doi: 10.1016/j.stem.2012.10.005
141. Kondoh H, Lleonart ME, Nakashima Y, Yokode M, Tanaka M, Bernard D, et al. A high glycolytic flux supports the proliferative potential of murine embryonic stem cells. *Antioxid Redox Signal*. (2006) 9:293–9. doi: 10.1089/ars.2007.9.ft-14
142. Moussaieff A, Rouleau M, Kitsberg D, Cohen M, Levy G, Barasch D, et al. Glycolysis-mediated changes in acetyl-coa and histone acetylation control the early differentiation of embryonic stem cells. *Cell Metab*. (2015) 21:392–402. doi: 10.1016/j.cmet.2015.02.002
143. Panopoulos AD, Yanes O, Ruiz S, Kida YS, Diep D, Tautenhahn R, et al. The metabolome of induced pluripotent stem cells reveals metabolic changes occurring in somatic cell reprogramming. *Cell Res*. (2012) 22:168–77. doi: 10.1038/cr.2011.177
144. Folmes CDL, Nelson TJ, Martinez-Fernandez A, Arrell DK, Lindor JZ, Dzeja PP, et al. Somatic oxidative bioenergetics transitions into pluripotency-dependent glycolysis to facilitate nuclear reprogramming. *Cell Metab*. (2011) 14:264–71. doi: 10.1016/j.cmet.2011.06.011
145. Zhu S, Li W, Zhou H, Wei W, Ambasudhan R, Lin T, et al. Reprogramming of human primary somatic cells by OCT4 and chemical compounds. *Cell Stem Cell* (2010) 7:651–5. doi: 10.1016/j.stem.2010.11.015
146. Xu X, Duan S, Yi F, Ocampo A, Liu GH, Izpisua Belmonte JC. Mitochondrial regulation in pluripotent stem cells. *Cell Metab*. (2013) 18:325–32. doi: 10.1016/j.cmet.2013.06.005
147. Prieto J, León M, Ponsoda X, Sendra R, Bort R, Ferrer-Lorente R, et al. Early ERK1/2 activation promotes DRP1-dependent mitochondrial fission necessary for cell reprogramming. *Nat Commun*. (2016)7:11124. doi: 10.1038/ncomms11124
148. Cho YM, Kwon S, Pak YK, Seol HW, Choi YM, Park do J, et al. Dynamic changes in mitochondrial biogenesis and antioxidant enzymes during the spontaneous differentiation of human embryonic stem cells. *Biochem Biophys Res Commun*. (2006) 348:1472–8. doi: 10.1016/j.bbrc.2006.08.020
149. Inoue SI, Noda S, Kashima K, Nakada K, Hayashi JI, Miyoshi H. Mitochondrial respiration defects modulate differentiation but not proliferation of hematopoietic stem and progenitor cells. *FEBS Lett*. (2010) 584:3402–9. doi: 10.1016/j.febslet.2010.06.036
150. Cai CL, Molkentin JD. The elusive progenitor cell in cardiac regeneration: slip slidin' away. *Circ Res*. (2017) 120:400–6. doi: 10.1161/CIRCRESAHA.116.309710
151. Li L, Xie T. Stem cell niche: structure and function. *Annu Rev Cell Dev Biol*. (2005) 21:605–31. doi: 10.1146/annurev.cellbio.21.012704.131525
152. Warburg O. Injuring of respiration the origin of cancer cells. *Science* (1956) 123:309–14. doi: 10.1126/science.123.3191.309
153. Munyon W, Merchant D. The relation between glucose utilization, lactic acid production and utilization and the growth cycle of L strain fibroblasts. *Exp Cell Res*. (1959) 17:490–98. doi: 10.1016/0014-4827(59)90069-2
154. Wang T, Marquardt C, Foker J. Aerobic glycolysis during lymphocyte proliferation. *Nature* (1976) 261:702–5. doi: 10.1038/261702a0
155. Hedeskov CJ. Early effects of phytohaemagglutinin on glucose metabolism of normal human lymphocytes. *Biochem J*. (1968) 110:373–80. doi: 10.1042/bj1100373
156. Lunt SY, Vander Heiden MG. Aerobic glycolysis: meeting the metabolic requirements of cell proliferation. *Annu Rev Cell Dev Biol*. (2011) 27:441–64. doi: 10.1146/annurev-cellbio-092910-154237
157. Board M, Lopez C, van den Bos C, Callaghan R, Clarke K, Carr C. Acetoacetate is a more efficient energy-yielding substrate for human mesenchymal stem cells than glucose and generates fewer reactive oxygen species. *Int J Biochem Cell Biol*. (2017) 88:75–83. doi: 10.1016/j.biocel.2017.05.007
158. Dos Santos F, Andrade PZ, Boura JS, Abecasis MM, Da Silva CL, Cabral JMS. *Ex vivo* expansion of human mesenchymal stem cells: a more effective cell proliferation kinetics and metabolism under hypoxia. *J Cell Physiol*. (2010) 223:27–35. doi: 10.1002/jcp.21987
159. Hosios AM, Hecht VC, Danai LV, Johnson MO, Rathmell JC, Steinhauser ML, et al. Amino acids rather than glucose account for the majority of cell mass in proliferating mammalian cells. *Dev Cell*. (2016) 36:540–9. doi: 10.1016/j.devcel.2016.02.012
160. Dai DF, Danoviz ME, Wiczer B, Laflamme MA, Tian R. Mitochondrial maturation in human pluripotent stem cell derived cardiomyocytes. *Stem Cells Int*. (2017) 2017:5153625. doi: 10.1155/2017/5153625
161. Birket MJ, Casini S, Kosmidis G, Elliott DA, Gerencser AA, Baartscheer A, et al. PGC-1α and reactive oxygen species regulate human embryonic stem cell-derived cardiomyocyte function. *Stem Cell Rep*. (2013) 1:560–74. doi: 10.1016/j.stemcr.2013.11.008
162. Wang Z, Yang Y, Xiang X, Zhu Y, Men J, He M. Estimation of the normal range of blood glucose in rats. *Wei Sheng Yan Jiu*. (2010) 39:133–7, 142.
163. Wolfensohn S, Lloyd M. *Handbook of Laboratory Animal Management and Welfare*. 3rd ed. Oxford: Blackwell Publishing Ltd (2003).
164. Perbellini F, Gomes RSM, Vieira S, Buchanan D, Malandraki-Miller S, Bruyneel A, et al. Chronic high-fat feeding affects the mesenchymal cell population expanded from adipose tissue but not cardiac atria. *Stem Cells Transl Med*. (2015) 4:1403–14. doi: 10.5966/sctm.2015-0024
165. Abdelmagid SA, Clarke SE, Nielsen DE, Badawi A, El-Sohemy A, Mutch DM, et al. Comprehensive profiling of plasma fatty acid concentrations in young healthy canadian adults. *PLoS ONE* (2015) 10:e0116195zzzz. doi: 10.1371/journal.pone.0116195
166. Vander Heiden MG, Cantley LC, Thompson CB. Understanding the Warburg effect: the metabolic requirements of cell proliferation. *Science* (2009) 324:1029–33. doi: 10.1126/science.1160809
167. Lee YK, Ng KM, Lai WH, Chan YC, Lau YM, Lian Q, et al. Calcium homeostasis in human induced pluripotent stem

cell-derived cardiomyocytes. *Stem Cell Rev*. (2011) 7:976–86. doi: 10.1007/s12015-011-9273-3
168. Kim C, Wong J, Wen J, Wang S, Wang C, Spiering S, et al. Studying arrhythmogenic right ventricular dysplasia with patient-specific iPSCs. *Nature* (2013) 494:105–10. doi: 10.1038/nature11799
169. Da Rocha AM, Campbell K, Mironov S, Jiang J, Mundada L, Guerrero-Serna G, et al. HiPSC-CM monolayer maturation state determines drug responsiveness in high throughput pro-arrhythmia screen. *Sci Rep*. (2017) 7:13834. doi: 10.1038/s41598-017-13590-y
170. Barr RL, Lopaschuk GD. Direct measurement of energy metabolism in the isolated working rat heart. *J Pharmacol Toxicol Methods* (1997) 38:11–7. doi: 10.1016/S1056-8719(97)86574-4
171. Belke DD, Larsen TS, Lopaschuk GD, Severson DL. Glucose and fatty acid metabolism in the isolated working mouse heart. *Am J Physiol*. (1999) 277(4 Pt 2):R1210–7. doi: 10.1152/ajpregu.1999.277.4.R1210
172. Jang DH, Greenwood JC, Spyres MB, Eckmann DM. Measurement of mitochondrial respiration and motility in acute care. *J Intensive Care Med*. (2017) 32:86–94. doi: 10.1177/0885066616658449
173. Brand MD, Nicholls DG. Assessing mitochondrial dysfunction in cells. *Biochem J*. (2011) 435(Pt 2): 297–312. doi: 10.1042/BJ20110162
174. Heather LC, Cole MA, Tan JJ, Ambrose LJA, Pope S, Abd-Jamil AH, et al. Metabolic adaptation to chronic hypoxia in cardiac mitochondria. *Basic Res Cardiol*. (2012) 107:268–79. doi: 10.1007/s00395-012-0268-2
175. Tan SC, Gomes RSM, Yeoh KK, Perbellini F, Malandraki-Miller S, Ambrose L, et al. Preconditioning of cardiosphere-derived cells with hypoxia or prolyl-4-hydroxylase inhibitors increases stemness and decreases reliance on oxidative metabolism. *Cell Transplant*. (2016) 25:35–53. doi: 10.3727/096368915X687697
176. Murry CE, Field LJ, Menasché P. Cell-based cardiac repair reflections at the 10-year point. *Circulation* (2005) 112:3174–83. doi: 10.1161/CIRCULATIONAHA.105.546218
177. Barile L, Messina E, Giacomello A, Marbán E. Endogenous cardiac stem cells. *Prog Cardiovasc Dis*. (2007) 50:31–48. doi: 10.1016/j.pcad.2007.03.005
178. Smits AM, van Vliet P, Metz CH, Korfage T, Sluijter JP, Doevendans PA, et al. Human cardiomyocyte progenitor cells differentiate into functional mature cardiomyocytes: an *in vitro* model for studying human cardiac physiology and pathophysiology. *Nat Protoc*. (2009) 4:232–43. doi: 10.1038/nprot.2008.229
179. Goumans MJ, de Boer TP, Smits AM, van Laake LW, van Vliet P, Metz CHG, et al. TGF-β1 induces efficient differentiation of human cardiomyocyte progenitor cells into functional cardiomyocytes *in vitro*. *Stem Cell Res*. (2008) 1:138–49. doi: 10.1016/j.scr.2008.02.003
180. Ye J, Boyle A, Shih H, Sievers RE, Zhang Y, Prasad M, et al. Sca-1 + cardiosphere-derived cells are enriched for isl1-expressing cardiac precursors and improve cardiac function after myocardial injury. *PLoS ONE* (2012) 7:e30329. doi: 10.1371/journal.pone.0030329
181. Smith AJ, Lewis FC, Aquila I, Waring CD, Nocera A, Agosti V, et al. Isolation and characterization of resident endogenous c-Kit+ cardiac stem cells from the adult mouse and rat heart. *Nat Protoc*. (2014) 9:1662–81. doi: 10.1038/nprot.2014.113
182. Matsuura K, Nagai T, Nishigaki N, Oyama T, Nishi J, Wada H, et al. Adult cardiac Sca-1-positive cells differentiate into beating cardiomyocytes. *J Biol Chem*. (2004) 279:11384–91. doi: 10.1074/jbc.M310822200
183. Oyama T, Nagai T, Wada H, Naito AT, Matsuura K, Iwanaga K, et al. Cardiac side population cells have a potential to migrate and differentiate into cardiomyocytes *in vitro* and *in vivo*. *J Cell Biol*. (2007) 176:329–41. doi: 10.1083/jcb.200603014
184. Fukuda K. Development of regenerative cardiomyocytes from mesenchymal stem cells for cardiovascular tissue engineering. *Artif Organs*. (2001) 25:187–93. doi: 10.1046/j.1525-1594.2001.025003187.x
185. Rangappa S, Fen C, Lee EH, Bongso A, Wei ESK. Transformation of adult mesenchymal stem cells isolated from the fatty tissue into cardiomyocytes. *Ann Thorac Surg*. (2003) 75:775–9. doi: 10.1016/S0003-4975(02)04568-X
186. Qian Q, Qian H, Zhang X, Zhu W, Yan Y, Ye S, et al. 5-azacytidine induces cardiac differentiation of human umbilical cord-derived mesenchymal stem cells by activating extracellular regulated kinase. *Stem Cells Dev*. (2012) 21:67–75. doi: 10.1089/scd.2010.0519
187. Xu W, Zhang X, Qian H, Zhu W, Sun X, Hu J, et al. Mesenchymal stem cells from adult human bone marrow differentiate into a cardiomyocyte phenotype *in vitro*. *Exp Biol Med*. (2004) 229:623–31. doi: 10.1177/153537020422900706
188. Naeem N, Haneef K, Kabir N, Iqbal H, Jamall S, Salim A. DNA methylation inhibitors, 5-azacytidine and zebularine potentiate the transdifferentiation of rat bone marrow mesenchymal stem cells into cardiomyocytes. *Cardiovasc Ther*. (2013) 31:201–9. doi: 10.1111/j.1755-5922.2012.00320.x
189. Bearzi C, Rota M, Hosoda T, Tillmanns J, Nascimbene A, De Angelis A, et al. Human cardiac stem cells. *Proc Natl Acad Sci USA*. (2007) 104:14068–73. doi: 10.1073/pnas.0706760104
190. Linke A, Muller P, Nurzynska D, Casarsa C, Torella D, Nascimbene A, et al. Stem cells in the dog heart are self-renewing, clonogenic, and multipotent and regenerate infarcted myocardium, improving cardiac function. *Proc Natl Acad Sci USA*. (2005) 102:8966–71. doi: 10.1073/pnas.0502678102
191. Stresemann C, Lyko F. Modes of action of the DNA methyltransferase inhibitors azacytidine and decitabine. *Int J Cancer* (2008) 123:8–13. doi: 10.1002/ijc.23607
192. Issa JPJ. DNA methylation as a therapeutic target in cancer. *Clin Cancer Res*. (2007) 13:1634–7. doi: 10.1158/1078-0432.CCR-06-2076
193. Kaur K, Yang J, Eisenberg CA, Eisenberg LM. 5-Azacytidine promotes the transdifferentiation of cardiac cells to skeletal myocytes. *Cell Reprog*. (2014) 16:1–7. doi: 10.1089/cell.2014.0021
194. Wan Safwani WKZ, Makpol S, Sathapan S, Chua KH. 5-Azacytidine is insufficient for cardiogenesis in human adipose-derived stem cells. *J Negat Results Biomed*. (2012) 11:3. doi: 10.1186/1477-5751-11-3
195. Takahashi T, Lord B, Schulze PC, Fryer RM, Sarang SS, Gullans SR, et al. Ascorbic acid enhances differentiation of embryonic stem cells into cardiac myocytes. *Circulation* (2003) 107:1912–6. doi: 10.1161/01.CIR.0000064899.53876.A3
196. Cao N, Liu Z, Chen Z, Wang J, Chen T, Zhao X, et al. Ascorbic acid enhances the cardiac differentiation of induced pluripotent stem cells through promoting the proliferation of cardiac progenitor cells. *Cell Res*. (2012) 22:219–36. doi: 10.1038/cr.2011.195
197. Choi KM, Seo YK, Yoon HH, Song KY, Kwon SY, Lee HS, et al. Effect of ascorbic acid on bone marrow-derived mesenchymal stem cell proliferation and differentiation. *J Biosci Bioeng*. (2008) 105:586–94. doi: 10.1263/jbb.105.586
198. Lim JY, Kim WH, Kim J, Park SI. Involvement of TGF-beta1 signaling in cardiomyocyte differentiation from P19CL6 cells. *Mol Cells* (2007) 24:431–6.
199. McCulloch CA, Tenenbaum HC. Dexamethasone induces proliferation and terminal differentiation of osteogenic cells in tissue culture. *Anat Rec*. (1986) 215:397–402. doi: 10.1002/ar.1092150410
200. Jaiswal N, Haynesworth SE, Caplan AI, Bruder SP. Osteogenic differentiation of purified, culture-expanded human mesenchymal stem cells *in vitro*. *J Cell Biochem*. (1997) 64:295–312. doi: 10.1002/(SICI)1097-4644(199702)64:2<295::AID-JCB12>3.0.CO;2-I
201. Hamidouche Z, Haÿ E, Vaudin P, Charbord P, Schüle R, Marie PJ, et al. FHL2 mediates dexamethasone-induced mesenchymal cell differentiation into osteoblasts by activating Wnt/beta-catenin signaling-dependent Runx2 expression. *FASEB J*. (2008) 22:3813–22. doi: 10.1096/fj.08-106302
202. Chang PL, Blair HC, Zhao X, Chien YW, Chen D, Tilden AB, et al. Comparison of fetal and adult marrow stromal cells in osteogenesis with and without glucocorticoids. *Connect Tissue Res*. (2006) 47:67–76. doi: 10.1080/03008200600584074
203. Kattman SJ, Witty AD, Gagliardi M, Dubois NC, Niapour M, Hotta A, et al. Stage-specific optimization of activin/nodal and BMP signaling promotes cardiac differentiation of mouse and human pluripotent stem cell lines. *Cell Stem Cell* (2011) 8:228–40. doi: 10.1016/j.stem.2010.12.008
204. Kehat I, Kenyagin-Karsenti D, Snir M, Segev H, Amit M, Gepstein A, et al. Human embryonic stem cells can differentiate into myocytes with structural and functional properties of cardiomyocytes. *J Clin Invest*. (2001) 108:407–14. doi: 10.1172/JCI200112131
205. Lian X, Zhang J, Zhu K, Kamp TJ, Palecek SP. Insulin inhibits cardiac mesoderm, not mesendoderm, formation during cardiac differentiation of

human pluripotent stem cells and modulation of canonical wnt signaling can rescue this inhibition. *Stem Cells* (2013) 31:447–57. doi: 10.1002/stem.1289
206. Lian X, Zhang J, Azarin SM, Zhu K, Hazeltine LB, Bao X, et al. Directed cardiomyocyte differentiation from human pluripotent stem cells by modulating Wnt/β-catenin signaling under fully defined conditions. *Nat Protoc.* (2013) 8:162–75. doi: 10.1038/nprot.2012.150
207. Lian X, Hsiao C, Wilson G, Zhu K, Hazeltine LB, Azarin SM, et al. Robust cardiomyocyte differentiation from human pluripotent stem cells via temporal modulation of canonical Wnt signaling. *Proc Natl Acad Sci USA*. (2012) 109:E1848–57. doi: 10.1073/pnas.1200250109
208. Paige SL, Osugi T, Afanasiev OK, Pabon L, Reinecke H, Murry CE. Endogenous wnt/β-Catenin signaling is required for cardiac differentiation in human embryonic stem cells. *PLoS ONE* (2010) 5:e11134. doi: 10.1371/journal.pone.0011134
209. Mummery CL, Zhang J, Ng ES, Elliott DA, Elefanty AG, Kamp TJ. Differentiation of human embryonic stem cells and induced pluripotent stem cells to cardiomyocytes: a methods overview. *Circ Res*. (2012) 111:344–58. doi: 10.1161/CIRCRESAHA.110.227512
210. Tzahor E. Wnt/β-Catenin signaling and cardiogenesis: timing does matter. *Dev Cell* (2007) 13:10–3. doi: 10.1016/j.devcel.2007.06.006
211. Kwon C, Arnold J, Hsiao EC, Taketo MM, Conklin BR, Srivastava D. Canonical Wnt signaling is a positive regulator of mammalian cardiac progenitors. *Proc Natl Acad Sci USA*. (2007) 104:10894–9. doi: 10.1073/pnas.0704044104
212. Lin L, Cui L, Zhou W, Dufort D, Zhang X, Cai CL, et al. beta-Catenin directly regulates Islet1 expression in cardiovascular progenitors and is required for multiple aspects of cardiogenesis. *Proc Natl Acad Sci USA*. (2007) 104:9313–8. doi: 10.1073/pnas.0700923104
213. Ueno S, Weidinger G, Osugi T, Kohn AD, Golob JL, Pabon L, et al. Biphasic role for Wnt/beta-catenin signaling in cardiac specification in zebrafish and embryonic stem cells. *Proc Natl Acad Sci USA*. (2007) 104:9685–90. doi: 10.1073/pnas.0702859104
214. Nathan E, Monovich A, Tirosh-Finkel L, Harrelson Z, Rousso T, Rinon A, et al. The contribution of Islet1-expressing splanchnic mesoderm cells to distinct branchiomeric muscles reveals significant heterogeneity in head muscle development. *Development* (2008) 135:647–57. doi: 10.1242/dev.007989
215. Zhang J, Wilson GF, Soerens AG, Koonce CH, Yu J, Palecek SP, et al. Functional cardiomyocytes derived from human induced pluripotent stem cells. *Circ Res.* (2009) 104:e30—41. doi: 10.1161/CIRCRESAHA.108.192237
216. Xu C, Police S, Rao N, Carpenter MK. Characterization and enrichment of cardiomyocytes derived from human embryonic stem cells. *Circ Res.* (2002) 91:501–8. doi: 10.1161/01.RES.0000035254.80718.91
217. Passier R, Oostwaard DW, Snapper J, Kloots J, Hassink RJ, Kuijk E, et al. Increased cardiomyocyte differentiation from human embryonic stem cells in serum-free cultures. *Stem Cells* (2005) 23:772–80. doi: 10.1634/stemcells.2004-0184
218. Laflamme MA, Gold J, Xu C, Hassanipour M, Rosler E, Police S, et al. Formation of human myocardium in the rat heart from human embryonic stem cells. *Am J Pathol*. (2005) 167:663–71. doi: 10.1016/S0002-9440(10)62041-X
219. Graichen R, Xu X, Braam SR, Balakrishnan T, Norfiza S, Sieh S, et al. Enhanced cardiomyogenesis of human embryonic stem cells by a small molecular inhibitor of p38 MAPK. *Differentiation* (2008) 76:357–70. doi: 10.1111/j.1432-0436.2007.00236.x
220. Freund C, Davis RP, Gkatzis K, Ward-van Oostwaard D, Mummery CL. The first reported generation of human induced pluripotent stem cells (iPS cells) and iPS cell-derived cardiomyocytes in the Netherlands. *Neth Heart J*. (2010) 18:51–4.
221. Yang L, Soonpaa MH, Adler ED, Roepke TK, Kattman SJ, Kennedy M, et al. Human cardiovascular progenitor cells develop from a KDR+ embryonic-stem-cell-derived population. *Nature* (2008) 453:524–8. doi: 10.1038/nature06894
222. Burridge PW, Matsa E, Shukla P, Lin ZC, Churko JM, Ebert AD, et al. Chemically defined generation of human cardiomyocytes. *Nat Methods* (2014) 11:855–60. doi: 10.1038/nmeth.2999
223. Zhang J, Klos M, Wilson GF, Herman AM, Lian X, Raval KK, et al. Extracellular matrix promotes highly efficient cardiac differentiation of human pluripotent stem cells: the matrix sandwich method. *Circ Res*. (2012) 111:1125–36. doi: 10.1161/CIRCRESAHA.112.273144
224. Zorzano A, Liesa M, Palacín M. Role of mitochondrial dynamics proteins in the pathophysiology of obesity and type 2 diabetes. *Int J Biochem Cell Biol*. (2009) 41:1846–54. doi: 10.1016/j.biocel.2009.02.004
225. Paltauf-Doburzynska J, Malli R, Graier WF. Hyperglycemic conditions affect shape and Ca2+ homeostasis of mitochondria in endothelial cells. *J Cardiovasc Pharmacol.* (2004) 44:423–36. doi: 10.1097/01.fjc.0000139449.64337.1b
226. Simsek T, Kocabas F, Zheng J, Deberardinis RJ, Mahmoud AI, Olson EN, et al. The distinct metabolic profile of hematopoietic stem cells reflects their location in a hypoxic niche. *Cell Stem Cell* (2010) 7:380–90. doi: 10.1016/j.stem.2010.07.011
227. Pattappa G, Heywood HK, de Bruijn JD, Lee DA. The metabolism of human mesenchymal stem cells during proliferation and differentiation. *J Cell Physiol*. (2011) 226:2562–70. doi: 10.1002/jcp.22605
228. Mathieu J, Zhang Z, Nelson A, Lamba DA, Reh TA, Ware C, et al. Hypoxia induces re-entry of committed cells into pluripotency. *Stem Cell*. (2013) 31:1737–48. doi: 10.1002/stem.1446
229. Ng KM, Lee YK, Chan YC, Lai WH, Fung ML, Li RA, et al. Exogenous expression of HIF-1 alpha promotes cardiac differentiation of embryonic stem cells. *J Mol Cell Cardiol.* (2010) 48:1129–37. doi: 10.1016/j.yjmcc.2010.01.015
230. Medley TL, Furtado M, Lam NT, Idrizi R, Williams D, Verma PJ, et al. Effect of oxygen on cardiac differentiation in mouse iPS cells: role of hypoxia inducible factor-1 and Wnt/beta-catenin signaling. *PLoS ONE* (2013) 8:e80280. doi: 10.1371/journal.pone.0080280
231. Gaber N, Gagliardi M, Patel P, Kinnear C, Zhang C, Chitayat D, et al. Fetal reprogramming and senescence in hypoplastic left heart syndrome and in human pluripotent stem cells during cardiac differentiation. *Am J Pathol*. (2013) 183:720–34. doi: 10.1016/j.ajpath.2013.05.022
232. Fynes K, Tostoes R, Ruban L, Weil B, Mason C, Veraitch FS. The differential effects of 2% oxygen preconditioning on the subsequent differentiation of mouse and human pluripotent stem cells. *Stem Cells Dev*. (2014) 23:1910–22. doi: 10.1089/scd.2013.0504
233. Sauer H, Rahimi G, Hescheler J, Wartenberg M. Role of reactive oxygen species and phosphatidylinositol 3-kinase in cardiomyocyte differentiation of embryonic stem cells. *FEBS Lett*. (2000) 476:218–23. doi: 10.1016/S0014-5793(00)01747-6
234. Li J, Stouffs M, Serrander L, Banfi B, Bettiol E, Charnay Y, et al. The NADPH oxidase NOX4 drives cardiac differentiation: role in regulating cardiac transcription factors and MAP kinase activation. *Mol Biol Cell* (2006) 17:3978–88. doi: 10.1091/mbc.e05-06-0532
235. Crespo FL, Sobrado VR, Gomez L, Cervera AM, McCreath KJ. Mitochondrial reactive oxygen species mediate cardiomyocyte formation from embryonic stem cells in high glucose. *Stem Cells* (2010) 28:1132–42. doi: 10.1002/stem.441
236. Lundy SD, Zhu WZ, Regnier M, Laflamme MA. Structural and functional maturation of cardiomyocytes derived from human pluripotent stem cells. *Stem Cells Dev*. (2013) 22:1991–2002. doi: 10.1089/scd.2012.0490
237. Chan YC, Ting S, Lee YK, Ng KM, Zhang J, Chen Z, et al. Electrical stimulation promotes maturation of cardiomyocytes derived from human embryonic stem cells. *J Cardiovasc Transl Res*. (2013) 6:989–99. doi: 10.1007/s12265-013-9510-z
238. Ruan JL, Tulloch NL, Razumova MV, Saiget M, Muskheli V, Pabon L, et al. Mechanical stress conditioning and electrical stimulation promote contractility and force maturation of induced pluripotent stem cell-derived human cardiac tissue. *Circulation* (2016) 134:1557–67. doi: 10.1161/CIRCULATIONAHA.114.014998
239. Yang X, Rodriguez M, Pabon L, Fischer KA, Reinecke H, Regnier M, et al. Tri-iodo-l-thyronine promotes the maturation of human cardiomyocytes-derived from induced pluripotent stem cells. *J Mol Cell Cardiol*. (2014) 72:296–304. doi: 10.1016/j.yjmcc.2014.04.005
240. Hazeltine LB, Simmons CS, Salick MR, Lian X, Badur MG, Han W, et al. Effects of substrate mechanics on contractility of cardiomyocytes generated

from human pluripotent stem cells. *Int J Cell Biol*. (2012) 2012:508294. doi: 10.1155/2012/508294
241. Lieu DK, Fu J, Chiamvimonvat N, Tung KWC, McNerney GP, Huser T, et al. Mechanism-based facilitated maturation of human pluripotent stem cell-derived cardiomyocytes. *Circ Arrhythmia Electrophysiol*. (2013) 6:191—201. doi: 10.1161/CIRCEP.111.973420
242. Liu J, Lieu DK, Siu CW, Fu JD, Tse HF, Li RA. Facilitated maturation of Ca2+ handling properties of human embryonic stem cell-derived cardiomyocytes by calsequestrin expression. *Am J Physiol Cell Physiol*. (2009) 297:C152—9. doi: 10.1152/ajpcell.00060.2009
243. Kuppusamy KT, Jones DC, Sperber H, Madan A, Fischer KA, Rodriguez ML, et al. Let-7 family of microRNA is required for maturation and adult-like metabolism in stem cell-derived cardiomyocytes. *Proc Natl Acad Sci USA*. (2015) 112:E2785–94. doi: 10.1073/pnas.1424042112
244. Zhang D, Shadrin IY, Lam J, Xian HQ, Snodgrass HR, Bursac N. Tissue-engineered cardiac patch for advanced functional maturation of human ESC-derived cardiomyocytes. *Biomaterials* (2013) 34:5813–20. doi: 10.1016/j.biomaterials.2013.04.026
245. Ulmer BM, Stoehr A, Schulze ML, Patel S, Gucek M, Mannhardt I, et al. Contractile work contributes to maturation of energy metabolism in hipsc-derived cardiomyocytes. *Stem Cell Rep*. (2018) 10:834–47. doi: 10.1016/j.stemcr.2018.01.039
246. Huebsch N, Loskill P, Deveshwar N, Spencer CI, Judge LM, Mandegar MA, et al. Miniaturized iPS-cell-derived cardiac muscles for physiologically relevant drug response analyses. *Sci Rep*. (2016) 6:24726. doi: 10.1038/srep24726
247. Besser RR, Ishahak M, Mayo V, Carbonero D, Claure I, Agarwal A. Engineered microenvironments for maturation of stem cell derived cardiac myocytes. *Theranostics* (2018) 8:124–40. doi: 10.7150/thno.19441
248. Drawnel FM, Boccardo S, Prummer M, Delobel F, Graff A, Weber M, et al. Disease modeling and phenotypic drug screening for diabetic cardiomyopathy using human induced pluripotent stem cells. *Cell Rep*. (2014) 9:810–20. doi: 10.1016/j.celrep.2014.09.055
249. Correia C, Koshkin A, Duarte P, Hu D, Teixeira A, Domian I, et al. Distinct carbon sources affect structural and functional maturation of cardiomyocytes derived from human pluripotent stem cells. *Sci Rep*. (2017) 7:8590. doi: 10.1038/s41598-017-08713-4
250. Rana P, Anson B, Engle S, Will Y. Characterization of human-induced pluripotent stem cell-derived cardiomyocytes: bioenergetics and utilization in safety screening. *Toxicol Sci*. (2012) 130:117–31. doi: 10.1093/toxsci/kfs233
251. Shimizu T. Fabrication of pulsatile cardiac tissue grafts using a novel 3-dimensional cell sheet manipulation technique and temperature-responsive cell culture surfaces. *Circ Res*. (2002) 90:40e—48. doi: 10.1161/hh0302.105722
252. Carrier RL, Papadaki M, Rupnick M, Schoen FJ, Bursac N, Langer R, et al. Cardiac tissue engineering: cell seeding, cultivation parameters, and tissue construct characterization. *Biotechnol Bioeng*. (1999) 64:580–9. doi: 10.1002/(SICI)1097-0290(19990905)64:5<580::AID-BIT8>3.0.CO;2-X
253. Leor J, Aboulafia-Etzion S, Dar A, Shapiro L, Barbash IM, Battler A, et al. Bioengineered cardiac grafts: a new approach to repair the infarcted myocardium? *Circulation* (2000) 102 (19 Suppl. 3):III56–61. doi: 10.1161/01.CIR.102.suppl_3.III-56
254. Li RK, Jia ZQ, Weisel RD, Mickle DAG, Choi A, Yau TM. Survival and function of bioengineered cardiac grafts. *Circulation* (1999) 100 (Suppl. 2):II-63–II-69.
255. Bursac N, Papadaki M, Cohen RJ, Schoen FJ, Eisenberg SR, Carrier R, et al. Cardiac muscle tissue engineering: toward an *in vitro* model for electrophysiological studies. *Am J Physiol*. (1999) 277:H433–44.
256. Kofidis T, de Bruin JL, Yamane T, Tanaka M, Lebl DR, Swijnenburg RJ, et al. Stimulation of paracrine pathways with growth factors enhances embryonic stem cell engraftment and host-specific differentiation in the heart after ischemic myocardial injury. *Circulation* (2005) 111:2486–93. doi: 10.1161/01.CIR.0000165063.09283.A8
257. Van Luyn MJA, Tio RA, Gallego Y Van Seijen XJ, Plantinga JA, De Leij LFMH, DeJongste MJL, et al. Cardiac tissue engineering: characteristics of in unison contracting two- and three-dimensional neonatal rat ventricle cell (co)-cultures. *Biomaterials* (2002) 23:4793–801. doi: 10.1016/S0142-9612(02)00230-2
258. Zimmermann WH, Fink C, Kralisch D, Remmers U, Weil J, Eschenhagen T. Three-dimensional engineered heart tissue from neonatal rat cardiac myocytes. *Biotechnol Bioeng*. (2000) 68:106–14. doi: 10.1002/(SICI)1097-0290(20000405)68:1<106::AID-BIT13>3.0.CO;2-3
259. Eschenhagen T, Fink C, Remmers U, Scholz H, Wattchow J, Weil J, et al. Three-dimensional reconstitution of embryonic cardiomyocytes in a collagen matrix: a new heart muscle model system. *FASEB J*. (1997) 11:683–94. doi: 10.1096/fasebj.11.8.9240969
260. Zimmermann WH, Schneiderbanger K, Schubert P, Didi M Munzel F, Heubach JF, et al. Tissue engineering of a differentiated cardiac muscle construct. *Circ Res*. (2002) 90:223–30. doi: 10.1161/hh0202.103644
261. Bian W, Badie N, Himel HD, Bursac N. Robust T-tubulation and maturation of cardiomyocytes using tissue-engineered epicardial mimetics. *Biomaterials* (2014) 35:3819–28. doi: 10.1016/j.biomaterials.2014.01.045
262. Zhang W, Kong CW, Tong MH, Chooi WH, Huang N, Li RA, et al. Maturation of human embryonic stem cell-derived cardiomyocytes (hESC-CMs) in 3D collagen matrix: effects of niche cell supplementation and mechanical stimulation. *Acta Biomater*. (2017) 49:204–17. doi: 10.1016/j.actbio.2016.11.058
263. Daley WP, Peters SB, Larsen M. Extracellular matrix dynamics in development and regenerative medicine. *J Cell Sci*. (2008) 121(Pt 3):255–64. doi: 10.1242/jcs.006064
264. Aszódi A, Legate KR, Nakchbandi I, Fässler R. What mouse mutants teach us about extracellular matrix function. *Annu Rev Cell Dev Biol*. (2006) 22:591–621. doi: 10.1146/annurev.cellbio.22.010305.104258
265. Radisic M, Park H, Shing H, Consi T, Schoen FJ, Langer R, et al. Functional assembly of engineered myocardium by electrical stimulation of cardiac myocytes cultured on scaffolds. *Proc Natl Acad Sci USA*. (2004) 101:18129–34. doi: 10.1073/pnas.0407817101
266. Zimmermann WH, Melnychenko I, Wasmeier G, Didie M, Naito H, Nixdorff U, et al. Engineered heart tissue grafts improve systolic and diastolic function in infarcted rat hearts. *Nat Med*. (2006) 12:452–8. doi: 10.1038/nm1394
267. Chen Q, Bruyneel A, Clarke K, Carr C, Czernuszka J. Collagen-based scaffolds for potential application of heart valve tissue engineering. *J Tissue Sci Eng*. (2012) S11:3–8. doi: 10.4172/2157-7552.S11-003
268. Hansen A, Eder A, Bonstrup M, Flato M, Mewe M, Schaaf S, et al. Development of a drug screening platform based on engineered heart tissue. *Circ Res*. (2010) 107:35–44. doi: 10.1161/CIRCRESAHA.109.211458
269. Christman KL, Vardanian AJ, Fang Q, Sievers RE, Fok HH, Lee RJ. Injectable fibrin scaffold improves cell transplant survival, reduces infarct expansion, and induces neovasculature formation in ischemic myocardium. *J Am Coll Cardiol*. (2004) 44:654–60. doi: 10.1016/j.jacc.2004.04.040
270. Khademhosseini A, Eng G, Yeh J, Kucharczyk PA, Langer R, Vunjak-Novakovic G, et al. Microfluidic patterning for fabrication of contractile cardiac organoids. *Biomed Microdevices* (2007) 9:149–57. doi: 10.1007/s10544-006-9013-7
271. Chen Q, Bruyneel A, Carr C, Czernuszka J. Bio-mechanical properties of novel bi-layer collagen-elastin scaffolds for heart valve tissue engineering. *Procedia Eng*. (2013) 59:247–54. doi: 10.1016/j.proeng.2013.05.118
272. Yu J, Lee AR, Lin WH, Lin CW, Wu YK, Tsai WB. Electrospun PLGA fibers incorporated with functionalized biomolecules for cardiac tissue engineering. *Tissue Eng Part A*. (2014) 20:1896–907. doi: 10.1089/ten.tea.2013.0008
273. Jacot JG, Kita-Matsuo H, Wei KA, Vincent Chen HS, Omens JH, Mercola M, et al. Cardiac myocyte force development during differentiation and maturation. *Ann NY Acad Sci*. (2010) 1188:121–7. doi: 10.1111/j.1749-6632.2009.05091.x
274. Nachlas ALY, Li S, Jha R, Singh M, Xu C, Davis ME. Human iPSC-derived mesenchymal stem cells encapsulated in PEGDA hydrogels mature into valve interstitial-like cells. *Acta Biomater*. (2018) 71:235–46. doi: 10.1016/j.actbio.2018.02.025
275. Chan AT, Karakas MF, Vakrou S, Afzal J, Rittenbach A, Lin X, et al. Hyaluronic acid-serum hydrogels rapidly restore metabolism of encapsulated stem cells and promote engraftment. *Biomaterials* (2015) 73:1–11. doi: 10.1016/j.biomaterials.2015.09.001
276. Ozawa T, Mickle DA, Weisel RD, Koyama N, Ozawa S, Li RK. Optimal biomaterial for creation of autologous cardiac grafts. *Circulation* (2002) 106(12 Suppl 1):I176–82. doi: 10.1161/01.cir.0000032901.55215.cc

277. Zong X, Bien H, Chung CY, Yin L, Fang D, Hsiao BS, et al. Electrospun fine-textured scaffolds for heart tissue constructs. *Biomaterials* (2005) 26:5330–8. doi: 10.1016/j.biomaterials.2005.01.052
278. Ott HC, Matthiesen TS, Goh SK, Black LD, Kren SM, Netoff TI, et al. Perfusion-decellularized matrix: using nature's platform to engineer a bioartificial heart. *Nat Med*. (2008) 14:213–21. doi: 10.1038/nm1684
279. Schaaf S, Shibamiya A, Mewe M, Eder A, Stöhr A, Hirt MN, et al. Human engineered heart tissue as a versatile tool in basic research and preclinical toxicology. *PLoS ONE* (2011) 6:e26397. doi: 10.1371/journal.pone.0026397
280. Weinberger F, Breckwoldt K, Pecha S, Kelly A, Geertz B, Starbatty J, et al. Cardiac repair in guinea pigs with human engineered heart tissue from induced pluripotent stem cells. *Sci Transl Med*. (2016) 8:363ra148. doi: 10.1126/scitranslmed.aaf8781
281. Mills RJ, Titmarsh DM, Koenig X, Parker BL, Ryall JG, Quaife-Ryan GA, et al. Functional screening in human cardiac organoids reveals a metabolic mechanism for cardiomyocyte cell cycle arrest. *Proc Natl Acad Sci USA*. (2017) 114:E8372–81. doi: 10.1073/pnas.1707316114
282. Amano Y, Nishiguchi A, Matsusaki M, Iseoka H, Miyagawa S, Sawa Y, et al. Development of vascularized iPSC derived 3D-cardiomyocyte tissues by filtration Layer-by-Layer technique and their application for pharmaceutical assays. *Acta Biomater*. (2016) 33:110–21. doi: 10.1016/j.actbio.2016.01.033
283. Kawatou M, Masumoto H, Fukushima H, Morinaga G, Sakata R, Ashihara T, et al. Modelling Torsade de Pointes arrhythmias *in vitro* in 3D human iPS cell-engineered heart tissue. *Nat Commun*. (2017) 8:1078. doi: 10.1038/s41467-017-01125-y

Conflict of Interest Statement: The authors declare that the research was conducted in the absence of any commercial or financial relationships that could be construed as a potential conflict of interest.

Copyright © 2018 Malandraki-Miller, Lopez, Al-Siddiqi and Carr. This is an open-access article distributed under the terms of the Creative Commons Attribution License (CC BY). The use, distribution or reproduction in other forums is permitted, provided the original author(s) and the copyright owner(s) are credited and that the original publication in this journal is cited, in accordance with accepted academic practice. No use, distribution or reproduction is permitted which does not comply with these terms.

International Journal of Biochemistry and Cell Biology 88 (2017) 75–83

Contents lists available at ScienceDirect

International Journal of Biochemistry and Cell Biology

journal homepage: www.elsevier.com/locate/biocel

Acetoacetate is a more efficient energy-yielding substrate for human mesenchymal stem cells than glucose and generates fewer reactive oxygen species

Mary Board[a,*], Colleen Lopez[b,1], Christian van den Bos[c], Richard Callaghan[d], Kieran Clarke[a], Carolyn Carr[a]

[a] Department of Physiology, Anatomy and Genetics, University of Oxford, South Parks Road, Oxford OX1 3 PG, United Kingdom
[b] California State University, San Marcos, USA
[c] Mares Ltd., Muensterstrasse 87, 48268 Greven, Germany
[d] Research School of Biology, ANU College of Medicine, Biology and the Environment, Australian National University, Canberra, Australia

ARTICLE INFO

Keywords:
Acetoacetate
Glycolysis
Oxidation
ROS
Stem cells

ABSTRACT

Stem cells have been assumed to demonstrate a reliance on anaerobic energy generation, suited to their hypoxic *in vivo* environment. However, we found that human mesenchymal stem cells (hMSCs) have an active oxidative metabolism with a range of substrates. More ATP was consistently produced from substrate oxidation than glycolysis by cultured hMSCs. Strong substrate preferences were shown with the ketone body, acetoacetate, being oxidised at up to 35 times the rate of glucose. ROS-generation was 45-fold lower during acetoacetate oxidation compared with glucose and substrate preference may be an adaptation to reduce oxidative stress. The UCP2 inhibitor, genipin, increased ROS production with either acetoacetate or glucose by 2-fold, indicating a role for UCP2 in suppressing ROS production. Addition of pyruvate stimulated acetoacetate oxidation and this combination increased ATP production 27-fold, compared with glucose alone, which has implications for growth medium composition. Oxygen tension during culture affected metabolism by hMSCs. Between passages 2 and 5, rates of both glycolysis and substrate-oxidation increased at least 2-fold for normoxic (20% O_2)- but not hypoxic (5% O_2)-cultured hMSCs, despite declining growth rates and no detectable signs of differentiation. Culture of the cells with 3-hydroxybutyrate abolished the increased rates of these pathways. These findings have implications for stem cell therapy, which necessarily involves *in vitro* culture of cells, since low passage number normoxic cultured stem cells show metabolic adaptations without detectable changes in stem-like status.

1. Introduction

The potential for stem cell therapy has received a great deal of popular and scientific attention over recent years with proposals that transplantation of cells could take the form of an acute treatment for myocardial infarction, for example, or a chronic treatment for neuro-degenerative disorders. Any form of therapy involves the extraction, storage and *in vitro* culture of cells raising the possibility that these processes (*in vitro* culture, in particular) would have an impact on the characteristics of the cells. Cytoskeletal and other phenotypic changes have been reported for mesenchymal stem cells in long-term culture of 40 passages (Vacanti et al., 2005) and this field has been reviewed by Bara et al. (2014). There is also the possibility that changes to the cells' energy metabolism occur and the present study investigates some aspects of this, allowing presentation of results indicating substrate selection and energy generation by human mesenchymal stem cells (hMSCs) under conditions of normoxic and physiologically relevant hypoxic culture between passages 2 and 5.

Cells in culture are normally exposed to glucose and glutamine and, occasionally, pyruvate in their growth media but a wider range of energy yielding substrates may be available to the cells *in vivo*. Plasma ketone body levels may reach or exceed 7 mM under conditions of starvation or a ketogenic diet, compared with normal levels in the fed state of around 0.1 mM (Hall et al., 1984). With ketone body levels of 7 mM, it may be that this species will be utilised by the stem cells to generate energy. Indeed, there are indications that stem cells *in vivo*

Abbreviations: hMS, Chuman mesenchymal stem cells; p2, passage 2; p5, passage 5

* Corresponding author.
E-mail address: mary.board@st-hildas.ox.ac.uk (M. Board).
[1] Present address: Research School of Biology, ANU College of Medicine, Biology and the Environment, Australian National University, Canberra, Australia.

http://dx.doi.org/10.1016/j.biocel.2017.05.007
Received 9 February 2017; Received in revised form 5 April 2017; Accepted 4 May 2017
Available online 05 May 2017
1357-2725/ © 2017 The Authors. Published by Elsevier Ltd. This is an open access article under the CC BY license (http://creativecommons.org/licenses/BY/4.0/).

may benefit from higher concentrations of ketone bodies which may influence their capacity to contribute to neurogenesis, among other processes (Lee et al., 2002a; Lee et al., 2002b). The potential contribution made to hMSC energy metabolism by the consumption of ketone bodies was investigated during the present study.

It is considered that mesenchymal stem cells *in vivo* occupy a hypoxic niche (Schofield, 1978; Crisan et al., 2008; Parmar et al., 2007; Suda et al., 2011) and that their energy yielding metabolism is likely to be correspondingly hypoxic and to include a reliance on the pathway of glycolysis for ATP generation (Pattappa et al., 2011; Simsek et al., 2010; reviewed by Gaspar et al., 2014). Much has been written about the relationship between hypoxia and differentiation of stem cells and suggestions have been made as to the adaptation and maintenance of hypoxic metabolism in these cells, including that they have immature and dysfunctional mitochondria (reviewed by Xu et al., 2013). We have assessed the contribution made to energy metabolism by the anaerobic glycolytic pathway and by the oxidative metabolism of hMSCs cultured *in vitro* under conditions of hypoxia (5% O_2) and normoxia (20% O_2). It is anticipated that stem cells would have a large ATP turnover to sustain, since these cells show a high rate of proliferation. (It has been estimated that the production of a single daughter *E.coli* cell accounts for the consumption of 2.36-2.9 × 10^{13} molecules of ATP (Hempfling and Mainzer, 1975; Farmer and Jones, 1975). The present study analysed a range of potential energy yielding substrates and calculated the contribution made to ATP synthesis in hMSCs growing in culture. Both the glucose and glutamine routinely included in growth medium can be used by these cells to generate ATP and pyruvate, where present, may also fulfil this role. The current study demonstrates the contributions made by these substrates and by the ketone body, acetoacetate, to ATP generation. The analysis represents a way of indicating which are potentially the most effective energy yielding substrates and thus what modifications to stem cell growth medium might be advantageous. The findings may also shed light on beneficial *in vivo* conditions for proliferation of stem cells in order to facilitate putative stem cell therapy.

Recent reports have indicated that the *in vitro* or *in vivo* consumption of ketone bodies by cells, particularly neurones, may represent an adaptation to alleviate oxidative stress (Fukao et al., 2004; Maalouf et al., 2009; Shimazu et al., 2013). Given the suggestions that stem cells reside in hypoxic niches *in vivo* partly to avoid generation of ROS (Suda et al., 2011), it may be that this cell-type would have a preference for a low ROS-generating substrate. Thus, we have measured rates of production of ROS by hMSCs after exposure to glucose and acetoacetate and assessed the effects of the UCP2-inhibitor, genipin, on production of ROS with different substrates.

2. Materials and methods

All consumables were purchased from Sigma Aldrich unless otherwise indicated.

2.1. Human mesenchymal stem cells

Stem cells were obtained from 3 sources: generous gifts from Lonza and Dr. Yasser El-Sherbini, Dept. of Biomedical Engineering, University of Oxford and purchased from Millipore.

2.1.1. Culture of cells

Cryopreserved cells were thawed, washed with growth medium and seeded at a density of 1 × 10^6 cells per 225 cm^2 with DMEM containing 2 mM ultra-glutamine, 5.5 mM glucose, 50 μg/ml gentamycin and 10% FBS (Lonza). Where 3-hydroxybutyrate (3-HB) was included in the growth medium, the concentration was 5 mM throughout. Cells were passaged at about 80% confluence. Cells for measurements of glycolysis or oxidation were seeded into 24-well plates at a density of 1 × 10^4 cells per well and used at 90% confluence. Cells were maintained in either normoxic culture with 20% O_2 tension or hypoxic culture with 5% O_2 tension in an oxygen tension controlled incubator. Previous workers have identified 5% O_2 as being a physiologically significant level of O_2 with respect to *in vivo* conditions for hMSCs, representing hypoxia (Pattappa et al., 2011).

2.2. Measurements of metabolic flux

2.2.1. Measurements of substrate-oxidation in 24-well plates

Cells were incubated for 90 min in the presence of a single radiolabelled substrate (with addition of unlabelled substrates where indicated) in DMEM (containing no pyruvate, glucose or glutamine) in a total volume of 0.5 mls. The concentrations of single substrates were: 5.5 mM glucose (considered similar to median human blood glucose concentration); 2 mM pyruvate (considered higher than endogenous pyruvate concentration from glucose metabolism and sufficient to stimulate activity of pyruvate dehydrogenase plus pyruvate carboxylase); 1 mM glutamine (considered similar to human blood glutamine concentrations); 10 mM acetoacetate (considered similar to intracellular acetoacetate concentrations produced from maximal blood ketone body concentrations). In addition, substrates incorporated radiolabels as follows: glucose: 21 MBq/mmol D-U-^{14}C-glucose (Perkin Elmer); pyruvate: 0.35MBq/mmol 1-^{14}C-pyruvate (American Radiochemicals); acetoacetate: 0.185MBq/mmol 3-^{14}C-acetoacetate (American Radiochemicals); glutamine: 1.2 MBq/mmol U-^{14}C-glutamine (Perkin Elmer). Evolved $^{14}CO_2$ was trapped and measured by the method of Collins et al. (1998), except that, after addition of perchloric acid to the wells, plates were gently agitated for 60 min to release dissolved $^{14}CO_2$. Filter papers containing trapped $^{14}CO_2$ were counted in Ecoscint (National Diagnostics) using a Tri-Carb 2800TR Liquid Scintillation Analyser. Preliminary measurements showed that rates of $^{14}CO_2$-production were linear for a period of at least 120 min under these conditions. Rates of ATP-production from individual substrates were calculated on the basis of mol/mol production as follows: glucose: 31; glutamine: 20; pyruvate: 12.5; acetoacetate: 20. For calculations of ATP-production from acetoacetate plus pyruvate, separate incubations were performed with ^{14}C-acetoacetate in the presence of unlabelled pyruvate and with ^{14}C-pyruvate in the presence of unlabelled acetoacetate. Rates of ATP-production from the labelled substrate were calculated for each condition and the results summed.

2.2.2. Measurements of glycolytic rate in 24 well plates

Glycolysis was measured as the production of ^3H_2O from 5-^{3}H-glucose, which occurs during the step catalysed by enolase. Cells were incubated with 5.5 mM glucose containing 17 MBq/mmol 5-^{3}H-glucose (Perkin Elmer) in DMEM without pyruvate, glutamine or glucose for 90 min in a total volume of 0.5mls. At 90 min, 0.2 mls of the medium was applied to a column (volume 1 ml) of Dowex-1-borate (prepared from Dowex-1-chloride by the method of Hammerstedt, 1973). Washing with 2 column volumes of water eluted the ^3H_2O which was counted for radioactivity (Tri-Carb 2800TR Liquid Scintillation Analyser).

2.2.3. Calculation of ATP yield

ATP yields were calculated from the following values: from glycolysis of glucose, it is assumed that 2 mol ATP will be produced per mole glucose glycolysed. For substrate oxidation measurements, it is assumed that full oxidation of each substrate takes place. Under these conditions, glucose oxidation will produce a mean value of 31 mol ATP/mol glucose when glucose is converted to CO_2 by the action of glycolysis, the pyruvate dehydrogenase reaction and reactions of the tricarboxylic acid cycle. It is assumed that cytosolic NADH generated from glycolysis will be re-oxidised due to the action of either the 3-phosphoglycerate or the malate-aspartate shuttles. Pyruvate oxidation generates 12.5 mol ATP/mol pyruvate when the substrate is fully converted to CO_2 by the actions of the pyruvate dehydrogenase reaction

and reactions of the tricarboxylic acid cycle. Acetoacetate oxidation generates 20 mol ATP/mol acetoacetate when the substrate is first split into acetyl coenzyme A which is fully converted to CO_2 by reactions of the tricarboxylic acid cycle. Glutamine oxidation generates 20 mol ATP/mol glutamine when the substrate is deaminated to α-ketoglutarate and α-ketoglutarate converted to pyruvate by reactions of the tricarboxylic acid cycle plus that of pyruvate carboxylase. The resulting pyruvate is then oxidised in the same way as exogenous pyruvate.

2.2.4. Measurement of reactive oxygen species

Cells were incubated under appropriate conditions in 24-well plates in a total volume of 0.2 ml for 90 min. At 90 min, ROS were assayed using an Oxiselect Amplex Red kit (Cell Biolabs, Inc.) according to the manufacturer's instructions. Where genipin was used, cells were pre-incubated for 24 h with 20 μM genipin.

2.3. Growth and differentiation experiments

2.3.1. Growth rates of hMSCs

At each passage (typically every 48 h), cell numbers were counted in a haemocytometer using Trypan Blue exclusion as a gauge of viability.

Please see Supplementary Information for measurements of mRNA production of marker proteins and differentiation of hMSCs into osteocytes, adipocytes and chondrocytes (Methods and Data).

2.4. Detection of UCP2 by western blotting

Western blots were performed under denaturing conditions. Cells were detached using trypsin, homogenised using a 21G needle, incubated for 5 min in a dri-block at 100 °C and centrifuged at 13,000 rpm for 10 min. Aliquots of the supernatant were assayed for protein concentration (Pierce BCA protein assay kit) and the remainder had 5% mercaptoethanol added before incubation for 5 min at 100 °C. Blots were performed by the method of Heather et al. (2011), where equal quantities of total cellular protein (25 μg) were loaded per well, proteins were stained with Ponceau's reagent and gels blocked with 5% milk powder. Loading of wells with equal amounts of protein allows normalisation of expression for comparative purposes and avoids the possibility that expression of housekeeping genes may change with passage number or with cell treatment protocol (Farmer et al., 1983; Gorr and Vogel, 2015). UCP2 protein was detected using rabbit polyclonal anti-human UCP2 antibody (5 μg/ml) purchased from Abcam and donkey anti-rabbit secondary antibody (to give a ratio of secondary: primary antibody of 1.6) allowed detection by exposure to X-ray film. Rainbow marker proteins (25–120 kDa) were used to assess molecular weight.

2.5. Data analysis

Data was analysed by single factor (Figs. 2 7a) or two factor (Fig. 1, 4 and 6) ANOVA.

3. Results

3.1. Oxidation of glucose, pyruvate, glutamine and acetoacetate

Oxidation rates for both glucose and acetoacetate rose with passage number for normoxic cultured cells (2-fold increase in glucose-oxidation rate and 2.6-fold increase in acetoacetate-oxidation rate) between passage 2 and passage 5 (p2-p5) whereas rates of oxidation of pyruvate and glutamine were not significantly different at the two passage numbers (Fig. 1A). Fig. 1 shows that acetoacetate was oxidised at a 27-fold higher rate than glucose at p2 and this rose to a 35-fold higher rate at p5. This increase was not seen for hypoxic-cultured cells, where the rate of oxidation of neither glucose nor acetoacetate was significantly different at p5 compared with p2, although that of pyruvate increased by 37%. Pyruvate and acetoacetate, which both feed directly into the mitochondrial TCA cycle, showed the highest rates of oxidation of all substrates for all culture conditions which indicates the functionality of the TCA cycle in these cells. When cells were cultured in the presence of 5 mM 3-hydroxybutyrate (3-HB) from passages 1–5, oxidation rates at passage 5 for normoxic cells were reduced by 4-fold for glucose and 3-fold for acetoacetate, giving an oxidation profile which more nearly resembled the 3-HB-free hypoxic condition than the 3-HB-free normoxic.

3.1.1. Oxidation of acetoacetate: effects of additional substrates

Adding glucose to acetoacetate oxidation experiments reduced the rate of acetoacetate oxidation by 8-fold (Fig. 2) for normoxic cultured cells, suggesting either that the presence of glucose has a suppressing effect on acetoacetate utilisation or that pyruvate from glucose competes with acetyl CoA from acetoacetate for oxidation by the TCA cycle. However, addition of pyruvate resulted in a 1.5-fold increase in rates of acetoacetate oxidation so that competition seems unlikely. Indeed, it could be that the pyruvate substrate is carboxylated to oxaloacetate as a result of intramitochondrial pyruvate carboxylase activity (as well as being decarboxylated to acetyl Coenzyme A by pyruvate dehydrogenase) in these cells, so that the presence of pyruvate may maintain the capacity of the TCA cycle enabling continued acetoacetate oxidation. This effect was consistent for cells of all passage numbers (results not shown). This action would explain the increase in acetoacetate oxidation rates seen when pyruvate is present (Fig. 2). Addition of malate had no significant effect on rates of pyruvate oxidation (data not shown), indicating that carboxylation of pyruvate is not the only route for oxidative metabolism of this substrate. This may explain the difference observed between the effects of glucose and those of pyruvate on acetoacetate oxidation, despite the fact that both substrates would be expected to give rise to intramitochondrial pyruvate. The higher concentrations of intramitochondrial pyruvate achieved when 2 mM pyruvate is the substrate may lead to appreciable activity of pyruvate carboxylase, while lower concentrations of pyruvate from glucose may not.

3.1.2. ATP production from substrate oxidation

Calculated rates of ATP production demonstrate that acetoacetate is the single most efficient substrate for ATP production by these cells, when full oxidation of the substrate is assumed (Fig. 3). Neither glucose nor glutamine, the usual additions to tissue culture medium, were as productive of ATP (glucose produced 17 times less ATP than acetoacetate alone and glutamine produced 38 times less). The presence of pyruvate may increase the capacity of the TCA cycle and, therefore, the yield of ATP from acetoacetate, making this the most productive substrate combination for energy yield by these cells.

3.1.3. Anaerobic metabolism of glucose: rates of glycolysis

Glycolytic rates were not significantly different for cells cultured under normoxic and hypoxic conditions at passage 2 (Fig. 4). However, more unexpected was the 1.9-fold rise in glycolytic rates seen for cells cultured under normoxia between passages 2 and 5. This effect was not seen for cells cultured under hypoxia and rates of glycolysis for hypoxic p5 cells were 37% lower than those for normoxic cultured cells. This mirrors the rise in oxidation rates seen for normoxic cultured cells (Fig. 1) and implies that energy yielding pathways are generally upregulated between the two passage numbers for cells cultured under 20% oxygen tension but not for cells cultured under 5% O_2 tension. When the cells were cultured with 3-HB, glycolytic rates at p5 were unchanged relative to p2. For cells cultured under hypoxia with 3-HB, glycolytic rates were significantly decreased by passage 5 (1.4-fold). The presence of 3-HB thus seems to have a suppressing effect on the increase in energy yielding metabolism which follows from normoxic culture for both aerobic and anaerobic pathways (Figs. 1 and 4). The

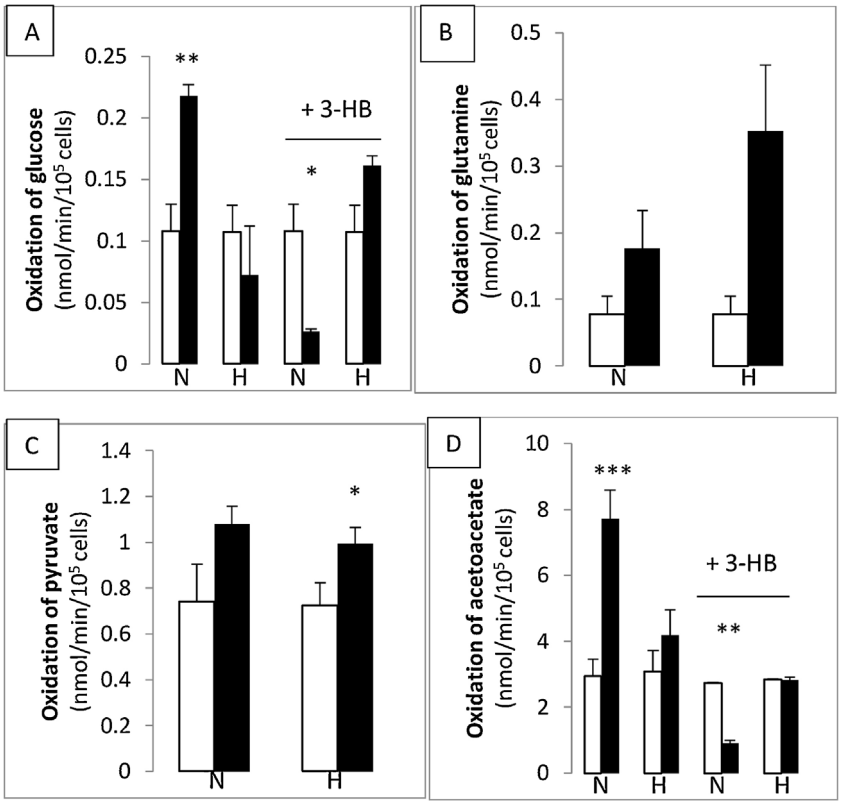

Fig. 1. Oxidation of energy yielding substrates by hMSCs.Rates of oxidation of 5.5 mM glucose (A); 1 mM glutamine (B); 2 mM pyruvate (C) and 10 mM acetoacetate (D) are shown for cells at passage 2 (open columns) and passage 5 (solid columns). Rates of substrate oxidation were measured in 24 well plates as the production of $^{14}CO_2$ from ^{14}C-labelled substrates. Cells were cultured as follows through passages 1–5: normoxia (20% O_2, N) or hypoxia (5% O_2, H) with 5 mM 3-HB, where indicated.n ≥ 5 for each column.*: $p < 0.05$, ** $p < 0.01$ and ***$p < 0.0001$ when substrate oxidation at p5 is compared with that at p2.

energy profile of cells cultured in the presence of 3-HB and 20% O_2 thus mimics that of cells cultured under hypoxic conditions.

3.1.4. ATP production from anaerobic and aerobic metabolism of glucose

Fig. 5 shows that normoxic cultured cells increase their calculated ATP production from both aerobic and anaerobic metabolism of glucose by a factor of 2 between passages 2 and 5. Interestingly, the proportion of ATP coming from each branch of metabolism remains constant (approximately 75% from glucose oxidation and 25% from glycolysis). Hypoxic cultured cells did not show the same increased rate of ATP generation and the inclusion of 3-HB in the culture medium of normoxic cells also reduced the passage-related increase in ATP generation producing a profile that resembles more closely that of hypoxic cultured cells than that of the normoxic. It would seem likely that the normoxic cultured cells increase their rate of ATP production either because they show increased rates of growth between passages 2 and 5 or because the cells are synthesising macromolecules in preparation for differentiation.

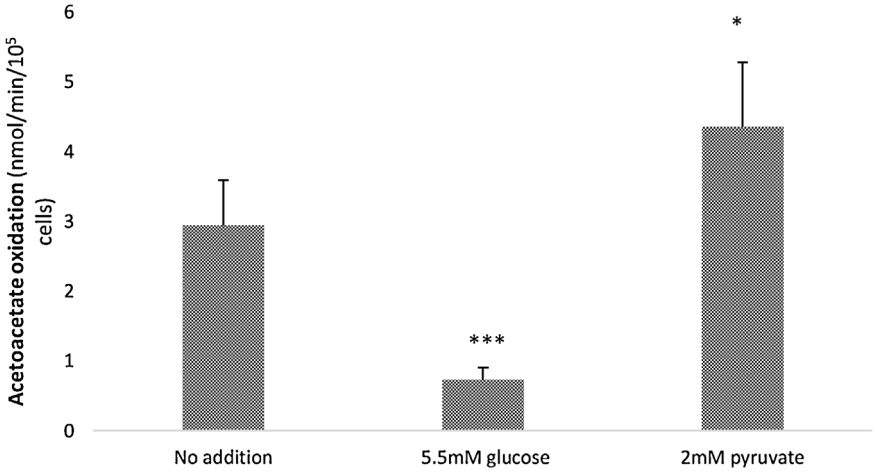

Fig. 2. Oxidation of acetoacetate by hMSCs: effects of additional substrates.Rates of oxidation of 10 mM acetoacetate containing a trace of 3-^{14}C-acetoacetate were measured in the presence of unlabelled 5.5 mM glucose or 2 mM pyruvate, where marked. Oxidation was measured in 24 well plates. Cells were passage 2, cultured under normoxic conditions.*: $p < 0.05$ and ***: $p < 0.0001$ compared with acetoacetate alone.

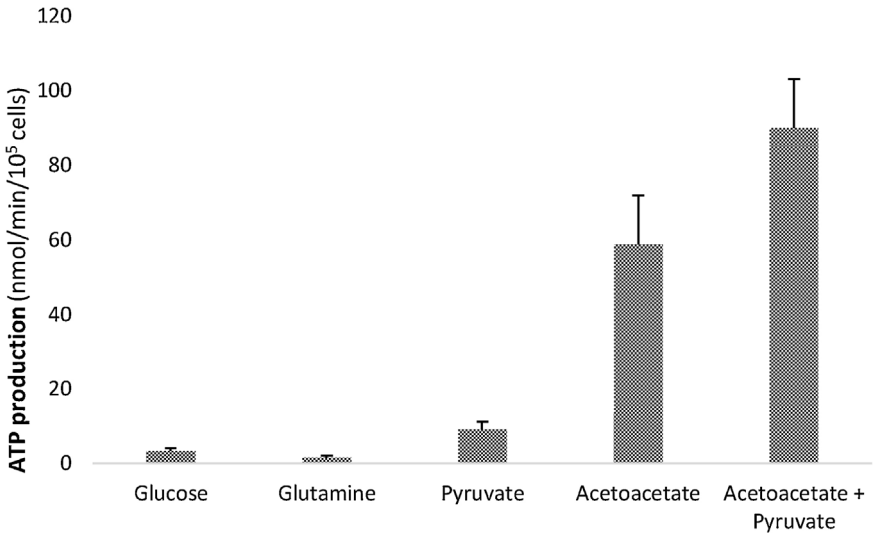

Fig. 3. Calculated rates of ATP production by hMSCs with oxidative substrates.Rates of ATP production from individual substrates were calculated on the basis of mol ATP produced/mol substrate oxidised. Assuming full oxidation of each mole of substrate converted to $CO_{2.}$, it is calculated that 1 mol of glucose will produce a mean value of 31 mol ATP; glutamine: 20; pyruvate: 12.5; acetoacetate: 20 (refer to Materials and Methods for complete explanation). For calculations of ATP production from acetoacetate plus pyruvate, separate incubations were performed with 10 mM acetoacetate labelled with ^{14}C-acetoacetate in the presence of unlabelled 2 mM pyruvate and with 2 mM pyruvate labelled with ^{14}C-pyruvate in the presence of unlabelled 10 mM acetoacetate. Rates of ATP production from the labelled substrate in each incubation were calculated and the results summed. Cells were passage 2, cultured under normoxic conditions.

3.2. Growth rates of hypoxic- and normoxic-cultured cells between passages 2 and 5

Fig. 6 demonstrates that growth rates declined with passage number for both normoxic and hypoxic culture conditions so that the cells were dividing at lower rates by passage 5 than at passage 2. This observation is true both for the normoxic cultured cells, which accelerate their rates of ATP production, and for the hypoxic cultured cells which do not.

3.2.1. Production of mRNA for markers of stem-like, hMSC and differentiated status

Markers of MSCs, general stem-like status or differentiation did not change for normoxic cultured cells between passage 2 and 5 (Table S1). Interestingly, the only changes were seen during hypoxic culture, where the cells show increased production of mRNA for the general markers of the stem-like state, Oct4, c-myc and Sox2 and of the osteocyte-specific protein, osteopontin. None of the other markers of osteocytes show similar changes and Halfon et al. (2011) have reported that MSCs lose their osteogenic potential after passages 5–6, although these authors probably cultured their cells under normoxic conditions. Wang et al. (2013) grew MSCs from human umbilical cord for 30 passages and found that multipotent markers were still expressed. For the cells of the present study, there are no clear indications that differentiation is underway by passage 5.

3.2.2. Differentiation of hMSCs along adipocytic, chondrocytic and osteocytic lineages

Cells grown under all conditions were assessed for their ability to differentiate at passage 6. All cells were successfully differentiated into adipocytes, chondrocytes and osteocytes and accumulation of intracellular fat, collagen and calcium were measured (Table S2). *Adipocyte differentiation*: intracellular fat accumulation was measured by Oil red O

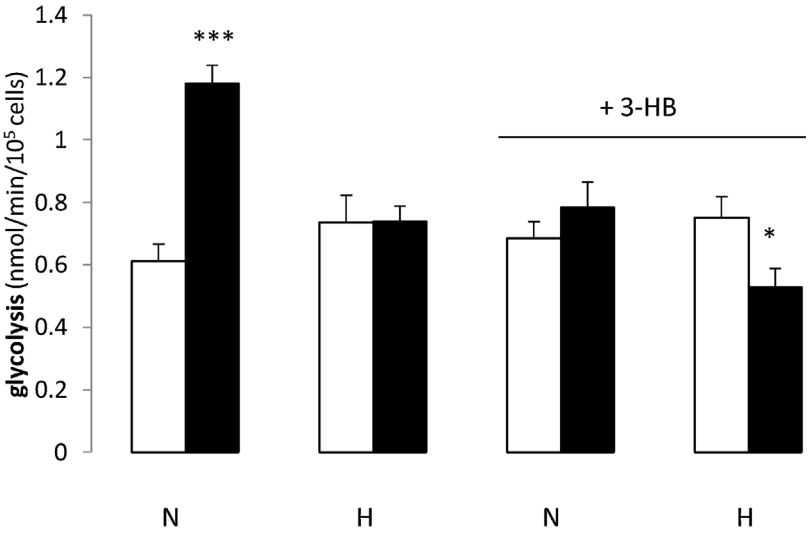

Fig. 4. Rates of glycolysis by hMSCs at passages 2 and 5.Rates of glycolysis were measured for hMSCs at passages 2 (open columns) and 5 (solid columns) when cultured through passages 1–5 under normoxia (20% O_2, N) or hypoxia (5% O_2, H) with 5 mM 3-HB, where indicated.Glycolytic rates were measured in 24-well plates as the production of ^3H_2O from 5-^{3}H-glucose by the method outlined in the Materials and Methods section.***: $p < 0.0001$ compared with normoxic cells at passage 2;*$p < 0.05$ compared with cells cultured under the same conditions at passage 2.

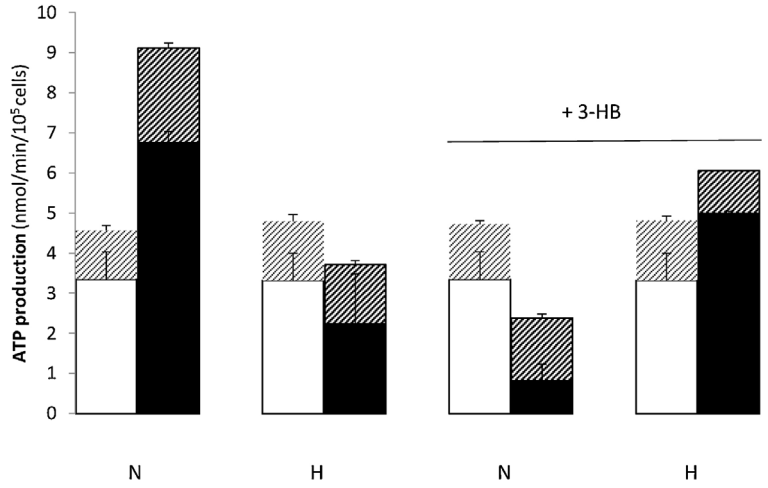

Fig. 5. Calculated rates of ATP production by hMSCs from glycolysis and from full oxidation of glucose.Rates of ATP production were calculated as previously (refer to Materials and Methods for full explanation) from the anaerobic (glycolysis) and aerobic (oxidation) pathways for glucose metabolism. Cells were cultured under normoxic conditions (20% O_2, N) or hypoxic (5% O_2, H) with 5 mM 3-HB, where indicated, through passages 1–5. ATP production from full oxidation of ^{14}C-labelled substrates is shown in the lower column of each data point and that from glycolysis is shown in the upper column. Measurements were made at passage 2 (open columns: oxidation; light patterning: glycolysis) and passage 5 (solid columns: oxidation; heavy patterning: glycolysis) for each culture condition.n ≥ 9.

staining and differentiated cells showed a mean 30% increase over control cells which were cultured as normal and not subjected to the differentiation protocol. *Chondrocyte differentiation*: production of collagen (assessed by Sirius red/fast green staining) showed a mean 45% increase over control cells. *Osteocyte differentiation*: intracellular calcium accumulated to a mean 44% increase over control cells for cells cultured under hypoxic conditions but to a mean 26% increase for cells cultured under normoxia. There were no significant effects of culture conditions, except in the case of osteocyte differentiation stated above. Thus, hMSCs cultured under all conditions used in the present study retain the capacity to differentiate along all three expected lineages.

3.3. Production of ROS by hMSCs incubated with glucose and acetoacetate

It has been suggested that consumption of ketone bodies by cells may be a mechanism for the avoidance of oxidative stress (Fukao et al., 2004; Maalouf et al., 2009). In order to investigate whether substrate availability has an influence on oxidative stress in hMSCs, levels of ROS were measured after incubation with either a glucose or an acetoacetate substrate (Fig. 7a). If the ROS production is considered relative to rates of substrate oxidation, then each mole of glucose oxidised generated 0.076 mol of ROS whereas each mole of acetoacetate oxidised generated 0.0017 mol of ROS, a 45-fold difference. It has been suggested that the activity of UCP2 may influence the production of ROS (Negre-Salvayre et al., 1997; Arsenijevic et al., 2000). Effects of the specific UCP2 inhibitor, genipin (Zhang et al., 2006), indicate that this observation may be true for the hMSCs of the present study. The presence of genipin resulted in a 2 −fold increase in ROS production with either a glucose or an acetoacetate substrate. It has been shown by Echtay et al. (2002) that UCP2 functions to carry the superoxide anion. If this function is common to the cells of the present study, UCP2 may well act to reduce intramitochondrial ROS production, perhaps in a substrate-independent manner.

3.3.1. Detection of human UCP2 by western blotting

The results of a Western blot using anti-human UCP2 antibody are shown in Fig. 7b. Cells cultured under all conditions show the presence of an approximately 66 kDa protein recognised by the antibody. The active UCP2 protein is a dimer composed of two subunits of approximately 32–35 kDa (reviewed by Ledesma et al., 2002). It has been shown for other members of the anion carrier superfamily that the two subunits may be covalently linked to form a functional unit (Trézéguet

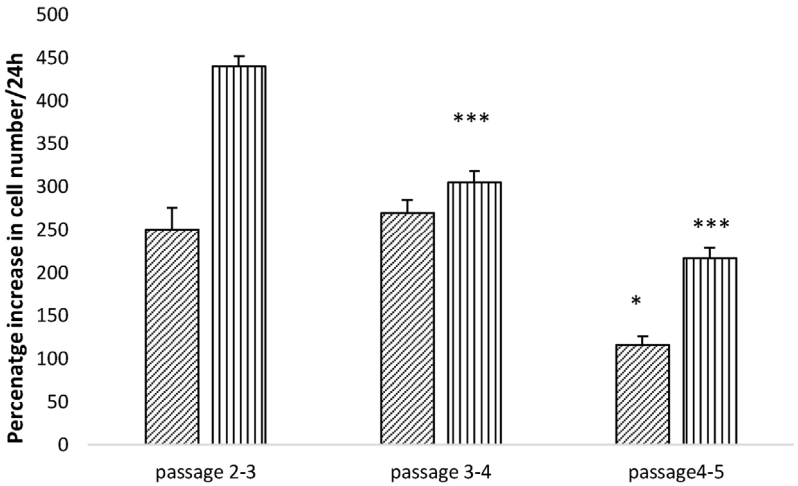

Fig. 6. Growth rates of hMSCs with passage number.HMSCs were cultured under normoxic (20% O_2, cross-hatched) or hypoxic (5% O_2, vertical lines) conditions. Cells were passaged every 48 h and cell numbers counted by haemocytometer, using Trypan Blue to assess viability.n = 4*: P < 0.05 compared with passage 2–3;*** p < 0.0001 compared with passage 2–3.

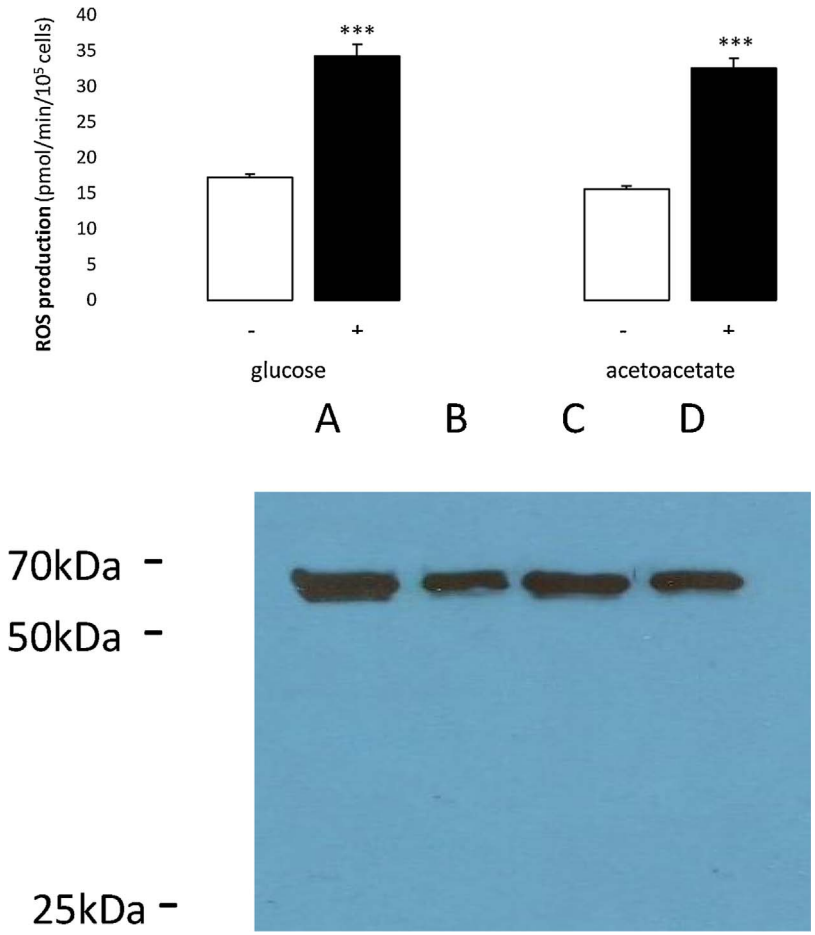

Fig. 7. a Production of ROS by hMSCs with glucose and acetoacetate: effects of genipin.hMSCs were cultured under normoxic conditions and were passage 5 at the time of assay. For measurements in the presence of genipin, cells were pre-incubated for 24 h with 20 μM genipin. Cells were incubated for 90 min in 24 well plates in the presence of either 5.5 mM glucose or 10 mM acetoacetate before measurement of ROS. Values were calculated for 6 replicates. The first column of each pair represents production in the absence of genipin (−, open columns) and the second column, with genipin (+, solid columns).***: $P < 0.0001$ for conditions with genipin compared with no addition.b Western Blot of hMSCs with anti-UCP2 antibody.Cell extracts were probed with anti-human UCP2 antibody and the probe detected using a secondary anti-rabbit antibody. Cells were cultured as follows: Lanes A and B under normoxic conditions and lanes C and D under hypoxic conditions. The presence of UCP2 protein was detected at passages 2 (lanes A and C) and 5 (lanes B and D).

et al., 2000). Jekabsons et al. (2003) also observed an approximately 64 kDa protein recognised by anti-human UCP2 antibody in their preparations of purified human UCP2. No band corresponding to the monomer is seen in the cells of the present study at any passage number between 2 and 5 (results for intermediate passage numbers not shown).

4. Discussion

A salient characteristic of hMSC metabolism in the present study is the high rate of acetoacetate oxidation seen at all passage numbers and under both normoxic and hypoxic culture. Not only does this indicate that the cells have a functional TCA cycle of a higher capacity than would be deduced from their oxidation of glucose but it also highlights the effectiveness of acetoacetate as a potential energy yielding substrate. Indeed, the combination of acetoacetate plus pyruvate proved to be the most successful in terms of calculated ATP yield. This observation has obvious implications for the design of growth medium for the culture of hMSCs. Glucose and glutamine, the usual substrates included in standard growth medium, are not as effective in producing ATP and it could be that the design of a medium incorporating both a ketone body and pyruvate may stimulate energy production by these cells. Since any form of stem cell therapy must involve the harvesting and *in vitro* culture of stem cells, this is something which may bear further scrutiny. The significance of pyruvate for cultured cells has been indicated by the observation that cells do not thrive in a pyruvate-free medium but succumb to oxidative stress (O'Donnell-Tormey et al., 1987). Furthermore, Alt et al. (2005) have suggested that stem cells *in vivo* may take up pyruvate released by other cells in the stroma. The results of the present study support this suggestion as an effective energetic approach by these cells. The pyruvate may aid the cells' metabolism by being carboxylated to oxaloacetate thus increasing the capacity of the TCA cycle and enabling increased oxidation of acetoacetate and other oxidative substrates.

Ketone bodies represent a fuel of intermediate and prolonged starvation, persisting at low levels in the blood in the fed state (approximately 0.1 mM) but rising after a fast of approximately 3–4 days in the human adult to levels that may be 70–80 times higher. Traditionally, ketone bodies have been regarded as a key fuel for neuronal tissues under these conditions. More recent reports have indicated that consumption of ketone bodies by cells, particularly neurones, may represent a way of reducing oxidative stress (Fukao et al., 2004; Maalouf et al., 2009) and it has been observed in general that stem cells tend to reside in an environment where there are low levels of ROS (Suda et al., 2011), which may be a strategy to aid their survival or their maintenance of the undifferentiated state. The current findings show that rates of ROS generation are 45-fold lower, on a mole ROS per mole substrate oxidised basis, with an acetoacetate substrate than they are with a glucose substrate. This may partly explain why oxidation of acetoacetate represents an appropriate metabolic strategy for these cells and may indicate a preference for an acetoacetate substrate when a range of substrates are available. Numerous recent reports have indicated a therapeutic role for a ketogenic diet, where a

high ratio of fat: carbohydrate intake stimulates ketone body production so that plasma levels may reach 6–8 mM (Musa-Veloso et al., 2006). Such reports range from neuronal protection (Maaloof et al., 2009; Kashiwaya et al., 2012; Laeger et al., 2010) and neurogenesis (Lee et al., 2002a; Lee et al., 2002b)to more general protection against age-related damage (Paoli et al., 2013; Paoli et al., 2014). The reduction in ROS produced with a ketone body substrate may represent one of the mechanisms underlying these effects. Since hMSCs have a high rate of proliferation and a higher rate of ATP synthesis from acetoacetate, there is scope for speculation as to whether the ketogenic diet may have further applications in assisting with putative therapies based around stem cell transplantation, such as those for neurodegenerative disorders.

The effects of the UCP2 inhibitor, genipin, in increasing rates of ROS production 2-fold with glucose or acetoacetate, indicate the potential role for UCP2 in reducing ROS production in hMSCs. It may not be the case that UCP2 functions to uncouple electron transport from phosphorylation of ADP (reviewed by Pecqueur et al., 2009) but a role in substrate selection, causing a shift from carbohydrate to lipid metabolism, has been suggested (reviewed by Nedergaard and Cannon, 2003), in addition to a putative role in superoxide anion export from the mitochondrion (Echtay et al., 2002). From the results of the present study, a potential role for UCP2 in indicating the availability of acetoacetate and enabling its mitochondrial transport and oxidation is possible and ought to be investigated. Moreover, both Bouillaud (2009) and Zhang et al. (2011) have suggested that UCP2 may decrease the oxidation rate of pyruvate, perhaps by shunting this substrate out of the mitochondrion (Zhang et al., 2011), thereby favouring glycolysis. We find that hMSCs oxidise little endogenous pyruvate from glucose compared with their capacity for oxidising exogenous pyruvate, which would support this view.

Normoxic culture of hMSCs in the present study results in a general increase in flux through energy yielding pathways between passage 2 and 5. This includes an increase of 1.9–fold in glycolytic flux and a 2–fold increase in rates of glucose-oxidation and 2.6–fold of acetoacetate. The reasons for this increased flux are not clear since they seem to be unrelated to either growth rate (which declines between passage 2 and 5) or to the onset of differentiation (shown by non-significant changes in mRNA levels for key markers over the same time-scale). This effect appears to be related to the oxygen tension since it is not reproduced by the cells cultured under hypoxic conditions, although cells cultured under normoxia with 3-HB also fail to show an increase in energy generation. One further possibility is that there are changes in expression or activity of UCP2 over this time-scale, changing the cells' substrate- and pathway-preferences and also perhaps changing anion transport activity. Western blots show that UCP2 is present at both passage 2 and passage 5. The possibility that the presence of oxygen at a 20% tension during long-term culture may alter rates of electron transport and production of ROS should be a subject for investigation. If this phenomenon is shown to be real, it would have implications for the long-term culture of stem cells under normoxic conditions for therapeutic or research purposes since any prolonged increase in ROS production may result in damage to DNA and higher rates of mutation and may account for the accumulation of genomic mutations observed by Wang et al. (2013) during long-term culture.

5. Conclusions

The consistent production of more ATP from oxidative pathways than from glycolysis by hMSCs indicated an active oxidative metabolism of high capacity. Thus, the occupancy of hypoxic niches by these cells does not curtail their oxidative capacity. The strong preference for the acetoacetate substrate shown by hMSCs, which may be necessary to reduce generation of ROS, means that this substrate should be considered for inclusion in growth medium. Up-regulation of both aerobic and anaerobic energy-yielding pathways when hMSCs were cultured in the presence of 20% O_2 indicates that metabolic changes occur during the standard culture of these cells which may have an impact on the cells' suitability for therapy.

Author contributions

MB had conceptual control of the overall project, devised and performed all experiments contributing to Figs. 1–7 and Table S2 and wrote the manuscript. CL performed the experiments presented in Table S1. CvdB had conceptual input into the project, proposing the experiments presented in Fig. 1 and facilitated the supply of materials. RC advised on experimental design for Fig. 1, provided facilities and assisted with the preparation of the manuscript. KC provided facilities. CC advised on experiments presented in Table S1, suggested experiments presented in Table S2 and provided facilities.

Acknowledgements

Consumables funding was provided by BHF grant no. PG/13/14/30216 and by Lonza. MB was supported by a Daphne Jackson Fellowship and sponsored by Make My Day Better. Funding sources had no involvement in the design or execution of the study nor in the writing of the manuscript. Grateful thanks are due to Dr. Rhys Evans for critical reading of the manuscript, to Dr. Yasser El-Sherbini for advice on differentiation experiments and to Maria Sousa Fialho for help with Western Blotting.

Appendix A. Supplementary data

Supplementary data associated with this article can be found, in the online version, at http://dx.doi.org/10.1016/j.biocel.2017.05.007.

References

Alt, R., Riemer, T., Fiehn, O., Niederwieser, D., Cross, M., 2005. Evidence for restricted glycolytic metabolism in primary CD133+ cells. Blood 106 (Abs. 1726).
Arsenijevic, D., Onuma, H., Percqueur, C., Raimbault, S., Manning, B.S., Miroux, B., Couplan, E., Alves-Guerra, M.C., Goubern, M., Surwit, R., Bouilaud, F., Richard, D., Collins, S., Ricquier, D., 2000. Disruption of the uncoupling protein-2 gene in mice reveals a role in immunity and reactive oxygen species production. Nat. Genet. 26, 435–439.
Bara, J.J., Richards, G.R., Alini, M., Stoddart, M., 2014. Concise review: bone marrow-Derived mesenchymal stem cells change phenotype following In vitro culture: implications for basic research and the clinic. Stem Cells 32 (7), 1713–1723.
Bouillaud, F., 2009. UCP2, not a physiologically relevant uncoupler but a glucose sparing switch impacting ROS production and glucose sensing. Biochim. Biophys. Acta 1787, 377–383.
Collins, C.L., Bode, B.P., Souba, W.W., Abcouwer, S.F., 1998. Multiwell $^{14}CO_2$-capture assay for evaluation of substrate oxidation rates of cells in culture. Biotechniques 24 (5), 803–808.
Crisan, M., Yap, S., Casteilla, L., Chen, C.W., Corselli, M., Park, T.S., 2008. A perivascular origin for mesenchymal stem cells in multiple human organs. Cell Stem Cell 3, 301–313.
Echtay, K.S., Roussel, D., St-Pierre, J., Jekabsons, M.B., Cadenas, S., Stuart, J.A., Harper, J.A., Roebuck, S.J., Morrison, A., Pickering, S., Clapham, J.C., Brand, M.D., 2002. Superoxide activates mitochondrial uncoupling proteins. Nature 415, 96–99.
Farmer, I.S., Jones, C.W., 1975. The energetics of *Escherichia coli* during aerobic growth in continuous culture. Eur. J. Biochem. 67 (1), 115–122.
Farmer, S.R., Wan, K.M., Ben-Ze'ev, A., Penman, S., 1983. Regulation of actin mRNA levels and translation responds to changes in cell configuration. Mol. Cell Biol. 3 (2), 182–189.
Fukao, T., Lopaschuk, G.D., Mitchell, G.A., 2004. Pathways and control of ketone body metabolism: on the fringe of lipid biochemistry. Prost. Leuk. EFA 70 (3), 243–251.
Gaspar, J.A., Doss, M.X., Hengstler, J.G., Cadenas, C., Hescheler, J., Sachinidis, A., 2014. Unique metabolic features of stem cells, cardiomyocytes, and their progenitors. Circ. Res. 114, 1346–1360.
Gorr, T.A., Vogel, J., 2015. Western blotting revisited: critical perusal of underappreciated technical issues Proteomics. Clin. Appl. 9 (3–4), 396–405.
Halfon, S., Abramov, N., Grinblat, B., Ginis, I., 2011. Markers distinguishing mesenchymal stem cells from fibroblasts are downregulated with passaging. Stem Cells Dev. 20 (1), 53–66.
Hall, S.E.H., Wastney, M.E., Bolton, T.M., Braaten, J.T., Berman, M., 1984. Ketone body kinetics in humans: the effects of insulin-dependent diabetes, obesity and starvation. J. Lipid Res. 25, 1184–1194.
Hammerstedt, R.H., 1973. The use of Dowex-1-borate to separate ^3H_2O from 2-^{3}H-

glucose. Anal. Biochem. 56, 292–293.
Heather, L.C., Howell, N.J., Emmanuel, Y., Cole, M.A., Frenneaux, M.P., Pagano, D., Clarke, K., 2011. Changes in cardiac substrate transporters and metabolic proteins mirror the metabolic shift in patients with aortic stenosis. PLoS One 6 (10), e26326.
Hempfling, W.P., Mainzer, S.E., 1975. Effects of varying the carbon source limiting growth on yield and maintenance characteristics of *Escherichia coli* in continuous culture. J. Bacteriol. 123 (3), 1076–1087.
Jekabsons, M.B., Echtay, K.S., Arechaga, I., Brand, M.D., 2003. Molecular properties of purified human uncoupling protein 2 refolded from bacterial inclusion bodies. J. Bioeng. Biomem. 35 (5), 409–418.
Kashiwaya, Y., Bergman, C., Lee, J.-H., Wan, R., King, M.T., Mughai, M.R., Okhun, E., Clarke, K., Mattson, M.P., Veech, R.L., 2012. A ketone ester diet exhibits anxiolytic and cognition-sparing properties, and lessens amyloid and tau pathologies in a mouse model of Alzheimer's disease. Neurobiol. Ageing 34 (6), 1530–1539.
Laeger, T., Metges, C.C., Kuhla, B., 2010. Role of β-hydroxybutyric acid in the central regulation of energy balance. Appetite 54 (3), 450–455.
Ledesma, A., Garcia de Lacoba, M., Rial, E., 2002. The mitochondrial uncoupling proteins. Genome Biol. 3 (12) (reviews 3015.9).
Lee, J., Duan, W., Mattson, M.P., 2002a. Evidence that brain-derived neurotrophic factor is required for basal neurogenesis and mediates, in part, the enhancement of neurogenesis by dietary restriction in the hippocampus of adult mice. J. Neurochem. 82 (6), 1367–1375.
Lee, J., Seroogy, K.B., Mattson, M.P., 2002b. Dietary restriction enhances neurotrophin expression and neurogenesis in the hippocampus of adult mice. J. Neurochem. 80 (3), 539–547.
Maalouf, M., Rho, J.M., Mattson, M.P., 2009. The neuroprotective properties of calorie restriction, the ketogenic diet, and ketone bodies. Brain Res. Rev. 59, 293–315.
Musa-Veloso, K., Likhodii, S.S., Rarama, E., Benoit, S., Liu, Y.-M., Chartrand, C., Curtis, D., Carmant, R., Lortie, L., Comeauc, A., Cunnane, F.J.E., 2006. Breath acetone predicts plasma ketone bodies in children with epilepsy on a ketogenic diet. Nutrition 22 (1), 1–8.
Nedergaard, J., Cannon, B., 2003. The 'novel' 'uncoupling' proteins UCP2 and UCP3: what do they really do? Pros and cons for suggested functions. Exp. Physiol. 88, 65–84.
Negre-Salvayre, A., Hirtz, C., Carrera, R., Cazenave, R., Troly, M., Salvayre, L., Penicaud, L., Casteilla, L., 1997. A role for uncoupling protein-2 as a regulator of mitochondrial hydrogen peroxide generation. FASEB J. 11, 809–815.
O'Donnell-Tormey, J., Nathan, C.F., Lanks, K., DeBoer, C.J., de la Harpe, J., 1987. Secretion of pyruvate: an antioxidant defense of mammalian cells. J. Exp. Med 165 (2), 500–514.
Paoli, A., Rubini, A., Volek, J.S., Grimaldi, K.A., 2013. Beyond weight loss: a review of the therapeutic uses of very-low-carbohydrate (ketogenic) diets. Eur. J. Clin. Nutr. 67, 789–796.
Paoli, A., Bianco, A., Daminani, E., Bosco, G., 2014. Ketogenic diet in neuromuscular and neurodegenerative diseases. Biomed. Res. Int. 2014, 474296.
Parmar, K., Mauch, P., Vergilio, J.A., Sackstein, R., Down, J.D., 2007. Distribution of hematopoietic stem cells in the bone marrow according to regional hypoxia. Proc. Natl. Acad. Sci. U. S. A. 104, 5431–5436.
Pattappa, G., Heywood, H.K., De Bruijn, J.D., Lee, D.A., 2011. The metabolism of human mesenchymal stem cells during proliferation and differentiation. J. Cell. Physiol. 226, 2562–2570.
Pecqueur, C., Alves-Guerra, C., Ricquier, D., Bouillaud, F., 2009. UCP2, a metabolic sensor coupling glucose oxidation to mitochondrial metabolism? IUBMB Life 61 (7), 762–767.
Schofield, R., 1978. The relationship between the spleen colony-forming cell and the haemopoietic stem cell. Blood Cells 4, 7–25.
Shimazu, T., Hirschey, M.D., Newman, J., He, W., Shirakawa, K., Le Moan, N., Grueter, C.A., Lim, H., Saunders, L.R., Stevens, R.D., Newgard, C.B., Farese, R.V. Jr., de Cabo, R., Ulrich, S., Akassoglou, K., Verdin, E., 2013. Suppression of oxidative stress by β-hydroxybutyrate an endogenous histone deacetylase inhibitor. Science 339, 211–214.
Simsek, T., Kocobas, F., Zheng, J., DeBarardinis, R.J., Mahmoud, A.I., Olson, E.N., Schneider, J.W., Zhang, C.C., Sadek, H.A., 2010. The distinct metabolic profile of hematopoietic stem cells reflects their location in a hypoxic niche. Cell Stem Cell 7 (3), 380–390.
Suda, T., Takubo, K., Semenza, G.L., 2011. Metabolic regulation of hematopoietic stem cells in the hypoxic niche. Cell Stem Cell 9 (4), 298–310.
Trézéguet, V., Le Saux, A., David, C., Gourdet, C., Fiore, C., Dianoux, A., Brandolin, G., Lauquin, G.J., 2000. A covalent tandem dimer of the mitochondrial ADP/ATP carrier is functional *in vivo*. Biochim. Biophys. Acta 1457 (1–2), 81–93.
Vacanti, V., Kong, E., Susuki, G., Sato, K., Canty, J.M., Lee, T., 2005. Phenotypic changes of adult porcine mesenchymal stem cells induced by prolonged passaging in culture. J. Cell Physiol. 205 (2), 194–201.
Wang, Y., Zhang, Z., Chi, Y., Zhang, Q., Xu, F., Yang, Z., Meng, L., Yang, S., Yan, S., Mao, A., Zhang, J., Yang, Y., Wang, S., Cui, J., Liang, L., Ji, Y., Han, Z.-B., Han, Fang, 2013. Long-term cultured mesenchymal stem cells frequently develop genomic mutations but do not undergo malignant transformation. Cell Death Dis. 4, 1–11.
Xu, X., Duan, S., Yi, F., Ocampo, A., Liu, G.-H., Belmonte, J.C.I., 2013. Mitochondrial regulation in pluripotent stem cells. Cell Metab. 18, 1–8.
Zhang, C.Y., Parton, L.E., Ye, C.P., Krauss, S., Shen, R., Lin, C.-T., Porco, J.A., Lowell, B.B., 2006. Genipin inhibits UCP2-mediated proton leak and acutely reverses obesity- and high glucose-induced β cell dysfunction in isolated pancreatic islets. Cell Metab. 3, 417–427.
Zhang, J., Khvorostov, I., Hong, J.S., Oktay, Y., Vergnes, L., Neubel, E., Wahjudi, P.N., Setoquchi, K., Wang, G., Do, A., Jung, H.J., McCaffery, J.M., Kurland, I.J., Reue, K., Lee, W.N., Koehler, C.M., Teitell, M.A., 2011. UCP2 regulates energy metabolism and differentiation potential of human pluripotent stem cells. EMBO J. 30 (24), 4860–4873.

References

[1] X. Yang, L. Pabon, and C. E. Murry, "Engineering adolescence: maturation of human pluripotent stem cell-derived cardiomyocytes," *Circ Res*, vol. 114, no. 3, pp. 511–23, 2014.

[2] C. for Disease Control and N. C. f. H. S. Prevention, "Multiple cause of death 1999-2015 on cdc wonder online database, released december 2016. data are from the multiple cause of death files, 1999-2015, as compiled from data provided by the 57 vital statistics jurisdictions through the vital statistics cooperative program.," 2016.

[3] M. Heron, "Deaths: Leading causes for 2014," report, U.S. Department of Health and Human Services, 2016.

[4] V. L. Roger, A. S. Go, D. M. Lloyd-Jones, E. J. Benjamin, J. D. Berry, W. B. Borden, D. M. Bravata, S. Dai, E. S. Ford, C. S. Fox, H. J. Fullerton, C. Gillespie, S. M. Hailpern, J. A. Heit, V. J. Howard, B. M. Kissela, S. J. Kittner, D. T. Lackland, J. H. Lichtman, L. D. Lisabeth, D. M. Makuc, G. M. Marcus, A. Marelli, D. B. Matchar, C. S. Moy, D. Mozaffarian, M. E. Mussolino, G. Nichol, N. P. Paynter, E. Z. Soliman, P. D. Sorlie, N. Sotoodehnia, T. N. Turan, S. S. Virani, N. D. Wong, D. Woo, M. B. Turner, C. American Heart Association Statistics, and S. Stroke Statistics, "Heart disease and stroke statistics–2012 update: a report from the american heart association," *Circulation*, vol. 125, no. 1, pp. e2–e220, 2012.

[5] R. S. Velagaleti, M. J. Pencina, J. M. Murabito, T. J. Wang, N. I. Parikh, R. B. D'Agostino, D. Levy, W. B. Kannel, and R. S. Vasan, "Long-term trends in the incidence of heart failure after myocardial infarction," *Circulation*, vol. 118, no. 20, pp. 2057–62, 2008.

[6] L. Hofstra, I. H. Liem, E. A. Dumont, H. H. Boersma, W. L. van Heerde, P. A. Doevendans, E. De Muinck, H. J. Wellens, G. J. Kemerink, C. P. Reutelingsperger, and G. A. Heidendal, "Visualisation of cell death in vivo in patients with acute myocardial infarction," *Lancet*, vol. 356, no. 9225, pp. 209–12, 2000.

[7] M. G. Sutton and N. Sharpe, "Left ventricular remodeling after myocardial infarction: pathophysiology and therapy," *Circulation*, vol. 101, no. 25, pp. 2981–8, 2000.

[8] R. P. Iyer, M. Jung, and M. L. Lindsey, "Mmp-9 signaling in the left ventricle following myocardial infarction," *Am J Physiol Heart Circ Physiol*, vol. 311, no. 1, pp. H190–8, 2016.

[9] R. Ellen Kreipke, Y. Wang, J. W. Miklas, J. Mathieu, and H. Ruohola-Baker, "Metabolic remodeling in early development and cardiomyocyte maturation," *Semin Cell Dev Biol*, vol. 52, pp. 84–92, 2016.

[10] E. L. Ongstad and R. G. Gourdie, "Can heart function lost to disease be regenerated by therapeutic targeting of cardiac scar tissue?," *Semin Cell Dev Biol*, vol. 58, pp. 41–54, 2016.

[11] K. Kurrelmeyer, D. Kalra, B. Bozkurt, F. Wang, Z. Dibbs, Y. Seta, G. Baumgarten, D. Engle, N. Sivasubramanian, and D. L. Mann, "Cardiac remodeling as a consequence and cause of progressive heart failure," *Clin Cardiol*, vol. 21, no. 12 Suppl 1, pp. I14–9, 1998.

[12] J. Levick, *An Introduction to Cardiovascular Physiology*. United Kingdom: Hodder Arnold, fifth edition ed., 2010.

[13] J. Z. Goldfinger and E. D. Adler, "End-of-life options for patients with

advanced heart failure," *Curr Heart Fail Rep*, vol. 7, no. 3, pp. 140–7, 2010.

[14] A. Kumar and C. P. Cannon, "Acute coronary syndromes: diagnosis and management, part i," *Mayo Clin Proc*, vol. 84, no. 10, pp. 917–38, 2009.

[15] A. Kumar and C. P. Cannon, "Acute coronary syndromes: Diagnosis and management, part ii," *Mayo Clin Proc*, vol. 84, no. 11, pp. 1021–36, 2009.

[16] J. K. Kirklin, D. C. Naftel, F. D. Pagani, R. L. Kormos, L. W. Stevenson, E. D. Blume, M. A. Miller, J. T. Baldwin, and J. B. Young, "Sixth intermacs annual report: a 10,000-patient database," *J Heart Lung Transplant*, vol. 33, no. 6, pp. 555–64, 2014.

[17] A. J. Perricone and R. S. Vander Heide, "Novel therapeutic strategies for ischemic heart disease," *Pharmacol Res*, vol. 89, pp. 36–45, 2014.

[18] Y. Toyoda, T. S. Guy, and A. Kashem, "Present status and future perspectives of heart transplantation," *Circ J*, vol. 77, no. 5, pp. 1097–110, 2013.

[19] M. A. Laflamme and C. E. Murry, "Heart regeneration," *Nature*, vol. 473, no. 7347, pp. 326–35, 2011.

[20] T. Borchardt and T. Braun, "Cardiovascular regeneration in non-mammalian model systems: what are the differences between newts and man?," *Thromb Haemost*, vol. 98, no. 2, pp. 311–8, 2007.

[21] J. O. Oberpriller and J. C. Oberpriller, "Response of the adult newt ventricle to injury," *J Exp Zool*, vol. 187, no. 2, pp. 249–53, 1974.

[22] D. Bader and J. O. Oberpriller, "Repair and reorganization of minced cardiac muscle in the adult newt (notophthalmus viridescens)," *J Morphol*, vol. 155, no. 3, pp. 349–57, 1978.

[23] F. Laube, M. Heister, C. Scholz, T. Borchardt, and T. Braun, "Re-programming of newt cardiomyocytes is induced by tissue regeneration," *J Cell Sci*, vol. 119, no. Pt 22, pp. 4719–29, 2006.

[24] K. D. Poss, L. G. Wilson, and M. T. Keating, "Heart regeneration in zebrafish," *Science*, vol. 298, no. 5601, pp. 2188–90, 2002.

[25] A. Lepilina, A. N. Coon, K. Kikuchi, J. E. Holdway, R. W. Roberts, C. G. Burns, and K. D. Poss, "A dynamic epicardial injury response supports progenitor cell activity during zebrafish heart regeneration," *Cell*, vol. 127, no. 3, pp. 607–19, 2006.

[26] K. Kikuchi, J. E. Holdway, A. A. Werdich, R. M. Anderson, Y. Fang, G. F. Egnaczyk, T. Evans, C. A. Macrae, D. Y. Stainier, and K. D. Poss, "Primary contribution to zebrafish heart regeneration by gata4(+) cardiomyocytes," *Nature*, vol. 464, no. 7288, pp. 601–5, 2010.

[27] C. Jopling, E. Sleep, M. Raya, M. Marti, A. Raya, and J. C. Izpisua Belmonte, "Zebrafish heart regeneration occurs by cardiomyocyte dedifferentiation and proliferation," *Nature*, vol. 464, no. 7288, pp. 606–9, 2010.

[28] K. Urbanek, F. Quaini, G. Tasca, D. Torella, C. Castaldo, B. Nadal-Ginard, A. Leri, J. Kajstura, E. Quaini, and P. Anversa, "Intense myocyte formation from cardiac stem cells in human cardiac hypertrophy," *Proc Natl Acad Sci U S A*, vol. 100, no. 18, pp. 10440–5, 2003.

[29] P. C. Hsieh, V. F. Segers, M. E. Davis, C. MacGillivray, J. Gannon, J. D. Molkentin, J. Robbins, and R. T. Lee, "Evidence from a genetic fate-mapping study that stem cells refresh adult mammalian cardiomyocytes after injury," *Nat Med*, vol. 13, no. 8, pp. 970–4, 2007.

[30] O. Bergmann, R. D. Bhardwaj, S. Bernard, S. Zdunek, F. Barnabe-Heider, S. Walsh, J. Zupicich, K. Alkass, B. A. Buchholz, H. Druid, S. Jovinge, and J. Frisen, "Evidence for cardiomyocyte renewal in humans," *Science*, vol. 324, no. 5923, pp. 98–102, 2009.

[31] J. Kajstura, A. Leri, N. Finato, C. Di Loreto, C. A. Beltrami, and P. Anversa, "Myocyte proliferation in end-stage cardiac failure in humans,"

Proc Natl Acad Sci U S A, vol. 95, no. 15, pp. 8801–5, 1998.

[32] O. Bergmann, R. D. Bhardwaj, S. Bernard, S. Zdunek, F. Barnabe-Heider, S. Walsh, J. Zupicich, K. Alkass, B. A. Buchholz, H. Druid, S. Jovinge, and J. Frisen, "Evidence for cardiomyocyte renewal in humans," *Science*, vol. 324, no. 5923, pp. 98–102, 2009.

[33] B. J. Gersh, R. D. Simari, A. Behfar, C. M. Terzic, and A. Terzic, "Cardiac cell repair therapy: a clinical perspective," *Mayo Clin Proc*, vol. 84, no. 10, pp. 876–92, 2009.

[34] F. B. Engel, *Heart Regeneration, Stem Cells and Beyond*. World Scientific Publishing Co, 2012.

[35] R. J. Hassink, K. B. Pasumarthi, H. Nakajima, M. Rubart, M. H. Soonpaa, A. B. de la Riviere, P. A. Doevendans, and L. J. Field, "Cardiomyocyte cell cycle activation improves cardiac function after myocardial infarction," *Cardiovasc Res*, vol. 78, no. 1, pp. 18–25, 2008.

[36] K. Malliaras, Y. Zhang, J. Seinfeld, G. Galang, E. Tseliou, K. Cheng, B. Sun, M. Aminzadeh, and E. Marban, "Cardiomyocyte proliferation and progenitor cell recruitment underlie therapeutic regeneration after myocardial infarction in the adult mouse heart," *EMBO Mol Med*, vol. 5, no. 2, pp. 191–209, 2013.

[37] K. Suzuki, B. Murtuza, N. Suzuki, R. T. Smolenski, and M. H. Yacoub, "Intracoronary infusion of skeletal myoblasts improves cardiac function in doxorubicin-induced heart failure," *Circulation*, vol. 104, no. 12 Suppl 1, pp. I213–7, 2001.

[38] S. Tomita, R. K. Li, R. D. Weisel, D. A. Mickle, E. J. Kim, T. Sakai, and Z. Q. Jia, "Autologous transplantation of bone marrow cells improves damaged heart function," *Circulation*, vol. 100, no. 19 Suppl, pp. II247–56, 1999.

[39] N. Nagaya, K. Kangawa, T. Itoh, T. Iwase, S. Murakami, Y. Miyahara, T. Fujii, M. Uematsu, H. Ohgushi, M. Yamagishi, T. Tokudome, H. Mori, K. Miyatake, and S. Kitamura, "Transplantation of mesenchymal stem cells improves cardiac function in a rat model of dilated cardiomyopathy," *Circulation*, vol. 112, no. 8, pp. 1128–35, 2005.

[40] J. Pouly, A. A. Hagege, J. T. Vilquin, A. Bissery, A. Rouche, P. Bruneval, D. Duboc, M. Desnos, M. Fiszman, Y. Fromes, and P. Menasche, "Does the functional efficacy of skeletal myoblast transplantation extend to nonischemic cardiomyopathy?," *Circulation*, vol. 110, no. 12, pp. 1626–31, 2004.

[41] K. L. He, G. H. Yi, W. Sherman, H. Zhou, G. P. Zhang, A. Gu, R. Kao, H. B. Haimes, J. Harvey, E. Roos, D. White, D. A. Taylor, J. Wang, and D. Burkhoff, "Autologous skeletal myoblast transplantation improved hemodynamics and left ventricular function in chronic heart failure dogs," *J Heart Lung Transplant*, vol. 24, no. 11, pp. 1940–9, 2005.

[42] G. V. Silva, S. Litovsky, J. A. Assad, A. L. Sousa, B. J. Martin, D. Vela, S. C. Coulter, J. Lin, J. Ober, W. K. Vaughn, R. V. Branco, E. M. Oliveira, R. He, Y. J. Geng, J. T. Willerson, and E. C. Perin, "Mesenchymal stem cells differentiate into an endothelial phenotype, enhance vascular density, and improve heart function in a canine chronic ischemia model," *Circulation*, vol. 111, no. 2, pp. 150–6, 2005.

[43] R. Waksman, J. Fournadjiev, R. Baffour, R. Pakala, D. Hellinga, L. Leborgne, H. Yazdi, E. Cheneau, R. Wolfram, R. Seabron, K. Horton, F. Kolodgie, R. Virmani, and E. Rivera, "Transepicardial autologous bone marrow-derived mononuclear cell therapy in a porcine model of chronically infarcted myocardium," *Cardiovasc Radiat Med*, vol. 5, no. 3, pp. 125–31, 2004.

[44] P. V. Johnston, T. Sasano, K. Mills, R. Evers, S. T. Lee, R. R. Smith, A. C. Lardo, S. Lai, C. Steenbergen, G. Gerstenblith, R. Lange, and E. Marban, "Engraftment, differentiation, and functional benefits of autologous cardiosphere-derived cells in

porcine ischemic cardiomyopathy," *Circulation*, vol. 120, no. 12, pp. 1075–83, 7 p following 1083, 2009.

[45] S. Ghostine, C. Carrion, L. C. Souza, P. Richard, P. Bruneval, J. T. Vilquin, B. Pouzet, K. Schwartz, P. Menasche, and A. A. Hagege, "Long-term efficacy of myoblast transplantation on regional structure and function after myocardial infarction," *Circulation*, vol. 106, no. 12 Suppl 1, pp. I131–6, 2002.

[46] J. C. Chachques, F. Duarte, B. Cattadori, A. Shafy, N. Lila, G. Chatellier, J. N. Fabiani, and A. F. Carpentier, "Angiogenic growth factors and/or cellular therapy for myocardial regeneration: a comparative study," *J Thorac Cardiovasc Surg*, vol. 128, no. 2, pp. 245–53, 2004.

[47] Y. W. Liu, B. Chen, X. Yang, J. A. Fugate, F. A. Kalucki, A. Futakuchi-Tsuchida, L. Couture, K. W. Vogel, C. A. Astley, A. Baldessari, J. Ogle, C. W. Don, Z. L. Steinberg, S. P. Seslar, S. A. Tuck, H. Tsuchida, A. V. Naumova, S. K. Dupras, M. S. Lyu, J. Lee, D. W. Hailey, H. Reinecke, L. Pabon, B. H. Fryer, W. R. MacLellan, R. S. Thies, and C. E. Murry, "Human embryonic stem cell-derived cardiomyocytes restore function in infarcted hearts of non-human primates," *Nat Biotechnol*, vol. 36, no. 7, pp. 597–605, 2018.

[48] P. Menasche, "Cell-based therapy for heart disease: a clinically oriented perspective," *Mol Ther*, vol. 17, no. 5, pp. 758–66, 2009.

[49] S. Dimmeler, J. Burchfield, and A. M. Zeiher, "Cell-based therapy of myocardial infarction," *Arterioscler Thromb Vasc Biol*, vol. 28, no. 2, pp. 208–16, 2008.

[50] C. Stamm, Y. H. Choi, B. Nasseri, and R. Hetzer, "A heart full of stem cells: the spectrum of myocardial progenitor cells in the postnatal heart," *Ther Adv Cardiovasc Dis*, vol. 3, no. 3, pp. 215–29, 2009.

[51] H. Jeong, H. W. Yim, H. J. Park, Y. Cho, H. Hong, N. J. Kim, and I. H. Oh, "Mesenchymal stem cell therapy for ischemic heart disease: Systematic review and meta-analysis," *Int J Stem Cells*, vol. 11, no. 1, pp. 1–12, 2018.

[52] M. Gyongyosi, P. M. Haller, D. J. Blake, and E. Martin Rendon, "Meta-analysis of cell therapy studies in heart failure and acute myocardial infarction," *Circ Res*, vol. 123, no. 2, pp. 301–308, 2018.

[53] S. A. Fisher, C. Doree, A. Mathur, and E. Martin-Rendon, "Meta-analysis of cell therapy trials for patients with heart failure," *Circ Res*, vol. 116, no. 8, pp. 1361–77, 2015.

[54] S. K. Sanganalmath and R. Bolli, "Cell therapy for heart failure: a comprehensive overview of experimental and clinical studies, current challenges, and future directions," *Circ Res*, vol. 113, no. 6, pp. 810–34, 2013.

[55] H. K. Awada, N. R. Johnson, and Y. Wang, "Dual delivery of vascular endothelial growth factor and hepatocyte growth factor coacervate displays strong angiogenic effects," *Macromol Biosci*, vol. 14, no. 5, pp. 679–86, 2014.

[56] D. A. M. Feyen, R. Gaetani, P. A. Doevendans, and J. P. G. Sluijter, "Stem cell-based therapy: Improving myocardial cell delivery," *Adv Drug Deliv Rev*, vol. 106, no. Pt A, pp. 104–115, 2016.

[57] E. Meng and T. Hoang, "Micro- and nano-fabricated implantable drug-delivery systems," *Ther Deliv*, vol. 3, no. 12, pp. 1457–67, 2012.

[58] M. Monaghan, U. Greiser, J. G. Wall, T. O'Brien, and A. Pandit, "Interference: an alternative therapy following acute myocardial infarction," *Trends Pharmacol Sci*, vol. 33, no. 12, pp. 635–45, 2012.

[59] S. Pascual-Gil, E. Garbayo, P. Diaz-Herraez, F. Prosper, and M. J. Blanco-Prieto, "Heart regeneration after myocardial infarction using synthetic biomaterials," *J Control Release*, vol. 203, pp. 23–38, 2015.

[60] V. Grimaldi, F. P. Mancini, A. Casamassimi, M. Al-Omran, A. Zullo, T. Infante, and C. Napoli, "Potential benefits of cell therapy in coronary heart disease," *J Cardiol*, vol. 62, no. 5, pp. 267–76, 2013.

[61] C. Cochain, K. M. Channon, and J. S. Silvestre, "Angiogenesis in the infarcted myocardium," *Antioxid Redox Signal*, vol. 18, no. 9, pp. 1100–13, 2013.

[62] N. G. Frangogiannis, "The inflammatory response in myocardial injury, repair, and remodelling," *Nat Rev Cardiol*, vol. 11, no. 5, pp. 255–65, 2014.

[63] K. J. Lavine, S. Epelman, K. Uchida, K. J. Weber, C. G. Nichols, J. D. Schilling, D. M. Ornitz, G. J. Randolph, and D. L. Mann, "Distinct macrophage lineages contribute to disparate patterns of cardiac recovery and remodeling in the neonatal and adult heart," *Proc Natl Acad Sci U S A*, vol. 111, no. 45, pp. 16029–34, 2014.

[64] A. Uygur and R. T. Lee, "Mechanisms of cardiac regeneration," *Dev Cell*, vol. 36, no. 4, pp. 362–74, 2016.

[65] L. Saludas, S. Pascual-Gil, F. Prosper, E. Garbayo, and M. Blanco-Prieto, "Hydrogel based approaches for cardiac tissue engineering," *Int J Pharm*, vol. 523, no. 2, pp. 454–475, 2017.

[66] J. T. Lam, A. Moretti, and K. L. Laugwitz, "Multipotent progenitor cells in regenerative cardiovascular medicine," *Pediatr Cardiol*, vol. 30, no. 5, pp. 690–8, 2009.

[67] V. F. Segers and R. T. Lee, "Stem-cell therapy for cardiac disease," *Nature*, vol. 451, no. 7181, pp. 937–42, 2008.

[68] P. A. Lalit, D. J. Hei, A. N. Raval, and T. J. Kamp, "Induced pluripotent stem cells for post-myocardial infarction repair: remarkable opportunities and challenges," *Circ Res*, vol. 114, no. 8, pp. 1328–45, 2014.

[69] A. A. Bruyneel, A. Sehgal, S. Malandraki-Miller, and C. Carr, "Stem cell therapy for the heart: Blind alley or magic bullet?," *J Cardiovasc Transl Res*, vol. 9, no. 5-6, pp. 405–418, 2016.

[70] S. Makino, K. Fukuda, S. Miyoshi, F. Konishi, H. Kodama, J. Pan, M. Sano, T. Takahashi, S. Hori, H. Abe, J. Hata, A. Umezawa, and S. Ogawa, "Cardiomyocytes can be generated from marrow stromal cells in vitro," *J Clin Invest*, vol. 103, no. 5, pp. 697–705, 1999.

[71] D. Orlic, J. Kajstura, S. Chimenti, I. Jakoniuk, S. M. Anderson, B. Li, J. Pickel, R. McKay, B. Nadal-Ginard, D. M. Bodine, A. Leri, and P. Anversa, "Bone marrow cells regenerate infarcted myocardium," *Nature*, vol. 410, no. 6829, pp. 701–5, 2001.

[72] H. Oh, S. B. Bradfute, T. D. Gallardo, T. Nakamura, V. Gaussin, Y. Mishina, J. Pocius, L. H. Michael, R. R. Behringer, D. J. Garry, M. L. Entman, and M. D. Schneider, "Cardiac progenitor cells from adult myocardium: homing, differentiation, and fusion after infarction," *Proc Natl Acad Sci U S A*, vol. 100, no. 21, pp. 12313–8, 2003.

[73] E. Messina, L. De Angelis, G. Frati, S. Morrone, S. Chimenti, F. Fiordaliso, M. Salio, M. Battaglia, M. V. Latronico, M. Coletta, E. Vivarelli, L. Frati, G. Cossu, and A. Giacomello, "Isolation and expansion of adult cardiac stem cells from human and murine heart," *Circ Res*, vol. 95, no. 9, pp. 911–21, 2004.

[74] C. A. Carr, D. J. Stuckey, J. J. Tan, S. C. Tan, R. S. Gomes, P. Camelliti, E. Messina, A. Giacomello, G. M. Ellison, and K. Clarke, "Cardiosphere-derived cells improve function in the infarcted rat heart for at least 16 weeks–an mri study," *PLoS One*, vol. 6, no. 10, p. e25669, 2011.

[75] N. Smart, S. Bollini, K. N. Dube, J. M. Vieira, B. Zhou, S. Davidson, D. Yellon, J. Riegler, A. N. Price, M. F. Lythgoe, W. T. Pu, and P. R. Riley, "De novo cardiomyocytes from within the activated adult heart after injury," *Nature*, vol. 474, no. 7353, pp. 640–4, 2011.

[76] M. A. Laflamme, K. Y. Chen, A. V. Naumova, V. Muskheli, J. A. Fugate, S. K. Dupras, H. Reinecke,

C. Xu, M. Hassanipour, S. Police, C. O'Sullivan, L. Collins, Y. Chen, E. Minami, E. A. Gill, S. Ueno, C. Yuan, J. Gold, and C. E. Murry, "Cardiomyocytes derived from human embryonic stem cells in pro-survival factors enhance function of infarcted rat hearts," *Nat Biotechnol*, vol. 25, no. 9, pp. 1015–24, 2007.

[77] S. Fernandes, A. V. Naumova, W. Z. Zhu, M. A. Laflamme, J. Gold, and C. E. Murry, "Human embryonic stem cell-derived cardiomyocytes engraft but do not alter cardiac remodeling after chronic infarction in rats," *J Mol Cell Cardiol*, vol. 49, no. 6, pp. 941–9, 2010.

[78] Y. Shiba, S. Fernandes, W. Z. Zhu, D. Filice, V. Muskheli, J. Kim, N. J. Palpant, J. Gantz, K. W. Moyes, H. Reinecke, B. Van Biber, T. Dardas, J. L. Mignone, A. Izawa, R. Hanna, M. Viswanathan, J. D. Gold, M. I. Kotlikoff, N. Sarvazyan, M. W. Kay, C. E. Murry, and M. A. Laflamme, "Human es-cell-derived cardiomyocytes electrically couple and suppress arrhythmias in injured hearts," *Nature*, vol. 489, no. 7415, pp. 322–5, 2012.

[79] J. J. Chong, X. Yang, C. W. Don, E. Minami, Y. W. Liu, J. J. Weyers, W. M. Mahoney, B. Van Biber, S. M. Cook, N. J. Palpant, J. A. Gantz, J. A. Fugate, V. Muskheli, G. M. Gough, K. W. Vogel, C. A. Astley, C. E. Hotchkiss, A. Baldessari, L. Pabon, H. Reinecke, E. A. Gill, V. Nelson, H. P. Kiem, M. A. Laflamme, and C. E. Murry, "Human embryonic-stem-cell-derived cardiomyocytes regenerate non-human primate hearts," *Nature*, vol. 510, no. 7504, pp. 273–7, 2014.

[80] L. Carpenter, C. Carr, C. T. Yang, D. J. Stuckey, K. Clarke, and S. M. Watt, "Efficient differentiation of human induced pluripotent stem cells generates cardiac cells that provide protection following myocardial infarction in the rat," *Stem Cells Dev*, vol. 21, no. 6, pp. 977–86, 2012.

[81] S. Kadota, L. Pabon, H. Reinecke, and C. E. Murry, "In vivo maturation of human induced pluripotent stem cell-derived cardiomyocytes in neonatal and adult rat hearts," *Stem Cell Reports*, vol. 8, no. 2, pp. 278–289, 2017.

[82] L. R. Zhao, W. M. Duan, M. Reyes, C. D. Keene, C. M. Verfaillie, and W. C. Low, "Human bone marrow stem cells exhibit neural phenotypes and ameliorate neurological deficits after grafting into the ischemic brain of rats," *Exp Neurol*, vol. 174, no. 1, pp. 11–20, 2002.

[83] E. Mezey, K. J. Chandross, G. Harta, R. A. Maki, and S. R. McKercher, "Turning blood into brain: cells bearing neuronal antigens generated in vivo from bone marrow," *Science*, vol. 290, no. 5497, pp. 1779–82, 2000.

[84] M. A. Eglitis and E. Mezey, "Hematopoietic cells differentiate into both microglia and macroglia in the brains of adult mice," *Proc Natl Acad Sci U S A*, vol. 94, no. 8, pp. 4080–5, 1997.

[85] T. R. Brazelton, F. M. Rossi, G. I. Keshet, and H. M. Blau, "From marrow to brain: expression of neuronal phenotypes in adult mice," *Science*, vol. 290, no. 5497, pp. 1775–9, 2000.

[86] G. Ferrari, G. Cusella-De Angelis, M. Coletta, E. Paolucci, A. Stornaiuolo, G. Cossu, and F. Mavilio, "Muscle regeneration by bone marrow-derived myogenic progenitors," *Science*, vol. 279, no. 5356, pp. 1528–30, 1998.

[87] E. Gussoni, Y. Soneoka, C. D. Strickland, E. A. Buzney, M. K. Khan, A. F. Flint, L. M. Kunkel, and R. C. Mulligan, "Dystrophin expression in the mdx mouse restored by stem cell transplantation," *Nature*, vol. 401, no. 6751, pp. 390–4, 1999.

[88] B. E. Petersen, W. C. Bowen, K. D. Patrene, W. M. Mars, A. K. Sullivan, N. Murase, S. S. Boggs, J. S. Greenberger, and J. P. Goff, "Bone marrow as a potential source of hepatic oval cells," *Science*, vol. 284, no. 5417, pp. 1168–70, 1999.

[89] N. D. Theise, S. Badve, R. Saxena, O. Henegariu, S. Sell, J. M. Crawford, and D. S. Krause, "Derivation of

hepatocytes from bone marrow cells in mice after radiation-induced myeloablation," *Hepatology*, vol. 31, no. 1, pp. 235–40, 2000.

[90] N. D. Theise, M. Nimmakayalu, R. Gardner, P. B. Illei, G. Morgan, L. Teperman, O. Henegariu, and D. S. Krause, "Liver from bone marrow in humans," *Hepatology*, vol. 32, no. 1, pp. 11–6, 2000.

[91] A. Kawamoto, T. Tkebuchava, J. Yamaguchi, H. Nishimura, Y. S. Yoon, C. Milliken, S. Uchida, O. Masuo, H. Iwaguro, H. Ma, A. Hanley, M. Silver, M. Kearney, D. W. Losordo, J. M. Isner, and T. Asahara, "Intramyocardial transplantation of autologous endothelial progenitor cells for therapeutic neovascularization of myocardial ischemia," *Circulation*, vol. 107, no. 3, pp. 461–8, 2003.

[92] A. Kawamoto, H. C. Gwon, H. Iwaguro, J. I. Yamaguchi, S. Uchida, H. Masuda, M. Silver, H. Ma, M. Kearney, J. M. Isner, and T. Asahara, "Therapeutic potential of ex vivo expanded endothelial progenitor cells for myocardial ischemia," *Circulation*, vol. 103, no. 5, pp. 634–7, 2001.

[93] T. Takahashi, C. Kalka, H. Masuda, D. Chen, M. Silver, M. Kearney, M. Magner, J. M. Isner, and T. Asahara, "Ischemia- and cytokine-induced mobilization of bone marrow-derived endothelial progenitor cells for neovascularization," *Nat Med*, vol. 5, no. 4, pp. 434–8, 1999.

[94] J. G. Shake, P. J. Gruber, W. A. Baumgartner, G. Senechal, J. Meyers, J. M. Redmond, M. F. Pittenger, and B. J. Martin, "Mesenchymal stem cell implantation in a swine myocardial infarct model: engraftment and functional effects," *Ann Thorac Surg*, vol. 73, no. 6, pp. 1919–25; discussion 1926, 2002.

[95] M. Kucia, B. Dawn, G. Hunt, Y. Guo, M. Wysoczynski, M. Majka, J. Ratajczak, F. Rezzoug, S. T. Ildstad, R. Bolli, and M. Z. Ratajczak, "Cells expressing early cardiac markers reside in the bone marrow and are mobilized into the peripheral blood after myocardial infarction," *Circ Res*, vol. 95, no. 12, pp. 1191–9, 2004.

[96] X. Guo, Y. Bai, L. Zhang, B. Zhang, N. Zagidullin, K. Carvalho, Z. Du, and B. Cai, "Cardiomyocyte differentiation of mesenchymal stem cells from bone marrow: new regulators and its implications," *Stem Cell Res Ther*, vol. 9, no. 1, p. 44, 2018.

[97] A. J. Wagers, R. I. Sherwood, J. L. Christensen, and I. L. Weissman, "Little evidence for developmental plasticity of adult hematopoietic stem cells," *Science*, vol. 297, no. 5590, pp. 2256–9, 2002.

[98] L. B. Balsam, A. J. Wagers, J. L. Christensen, T. Kofidis, I. L. Weissman, and R. C. Robbins, "Haematopoietic stem cells adopt mature haematopoietic fates in ischaemic myocardium," *Nature*, vol. 428, no. 6983, pp. 668–73, 2004.

[99] C. E. Murry, M. H. Soonpaa, H. Reinecke, H. Nakajima, H. O. Nakajima, M. Rubart, K. B. Pasumarthi, J. I. Virag, S. H. Bartelmez, V. Poppa, G. Bradford, J. D. Dowell, D. A. Williams, and L. J. Field, "Haematopoietic stem cells do not transdifferentiate into cardiac myocytes in myocardial infarcts," *Nature*, vol. 428, no. 6983, pp. 664–8, 2004.

[100] G. Vassilopoulos and D. W. Russell, "Cell fusion: an alternative to stem cell plasticity and its therapeutic implications," *Curr Opin Genet Dev*, vol. 13, no. 5, pp. 480–5, 2003.

[101] K. R. Chien, "Stem cells: lost in translation," *Nature*, vol. 428, no. 6983, pp. 607–8, 2004.

[102] D. Orlic, "Adult bm stem cells regenerate mouse myocardium," *Cytotherapy*, vol. 4, no. 6, pp. 521–5, 2002.

[103] D. Orlic, "Adult bone marrow stem cells regenerate myocardium in ischemic heart disease," *Ann N Y Acad Sci*, vol. 996, pp. 152–7, 2003.

[104] R. Liao, O. Pfister, M. Jain, and F. Mouquet, "The bone marrow–cardiac axis of myocardial regeneration," *Prog Cardiovasc Dis*, vol. 50, no. 1, pp. 18–30, 2007.

[105] A. A. Kocher, M. D. Schuster, M. J. Szabolcs, S. Takuma, D. Burkhoff, J. Wang, S. Homma, N. M. Edwards, and S. Itescu, "Neovascularization of ischemic myocardium by human bone-marrow-derived angioblasts prevents cardiomyocyte apoptosis, reduces remodeling and improves cardiac function," *Nat Med*, vol. 7, no. 4, pp. 430–6, 2001.

[106] A. A. Mangi, N. Noiseux, D. Kong, H. He, M. Rezvani, J. S. Ingwall, and V. J. Dzau, "Mesenchymal stem cells modified with akt prevent remodeling and restore performance of infarcted hearts," *Nat Med*, vol. 9, no. 9, pp. 1195–201, 2003.

[107] C. Toma, M. F. Pittenger, K. S. Cahill, B. J. Byrne, and P. D. Kessler, "Human mesenchymal stem cells differentiate to a cardiomyocyte phenotype in the adult murine heart," *Circulation*, vol. 105, no. 1, pp. 93–8, 2002.

[108] F. Mouquet, O. Pfister, M. Jain, A. Oikonomopoulos, S. Ngoy, R. Summer, A. Fine, and R. Liao, "Restoration of cardiac progenitor cells after myocardial infarction by self-proliferation and selective homing of bone marrow-derived stem cells," *Circ Res*, vol. 97, no. 11, pp. 1090–2, 2005.

[109] S. Fazel, M. Cimini, L. Chen, S. Li, D. Angoulvant, P. Fedak, S. Verma, R. D. Weisel, A. Keating, and R. K. Li, "Cardioprotective c-kit+ cells are from the bone marrow and regulate the myocardial balance of angiogenic cytokines," *J Clin Invest*, vol. 116, no. 7, pp. 1865–77, 2006.

[110] F. S. Loffredo, M. L. Steinhauser, J. Gannon, and R. T. Lee, "Bone marrow-derived cell therapy stimulates endogenous cardiomyocyte progenitors and promotes cardiac repair," *Cell Stem Cell*, vol. 8, no. 4, pp. 389–98, 2011.

[111] K. E. Hatzistergos, H. Quevedo, B. N. Oskouei, Q. Hu, G. S. Feigenbaum, I. S. Margitich, R. Mazhari, A. J. Boyle, J. P. Zambrano, J. E. Rodriguez, R. Dulce, P. M. Pattany, D. Valdes, C. Revilla, A. W. Heldman, I. McNiece, and J. M. Hare, "Bone marrow mesenchymal stem cells stimulate cardiac stem cell proliferation and differentiation," *Circ Res*, vol. 107, no. 7, pp. 913–22, 2010.

[112] A. Abdel-Latif, R. Bolli, I. M. Tleyjeh, V. M. Montori, E. C. Perin, C. A. Hornung, E. K. Zuba-Surma, M. Al-Mallah, and B. Dawn, "Adult bone marrow-derived cells for cardiac repair: a systematic review and meta-analysis," *Arch Intern Med*, vol. 167, no. 10, pp. 989–97, 2007.

[113] C. Breymann, D. Schmidt, and S. P. Hoerstrup, "Umbilical cord cells as a source of cardiovascular tissue engineering," *Stem Cell Rev*, vol. 2, no. 2, pp. 87–92, 2006.

[114] C. H. Fang, J. Jin, J. H. Joe, Y. S. Song, B. I. So, S. M. Lim, G. J. Cheon, S. K. Woo, J. C. Ra, Y. Y. Lee, and K. S. Kim, "In vivo differentiation of human amniotic epithelial cells into cardiomyocyte-like cells and cell transplantation effect on myocardial infarction in rats: comparison with cord blood and adipose tissue-derived mesenchymal stem cells," *Cell Transplant*, vol. 21, no. 8, pp. 1687–96, 2012.

[115] J. M. Gimble, A. J. Katz, and B. A. Bunnell, "Adipose-derived stem cells for regenerative medicine," *Circ Res*, vol. 100, no. 9, pp. 1249–60, 2007.

[116] B. Li, Q. Zeng, H. Wang, S. Shao, X. Mao, F. Zhang, S. Li, and Z. Guo, "Adipose tissue stromal cells transplantation in rats of acute myocardial infarction," *Coron Artery Dis*, vol. 18, no. 3, pp. 221–7, 2007.

[117] C. Valina, K. Pinkernell, Y. H. Song, X. Bai, S. Sadat, R. J. Campeau, T. H. Le Jemtel, and E. Alt, "Intracoronary administration of autologous adipose tissue-derived stem cells improves left ventricular function, perfusion, and remodelling after acute myocardial infarction," *Eur Heart J*, vol. 28, no. 21, pp. 2667–77, 2007.

[118] P. De Coppi, J. Bartsch, G., M. M. Siddiqui, T. Xu, C. C. Santos, L. Perin, G. Mostoslavsky, A. C. Serre, E. Y. Snyder, J. J. Yoo, M. E. Furth, S. Soker, and A. Atala, "Isolation of amniotic stem cell lines with potential

for therapy," *Nat Biotechnol*, vol. 25, no. 1, pp. 100–6, 2007.

[119] A. P. Beltrami, L. Barlucchi, D. Torella, M. Baker, F. Limana, S. Chimenti, H. Kasahara, M. Rota, E. Musso, K. Urbanek, A. Leri, J. Kajstura, B. Nadal-Ginard, and P. Anversa, "Adult cardiac stem cells are multipotent and support myocardial regeneration," *Cell*, vol. 114, no. 6, pp. 763–76, 2003.

[120] J. P. Veinot, W. Prichett-Pejic, J. Song, G. Waghray, W. Parks, T. G. Mesana, and M. Ruel, "Cd117-positive cells and mast cells in adult human cardiac valves–observations and implications for the creation of bioengineered grafts," *Cardiovasc Pathol*, vol. 15, no. 1, pp. 36–40, 2006.

[121] J. Sandstedt, M. Jonsson, A. Lindahl, A. Jeppsson, and J. Asp, "C-kit+ cd45- cells found in the adult human heart represent a population of endothelial progenitor cells," *Basic Res Cardiol*, vol. 105, no. 4, pp. 545–56, 2010.

[122] G. M. Ellison, C. Vicinanza, A. J. Smith, I. Aquila, A. Leone, C. D. Waring, B. J. Henning, G. G. Stirparo, R. Papait, M. Scarfo, V. Agosti, G. Viglietto, G. Condorelli, C. Indolfi, S. Ottolenghi, D. Torella, and B. Nadal-Ginard, "Adult c-kit(pos) cardiac stem cells are necessary and sufficient for functional cardiac regeneration and repair," *Cell*, vol. 154, no. 4, pp. 827–42, 2013.

[123] N. Sultana, L. Zhang, J. Yan, J. Chen, W. Cai, S. Razzaque, D. Jeong, W. Sheng, L. Bu, M. Xu, G. Y. Huang, R. J. Hajjar, B. Zhou, A. Moon, and C. L. Cai, "Resident c-kit(+) cells in the heart are not cardiac stem cells," *Nat Commun*, vol. 6, p. 8701, 2015.

[124] J. D. Molkentin and S. R. Houser, "Are resident c-kit+ cardiac stem cells really all that are needed to mend a broken heart?," *Circ Res*, vol. 113, no. 9, pp. 1037–9, 2013.

[125] J. H. van Berlo, O. Kanisicak, M. Maillet, R. J. Vagnozzi, J. Karch, S. C. Lin, R. C. Middleton, E. Marban, and J. D. Molkentin, "c-kit+ cells minimally contribute cardiomyocytes to the heart," *Nature*, vol. 509, no. 7500, pp. 337–41, 2014.

[126] R. Bolli, A. R. Chugh, D. D'Amario, J. H. Loughran, M. F. Stoddard, S. Ikram, G. M. Beache, S. G. Wagner, A. Leri, T. Hosoda, F. Sanada, J. B. Elmore, P. Goichberg, D. Cappetta, N. K. Solankhi, I. Fahsah, D. G. Rokosh, M. S. Slaughter, J. Kajstura, and P. Anversa, "Cardiac stem cells in patients with ischaemic cardiomyopathy (scipio): initial results of a randomised phase 1 trial," *Lancet*, vol. 378, no. 9806, pp. 1847–57, 2011.

[127] E. The Lancet, "Expression of concern: the scipio trial," *Lancet*, vol. 383, no. 9925, p. 1279, 2014.

[128] X. Wang, Q. Hu, Y. Nakamura, J. Lee, G. Zhang, A. H. From, and J. Zhang, "The role of the sca-1+/cd31- cardiac progenitor cell population in postinfarction left ventricular remodeling," *Stem Cells*, vol. 24, no. 7, pp. 1779–88, 2006.

[129] S. Uchida, P. De Gaspari, S. Kostin, K. Jenniches, A. Kilic, Y. Izumiya, I. Shiojima, K. Grosse Kreymborg, H. Renz, K. Walsh, and T. Braun, "Sca1-derived cells are a source of myocardial renewal in the murine adult heart," *Stem Cell Reports*, vol. 1, no. 5, pp. 397–410, 2013.

[130] B. Bailey, J. Fransioli, N. A. Gude, J. Alvarez, R., X. Zhang, A. B. Gustafsson, and M. A. Sussman, "Sca-1 knockout impairs myocardial and cardiac progenitor cell function," *Circ Res*, vol. 111, no. 6, pp. 750–60, 2012.

[131] H. H. Chan, Z. Meher Homji, R. S. Gomes, D. Sweeney, G. N. Thomas, J. J. Tan, H. Zhang, F. Perbellini, D. J. Stuckey, S. M. Watt, D. Taggart, K. Clarke, E. Martin-Rendon, and C. A. Carr, "Human cardiosphere-derived cells from patients with chronic ischaemic heart disease can be routinely expanded from atrial but not epicardial ventricular biopsies," *J Cardiovasc Transl Res*, vol. 5, no. 5, pp. 678–87, 2012.

[132] L. C. Hsiao, F. Perbellini, R. S. Gomes, J. J. Tan, S. Vieira, G. Faggian,

K. Clarke, and C. A. Carr, "Murine cardiosphere-derived cells are impaired by age but not by cardiac dystrophic dysfunction," *Stem Cells Dev*, vol. 23, no. 9, pp. 1027–36, 2014.

[133] F. Perbellini, R. S. Gomes, S. Vieira, D. Buchanan, S. Malandraki-Miller, A. A. Bruyneel, L. Sousa Fialho Mda, V. Ball, K. Clarke, G. Faggian, and C. A. Carr, "Chronic high-fat feeding affects the mesenchymal cell population expanded from adipose tissue but not cardiac atria," *Stem Cells Transl Med*, vol. 4, no. 12, pp. 1403–14, 2015.

[134] I. Chimenti, E. Forte, F. Angelini, E. Messina, and A. Giacomello, "Biochemistry and biology: heart-to-heart to investigate cardiac progenitor cells," *Biochim Biophys Acta*, vol. 1830, no. 2, pp. 2459–69, 2013.

[135] I. Chimenti, R. R. Smith, T. S. Li, G. Gerstenblith, E. Messina, A. Giacomello, and E. Marban, "Relative roles of direct regeneration versus paracrine effects of human cardiosphere-derived cells transplanted into infarcted mice," *Circ Res*, vol. 106, no. 5, pp. 971–80, 2010.

[136] C. Bearzi, M. Rota, T. Hosoda, J. Tillmanns, A. Nascimbene, A. De Angelis, S. Yasuzawa-Amano, I. Trofimova, R. W. Siggins, N. Lecapitaine, S. Cascapera, A. P. Beltrami, D. A. D'Alessandro, E. Zias, F. Quaini, K. Urbanek, R. E. Michler, R. Bolli, J. Kajstura, A. Leri, and P. Anversa, "Human cardiac stem cells," *Proc Natl Acad Sci U S A*, vol. 104, no. 35, pp. 14068–73, 2007.

[137] T. Sano, D. Ousaka, T. Goto, S. Ishigami, K. Hirai, S. Kasahara, S. Ohtsuki, S. Sano, and H. Oh, "Impact of cardiac progenitor cells on heart failure and survival in single ventricle congenital heart disease," *Circ Res*, vol. 122, no. 7, pp. 994–1005, 2018.

[138] J. A. Thomson, J. Itskovitz-Eldor, S. S. Shapiro, M. A. Waknitz, J. J. Swiergiel, V. S. Marshall, and J. M. Jones, "Embryonic stem cell lines derived from human blastocysts," *Science*, vol. 282, no. 5391, pp. 1145–7, 1998.

[139] S. E. Harding, N. N. Ali, M. Brito-Martins, and J. Gorelik, "The human embryonic stem cell-derived cardiomyocyte as a pharmacological model," *Pharmacol Ther*, vol. 113, no. 2, pp. 341–53, 2007.

[140] O. Caspi, I. Huber, I. Kehat, M. Habib, G. Arbel, A. Gepstein, L. Yankelson, D. Aronson, R. Beyar, and L. Gepstein, "Transplantation of human embryonic stem cell-derived cardiomyocytes improves myocardial performance in infarcted rat hearts," *J Am Coll Cardiol*, vol. 50, no. 19, pp. 1884–93, 2007.

[141] L. W. van Laake, R. Passier, P. A. Doevendans, and C. L. Mummery, "Human embryonic stem cell-derived cardiomyocytes and cardiac repair in rodents," *Circ Res*, vol. 102, no. 9, pp. 1008–10, 2008.

[142] M. A. Laflamme, J. Gold, C. Xu, M. Hassanipour, E. Rosler, S. Police, V. Muskheli, and C. E. Murry, "Formation of human myocardium in the rat heart from human embryonic stem cells," *Am J Pathol*, vol. 167, no. 3, pp. 663–71, 2005.

[143] W. H. Zimmermann, "Embryonic and embryonic-like stem cells in heart muscle engineering," *J Mol Cell Cardiol*, vol. 50, no. 2, pp. 320–6, 2011.

[144] L. Ye, C. Swingen, and J. Zhang, "Induced pluripotent stem cells and their potential for basic and clinical sciences," *Curr Cardiol Rev*, vol. 9, no. 1, pp. 63–72, 2013.

[145] S. J. Park, S. A. Lee, N. Prasain, D. Bae, H. Kang, T. Ha, J. S. Kim, K. S. Hong, C. Mantel, S. H. Moon, H. E. Broxmeyer, and M. R. Lee, "Metabolome profiling of partial and fully reprogrammed induced pluripotent stem cells," *Stem Cells Dev*, 2017.

[146] T. Halevy and A. Urbach, "Comparing esc and ipsc-based models for human genetic disorders," *J Clin Med*, vol. 3, no. 4, pp. 1146–62, 2014.

[147] J. Bilic and J. C. Izpisua Belmonte, "Concise review: Induced pluripotent stem cells versus embryonic stem cells: close enough or yet too far apart?,"

Stem Cells, vol. 30, no. 1, pp. 33–41, 2012.

[148] K. Takahashi, K. Tanabe, M. Ohnuki, M. Narita, T. Ichisaka, K. Tomoda, and S. Yamanaka, "Induction of pluripotent stem cells from adult human fibroblasts by defined factors," *Cell*, vol. 131, no. 5, pp. 861–72, 2007.

[149] K. Takahashi and S. Yamanaka, "Induction of pluripotent stem cells from mouse embryonic and adult fibroblast cultures by defined factors," *Cell*, vol. 126, no. 4, pp. 663–76, 2006.

[150] G. Bahadur and M. Morrison, "Patenting human pluripotent cells: balancing commercial, academic and ethical interests," *Hum Reprod*, vol. 25, no. 1, pp. 14–21, 2010.

[151] A. Plomer, K. S. Taymor, and C. T. Scott, "Challenges to human embryonic stem cell patents," *Cell Stem Cell*, vol. 2, no. 1, pp. 13–7, 2008.

[152] M. Rao and M. L. Condic, "Alternative sources of pluripotent stem cells: scientific solutions to an ethical dilemma," *Stem Cells Dev*, vol. 17, no. 1, pp. 1–10, 2008.

[153] D. Sinnecker, A. Goedel, K. L. Laugwitz, and A. Moretti, "Induced pluripotent stem cell-derived cardiomyocytes: a versatile tool for arrhythmia research," *Circ Res*, vol. 112, no. 6, pp. 961–8, 2013.

[154] D. B. Resnik, "The commercialization of human stem cells: ethical and policy issues," *Health Care Anal*, vol. 10, no. 2, pp. 127–54, 2002.

[155] V. K. Singh, M. Kalsan, N. Kumar, A. Saini, and R. Chandra, "Induced pluripotent stem cells: applications in regenerative medicine, disease modeling, and drug discovery," *Front Cell Dev Biol*, vol. 3, p. 2, 2015.

[156] P. Hou, Y. Li, X. Zhang, C. Liu, J. Guan, H. Li, T. Zhao, J. Ye, W. Yang, K. Liu, J. Ge, J. Xu, Q. Zhang, Y. Zhao, and H. Deng, "Pluripotent stem cells induced from mouse somatic cells by small-molecule compounds," *Science*, vol. 341, no. 6146, pp. 651–4, 2013.

[157] Y. Shi, H. Inoue, J. C. Wu, and S. Yamanaka, "Induced pluripotent stem cell technology: a decade of progress," *Nat Rev Drug Discov*, vol. 16, no. 2, pp. 115–130, 2017.

[158] I. Karakikes, M. Ameen, V. Termglinchan, and J. C. Wu, "Human induced pluripotent stem cell-derived cardiomyocytes: insights into molecular, cellular, and functional phenotypes," *Circ Res*, vol. 117, no. 1, pp. 80–8, 2015.

[159] S. R. Braam, R. Passier, and C. L. Mummery, "Cardiomyocytes from human pluripotent stem cells in regenerative medicine and drug discovery," *Trends Pharmacol Sci*, vol. 30, no. 10, pp. 536–45, 2009.

[160] J. S. Leyton-Mange and D. J. Milan, "Pluripotent stem cells as a platform for cardiac arrhythmia drug screening," *Curr Treat Options Cardiovasc Med*, vol. 16, no. 9, p. 334, 2014.

[161] M. Grskovic, A. Javaherian, B. Strulovici, and G. Q. Daley, "Induced pluripotent stem cells–opportunities for disease modelling and drug discovery," *Nat Rev Drug Discov*, vol. 10, no. 12, pp. 915–29, 2011.

[162] S. Sharmin, A. Taguchi, Y. Kaku, Y. Yoshimura, T. Ohmori, T. Sakuma, M. Mukoyama, T. Yamamoto, H. Kurihara, and R. Nishinakamura, "Human induced pluripotent stem cellderived podocytes mature into vascularized glomeruli upon experimental transplantation," *Journal of the American Society of Nephrology*, p. ASN. 2015010096, 2015.

[163] T. Takebe, K. Sekine, M. Enomura, H. Koike, M. Kimura, T. Ogaeri, R. R. Zhang, Y. Ueno, Y. W. Zheng, N. Koike, S. Aoyama, Y. Adachi, and H. Taniguchi, "Vascularized and functional human liver from an ipsc-derived organ bud transplant," *Nature*, vol. 499, no. 7459, pp. 481–4, 2013.

[164] D. A. Robinton and G. Q. Daley, "The promise of induced pluripotent stem cells in research and therapy," *Nature*, vol. 481, no. 7381, pp. 295–305, 2012.

[165] D. Huangfu, R. Maehr, W. Guo, A. Eijkelenboom, M. Snitow, A. E. Chen, and D. A. Melton, "Induction of pluripotent stem cells by defined factors is greatly improved by small-molecule compounds," *Nat Biotechnol*, vol. 26, no. 7, pp. 795–7, 2008.

[166] T. Kondo, M. Asai, K. Tsukita, Y. Kutoku, Y. Ohsawa, Y. Sunada, K. Imamura, N. Egawa, N. Yahata, K. Okita, K. Takahashi, I. Asaka, T. Aoi, A. Watanabe, K. Watanabe, C. Kadoya, R. Nakano, D. Watanabe, K. Maruyama, O. Hori, S. Hibino, T. Choshi, T. Nakahata, H. Hioki, T. Kaneko, M. Naitoh, K. Yoshikawa, S. Yamawaki, S. Suzuki, R. Hata, S. Ueno, T. Seki, K. Kobayashi, T. Toda, K. Murakami, K. Irie, W. L. Klein, H. Mori, T. Asada, R. Takahashi, N. Iwata, S. Yamanaka, and H. Inoue, "Modeling alzheimer's disease with ipscs reveals stress phenotypes associated with intracellular abeta and differential drug responsiveness," *Cell Stem Cell*, vol. 12, no. 4, pp. 487–96, 2013.

[167] T. Yagi, D. Ito, Y. Okada, W. Akamatsu, Y. Nihei, T. Yoshizaki, S. Yamanaka, H. Okano, and N. Suzuki, "Modeling familial alzheimer's disease with induced pluripotent stem cells," *Hum Mol Genet*, vol. 20, no. 23, pp. 4530–9, 2011.

[168] M. A. Israel, S. H. Yuan, C. Bardy, S. M. Reyna, Y. Mu, C. Herrera, M. P. Hefferan, S. Van Gorp, K. L. Nazor, F. S. Boscolo, C. T. Carson, L. C. Laurent, M. Marsala, F. H. Gage, A. M. Remes, E. H. Koo, and L. S. Goldstein, "Probing sporadic and familial alzheimer's disease using induced pluripotent stem cells," *Nature*, vol. 482, no. 7384, pp. 216–20, 2012.

[169] G. Woodruff, J. E. Young, F. J. Martinez, F. Buen, A. Gore, J. Kinaga, Z. Li, S. H. Yuan, K. Zhang, and L. S. Goldstein, "The presenilin-1 deltae9 mutation results in reduced gamma-secretase activity, but not total loss of ps1 function, in isogenic human stem cells," *Cell Rep*, vol. 5, no. 4, pp. 974–85, 2013.

[170] J. Mertens, K. Stuber, P. Wunderlich, J. Ladewig, J. C. Kesavan, R. Vandenberghe, M. Vandenbulcke, P. van Damme, J. Walter, O. Brustle, and P. Koch, "App processing in human pluripotent stem cell-derived neurons is resistant to nsaid-based gamma-secretase modulation," *Stem Cell Reports*, vol. 1, no. 6, pp. 491–8, 2013.

[171] J. K. Lee, H. K. Jin, M. H. Park, B. R. Kim, P. H. Lee, H. Nakauchi, J. E. Carter, X. He, E. H. Schuchman, and J. S. Bae, "Acid sphingomyelinase modulates the autophagic process by controlling lysosomal biogenesis in alzheimer's disease," *J Exp Med*, vol. 211, no. 8, pp. 1551–70, 2014.

[172] L. Duan, B. J. Bhattacharyya, A. Belmadani, L. Pan, R. J. Miller, and J. A. Kessler, "Stem cell derived basal forebrain cholinergic neurons from alzheimer's disease patients are more susceptible to cell death," *Mol Neurodegener*, vol. 9, p. 3, 2014.

[173] C. R. Muratore, H. C. Rice, P. Srikanth, D. G. Callahan, T. Shin, L. N. Benjamin, D. M. Walsh, D. J. Selkoe, and T. L. Young-Pearse, "The familial alzheimer's disease appv717i mutation alters app processing and tau expression in ipsc-derived neurons," *Hum Mol Genet*, vol. 23, no. 13, pp. 3523–36, 2014.

[174] V. Mahairaki, J. Ryu, A. Peters, Q. Chang, T. Li, T. S. Park, P. W. Burridge, J. Talbot, C. C., L. Asnaghi, L. J. Martin, E. T. Zambidis, and V. E. Koliatsos, "Induced pluripotent stem cells from familial alzheimer's disease patients differentiate into mature neurons with amyloidogenic properties," *Stem Cells Dev*, vol. 23, no. 24, pp. 2996–3010, 2014.

[175] Q. Liu, S. Waltz, G. Woodruff, J. Ouyang, M. A. Israel, C. Herrera, F. Sarsoza, R. E. Tanzi, E. H. Koo, J. M. Ringman, L. S. Goldstein, S. L. Wagner, and S. H. Yuan, "Effect of potent gamma-secretase modulator in human neurons derived from multiple presenilin 1-induced pluripotent stem cell mutant carriers," *JAMA Neurol*, vol. 71, no. 12, pp. 1481–9, 2014.

[176] J. E. Young, J. Boulanger-Weill, D. A. Williams, G. Woodruff, F. Buen, A. C. Revilla, C. Herrera, M. A.

Israel, S. H. Yuan, S. D. Edland, and L. S. Goldstein, "Elucidating molecular phenotypes caused by the sorl1 alzheimer's disease genetic risk factor using human induced pluripotent stem cells," *Cell Stem Cell*, vol. 16, no. 4, pp. 373–85, 2015.

[177] A. M. Hossini, M. Megges, A. Prigione, B. Lichtner, M. R. Toliat, W. Wruck, F. Schroter, P. Nuernberg, H. Kroll, E. Makrantonaki, C. C. Zouboulis, and J. Adjaye, "Induced pluripotent stem cell-derived neuronal cells from a sporadic alzheimer's disease donor as a model for investigating ad-associated gene regulatory networks," *BMC Genomics*, vol. 16, p. 84, 2015.

[178] S. Moore, L. D. Evans, T. Andersson, E. Portelius, J. Smith, T. B. Dias, N. Saurat, A. McGlade, P. Kirwan, K. Blennow, J. Hardy, H. Zetterberg, and F. J. Livesey, "App metabolism regulates tau proteostasis in human cerebral cortex neurons," *Cell Rep*, vol. 11, no. 5, pp. 689–96, 2015.

[179] M. C. Liao, C. R. Muratore, T. M. Gierahn, S. E. Sullivan, P. Srikanth, P. L. De Jager, J. C. Love, and T. L. Young-Pearse, "Single-cell detection of secreted abeta and sappalpha from human ipsc-derived neurons and astrocytes," *J Neurosci*, vol. 36, no. 5, pp. 1730–46, 2016.

[180] M. Lin, E. Pedrosa, A. Shah, A. Hrabovsky, S. Maqbool, D. Zheng, and H. M. Lachman, "Rna-seq of human neurons derived from ips cells reveals candidate long non-coding rnas involved in neurogenesis and neuropsychiatric disorders," *PLoS One*, vol. 6, no. 9, p. e23356, 2011.

[181] K. J. Brennand, A. Simone, J. Jou, C. Gelboin-Burkhart, N. Tran, S. Sangar, Y. Li, Y. Mu, G. Chen, D. Yu, S. McCarthy, J. Sebat, and F. H. Gage, "Modelling schizophrenia using human induced pluripotent stem cells," *Nature*, vol. 473, no. 7346, pp. 221–5, 2011.

[182] Z. Wen, H. N. Nguyen, Z. Guo, M. A. Lalli, X. Wang, Y. Su, N. S. Kim, K. J. Yoon, J. Shin, C. Zhang, G. Makri, D. Nauen, H. Yu, E. Guzman, C. H. Chiang, N. Yoritomo, K. Kaibuchi, J. Zou, K. M. Christian, L. Cheng, C. A. Ross, R. L. Margolis, G. Chen, K. S. Kosik, H. Song, and G. L. Ming, "Synaptic dysregulation in a human ips cell model of mental disorders," *Nature*, vol. 515, no. 7527, pp. 414–8, 2014.

[183] H. N. Nguyen, B. Byers, B. Cord, A. Shcheglovitov, J. Byrne, P. Gujar, K. Kee, B. Schule, R. E. Dolmetsch, W. Langston, T. D. Palmer, and R. R. Pera, "Lrrk2 mutant ipsc-derived da neurons demonstrate increased susceptibility to oxidative stress," *Cell Stem Cell*, vol. 8, no. 3, pp. 267–80, 2011.

[184] O. Cooper, H. Seo, S. Andrabi, C. Guardia-Laguarta, J. Graziotto, M. Sundberg, J. R. McLean, L. Carrillo-Reid, Z. Xie, T. Osborn, G. Hargus, M. Deleidi, T. Lawson, H. Bogetofte, E. Perez-Torres, L. Clark, C. Moskowitz, J. Mazzulli, L. Chen, L. Volpicelli-Daley, N. Romero, H. Jiang, R. J. Uitti, Z. Huang, G. Opala, L. A. Scarffe, V. L. Dawson, C. Klein, J. Feng, O. A. Ross, J. Q. Trojanowski, V. M. Lee, K. Marder, D. J. Surmeier, Z. K. Wszolek, S. Przedborski, D. Krainc, T. M. Dawson, and O. Isacson, "Pharmacological rescue of mitochondrial deficits in ipsc-derived neural cells from patients with familial parkinson's disease," *Sci Transl Med*, vol. 4, no. 141, p. 141ra90, 2012.

[185] J. D. Miller, Y. M. Ganat, S. Kishinevsky, R. L. Bowman, B. Liu, E. Y. Tu, P. K. Mandal, E. Vera, J. W. Shim, S. Kriks, T. Taldone, N. Fusaki, M. J. Tomishima, D. Krainc, T. A. Milner, D. J. Rossi, and L. Studer, "Human ipsc-based modeling of late-onset disease via progerin-induced aging," *Cell Stem Cell*, vol. 13, no. 6, pp. 691–705, 2013.

[186] F. Soldner, Y. Stelzer, C. S. Shivalila, B. J. Abraham, J. C. Latourelle, M. I. Barrasa, J. Goldmann, R. H. Myers, R. A. Young, and R. Jaenisch, "Parkinson-associated risk variant in distal enhancer of alpha-synuclein modulates target gene expression," *Nature*, vol. 533, no. 7601, pp. 95–9, 2016.

[187] P. Seibler, J. Graziotto, H. Jeong, F. Simunovic, C. Klein, and D. Krainc, "Mitochondrial parkin recruitment is

impaired in neurons derived from mutant pink1 induced pluripotent stem cells," *J Neurosci*, vol. 31, no. 16, pp. 5970–6, 2011.

[188] M. J. Devine, M. Ryten, P. Vodicka, A. J. Thomson, T. Burdon, H. Houlden, F. Cavaleri, M. Nagano, N. J. Drummond, J. W. Taanman, A. H. Schapira, K. Gwinn, J. Hardy, P. A. Lewis, and T. Kunath, "Parkinson's disease induced pluripotent stem cells with triplication of the alpha-synuclein locus," *Nat Commun*, vol. 2, p. 440, 2011.

[189] Y. Imaizumi, Y. Okada, W. Akamatsu, M. Koike, N. Kuzumaki, H. Hayakawa, T. Nihira, T. Kobayashi, M. Ohyama, S. Sato, M. Takanashi, M. Funayama, A. Hirayama, T. Soga, T. Hishiki, M. Suematsu, T. Yagi, D. Ito, A. Kosakai, K. Hayashi, M. Shouji, A. Nakanishi, N. Suzuki, Y. Mizuno, N. Mizushima, M. Amagai, Y. Uchiyama, H. Mochizuki, N. Hattori, and H. Okano, "Mitochondrial dysfunction associated with increased oxidative stress and alpha-synuclein accumulation in park2 ipsc-derived neurons and postmortem brain tissue," *Mol Brain*, vol. 5, p. 35, 2012.

[190] H. Jiang, Y. Ren, E. Y. Yuen, P. Zhong, M. Ghaedi, Z. Hu, G. Azabdaftari, K. Nakaso, Z. Yan, and J. Feng, "Parkin controls dopamine utilization in human midbrain dopaminergic neurons derived from induced pluripotent stem cells," *Nat Commun*, vol. 3, p. 668, 2012.

[191] A. Sanchez-Danes, Y. Richaud-Patin, I. Carballo-Carbajal, S. Jimenez-Delgado, C. Caig, S. Mora, C. Di Guglielmo, M. Ezquerra, B. Patel, A. Giralt, J. M. Canals, M. Memo, J. Alberch, J. Lopez-Barneo, M. Vila, A. M. Cuervo, E. Tolosa, A. Consiglio, and A. Raya, "Disease-specific phenotypes in dopamine neurons from human ips-based models of genetic and sporadic parkinson's disease," *EMBO Mol Med*, vol. 4, no. 5, pp. 380–95, 2012.

[192] C. Y. Chung, V. Khurana, P. K. Auluck, D. F. Tardiff, J. R. Mazzulli, F. Soldner, V. Baru, Y. Lou, Y. Freyzon, S. Cho, A. E. Mungenast, J. Muffat, M. Mitalipova, M. D. Pluth, N. T. Jui, B. Schule, S. J. Lippard, L. H. Tsai, D. Krainc, S. L. Buchwald, R. Jaenisch, and S. Lindquist, "Identification and rescue of alpha-synuclein toxicity in parkinson patient-derived neurons," *Science*, vol. 342, no. 6161, pp. 983–7, 2013.

[193] P. Reinhardt, B. Schmid, L. F. Burbulla, D. C. Schondorf, L. Wagner, M. Glatza, S. Hoing, G. Hargus, S. A. Heck, A. Dhingra, G. Wu, S. Muller, K. Brockmann, T. Kluba, M. Maisel, R. Kruger, D. Berg, Y. Tsytsyura, C. S. Thiel, O. E. Psathaki, J. Klingauf, T. Kuhlmann, M. Klewin, H. Muller, T. Gasser, H. R. Scholer, and J. Sterneckert, "Genetic correction of a lrrk2 mutation in human ipscs links parkinsonian neurodegeneration to erk-dependent changes in gene expression," *Cell Stem Cell*, vol. 12, no. 3, pp. 354–67, 2013.

[194] S. D. Ryan, N. Dolatabadi, S. F. Chan, X. Zhang, M. W. Akhtar, J. Parker, F. Soldner, C. R. Sunico, S. Nagar, M. Talantova, B. Lee, K. Lopez, A. Nutter, B. Shan, E. Molokanova, Y. Zhang, X. Han, T. Nakamura, E. Masliah, r. Yates, J. R., N. Nakanishi, A. Y. Andreyev, S. Okamoto, R. Jaenisch, R. Ambasudhan, and S. A. Lipton, "Isogenic human ipsc parkinson's model shows nitrosative stress-induced dysfunction in mef2-pgc1alpha transcription," *Cell*, vol. 155, no. 6, pp. 1351–64, 2013.

[195] E. M. Hartfield, M. Yamasaki-Mann, H. J. Ribeiro Fernandes, J. Vowles, W. S. James, S. A. Cowley, and R. Wade-Martins, "Physiological characterisation of human ips-derived dopaminergic neurons," *PLoS One*, vol. 9, no. 2, p. e87388, 2014.

[196] D. C. Schondorf, M. Aureli, F. E. McAllister, C. J. Hindley, F. Mayer, B. Schmid, S. P. Sardi, M. Valsecchi, S. Hoffmann, L. K. Schwarz, U. Hedrich, D. Berg, L. S. Shihabuddin, J. Hu, J. Pruszak, S. P. Gygi, S. Sonnino, T. Gasser, and M. Deleidi, "ipsc-derived neurons from gba1-associated parkinson's disease patients show autophagic defects and

impaired calcium homeostasis," *Nat Commun*, vol. 5, p. 4028, 2014.

[197] U. Dettmer, A. J. Newman, F. Soldner, E. S. Luth, N. C. Kim, V. E. von Saucken, J. B. Sanderson, R. Jaenisch, T. Bartels, and D. Selkoe, "Parkinson-causing alpha-synuclein missense mutations shift native tetramers to monomers as a mechanism for disease initiation," *Nat Commun*, vol. 6, p. 7314, 2015.

[198] R. Fernandez-Santiago, I. Carballo-Carbajal, G. Castellano, R. Torrent, Y. Richaud, A. Sanchez-Danes, R. Vilarrasa-Blasi, A. Sanchez-Pla, J. L. Mosquera, J. Soriano, J. Lopez-Barneo, J. M. Canals, J. Alberch, A. Raya, M. Vila, A. Consiglio, J. I. Martin-Subero, M. Ezquerra, and E. Tolosa, "Aberrant epigenome in ipsc-derived dopaminergic neurons from parkinson's disease patients," *EMBO Mol Med*, vol. 7, no. 12, pp. 1529–46, 2015.

[199] Y. Ren, H. Jiang, Z. Hu, K. Fan, J. Wang, S. Janoschka, X. Wang, S. Ge, and J. Feng, "Parkin mutations reduce the complexity of neuronal processes in ipsc-derived human neurons," *Stem Cells*, vol. 33, no. 1, pp. 68–78, 2015.

[200] A. Shaltouki, R. Sivapatham, Y. Pei, A. A. Gerencser, O. Momcilovic, M. S. Rao, and X. Zeng, "Mitochondrial alterations by parkin in dopaminergic neurons using park2 patient-specific and park2 knockout isogenic ipsc lines," *Stem Cell Reports*, vol. 4, no. 5, pp. 847–59, 2015.

[201] E. Aflaki, D. K. Borger, N. Moaven, B. K. Stubblefield, S. A. Rogers, S. Patnaik, F. J. Schoenen, W. Westbroek, W. Zheng, P. Sullivan, H. Fujiwara, R. Sidhu, Z. M. Khaliq, G. J. Lopez, D. S. Goldstein, D. S. Ory, J. Marugan, and E. Sidransky, "A new glucocerebrosidase chaperone reduces alpha-synuclein and glycolipid levels in ipsc-derived dopaminergic neurons from patients with gaucher disease and parkinsonism," *J Neurosci*, vol. 36, no. 28, pp. 7441–52, 2016.

[202] M. Nagai, D. B. Re, T. Nagata, A. Chalazonitis, T. M. Jessell, H. Wichterle, and S. Przedborski, "Astrocytes expressing als-linked mutated sod1 release factors selectively toxic to motor neurons," *Nat Neurosci*, vol. 10, no. 5, pp. 615–22, 2007.

[203] F. P. Di Giorgio, M. A. Carrasco, M. C. Siao, T. Maniatis, and K. Eggan, "Non-cell autonomous effect of glia on motor neurons in an embryonic stem cell-based als model," *Nat Neurosci*, vol. 10, no. 5, pp. 608–14, 2007.

[204] M. C. Marchetto, A. R. Muotri, Y. Mu, A. M. Smith, G. G. Cezar, and F. H. Gage, "Non-cell-autonomous effect of human sod1 g37r astrocytes on motor neurons derived from human embryonic stem cells," *Cell Stem Cell*, vol. 3, no. 6, pp. 649–57, 2008.

[205] A. M. Haidet-Phillips, M. E. Hester, C. J. Miranda, K. Meyer, L. Braun, A. Frakes, S. Song, S. Likhite, M. J. Murtha, K. D. Foust, M. Rao, A. Eagle, A. Kammesheidt, A. Christensen, J. R. Mendell, A. H. Burghes, and B. K. Kaspar, "Astrocytes from familial and sporadic als patients are toxic to motor neurons," *Nat Biotechnol*, vol. 29, no. 9, pp. 824–8, 2011.

[206] A. D. Ebert, J. Yu, J. Rose, F. F., V. B. Mattis, C. L. Lorson, J. A. Thomson, and C. N. Svendsen, "Induced pluripotent stem cells from a spinal muscular atrophy patient," *Nature*, vol. 457, no. 7227, pp. 277–80, 2009.

[207] J. Mariani, G. Coppola, P. Zhang, A. Abyzov, L. Provini, L. Tomasini, M. Amenduni, A. Szekely, D. Palejev, M. Wilson, M. Gerstein, E. L. Grigorenko, K. Chawarska, K. A. Pelphrey, J. R. Howe, and F. M. Vaccarino, "Foxg1-dependent dysregulation of gaba/glutamate neuron differentiation in autism spectrum disorders," *Cell*, vol. 162, no. 2, pp. 375–390, 2015.

[208] J. Mertens, Q. W. Wang, Y. Kim, D. X. Yu, S. Pham, B. Yang, Y. Zheng, K. E. Diffenderfer, J. Zhang, S. Soltani, T. Eames, S. T. Schafer, L. Boyer, M. C. Marchetto, J. I. Nurnberger, J. R. Calabrese, K. J. Odegaard, M. J. McCarthy, P. P. Zandi, M. Alda, C. M.

Nievergelt, S. Pharmacogenomics of Bipolar Disorder, S. Mi, K. J. Brennand, J. R. Kelsoe, F. H. Gage, and J. Yao, "Differential responses to lithium in hyperexcitable neurons from patients with bipolar disorder," *Nature*, vol. 527, no. 7576, pp. 95–9, 2015.

[209] H. Inoue and S. Yamanaka, "The use of induced pluripotent stem cells in drug development," *Clin Pharmacol Ther*, vol. 89, no. 5, pp. 655–61, 2011.

[210] M. F. Burkhardt, F. J. Martinez, S. Wright, C. Ramos, D. Volfson, M. Mason, J. Garnes, V. Dang, J. Lievers, U. Shoukat-Mumtaz, R. Martinez, H. Gai, R. Blake, E. Vaisberg, M. Grskovic, C. Johnson, S. Irion, J. Bright, B. Cooper, L. Nguyen, I. Griswold-Prenner, and A. Javaherian, "A cellular model for sporadic als using patient-derived induced pluripotent stem cells," *Mol Cell Neurosci*, vol. 56, pp. 355–64, 2013.

[211] J. Lord, A. J. Lu, and C. Cruchaga, "Identification of rare variants in alzheimer's disease," *Front Genet*, vol. 5, p. 369, 2014.

[212] J. Bright, S. Hussain, V. Dang, S. Wright, B. Cooper, T. Byun, C. Ramos, A. Singh, G. Parry, N. Stagliano, and I. Griswold-Prenner, "Human secreted tau increases amyloid-beta production," *Neurobiol Aging*, vol. 36, no. 2, pp. 693–709, 2015.

[213] G. Lee, C. N. Ramirez, H. Kim, N. Zeltner, B. Liu, C. Radu, B. Bhinder, Y. J. Kim, I. Y. Choi, B. Mukherjee-Clavin, H. Djaballah, and L. Studer, "Large-scale screening using familial dysautonomia induced pluripotent stem cells identifies compounds that rescue ikbkap expression," *Nat Biotechnol*, vol. 30, no. 12, pp. 1244–8, 2012.

[214] X. Xu, Y. Lei, J. Luo, J. Wang, S. Zhang, X. J. Yang, M. Sun, E. Nuwaysir, G. Fan, J. Zhao, L. Lei, and Z. Zhong, "Prevention of beta-amyloid induced toxicity in human ips cell-derived neurons by inhibition of cyclin-dependent kinases and associated cell cycle events," *Stem Cell Res*, vol. 10, no. 2, pp. 213–27, 2013.

[215] S. Hoing, Y. Rudhard, P. Reinhardt, M. Glatza, M. Stehling, G. Wu, C. Peiker, A. Bocker, J. A. Parga, E. Bunk, J. C. Schwamborn, M. Slack, J. Sterneckert, and H. R. Scholer, "Discovery of inhibitors of microglial neurotoxicity acting through multiple mechanisms using a stem-cell-based phenotypic assay," *Cell Stem Cell*, vol. 11, no. 5, pp. 620–32, 2012.

[216] N. A. Naryshkin, M. Weetall, A. Dakka, J. Narasimhan, X. Zhao, Z. Feng, K. K. Ling, G. M. Karp, H. Qi, M. G. Woll, G. Chen, N. Zhang, V. Gabbeta, P. Vazirani, A. Bhattacharyya, B. Furia, N. Risher, J. Sheedy, R. Kong, J. Ma, A. Turpoff, C. S. Lee, X. Zhang, Y. C. Moon, P. Trifillis, E. M. Welch, J. M. Colacino, J. Babiak, N. G. Almstead, S. W. Peltz, L. A. Eng, K. S. Chen, J. L. Mull, M. S. Lynes, L. L. Rubin, P. Fontoura, L. Santarelli, D. Haehnke, K. D. McCarthy, R. Schmucki, M. Ebeling, M. Sivaramakrishnan, C. P. Ko, S. V. Paushkin, H. Ratni, I. Gerlach, A. Ghosh, and F. Metzger, "Motor neuron disease. smn2 splicing modifiers improve motor function and longevity in mice with spinal muscular atrophy," *Science*, vol. 345, no. 6197, pp. 688–93, 2014.

[217] A. Mullard, "Stem-cell discovery platforms yield first clinical candidates," *Nat Rev Drug Discov*, vol. 14, no. 9, pp. 589–91, 2015.

[218] E. A. Kimbrel and R. Lanza, "Current status of pluripotent stem cells: moving the first therapies to the clinic," *Nat Rev Drug Discov*, vol. 14, no. 10, pp. 681–92, 2015.

[219] J. Hanna, M. Wernig, S. Markoulaki, C. W. Sun, A. Meissner, J. P. Cassady, C. Beard, T. Brambrink, L. C. Wu, T. M. Townes, and R. Jaenisch, "Treatment of sickle cell anemia mouse model with ips cells generated from autologous skin," *Science*, vol. 318, no. 5858, pp. 1920–3, 2007.

[220] M. Wernig, J. P. Zhao, J. Pruszak, E. Hedlund, D. Fu, F. Soldner, V. Broccoli, M. Constantine-Paton, O. Isacson, and R. Jaenisch, "Neurons

derived from reprogrammed fibroblasts functionally integrate into the fetal brain and improve symptoms of rats with parkinson's disease," *Proc Natl Acad Sci U S A*, vol. 105, no. 15, pp. 5856–61, 2008.

[221] D. Xu, Z. Alipio, L. M. Fink, D. M. Adcock, J. Yang, D. C. Ward, and Y. Ma, "Phenotypic correction of murine hemophilia a using an ips cell-based therapy," *Proc Natl Acad Sci U S A*, vol. 106, no. 3, pp. 808–13, 2009.

[222] H. J. Chi, S. Gao, X. C. Yang, J. Cai, W. S. Zhao, H. Sun, and Y. J. Geng, "Clinical application of induced pluripotent stem cells in cardiovascular medicine," *Cardiology*, vol. 131, no. 4, pp. 236–44, 2015.

[223] C. Mauritz, A. Martens, S. V. Rojas, T. Schnick, C. Rathert, N. Schecker, S. Menke, S. Glage, R. Zweigerdt, A. Haverich, U. Martin, and I. Kutschka, "Induced pluripotent stem cell (ipsc)-derived flk-1 progenitor cells engraft, differentiate, and improve heart function in a mouse model of acute myocardial infarction," *Eur Heart J*, vol. 32, no. 21, pp. 2634–41, 2011.

[224] J. Dahlmann, G. Awad, C. Dolny, S. Weinert, K. Richter, K. D. Fischer, T. Munsch, V. Lessmann, M. Volleth, M. Zenker, Y. Chen, C. Merkl, A. Schnieke, H. Baraki, I. Kutschka, and G. Kensah, "Generation of functional cardiomyocytes from rat embryonic and induced pluripotent stem cells using feeder-free expansion and differentiation in suspension culture," *PLoS One*, vol. 13, no. 3, p. e0192652, 2018.

[225] X. Zhao, H. Chen, D. Xiao, H. Yang, I. Itzhaki, X. Qin, T. Chour, A. Aguirre, K. Lehmann, Y. Kim, P. Shukla, A. Holmstrom, J. Z. Zhang, Y. Zhuge, B. C. Ndoye, M. Zhao, E. Neofytou, W. H. Zimmermann, M. Jain, and J. C. Wu, "Comparison of non-human primate versus human induced pluripotent stem cell-derived cardiomyocytes for treatment of myocardial infarction," *Stem Cell Reports*, vol. 10, no. 2, pp. 422–435, 2018.

[226] Q. Zhang, J. Jiang, P. Han, Q. Yuan, J. Zhang, X. Zhang, Y. Xu, H. Cao, Q. Meng, L. Chen, T. Tian, X. Wang, P. Li, J. Hescheler, G. Ji, and Y. Ma, "Direct differentiation of atrial and ventricular myocytes from human embryonic stem cells by alternating retinoid signals," *Cell Res*, vol. 21, no. 4, pp. 579–87, 2011.

[227] R. Duelen and M. Sampaolesi, "Stem cell technology in cardiac regeneration: A pluripotent stem cell promise," *EBioMedicine*, vol. 16, pp. 30–40, 2017.

[228] T. J. Nelson, A. Martinez-Fernandez, S. Yamada, C. Perez-Terzic, Y. Ikeda, and A. Terzic, "Repair of acute myocardial infarction by human stemness factors induced pluripotent stem cells," *Circulation*, vol. 120, no. 5, pp. 408–16, 2009.

[229] L. Ye, Y. H. Chang, Q. Xiong, P. Zhang, L. Zhang, P. Somasundaram, M. Lepley, C. Swingen, L. Su, J. S. Wendel, J. Guo, A. Jang, D. Rosenbush, L. Greder, J. R. Dutton, J. Zhang, T. J. Kamp, D. S. Kaufman, Y. Ge, and J. Zhang, "Cardiac repair in a porcine model of acute myocardial infarction with human induced pluripotent stem cell-derived cardiovascular cells," *Cell Stem Cell*, vol. 15, no. 6, pp. 750–61, 2014.

[230] A. Chow, D. J. Stuckey, E. Kidher, M. Rocco, R. J. Jabbour, C. A. Mansfield, A. Darzi, S. E. Harding, M. M. Stevens, and T. Athanasiou, "Human induced pluripotent stem cell-derived cardiomyocyte encapsulating bioactive hydrogels improve rat heart function post myocardial infarction," *Stem Cell Reports*, vol. 9, no. 5, pp. 1415–1422, 2017.

[231] C. W. van den Berg, S. Okawa, S. M. Chuva de Sousa Lopes, L. van Iperen, R. Passier, S. R. Braam, L. G. Tertoolen, A. del Sol, R. P. Davis, and C. L. Mummery, "Transcriptome of human foetal heart compared with cardiomyocytes from pluripotent stem cells," *Development*, vol. 142, no. 18, pp. 3231–8, 2015.

[232] A. C. Fijnvandraat, A. C. van Ginneken, P. A. de Boer, J. M.

Ruijter, V. M. Christoffels, A. F. Moorman, and R. H. Lekanne Deprez, "Cardiomyocytes derived from embryonic stem cells resemble cardiomyocytes of the embryonic heart tube," *Cardiovasc Res*, vol. 58, no. 2, pp. 399–409, 2003.

[233] A. Novak, L. Barad, N. Zeevi-Levin, R. Shick, R. Shtrichman, A. Lorber, J. Itskovitz-Eldor, and O. Binah, "Cardiomyocytes generated from cpvtd307h patients are arrhythmogenic in response to beta-adrenergic stimulation," *J Cell Mol Med*, vol. 16, no. 3, pp. 468–82, 2012.

[234] C. Mummery, D. Ward-van Oostwaard, P. Doevendans, R. Spijker, S. van den Brink, R. Hassink, M. van der Heyden, T. Opthof, M. Pera, A. B. de la Riviere, R. Passier, and L. Tertoolen, "Differentiation of human embryonic stem cells to cardiomyocytes: role of coculture with visceral endoderm-like cells," *Circulation*, vol. 107, no. 21, pp. 2733–40, 2003.

[235] F. B. Bedada, M. Wheelwright, and J. M. Metzger, "Maturation status of sarcomere structure and function in human ipsc-derived cardiac myocytes," *Biochim Biophys Acta*, vol. 1863, no. 7 Pt B, pp. 1829–38, 2016.

[236] T. J. Kolanowski, C. L. Antos, and K. Guan, "Making human cardiomyocytes up to date: Derivation, maturation state and perspectives," *Int J Cardiol*, vol. 241, pp. 379–386, 2017.

[237] M. G. Vander Heiden, L. C. Cantley, and C. B. Thompson, "Understanding the warburg effect: the metabolic requirements of cell proliferation," *Science*, vol. 324, no. 5930, pp. 1029–33, 2009.

[238] S. Varum, A. S. Rodrigues, M. B. Moura, O. Momcilovic, C. A. t. Easley, J. Ramalho-Santos, B. Van Houten, and G. Schatten, "Energy metabolism in human pluripotent stem cells and their differentiated counterparts," *PLoS One*, vol. 6, no. 6, p. e20914, 2011.

[239] T. Schwarzer, Michael; Doenst, *The Scientists's Guide to Cardiac Metabolism*. Academic Press, 1st ed., 2016.

[240] R. J. Bing, A. Siegel, I. Ungar, and M. Gilbert, "Metabolism of the human heart.," *Am J Med.*, vol. 16, no. 4, pp. 504–15, 1954.

[241] S. Neubauer, "The failing heart–an engine out of fuel," *N Engl J Med*, vol. 356, no. 11, pp. 1140–51, 2007.

[242] J. R. Neely and H. E. Morgan, "Relationship between carbohydrate and lipid metabolism and the energy balance of heart muscle," *Annu Rev Physiol*, vol. 36, pp. 413–59, 1974.

[243] J. R. Neely, A. J. Liedtke, J. T. Whitmer, and M. J. Rovetto, "Relationship between coronary flow and adenosine triphosphate production from glycolysis and oxidative metabolism," *Recent Adv Stud Cardiac Struct Metab*, vol. 8, pp. 301–21, 1975.

[244] V. M. C. Madeira, "Overview of mitochondrial bioenergetics," *Methods Mol Biol*, vol. 1782, pp. 1–6, 2018.

[245] S. Jitrapakdee, M. E. Walker, and J. C. Wallace, "Identification of novel alternatively spliced pyruvate carboxylase mrnas with divergent 5'-untranslated regions which are expressed in a tissue-specific manner," *Biochem Biophys Res Commun*, vol. 223, no. 3, pp. 695–700, 1996.

[246] I. D. Wexler, Y. Du, M. V. Lisgaris, S. K. Mandal, S. O. Freytag, B. S. Yang, T. C. Liu, M. Kwon, M. S. Patel, and D. S. Kerr, "Primary amino acid sequence and structure of human pyruvate carboxylase," *Biochim Biophys Acta*, vol. 1227, no. 1-2, pp. 46–52, 1994.

[247] M. Weller, "http://www.handwrittentutorials.com," *webpage*, 2013.

[248] G. Lopaschuk, "The role of fatty acid oxidation in cardiac ischemia and reperfusion.," *Advanced Studies in Medicine*, vol. 4, pp. 1093–129, 2004.

[249] G. D. Lopaschuk, J. R. Ussher, C. D. Folmes, J. S. Jaswal, and W. C. Stanley, "Myocardial fatty acid

metabolism in health and disease," *Physiol Rev*, vol. 90, no. 1, pp. 207–58, 2010.

[250] W. C. Stanley, F. A. Recchia, and G. D. Lopaschuk, "Myocardial substrate metabolism in the normal and failing heart," *Physiol Rev*, vol. 85, no. 3, pp. 1093–129, 2005.

[251] J. G. Salway, *Metabolism at a glance*. Wiley-Blackwell, 4th edition ed., 2017.

[252] I. Darvey, "What factors are responsible for the greater yield of atp per carbon atom when fatty acids are completely oxidised to co2 and water compared with glucose?," *Biochemical Education*, no. 27, pp. 209–210, 1999.

[253] R. J. Bing, A. Siegel, I. Ungar, and M. Gilbert, "Metabolism of the human heart. ii. studies on fat, ketone and amino acid metabolism," *Am J Med*, vol. 16, no. 4, pp. 504–15, 1954.

[254] G. J. van der Vusse, J. F. Glatz, H. C. Stam, and R. S. Reneman, "Fatty acid homeostasis in the normoxic and ischemic heart," *Physiol Rev*, vol. 72, no. 4, pp. 881–940, 1992.

[255] H. L. Evans RD, *Metabolic pathways and abnormalities*. Surg., Elsevier Ltd, 2016.

[256] M. A. Cole, A. H. Abd Jamil, L. C. Heather, A. J. Murray, E. R. Sutton, M. Slingo, L. Sebag-Montefiore, S. C. Tan, D. Aksentijevic, O. S. Gildea, D. J. Stuckey, K. K. Yeoh, C. A. Carr, R. D. Evans, E. Aasum, C. J. Schofield, P. J. Ratcliffe, S. Neubauer, P. A. Robbins, and K. Clarke, "On the pivotal role of pparalpha in adaptation of the heart to hypoxia and why fat in the diet increases hypoxic injury," *FASEB J*, vol. 30, no. 8, pp. 2684–97, 2016.

[257] H. Taegtmeyer, M. E. Young, G. D. Lopaschuk, E. D. Abel, H. Brunengraber, V. Darley-Usmar, C. Des Rosiers, R. Gerszten, J. F. Glatz, J. L. Griffin, R. J. Gropler, H. G. Holzhuetter, J. R. Kizer, E. D. Lewandowski, C. R. Malloy, S. Neubauer, L. R. Peterson, M. A. Portman, F. A. Recchia, J. E. Van Eyk, T. J. Wang, and S. American Heart Association Council on Basic Cardiovascular, "Assessing cardiac metabolism: A scientific statement from the american heart association," *Circ Res*, vol. 118, no. 10, pp. 1659–701, 2016.

[258] J. W. Kim, I. Tchernyshyov, G. L. Semenza, and C. V. Dang, "Hif-1-mediated expression of pyruvate dehydrogenase kinase: a metabolic switch required for cellular adaptation to hypoxia," *Cell Metab*, vol. 3, no. 3, pp. 177–85, 2006.

[259] P. J. Randle, P. B. Garland, C. N. Hales, and E. A. Newsholme, "The glucose fatty-acid cycle. its role in insulin sensitivity and the metabolic disturbances of diabetes mellitus," *Lancet*, vol. 1, no. 7285, pp. 785–9, 1963.

[260] L. Hue and H. Taegtmeyer, "The randle cycle revisited: a new head for an old hat," *Am J Physiol Endocrinol Metab*, vol. 297, no. 3, pp. E578–91, 2009.

[261] G. D. Lopaschuk and J. S. Jaswal, "Energy metabolic phenotype of the cardiomyocyte during development, differentiation, and postnatal maturation," *J Cardiovasc Pharmacol*, vol. 56, no. 2, pp. 130–40, 2010.

[262] L. Lai, T. C. Leone, C. Zechner, P. J. Schaeffer, S. M. Kelly, D. P. Flanagan, D. M. Medeiros, A. Kovacs, and D. P. Kelly, "Transcriptional coactivators pgc-1alpha and pgc-lbeta control overlapping programs required for perinatal maturation of the heart," *Genes Dev*, vol. 22, no. 14, pp. 1948–61, 2008.

[263] J. Kolwicz, S. C., S. Purohit, and R. Tian, "Cardiac metabolism and its interactions with contraction, growth, and survival of cardiomyocytes," *Circ Res*, vol. 113, no. 5, pp. 603–16, 2013.

[264] G. D. Lopaschuk, R. L. Collins-Nakai, and T. Itoi, "Developmental changes in energy substrate use by the heart," *Cardiovasc Res*, vol. 26, no. 12, pp. 1172–80, 1992.

[265] F. C. Battaglia and G. Meschia, "Principal substrates of fetal metabolism," *Physiol Rev*, vol. 58, no. 2, pp. 499–527, 1978.

[266] R. A. Breckenridge, I. Piotrowska, K. E. Ng, T. J. Ragan, J. A. West, S. Kotecha, N. Towers, M. Bennett, P. C. Kienesberger, R. T. Smolenski, H. K. Siddall, J. L. Offer, M. M. Mocanu, D. M. Yelon, J. R. Dyck, J. L. Griffin, A. Y. Abramov, A. P. Gould, and T. J. Mohun, "Hypoxic regulation of hand1 controls the fetal-neonatal switch in cardiac metabolism," *PLoS Biol*, vol. 11, no. 9, p. e1001666, 2013.

[267] G. D. Lopaschuk, M. A. Spafford, and D. R. Marsh, "Glycolysis is predominant source of myocardial atp production immediately after birth," *Am J Physiol*, vol. 261, no. 6 Pt 2, pp. H1698–705, 1991.

[268] S. Malandraki-Miller, C. A. Lopez, H. Al-Siddiqi, and C. A. Carr, "Changing metabolism in differentiating cardiac progenitor cellscan stem cells become metabolically flexible cardiomyocytes?," *Frontiers in Cardiovascular Medicine*, vol. 5, no. 119, 2018.

[269] B. N. Puente, W. Kimura, S. A. Muralidhar, J. Moon, J. F. Amatruda, K. L. Phelps, D. Grinsfelder, B. A. Rothermel, R. Chen, J. A. Garcia, C. X. Santos, S. Thet, E. Mori, M. T. Kinter, P. M. Rindler, S. Zacchigna, S. Mukherjee, D. J. Chen, A. I. Mahmoud, M. Giacca, P. S. Rabinovitch, A. Aroumougame, A. M. Shah, L. I. Szweda, and H. A. Sadek, "The oxygen-rich postnatal environment induces cardiomyocyte cell-cycle arrest through dna damage response," *Cell*, vol. 157, no. 3, pp. 565–79, 2014.

[270] A. I. Mahmoud, F. Kocabas, S. A. Muralidhar, W. Kimura, A. S. Koura, S. Thet, E. R. Porrello, and H. A. Sadek, "Meis1 regulates postnatal cardiomyocyte cell cycle arrest," *Nature*, vol. 497, no. 7448, pp. 249–253, 2013.

[271] G. Attardi and G. Schatz, "Biogenesis of mitochondria," *Annu Rev Cell Biol*, vol. 4, pp. 289–333, 1988.

[272] F. Mayor and J. M. Cuezva, "Hormonal and metabolic changes in the perinatal period," *Biol Neonate*, vol. 48, no. 4, pp. 185–96, 1985.

[273] I. Menendez-Montes, B. Escobar, B. Palacios, M. J. Gomez, J. L. Izquierdo-Garcia, L. Flores, L. J. Jimenez-Borreguero, J. Aragones, J. Ruiz-Cabello, M. Torres, and S. Martin-Puig, "Myocardial vhl-hif signaling controls an embryonic metabolic switch essential for cardiac maturation," *Dev Cell*, vol. 39, no. 6, pp. 724–739, 2016.

[274] J. J. Lehman, P. M. Barger, A. Kovacs, J. E. Saffitz, D. M. Medeiros, and D. P. Kelly, "Peroxisome proliferator-activated receptor gamma coactivator-1 promotes cardiac mitochondrial biogenesis," *J Clin Invest*, vol. 106, no. 7, pp. 847–56, 2000.

[275] C. A. Virbasius, J. V. Virbasius, and R. C. Scarpulla, "Nrf-1, an activator involved in nuclear-mitochondrial interactions, utilizes a new dna-binding domain conserved in a family of developmental regulators," *Genes Dev*, vol. 7, no. 12A, pp. 2431–45, 1993.

[276] S. Chung, P. P. Dzeja, R. S. Faustino, C. Perez-Terzic, A. Behfar, and A. Terzic, "Mitochondrial oxidative metabolism is required for the cardiac differentiation of stem cells," *Nat Clin Pract Cardiovasc Med*, vol. 4 Suppl 1, pp. S60–7, 2007.

[277] N. G. Larsson, J. Wang, H. Wilhelmsson, A. Oldfors, P. Rustin, M. Lewandoski, G. S. Barsh, and D. A. Clayton, "Mitochondrial transcription factor a is necessary for mtdna maintenance and embryogenesis in mice," *Nat Genet*, vol. 18, no. 3, pp. 231–6, 1998.

[278] P. B. Bushdid, H. Osinska, R. R. Waclaw, J. D. Molkentin, and K. E. Yutzey, "Nfatc3 and nfatc4 are required for cardiac development and mitochondrial function," *Circ Res*, vol. 92, no. 12, pp. 1305–13, 2003.

[279] Z. Wu, P. Puigserver, U. Andersson, C. Zhang, G. Adelmant, V. Mootha, A. Troy, S. Cinti, B. Lowell, R. C. Scarpulla, and B. M. Spiegelman, "Mechanisms controlling mitochondrial biogenesis and respiration through the thermogenic coactivator pgc-1," *Cell*, vol. 98, no. 1, pp. 115–24, 1999.

[280] J. C. Yoon, P. Puigserver, G. Chen, J. Donovan, Z. Wu, J. Rhee, G. Adelmant, J. Stafford, C. R. Kahn, D. K. Granner, C. B. Newgard, and B. M. Spiegelman, "Control of hepatic gluconeogenesis through the transcriptional coactivator pgc-1," *Nature*, vol. 413, no. 6852, pp. 131–8, 2001.

[281] V. K. Mootha, C. Handschin, D. Arlow, X. Xie, J. St Pierre, S. Sihag, W. Yang, D. Altshuler, P. Puigserver, N. Patterson, P. J. Willy, I. G. Schulman, R. A. Heyman, E. S. Lander, and B. M. Spiegelman, "Erralpha and gabpa/b specify pgc-1alpha-dependent oxidative phosphorylation gene expression that is altered in diabetic muscle," *Proc Natl Acad Sci U S A*, vol. 101, no. 17, pp. 6570–5, 2004.

[282] J. M. Huss, I. P. Torra, B. Staels, V. Giguere, and D. P. Kelly, "Estrogen-related receptor alpha directs peroxisome proliferator-activated receptor alpha signaling in the transcriptional control of energy metabolism in cardiac and skeletal muscle," *Mol Cell Biol*, vol. 24, no. 20, pp. 9079–91, 2004.

[283] T. Wang, C. McDonald, N. B. Petrenko, M. Leblanc, T. Wang, V. Giguere, R. M. Evans, V. V. Patel, and L. Pei, "Estrogen-related receptor alpha (erralpha) and errgamma are essential coordinators of cardiac metabolism and function," *Mol Cell Biol*, vol. 35, no. 7, pp. 1281–98, 2015.

[284] W. A. Alaynick, R. P. Kondo, W. Xie, W. He, C. R. Dufour, M. Downes, J. W. Jonker, W. Giles, R. K. Naviaux, V. Giguere, and R. M. Evans, "Errgamma directs and maintains the transition to oxidative metabolism in the postnatal heart," *Cell Metab*, vol. 6, no. 1, pp. 13–24, 2007.

[285] S. H. Lee, P. L. Wolf, R. Escudero, R. Deutsch, S. W. Jamieson, and P. A. Thistlethwaite, "Early expression of angiogenesis factors in acute myocardial ischemia and infarction," *N Engl J Med*, vol. 342, no. 9, pp. 626–33, 2000.

[286] H. R. Cross, L. H. Opie, G. K. Radda, and K. Clarke, "Is a high glycogen content beneficial or detrimental to the ischemic rat heart? a controversy resolved," *Circ Res*, vol. 78, no. 3, pp. 482–91, 1996.

[287] G. L. Semenza, "Hypoxia-inducible factor 1 and cardiovascular disease," *Annu Rev Physiol*, vol. 76, pp. 39–56, 2014.

[288] L. C. Heather, C. A. Carr, D. J. Stuckey, S. Pope, K. J. Morten, E. E. Carter, L. M. Edwards, and K. Clarke, "Critical role of complex iii in the early metabolic changes following myocardial infarction," *Cardiovasc Res*, vol. 85, no. 1, pp. 127–36, 2010.

[289] M. S. Dodd, H. J. Atherton, C. A. Carr, D. J. Stuckey, J. A. West, J. L. Griffin, G. K. Radda, K. Clarke, L. C. Heather, and D. J. Tyler, "Impaired in vivo mitochondrial krebs cycle activity after myocardial infarction assessed using hyperpolarized magnetic resonance spectroscopy," *Circ Cardiovasc Imaging*, vol. 7, no. 6, pp. 895–904, 2014.

[290] V. G. Sharov, A. V. Todor, N. Silverman, S. Goldstein, and H. N. Sabbah, "Abnormal mitochondrial respiration in failed human myocardium," *J Mol Cell Cardiol*, vol. 32, no. 12, pp. 2361–7, 2000.

[291] G. Gong, J. Liu, P. Liang, T. Guo, Q. Hu, K. Ochiai, M. Hou, Y. Ye, X. Wu, A. Mansoor, A. H. From, K. Ugurbil, R. J. Bache, and J. Zhang, "Oxidative capacity in failing hearts," *Am J Physiol Heart Circ Physiol*, vol. 285, no. 2, pp. H541–8, 2003.

[292] J. Casademont and O. Miro, "Electron transport chain defects in heart failure," *Heart Fail Rev*, vol. 7, no. 2, pp. 131–9, 2002.

[293] A. F. Quigley, R. M. Kapsa, D. Esmore, G. Hale, and E. Byrne, "Mitochondrial respiratory chain activity in idiopathic dilated cardiomyopathy," *J Card Fail*, vol. 6, no. 1, pp. 47–55, 2000.

[294] J. Marin-Garcia, M. J. Goldenthal, and G. W. Moe, "Mitochondrial pathology in cardiac failure," *Cardiovasc Res*, vol. 49, no. 1, pp. 17–26, 2001.

[295] V. G. Sharov, A. Goussev, M. Lesch, S. Goldstein, and H. N. Sabbah, "Abnormal mitochondrial function in myocardium of dogs with chronic heart failure," *J Mol Cell Cardiol*, vol. 30, no. 9, pp. 1757–62, 1998.

[296] H. Taegtmeyer, S. Sen, and D. Vela, "Return to the fetal gene program: a suggested metabolic link to gene expression in the heart," *Ann N Y Acad Sci*, vol. 1188, pp. 191–8, 2010.

[297] H. S. Leong, M. Grist, H. Parsons, R. B. Wambolt, G. D. Lopaschuk, R. Brownsey, and M. F. Allard, "Accelerated rates of glycolysis in the hypertrophied heart: are they a methodological artifact?," *Am J Physiol Endocrinol Metab*, vol. 282, no. 5, pp. E1039–45, 2002.

[298] E. R. Kreipke, Y. Wang, J. W. Miklas, J. Mathieu, and H. Ruohola-Baker, "Metabolic remodeling in early development and cardiomyocyte maturation," *Semin Cell Dev Biol*, vol. 52, pp. 84–92, 2016.

[299] G. Fragasso, "Deranged cardiac metabolism and the pathogenesis of heart failure," *Card Fail Rev*, vol. 2, no. 1, pp. 8–13, 2016.

[300] V. Carubelli, A. I. Castrini, V. Lazzarini, M. Gheorghiade, M. Metra, and C. Lombardi, "Amino acids and derivatives, a new treatment of chronic heart failure?," *Heart Fail Rev*, vol. 20, no. 1, pp. 39–51, 2015.

[301] A. R. Wende, M. K. Brahma, G. R. McGinnis, and M. E. Young, "Metabolic origins of heart failure," *JACC Basic Transl Sci*, vol. 2, no. 3, pp. 297–310, 2017.

[302] L. Lai, T. C. Leone, M. P. Keller, O. J. Martin, A. T. Broman, J. Nigro, K. Kapoor, T. R. Koves, R. Stevens, O. R. Ilkayeva, R. B. Vega, A. D. Attie, D. M. Muoio, and D. P. Kelly, "Energy metabolic reprogramming in the hypertrophied and early stage failing heart: a multisystems approach," *Circ Heart Fail*, vol. 7, no. 6, pp. 1022–31, 2014.

[303] H. Sun, K. C. Olson, C. Gao, D. A. Prosdocimo, M. Zhou, Z. Wang, D. Jeyaraj, J. Y. Youn, S. Ren, Y. Liu, C. D. Rau, S. Shah, O. Ilkayeva, W. J. Gui, N. S. William, R. M. Wynn, C. B. Newgard, H. Cai, X. Xiao, D. T. Chuang, P. C. Schulze, C. Lynch, M. K. Jain, and Y. Wang, "Catabolic defect of branched-chain amino acids promotes heart failure," *Circulation*, vol. 133, no. 21, pp. 2038–49, 2016.

[304] W. Wang, F. Zhang, Y. Xia, S. Zhao, W. Yan, H. Wang, Y. Lee, C. Li, L. Zhang, K. Lian, E. Gao, H. Cheng, and L. Tao, "Defective branched chain amino acid catabolism contributes to cardiac dysfunction and remodeling following myocardial infarction," *Am J Physiol Heart Circ Physiol*, vol. 311, no. 5, pp. H1160–H1169, 2016.

[305] T. Li, Z. Zhang, J. Kolwicz, S. C., L. Abell, N. D. Roe, M. Kim, B. Zhou, Y. Cao, J. Ritterhoff, H. Gu, D. Raftery, H. Sun, and R. Tian, "Defective branched-chain amino acid catabolism disrupts glucose metabolism and sensitizes the heart to ischemia-reperfusion injury," *Cell Metab*, vol. 25, no. 2, pp. 374–385, 2017.

[306] A. K. Biala, R. Dhingra, and L. A. Kirshenbaum, "Mitochondrial dynamics: Orchestrating the journey to advanced age," *J Mol Cell Cardiol*, vol. 83, pp. 37–43, 2015.

[307] E. J. Lesnefsky, T. I. Gudz, S. Moghaddas, C. T. Migita, M. Ikeda-Saito, P. J. Turkaly, and C. L. Hoppel, "Aging decreases electron transport complex iii activity in heart interfibrillar mitochondria by alteration of the cytochrome c binding site," *J Mol Cell Cardiol*, vol. 33, no. 1, pp. 37–47, 2001.

[308] N. Shyh-Chang, G. Q. Daley, and L. C. Cantley, "Stem cell metabolism in tissue development and aging," *Development*, vol. 140, no. 12, pp. 2535–47, 2013.

[309] D. K. Gardner and A. J. Harvey, "Blastocyst metabolism," *Reprod Fertil Dev*, vol. 27, no. 4, pp. 638–54, 2015.

[310] H. Kondoh, M. E. Lleonart, Y. Nakashima, M. Yokode, M. Tanaka, D. Bernard, J. Gil, and D. Beach, "A high glycolytic flux supports the proliferative potential of murine

embryonic stem cells," *Antioxid Redox Signal*, vol. 9, no. 3, pp. 293–9, 2007.

[311] A. Moussaieff, M. Rouleau, D. Kitsberg, M. Cohen, G. Levy, D. Barasch, A. Nemirovski, S. Shen-Orr, I. Laevsky, M. Amit, D. Bomze, B. Elena-Herrmann, T. Scherf, M. Nissim-Rafinia, S. Kempa, J. Itskovitz-Eldor, E. Meshorer, D. Aberdam, and Y. Nahmias, "Glycolysis-mediated changes in acetyl-coa and histone acetylation control the early differentiation of embryonic stem cells," *Cell Metab*, vol. 21, no. 3, pp. 392–402, 2015.

[312] A. D. Panopoulos, O. Yanes, S. Ruiz, Y. S. Kida, D. Diep, R. Tautenhahn, A. Herrerias, E. M. Batchelder, N. Plongthongkum, M. Lutz, W. T. Berggren, K. Zhang, R. M. Evans, G. Siuzdak, and J. C. Izpisua Belmonte, "The metabolome of induced pluripotent stem cells reveals metabolic changes occurring in somatic cell reprogramming," *Cell Res*, vol. 22, no. 1, pp. 168–77, 2012.

[313] C. D. Folmes, T. J. Nelson, A. Martinez-Fernandez, D. K. Arrell, J. Z. Lindor, P. P. Dzeja, Y. Ikeda, C. Perez-Terzic, and A. Terzic, "Somatic oxidative bioenergetics transitions into pluripotency-dependent glycolysis to facilitate nuclear reprogramming," *Cell Metab*, vol. 14, no. 2, pp. 264–71, 2011.

[314] X. Xu, S. Duan, F. Yi, A. Ocampo, G. H. Liu, and J. C. Izpisua Belmonte, "Mitochondrial regulation in pluripotent stem cells," *Cell Metab*, vol. 18, no. 3, pp. 325–32, 2013.

[315] J. Prieto, M. Leon, X. Ponsoda, R. Sendra, R. Bort, R. Ferrer-Lorente, A. Raya, C. Lopez-Garcia, and J. Torres, "Early erk1/2 activation promotes drp1-dependent mitochondrial fission necessary for cell reprogramming," *Nat Commun*, vol. 7, p. 11124, 2016.

[316] Y. M. Cho, S. Kwon, Y. K. Pak, H. W. Seol, Y. M. Choi, D. J. Park, K. S. Park, and H. K. Lee, "Dynamic changes in mitochondrial biogenesis and antioxidant enzymes during the spontaneous differentiation of human embryonic stem cells," *Biochem Biophys Res Commun*, vol. 348, no. 4, pp. 1472–8, 2006.

[317] S. Inoue, S. Noda, K. Kashima, K. Nakada, J. Hayashi, and H. Miyoshi, "Mitochondrial respiration defects modulate differentiation but not proliferation of hematopoietic stem and progenitor cells," *FEBS Lett*, vol. 584, no. 15, pp. 3402–9, 2010.

[318] L. Li and T. Xie, "Stem cell niche: structure and function," *Annu Rev Cell Dev Biol*, vol. 21, pp. 605–31, 2005.

[319] O. Warburg, "On the origin of cancer cells," *Science*, vol. 123, no. 3191, pp. 309–14, 1956.

[320] T. Wang, C. Marquardt, and J. Foker, "Aerobic glycolysis during lymphocyte proliferation," *Nature*, vol. 261, no. 5562, pp. 702–5, 1976.

[321] C. J. Hedeskov, "Early effects of phytohaemagglutinin on glucose metabolism of normal human lymphocytes," *Biochem J*, vol. 110, no. 2, pp. 373–80, 1968.

[322] W. H. Munyon and D. J. Merchant, "The relation between glucose utilization, lactic acid production and utilization and the growth cycle of l strain fibroblasts," *Exp Cell Res*, vol. 17, no. 3, pp. 490–8, 1959.

[323] M. J. Bissell, C. Hatie, and H. Rubin, "Patterns of glucose metabolism in normal and virus-transformed chick cells in tissue culture," *J Natl Cancer Inst*, vol. 49, no. 2, pp. 555–65, 1972.

[324] M. Harris, *The Chemical Basis of Development*. Baltimore: Johns Hopkins University Press, 1958.

[325] S. Y. Lunt and M. G. Vander Heiden, "Aerobic glycolysis: meeting the metabolic requirements of cell proliferation," *Annu Rev Cell Dev Biol*, vol. 27, pp. 441–64, 2011.

[326] M. Board, C. Lopez, C. van den Bos, R. Callaghan, K. Clarke, and C. Carr, "Acetoacetate is a more efficient energy-yielding substrate for human mesenchymal stem cells than

glucose and generates fewer reactive oxygen species," *Int J Biochem Cell Biol*, vol. 88, pp. 75–83, 2017.

[327] F. Dos Santos, P. Z. Andrade, J. S. Boura, M. M. Abecasis, C. L. da Silva, and J. M. Cabral, "Ex vivo expansion of human mesenchymal stem cells: a more effective cell proliferation kinetics and metabolism under hypoxia," *J Cell Physiol*, vol. 223, no. 1, pp. 27–35, 2010.

[328] D. F. Dai, M. E. Danoviz, B. Wiczer, M. A. Laflamme, and R. Tian, "Mitochondrial maturation in human pluripotent stem cell derived cardiomyocytes," *Stem Cells Int*, vol. 2017, p. 5153625, 2017.

[329] M. J. Birket, S. Casini, G. Kosmidis, D. A. Elliott, A. A. Gerencser, A. Baartscheer, C. Schumacher, P. G. Mastroberardino, A. G. Elefanty, E. G. Stanley, and C. L. Mummery, "Pgc-1alpha and reactive oxygen species regulate human embryonic stem cell-derived cardiomyocyte function," *Stem Cell Reports*, vol. 1, no. 6, pp. 560–74, 2013.

[330] Z. Wang, Y. Yang, X. Xiang, Y. Zhu, J. Men, and M. He, "[estimation of the normal range of blood glucose in rats]," *Wei Sheng Yan Jiu*, vol. 39, no. 2, pp. 133–7, 142, 2010.

[331] L. M. Wolfensohn S, *Handbook of Laboratory Animal Management and Welfare.* lackwell Publishing Ltd, third ed., 2003.

[332] S. A. Abdelmagid, S. E. Clarke, D. E. Nielsen, A. Badawi, A. El-Sohemy, D. M. Mutch, and D. W. Ma, "Comprehensive profiling of plasma fatty acid concentrations in young healthy canadian adults," *PLoS One*, vol. 10, no. 2, p. e0116195, 2015.

[333] C. M. Kummitha, S. C. Kalhan, G. M. Saidel, and N. Lai, "Relating tissue/organ energy expenditure to metabolic fluxes in mouse and human: experimental data integrated with mathematical modeling," *Physiol Rep*, vol. 2, no. 9, 2014.

[334] T. El Bacha, M. Luz, and A. Da Poian, "Dynamic adaptation of nutrient utilization in humans.," *Nature Education*, vol. 3, no. 9, p. 8, 2010.

[335] S. L. Berg JM, Tymoczko JL, *Biochemistry. 5th edition.* Biochemistry, New York: W H Freeman, 5th edition ed., 2002.

[336] I. Kehat, L. Khimovich, O. Caspi, A. Gepstein, R. Shofti, G. Arbel, I. Huber, J. Satin, J. Itskovitz-Eldor, and L. Gepstein, "Electromechanical integration of cardiomyocytes derived from human embryonic stem cells," *Nat Biotechnol*, vol. 22, no. 10, pp. 1282–9, 2004.

[337] T. Xue, H. C. Cho, F. G. Akar, S. Y. Tsang, S. P. Jones, E. Marban, G. F. Tomaselli, and R. A. Li, "Functional integration of electrically active cardiac derivatives from genetically engineered human embryonic stem cells with quiescent recipient ventricular cardiomyocytes: insights into the development of cell-based pacemakers," *Circulation*, vol. 111, no. 1, pp. 11–20, 2005.

[338] Y. K. Lee, K. M. Ng, W. H. Lai, Y. C. Chan, Y. M. Lau, Q. Lian, H. F. Tse, and C. W. Siu, "Calcium homeostasis in human induced pluripotent stem cell-derived cardiomyocytes," *Stem Cell Rev*, vol. 7, no. 4, pp. 976–86, 2011.

[339] J. Satin, I. Itzhaki, S. Rapoport, E. A. Schroder, L. Izu, G. Arbel, R. Beyar, C. W. Balke, J. Schiller, and L. Gepstein, "Calcium handling in human embryonic stem cell-derived cardiomyocytes," *Stem Cells*, vol. 26, no. 8, pp. 1961–72, 2008.

[340] M. Brito-Martins, S. E. Harding, and N. N. Ali, "beta(1)- and beta(2)-adrenoceptor responses in cardiomyocytes derived from human embryonic stem cells: comparison with failing and non-failing adult human heart," *Br J Pharmacol*, vol. 153, no. 4, pp. 751–9, 2008.

[341] C. Kim, J. Wong, J. Wen, S. Wang, C. Wang, S. Spiering, N. G. Kan, S. Forcales, P. L. Puri, T. C. Leone, J. E. Marine, H. Calkins, D. P. Kelly, D. P. Judge, and H. S. Chen, "Studying arrhythmogenic right ventricular dysplasia with patient-specific ipscs," *Nature*, vol. 494, no. 7435, pp. 105–10, 2013.

[342] C. Denning, V. Borgdorff, J. Crutchley, K. S. Firth, V. George, S. Kalra, A. Kondrashov, M. D. Hoang, D. Mosqueira, A. Patel, L. Prodanov, D. Rajamohan, W. C. Skarnes, J. G. Smith, and L. E. Young, "Cardiomyocytes from human pluripotent stem cells: From laboratory curiosity to industrial biomedical platform," *Biochim Biophys Acta*, vol. 1863, no. 7 Pt B, pp. 1728–48, 2016.

[343] A. M. da Rocha, K. Campbell, S. Mironov, J. Jiang, L. Mundada, G. Guerrero-Serna, J. Jalife, and T. J. Herron, "hipsc-cm monolayer maturation state determines drug responsiveness in high throughput pro-arrhythmia screen," *Sci Rep*, vol. 7, no. 1, p. 13834, 2017.

[344] C. L. Collins, B. P. Bode, W. W. Souba, and S. F. Abcouwer, "Multiwell 14co2-capture assay for evaluation of substrate oxidation rates of cells in culture," *Biotechniques*, vol. 24, no. 5, pp. 803–8, 1998.

[345] R. L. Barr and G. D. Lopaschuk, "Direct measurement of energy metabolism in the isolated working rat heart," *J Pharmacol Toxicol Methods*, vol. 38, no. 1, pp. 11–7, 1997.

[346] D. D. Belke, T. S. Larsen, G. D. Lopaschuk, and D. L. Severson, "Glucose and fatty acid metabolism in the isolated working mouse heart," *Am J Physiol*, vol. 277, no. 4 Pt 2, pp. R1210–7, 1999.

[347] D. H. Jang, J. C. Greenwood, M. B. Spyres, and D. M. Eckmann, "Measurement of mitochondrial respiration and motility in acute care: Sepsis, trauma, and poisoning," *J Intensive Care Med*, vol. 32, no. 1, pp. 86–94, 2017.

[348] M. D. Brand and D. G. Nicholls, "Assessing mitochondrial dysfunction in cells," *Biochem J*, vol. 435, no. 2, pp. 297–312, 2011.

[349] L. C. Heather, M. A. Cole, J. J. Tan, L. J. Ambrose, S. Pope, A. H. Abd-Jamil, E. E. Carter, M. S. Dodd, K. K. Yeoh, C. J. Schofield, and K. Clarke, "Metabolic adaptation to chronic hypoxia in cardiac mitochondria," *Basic Res Cardiol*, vol. 107, no. 3, p. 268, 2012.

[350] S. C. Tan, R. S. Gomes, K. K. Yeoh, F. Perbellini, S. Malandraki-Miller, L. Ambrose, L. C. Heather, G. Faggian, C. J. Schofield, K. E. Davies, K. Clarke, and C. A. Carr, "Preconditioning of cardiosphere-derived cells with hypoxia or prolyl-4-hydroxylase inhibitors increases stemness and decreases reliance on oxidative metabolism," *Cell Transplant*, vol. 25, no. 1, pp. 35–53, 2016.

[351] S. J. Kattman, A. D. Witty, M. Gagliardi, N. C. Dubois, M. Niapour, A. Hotta, J. Ellis, and G. Keller, "Stage-specific optimization of activin/nodal and bmp signaling promotes cardiac differentiation of mouse and human pluripotent stem cell lines," *Cell Stem Cell*, vol. 8, no. 2, pp. 228–40, 2011.

[352] I. Kehat, D. Kenyagin-Karsenti, M. Snir, H. Segev, M. Amit, A. Gepstein, E. Livne, O. Binah, J. Itskovitz-Eldor, and L. Gepstein, "Human embryonic stem cells can differentiate into myocytes with structural and functional properties of cardiomyocytes," *J Clin Invest*, vol. 108, no. 3, pp. 407–14, 2001.

[353] X. Lian, J. Zhang, K. Zhu, T. J. Kamp, and S. P. Palecek, "Insulin inhibits cardiac mesoderm, not mesendoderm, formation during cardiac differentiation of human pluripotent stem cells and modulation of canonical wnt signaling can rescue this inhibition," *Stem Cells*, vol. 31, no. 3, pp. 447–57, 2013.

[354] X. Lian, J. Zhang, S. M. Azarin, K. Zhu, L. B. Hazeltine, X. Bao, C. Hsiao, T. J. Kamp, and S. P. Palecek, "Directed cardiomyocyte differentiation from human pluripotent stem cells by modulating wnt/beta-catenin signaling under fully defined conditions," *Nat Protoc*, vol. 8, no. 1, pp. 162–75, 2013.

[355] X. Lian, C. Hsiao, G. Wilson, K. Zhu, L. B. Hazeltine, S. M. Azarin, K. K. Raval, J. Zhang, T. J. Kamp, and S. P. Palecek, "Robust cardiomyocyte differentiation from human pluripotent

stem cells via temporal modulation of canonical wnt signaling," *Proc Natl Acad Sci U S A*, vol. 109, no. 27, pp. E1848–57, 2012.

[356] S. L. Paige, T. Osugi, O. K. Afanasiev, L. Pabon, H. Reinecke, and C. E. Murry, "Endogenous wnt/beta-catenin signaling is required for cardiac differentiation in human embryonic stem cells," *PLoS One*, vol. 5, no. 6, p. e11134, 2010.

[357] L. Yang, M. H. Soonpaa, E. D. Adler, T. K. Roepke, S. J. Kattman, M. Kennedy, E. Henckaerts, K. Bonham, G. W. Abbott, R. M. Linden, L. J. Field, and G. M. Keller, "Human cardiovascular progenitor cells develop from a kdr+ embryonic-stem-cell-derived population," *Nature*, vol. 453, no. 7194, pp. 524–8, 2008.

[358] C. Xu, S. Police, N. Rao, and M. K. Carpenter, "Characterization and enrichment of cardiomyocytes derived from human embryonic stem cells," *Circ Res*, vol. 91, no. 6, pp. 501–8, 2002.

[359] R. Passier, D. W. Oostwaard, J. Snapper, J. Kloots, R. J. Hassink, E. Kuijk, B. Roelen, A. B. de la Riviere, and C. Mummery, "Increased cardiomyocyte differentiation from human embryonic stem cells in serum-free cultures," *Stem Cells*, vol. 23, no. 6, pp. 772–80, 2005.

[360] R. Graichen, X. Xu, S. R. Braam, T. Balakrishnan, S. Norfiza, S. Sieh, S. Y. Soo, S. C. Tham, C. Mummery, A. Colman, R. Zweigerdt, and B. P. Davidson, "Enhanced cardiomyogenesis of human embryonic stem cells by a small molecular inhibitor of p38 mapk," *Differentiation*, vol. 76, no. 4, pp. 357–70, 2008.

[361] P. W. Burridge, E. Matsa, P. Shukla, Z. C. Lin, J. M. Churko, A. D. Ebert, F. Lan, S. Diecke, B. Huber, N. M. Mordwinkin, J. R. Plews, O. J. Abilez, B. Cui, J. D. Gold, and J. C. Wu, "Chemically defined generation of human cardiomyocytes," *Nat Methods*, vol. 11, no. 8, pp. 855–60, 2014.

[362] J. Zhang, G. F. Wilson, A. G. Soerens, C. H. Koonce, J. Yu, S. P. Palecek, J. A. Thomson, and T. J. Kamp, "Functional cardiomyocytes derived from human induced pluripotent stem cells," *Circ Res*, vol. 104, no. 4, pp. e30–41, 2009.

[363] C. Xu, S. Police, N. Rao, and M. K. Carpenter, "Characterization and enrichment of cardiomyocytes derived from human embryonic stem cells," *Circ Res*, vol. 91, no. 6, pp. 501–8, 2002.

[364] C. Freund, R. P. Davis, K. Gkatzis, D. Ward-van Oostwaard, and C. L. Mummery, "The first reported generation of human induced pluripotent stem cells (ips cells) and ips cell-derived cardiomyocytes in the netherlands," *Neth Heart J*, vol. 18, no. 1, pp. 51–4, 2010.

[365] J. Zhang, M. Klos, G. F. Wilson, A. M. Herman, X. Lian, K. K. Raval, M. R. Barron, L. Hou, A. G. Soerens, J. Yu, S. P. Palecek, G. E. Lyons, J. A. Thomson, T. J. Herron, J. Jalife, and T. J. Kamp, "Extracellular matrix promotes highly efficient cardiac differentiation of human pluripotent stem cells: the matrix sandwich method," *Circ Res*, vol. 111, no. 9, pp. 1125–36, 2012.

[366] N. Cao, H. Liang, J. Huang, J. Wang, Y. Chen, Z. Chen, and H. T. Yang, "Highly efficient induction and long-term maintenance of multipotent cardiovascular progenitors from human pluripotent stem cells under defined conditions," *Cell Res*, vol. 23, no. 9, pp. 1119–32, 2013.

[367] T. Simsek, F. Kocabas, J. Zheng, R. J. Deberardinis, A. I. Mahmoud, E. N. Olson, J. W. Schneider, C. C. Zhang, and H. A. Sadek, "The distinct metabolic profile of hematopoietic stem cells reflects their location in a hypoxic niche," *Cell Stem Cell*, vol. 7, no. 3, pp. 380–90, 2010.

[368] G. Pattappa, H. K. Heywood, J. D. de Bruijn, and D. A. Lee, "The metabolism of human mesenchymal stem cells during proliferation and differentiation," *J Cell Physiol*, vol. 226, no. 10, pp. 2562–70, 2011.

[369] J. Mathieu, Z. Zhang, A. Nelson, D. A. Lamba, T. A. Reh, C. Ware, and H. Ruohola-Baker, "Hypoxia induces re-entry of committed cells into pluripotency," *Stem Cells*, vol. 31, no. 9, pp. 1737–48, 2013.

[370] K. M. Ng, Y. K. Lee, Y. C. Chan, W. H. Lai, M. L. Fung, R. A. Li, C. W. Siu, and H. F. Tse, "Exogenous expression of hif-1 alpha promotes cardiac differentiation of embryonic stem cells," *J Mol Cell Cardiol*, vol. 48, no. 6, pp. 1129–37, 2010.

[371] T. L. Medley, M. Furtado, N. T. Lam, R. Idrizi, D. Williams, P. J. Verma, M. Costa, and D. M. Kaye, "Effect of oxygen on cardiac differentiation in mouse ips cells: role of hypoxia inducible factor-1 and wnt/beta-catenin signaling," *PLoS One*, vol. 8, no. 11, p. e80280, 2013.

[372] N. Gaber, M. Gagliardi, P. Patel, C. Kinnear, C. Zhang, D. Chitayat, P. Shannon, E. Jaeggi, U. Tabori, G. Keller, and S. Mital, "Fetal reprogramming and senescence in hypoplastic left heart syndrome and in human pluripotent stem cells during cardiac differentiation," *Am J Pathol*, vol. 183, no. 3, pp. 720–34, 2013.

[373] K. Fynes, R. Tostoes, L. Ruban, B. Weil, C. Mason, and F. S. Veraitch, "The differential effects of 2differentiation of mouse and human pluripotent stem cells," *Stem Cells Dev*, vol. 23, no. 16, pp. 1910–22, 2014.

[374] H. Sauer, G. Rahimi, J. Hescheler, and M. Wartenberg, "Role of reactive oxygen species and phosphatidylinositol 3-kinase in cardiomyocyte differentiation of embryonic stem cells," *FEBS Lett*, vol. 476, no. 3, pp. 218–23, 2000.

[375] J. Li, M. Stouffs, L. Serrander, B. Banfi, E. Bettiol, Y. Charnay, K. Steger, K. H. Krause, and M. E. Jaconi, "The nadph oxidase nox4 drives cardiac differentiation: Role in regulating cardiac transcription factors and map kinase activation," *Mol Biol Cell*, vol. 17, no. 9, pp. 3978–88, 2006.

[376] M. J. Birket, S. Casini, G. Kosmidis, D. A. Elliott, A. A. Gerencser, A. Baartscheer, C. Schumacher, P. G. Mastroberardino, A. G. Elefanty, E. G. Stanley, and C. L. Mummery, "Pgc-1alpha and reactive oxygen species regulate human embryonic stem cell-derived cardiomyocyte function," *Stem Cell Reports*, vol. 1, no. 6, pp. 560–74, 2013.

[377] F. L. Crespo, V. R. Sobrado, L. Gomez, A. M. Cervera, and K. J. McCreath, "Mitochondrial reactive oxygen species mediate cardiomyocyte formation from embryonic stem cells in high glucose," *Stem Cells*, vol. 28, no. 7, pp. 1132–42, 2010.

[378] S. D. Lundy, W. Z. Zhu, M. Regnier, and M. A. Laflamme, "Structural and functional maturation of cardiomyocytes derived from human pluripotent stem cells," *Stem Cells Dev*, vol. 22, no. 14, pp. 1991–2002, 2013.

[379] V. J. Bhute, X. Bao, K. K. Dunn, K. R. Knutson, E. C. McCurry, G. Jin, W. H. Lee, S. Lewis, A. Ikeda, and S. P. Palecek, "Metabolomics identifies metabolic markers of maturation in human pluripotent stem cell-derived cardiomyocytes," *Theranostics*, vol. 7, no. 7, pp. 2078–2091, 2017.

[380] Y. C. Chan, S. Ting, Y. K. Lee, K. M. Ng, J. Zhang, Z. Chen, C. W. Siu, S. K. Oh, and H. F. Tse, "Electrical stimulation promotes maturation of cardiomyocytes derived from human embryonic stem cells," *J Cardiovasc Transl Res*, vol. 6, no. 6, pp. 989–99, 2013.

[381] A. Mihic, J. Li, Y. Miyagi, M. Gagliardi, S. H. Li, J. Zu, R. D. Weisel, G. Keller, and R. K. Li, "The effect of cyclic stretch on maturation and 3d tissue formation of human embryonic stem cell-derived cardiomyocytes," *Biomaterials*, vol. 35, no. 9, pp. 2798–808, 2014.

[382] J. L. Ruan, N. L. Tulloch, M. V. Razumova, M. Saiget, V. Muskheli, L. Pabon, H. Reinecke, M. Regnier, and C. E. Murry, "Mechanical stress conditioning and electrical stimulation promote contractility and force maturation of induced pluripotent stem cell-derived human cardiac tissue," *Circulation*, vol. 134, no. 20, pp. 1557–1567, 2016.

[383] J. Liu, D. K. Lieu, C. W. Siu, J. D. Fu, H. F. Tse, and R. A. Li, "Facilitated maturation of ca2+ handling properties of human embryonic stem cell-derived cardiomyocytes by calsequestrin expression," *Am J Physiol Cell Physiol*, vol. 297, no. 1, pp. C152–9, 2009.

[384] D. K. Lieu, J. D. Fu, N. Chiamvimonvat, K. C. Tung, G. P. McNerney, T. Huser, G. Keller, C. W. Kong, and R. A. Li, "Mechanism-based facilitated maturation of human pluripotent stem cell-derived cardiomyocytes," *Circ Arrhythm Electrophysiol*, vol. 6, no. 1, pp. 191–201, 2013.

[385] L. B. Hazeltine, C. S. Simmons, M. R. Salick, X. Lian, M. G. Badur, W. Han, S. M. Delgado, T. Wakatsuki, W. C. Crone, B. L. Pruitt, and S. P. Palecek, "Effects of substrate mechanics on contractility of cardiomyocytes generated from human pluripotent stem cells," *Int J Cell Biol*, vol. 2012, p. 508294, 2012.

[386] X. Yang, M. Rodriguez, L. Pabon, K. A. Fischer, H. Reinecke, M. Regnier, N. J. Sniadecki, H. Ruohola-Baker, and C. E. Murry, "Tri-iodo-l-thyronine promotes the maturation of human cardiomyocytes-derived from induced pluripotent stem cells," *J Mol Cell Cardiol*, vol. 72, pp. 296–304, 2014.

[387] W. Zhang, C. W. Kong, M. H. Tong, W. H. Chooi, N. Huang, R. A. Li, and B. P. Chan, "Maturation of human embryonic stem cell-derived cardiomyocytes (hesc-cms) in 3d collagen matrix: Effects of niche cell supplementation and mechanical stimulation," *Acta Biomater*, vol. 49, pp. 204–217, 2017.

[388] N. Huebsch, P. Loskill, N. Deveshwar, C. I. Spencer, L. M. Judge, M. A. Mandegar, C. B. Fox, T. M. Mohamed, Z. Ma, A. Mathur, A. M. Sheehan, A. Truong, M. Saxton, J. Yoo, D. Srivastava, T. A. Desai, P. L. So, K. E. Healy, and B. R. Conklin, "Miniaturized ips-cell-derived cardiac muscles for physiologically relevant drug response analyses," *Sci Rep*, vol. 6, p. 24726, 2016.

[389] D. Zhang, I. Y. Shadrin, J. Lam, H. Q. Xian, H. R. Snodgrass, and N. Bursac, "Tissue-engineered cardiac patch for advanced functional maturation of human esc-derived cardiomyocytes," *Biomaterials*, vol. 34, no. 23, pp. 5813–20, 2013.

[390] B. M. Ulmer, A. Stoehr, M. L. Schulze, S. Patel, M. Gucek, I. Mannhardt, S. Funcke, E. Murphy, T. Eschenhagen, and A. Hansen, "Contractile work contributes to maturation of energy metabolism in hipsc-derived cardiomyocytes," *Stem Cell Reports*, vol. 10, no. 3, pp. 834–847, 2018.

[391] R. R. Besser, M. Ishahak, V. Mayo, D. Carbonero, I. Claure, and A. Agarwal, "Engineered microenvironments for maturation of stem cell derived cardiac myocytes," *Theranostics*, vol. 8, no. 1, pp. 124–140, 2018.

[392] A. Zorzano, M. Liesa, and M. Palacin, "Role of mitochondrial dynamics proteins in the pathophysiology of obesity and type 2 diabetes," *Int J Biochem Cell Biol*, vol. 41, no. 10, pp. 1846–54, 2009.

[393] J. Paltauf-Doburzynska, R. Malli, and W. F. Graier, "Hyperglycemic conditions affect shape and ca2+ homeostasis of mitochondria in endothelial cells," *J Cardiovasc Pharmacol*, vol. 44, no. 4, pp. 423–36, 2004.

[394] K. T. Kuppusamy, D. C. Jones, H. Sperber, A. Madan, K. A. Fischer, M. L. Rodriguez, L. Pabon, W. Z. Zhu, N. L. Tulloch, X. Yang, N. J. Sniadecki, M. A. Laflamme, W. L. Ruzzo, C. E. Murry, and H. Ruohola-Baker, "Let-7 family of microrna is required for maturation and adult-like metabolism in stem cell-derived cardiomyocytes," *Proc Natl Acad Sci U S A*, vol. 112, no. 21, pp. E2785–94, 2015.

[395] F. M. Drawnel, S. Boccardo, M. Prummer, F. Delobel, A. Graff, M. Weber, R. Gerard, L. Badi, T. Kam-Thong, L. Bu, X. Jiang, J. C. Hoflack, A. Kiialainen, E. Jeworutzki, N. Aoyama, C. Carlson, M. Burcin, G. Gromo, M. Boehringer, H. Stahlberg, B. J. Hall, M. C.

Magnone, K. Kolaja, K. R. Chien, J. Bailly, and R. Iacone, "Disease modeling and phenotypic drug screening for diabetic cardiomyopathy using human induced pluripotent stem cells," *Cell Rep*, vol. 9, no. 3, pp. 810–21, 2014.

[396] C. Correia, A. Koshkin, P. Duarte, D. Hu, A. Teixeira, I. Domian, M. Serra, and P. M. Alves, "Distinct carbon sources affect structural and functional maturation of cardiomyocytes derived from human pluripotent stem cells," *Sci Rep*, vol. 7, no. 1, p. 8590, 2017.

[397] R. J. Mills, D. M. Titmarsh, X. Koenig, B. L. Parker, J. G. Ryall, G. A. Quaife-Ryan, H. K. Voges, M. P. Hodson, C. Ferguson, L. Drowley, A. T. Plowright, E. J. Needham, Q. D. Wang, P. Gregorevic, M. Xin, W. G. Thomas, R. G. Parton, L. K. Nielsen, B. S. Launikonis, D. E. James, D. A. Elliott, E. R. Porrello, and J. E. Hudson, "Functional screening in human cardiac organoids reveals a metabolic mechanism for cardiomyocyte cell cycle arrest," *Proc Natl Acad Sci U S A*, vol. 114, no. 40, pp. E8372–E8381, 2017.

[398] P. Rana, B. Anson, S. Engle, and Y. Will, "Characterization of human-induced pluripotent stem cell-derived cardiomyocytes: bioenergetics and utilization in safety screening," *Toxicol Sci*, vol. 130, no. 1, pp. 117–31, 2012.

[399] J. Y. Wen, C. Y. Wei, K. Shah, J. Wong, C. Wang, and H. S. Chen, "Maturation-based model of arrhythmogenic right ventricular dysplasia using patient-specific induced pluripotent stem cells," *Circ J*, vol. 79, no. 7, pp. 1402–8, 2015.

[400] A. Moretti, M. Bellin, A. Welling, C. B. Jung, J. T. Lam, L. Bott-Flugel, T. Dorn, A. Goedel, C. Hohnke, F. Hofmann, M. Seyfarth, D. Sinnecker, A. Schomig, and K. L. Laugwitz, "Patient-specific induced pluripotent stem-cell models for long-qt syndrome," *N Engl J Med*, vol. 363, no. 15, pp. 1397–409, 2010.

[401] W. Bian, N. Badie, H. D. t. Himel, and N. Bursac, "Robust t-tubulation and maturation of cardiomyocytes using tissue-engineered epicardial mimetics," *Biomaterials*, vol. 35, no. 12, pp. 3819–28, 2014.

[402] T. Shimizu, M. Yamato, Y. Isoi, T. Akutsu, T. Setomaru, K. Abe, A. Kikuchi, M. Umezu, and T. Okano, "Fabrication of pulsatile cardiac tissue grafts using a novel 3-dimensional cell sheet manipulation technique and temperature-responsive cell culture surfaces," *Circ Res*, vol. 90, no. 3, p. e40, 2002.

[403] R. L. Carrier, M. Papadaki, M. Rupnick, F. J. Schoen, N. Bursac, R. Langer, L. E. Freed, and G. Vunjak-Novakovic, "Cardiac tissue engineering: cell seeding, cultivation parameters, and tissue construct characterization," *Biotechnol Bioeng*, vol. 64, no. 5, pp. 580–9, 1999.

[404] J. Leor, S. Aboulafia-Etzion, A. Dar, L. Shapiro, I. M. Barbash, A. Battler, Y. Granot, and S. Cohen, "Bioengineered cardiac grafts: A new approach to repair the infarcted myocardium?," *Circulation*, vol. 102, no. 19 Suppl 3, pp. III56–61, 2000.

[405] R. K. Li, Z. Q. Jia, R. D. Weisel, D. A. Mickle, A. Choi, and T. M. Yau, "Survival and function of bioengineered cardiac grafts," *Circulation*, vol. 100, no. 19 Suppl, pp. II63–9, 1999.

[406] N. Bursac, M. Papadaki, R. J. Cohen, F. J. Schoen, S. R. Eisenberg, R. Carrier, G. Vunjak-Novakovic, and L. E. Freed, "Cardiac muscle tissue engineering: toward an in vitro model for electrophysiological studies," *Am J Physiol*, vol. 277, no. 2 Pt 2, pp. H433–44, 1999.

[407] T. Kofidis, J. L. de Bruin, T. Yamane, M. Tanaka, D. R. Lebl, R. J. Swijnenburg, I. L. Weissman, and R. C. Robbins, "Stimulation of paracrine pathways with growth factors enhances embryonic stem cell engraftment and host-specific differentiation in the heart after ischemic myocardial injury," *Circulation*, vol. 111, no. 19, pp. 2486–93, 2005.

[408] M. J. van Luyn, R. A. Tio, X. J. Gallego y van Seijen, J. A. Plantinga,

L. F. de Leij, M. J. DeJongste, and P. B. van Wachem, "Cardiac tissue engineering: characteristics of in unison contracting two- and three-dimensional neonatal rat ventricle cell (co)-cultures," *Biomaterials*, vol. 23, no. 24, pp. 4793–801, 2002.

[409] W. H. Zimmermann, C. Fink, D. Kralisch, U. Remmers, J. Weil, and T. Eschenhagen, "Three-dimensional engineered heart tissue from neonatal rat cardiac myocytes," *Biotechnol Bioeng*, vol. 68, no. 1, pp. 106–14, 2000.

[410] T. Eschenhagen, C. Fink, U. Remmers, H. Scholz, J. Wattchow, J. Weil, W. Zimmermann, H. H. Dohmen, H. Schafer, N. Bishopric, T. Wakatsuki, and E. L. Elson, "Three-dimensional reconstitution of embryonic cardiomyocytes in a collagen matrix: a new heart muscle model system," *FASEB J*, vol. 11, no. 8, pp. 683–94, 1997.

[411] W. H. Zimmermann, K. Schneiderbanger, P. Schubert, M. Didie, F. Munzel, J. F. Heubach, S. Kostin, W. L. Neuhuber, and T. Eschenhagen, "Tissue engineering of a differentiated cardiac muscle construct," *Circ Res*, vol. 90, no. 2, pp. 223–30, 2002.

[412] Y. Miyahara, N. Nagaya, M. Kataoka, B. Yanagawa, K. Tanaka, H. Hao, K. Ishino, H. Ishida, T. Shimizu, K. Kangawa, S. Sano, T. Okano, S. Kitamura, and H. Mori, "Monolayered mesenchymal stem cells repair scarred myocardium after myocardial infarction," *Nat Med*, vol. 12, no. 4, pp. 459–65, 2006.

[413] Y. Sawa, S. Miyagawa, T. Sakaguchi, T. Fujita, A. Matsuyama, A. Saito, T. Shimizu, and T. Okano, "Tissue engineered myoblast sheets improved cardiac function sufficiently to discontinue lvas in a patient with dcm: report of a case," *Surg Today*, vol. 42, no. 2, pp. 181–4, 2012.

[414] H. C. Ott, T. S. Matthiesen, S. K. Goh, L. D. Black, S. M. Kren, T. I. Netoff, and D. A. Taylor, "Perfusion-decellularized matrix: using nature's platform to engineer a bioartificial heart," *Nat Med*, vol. 14, no. 2, pp. 213–21, 2008.

[415] W. Erdbrugger, W. Konertz, P. M. Dohmen, S. Posner, H. Ellerbrok, O. E. Brodde, H. Robenek, D. Modersohn, A. Pruss, S. Holinski, M. Stein-Konertz, and G. Pauli, "Decellularized xenogenic heart valves reveal remodeling and growth potential in vivo," *Tissue Eng*, vol. 12, no. 8, pp. 2059–68, 2006.

[416] Y. Duan, Z. Liu, J. O'Neill, L. Q. Wan, D. O. Freytes, and G. Vunjak-Novakovic, "Hybrid gel composed of native heart matrix and collagen induces cardiac differentiation of human embryonic stem cells without supplemental growth factors," *J Cardiovasc Transl Res*, vol. 4, no. 5, pp. 605–15, 2011.

[417] T. Y. Lu, B. Lin, J. Kim, M. Sullivan, K. Tobita, G. Salama, and L. Yang, "Repopulation of decellularized mouse heart with human induced pluripotent stem cell-derived cardiovascular progenitor cells," *Nat Commun*, vol. 4, p. 2307, 2013.

[418] M. J. Robertson, J. L. Dries-Devlin, S. M. Kren, J. S. Burchfield, and D. A. Taylor, "Optimizing recellularization of whole decellularized heart extracellular matrix," *PLoS One*, vol. 9, no. 2, p. e90406, 2014.

[419] H. Kitahara, H. Yagi, K. Tajima, K. Okamoto, A. Yoshitake, R. Aeba, M. Kudo, I. Kashima, S. Kawaguchi, A. Hirano, M. Kasai, Y. Akamatsu, H. Oka, Y. Kitagawa, and H. Shimizu, "Heterotopic transplantation of a decellularized and recellularized whole porcine heart," *Interact Cardiovasc Thorac Surg*, vol. 22, no. 5, pp. 571–9, 2016.

[420] D. T. Nguyen, M. O'Hara, C. Graneli, R. Hicks, T. Miliotis, A. C. Nystrom, S. Hansson, P. Davidsson, L. M. Gan, M. C. Magnone, M. Althage, and S. Heydarkhan-Hagvall, "Humanizing miniature hearts through 4-flow cannulation perfusion decellularization and recellularization," *Sci Rep*, vol. 8, no. 1, p. 7458, 2018.

[421] W. P. Daley, S. B. Peters, and M. Larsen, "Extracellular matrix dynamics in development and

regenerative medicine," *J Cell Sci*, vol. 121, no. Pt 3, pp. 255–64, 2008.

[422] A. Aszodi, K. R. Legate, I. Nakchbandi, and R. Fassler, "What mouse mutants teach us about extracellular matrix function," *Annu Rev Cell Dev Biol*, vol. 22, pp. 591–621, 2006.

[423] M. Radisic, H. Park, H. Shing, T. Consi, F. J. Schoen, R. Langer, L. E. Freed, and G. Vunjak-Novakovic, "Functional assembly of engineered myocardium by electrical stimulation of cardiac myocytes cultured on scaffolds," *Proc Natl Acad Sci U S A*, vol. 101, no. 52, pp. 18129–34, 2004.

[424] W. H. Zimmermann, I. Melnychenko, G. Wasmeier, M. Didie, H. Naito, U. Nixdorff, A. Hess, L. Budinsky, K. Brune, B. Michaelis, S. Dhein, A. Schwoerer, H. Ehmke, and T. Eschenhagen, "Engineered heart tissue grafts improve systolic and diastolic function in infarcted rat hearts," *Nat Med*, vol. 12, no. 4, pp. 452–8, 2006.

[425] Q. Chen, A. Bruyneel, K. Clarke, C. Carr, and J. Czernuszka, "Collagen-based scaffolds for potential application of heart valve tissue engineering," *Journal of Tissue Science and Engineering*, vol. 2013, 2013.

[426] A. Hansen, A. Eder, M. Bonstrup, M. Flato, M. Mewe, S. Schaaf, B. Aksehirlioglu, A. P. Schwoerer, J. Uebeler, and T. Eschenhagen, "Development of a drug screening platform based on engineered heart tissue," *Circ Res*, vol. 107, no. 1, pp. 35–44, 2010.

[427] K. L. Christman, A. J. Vardanian, Q. Fang, R. E. Sievers, H. H. Fok, and R. J. Lee, "Injectable fibrin scaffold improves cell transplant survival, reduces infarct expansion, and induces neovasculature formation in ischemic myocardium," *J Am Coll Cardiol*, vol. 44, no. 3, pp. 654–60, 2004.

[428] A. Khademhosseini, G. Eng, J. Yeh, P. A. Kucharczyk, R. Langer, G. Vunjak-Novakovic, and M. Radisic, "Microfluidic patterning for fabrication of contractile cardiac organoids," *Biomed Microdevices*, vol. 9, no. 2, pp. 149–57, 2007.

[429] Q. Chen, A. Bruyneel, C. Carr, and J. Czernuszka, "Bio-mechanical properties of novel bi-layer collagen-elastin scaffolds for heart valve tissue engineering," *Procedia Engineering*, vol. 59, pp. 247–254, 2013.

[430] Y. Wang, X. C. Liu, J. Zhao, X. R. Kong, R. F. Shi, X. B. Zhao, C. X. Song, T. J. Liu, and F. Lu, "Degradable plga scaffolds with basic fibroblast growth factor: experimental studies in myocardial revascularization," *Tex Heart Inst J*, vol. 36, no. 2, pp. 89–97, 2009.

[431] X. Zong, H. Bien, C. Y. Chung, L. Yin, D. Fang, B. S. Hsiao, B. Chu, and E. Entcheva, "Electrospun fine-textured scaffolds for heart tissue constructs," *Biomaterials*, vol. 26, no. 26, pp. 5330–8, 2005.

[432] J. Yu, A. R. Lee, W. H. Lin, C. W. Lin, Y. K. Wu, and W. B. Tsai, "Electrospun plga fibers incorporated with functionalized biomolecules for cardiac tissue engineering," *Tissue Eng Part A*, vol. 20, no. 13-14, pp. 1896–907, 2014.

[433] T. Ozawa, D. A. Mickle, R. D. Weisel, N. Koyama, S. Ozawa, and R. K. Li, "Optimal biomaterial for creation of autologous cardiac grafts," *Circulation*, vol. 106, no. 12 Suppl 1, pp. I176–82, 2002.

[434] N. Davidenko, T. Gibb, C. Schuster, S. M. Best, J. J. Campbell, C. J. Watson, and R. E. Cameron, "Biomimetic collagen scaffolds with anisotropic pore architecture," *Acta Biomater*, vol. 8, no. 2, pp. 667–76, 2012.

[435] E. Shin, S. Choi, D. Singh, S. Zo, Y. Lee, J. Kim, and S. Han, "Cellulose," *Mater.*, 2014.

[436] R. Gaetani, D. A. Feyen, V. Verhage, R. Slaats, E. Messina, K. L. Christman, A. Giacomello, P. A. Doevendans, and J. P. Sluijter, "Epicardial application of cardiac progenitor cells in a 3d-printed gelatin/hyaluronic acid patch preserves cardiac function after

myocardial infarction," *Biomaterials*, vol. 61, pp. 339–48, 2015.

[437] P. Joanne, M. Kitsara, S. E. Boitard, H. Naemetalla, V. Vanneaux, M. Pernot, J. Larghero, P. Forest, Y. Chen, P. Menasche, and O. Agbulut, "Nanofibrous clinical-grade collagen scaffolds seeded with human cardiomyocytes induces cardiac remodeling in dilated cardiomyopathy," *Biomaterials*, vol. 80, pp. 157–168, 2016.

[438] R. Hufenus, F. Reifler, K. Maniura-Weber, Spierings, and M. Zinn, "Macromol.," *Mater. Eng.*, 2012.

[439] A. Hasan, R. Waters, B. Roula, R. Dana, S. Yara, T. Alexandre, and A. Paul, "Engineered biomaterials to enhance stem cell-based cardiac tissue engineering and therapy," *Macromol Biosci*, vol. 16, no. 7, pp. 958–77, 2016.

[440] F. E. Herrmann, A. Lehner, T. Hollweck, U. Haas, C. Fano, D. Fehrenbach, R. Kozlik-Feldmann, E. Wintermantel, G. Eissner, C. Hagl, and B. Akra, "In vitro biological and mechanical evaluation of various scaffold materials for myocardial tissue engineering," *J Biomed Mater Res A*, vol. 102, no. 4, pp. 958–66, 2014.

[441] J. C. Ashworth, M. Mehr, P. G. Buxton, S. M. Best, and R. E. Cameron, "Cell invasion in collagen scaffold architectures, characterized by percolation theory," *Adv Healthc Mater*, vol. 4, no. 9, pp. 1317–21, 2015.

[442] I. Jun, H. S. Han, J. R. Edwards, and H. Jeon, "Electrospun fibrous scaffolds for tissue engineering: Viewpoints on architecture and fabrication," *Int J Mol Sci*, vol. 19, no. 3, 2018.

[443] J. Zhu and R. E. Marchant, "Design properties of hydrogel tissue-engineering scaffolds," *Expert Rev Med Devices*, vol. 8, no. 5, pp. 607–26, 2011.

[444] K. L. Fujimoto, Z. Ma, D. M. Nelson, R. Hashizume, J. Guan, K. Tobita, and W. R. Wagner, "Synthesis, characterization and therapeutic efficacy of a biodegradable, thermoresponsive hydrogel designed for application in chronic infarcted myocardium," *Biomaterials*, vol. 30, no. 26, pp. 4357–68, 2009.

[445] R. Lakshmanan, U. M. Krishnan, and S. Sethuraman, "Polymeric scaffold aided stem cell therapeutics for cardiac muscle repair and regeneration," *Macromol Biosci*, vol. 13, no. 9, pp. 1119–34, 2013.

[446] C. Fink, S. Ergun, D. Kralisch, U. Remmers, J. Weil, and T. Eschenhagen, "Chronic stretch of engineered heart tissue induces hypertrophy and functional improvement," *FASEB J*, vol. 14, no. 5, pp. 669–79, 2000.

[447] S. Schaaf, A. Shibamiya, M. Mewe, A. Eder, A. Stohr, M. N. Hirt, T. Rau, W. H. Zimmermann, L. Conradi, T. Eschenhagen, and A. Hansen, "Human engineered heart tissue as a versatile tool in basic research and preclinical toxicology," *PLoS One*, vol. 6, no. 10, p. e26397, 2011.

[448] F. Weinberger, K. Breckwoldt, S. Pecha, A. Kelly, B. Geertz, J. Starbatty, T. Yorgan, K. H. Cheng, K. Lessmann, T. Stolen, M. Scherrer-Crosbie, G. Smith, H. Reichenspurner, A. Hansen, and T. Eschenhagen, "Cardiac repair in guinea pigs with human engineered heart tissue from induced pluripotent stem cells," *Sci Transl Med*, vol. 8, no. 363, p. 363ra148, 2016.

[449] Y. Amano, A. Nishiguchi, M. Matsusaki, H. Iseoka, S. Miyagawa, Y. Sawa, M. Seo, T. Yamaguchi, and M. Akashi, "Development of vascularized ipsc derived 3d-cardiomyocyte tissues by filtration layer-by-layer technique and their application for pharmaceutical assays," *Acta Biomater*, vol. 33, pp. 110–21, 2016.

[450] M. Kawatou, H. Masumoto, H. Fukushima, G. Morinaga, R. Sakata, T. Ashihara, and J. K. Yamashita, "Modelling torsade de pointes arrhythmias in vitro in 3d human ips cell-engineered heart tissue," *Nat Commun*, vol. 8, no. 1, p. 1078, 2017.

[451] K. Breckwoldt, D. Letuffe-Breniere, I. Mannhardt, T. Schulze, B. Ulmer,

T. Werner, A. Benzin, B. Klampe, M. C. Reinsch, S. Laufer, A. Shibamiya, M. Prondzynski, G. Mearini, D. Schade, S. Fuchs, C. Neuber, E. Kramer, U. Saleem, M. L. Schulze, M. L. Rodriguez, T. Eschenhagen, and A. Hansen, "Differentiation of cardiomyocytes and generation of human engineered heart tissue," *Nat Protoc*, vol. 12, no. 6, pp. 1177–1197, 2017.

[452] K. J. Livak and T. D. Schmittgen, "Analysis of relative gene expression data using real-time quantitative pcr and the 2(-delta delta c(t)) method," *Methods*, vol. 25, no. 4, pp. 402–8, 2001.

[453] O. Gavet and J. Pines, "Progressive activation of cyclinb1-cdk1 coordinates entry to mitosis," *Dev Cell*, vol. 18, no. 4, pp. 533–43, 2010.

[454] R. L. Barr and G. D. Lopaschuk, "Methodology for measuring in vitro/ex vivo cardiac energy metabolism," *J Pharmacol Toxicol Methods*, vol. 43, no. 2, pp. 141–52, 2000.

[455] G. D. Lopaschuk and R. L. Barr, "Measurements of fatty acid and carbohydrate metabolism in the isolated working rat heart," *Mol Cell Biochem*, vol. 172, no. 1-2, pp. 137–47, 1997.

[456] T. TeSlaa and M. A. Teitell, "Techniques to monitor glycolysis," *Methods Enzymol*, vol. 542, pp. 91–114, 2014.

[457] N. B. Stottrup, B. Lofgren, R. D. Birkler, J. M. Nielsen, L. Wang, C. A. Caldarone, S. B. Kristiansen, H. Contractor, M. Johannsen, H. E. Botker, and T. T. Nielsen, "Inhibition of the malate-aspartate shuttle by pre-ischaemic aminooxyacetate loading of the heart induces cardioprotection," *Cardiovasc Res*, vol. 88, no. 2, pp. 257–66, 2010.

[458] J. Walborg, E. F. and R. S. Lantz, "Separation and quantitation of saccharides by ion-exchange chromatography utilizing boric acid-glycerol buffers," *Anal Biochem*, vol. 22, no. 1, pp. 123–33, 1968.

[459] R. H. Hammerstedt, "The use of dowex-1-borate to separate 3hoh from 2-3h-glucose," *Anal Biochem*, vol. 56, no. 1, pp. 292–3, 1973.

[460] C. E. Kight and S. E. Fleming, "Oxidation of glucose carbon entering the tca cycle is reduced by glutamine in small intestine epithelial cells," *Am J Physiol*, vol. 268, no. 6 Pt 1, pp. G879–88, 1995.

[461] J. M. Passmann, N. S. Radin, and J. A. Cooper, "Liquid scintillation technique for measuring carbon-14-dioxide activity," *Analytical Chemistry*, vol. 28, no. 4, pp. 484–486, 1956.

[462] B. Chance and G. R. Williams, "Respiratory enzymes in oxidative phosphorylation. iii. the steady state," *J Biol Chem*, vol. 217, no. 1, pp. 409–27, 1955.

[463] A. A. Gerencser, A. Neilson, S. W. Choi, U. Edman, N. Yadava, R. J. Oh, D. A. Ferrick, D. G. Nicholls, and M. D. Brand, "Quantitative microplate-based respirometry with correction for oxygen diffusion," *Anal Chem*, vol. 81, no. 16, pp. 6868–78, 2009.

[464] J. Zhang, E. Nuebel, D. R. Wisidagama, K. Setoguchi, J. S. Hong, C. M. Van Horn, S. S. Imam, L. Vergnes, C. S. Malone, C. M. Koehler, and M. A. Teitell, "Measuring energy metabolism in cultured cells, including human pluripotent stem cells and differentiated cells," *Nat Protoc*, vol. 7, no. 6, pp. 1068–85, 2012.

[465] B. G. Hill, B. P. Dranka, L. Zou, J. C. Chatham, and V. M. Darley-Usmar, "Importance of the bioenergetic reserve capacity in response to cardiomyocyte stress induced by 4-hydroxynonenal," *Biochem J*, vol. 424, no. 1, pp. 99–107, 2009.

[466] C. Y. Logan and R. Nusse, "The wnt signaling pathway in development and disease," *Annu Rev Cell Dev Biol*, vol. 20, pp. 781–810, 2004.

[467] T. Reya and H. Clevers, "Wnt signalling in stem cells and cancer," *Nature*, vol. 434, no. 7035, pp. 843–50, 2005.

[468] T. P. Yamaguchi, "Heads or tails: Wnts and anterior-posterior patterning," *Curr Biol*, vol. 11, no. 17, pp. R713–24, 2001.

[469] D. Kimelman, "Mesoderm induction: from caps to chips," *Nat Rev Genet*, vol. 7, no. 5, pp. 360–72, 2006.

[470] M. J. Marvin, G. Di Rocco, A. Gardiner, S. M. Bush, and A. B. Lassar, "Inhibition of wnt activity induces heart formation from posterior mesoderm," *Genes Dev*, vol. 15, no. 3, pp. 316–27, 2001.

[471] V. A. Schneider and M. Mercola, "Wnt antagonism initiates cardiogenesis in xenopus laevis," *Genes Dev*, vol. 15, no. 3, pp. 304–15, 2001.

[472] E. Tzahor and A. B. Lassar, "Wnt signals from the neural tube block ectopic cardiogenesis," *Genes Dev*, vol. 15, no. 3, pp. 255–60, 2001.

[473] X. Wu, K. Golden, and R. Bodmer, "Heart development in drosophila requires the segment polarity gene wingless," *Dev Biol*, vol. 169, no. 2, pp. 619–28, 1995.

[474] M. Park, X. Wu, K. Golden, J. D. Axelrod, and R. Bodmer, "The wingless signaling pathway is directly involved in drosophila heart development," *Dev Biol*, vol. 177, no. 1, pp. 104–16, 1996.

[475] A. T. Naito, H. Akazawa, H. Takano, T. Minamino, T. Nagai, H. Aburatani, and I. Komuro, "Phosphatidylinositol 3-kinase-akt pathway plays a critical role in early cardiomyogenesis by regulating canonical wnt signaling," *Circ Res*, vol. 97, no. 2, pp. 144–51, 2005.

[476] T. Nakamura, M. Sano, Z. Songyang, and M. D. Schneider, "A wnt- and beta -catenin-dependent pathway for mammalian cardiac myogenesis," *Proc Natl Acad Sci U S A*, vol. 100, no. 10, pp. 5834–9, 2003.

[477] A. T. Naito, I. Shiojima, H. Akazawa, K. Hidaka, T. Morisaki, A. Kikuchi, and I. Komuro, "Developmental stage-specific biphasic roles of wnt/beta-catenin signaling in cardiomyogenesis and hematopoiesis," *Proc Natl Acad Sci U S A*, vol. 103, no. 52, pp. 19812–7, 2006.

[478] C. Freund, D. Ward-van Oostwaard, J. Monshouwer-Kloots, S. van den Brink, M. van Rooijen, X. Xu, R. Zweigerdt, C. Mummery, and R. Passier, "Insulin redirects differentiation from cardiogenic mesoderm and endoderm to neuroectoderm in differentiating human embryonic stem cells," *Stem Cells*, vol. 26, no. 3, pp. 724–33, 2008.

[479] X. Q. Xu, R. Graichen, S. Y. Soo, T. Balakrishnan, S. N. Rahmat, S. Sieh, S. C. Tham, C. Freund, J. Moore, C. Mummery, A. Colman, R. Zweigerdt, and B. P. Davidson, "Chemically defined medium supporting cardiomyocyte differentiation of human embryonic stem cells," *Differentiation*, vol. 76, no. 9, pp. 958–70, 2008.

[480] S. Gessert and M. Kuhl, "The multiple phases and faces of wnt signaling during cardiac differentiation and development," *Circ Res*, vol. 107, no. 2, pp. 186–99, 2010.

[481] D. Quiat, K. A. Voelker, J. Pei, N. V. Grishin, R. W. Grange, R. Bassel-Duby, and E. N. Olson, "Concerted regulation of myofiber-specific gene expression and muscle performance by the transcriptional repressor sox6," *Proc Natl Acad Sci U S A*, vol. 108, no. 25, pp. 10196–201, 2011.

[482] S. Schiaffino and C. Reggiani, "Molecular diversity of myofibrillar proteins: gene regulation and functional significance," *Physiol Rev*, vol. 76, no. 2, pp. 371–423, 1996.

[483] M. Yeager, "Structure of cardiac gap junction intercellular channels," *J Struct Biol*, vol. 121, no. 2, pp. 231–45, 1998.

[484] H. M. van der Velden and H. J. Jongsma, "Cardiac gap junctions and connexins: their role in atrial fibrillation and potential as therapeutic targets," *Cardiovasc Res*, vol. 54, no. 2, pp. 270–9, 2002.

[485] J. C. Cheng, H. M. Chang, L. Fang, Y. P. Sun, and P. C. Leung, "Tgf-beta1 up-regulates connexin43 expression:

a potential mechanism for human trophoblast cell differentiation," *J Cell Physiol*, vol. 230, no. 7, pp. 1558–66, 2015.

[486] M. Oyamada, K. Takebe, A. Endo, S. Hara, and Y. Oyamada, "Connexin expression and gap-junctional intercellular communication in es cells and ips cells," *Front Pharmacol*, vol. 4, p. 85, 2013.

[487] L. A. Boyer, T. I. Lee, M. F. Cole, S. E. Johnstone, S. S. Levine, J. P. Zucker, M. G. Guenther, R. M. Kumar, H. L. Murray, R. G. Jenner, D. K. Gifford, D. A. Melton, R. Jaenisch, and R. A. Young, "Core transcriptional regulatory circuitry in human embryonic stem cells," *Cell*, vol. 122, no. 6, pp. 947–56, 2005.

[488] M. J. Bround, R. Wambolt, D. S. Luciani, J. E. Kulpa, B. Rodrigues, R. W. Brownsey, M. F. Allard, and J. D. Johnson, "Cardiomyocyte atp production, metabolic flexibility, and survival require calcium flux through cardiac ryanodine receptors in vivo," *J Biol Chem*, vol. 288, no. 26, pp. 18975–86, 2013.

[489] D. F. McKillop and M. A. Geeves, "Regulation of the interaction between actin and myosin subfragment 1: evidence for three states of the thin filament," *Biophys J*, vol. 65, no. 2, pp. 693–701, 1993.

[490] T. Harigaya, S. Sakai, and K. Kohmoto, "Induction of mammary prolactin receptors and lactose synthesis after ovariectomy in the pregnant mouse," *Endocrinol Jpn*, vol. 25, no. 2, pp. 157–61, 1978.

[491] A. M. Katz, *Physiology of the Heart*. Lippincott Williams and Wilkins., 4th edition ed., 2005.

[492] A. L. Olson and J. E. Pessin, "Structure, function, and regulation of the mammalian facilitative glucose transporter gene family," *Annu Rev Nutr*, vol. 16, pp. 235–56, 1996.

[493] C. Depre, J. L. Vanoverschelde, and H. Taegtmeyer, "Glucose for the heart," *Circulation*, vol. 99, no. 4, pp. 578–88, 1999.

[494] A. Onay-Besikci, "Regulation of cardiac energy metabolism in newborn," *Mol Cell Biochem*, vol. 287, no. 1-2, pp. 1–11, 2006.

[495] L. H. Young, D. L. Coven, and r. Russell, R. R., "Cellular and molecular regulation of cardiac glucose transport," *J Nucl Cardiol*, vol. 7, no. 3, pp. 267–76, 2000.

[496] T. Doenst, T. D. Nguyen, and E. D. Abel, "Cardiac metabolism in heart failure: implications beyond atp production," *Circ Res*, vol. 113, no. 6, pp. 709–24, 2013.

[497] M. A. Giorgi, R. Bolanos, C. D. Gonzalez, and G. Di Girolamo, "Qt interval prolongation: preclinical and clinical testing arrhythmogenesis in drugs and regulatory implications," *Curr Drug Saf*, vol. 5, no. 1, pp. 54–7, 2010.

[498] M. Rakhshandehroo, B. Knoch, M. Muller, and S. Kersten, "Peroxisome proliferator-activated receptor alpha target genes," *PPAR Res*, vol. 2010, 2010.

[499] Y. C. Long, Z. Cheng, K. D. Copps, and M. F. White, "Insulin receptor substrates irs1 and irs2 coordinate skeletal muscle growth and metabolism via the akt and ampk pathways," *Mol Cell Biol*, vol. 31, no. 3, pp. 430–41, 2011.

[500] M. F. White and C. R. Kahn, "The insulin signaling system," *J Biol Chem*, vol. 269, no. 1, pp. 1–4, 1994.

[501] X. J. Sun, L. M. Wang, Y. Zhang, L. Yenush, J. Myers, M. G., E. Glasheen, W. S. Lane, J. H. Pierce, and M. F. White, "Role of irs-2 in insulin and cytokine signalling," *Nature*, vol. 377, no. 6545, pp. 173–7, 1995.

[502] L. Yenush and M. F. White, "The irs-signalling system during insulin and cytokine action," *Bioessays*, vol. 19, no. 6, pp. 491–500, 1997.

[503] Y. Qi, Z. Xu, Q. Zhu, C. Thomas, R. Kumar, H. Feng, D. E. Dostal, M. F. White, K. M. Baker, and S. Guo, "Myocardial loss of irs1 and irs2 causes heart failure and is controlled by p38alpha mapk during

insulin resistance," *Diabetes*, vol. 62, no. 11, pp. 3887–900, 2013.

[504] Y. M. Taylor PM, Cass AEG, "Extracellular matrix scaffolds for tissue engineering heart valves.," *Prog Pediatr Cardiol*, no. 21, pp. 219–225, 2006.

[505] S. Ueno, G. Weidinger, T. Osugi, A. D. Kohn, J. L. Golob, L. Pabon, H. Reinecke, R. T. Moon, and C. E. Murry, "Biphasic role for wnt/beta-catenin signaling in cardiac specification in zebrafish and embryonic stem cells," *Proc Natl Acad Sci U S A*, vol. 104, no. 23, pp. 9685–90, 2007.

[506] A. F. Bayomy, M. Bauer, Y. Qiu, and R. Liao, "Regeneration in heart disease-is ecm the key?," *Life Sci*, vol. 91, no. 17-18, pp. 823–7, 2012.

[507] R. Csepregi, B. Lemli, S. Kunsagi-Mate, L. Szente, T. Koszegi, B. Nemeti, and M. Poor, "Complex formation of resorufin and resazurin with beta-cyclodextrins: Can cyclodextrins interfere with a resazurin cell viability assay?," *Molecules*, vol. 23, no. 2, 2018.

[508] C. F. Bentzinger, Y. X. Wang, J. von Maltzahn, V. D. Soleimani, H. Yin, and M. A. Rudnicki, "Fibronectin regulates wnt7a signaling and satellite cell expansion," *Cell Stem Cell*, vol. 12, no. 1, pp. 75–87, 2013.

[509] P. Cheng, P. Andersen, D. Hassel, B. L. Kaynak, P. Limphong, L. Juergensen, C. Kwon, and D. Srivastava, "Fibronectin mediates mesendodermal cell fate decisions," *Development*, vol. 140, no. 12, pp. 2587–96, 2013.

[510] S. Sa, L. Wong, and K. E. McCloskey, "Combinatorial fibronectin and laminin signaling promote highly efficient cardiac differentiation of human embryonic stem cells," *Biores Open Access*, vol. 3, no. 4, pp. 150–61, 2014.

[511] K. H. Narsinh, N. Sun, V. Sanchez-Freire, A. S. Lee, P. Almeida, S. Hu, T. Jan, K. D. Wilson, D. Leong, J. Rosenberg, M. Yao, R. C. Robbins, and J. C. Wu, "Single cell transcriptional profiling reveals heterogeneity of human induced pluripotent stem cells," *J Clin Invest*, vol. 121, no. 3, pp. 1217–21, 2011.

[512] C. Y. Ivashchenko, G. C. Pipes, I. M. Lozinskaya, Z. Lin, X. Xiaoping, S. Needle, E. T. Grygielko, E. Hu, J. R. Toomey, J. J. Lepore, and R. N. Willette, "Human-induced pluripotent stem cell-derived cardiomyocytes exhibit temporal changes in phenotype," *Am J Physiol Heart Circ Physiol*, vol. 305, no. 6, pp. H913–22, 2013.

[513] I. Piccini, J. Rao, G. Seebohm, and B. Greber, "Human pluripotent stem cell-derived cardiomyocytes: Genome-wide expression profiling of long-term in vitro maturation in comparison to human heart tissue," *Genom Data*, vol. 4, pp. 69–72, 2015.

[514] C. B. Jung, A. Moretti, M. Mederos y Schnitzler, L. Iop, U. Storch, M. Bellin, T. Dorn, S. Ruppenthal, S. Pfeiffer, A. Goedel, R. J. Dirschinger, M. Seyfarth, J. T. Lam, D. Sinnecker, T. Gudermann, P. Lipp, and K. L. Laugwitz, "Dantrolene rescues arrhythmogenic ryr2 defect in a patient-specific stem cell model of catecholaminergic polymorphic ventricular tachycardia," *EMBO Mol Med*, vol. 4, no. 3, pp. 180–91, 2012.

[515] K. K. Linask and J. W. Lash, "A role for fibronectin in the migration of avian precardiac cells. i. dose-dependent effects of fibronectin antibody," *Dev Biol*, vol. 129, no. 2, pp. 315–23, 1988.

[516] K. P. Hanson, J. P. Jung, Q. A. Tran, S. P. Hsu, R. Iida, V. Ajeti, P. J. Campagnola, K. W. Eliceiri, J. M. Squirrell, G. E. Lyons, and B. M. Ogle, "Spatial and temporal analysis of extracellular matrix proteins in the developing murine heart: a blueprint for regeneration," *Tissue Eng Part A*, vol. 19, no. 9-10, pp. 1132–43, 2013.

[517] H. Yang, T. K. Borg, H. Liu, and B. Z. Gao, "Interactive relationship between basement-membrane development and sarcomerogenesis in single cardiomyocytes," *Exp Cell Res*, vol. 330, no. 1, pp. 222–32, 2015.

[518] A. H. Fong, M. Romero-Lopez, C. M. Heylman, M. Keating, D. Tran, A. Sobrino, A. Q. Tran, H. H. Pham, C. Fimbres, P. D. Gershon, E. L. Botvinick, S. C. George, and C. C. Hughes, "Three-dimensional adult cardiac extracellular matrix promotes maturation of human induced pluripotent stem cell-derived cardiomyocytes," *Tissue Eng Part A*, vol. 22, no. 15-16, pp. 1016–25, 2016.

[519] B. L. Farrugia, M. S. Lord, J. M. Whitelock, and J. Melrose, "Harnessing chondroitin sulphate in composite scaffolds to direct progenitor and stem cell function for tissue repair," *Biomater Sci*, vol. 6, no. 5, pp. 947–957, 2018.

[520] F. Saporito, G. Sandri, C. M. Bonferoni, S. Rossi, L. Malavasi, C. Del Fante, B. Vigani, L. Black, and F. Ferrari, "Electrospun gelatinchondroitin sulfate scaffolds loaded with platelet lysate promote immature cardiomyocyte proliferation," *Polymers*, vol. 10, no. 2, p. 208, 2018.

[521] S. D. Bird, P. A. Doevendans, M. A. van Rooijen, A. Brutel de la Riviere, R. J. Hassink, R. Passier, and C. L. Mummery, "The human adult cardiomyocyte phenotype," *Cardiovasc Res*, vol. 58, no. 2, pp. 423–34, 2003.

[522] W. Z. Zhu, Y. Xie, K. W. Moyes, J. D. Gold, B. Askari, and M. A. Laflamme, "Neuregulin/erbb signaling regulates cardiac subtype specification in differentiating human embryonic stem cells," *Circ Res*, vol. 107, no. 6, pp. 776–86, 2010.

[523] E. Drouin, F. Charpentier, C. Gauthier, K. Laurent, and H. Le Marec, "Electrophysiologic characteristics of cells spanning the left ventricular wall of human heart: evidence for presence of m cells," *J Am Coll Cardiol*, vol. 26, no. 1, pp. 185–92, 1995.

[524] S. Kadota, I. Minami, N. Morone, J. E. Heuser, K. Agladze, and N. Nakatsuji, "Development of a reentrant arrhythmia model in human pluripotent stem cell-derived cardiac cell sheets," *Eur Heart J*, vol. 34, no. 15, pp. 1147–56, 2013.

[525] F. Pillekamp, M. Haustein, M. Khalil, M. Emmelheinz, R. Nazzal, R. Adelmann, F. Nguemo, O. Rubenchyk, K. Pfannkuche, M. Matzkies, M. Reppel, W. Bloch, K. Brockmeier, and J. Hescheler, "Contractile properties of early human embryonic stem cell-derived cardiomyocytes: beta-adrenergic stimulation induces positive chronotropy and lusitropy but not inotropy," *Stem Cells Dev*, vol. 21, no. 12, pp. 2111–21, 2012.

[526] E. J. Smart and X. A. Li, "Hyperglycemia: cell death in a cave," *Biochim Biophys Acta*, vol. 1772, no. 5, pp. 524–6, 2007.

[527] X. F. Deng, D. G. Rokosh, and P. C. Simpson, "Autonomous and growth factor-induced hypertrophy in cultured neonatal mouse cardiac myocytes. comparison with rat," *Circ Res*, vol. 87, no. 9, pp. 781–8, 2000.

[528] H. Ito, M. Hiroe, Y. Hirata, M. Tsujino, S. Adachi, M. Shichiri, A. Koike, A. Nogami, and F. Marumo, "Insulin-like growth factor-i induces hypertrophy with enhanced expression of muscle specific genes in cultured rat cardiomyocytes," *Circulation*, vol. 87, no. 5, pp. 1715–21, 1993.

[529] C. Montessuit, T. Palma, C. Viglino, C. Pellieux, and R. Lerch, "Effects of insulin-like growth factor-i on the maturation of metabolism in neonatal rat cardiomyocytes," *Pflugers Arch*, vol. 452, no. 4, pp. 380–6, 2006.

[530] J. D. Fu, S. N. Rushing, D. K. Lieu, C. W. Chan, C. W. Kong, L. Geng, K. D. Wilson, N. Chiamvimonvat, K. R. Boheler, J. C. Wu, G. Keller, R. J. Hajjar, and R. A. Li, "Distinct roles of microrna-1 and -499 in ventricular specification and functional maturation of human embryonic stem cell-derived cardiomyocytes," *PLoS One*, vol. 6, no. 11, p. e27417, 2011.

[531] T. E. Callis, K. Pandya, H. Y. Seok, R. H. Tang, M. Tatsuguchi, Z. P. Huang, J. F. Chen, Z. Deng, B. Gunn, J. Shumate, M. S. Willis, C. H. Selzman, and D. Z. Wang, "Microrna-208a is a regulator of cardiac hypertrophy and conduction in mice," *J Clin Invest*, vol. 119, no. 9, pp. 2772–86, 2009.

[532] E. van Rooij, L. B. Sutherland, X. Qi, J. A. Richardson, J. Hill, and E. N. Olson, "Control of stress-dependent cardiac growth and gene expression by a microrna," *Science*, vol. 316, no. 5824, pp. 575–9, 2007.

[533] S. Mandard, M. Muller, and S. Kersten, "Peroxisome proliferator-activated receptor alpha target genes," *Cell Mol Life Sci*, vol. 61, no. 4, pp. 393–416, 2004.

[534] O. Braissant, F. Foufelle, C. Scotto, M. Dauca, and W. Wahli, "Differential expression of peroxisome proliferator-activated receptors (ppars): tissue distribution of ppar-alpha, -beta, and -gamma in the adult rat," *Endocrinology*, vol. 137, no. 1, pp. 354–66, 1996.

[535] P. Escher, O. Braissant, S. Basu-Modak, L. Michalik, W. Wahli, and B. Desvergne, "Rat ppars: quantitative analysis in adult rat tissues and regulation in fasting and refeeding," *Endocrinology*, vol. 142, no. 10, pp. 4195–202, 2001.

[536] D. Auboeuf, J. Rieusset, L. Fajas, P. Vallier, V. Frering, J. P. Riou, B. Staels, J. Auwerx, M. Laville, and H. Vidal, "Tissue distribution and quantification of the expression of mrnas of peroxisome proliferator-activated receptors and liver x receptor-alpha in humans: no alteration in adipose tissue of obese and niddm patients," *Diabetes*, vol. 46, no. 8, pp. 1319–27, 1997.

[537] O. Braissant and W. Wahli, "Differential expression of peroxisome proliferator-activated receptor-alpha, -beta, and -gamma during rat embryonic development," *Endocrinology*, vol. 139, no. 6, pp. 2748–54, 1998.

[538] M. Loviscach, N. Rehman, L. Carter, S. Mudaliar, P. Mohadeen, T. P. Ciaraldi, J. H. Veerkamp, and R. R. Henry, "Distribution of peroxisome proliferator-activated receptors (ppars) in human skeletal muscle and adipose tissue: relation to insulin action," *Diabetologia*, vol. 43, no. 3, pp. 304–11, 2000.

[539] P. Ferre, "The biology of peroxisome proliferator-activated receptors: relationship with lipid metabolism and insulin sensitivity," *Diabetes*, vol. 53 Suppl 1, pp. S43–50, 2004.

[540] K. Schoonjans, B. Staels, and J. Auwerx, "Role of the peroxisome proliferator-activated receptor (ppar) in mediating the effects of fibrates and fatty acids on gene expression," *J Lipid Res*, vol. 37, no. 5, pp. 907–25, 1996.

[541] B. P. Kota, T. H. Huang, and B. D. Roufogalis, "An overview on biological mechanisms of ppars," *Pharmacol Res*, vol. 51, no. 2, pp. 85–94, 2005.

[542] J. P. Berger, T. E. Akiyama, and P. T. Meinke, "Ppars: therapeutic targets for metabolic disease," *Trends Pharmacol Sci*, vol. 26, no. 5, pp. 244–51, 2005.

[543] D. Bishop-Bailey, "Peroxisome proliferator-activated receptors in the cardiovascular system," *Br J Pharmacol*, vol. 129, no. 5, pp. 823–34, 2000.

[544] L. Michalik, B. Desvergne, C. Dreyer, M. Gavillet, R. N. Laurini, and W. Wahli, "Ppar expression and function during vertebrate development," *Int J Dev Biol*, vol. 46, no. 1, pp. 105–14, 2002.

[545] B. Grygiel-Gorniak, "Peroxisome proliferator-activated receptors and their ligands: nutritional and clinical implications–a review," *Nutr J*, vol. 13, p. 17, 2014.

[546] R. Bordet, T. Ouk, O. Petrault, P. Gele, S. Gautier, M. Laprais, D. Deplanque, P. Duriez, B. Staels, J. C. Fruchart, and M. Bastide, "Ppar: a new pharmacological target for neuroprotection in stroke and neurodegenerative diseases," *Biochem Soc Trans*, vol. 34, no. Pt 6, pp. 1341–6, 2006.

[547] S. Kersten, B. Desvergne, and W. Wahli, "Roles of ppars in health and disease," *Nature*, vol. 405, no. 6785, pp. 421–4, 2000.

[548] J. M. Thorp and W. S. Waring, "Modification of metabolism and

distribution of lipids by ethyl chlorophenoxyisobutyrate," *Nature*, vol. 194, pp. 948–9, 1962.

[549] T. M. Willson, P. J. Brown, D. D. Sternbach, and B. R. Henke, "The ppars: from orphan receptors to drug discovery," *J Med Chem*, vol. 43, no. 4, pp. 527–50, 2000.

[550] J. Berger and D. E. Moller, "The mechanisms of action of ppars," *Annu Rev Med*, vol. 53, pp. 409–35, 2002.

[551] J. C. Fruchart, P. Duriez, and B. Staels, "[molecular mechanism of action of the fibrates]," *J Soc Biol*, vol. 193, no. 1, pp. 67–75, 1999.

[552] S. A. Kliewer, S. S. Sundseth, S. A. Jones, P. J. Brown, G. B. Wisely, C. S. Koble, P. Devchand, W. Wahli, T. M. Willson, J. M. Lenhard, and J. M. Lehmann, "Fatty acids and eicosanoids regulate gene expression through direct interactions with peroxisome proliferator-activated receptors alpha and gamma," *Proc Natl Acad Sci U S A*, vol. 94, no. 9, pp. 4318–23, 1997.

[553] H. E. Xu, M. H. Lambert, V. G. Montana, D. J. Parks, S. G. Blanchard, P. J. Brown, D. D. Sternbach, J. M. Lehmann, G. B. Wisely, T. M. Willson, S. A. Kliewer, and M. V. Milburn, "Molecular recognition of fatty acids by peroxisome proliferator-activated receptors," *Mol Cell*, vol. 3, no. 3, pp. 397–403, 1999.

[554] W. S. Lee and J. Kim, "Peroxisome proliferator-activated receptors and the heart: Lessons from the past and future directions," *PPAR Res*, vol. 2015, p. 271983, 2015.

[555] G. Krey, O. Braissant, F. L'Horset, E. Kalkhoven, M. Perroud, M. G. Parker, and W. Wahli, "Fatty acids, eicosanoids, and hypolipidemic agents identified as ligands of peroxisome proliferator-activated receptors by coactivator-dependent receptor ligand assay," *Mol Endocrinol*, vol. 11, no. 6, pp. 779–91, 1997.

[556] B. M. Forman, J. Chen, and R. M. Evans, "Hypolipidemic drugs, polyunsaturated fatty acids, and eicosanoids are ligands for peroxisome proliferator-activated receptors alpha and delta," *Proc Natl Acad Sci U S A*, vol. 94, no. 9, pp. 4312–7, 1997.

[557] S. Kersten, "Integrated physiology and systems biology of pparalpha," *Mol Metab*, vol. 3, no. 4, pp. 354–71, 2014.

[558] R. M. Kaikaus, N. M. Bass, and R. K. Ockner, "Functions of fatty acid binding proteins," *Experientia*, vol. 46, no. 6, pp. 617–30, 1990.

[559] M. Furuhashi and G. S. Hotamisligil, "Fatty acid-binding proteins: role in metabolic diseases and potential as drug targets," *Nat Rev Drug Discov*, vol. 7, no. 6, pp. 489–503, 2008.

[560] C. Wolfrum, C. M. Borrmann, T. Borchers, and F. Spener, "Fatty acids and hypolipidemic drugs regulate peroxisome proliferator-activated receptors alpha - and gamma-mediated gene expression via liver fatty acid binding protein: a signaling path to the nucleus," *Proc Natl Acad Sci U S A*, vol. 98, no. 5, pp. 2323–8, 2001.

[561] N. S. Tan, N. S. Shaw, N. Vinckenbosch, P. Liu, R. Yasmin, B. Desvergne, W. Wahli, and N. Noy, "Selective cooperation between fatty acid binding proteins and peroxisome proliferator-activated receptors in regulating transcription," *Mol Cell Biol*, vol. 22, no. 14, pp. 5114–27, 2002.

[562] L. Ding, X. Liang, D. Zhu, and Y. Lou, "Peroxisome proliferator-activated receptor alpha is involved in cardiomyocyte differentiation of murine embryonic stem cells in vitro," *Cell Biol Int*, vol. 31, no. 9, pp. 1002–9, 2007.

[563] V. Chandra, P. Huang, Y. Hamuro, S. Raghuram, Y. Wang, T. P. Burris, and F. Rastinejad, "Structure of the intact ppar-gamma-rxr- nuclear receptor complex on dna," *Nature*, vol. 456, no. 7220, pp. 350–6, 2008.

[564] D. L. van der Meer, T. Degenhardt, S. Vaisanen, P. J. de Groot, M. Heinaniemi, S. C. de Vries, M. Muller, C. Carlberg, and S. Kersten, "Profiling of promoter occupancy by pparalpha in human

hepatoma cells via chip-chip analysis," *Nucleic Acids Res*, vol. 38, no. 9, pp. 2839–50, 2010.

[565] Y. Guan, "Peroxisome proliferator-activated receptor family and its relationship to renal complications of the metabolic syndrome," *J Am Soc Nephrol*, vol. 15, no. 11, pp. 2801–15, 2004.

[566] J. E. Noonan, A. J. Jenkins, J. X. Ma, A. C. Keech, J. J. Wang, and E. L. Lamoureux, "An update on the molecular actions of fenofibrate and its clinical effects on diabetic retinopathy and other microvascular end points in patients with diabetes," *Diabetes*, vol. 62, no. 12, pp. 3968–75, 2013.

[567] H. Keller, P. R. Devchand, M. Perroud, and W. Wahli, "Ppar alpha structure-function relationships derived from species-specific differences in responsiveness to hypolipidemic agents," *Biol Chem*, vol. 378, no. 7, pp. 651–5, 1997.

[568] A. Bernardes, P. C. Souza, J. R. Muniz, C. G. Ricci, S. D. Ayers, N. M. Parekh, A. S. Godoy, D. B. Trivella, P. Reinach, P. Webb, M. S. Skaf, and I. Polikarpov, "Molecular mechanism of peroxisome proliferator-activated receptor alpha activation by wy14643: a new mode of ligand recognition and receptor stabilization," *J Mol Biol*, vol. 425, no. 16, pp. 2878–93, 2013.

[569] A. Bernardes, P. C. Souza, J. R. Muniz, C. G. Ricci, S. D. Ayers, N. M. Parekh, A. S. Godoy, D. B. Trivella, P. Reinach, P. Webb, M. S. Skaf, and I. Polikarpov, "Molecular mechanism of peroxisome proliferator-activated receptor alpha activation by wy14643: a new mode of ligand recognition and receptor stabilization," *J Mol Biol*, vol. 425, no. 16, pp. 2878–93, 2013.

[570] A. A. Santilli, A. C. Scotese, and R. M. Tomarelli, "A potent antihypercholesterolemic agent: (4-chloro-6-(2,3-xylidino)-2-pyrimidinylthio) acetic acid (wy-14643)," *Experientia*, vol. 30, no. 10, pp. 1110–1, 1974.

[571] G. Wolkart, A. Schrammel, K. Dorffel, G. Haemmerle, R. Zechner, and B. Mayer, "Cardiac dysfunction in adipose triglyceride lipase deficiency: treatment with a pparalpha agonist," *Br J Pharmacol*, vol. 165, no. 2, pp. 380–9, 2012.

[572] C. Mascaro, E. Acosta, J. A. Ortiz, P. F. Marrero, F. G. Hegardt, and D. Haro, "Control of human muscle-type carnitine palmitoyltransferase i gene transcription by peroxisome proliferator-activated receptor," *J Biol Chem*, vol. 273, no. 15, pp. 8560–3, 1998.

[573] J. M. Brandt, F. Djouadi, and D. P. Kelly, "Fatty acids activate transcription of the muscle carnitine palmitoyltransferase i gene in cardiac myocytes via the peroxisome proliferator-activated receptor alpha," *J Biol Chem*, vol. 273, no. 37, pp. 23786–92, 1998.

[574] M. J. Barrero, N. Camarero, P. F. Marrero, and D. Haro, "Control of human carnitine palmitoyltransferase ii gene transcription by peroxisome proliferator-activated receptor through a partially conserved peroxisome proliferator-responsive element," *Biochem J*, vol. 369, no. Pt 3, pp. 721–9, 2003.

[575] T. Gulick, S. Cresci, T. Caira, D. D. Moore, and D. P. Kelly, "The peroxisome proliferator-activated receptor regulates mitochondrial fatty acid oxidative enzyme gene expression," *Proc Natl Acad Sci U S A*, vol. 91, no. 23, pp. 11012–6, 1994.

[576] D. M. Muoio, P. S. MacLean, D. B. Lang, S. Li, J. A. Houmard, J. M. Way, D. A. Winegar, J. C. Corton, G. L. Dohm, and W. E. Kraus, "Fatty acid homeostasis and induction of lipid regulatory genes in skeletal muscles of peroxisome proliferator-activated receptor (ppar) alpha knock-out mice. evidence for compensatory regulation by ppar delta," *J Biol Chem*, vol. 277, no. 29, pp. 26089–97, 2002.

[577] M. C. Sugden, K. Bulmer, G. F. Gibbons, and M. J. Holness, "Role of peroxisome proliferator-activated receptor-alpha in the mechanism underlying changes in renal pyruvate dehydrogenase kinase isoform 4 protein expression in starvation and after refeeding," *Arch Biochem*

Biophys, vol. 395, no. 2, pp. 246–52, 2001.

[578] K. Motojima, P. Passilly, J. M. Peters, F. J. Gonzalez, and N. Latruffe, "Expression of putative fatty acid transporter genes are regulated by peroxisome proliferator-activated receptor alpha and gamma activators in a tissue- and inducer-specific manner," *J Biol Chem*, vol. 273, no. 27, pp. 16710–4, 1998.

[579] M. E. Young, S. Patil, J. Ying, C. Depre, H. S. Ahuja, G. L. Shipley, S. M. Stepkowski, P. J. Davies, and H. Taegtmeyer, "Uncoupling protein 3 transcription is regulated by peroxisome proliferator-activated receptor (alpha) in the adult rodent heart," *FASEB J*, vol. 15, no. 3, pp. 833–45, 2001.

[580] K. Schoonjans, M. Watanabe, H. Suzuki, A. Mahfoudi, G. Krey, W. Wahli, P. Grimaldi, B. Staels, T. Yamamoto, and J. Auwerx, "Induction of the acyl-coenzyme a synthetase gene by fibrates and fatty acids is mediated by a peroxisome proliferator response element in the c promoter," *J Biol Chem*, vol. 270, no. 33, pp. 19269–76, 1995.

[581] M. H. Hsu, U. Savas, K. J. Griffin, and E. F. Johnson, "Identification of peroxisome proliferator-responsive human genes by elevated expression of the peroxisome proliferator-activated receptor alpha in hepg2 cells," *J Biol Chem*, vol. 276, no. 30, pp. 27950–8, 2001.

[582] T. Aoyama, J. M. Peters, N. Iritani, T. Nakajima, K. Furihata, T. Hashimoto, and F. J. Gonzalez, "Altered constitutive expression of fatty acid-metabolizing enzymes in mice lacking the peroxisome proliferator-activated receptor alpha (pparalpha)," *J Biol Chem*, vol. 273, no. 10, pp. 5678–84, 1998.

[583] M. Rakhshandehroo, G. Hooiveld, M. Muller, and S. Kersten, "Comparative analysis of gene regulation by the transcription factor pparalpha between mouse and human," *PLoS One*, vol. 4, no. 8, p. e6796, 2009.

[584] M. Rakhshandehroo, L. M. Sanderson, M. Matilainen, R. Stienstra, C. Carlberg, P. J. de Groot, M. Muller, and S. Kersten, "Comprehensive analysis of pparalpha-dependent regulation of hepatic lipid metabolism by expression profiling," *PPAR Res*, vol. 2007, p. 26839, 2007.

[585] B. N. Finck, "The ppar regulatory system in cardiac physiology and disease," *Cardiovasc Res*, vol. 73, no. 2, pp. 269–77, 2007.

[586] F. Sharifpanah, M. Wartenberg, M. Hannig, H. M. Piper, and H. Sauer, "Peroxisome proliferator-activated receptor alpha agonists enhance cardiomyogenesis of mouse es cells by utilization of a reactive oxygen species-dependent mechanism," *Stem Cells*, vol. 26, no. 1, pp. 64–71, 2008.

[587] L. Ding, X. G. Liang, and Y. J. Lou, "Time-dependence of cardiomyocyte differentiation disturbed by peroxisome proliferator-activated receptor alpha inhibitor gw6471 in murine embryonic stem cells in vitro," *Acta Pharmacol Sin*, vol. 28, no. 5, pp. 634–42, 2007.

[588] P. M. Barger and D. P. Kelly, "Ppar signaling in the control of cardiac energy metabolism," *Trends Cardiovasc Med*, vol. 10, no. 6, pp. 238–45, 2000.

[589] K. A. van der Lee, M. M. Vork, J. E. De Vries, P. H. Willemsen, J. F. Glatz, R. S. Reneman, G. J. Van der Vusse, and M. Van Bilsen, "Long-chain fatty acid-induced changes in gene expression in neonatal cardiac myocytes," *J Lipid Res*, vol. 41, no. 1, pp. 41–7, 2000.

[590] L. Cheng, G. Ding, Q. Qin, Y. Xiao, D. Woods, Y. E. Chen, and Q. Yang, "Peroxisome proliferator-activated receptor delta activates fatty acid oxidation in cultured neonatal and adult cardiomyocytes," *Biochem Biophys Res Commun*, vol. 313, no. 2, pp. 277–86, 2004.

[591] A. J. Gilde, K. A. van der Lee, P. H. Willemsen, G. Chinetti, F. R. van der Leij, G. J. van der Vusse, B. Staels, and M. van Bilsen, "Peroxisome proliferator-activated receptor (ppar)

alpha and pparbeta/delta, but not ppargamma, modulate the expression of genes involved in cardiac lipid metabolism," *Circ Res*, vol. 92, no. 5, pp. 518–24, 2003.

[592] F. Djouadi, C. J. Weinheimer, J. E. Saffitz, C. Pitchford, J. Bastin, F. J. Gonzalez, and D. P. Kelly, "A gender-related defect in lipid metabolism and glucose homeostasis in peroxisome proliferator- activated receptor alpha- deficient mice," *J Clin Invest*, vol. 102, no. 6, pp. 1083–91, 1998.

[593] F. Djouadi, J. M. Brandt, C. J. Weinheimer, T. C. Leone, F. J. Gonzalez, and D. P. Kelly, "The role of the peroxisome proliferator-activated receptor alpha (ppar alpha) in the control of cardiac lipid metabolism," *Prostaglandins Leukot Essent Fatty Acids*, vol. 60, no. 5-6, pp. 339–43, 1999.

[594] M. Van Bilsen, J. E. de Vries, and G. J. Van der Vusse, "Long-term effects of fatty acids on cell viability and gene expression of neonatal cardiac myocytes," *Prostaglandins Leukot Essent Fatty Acids*, vol. 57, no. 1, pp. 39–45, 1997.

[595] B. N. Finck, J. J. Lehman, T. C. Leone, M. J. Welch, M. J. Bennett, A. Kovacs, X. Han, R. W. Gross, R. Kozak, G. D. Lopaschuk, and D. P. Kelly, "The cardiac phenotype induced by pparalpha overexpression mimics that caused by diabetes mellitus," *J Clin Invest*, vol. 109, no. 1, pp. 121–30, 2002.

[596] P. Wu, J. M. Peters, and R. A. Harris, "Adaptive increase in pyruvate dehydrogenase kinase 4 during starvation is mediated by peroxisome proliferator-activated receptor alpha," *Biochem Biophys Res Commun*, vol. 287, no. 2, pp. 391–6, 2001.

[597] A. J. Murray, M. Panagia, D. Hauton, G. F. Gibbons, and K. Clarke, "Plasma free fatty acids and peroxisome proliferator-activated receptor alpha in the control of myocardial uncoupling protein levels," *Diabetes*, vol. 54, no. 12, pp. 3496–502, 2005.

[598] M. P. Thompson and D. Kim, "Links between fatty acids and expression of ucp2 and ucp3 mrnas," *FEBS Lett*, vol. 568, no. 1-3, pp. 4–9, 2004.

[599] M. M. Rhead, G. Eglinton, G. H. Draffan, and P. J. England, "Conversion of oleic acid to saturated fatty acids in severn estuary sediments," *Nature*, vol. 232, no. 5309, pp. 327–30, 1971.

[600] C. T. Jones and T. P. Rolph, "Metabolism during fetal life: a functional assessment of metabolic development," *Physiol Rev*, vol. 65, no. 2, pp. 357–430, 1985.

[601] E. Poon, W. Keung, Y. Liang, R. Ramalingam, B. Yan, S. Zhang, A. Chopra, J. Moore, A. Herren, D. K. Lieu, H. S. Wong, Z. Weng, O. T. Wong, Y. W. Lam, G. F. Tomaselli, C. Chen, K. R. Boheler, and R. A. Li, "Proteomic analysis of human pluripotent stem cell-derived, fetal, and adult ventricular cardiomyocytes reveals pathways crucial for cardiac metabolism and maturation," *Circ Cardiovasc Genet*, vol. 8, no. 3, pp. 427–36, 2015.

[602] B. N. Finck, "Effects of pparalpha on cardiac glucose metabolism: a transcriptional equivalent of the glucose-fatty acid cycle?," *Expert Rev Cardiovasc Ther*, vol. 4, no. 2, pp. 161–71, 2006.

[603] J. Pfleger, M. He, and M. Abdellatif, "Mitochondrial complex ii is a source of the reserve respiratory capacity that is regulated by metabolic sensors and promotes cell survival," *Cell Death Dis*, vol. 6, p. e1835, 2015.

[604] H. Naito, I. Melnychenko, M. Didie, K. Schneiderbanger, P. Schubert, S. Rosenkranz, T. Eschenhagen, and W. H. Zimmermann, "Optimizing engineered heart tissue for therapeutic applications as surrogate heart muscle," *Circulation*, vol. 114, no. 1 Suppl, pp. I72–8, 2006.

[605] G. Kensah, A. Roa Lara, J. Dahlmann, R. Zweigerdt, K. Schwanke, J. Hegermann, D. Skvorc, A. Gawol, A. Azizian, S. Wagner, L. S. Maier, A. Krause, G. Drager, M. Ochs, A. Haverich, I. Gruh, and U. Martin,

"Murine and human pluripotent stem cell-derived cardiac bodies form contractile myocardial tissue in vitro," *Eur Heart J*, vol. 34, no. 15, pp. 1134–46, 2013.

[606] C. P. Jackman, A. L. Carlson, and N. Bursac, "Dynamic culture yields engineered myocardium with near-adult functional output," *Biomaterials*, vol. 111, pp. 66–79, 2016.

[607] K. Baar, "New dimensions in tissue engineering: possible models for human physiology," *Exp Physiol*, vol. 90, no. 6, pp. 799–806, 2005.

[608] T. Eschenhagen and W. H. Zimmermann, "Engineering myocardial tissue," *Circ Res*, vol. 97, no. 12, pp. 1220–31, 2005.

[609] W. H. Zimmermann, M. Didie, G. H. Wasmeier, U. Nixdorff, A. Hess, I. Melnychenko, O. Boy, W. L. Neuhuber, M. Weyand, and T. Eschenhagen, "Cardiac grafting of engineered heart tissue in syngenic rats," *Circulation*, vol. 106, no. 12 Suppl 1, pp. I151–7, 2002.

[610] A. Stohr, F. W. Friedrich, F. Flenner, B. Geertz, A. Eder, S. Schaaf, M. N. Hirt, J. Uebeler, S. Schlossarek, L. Carrier, A. Hansen, and T. Eschenhagen, "Contractile abnormalities and altered drug response in engineered heart tissue from mybpc3-targeted knock-in mice," *J Mol Cell Cardiol*, vol. 63, pp. 189–98, 2013.

[611] W. J. de Lange, A. C. Grimes, L. F. Hegge, and J. C. Ralphe, "Ablation of cardiac myosin-binding protein-c accelerates contractile kinetics in engineered cardiac tissue," *J Gen Physiol*, vol. 141, no. 1, pp. 73–84, 2013.

[612] W. J. de Lange, L. F. Hegge, A. C. Grimes, C. W. Tong, T. M. Brost, R. L. Moss, and J. C. Ralphe, "Neonatal mouse-derived engineered cardiac tissue: a novel model system for studying genetic heart disease," *Circ Res*, vol. 109, no. 1, pp. 8–19, 2011.

[613] M. Tiburcy, J. E. Hudson, P. Balfanz, S. Schlick, T. Meyer, M. L. Chang Liao, E. Levent, F. Raad, S. Zeidler, E. Wingender, J. Riegler, M. Wang, J. D. Gold, I. Kehat, E. Wettwer, U. Ravens, P. Dierickx, L. W. van Laake, M. J. Goumans, S. Khadjeh, K. Toischer, G. Hasenfuss, L. A. Couture, A. Unger, W. A. Linke, T. Araki, B. Neel, G. Keller, L. Gepstein, J. C. Wu, and W. H. Zimmermann, "Defined engineered human myocardium with advanced maturation for applications in heart failure modeling and repair," *Circulation*, vol. 135, no. 19, pp. 1832–1847, 2017.

[614] M. N. Hirt, N. A. Sorensen, L. M. Bartholdt, J. Boeddinghaus, S. Schaaf, A. Eder, I. Vollert, A. Stohr, T. Schulze, A. Witten, M. Stoll, A. Hansen, and T. Eschenhagen, "Increased afterload induces pathological cardiac hypertrophy: a new in vitro model," *Basic Res Cardiol*, vol. 107, no. 6, p. 307, 2012.

[615] M. D. Lemoine, I. Mannhardt, K. Breckwoldt, M. Prondzynski, F. Flenner, B. Ulmer, M. N. Hirt, C. Neuber, A. Horvath, B. Kloth, H. Reichenspurner, S. Willems, A. Hansen, T. Eschenhagen, and T. Christ, "Human ipsc-derived cardiomyocytes cultured in 3d engineered heart tissue show physiological upstroke velocity and sodium current density," *Sci Rep*, vol. 7, no. 1, p. 5464, 2017.

[616] A. Eder, A. Hansen, J. Uebeler, T. Schulze, C. Neuber, S. Schaaf, L. Yuan, T. Christ, M. A. Vos, and T. Eschenhagen, "Effects of proarrhythmic drugs on relaxation time and beating pattern in rat engineered heart tissue," *Basic Res Cardiol*, vol. 109, no. 6, p. 436, 2014.

[617] I. Mannhardt, K. Breckwoldt, D. Letuffe-Breniere, S. Schaaf, H. Schulz, C. Neuber, A. Benzin, T. Werner, A. Eder, T. Schulze, B. Klampe, T. Christ, M. N. Hirt, N. Huebner, A. Moretti, T. Eschenhagen, and A. Hansen, "Human engineered heart tissue: Analysis of contractile force," *Stem Cell Reports*, vol. 7, no. 1, pp. 29–42, 2016.

[618] S. Schaaf, A. Eder, I. Vollert, A. Stohr, A. Hansen, and T. Eschenhagen,

"Generation of strip-format fibrin-based engineered heart tissue (eht)," *Methods Mol Biol*, vol. 1181, pp. 121–9, 2014.

[619] A. Stoehr, C. Neuber, C. Baldauf, I. Vollert, F. W. Friedrich, F. Flenner, L. Carrier, A. Eder, S. Schaaf, M. N. Hirt, B. Aksehirlioglu, C. W. Tong, A. Moretti, T. Eschenhagen, and A. Hansen, "Automated analysis of contractile force and ca2+ transients in engineered heart tissue," *Am J Physiol Heart Circ Physiol*, vol. 306, no. 9, pp. H1353–63, 2014.

[620] I. Mannhardt, U. Saleem, A. Benzin, T. Schulze, B. Klampe, T. Eschenhagen, and A. Hansen, "Automated contraction analysis of human engineered heart tissue for cardiac drug safety screening," *J Vis Exp*, no. 122, 2017.

[621] A. U. Uzun, I. Mannhardt, K. Breckwoldt, A. Horvath, S. S. Johannsen, A. Hansen, T. Eschenhagen, and T. Christ, "Ca(2+)-currents in human induced pluripotent stem cell-derived cardiomyocytes effects of two different culture conditions," *Front Pharmacol*, vol. 7, p. 300, 2016.

[622] Z. Li, X. Guo, S. Matsushita, and J. Guan, "Differentiation of cardiosphere-derived cells into a mature cardiac lineage using biodegradable poly(n-isopropylacrylamide) hydrogels," *Biomaterials*, vol. 32, no. 12, pp. 3220–32, 2011.

[623] K. Wittmann, K. Storck, C. Muhr, H. Mayer, S. Regn, R. Staudenmaier, H. Wiese, G. Maier, P. Bauer-Kreisel, and T. Blunk, "Development of volume-stable adipose tissue constructs using polycaprolactone-based polyurethane scaffolds and fibrin hydrogels," *J Tissue Eng Regen Med*, vol. 10, no. 10, pp. E409–E418, 2016.

[624] K. Nagamine, T. Kawashima, S. Sekine, Y. Ido, M. Kanzaki, and M. Nishizawa, "Spatiotemporally controlled contraction of micropatterned skeletal muscle cells on a hydrogel sheet," *Lab Chip*, vol. 11, no. 3, pp. 513–7, 2011.

[625] D. L. Brutsaert, "Cardiac endothelial-myocardial signaling: its role in cardiac growth, contractile performance, and rhythmicity," *Physiol Rev*, vol. 83, no. 1, pp. 59–115, 2003.

[626] A. C. Nag and R. Zak, "Dissociation of adult mammalian heart into single cell suspension: an ultrastructural study," *J Anat*, vol. 129, no. Pt 3, pp. 541–59, 1979.

[627] M. Radisic, M. Euloth, L. Yang, R. Langer, L. E. Freed, and G. Vunjak-Novakovic, "High-density seeding of myocyte cells for cardiac tissue engineering," *Biotechnol Bioeng*, vol. 82, no. 4, pp. 403–14, 2003.

[628] S. Tohyama, F. Hattori, M. Sano, T. Hishiki, Y. Nagahata, T. Matsuura, H. Hashimoto, T. Suzuki, H. Yamashita, Y. Satoh, T. Egashira, T. Seki, N. Muraoka, H. Yamakawa, Y. Ohgino, T. Tanaka, M. Yoichi, S. Yuasa, M. Murata, M. Suematsu, and K. Fukuda, "Distinct metabolic flow enables large-scale purification of mouse and human pluripotent stem cell-derived cardiomyocytes," *Cell Stem Cell*, vol. 12, no. 1, pp. 127–37, 2013.

[629] Y. Zhang, Y. Cheng, C. Chen, Q. Liu, X. Bi, L. Duan, J. Liu, M. Wan, L. Huang, and K. Hu, "Cd36 upregulation in ht-29 tumor cells cultured on 3d multicellular spheroids culturing platform based on anisotropic magnetic hydrogel," *J Biomed Nanotechnol*, vol. 14, no. 3, pp. 594–600, 2018.

[630] D. Kim, E. Monaco, A. Maki, A. S. de Lima, H. J. Kong, W. L. Hurley, and M. B. Wheeler, "Morphologic and transcriptomic comparison of adipose- and bone-marrow-derived porcine stem cells cultured in alginate hydrogels," *Cell Tissue Res*, vol. 341, no. 3, pp. 359–70, 2010.

[631] K. Sekine, A. Revzin, R. G. Tompkins, and M. Toner, "Panning of multiple subsets of leukocytes on antibody-decorated poly(ethylene) glycol-coated glass slides," *J Immunol Methods*, vol. 313, no. 1-2, pp. 96–109, 2006.

[632] M. Guvendiren, M. Perepelyuk, R. G. Wells, and J. A. Burdick, "Hydrogels with differential and patterned mechanics to study stiffness-mediated myofibroblastic differentiation of hepatic stellate cells," *J Mech Behav Biomed Mater*, vol. 38, pp. 198–208, 2014.

[633] M. E. L. Lago, L. P. da Silva, C. Henriques, A. F. Carvalho, R. L. Reis, and A. P. Marques, "Generation of gellan gum-based adipose-like microtissues," *Bioengineering (Basel)*, vol. 5, no. 3, 2018.

[634] M. Patel, H. J. Moon, Y. Ko du, and B. Jeong, "Composite system of graphene oxide and polypeptide thermogel as an injectable 3d scaffold for adipogenic differentiation of tonsil-derived mesenchymal stem cells," *ACS Appl Mater Interfaces*, vol. 8, no. 8, pp. 5160–9, 2016.

[635] C. Robertson, D. D. Tran, and S. C. George, "Concise review: maturation phases of human pluripotent stem cell-derived cardiomyocytes," *Stem Cells*, vol. 31, no. 5, pp. 829–37, 2013.

[636] N. E. Buroker, X. H. Ning, and M. Portman, "Cardiac pparalpha protein expression is constant as alternate nuclear receptors and pgc-1 coordinately increase during the postnatal metabolic transition," *PPAR Res*, vol. 2008, p. 279531, 2008.

[637] J. England and S. Loughna, "Heavy and light roles: myosin in the morphogenesis of the heart," *Cell Mol Life Sci*, vol. 70, no. 7, pp. 1221–39, 2013.

[638] K. Osafune, L. Caron, M. Borowiak, R. J. Martinez, C. S. Fitz-Gerald, Y. Sato, C. A. Cowan, K. R. Chien, and D. A. Melton, "Marked differences in differentiation propensity among human embryonic stem cell lines," *Nat Biotechnol*, vol. 26, no. 3, pp. 313–5, 2008.

[639] P. W. Burridge, D. Anderson, H. Priddle, M. D. Barbadillo Munoz, S. Chamberlain, C. Allegrucci, L. E. Young, and C. Denning, "Improved human embryonic stem cell embryoid body homogeneity and cardiomyocyte differentiation from a novel v-96 plate aggregation system highlights interline variability," *Stem Cells*, vol. 25, no. 4, pp. 929–38, 2007.

[640] P. W. Burridge, G. Keller, J. D. Gold, and J. C. Wu, "Production of de novo cardiomyocytes: human pluripotent stem cell differentiation and direct reprogramming," *Cell Stem Cell*, vol. 10, no. 1, pp. 16–28, 2012.

[641] D. P. Francis, M. Mielewczik, D. Zargaran, and G. D. Cole, "Autologous bone marrow-derived stem cell therapy in heart disease: discrepancies and contradictions," *Int J Cardiol*, vol. 168, no. 4, pp. 3381–403, 2013.

[642] C. Frantz, K. M. Stewart, and V. M. Weaver, "The extracellular matrix at a glance," *J Cell Sci*, vol. 123, no. Pt 24, pp. 4195–200, 2010.

[643] K. L. Fujimoto, K. Tobita, W. D. Merryman, J. Guan, N. Momoi, D. B. Stolz, M. S. Sacks, B. B. Keller, and W. R. Wagner, "An elastic, biodegradable cardiac patch induces contractile smooth muscle and improves cardiac remodeling and function in subacute myocardial infarction," *J Am Coll Cardiol*, vol. 49, no. 23, pp. 2292–300, 2007.

[644] V. Fuster, "Global burden of cardiovascular disease: time to implement feasible strategies and to monitor results," *J Am Coll Cardiol*, vol. 64, no. 5, pp. 520–2, 2014.

[645] S. A. Fisher, C. Doree, D. P. Taggart, A. Mathur, and E. Martin-Rendon, "Cell therapy for heart disease: Trial sequential analyses of two cochrane reviews," *Clin Pharmacol Ther*, vol. 100, no. 1, pp. 88–101, 2016.

[646] T. Force and K. L. Kolaja, "Cardiotoxicity of kinase inhibitors: the prediction and translation of preclinical models to clinical outcomes," *Nat Rev Drug Discov*, vol. 10, no. 2, pp. 111–26, 2011.

[647] S. A. Fisher, H. Zhang, C. Doree, A. Mathur, and E. Martin-Rendon, "Stem cell treatment for acute myocardial infarction," *Cochrane Database Syst Rev*, no. 9, p. CD006536, 2015.

[648] M. A. Gaballa, J. N. Sunkomat, H. Thai, E. Morkin, G. Ewy, and S. Goldman, "Grafting an acellular 3-dimensional collagen scaffold onto a non-transmural infarcted myocardium induces neo-angiogenesis and reduces cardiac remodeling," *J Heart Lung Transplant*, vol. 25, no. 8, pp. 946–54, 2006.

[649] J. D. Tugwood, I. Issemann, R. G. Anderson, K. R. Bundell, W. L. McPheat, and S. Green, "The mouse peroxisome proliferator activated receptor recognizes a response element in the 5' flanking sequence of the rat acyl coa oxidase gene," *EMBO J*, vol. 11, no. 2, pp. 433–9, 1992.

[650] T. Helledie, L. Grontved, S. S. Jensen, P. Kiilerich, L. Rietveld, T. Albrektsen, M. S. Boysen, J. Nohr, L. K. Larsen, J. Fleckner, H. G. Stunnenberg, K. Kristiansen, and S. Mandrup, "The gene encoding the acyl-coa-binding protein is activated by peroxisome proliferator-activated receptor gamma through an intronic response element functionally conserved between humans and rodents," *J Biol Chem*, vol. 277, no. 30, pp. 26821–30, 2002.

[651] N. Vu-Dac, K. Schoonjans, B. Laine, J. C. Fruchart, J. Auwerx, and B. Staels, "Negative regulation of the human apolipoprotein a-i promoter by fibrates can be attenuated by the interaction of the peroxisome proliferator-activated receptor with its response element," *J Biol Chem*, vol. 269, no. 49, pp. 31012–8, 1994.

[652] N. Vu-Dac, K. Schoonjans, V. Kosykh, J. Dallongeville, J. C. Fruchart, B. Staels, and J. Auwerx, "Fibrates increase human apolipoprotein a-ii expression through activation of the peroxisome proliferator-activated receptor," *J Clin Invest*, vol. 96, no. 2, pp. 741–50, 1995.

[653] N. Vu-Dac, P. Gervois, H. Jakel, M. Nowak, E. Bauge, H. Dehondt, B. Staels, L. A. Pennacchio, E. M. Rubin, J. Fruchart-Najib, and J. C. Fruchart, "Apolipoprotein a5, a crucial determinant of plasma triglyceride levels, is highly responsive to peroxisome proliferator-activated receptor alpha activators," *J Biol Chem*, vol. 278, no. 20, pp. 17982–5, 2003.

[654] X. Prieur, H. Coste, and J. C. Rodriguez, "The human apolipoprotein av gene is regulated by peroxisome proliferator-activated receptor-alpha and contains a novel farnesoid x-activated receptor response element," *J Biol Chem*, vol. 278, no. 28, pp. 25468–80, 2003.

[655] R. Hertz, J. Bishara-Shieban, and J. Bar-Tana, "Mode of action of peroxisome proliferators as hypolipidemic drugs. suppression of apolipoprotein c-iii," *J Biol Chem*, vol. 270, no. 22, pp. 13470–5, 1995.

[656] B. Zhang, S. L. Marcus, F. G. Sajjadi, K. Alvares, J. K. Reddy, S. Subramani, R. A. Rachubinski, and J. P. Capone, "Identification of a peroxisome proliferator-responsive element upstream of the gene encoding rat peroxisomal enoyl-coa hydratase/3-hydroxyacyl-coa dehydrogenase," *Proc Natl Acad Sci U S A*, vol. 89, no. 16, pp. 7541–5, 1992.

[657] O. Bardot, T. C. Aldridge, N. Latruffe, and S. Green, "Ppar-rxr heterodimer activates a peroxisome proliferator response element upstream of the bifunctional enzyme gene," *Biochem Biophys Res Commun*, vol. 192, no. 1, pp. 37–45, 1993.

[658] S. L. Marcus, K. S. Miyata, B. Zhang, S. Subramani, R. A. Rachubinski, and J. P. Capone, "Diverse peroxisome proliferator-activated receptors bind to the peroxisome proliferator-responsive elements of the rat hydratase/dehydrogenase and fatty acyl-coa oxidase genes but differentially induce expression," *Proc Natl Acad Sci U S A*, vol. 90, no. 12, pp. 5723–7, 1993.

[659] D. L. Kroetz, P. Yook, P. Costet, P. Bianchi, and T. Pineau, "Peroxisome proliferator-activated receptor alpha controls the hepatic cyp4a induction adaptive response to starvation and diabetes," *J Biol Chem*, vol. 273, no. 47, pp. 31581–9, 1998.

[660] A. S. Muerhoff, K. J. Griffin, and E. F. Johnson, "The peroxisome

proliferator-activated receptor mediates the induction of cyp4a6, a cytochrome p450 fatty acid omega-hydroxylase, by clofibric acid," *J Biol Chem*, vol. 267, no. 27, pp. 19051–3, 1992.

[661] E. F. Johnson, C. N. Palmer, K. J. Griffin, and M. H. Hsu, "Role of the peroxisome proliferator-activated receptor in cytochrome p450 4a gene regulation," *FASEB J*, vol. 10, no. 11, pp. 1241–8, 1996.

[662] S. K. Cheema and L. B. Agellon, "The murine and human cholesterol 7alpha-hydroxylase gene promoters are differentially responsive to regulation by fatty acids mediated via peroxisome proliferator-activated receptor alpha," *J Biol Chem*, vol. 275, no. 17, pp. 12530–6, 2000.

[663] M. C. Hunt, Y. Z. Yang, G. Eggertsen, C. M. Carneheim, M. Gafvels, C. Einarsson, and S. E. Alexson, "The peroxisome proliferator-activated receptor alpha (pparalpha) regulates bile acid biosynthesis," *J Biol Chem*, vol. 275, no. 37, pp. 28947–53, 2000.

[664] C. Tang, H. P. Cho, M. T. Nakamura, and S. D. Clarke, "Regulation of human delta-6 desaturase gene transcription: identification of a functional direct repeat-1 element," *J Lipid Res*, vol. 44, no. 4, pp. 686–95, 2003.

[665] H. Poirier, I. Niot, M. C. Monnot, O. Braissant, C. Meunier-Durmort, P. Costet, T. Pineau, W. Wahli, T. M. Willson, and P. Besnard, "Differential involvement of peroxisome-proliferator-activated receptors alpha and delta in fibrate and fatty-acid-mediated inductions of the gene encoding liver fatty-acid-binding protein in the liver and the small intestine," *Biochem J*, vol. 355, no. Pt 2, pp. 481–8, 2001.

[666] G. Martin, K. Schoonjans, A. M. Lefebvre, B. Staels, and J. Auwerx, "Coordinate regulation of the expression of the fatty acid transport protein and acyl-coa synthetase genes by pparalpha and ppargamma activators," *J Biol Chem*, vol. 272, no. 45, pp. 28210–7, 1997.

[667] K. Schoonjans, J. Peinado-Onsurbe, A. M. Lefebvre, R. A. Heyman, M. Briggs, S. Deeb, B. Staels, and J. Auwerx, "Pparalpha and ppargamma activators direct a distinct tissue-specific transcriptional response via a ppre in the lipoprotein lipase gene," *EMBO J*, vol. 15, no. 19, pp. 5336–48, 1996.

[668] K. A. Tobin, H. H. Steineger, S. Alberti, O. Spydevold, J. Auwerx, J. A. Gustafsson, and H. I. Nebb, "Cross-talk between fatty acid and cholesterol metabolism mediated by liver x receptor-alpha," *Mol Endocrinol*, vol. 14, no. 5, pp. 741–52, 2000.

[669] J. C. Rodriguez, G. Gil-Gomez, F. G. Hegardt, and D. Haro, "Peroxisome proliferator-activated receptor mediates induction of the mitochondrial 3-hydroxy-3-methylglutaryl-coa synthase gene by fatty acids," *J Biol Chem*, vol. 269, no. 29, pp. 18767–72, 1994.

[670] A. Y. Tu and J. J. Albers, "Functional analysis of the transcriptional activity of the mouse phospholipid transfer protein gene," *Biochem Biophys Res Commun*, vol. 287, no. 4, pp. 921–6, 2001.

[671] C. W. Miller and J. M. Ntambi, "Peroxisome proliferators induce mouse liver stearoyl-coa desaturase 1 gene expression," *Proc Natl Acad Sci U S A*, vol. 93, no. 18, pp. 9443–8, 1996.

[672] D. Lopez, R. B. Irby, and M. P. McLean, "Peroxisome proliferator-activated receptor alpha induces rat sterol carrier protein x promoter activity through two peroxisome proliferator-response elements," *Mol Cell Endocrinol*, vol. 205, no. 1-2, pp. 169–84, 2003.

[673] H. Y. Yoo, M. S. Chang, and H. M. Rho, "Induction of the rat cu/zn superoxide dismutase gene through the peroxisome proliferator-responsive element by arachidonic acid," *Gene*, vol. 234, no. 1, pp. 87–91, 1999.

[674] R. Hertz, M. Seckbach, M. M. Zakin, and J. Bar-Tana, "Transcriptional suppression of the transferrin

gene by hypolipidemic peroxisome proliferators," *J Biol Chem*, vol. 271, no. 1, pp. 218–24, 1996.

[675] V. Nicolas-Frances, V. K. Dasari, E. Abruzzi, T. Osumi, and N. Latruffe, "The peroxisome proliferator response element (ppre) present at positions -681/-669 in the rat liver 3-ketoacyl-coa thiolase b gene functionally interacts differently with pparalpha and hnf-4," *Biochem Biophys Res Commun*, vol. 269, no. 2, pp. 347–51, 2000.

[676] O. Barbier, L. Villeneuve, V. Bocher, C. Fontaine, I. P. Torra, C. Duhem, V. Kosykh, J. C. Fruchart, C. Guillemette, and B. Staels, "The udp-glucuronosyltransferase 1a9 enzyme is a peroxisome proliferator-activated receptor alpha and gamma target gene," *J Biol Chem*, vol. 278, no. 16, pp. 13975–83, 2003.

[677] M. J. Barbera, A. Schluter, N. Pedraza, R. Iglesias, F. Villarroya, and M. Giralt, "Peroxisome proliferator-activated receptor alpha activates transcription of the brown fat uncoupling protein-1 gene. a link between regulation of the thermogenic and lipid oxidation pathways in the brown fat cell," *J Biol Chem*, vol. 276, no. 2, pp. 1486–93, 2001.

[678] M. C. Hunt, P. J. Lindquist, J. M. Peters, F. J. Gonzalez, U. Diczfalusy, and S. E. Alexson, "Involvement of the peroxisome proliferator-activated receptor alpha in regulating long-chain acyl-coa thioesterases," *J Lipid Res*, vol. 41, no. 5, pp. 814–23, 2000.

[679] M. E. Young, G. W. Goodwin, J. Ying, P. Guthrie, C. R. Wilson, F. A. Laws, and H. Taegtmeyer, "Regulation of cardiac and skeletal muscle malonyl-coa decarboxylase by fatty acids," *Am J Physiol Endocrinol Metab*, vol. 280, no. 3, pp. E471–9, 2001.

[680] F. M. Campbell, R. Kozak, A. Wagner, J. Y. Altarejos, J. R. Dyck, D. D. Belke, D. L. Severson, D. P. Kelly, and G. D. Lopaschuk, "A role for peroxisome proliferator-activated receptor alpha (pparalpha) in the control of cardiac malonyl-coa levels: reduced fatty acid oxidation rates and increased glucose oxidation rates in the hearts of mice lacking pparalpha are associated with higher concentrations of malonyl-coa and reduced expression of malonyl-coa decarboxylase," *J Biol Chem*, vol. 277, no. 6, pp. 4098–103, 2002.

[681] T. Kok, H. Wolters, V. W. Bloks, R. Havinga, P. L. Jansen, B. Staels, and F. Kuipers, "Induction of hepatic abc transporter expression is part of the pparalpha-mediated fasting response in the mouse," *Gastroenterology*, vol. 124, no. 1, pp. 160–71, 2003.

[682] A. D. Edgar, C. Tomkiewicz, P. Costet, C. Legendre, M. Aggerbeck, J. Bouguet, B. Staels, C. Guyomard, T. Pineau, and R. Barouki, "Fenofibrate modifies transaminase gene expression via a peroxisome proliferator activated receptor alpha-dependent pathway," *Toxicol Lett*, vol. 98, no. 1-2, pp. 13–23, 1998.

[683] S. Kersten, S. Mandard, P. Escher, F. J. Gonzalez, S. Tafuri, B. Desvergne, and W. Wahli, "The peroxisome proliferator-activated receptor alpha regulates amino acid metabolism," *FASEB J*, vol. 15, no. 11, pp. 1971–8, 2001.

[684] J. C. Corton, L. Q. Fan, S. Brown, S. P. Anderson, C. Bocos, R. C. Cattley, A. Mode, and J. A. Gustafsson, "Down-regulation of cytochrome p450 2c family members and positive acute-phase response gene expression by peroxisome proliferator chemicals," *Mol Pharmacol*, vol. 54, no. 3, pp. 463–73, 1998.

[685] S. P. Anderson, L. Yoon, E. B. Richard, C. S. Dunn, R. C. Cattley, and J. C. Corton, "Delayed liver regeneration in peroxisome proliferator-activated receptor-alpha-null mice," *Hepatology*, vol. 36, no. 3, pp. 544–54, 2002.

[686] T. B. Barclay, J. M. Peters, M. B. Sewer, L. Ferrari, F. J. Gonzalez, and E. T. Morgan, "Modulation of cytochrome p-450 gene expression in endotoxemic mice is tissue specific and peroxisome proliferator-activated receptor-alpha dependent," *J*

Pharmacol Exp Ther, vol. 290, no. 3, pp. 1250–7, 1999.

[687] T. C. Leone, C. J. Weinheimer, and D. P. Kelly, "A critical role for the peroxisome proliferator-activated receptor alpha (pparalpha) in the cellular fasting response: the pparalpha-null mouse as a model of fatty acid oxidation disorders," *Proc Natl Acad Sci U S A*, vol. 96, no. 13, pp. 7473–8, 1999.

[688] S. S. Lee, T. Pineau, J. Drago, E. J. Lee, J. W. Owens, D. L. Kroetz, P. M. Fernandez-Salguero, H. Westphal, and F. J. Gonzalez, "Targeted disruption of the alpha isoform of the peroxisome proliferator-activated receptor gene in mice results in abolishment of the pleiotropic effects of peroxisome proliferators," *Mol Cell Biol*, vol. 15, no. 6, pp. 3012–22, 1995.

[689] G. S. Yu, Y. C. Lu, and T. Gulick, "Co-regulation of tissue-specific alternative human carnitine palmitoyltransferase ibeta gene promoters by fatty acid enzyme substrate," *J Biol Chem*, vol. 273, no. 49, pp. 32901–9, 1998.

[690] T. Hashimoto, T. Fujita, N. Usuda, W. Cook, C. Qi, J. M. Peters, F. J. Gonzalez, A. V. Yeldandi, M. S. Rao, and J. K. Reddy, "Peroxisomal and mitochondrial fatty acid beta-oxidation in mice nullizygous for both peroxisome proliferator-activated receptor alpha and peroxisomal fatty acyl-coa oxidase. genotype correlation with fatty liver phenotype," *J Biol Chem*, vol. 274, no. 27, pp. 19228–36, 1999.

[691] M. J. Holness, N. D. Smith, K. Bulmer, T. Hopkins, G. F. Gibbons, and M. C. Sugden, "Evaluation of the role of peroxisome-proliferator-activated receptor alpha in the regulation of cardiac pyruvate dehydrogenase kinase 4 protein expression in response to starvation, high-fat feeding and hyperthyroidism," *Biochem J*, vol. 364, no. Pt 3, pp. 687–94, 2002.

[692] S. M. Post, H. Duez, P. P. Gervois, B. Staels, F. Kuipers, and H. M. Princen, "Fibrates suppress bile acid synthesis via peroxisome proliferator-activated receptor-alpha-mediated downregulation of cholesterol 7alpha-hydroxylase and sterol 27-hydroxylase expression," *Arterioscler Thromb Vasc Biol*, vol. 21, no. 11, pp. 1840–5, 2001.

[693] M. Arand, M. W. Coughtrie, B. Burchell, F. Oesch, and L. W. Robertson, "Selective induction of bilirubin udp-glucuronosyl-transferase by perfluorodecanoic acid," *Chem Biol Interact*, vol. 77, no. 1, pp. 97–105, 1991.

[694] H. Guillou, P. Martin, S. Jan, S. D'Andrea, A. Roulet, D. Catheline, V. Rioux, T. Pineau, and P. Legrand, "Comparative effect of fenofibrate on hepatic desaturases in wild-type and peroxisome proliferator-activated receptor alpha-deficient mice," *Lipids*, vol. 37, no. 10, pp. 981–9, 2002.

[695] K. Yamazaki, J. Kuromitsu, and I. Tanaka, "Microarray analysis of gene expression changes in mouse liver induced by peroxisome proliferator-activated receptor alpha agonists," *Biochem Biophys Res Commun*, vol. 290, no. 3, pp. 1114–22, 2002.

[696] S. Kersten, S. Mandard, N. S. Tan, P. Escher, D. Metzger, P. Chambon, F. J. Gonzalez, B. Desvergne, and W. Wahli, "Characterization of the fasting-induced adipose factor fiaf, a novel peroxisome proliferator-activated receptor target gene," *J Biol Chem*, vol. 275, no. 37, pp. 28488–93, 2000.

[697] M. Kockx, P. P. Gervois, P. Poulain, B. Derudas, J. M. Peters, F. J. Gonzalez, H. M. Princen, T. Kooistra, and B. Staels, "Fibrates suppress fibrinogen gene expression in rodents via activation of the peroxisome proliferator-activated receptor-alpha," *Blood*, vol. 93, no. 9, pp. 2991–8, 1999.

[698] N. Macdonald, K. Barrow, R. Tonge, M. Davison, R. A. Roberts, and S. Chevalier, "Pparalpha-dependent alteration of grp94 expression in mouse hepatocytes," *Biochem Biophys Res Commun*, vol. 277, no. 3, pp. 699–704, 2000.

[699] A. Foliot and P. Beaune, "Effects of microsomal enzyme inducers on

glutathione s-transferase isoenzymes in livers of rats and hamsters," *Biochem Pharmacol*, vol. 48, no. 2, pp. 293–300, 1994.

[700] S. Hasmall, G. Orphanides, N. James, W. Pennie, K. Hedley, A. Soames, I. Kimber, and R. Roberts, "Downregulation of lactoferrin by pparalpha ligands: role in perturbation of hepatocyte proliferation and apoptosis," *Toxicol Sci*, vol. 68, no. 2, pp. 304–13, 2002.

[701] T. Kok, V. W. Bloks, H. Wolters, R. Havinga, P. L. Jansen, B. Staels, and F. Kuipers, "Peroxisome proliferator-activated receptor alpha (pparalpha)-mediated regulation of multidrug resistance 2 (mdr2) expression and function in mice," *Biochem J*, vol. 369, no. Pt 3, pp. 539–47, 2003.

[702] M. C. Hunt, K. Solaas, B. F. Kase, and S. E. Alexson, "Characterization of an acyl-coa thioesterase that functions as a major regulator of peroxisomal lipid metabolism," *J Biol Chem*, vol. 277, no. 2, pp. 1128–38, 2002.

[703] M. C. Sugden, K. Bulmer, G. F. Gibbons, B. L. Knight, and M. J. Holness, "Peroxisome-proliferator-activated receptor-alpha (pparalpha) deficiency leads to dysregulation of hepatic lipid and carbohydrate metabolism by fatty acids and insulin," *Biochem J*, vol. 364, no. Pt 2, pp. 361–8, 2002.

[704] P. Mardones, A. Pilon, M. Bouly, D. Duran, T. Nishimoto, H. Arai, K. F. Kozarsky, M. Altayo, J. F. Miquel, G. Luc, V. Clavey, B. Staels, and A. Rigotti, "Fibrates down-regulate hepatic scavenger receptor class b type i protein expression in mice," *J Biol Chem*, vol. 278, no. 10, pp. 7884–90, 2003.

[705] S. Kersten, J. Seydoux, J. M. Peters, F. J. Gonzalez, B. Desvergne, and W. Wahli, "Peroxisome proliferator-activated receptor alpha mediates the adaptive response to fasting," *J Clin Invest*, vol. 103, no. 11, pp. 1489–98, 1999.

[706] M. B. Armstrong and H. C. Towle, "Polyunsaturated fatty acids stimulate hepatic ucp-2 expression via a pparalpha-mediated pathway," *Am J Physiol Endocrinol Metab*, vol. 281, no. 6, pp. E1197–204, 2001.

[707] N. Tsuboyama-Kasaoka, M. Takahashi, H. Kim, and O. Ezaki, "Up-regulation of liver uncoupling protein-2 mrna by either fish oil feeding or fibrate administration in mice," *Biochem Biophys Res Commun*, vol. 257, no. 3, pp. 879–85, 1999.

[708] P. Delerive, K. De Bosscher, S. Besnard, W. Vanden Berghe, J. M. Peters, F. J. Gonzalez, J. C. Fruchart, A. Tedgui, G. Haegeman, and B. Staels, "Peroxisome proliferator-activated receptor alpha negatively regulates the vascular inflammatory gene response by negative cross-talk with transcription factors nf-kappab and ap-1," *J Biol Chem*, vol. 274, no. 45, pp. 32048–54, 1999.

[709] Y. Fukui and K. Motojima, "Expression of resistin in the adipose tissue is modulated by various factors including peroxisome proliferator-activated receptor alpha," *Diabetes Obes Metab*, vol. 4, no. 5, pp. 342–5, 2002.

[710] J. M. Peters, T. Aoyama, A. M. Burns, and F. J. Gonzalez, "Bezafibrate is a dual ligand for pparalpha and pparbeta: studies using null mice," *Biochim Biophys Acta*, vol. 1632, no. 1-3, pp. 80–9, 2003.

[711] L. Q. Fan, R. C. Cattley, and J. C. Corton, "Tissue-specific induction of 17 beta-hydroxysteroid dehydrogenase type iv by peroxisome proliferator chemicals is dependent on the peroxisome proliferator-activated receptor alpha," *J Endocrinol*, vol. 158, no. 2, pp. 237–46, 1998.

[712] G. Chinetti, F. G. Gbaguidi, S. Griglio, Z. Mallat, M. Antonucci, P. Poulain, J. Chapman, J. C. Fruchart, A. Tedgui, J. Najib-Fruchart, and B. Staels, "Cla-1/sr-bi is expressed in atherosclerotic lesion macrophages and regulated by activators of peroxisome proliferator-activated receptors," *Circulation*, vol. 101, no. 20, pp. 2411–7, 2000.

[713] M. J. Holness, K. Bulmer, G. F. Gibbons, and M. C. Sugden, "Up-regulation of pyruvate dehydrogenase kinase isoform 4 (pdk4) protein expression in oxidative skeletal muscle does not require the obligatory participation of peroxisome-proliferator-activated receptor alpha (pparalpha)," *Biochem J*, vol. 366, no. Pt 3, pp. 839–46, 2002.